

Alps
Adria
Acoustics
Association

The 8th Congress of the Alps Adria Acoustics Association

20-21 September 2018, Zagreb, Croatia

Conference Proceedings

ISBN 978-953-95097-2-7

Hrvatsko akustičko društvo
HAD
Acoustical Society of Croatia



Title: The 8th Congress of the Alps Adria Acoustics Association – Conference Proceedings

Publisher: Hrvatsko akustičko društvo (HAD)
Acoustical Society of Croatia (ASC)

Editors: Marko Horvat, Miljenko Krhen

Year: 2018

Published in: Zagreb, Croatia

ISBN: 978-953-95097-2-7

Editors' Note

The requirements on the layout of the manuscripts to be published in these Conference Proceedings were given in advance in form of a template. Nevertheless, in some cases, these requirements were not followed strictly, and the resulting manuscripts deviate from them to some extent. The final layout and the content of the manuscripts is the sole responsibility of the authors. The editors could not correct spelling or other errors, nor could they proof the language style. Therefore, the readers are asked to excuse any errors that may have resulted for reasons stated above. The editors are not responsible for the statements and opinions given in this publication.

Organizing institution

Acoustical Society of Croatia
(Hrvatsko akustičko društvo, HAD)
Unska 3
HR-10000 Zagreb,
Croatia

Hrvatsko akustičko društvo
HAD
Acoustical Society of Croatia

Contact

Congress Secretariat

E-mail: info@alpsadriaacoustics.eu
Phone: +38516129833
(chairperson)

Postal address:
Hrvatsko akustičko društvo
Unska 3, HR-10000 Zagreb
Croatia

Congress website www.alpsadriaacoustics.eu

Congress venue

Faculty of Transport and Traffic Sciences
University of Zagreb
Campus Borongaj (Object 69),
Borongajska 83f, 10000 Zagreb,
Croatia

Congress Committees

Organizing Committee

Prof. Dr. Tino Bucak
Prof. Dr. Mirko Čudina
Prof. Dr. Siniša Fajt
Doc. Dr. Marko Horvat
Prof. Dr. Kristian Jambrošić
Dipl. Ing. Fabio Kaiser
Dr. Miljenko Krhen
Prof. Dr. Antonio Petošić
Prof. Dr. Jurij Prezelj
Doc. Dr. Davor Sumpor
Prof. Mag. Gregor Widholm

Scientific Committee

Doc. Dr. Samo Beguš
Prof. Dr. Tino Bucak
Prof. Dr. Mirko Čudina
Dr. Ferdinand Deželak
Prof. Dr. Ivan Đurek
Prof. Dr. Siniša Fajt
Dr. Martin Hagmüller
Doc. Dr. Marko Horvat
Prof. Dr. Kristian Jambrošić
Dipl. Ing. Fabio Kaiser
Dr. Miljenko Krhen
Prof. Dr. Antonio Petošić
Prof. Dr. Jurij Prezelj
Mag. Mihael Ramšak
Doc. Dr. Davor Sumpor
Prof. Dr. Holger Waubke
Prof. Mag. Gregor Widholm

The 8th Congress of the Alps Adria Acoustics Association is co-organized by:

University of Zagreb, Faculty of Electrical Engineering and Computing

University of Zagreb, Faculty of Transport and Traffic Sciences

as a joint meeting with:

Austrian Acoustics Association

Slovenian Acoustical Society

under the auspices of:

European Acoustics Association

Croatian Academy of Engineering

and endorsed by:

Croatian Ergonomics Society

The congress is sponsored by:

International Commission for Acoustics

P-Audio

Storm Computers

Belmet 97

Welcome to the 8th Congress of the Alps Adria Acoustics Association!

The 8th Congress of the Alps Adria Acoustics Association will be held at the University of Zagreb in Zagreb, Croatia, from 20 to 21 September 2018.

The Alps Adria Acoustics Association (AAAA) was founded by the acoustical societies of Austria, Croatia and Slovenia in 2002 as a new regional association of scientists, experts and educators in the field of acoustics. The original goal was to promote all aspects of research in the field of acoustics in the whole of the region, and beyond. In addition, the aim was to improve the overall cooperation among the founding countries and their respective national societies.

Every two years one of the three founding societies of the AAAA organizes a scientific congress on acoustics. The main goal of these congresses is to bring together acousticians from Croatia, Austria and Slovenia, as well as from other European countries, in order to exchange knowledge, share research outcomes and strengthen cooperation for the benefit of the whole region. National and international experts present a number of scientific and applied papers on their research and professional activities in all fields of acoustics. Congress topics cover architectural and building acoustics, auditory and speech acoustics, environmental and transportation noise, machinery noise and vibration control, computational acoustics, electroacoustics, legislation in acoustics, musical acoustics, measurement techniques, non-linear acoustics, psychoacoustics and perception of sound, signal processing, sound generation and radiation, ultrasonics, hydroacoustics, etc.

The programme of the 8th Congress of AAAA includes two very interesting keynote talks given by prof. dr. Monika Rychtáriková and prof. dr. Jurij Prezelj, as well as 48 oral presentations of scientific papers with topics covering the interests of both the scientific community and the industry. Moreover, a roundtable discussion on noise legislation, its implementation in national laws and discovered challenges for experts and companies is organised as well.

Full papers based on abstracts that have been reviewed and accepted by two independent reviewers will be published in the Congress Proceedings, to be distributed to all Congress participants.

The 2018 Congress from the AAAA series is organized by the Acoustics Society of Croatia (HAD) acting on behalf of the Alps Adria Acoustics Association, and is certified as a symposium supported by the European Acoustics Association.

I look forward to meeting you in Zagreb in September 2018!

Kristian Jambrošić,
Congress Chair

Programme overview

Thursday, 20 September 2018

08:00 – 09:00	Registration		*08:00 – 09:00*
09:00 – 09:30	Opening ceremony		*09:00 – 09:30*
09:30 – 10:30	Keynote lecture 1		*09:30 – 10:30*
10:30 – 11:00	Coffee break		*10:30 – 11:00*
11:00 – 11:20	Building Acoustics	Electroacoustics	*11:00 – 11:20*
11:20 – 11:40			*11:20 – 11:40*
11:40 – 12:00		Signal processing	*11:40 – 12:00*
12:00 – 12:20			*12:00 – 12:20*
12:20 – 12:40			*12:20 – 12:40*
12:40 – 13:00	Ultrasound		*12:40 – 13:00*
13:00 – 14:00	Lunch		*13:00 – 14:00*
14:00 – 14:20	Musical acoustics	Measurement techniques	*14:00 – 14:20*
14:20 – 14:40			*14:20 – 14:40*
14:40 – 15:00	Room acoustics		*14:40 – 15:00*
15:00 – 15:20			*15:00 – 15:20*
15:20 – 15:40		Acoustic applications	*15:20 – 15:40*
15:40 – 16:00			*15:40 – 16:00*
16:00 – 16:30	Coffee break		*16:00 – 16:30*
16:30 – 16:50	Room acoustics (continued)	Noise	*16:30 – 16:50*
16:50 – 17:10			*16:50 – 17:10*
17:10 – 17:30			*17:10 – 17:30*
17:30 – 17:50			*17:30 – 17:50*
17:50 – 18:10			*17:50 – 18:10*
18:10 – 18:30			*18:10 – 18:30*
19:30 – 23:00	Conference dinner		19:30 – 23:00

Friday, 21 September 2018

08:00 – 09:00	Registration		*08:00 – 09:00*
09:00 – 10:00	Keynote lecture 2		*09:00 – 10:00*
10:00 – 10:30	Coffee break		*10:00 – 10:30*
10:30 – 10:50	Room acoustics (continued)	Diagnostics and monitoring	*10:30 – 10:50*
10:50 – 11:10			*10:50 – 11:10*
11:10 – 11:30			*11:10 – 11:30*
11:30 – 11:50	Sound quality		*11:30 – 11:50*
11:50 – 12:10			*11:50 – 12:10*
12:10 – 12:30			*12:10 – 12:30*
12:30 – 13:30	Lunch		*12:30 – 13:30*
13:30 – 16:30	Roundtable		*13:30 – 16:30*
16:30 – 17:00	Closing ceremony		*16:30 – 17:00*

Detailed programme

Thursday, 20 September 2018

8:00 – 9:00	Registration	
9:00 – 9:30	**Opening ceremony**	
9:30 – 10:30	**Keynote lecture** **Echolocation of people – what we know until now** *Prof. dr. Monika Rychtáriková, KU Leuven, Faculty of Architecture*	
10:30 – 11:00	**Coffee break**	
	Building Acoustics	**Room 1**
11:00 – 11:20	*Franz Dolezal, Niko Kumer* Semiempirical model for prediction of weighted sound reduction index of cross laminated timber walls with external thermal insulation composite systems	
11:20 – 11:40	*Maximilian Neusser, Herbert Müllner* The influence of secondary wall details on new descriptors for sound insulation of leightweight wall constructions	
11:40 – 12:00	*Daniel Urbán, N.B. Roozen, Monika Rychtáriková* The discussion on sound insulation performance of façades in Slovakia	
12:00 – 12:20	*Beata Mesterhazy, Attila Balazs Nagy* The effect of power socket holes on the sound insulation of walls	
12:20 – 12:40	*Zoltán Horváth* CDM experiences with different issues in building acoustics	
	Ultrasound	**Room 1**
12:40 – 13:00	*Petar Frančer, Iva Brkić, Antonio Petošić* Electromechanical and acoustical characterization of piezoceramic elements and ultrasound transducers	

* * *

	Electroacoustics	**Room 2**
11:00 – 11:20	*Tin Obradović, Siniša Fajt, Vladimir Olujić* Design, Modeling and Implementation of the Guitar Audio Interface	
11:20 – 11:40	*Tilen Mramor, Danijel Svenšek, Jurij Prezelj* Nonlinear response of loudspeakers	
	Signal processing	**Room 2**
11:40 – 12:00	*Holger Waubke* Single degree of freedom systems with Bouc hysteresis and filtered white noise	
12:00 – 12:20	*Ivan Djurek, Elena Maganić, Mia Suhanek* Music dynamic range of FM radio stations in Zagreb	

12:20 – 12:40 *Andrea Andrijašević*
Blind estimation of reverberation time – it is how you say it that matters

12:40 – 13:00 *Davor Šušković, Siniša Fajt, Domagoj Matić*
Speech intelligibility improvement for hearing impaired with hearing instruments and FM systems

13:00 – 14:00 **Lunch**

Musical acoustics **Room 1**

14:00 – 14:20 *Péter Fiala, Bence Szaksz*
Modelling collision problems in model-based sound synthesis of string instruments

14:20 – 14:40 *Nikola Kudrna, Kristian Jambrošić*
Granular sound synthesis

Room acoustics **Room 1**

14:40 – 15:00 *Kristian Jambrošić, Marko Horvat*
Acoustics of contemporary churches in Croatia

15:00 – 15:20 *Jonas Schira*
Enhancement of bass frequency absorption in fabric-based absorbers

15:20 – 15:40 *Çiğdem Türk*
The applicability of acoustic design approaches in early design stage by architects

15:40 – 16:00 *Rok Prislan, Daniel Svenšek*
Ray-tracing semiclassical (RTS) frequency response modeling for local- and extended- reaction boundaries

* * *

Measurement techniques **Room 2**

14:00 – 14:20 *Matej Tomc, Aleš Magajne, Samo Beguš, Gregor Geršak*
Physiology of monaural and binaural measurements of infrasound

14:20 – 14:40 *Biljana Tanatarec*
Evaluation of commercial software used for acoustic measurements

14:40 – 15:00 *Antonio Petošić, Petar Frančљek, Mario Štrbac, Peter Zátko, Daniel Urbán, Daniel Szabó*
Measurement uncertainty in the field of environmental noise and building acoustic measurements: experience from interlaboratory comparisons

15:00 – 15:20 *Antonio Petošić, Sanja Grubeša, Slobodan Šodolović, Petar Frančљek*
Acoustic performance of large parallel baffled silencers by using in-situ measurement method

Acoustic applications **Room 2**

15:20 – 15:40 *Mario Kalac, Paula Rinkovec, Josip Nimac, Miljenko Krhen*
Realization of audio guidance system

16:00 – 16:30 **Coffee break**

	Room acoustics (continued)	**Room 1**
16:30 – 16:50	*Siniša Fajt, Miljenko Krhen, Fabijan Žunić* Optimal reverberation time	
16:50 – 17:10	*Miljenko Krhen, Siniša Fajt, Fabijan Žunić* Audio signal processing in acoustically different rooms	
17:10 – 17:30	*Paulína Šujanová, Herbert Muellner* Development of acoustic parameter calculation tool for BIM supporting architectural design tools	
17:30 – 17:50	*Nika Šubic, Roman Kunič* Room acoustics calculator for educational and design purposes	
17:50 – 18:10	*Louena Shtrepi* Diffusive surface design guidelines	
18:10 – 18:30	*Vladimir Olujić, Siniša Fajt, Tin Obradović* Optimization of the acoustic quality of the listening room	

* * *

	Noise	**Room 2**
16:30 – 16:50	*Konca Saher* Rain noise sound intensity testing – London 2012 Olympics International Broadcasting Center case study	
16:50 – 17:10	*Ezgi Dadas, Fusun Demirel* Noise Protection in Industrial Buildings: Architectural Design Strategies	
17:10 – 17:30	*Ferdinand Deželak* Bad practice of one acoustical expert opinion	
17:30 – 17:50	*Gerald Schleinzer, David Thompson* Roll2Rail – New methods for pass-by noise certification of trains - part 2	
17:50 – 18:10	*David Fujs, Tino Bucak, Davor Franjković* Experimental assessment of aerodynamic noise on an airfoil surface	
18:10 – 18:30	*Dominik Jerinić, Marko Maradin, Tino Bucak* External noise analysis of supersonic fighter aircraft MiG-21 UMD	

Friday, 21 September 2018

8:00 – 9:00	Registration	
9:00 – 10:00	**Keynote lecture** **Application of non-standard measurement equipment for acoustic measurements** *Prof. dr. Jurij Prezelj, University of Ljubljana, Faculty of Mechanical Engineering*	
10:00 – 10:30	**Coffee break**	
	Room acoustics (continued)	**Room 1**
10:30 – 10:50	*Fatma Yelkenci Sert, Özgül Yılmaz Karaman* The case study on user satisfaction in relation to comfort conditions in manisa mosques: Çeşnigir mosque, Ivaz Paşa mosque, Sultan mosque and Hatuniye mosque	

10:50 – 11:10 *Goran Pavić, Liangfen Du*
Coupling of sound spaces by the Acoustical Surface Impedance approach

11:10 – 11:30 *Luka Čurović, Jure Murovec, Tadej Novaković, Jurij Prezelj*
Analysis of reverberation time in narrow band spectral resolution

Sound quality **Room 1**

11:30 – 11:50 *Tadej Novaković, Jurij Prezelj, Luka Čurović, Jure Murovec*
Subjective and objective noise analysis of new centrifugal impeller design

11:50 – 12:10 *Manuel Pürscher, Stefan Schöpf, Peter Fischer*
NVH signal analysis via pattern recognition ANNs: automotive brake creep groan as case study

12:10 – 12:30 *Severin Huemer-Kals, Manuel Pürscher, Peter Fischer*
Linearized simulative approach for the investigation of a friction-induced low-frequency oscillation phenomenon within passenger vehicle front axles

* * *

Diagnostics and monitoring **Room 2**

10:30 – 10:50 *Jurij Gostiša, Marko Hočevar*
Aeroacoustic investigation of the forward-curved fan inlet flow field

10:50 – 11:10 *Aleš Belšak, Jurij Prezelj*
Dedicated wavelet analysis for crack identification in gears

11:10 – 11:30 *Aleš Belšak, Mario Hirz*
Vibration analysis of multi-plate clutches for vehicles

11:30 – 11:50 *Ivan Vican, Gordan Kreković, Kristian Jambrošić*
Relevance of empirical mode decomposition for fetal heartbeat detection on smartphone devices

11:50 – 12:10 *Jure Murovec, Luka Čurović, Tadej Novaković, Jurij Prezelj*
Psychoacoustic approach for detection of cavitation in a centrifugal pump

12:10 – 12:30 *Tomaž Berlec, Jurij Prezelj, Janez Kušar*
Monitoring of production cell, based on noise and vibration signals

12:30 – 13:30 **Lunch**

13:30 – 16:30 **Roundtable “Noise legislation, its implementation in national laws and discovered challenges”** (with coffee break)

16:30 – 17:00 **Closing ceremony**

Keynote papers

ECHOLOCATION OF PEOPLE – WHAT WE KNOW UNTIL NOW

Monika Rychtáriková

KU Leuven, Faculty of Architecture, monika.rychtarikova@kuleuven.be

Abstract: *Although the main mechanisms of sound source localization is already quite well understood, much less is known about the auditory process of human acoustic self-localization and echolocation. Next to the haptic input, visually impaired people experience by probing the environment with a white cane, extract spatial information from sounds already present in a given space, or from the echo's of an impulsive self-produced sound such as finger snap, white cane tick or oral click, and use this spatial information to create a mental 3D map of their environment, where they are in it, and the distance to possible obstacles, pathways or portals.*
Only recently, it has been shown that experienced human echolocators develop the necessary neural circuitry to sense the strong early reflections of walls, and to distinguish them from the noisy and confusing mishmash of late-arriving weaker echo's. Humans, blind or sighted alike, can also learn to use echolocation by either using ambient sounds or by emitting sounds such as oral clicks, cane hits, or by means of portable clicking devices, listening to the echoes and interpreting the resulting patterns. When using ambient sounds, this ability is usually referred to as passive echolocation and in cases in which a person generates the sounds him/her-self, it is referred to as active echolocation.
This paper brings a state-of-the art knowledge on acoustic orientation and echolocation of humans.

Key words: echolocation, self-localization

8th Congress of the Alps Adria Acoustics Association
Zagreb, Croatia
20 – 21 September 2018

Hrvatsko akustičko društvo
HAD
Acoustical Society of Croatia

Application of non-standard measurement equipment for acoustic measurements

Jurij Prezelj

University of Ljubljana, Faculty of mechanical engineering (jurij.prezelj@fs.uni-lj.si)

Abstract: *The role of international acoustics standards is to provide comparable measurement results. They recommend conditions of acoustic environment, measurement procedures, required properties of the measuring equipment and conditions of the samples to be measured. Requirements to the appropriate measuring equipment are particularly strict in these standards. Measurement results, based on standard procedures, provide reproducible results, but they often do not contain data which might be of particular importance for the customer. Customers of acoustic measurements usually expect results to be reported in a way to help them with improving of their products or at the planning of noise reduction measures. This paper demonstrates how to use uncalibrated low cost measuring equipment and incorporate it into standardized procedures to satisfy the requirements of customers and perhaps even accreditation bodies.*

Key words: Deconvolution, Frequency Response Compensation, Linearity, Microphone pairing, Microphone Array Calibration, Immission Directivity, Uncalibrated Equipment, Traceability to SI units

1. INTRODUCTION

Acoustics deals with sound. Sound can be imagined as a propagation of pressure disturbance in the media within the area of observed space. Measurements in acoustics are limited to a fixed observation point. The first scientific insights about the sound were based on the frequency analysis, until 1900s. Sound pressure signals, as known today, were not available at the time, and only relative amplitudes of sound pressure could be compared or measured. In order to achieve a traceability of sound pressure to SI units a primary standard for calibration was needed. A calibration of microphones based on a Rayleigh disc in an impedance tube was the first calibration method, achieving a traceability of sound pressure to the SI units. As a primary standard it was used until 1970-s. Pistonphones and sound calibrators are commonly used today for laboratory calibration of measurement microphones. Reciprocity calibration is currently the favored primary standard for calibration of measurement microphones. Both, the calibration of measurement microphones and the traceability of sound pressure to the SI units enabled development of measuring techniques in acoustics and consequently their standardization.

2. STANDARDS

Standards provide people and organizations with a basis for mutual understanding, and are used as a tool to facilitate communication, measurement, commerce and manufacturing. They ensure that products, systems and measurement equipment are compatible and interoperable.
Standards form the basis for the introduction of new technologies and innovations, and ensure that products, their components and services supplied by different companies are mutually compatible. Standards also spread the knowledge within the industries, where products and processes supplied by various providers must interact with one another. Standardization is a voluntary cooperation among industry, consumers, public authorities, researchers and other interested parties for the development of technical specifications based on consensus.
Since 1945 number of international bodies publishing standard from the field of acoustics increased dramatically; ISO, IEC, IEEE, CEN, AES, etc. Standardization is identified in Horizon 2020 as one of the innovation-support measures by bridging the gap between research and the market, and helping the fast and easy transfer of research results to the European and international market.

2.1 Standards in Acoustics

Purpose and guidance of the standards in the field of the acoustic is different as for example the purpose of the standards in the field of digital communications. Nevertheless, ISO as most recognizable publisher of international standards has published 206 standards in the field of acoustics, and 39 standards are being developed at the moment, under three acoustic sections;

1) ISO/TCSC1 Noise: 125 published standards and 26 under development
2) ISO/TCSC2 Building Acoustics: 50 published standards and 9 under development
3) ISO/TCSC3 Underwater acoustics: 3 published standards and 2 under development

At the moment even standards from subjective psychoacoustics are being developed as for example: a) ISO/TS 12913-2: Soundscape - Part 2: Data collection and reporting requirements, and ISO/NP TS 15666: Assessment of noise annoyance by means of social and socio-acoustic surveys. Regardless to ISO sections, standards from the field of acoustics can be classified into three distinctive groups:

a) **Basic standards**, which define acoustic quantities, as for example the human hearing threshold of sound pressure, free field conditions, time constants fast, slow and impulse for effective RMS pressure, "A" and "C" frequency weighting, calculations of Equivalent level, percentile, psychoacoustic features,…
b) **Standards for measurement equipment**, which define requirements for measurement equipment. At the same time these standards classify measurement equipment into classes intended for different types of measurements.
c) Standards for **Measurement procedure** which are intended for achieving repeatability and reproducibility of results between different laboratories. These standards define:
    a. Measurement procedure, as for example 1) Sampling with number of microphones or/and their location, length of the sampled noise/sound signal, number of repetitions, 2) Sample with its operating condition, 3) Acoustic environment as for example free field, reverberant field, background noise, …etc)
    b. Measurement equipment
    c. Calculation algorithms of measured acoustic parameters with measurement uncertainty
    d. Reporting

Only all three groups of standards together provide credible measurement results. Repeatability and inter-laboratory comparison of results can be achieved within a narrow interval of measuring uncertainty, with high probability of true value in this interval, by following to standards by the letter. In this way reproducibility and traceability to international SI units is ensured.

2.2 Drawback of standardized work

Real physical domain of acoustic has different time scales and different spatial scales resulting in a large range of scales. Spatial scale of environmental noise of the city is 10^4 m, with a time constant of one year ($3*10^7$ sec). This scale is an example of the largest and longest scale of observation in acoustics, (except the acoustic of the sun and planets). Small spark in the electric motor with a dimension around 10^{-4} m generates noise and sound signal which should be sampled with 100 kHz, (time constant 10^{-5} sec). Spark is an example of the smallest and shortest time scales for acoustic is air. Acoustic emission however has even smaller scales in space and in time, but we will limit ourselves to sound in air. Upon space and time scale differences, we have sound pressure amplitude ranging from $2*10^{-5}$ Pa (hearing threshold) up to 10^3 Pa (amplitude of the gun at 0.3 m) and wavelengths of sound in air, ranging from 17,2 m down to 0,0172 m.

Large ranges of a spatial scale, and of a time scale, inevitable leads towards a large number of standards, each one for a limited purpose. The first ambiguity occurs with a selection of proper standard, which might be confusing for an uneducated customer. For example, 47 standards are available for measurement of sound power, 5 standards are available for measurement of sound absorption. A question emerges; where is the limit for the number of standards, and where is the place for common sense measurements, and how to trust such results? Is the future in increasing the number of standards, specialized for every single possible application?

A strict following to the standards generally provides traceable and valid results, but at the same time provides only results defined in standard. If more detailed information about sound/noise source or about the propagation path, or about acoustic sample is needed, a report from accredited laboratory may not provide adequate information for acoustic engineers.

There is no standard available for acoustic measurements of nonstandard methods, since there is no standard for common sense. However, there is Good Laboratory Practice guideline, which was introduced in 1972 in New Zealand and in Denmark, dedicated for industrial biochemical laboratories. Such approaches lead towards establishing the ILAC and national and international accreditation bodies like SA, HAA, AA.

Internationally accepted standards sometimes make no sense. For example:

a. Inconsistency between IEC 61672-1 and IEC 61672-2 in relation to Peak C sound levels. While Clause 17 in IEC 61672-2 states that Peak C shall be tested, the IEC 61672-1 states that the SLMs may have Peak C capability i.e. the peak C capability is not mandatory. Adding the words ‘if available’ in IEC 61672-2 can remove this ambiguity.
b. ISO 3745:2012, ISO 3746:2010 and ISO 3744:2010; Why measurement locations of microphones for Lw measurement are so precisely defined, yet orientation of the source within the control volume is arbitrary?

c. ISO 1996-2:2016: Why is necessary to place wind measuring device on the precise height of 10 m, yet there is no guideline where to measure it? All details are given for measurement duration, sound field corrections, calculation and evaluation, yet no recommendation for microphone location.
d. Legislation might contain stupidities as well. For example, noise level in the dwelling should be measured at the center of the room (Slovenian legislation).
e. Equipment demanded by the standards is usually a class above practically needed. Why do we need environmental noise with instruments of type 1?
f. Demands for measurement equipment are sometimes exaggerated.

The question appears: When and how to perform valid measurements outside the scope of the subjected standard and not achieving all of its requirements, but still provide credible results?

The first problem, when following to the demands of the standard, which often arises, is measurement equipment, including microphones, measurement amplifiers and software application. In this paper we will focus into an implementation of nonstandard measurement equipment into standard operating procedures.

3. MEASUREMENT EQUIPMENT

During the design process of an experiment or a measurement procedure, the first question should be: Are measured values based on the traceability to absolute sound pressure? Is it necessary to establish the traceability of measuring equipment to SI units? The answer depends on acoustic parameter to be measured and is given in table 1:

Table 1: Is the traceability to SI units required to provide a valid result?

Area of acoustic measurements	Traceability requirement
Building acoustic (sound insulation)	NO
Sound power Lw	YES
Sound Power - comparison method	NO
Sound absorption	NO
Environmental noise Ldvn	YES
Reverberation time T60	NO
Human hearing	YES
Sound event recognition	NO
Hearing protection devices	NO

Some standards require equipment with specifications which are highly exaggerated for the purpose of measurement, as for example:

1. Sound power measure with the comparison method ISO 3741:2010 demands implementation of instruments of type 1, although there is practical no background for that. Method itself can be used to calibrate an uncalibrated measuring system.
2. Laboratory measurements procedure for ducted silencer according to ISO 7235:2003 demands measuring equipment of type 1 yet all the quantities are calculated from difference in SPL, which could be performed from the same microphone.
3. Measurement of sound insulation in building acoustics ISO 16283-1:2014 are based on the difference between two averaged values of SPL, obtained with the same microphone.
4. Can measurement of sound absorption in the reverberation room complying with the ISO 354:2003, be performed with non-calibrated equipment in less defined acoustic conditions? Yes they can, and more
5. Other examples can be given….

If there is no need to ascertain the traceability to SI units, because results are based on a relative comparison between two consecutive measurements, what kind of measuring equipment can we use? To validate its suitability, four parameters of measuring system should be examined:

1. Linear amplitude response (Background noise vs. Harmonic distortion)
2. Linear frequency response (Low frequency range limit Hi frequency range limit)
3. Phase match in case of multichannel measuring system
4. Directivity pattern

3.1. Linear amplitude response

Linearity of an amplitude response is the most important parameter, which defines a range between the lowest and the highest level. When using low cost measuring equipment, like sound card and back-electret microphone, it is not enough to calibrate the system at a single frequency at single amplitude. It is eminent to check the level of system noise and to set the amplification at different positions in the measuring chain. Different combination of amplification at different elements of measuring system can influence the dynamic range. If amplification is set to 100 % of AD converter with the calibrator for 94 dB at 1 kHz, sound card with 16 bit resolution will provide measuring range from the microphone self-noise up to 94 dB. If the amplification is set to 0,1% of AD converter with the calibrator for 94 dB at 1 kHz, sound card with 16 bit resolution will provide measuring range from microphone self-noise level up to measured sound level of 114 dB. If amplification is set to 0,01% of AD converter with calibrator for 94 dB at 1 kHz sound card will provide measuring range from its AD self-noise level 38 dB up to output from the microphone 134 dB. However this is usually over the low cost microphone linearity limit. Behringer ECM 8000 and T-BONE as example of low cost measuring microphones for less than 80 Eur in combination with USB microphone preamplifier with integrated sound card are discussed in this paper, together with a back-electret cartridge for 1 Eur. Results of amplitude linearity is presented in Fig.1. Low cost microphone provides linear response from 25 dB up to 105 dB. It should be noted that first harmonics from low cost microphone are for approximately 4-7 dB higher. The first harmonic increases for 20 dB if the SPL level increases from 98 dB to over 102 dB.

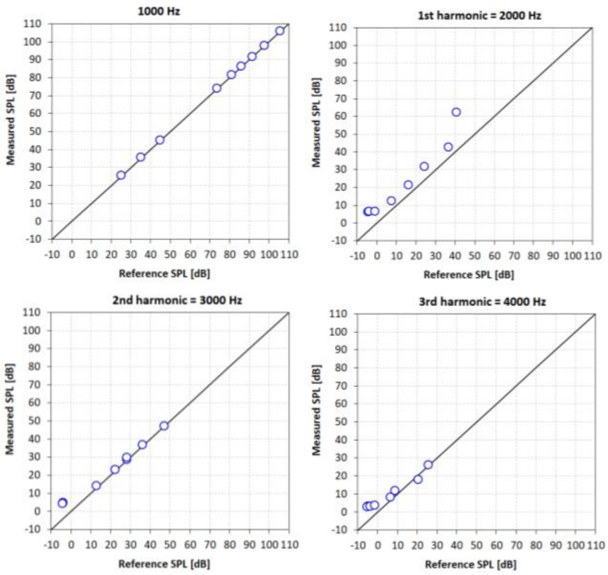

Fig. 1. Linearity of the low cost microphone at 1000 Hz and higher harmonics compared to a reference B&K microphone type 4190

If low cost measurement equipment is used we should check the linearity of its response and be careful not to overload it due to inception of harmonic distortion.

3.2 Flat Frequency Response

Measurement systems in acoustic are electromechanical systems transforming thermodynamic energy of the media (hydraulic power: $P_{hyd}=Q\Delta p$), into electrical energy (electrical power $P_{el}=IU$). Electrical signal $y(t)$ should be a copy of an acoustical signal $x(t)$, the transfer function $W(\tau)$ should be exactly 1, hence measurement system should have an ideal Dirac impulse response. Measuring systems in acoustics is therefore a Linear Time Invariant Electro Mechanical (LTIEM) system.

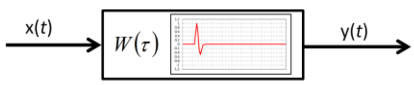

Fig. 2. Arbitrary LTIEM system of quantity $x(t)$, characterized with transfer function in time domain, that is with the impulse response W and output signal $y(t)$

Demand for a flat frequency response of measuring equipment is a mathematical consequence of a wish for a measuring system to have an ideal Dirac impulse response. We can write an Equation for correlating output from the system with the input into the system using impulse response W(τ), also known as convolution given in Eq.1. Convolution for a discrete system can be written using vectors, where vector $\mathbf{x}(n)$ represent an input signal history started at time n, $\mathbf{W}$ is an impulse response written in vector form containing M values, and y(n) is an output from the system at time n:

$$y(t)=x(t)*W(\tau)=\int_{-\infty}^{\infty}x(t-\tau)W(\tau)d\tau \tag{1}$$

$$y(n)=\mathbf{x}(n)*\mathbf{W}=\sum_{j=0}^{M}\mathbf{x}(n-j)\mathbf{W}_j \tag{2}$$

Convolution theorem states that that the convolution between two signals is equal to the product of their Fourier transformations as given by Eq.5 and Eq.6;

$$x(t)*W(\tau)=W(\tau)*x(t)=F\{x(t)\}F\{W(\tau)\} \tag{3}$$

$$x(t)*W(\tau)=X(\omega)W(\omega) \tag{4}$$

Commutative property of convolution given in Eq.5 is very important

$$y(t)=x(t)*W(\tau)=W(\tau)*x(t) \tag{5}$$

Now we can define an inverse system $\mathbf{W}^{-1}(\tau)$ which can compensate an error of original system $\mathbf{W}(\tau)$, as depicted in Fig.3. Combined system must have an ideal Dirac impulse response $\delta(\tau)$, Eq.6:

$$W(\tau)*W^{-1}(\tau)=W^{-1}(\tau)*W(\tau)=\delta(\tau) \tag{6}$$

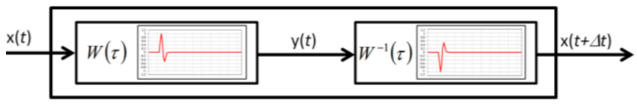

Fig. 3. LTIEM system and its inverse system

$$y(n)=\sum_{k=0}^{N}\mathbf{W}_k\mathbf{x}(n-k) \tag{7}$$

$$x(n+n_0)=\sum_{k=0}^{N}\sum_{j=0}^{N}\mathbf{W}_k\mathbf{W}_j^{-1}\mathbf{x}(n-k-j) \tag{8}$$

$$\boldsymbol{\delta}=\mathbf{W}*\mathbf{W}^{-1} \tag{9}$$

Mathematical theory is simple and clear; however there are problems and limitations with defining the inverse system $\mathbf{W}^{-1}$. Causality, time delay, linearity and stability are most important limitations. More methods can be implemented for determination of inverse system; that is for the compensation of the electromechanical system:

1. Direct deconvolution
2. Inverse Fourier Transformation
3. Adaptive LMS algorithm for FIR filter

3.2.1 Deconvolution using system of linear equations

Direct deconvolution is based on solving the system of linear equations. Convolution of measurement system impulse response and its inverse system should provide a Dirac function, because output from the measuring system should be a perfect copy of input into the system, as given in Eq.(9). Based on the definition of convolution we can write a set of linear equation as given in Eq (10), below.

$$\begin{Vmatrix}1\\0\\0\\:\\0\end{Vmatrix} = \begin{Vmatrix} w(1) & 0 & 0 & \ldots & 0 \\ w(2) & w(1) & 0 & \ldots & 0 \\ w(3) & w(2) & w(1) & \ldots & 0 \\ : & : & : & \ldots & : \\ w(N) & w(N-1) & w(N-2) & \ldots & h(1) \end{Vmatrix} * \begin{Vmatrix} w_{inv}(1) \\ w_{inv}(2) \\ w_{inv}(3) \\ : \\ w_{inv}(N) \end{Vmatrix}$$

This system can be easily solved. Solutions for the first five values of inverse impulse response are given in the set of equation, Eq.11. From this set of equations we can see that any delay in the original impulse response causes instability due to zero values in the denominator. Therefore, only the causal part of the impulse response should be considered when using direct deconvolution, as for two given examples in Fig.4, where red impulse responses depict original impulse responses of the LTIEM systems and blue impulse responses depicts its inverse system.

$$\begin{aligned}
w_{inv}(1) &= -\frac{-w(1)}{w^2(1)} \\
w_{inv}(2) &= -\frac{w(2)}{w^2(1)} \\
w_{inv}(3) &= -\frac{w(3)}{w^2(1)} + \frac{w^2(2)}{w^3(1)} \\
w_{inv}(4) &= -\frac{w(4)}{w^2(1)} + \frac{2w(2)w(3)}{w^3(1)} - \frac{w^3(2)}{w^4(1)} \\
w_{inv}(5) &= -\frac{w(5)}{w^2(1)} + \frac{2w(2)w(4)+w^2(3)}{w^3(1)} - \frac{3w^2(2)w(3)}{w^4(1)} + \frac{w^4(2)}{w^5(1)}
\end{aligned} \qquad (11)$$

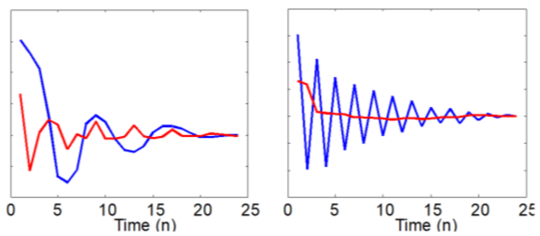

Fig. 4. Examples of two LTIEM impulse responses (red curves) and three corresponding impulse responses of their inverse systems (blue curves)

If moderate instability occurs we can compensate it simply by subtraction of its baseline by using polynomial or any other fitting as shown in Fig.5. Inverse impulse response is presented in Fig.5A. We eliminated the divergence by subtracting the baseline, results are presented in Fig.5B. The baseline was determined with polynomial curve fitting. First part of calculated inverse impulse response is presented in Fig.5

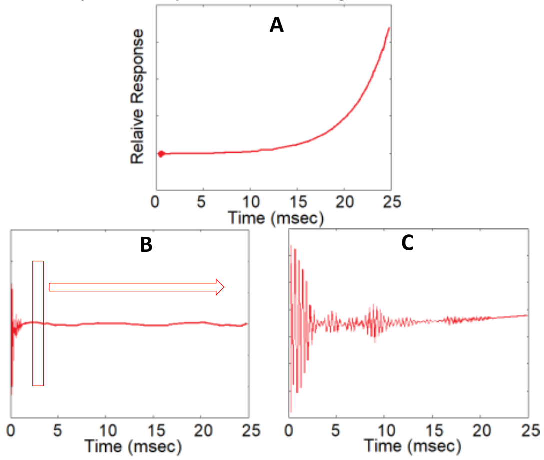

Fig.5. Compensation of moderate instability during calculation of inverse system impulse response

3.2.2 Inverse FFT

Borel's convolution theorem states: "Fourier transform of the convolution ***y*** = ***H**x** is equal to the product of Fourier transforms of functions ***H*** and ***x***, respectively:

$$y(\omega) = H(\omega)x(\omega) \qquad (12)$$

$$H^{-1}(\omega) = \frac{1}{H(\omega)} \qquad (13)$$

$$x(t) = \frac{1}{2\pi}\int_{-\infty}^{\infty}\left(\frac{y(\omega)}{H(\omega)} - \frac{n(\omega)}{H(\omega)}\right)e^{i\omega t}d\omega \qquad (14)$$

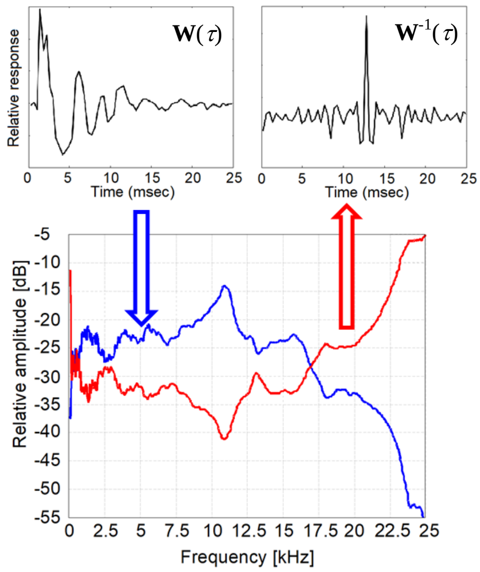

Fig.6. Impulse response **W**(τ) of the system with its frequency response, and inverse frequency response with its inverse Fourier transform in the form of inverse impulse response **W**$^{-1}$(τ)

In Fig. 6 we can see impulse response $\mathbf{W}(\tau)$ and its inverse impulse response $\mathbf{W}^{-1}(\tau)$ obtained with inverse Fourier transformation. Amplitude axis is logarithmic; therefore multiplication is substituted with summation. Sum of the frequency response and inverse frequency response is constant. Compensation filter has an amplitude of amplification in high frequency range over 10 dB.

The cause for instability of direct method is now obvious. It originates from the fact that it is impossible to compensate a zero response of the system with an infinite amplification of the compensation filter. This means that compensation can be performed in frequency range limited by a dynamic range of the compensated measuring system. Dynamic response is lower for the amplitude of the compensation.

3.2.3 Adaptive LMS algorithm for FIR filter

Foundation of digital signal processing is Finite Impulse Response (FIR) filter. FIR filter is a direct implementation of convolution integral into digital domain, as given in Eq.7. Values of FIR filter coefficients already represent its impulse response. Therefore FIR filter can be used to model any real physical LTIEM system. To find an impulse response of real physical LTIEM system (marked with **A**) in Fig.7, we can use Least Mean Square (LMS) adaptive algorithm. Coefficients of FIR filter are being updated with a rate defined by the convergence coefficient μ, until the output from the FIR filter **W** is a perfect reproduction (at least with minimum error e) of the output from the real physical system **A.** FIR filter could be interpreted as a single layer neural network with N inputs and N outputs based on a very large learning database.

$$\mathbf{W}(n+1) = \mathbf{W}(n) + \mu \mathbf{x}(n) e(n) \tag{15}$$

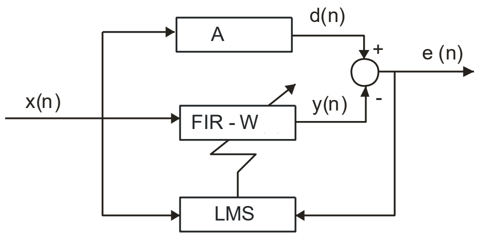

Fig. 7. LMS algorithm used for identification of real physical system **A** with adaptive FIR filter **W**

By a simple rearrangement of the basic adaptive LMS algorithm for LTIEM system, we can apply it for adaptive search of inverse system impulse response, as shown in Fig.8. If block A represents a real physical LTIEM system, then will the adaptive filter W converge to its inverse system A^{-1}. Because the adaptive LMS algorithm cannot predict the signal, a delay should be integrated into such system. Delay z^{-n} should be at least as long as the delay of the real physical LTIEM which is to be compensated. Delay can be however much longer, for example as long as whole impulse response of the original system.

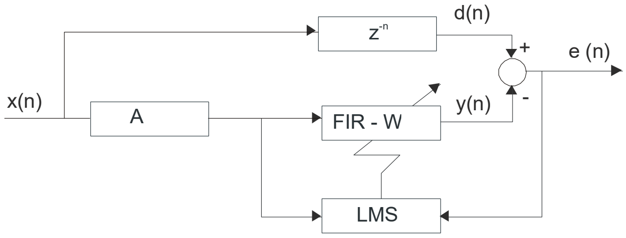

Fig.7. Identification the inverse system of the system **A**, using LMS algorithm

4. IMPLEMENTATION OF DECONVOLUTION

Deconvolution is a mathematical term for calculating the inverse impulse response. Inverse impulse response is useful because compensates both; frequency response and phase mismatch. An implementation of deconvolution can be demonstrated by the compensation of loudspeaker frequency response.

4.1 LOUDSPEAKER FREQUENCY RESPONSE COMPENSATION

Three small full-range designs of loudspeakers were measured with a laboratory grade type 1 reference microphone B&K type 4190, a vintage measuring preamplifier B&K type 3636 and a 24 bit sound card. Deconvolution was calculated using inverse Fourier transformation and adaptive LMS algorithm. Example of two calculated inverse impulse responses by using two different methods is presented in Fig. 9.

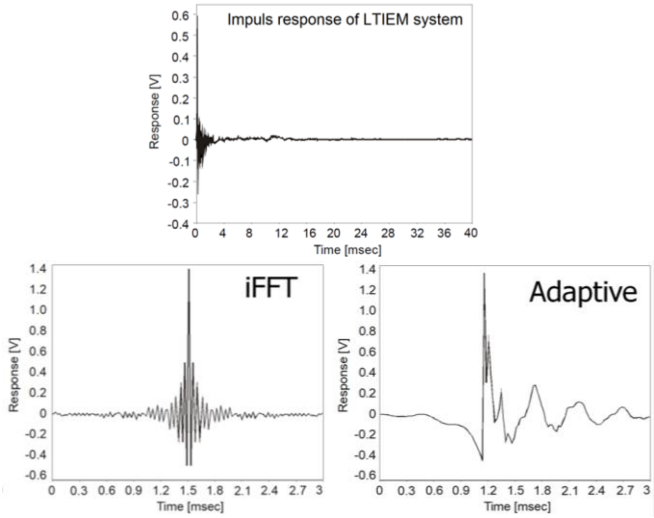

Fig.9. Impulse response of a LTIEM system and two corresponding inverse impulse responses obtained with the iFFT and the adaptive LMS algorithm

It is interesting that two inverse impulse responses, marked with iFFT and Adaptive in Fig.9, calculated with two different methods, from the same impulse response and for the same purpose with approximately similar compensation capabilities, are completely different and unrecognizable to each other in time domain. Results of compensation for three different loudspeakers are presented in Fig.10 and Fig.11. Black curves in Figs.10 and 11 represent their original frequency response functions without compensation from 100Hz up to 20 kHz. Their frequency response functions after the adaptive compensation with different sizes of FIR filter are presented in colors (blue 32, green 128 and red 512). Curves are just shifted, for the presentation purpose, the amplitude of SPL after the compensation remains on the same level.

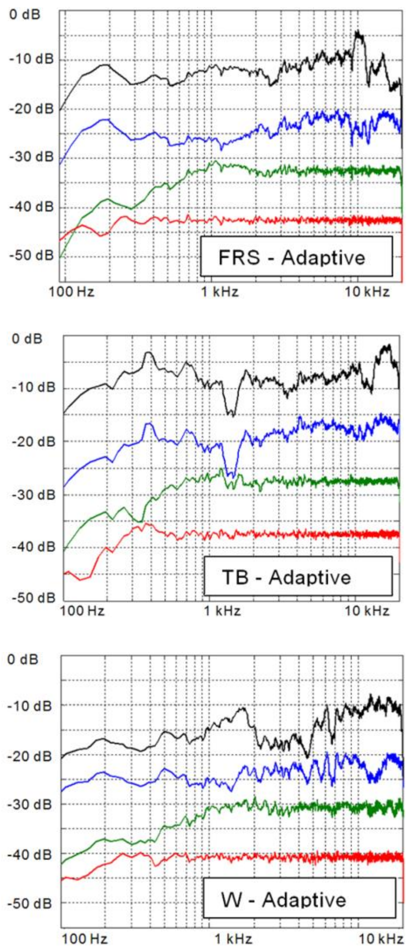

Fig. 10. FRF of three different loudspeakers without compensation (black) and with adaptive compensation in color, (blue 32, green 128 and red 512)

An attractive feature of adaptive compensation can be observed from Fig.10. Small size compensation filter affects only higher frequency range, while frequency response below the FIR filter frequency limit remains practically unaffected. Compensation filter of FIR filter size 32 already enables considerable improvement if original FRF is not flat only in the highest frequency range Filter of size 512 enables very good compensation down to 300 Hz in all three examples. The effect of compensation with so long filter is expected to go down to 100 Hz.

Results of compensation based on the inverse Fourier transformation are presented in Fig. 11. By comparing these results to results of compensation using adaptive method, it can be seen that small filter size affects the frequency range in wide frequency range. This is a contrast to adaptive method, where compensation is applied only in frequency range where its effect is significant.

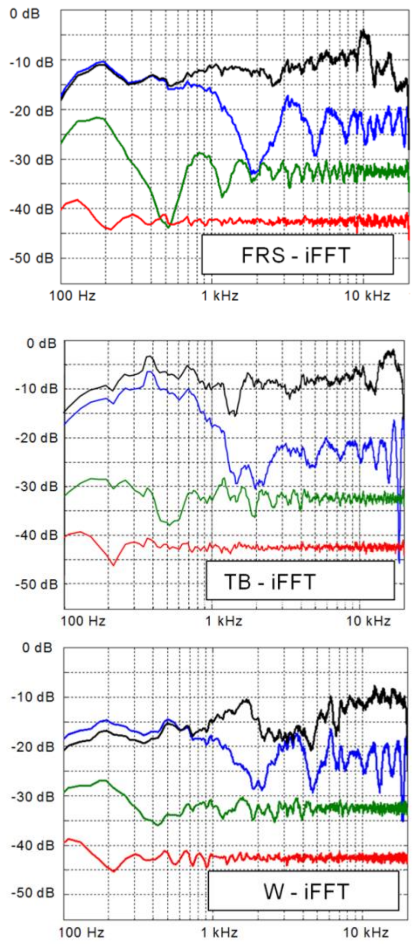

Fig. 11. FRF of three different loudspeakers without compensation (black) and with iFFT compensation in color, (blue 32, green 128 and red 512)

Based on our results and experiences we concluded, that deconvolution, based on adaptive FIR filter using LMS algorithm provides inverse system with the most promising compensation properties.

4.2 FREQUENCY and PHASE RESPONSE COMPENSATION of MICROPHONES

Sound intensity is the basic acoustic quantity, composed from acoustic particle velocity vector **v**(t) and sound pressure scalar p(t). At the moment two methods are readily available for its measurements; first one is based on the Microflown acoustic particle velocity sensor, and second one is based on two-microphone method. Microflown particle velocity sensor is based on hot-wire technology, patented in 2000. Two-microphone method is well established in the acoustic community. Different methods of sound power measurements, sound insulation measurement utilizing sound intensity probe as standardized measuring equipment.

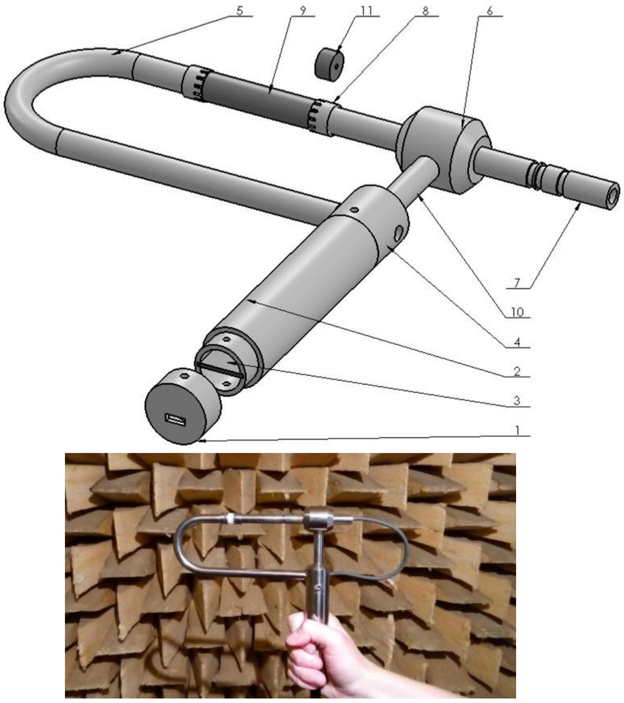

Fig.12. Prototype of the sound intensity probe based on two low cost microphones

The main challenge of sound intensity probe design is to achieve perfect amplitude and phase match between two microphones, (old school words). Both microphones must provide identical signal when exposed to the same sound pressure field. Challenge is traditionally solved by microphone pairing, resulting in extremely costly equipment. Is it possible to compensate two low cost microphones to overcome such a problem using deconvolution? To answer this question a prototype has been developed, Fig 12. Its main features are:

a. AD converter (sound card) within the handle (2,3)
b. Direct connectivity via USB to the PC, using window drivers for sound card (1), Application written in LabView.
c. Microphone (8), holder (7), easy exchange of spacers (9, 11), with zero length spacer for calculation of compensation.

Before the start of intensity measurement, microphones are positioned together with the zero spacer. During such configuration signals from both microphones should be identical. One microphone is selected as the reference, and the second is compensated to provide identical signal for identical sound pressure excitation. Results of microphone matching are presented in figure 14, where signals from two microphones can be seen before compensation (above) and after the compensation (below).

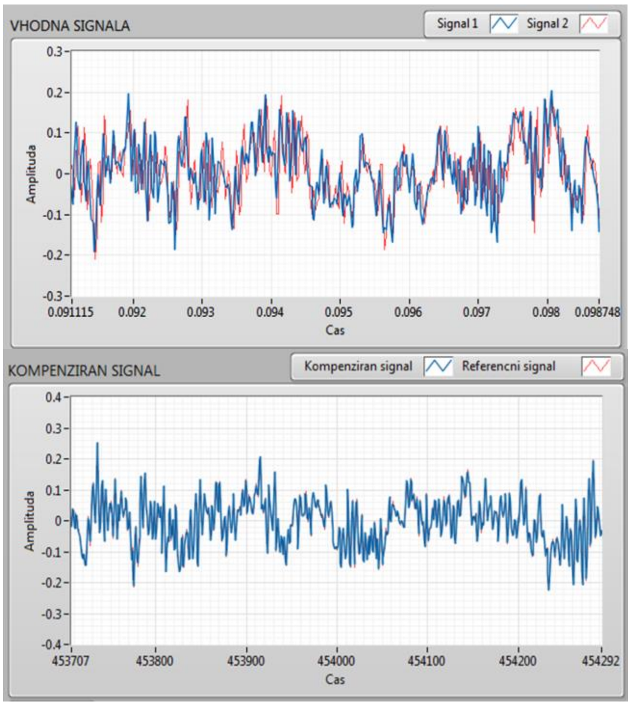

Fig.13. Signals from two microphones excited with the identical sound pressure, before compensation above and after compensation below

LMS algorithm can be used for deconvolution; that is for identification of inverse impulse response of measurement system. Implementation of delay into the adaptive algorithm enables matching of two similar microphones. LMS algorithm actually calculates an inverse of the transfer function between two microphones. Fig. 14 shows the amplitude response of transfer function between two microphones in the same sound pressure filed, before (black line with squares) and after compensation, (dotted line with red triangles). Fig.15 shows the phase shift between two microphones in the same sound pressure filed, before compensation (black line) and after compensation, (blue line).

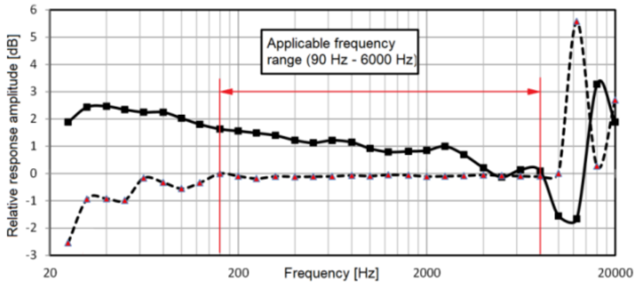

Fig. 14. Amplitude response of transfer function between two microphones in the same sound pressure filed, before (black line with squares) and after compensation, (dotted line with red triangles).

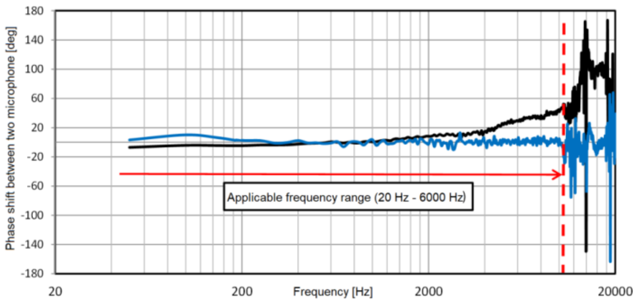

Fig.15. Amplitude response of transfer function between two microphones in the same sound pressure filed, before (black line with squares) and after compensation, (dotted line with red triangles)

In order to confirm the capabilities of adaptive LMS compensation for microphone pairing, the sound intensity probe was tested for directivity. Directivity pattern at different frequencies of the Intensity probe using two 1$ microphones, with adaptive compensation using LMS algorithm is depicted in Fig 16. Shape of the directivity was measured for half the plane. Curves in the shape of an "8" indicate that sound intensity probe is working accordingly to the theory. Different amplitudes are result of using a simple loudspeaker as a broadband noise source, which was not compensated to have flat response.

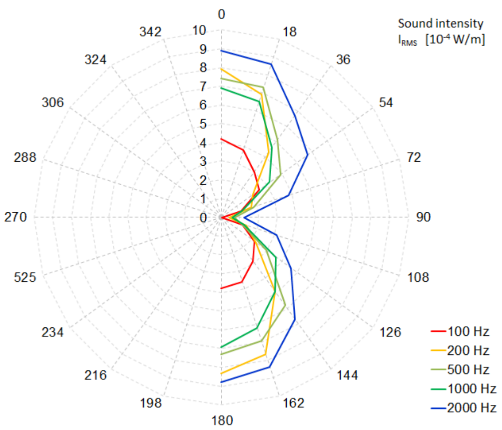

Fig.16. Directivity plot of sound intensity probe, based on low cost microphones and adaptive compensation using LMS algorithm

1$ microphones can obviously be compensated for a frequency response and for a phase response, to the matching level, which enables using them in an Intensity probe. However, an additional calibration step for compensation is needed before starting the intensity measurements.

4.3. IMPLEMENTATION of COMPENSATION in BEAMFORMING MICROPHONE ARRAY

Encouraged by the results with microphone compensation for sound intensity probe, we expanded the research on microphone array for beamforming. Focus was given to 1D beamforming, for detection of noise source direction in horizontal plane. Different geometries of microphone arrays have been theoretically and numerically tested. Results are presented for linear array with 8 microphones and for circular and triangular array with 24 microphones, as shown in Fig.17.

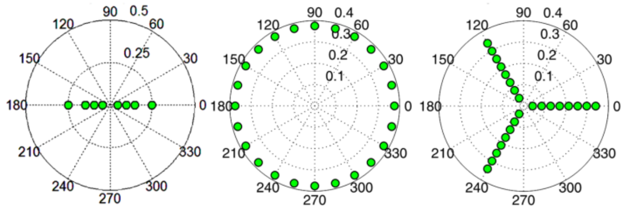

Fig.17. Different geometry of microphone array, Linear (LIN), circular (CIR) and cross (CRS)

Theoretical signal to noise ratio of three microphone array geometries, with ideal microphones, is presented in Fig.18, as well as indication of applicable frequency range, for noise source direction identification. A linear 8 microphone array of 0.5 m length provides very nice results, in frequency range from 400 Hz up to 4000 Hz, unfortunately only in the half plane from 0-180 deg. Circular array with 24 ideal microphones provides noise source identification around 360 degrees, however side lobes are densely populated. Triangular array provides response with less side lobes, however, two side lobes are very pronounced making it hard to implement.

Simulation results of signal to noise ratio for linear array with amplitude and phase shifted signals, accordingly to measured transfer functions of available microphones are depicted in Fig.19 above. Due to amplitude and phase mismatch, the number of side-lobes increases and lobes are broader, resulting in blunter acoustic picture. After the implementation of frequency response and phase mismatch compensation, using adaptive LMS algorithm, simulation results for signal to noise ratio significantly improved. After the implementation of adaptive compensation, only one additional side-lobe at each side of the main lobe remained in the signal to noise diagram.

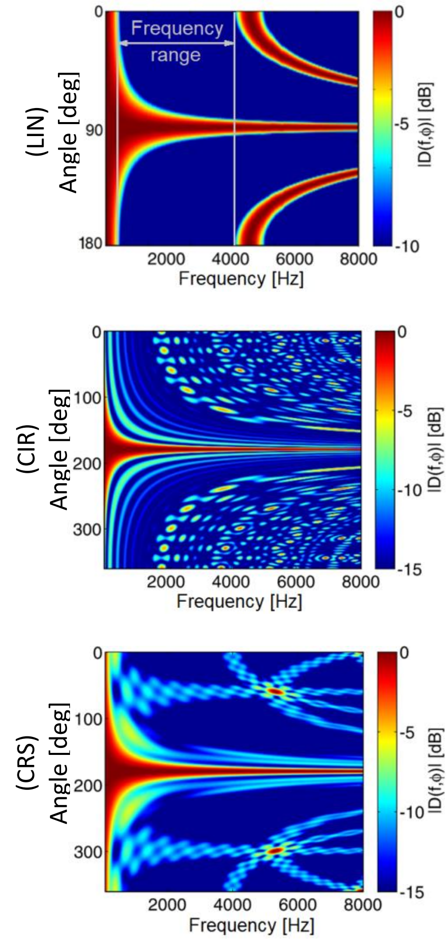

Fig.18. Signal to noise ratio for three microphone array geometries; Linear (LIN), Circular (CIR), and Cross (CRS)

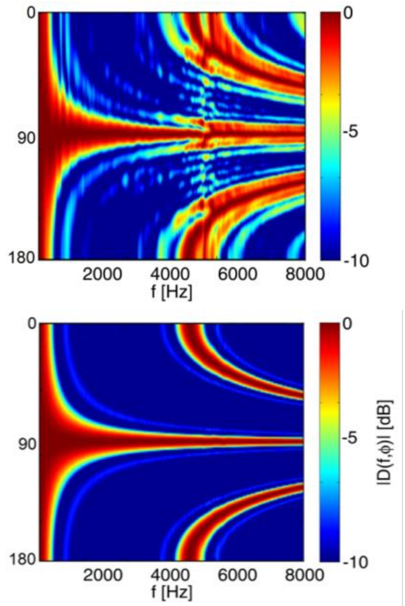

Fig.19. Signal to noise ratio of linear array; without microphone compensation above, with adaptive LMS compensation below

Encouraged by simulation results, an acoustic camera was designed, as shown in Fig. 20. An example of the acoustic picture of a piston compressor and acoustic picture of a vacuum cleaner with electric saw are presented in Fig. 21.

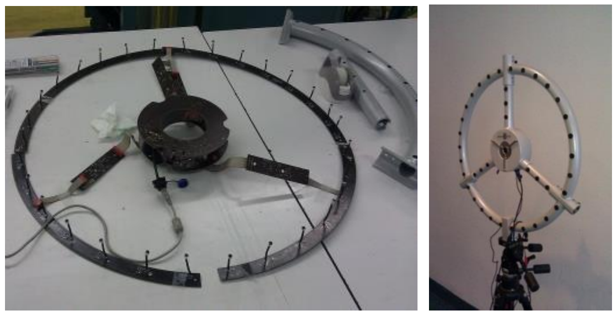

Fig.20. Circular microphone array based on 32 low cost microphones and the compensation algorithm

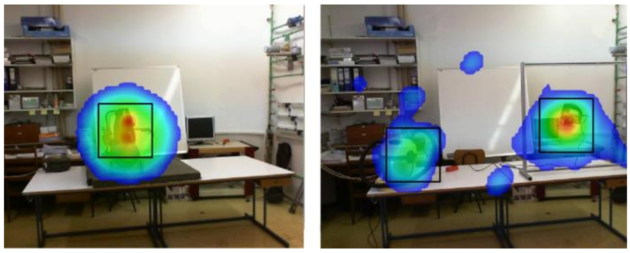

Fig.21. An example of acoustic picture, based on a sum and delay algorithm in frequency domain, obtained from 32 signals, provided by low cost microphones, compensated with the adaptive LMS algorithm.

We can conclude that low cost measurement systems can be implemented for use in a variety of different applications. Their disadvantage is additional time to compensate them and knowledge database needed to do so.

5. MICROPHONE ARRAY FOR ENVIRONMENTAL NOISE MONITORING

A new application has been developed as an answer to the question; how to integrate a nonstandard measuring method of environmental noise into an operating procedure of standardized method, to satisfy strict demands of accreditation offices, government officials, and to maintain the traceability to SI units.

The application has been developed around the core idea, that an instantaneous noise level at any given measurement location can be divided / allocated / attributed to many partial sources surrounding the measurement location. Theoretically we can place an arbitrary number of uncorrelated noise sources with equal sound power at equal distance from the Immission point, yet at different directions. Equivalent noise level is defined in Eq.17, where $Lp(t)$ represents instantaneous sound pressure level, provided by the calibrated sound level meter. Instantaneous sound pressure level can be additionally attributed with Immission directivity, and we can write $Lp(\varphi,t)$. Immission directivity needs to be defined according to Eq.18 in order to maintain the traceability of results. Equivalent level, based on the Immission directivity, can be now redefined according to Eq.19.

$$L_{Aeq}(T) = 10\log\left[\frac{1}{T}\int_0^T 10^{\frac{Lp(t)}{10}}\,dt\right] \tag{17}$$

$$L_p(t) = 10\log\left[\frac{1}{2\pi}\int_0^{2\pi} 10^{\frac{Lp(\varphi,t)}{10}}\,d\varphi\right] \tag{18}$$

$$L_{Aeq}(T) = 10\log\left[\frac{1}{2\pi}\int_0^T\int_0^{2\pi} 10^{\frac{Lp(\varphi,t)}{10}}\,d\varphi dt\right] \tag{19}$$

Overall noise level at the Immission point is a sum of contributions from theoretical noise sources, evenly allocated around the Immission center, as depicted in Fig.22 and Fig.23. Red curve represents Immission directivity for different numbers of noise sources with equal sound power around the Immission point, and blue curve represents the level detected by the omnidirectional measurement microphone, which is calibrated and provides traceability to SI units.
Two uncorrelated noise sources (NS) of equal power add 3 dB, 10 uncorrelated sources NS add 10 dB. By increasing the number of sources to infinity and dividing 360 degrees to infinite number of infinitesimally small angles.

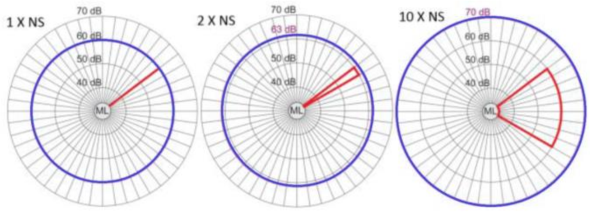

Fig.22. Red curve presents immission directivity; blue curve represents result obtained from omnidirectional microphone.

Theory seems to be consistent, yet nobody ever thought about such understanding of noise measurements, because no hardware was available for measuring $L(t,\varphi)$. Application of array with large number of microphones in combination with Beamforming seems to be a perfect candidate for calculation of noise Immission directivity. Microphone array with 33 microphones, placed in a combination of circle and triangular array provides signal to noise ratio for detection of dominant noise source direction over 10 dB in frequency range from 200 Hz up to 12 kHz. An example of Immission directivity, obtained with MEMS microphone array is presented in Fig. 23.

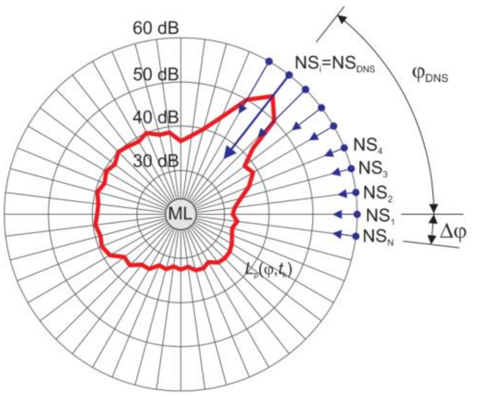

Fig.23. Results of Immission directivity measurement using microphone array with 33 MEMS microphones

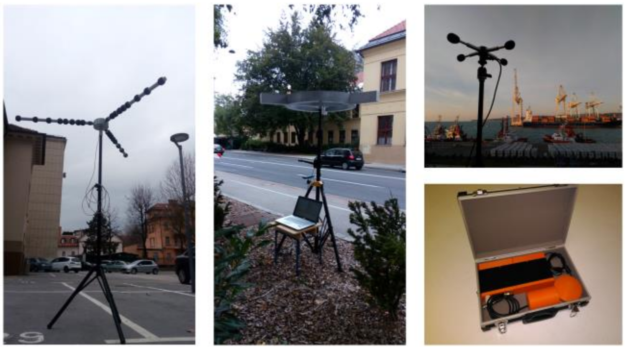

Fig.24. Evolution of hardware for Immission directivity measurements. Triangular array with low cost microphones (Left), microphone array with 33 MEMS microphones (center), state of the art measuring system for Immission directivity (right)

Acoustics is subjected to randomness. On the very small scale, the Brownian motion of infinite number of air particles generates pressure and influences the microphone noise. On the much larger scale, observing environmental noise in the city, we also have infinite number of small noise sources with different power levels, influencing our measurements of sound pressure level. Statistical approach is important towards understanding the environmental noise. We can argue, that at a given position in space, in a discrete time interval d*T*, only one of the noise sources is dominant, even if for a fraction of a dB level. By taking into account a very large number of intervals d*T* and statistical analysis of dominant noise sources spatial distribution, we can get the Immission directivity. We just need to confirm the hypothesis that discretization of noise level (based on a typical time constant of 125 msec) on many noise levels with much shorter time scale of 5 msec, and attribution of directivity with a single value to this shorter levels, provides a statistical distribution of noise Immission directivity in a larger time scale, (1 minute for example). The logic behind this is similar to observation of wave formation produced by an electron in a double slit experiment. Therefore a measurement system was designed, based on 4 microphones and sound intensity algorithm, providing the detection of dominant direction within 10 milliseconds, approximately 2000 samples at 200 kHz sampling. To each measured value of SPL, performed by a calibrated instrument, we can attribute Immission directivity, and by following the equations, traceability of results is guaranteed. Examples of results of proposed application for monitoring the noise around port of Koper are depicted in Fig. 25.

Fig.25. Immission directivity, obtained with up-to-date system, based on four microphones, based on intensity algorithm

6. CONCLUSIONS:

Deconvolution based on adaptive LMS algorithm for inverse FIR filter design can be implemented for frequency response and for phase response compensation. All Linear Time Invariant Electromechanical systems can be compensated, including loudspeakers and microphones. Traceability of measured results to SI units cannot be achieved with such approach, although results are credible.
In order to achieve traceability of practical results, nonstandard measurement procedures and equipment should be integrated into the operating procedures based on standardized methods.

7. REFERENCES

[1.] J.Prezelj, et.al., Electromechanical system frequency response equalization using three different methods. Mechanical systems and signal processing: MSSP, 2007, Vol. (21), No. 1, pp. 573-590.
[2.] S.Levičar, Implementation of adaptive algorithms for microphone compensation used in sound intensity probe, Master Thesis, University of Ljubljana, Faculty of mechanical engineering, 2016
[3.] P.Lipar, et.al., Calibration procedure of the phased microphone array, Proceedings of the 7th AAAA Congress on Sound and Vibration, Ljubljana, Slovenia, 22nd and 23rd September 2016. pp. 273-282
[4.] J.Murovec, et.al., Microphone array based automated environmental noise measurement system. Applied acoustics, 2018, vol. 141, str. 106-114,
[5.] J.Prezelj,et.al., Test signal for identification of nonlinear response in electromechanical system, 6th Congress of the Alps Adria Acoustics Association, October 16th and 17th 2014, Graz
[6.] J.Prezelj,et.al., Assessment of electromechanical system nonlinear response in time domain, Taktons 2013, Second International Acoustics and Audio Engineering Conference, November 13th - 16th, 2013, Novi Sad Serbia. Audio Engineering Society, pp. 33-36
[7.] J.Prezelj, et.al., Traffic noise modelling and measurement : inter-laboratory comparison. Applied acoustics, Dec. 2017, vol. 127, str. 160-168
[8.] J.Prezelj, et.al., On acoustic very near field measurements. Mechanical systems and signal processing : MSSP 2013, vol. 40, no. 1, str. 194-207,
[9.] J.Prezelj, Directivity measurements of environmental noise Immission, Euronoise 2018, Heraklion, Crete, pp. 711-718,

Contributed papers

REALIZATION OF AUDIO GUIDANCE SYSTEM

Mario Kalac, Paula Rinkovec, Josip Nimac, Miljenko Krhen

University of Zagreb, Faculty of Electrical Engineering and Computing

Abstract: Due to the lack of description and information about the displayed exhibits, visiting a museum can nowadays be not as interesting as one would hope. It is often the case that visitors cannot fully comprehend the significance of what is in front of them. In the scope of this paper, an audio guide had been developed, with the intention of providing visitors with a better experience. By scanning QR codes using the Audiseum mobile application visitors gain access to exhibits' descriptions in audio and text. Museum administrators are provided with a web interface through which they can manage all of the museums exhibits. Audiseum audio guide system is beneficial for both museums and their visitors, since it provides visitors with an easily accessible audio guide and museums with the better quality of service.

Keywords: museum, audio guidance system, mobile application, web application, QR codes

1. INTRODUCTION

When visiting a museum, most visitors do not only want to look at the exhibits and walk by, but rather find out more about them, their origin and history. Not everyone has the opportunity to be accompanied by a museum guide during their visit since that would be expensive for both the museum and its visitors. With that in mind, an audio guidance system, consisting of mobile and web application, was developed. This system allows the museum to generate QR codes that are placed next to the corresponding exhibit. By scanning a QR code using the mobile application, visitors gain access to an audio and textual description of the exhibit. Using this system improves the quality of the museum experience and makes it more interesting.

2. USED TECHNOLOGIES

2.1. Java

Programming language used for development of the mobile application is Java, a class-based and object-oriented language. It is founded on a principle „*write once, run everywhere*“, which enables compiled Java code to be run on all platforms supporting Java without recompilation [1].

2.2. HTML

Hypertext Markup Language (HTML) is a semantic language used for defining content and structure of web pages and web applications. HTML pages are built using HTML elements that are defined by tags. Tags are interpreted by a browser and rendered onto the screen [2].

2.3. CSS

Cascading Style Sheets (CSS) is a presentational language used to define layout and style of HTML elements. This allows separation of content and style of the web page [3].

2.4. Bootstrap

Bootstrap is a library that makes designing of web pages significantly easier. It offers a wide variety of templates for tables, navigation, forms, buttons and many more. The main advantage of using Bootstrap is the ability to easily create responsive web pages [4].

2.5. Django

Server-side of audio guidance system is built with Django, a Python based framework that allows fast and pragmatic development.

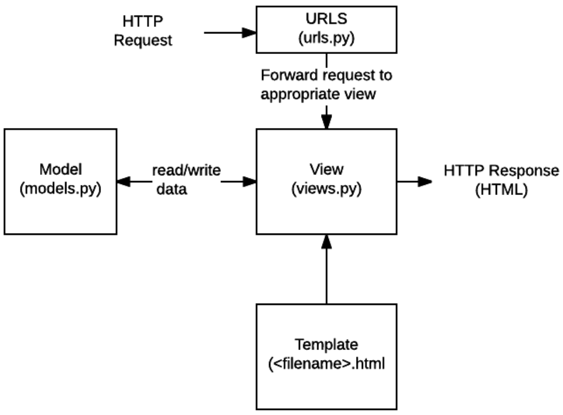

Fig. 1. Django MVT architecture [5]

Django implements Model View Template (MVT) architecture, shown on Figure 1.
URLs is a helper component that receives and routes HTTP requests to the appropriate view.
View is a class or function which handles HTTP requests by accessing the data using Django models and forwards it to the template.
Models are classes representing the structure of database entities.
Templates are files that define the basic structure of a document with placeholders for the actual data received from the view [5].

2.1. PostgreSQL

Database that is used is PosgreSQL, a free open-source object-relational database that works on all major operating systems [6].

3. SYSTEM ARCHITECTURE

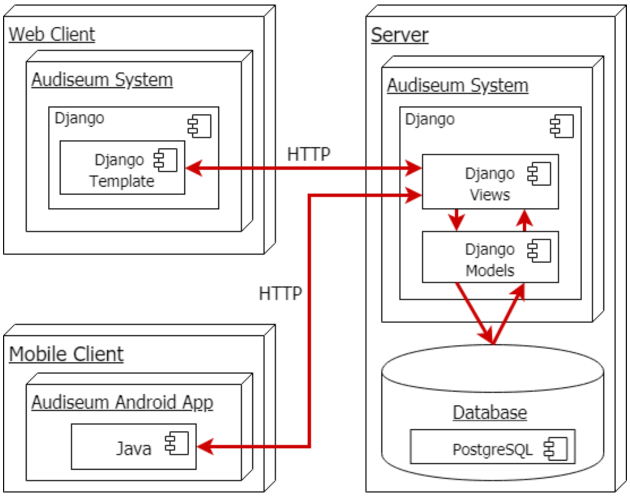

Fig. 2. Component diagram

Main components of Audiseum Audio Guidance System, that is divided into three parts: server, web application and mobile application, are shown on Figure 2. By accessing mobile or web application, user initiates an action which triggers the sending of an HTTP request towards the server. After receiving the HTTP request, the URL router delegates the request to the appropriate Django View class, which then calls the suitable Django Model class. The required data is then fetched and returned to the View class using the built-in mechanism of the Django Model. Django View class sends the data back to the client in a form of an HTTP response, and additionally when responding to a request from the web application populates the Template with the appropriate data.

4. WORKFLOW

4.1. Mobile application

The Audiseum mobile application is available for visitors to download free of charge. It allows them to scan the exhibits' QR codes and gain access to audio and textual description of the exhibits.

4.2. Web application

Besides previously mentioned mobile application the Audiseum web application is available to both visitors and museum staff.
Visitors can view all exhibits and filter them by predefined categories. They can also view a detailed description of each exhibit and listen to the accompanied audio recording.
The museums administrators can additionally, with all of the above, add new exhibits and edit or delete the existing ones.

5. CONCLUSION

Audiseum audio guidance system was developed with the purpose of making museum visits more interesting. It offers visitors the opportunity to find out more about the museums exhibits in a form of audio and textual description. Future improvements of the system include iOS application and descriptions in multiple languages. The Audiseum system is useful for both museums and their visitors, providing them with an easily accessible audio guide and lowering costs for museums.

6. REFERENCES

[1] Wikipedia, "Java (programming language)." [Online]. Available: https://en.wikipedia.org/wiki/Java_(programming_language). [Accessed: 07-Jun-2018].

[2] Wikipedia, "HTML." [Online]. Available: https://en.wikipedia.org/wiki/HTML. [Accessed: 07-Jun-2018].

[3] Wikipedia, "Cascading Style Sheets." [Online]. Available: https://en.wikipedia.org/wiki/Cascading_Style_Sheets. [Accessed: 07-Jun-2018].

[4] Wikipedia, "Bootstrap (frontend framework)." [Online]. Available: https://en.wikipedia.org/wiki/Bootstrap_(front-end_framework). [Accessed: 07-Jun-2018].

[5] MDN Web Docs, "Django introduction." [Online]. Available: https://developer.mozilla.org/en-US/docs/Learn/Server-side/Django/Introduction. [Accessed: 07-Jun-2018].

[6] "PostgreSQL: About." [Online]. Available: https://www.postgresql.org/about/. [Accessed: 07-Jun-2018].

8th Congress of the Alps Adria Acoustics Association
Zagreb, Croatia
20 – 21 September 2018

Hrvatsko akustičko društvo
HAD
Acoustical Society of Croatia

SEMIEMPIRICAL MODEL FOR PREDICTION OF WEIGHTED SOUND REDUCTION INDEX OF CROSS LAMINATED TIMBER WALLS WITH EXTERNAL THERMAL INSULATION COMPOSITE SYSTEMS

Franz Dolezal[1], Niko Kumer[2]

[1]IBO - Austrian Institute for Building and Ecology, 1090 Vienna, franz.dolezal@ibo.at
[2]Stora Enso Wood Products, Austria, 9462 Bad St. Leonhard, niko.kumer@storaenso.at

Abstract: *Since solid wood structures made of Cross Laminated Timber (CLT) are more frequently applied for multi storey residential buildings, the demand for reliable prediction of sound insulation is increasing. In Austria, the national standard for prediction of sound insulation is currently under revision. Therefore a reliable, simplyfied method for prediction of exterior walls made of CLT and ETICS (external thermal insulation composite systems) is needed, in order to be integrated in the next issue of this standard, since the use of ETICS is the most common method of thermal insulation for exterior walls in Austria.*

Key words: sound reduction index, exterior walls, CLT, cross laminated timber, ETICS

1. INTRODUCTION

Thermal insulation is an essential component of the characteristic exterior building element used in Austria since local climate is defined by cold winters and, due to climate change, hot, humid summers. One method for increasing energy performance and reducing environmental impact of buildings are external thermal insulation composite systems (ETICS). These systems substantially improve thermal resistance and reduce energy losses of external walls. Due to financial reasons, the use of ETICS is the most common way of thermal insulation for exterior walls in Austria. But ETICS also have an impact on acoustic behaviour of the component, which have been closely investigated during the last decades [1-7]. Interest in these studies was focused on combination with mineral structures, since these materials usually were the carrier constructions. A relatively new base wall structure, and not that good investigated in combination with ETICS, is cross laminated timber (CLT). CLT is a prefabricated wood product, developed more than twenty years ago in Austria. It is made of at least three layers of orthogonally arranged timber boards, glued together with organic adhesives with thicknesses from 60 to 400 mm. Because of its favorable properties and sustainability performance concerning global warming mitigation, it is nowadays frequently applied in buildings as walls or floors. CLT is quite a new material and acoustic research is still in progress. Since CLT has lower mass than mineral structures, ordinary prediction models based on huge mass differences between the components cannot be applied on the specific combination of CLT and ETICS.

2. ACOUSTIC BEHAVIOR OF THE COMPONENTS AND MOUNTING CONDITIONS

2.1. Acoustic performance of CLT

CLT plates can neither be assigned as heavy nor as lightweight, multilayered elements. Whilst acoustic requirements are fulfilled by mass of heavy elements or low bending stiffness of the planking of post and beam structures, solid wood elements cannot be classified in one of these categories. Generally sound insulation is decreasing around the critical frequency. Heavy elements show this decline at very low, lightweight elements at very high frequencies.
In both cases it can be found outside the building acoustics frequency range. At CLT structures the critical frequency is situated between 100 and 500 Hz, which is exactly in the relevant frequency range. This is a fact which has to be considered whilst configuration of the building element in order to assure a satisfying level of sound insulation and noise protection [8].
According to [9] a CLT plate can exhibit large differences in modulus of elasticity between its major and minor axis what leads to different critical frequencies. This property of CLT leads to the fact, that there is no single dip in the

sound insulation spectrum in a narrow frequency band, but a range with increased sound transmission between these two critical frequencies. Depending on the ratio between the deflection stiffness in the longitudinal direction and that in the transverse direction, this "coincidence region" can extend from a few third-octave bands up to a few octave bands, leading to increased sound transmission in this range [10].

2.2. Acoustic performance of ETICS

Application of ETICS affects significantly the acoustic behavior of the external wall component. Due to the mass-spring-mass system, formed by the basic wall, the thermal insulation and the light exterior plaster, the system inherent resonance effect leads to reduced sound insulation around the resonance frequency and increased sound insulation in the higher frequency range. According to [11], changes in single number rating due to the combined impact of ETICS at high frequencies and the resonance frequency vary from -8 to +19 dB. Main drivers of the acoustic performance seem to be the sound insulation spectrum of the carrier wall, the dynamic stiffness of the thermal insulation layer and the mass of the external plaster layer.

2.3. Determination of dynamic behavior of insulation material

The main property of a thermal insulation material used for ETICS in terms of acoustic, is the dynamic stiffness s' (MN/m^3). It is defined as the ratio between dynamic force to the dynamic displacement and has a major impact on airborne sound insulation properties of the exterior wall where this insulation material is mounted to. The sound reduction index spectrum of an exterior wall with ETICS, compared to a sole CLT plate, shows a dip at the mass-spring-mass resonant frequency due to the masses of CLT and the exterior plaster and the insulation layer acting as the spring.
Methodology of how to determine s' is specified in EN 29052-1 [12]. Nevertheless a round robin test in 2016 showed differences up to 55 % [13] in results when standardized methods are applied and even up to 300 % when plaster layer and sealant material is not processed with the same precision. Considering this, even measurement results of s' do not seem to be entirely reliable, what unfortunately must lead to an impact on accuracy of prediction results as well.

3. METHODLOGY

At the beginning, a compilation of sound measurement results for CLT by Stora Enso was carried out. The aim was to find a relation between thickness of the CLT-plate (which means the mass of the plate) and the sound insulation properties of the element in order to create an equivalent to Berger´s Mass Law which is successfully applied to heavy mineral structures according to [14]. This new "mass law for CLT" formula allows the determination of the weighted sound reduction index R_W for the CLT basic wall, as a prerequisite for the calculation with ETICS. The next step is the creation of a comprehensive database for the weighted sound reduction index R_W of exterior walls made of CLT with ETICS. Based on these databases and under consideration of the fact that a couple of parameters can be varied in this system, the particular resonant frequency f_r, according to equation 1, provides a basis for the calculation with the dynamic stiffness of the insulation material s', the mass of the CLT wall m'_{CLT} and the mass of the plaster $m'_{plaster}$.

$$f_R = \frac{1}{2\pi} * \sqrt{s' * (\frac{1}{m'_{CLT}} + \frac{1}{m'_{plaster}})} \ in\ Hz \qquad (1)$$

Different existing prediction models were applied and compared to measurement results. Since dynamic stiffness is the most critical parameter concerning indication and accuracy of determination, measurement results without reliable specification of s' were excluded from the model. Finally standard deviation of the new single number value prediction model for CLT with ETICS was verified and limits of application defined.

4. EXISTING PREDICTION MODELS

4.1. Prediction models for airborne sound insulation of CLT plates

Prediction models for airborne sound insulation spectra of CLT have been developed i.a. by Stora Enso, published in [9]. The model is based on a modular system adding e.g. various floor packages and ceiling packages to the CLT structural system by Stora Enso. The model build up is made in order to perform fast and efficient updates as soon as new products are implemented or material characteristics are changed. A detailed description of the model is not published.
A single number value model for prediction of weighted sound reduction index of lightweight wooden plates is provided in EN 13986 [15]. The particular acoustic behavior of different installation angles and, thus, different applications of CLT plates cannot be adressed with this formula.
Another method which seem to be appropriate is the british mass law equation given in [14], though it requires a minimum mass of the specimen of 50 kg/m². This standard offers four different mass laws, always with slightly different results. Usually they are designed for

higher masses (m' > 100 kg/m²) and heavy mineral components, except from the british one. Application of the other mass laws on CLT elements do not lead to reasonable results. Finally a comprehensive method to predict the single number value of wood components was developed by Holtz et al. [2]. Emphasis was placed on wood frame constructions, but solid wood elements were taken into account as well.

4.2. Prediction models for sound insulation of external walls with ETICS

The most famous and widely used method of predictiingf the airborne sound insulation of ETICS has been developed by Scholl in [1] and Weber et al. in [16]. This method has been refined, recently published in [7], and is used in a simplified version in [14] as well. Calculation is limited to heavy and semi-heavy (vertically perforated bricks) mineral structures. Nevertheless, special cases are adressed as well like double layer ETICS (refurbishments) and very thick insulation layers (e.g. as necessary for passive houses). Since mass differences between the resonant masses (basic wall and plaster) are high, resonant frequency is calculated with equation 2, where f_R is the resonant frequency of the system and m''_p the mass of the plaster.

$$f_R = 160\sqrt{\frac{s'}{m''_p}}\ \ in\ Hz \qquad (2)$$

The aim of the method is to obtain ΔR_w (the improvement of the weighted sound reduction index R_w), which is the difference between $R_{w,0}$ of the sole CLT element and R_w of the element with ETICS. Basic calculation is carried out without anchor plugs, with glue application covering 40 % of the surface and a $R_{w,0}$ of the raw wall without ETICS of 53 dB. All deviations from these default values are taken into account with correction terms. However, this method seems to be widely used, but it is not suitable for semi-lightweight structures like CLT.

4.3. Single number prediction model for ETICS on solid wood structures

Apart from the prediction of airborne sound insulation of CLT, methodology of [2] offers prediction results for different mounting conditions of ETICS and additional internal installation walls as well. Once the $R_{w,0}$ of the CLT basic wall is determined, an equation for the improvement of the sound insulation with ETICS is applied. Only Mineral wool and wood fibre insulation boards are covered with this method. Calculation is based on the resonance frequency (equation 1) of the system, and additional correction terms for applications on solid wood elements and mounting conditions of the ETICS with amount of glue and anchors.

5. PREDICTION MODEL

This new model is exclusively developed for the application on CLT basic walls with thermal and acoustical improvement with ETICS. Therefore complexity, compared to existing models, could be reduced, since only one single type of basic wall had to be covered.

5.1. Prediction model for airborne sound insulation of CLT plates

In order to start with a comprehensive database, several measurement results of airborne sound insulation of CLT plates have been provided by Stora Enso and other databases. Figure 1 shows mean values of R_w for different thicknesses (corresponds to the different masses) of CLT plates and variance if more measurements were carried out for one single type.

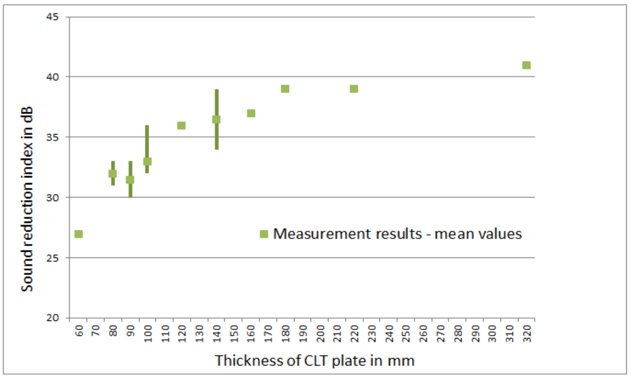

Fig.1. Measurement results (mean values and variance) for airborne sound insulation of CLT plates

Mass of the plate is calculated from thickness and an average density ρ of 440 kg/m³. This is the basis for the equations of weighted sound reduction index R_w of the CLT plate. Furthermore it is considered, that the installation angle has an impact on R_w, so two equations have been developed (one for walls and one for floors), taking the usual thicknesses of the particular application into account. “Mass laws for CLT” is derived from mean values of available measurement results, excluding peculiar outliers. Results are given in equation 3 for walls and equation 4 for CLT floors with the respective thicknesses mentioned, for which the equation can be applied to.

$$R_{w,CLT,wall} = 25{,}1\ \lg m'_{CLT} - 8{,}1\ \ in\ dB \qquad (3)$$

applicable for CLT from 60 to 150 mm

$$R_{w,CLT,floor} = 12{,}2\ \lg m'_{CLT} + 15\ \ in\ dB \qquad (4)$$

applicable for CLT from 120 to 320 mm

Figure 2 shows the results of the two equations graphically in relation to the measurement results. Previously mentioned standardized equations [14, 15] and calculation model according to [2] have also been calculated and are pictured as well.

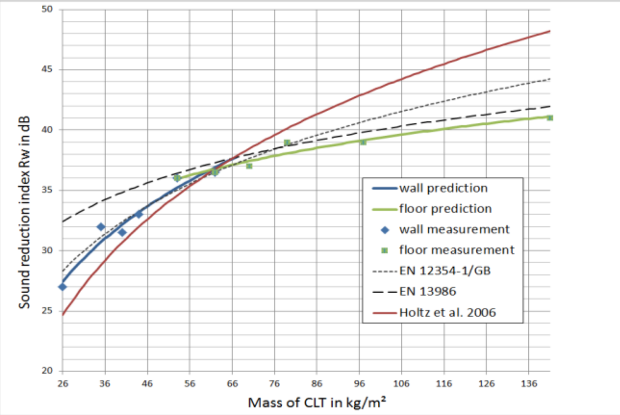

Fig.2. Measurement results of R_w of CLT and results from different prediction models

5.2. Prediction model for airborne sound insulation of CLT plates with ETICS

For this CLT+ETICS model, only measurement data were used which could provide reliably measured values of the dynamic stiffness of the applied insulation material. So special emphasis was given on material properties of the layers of the investigated building components. Measurement results were provided by Stora Enso. Once R_w of CLT is calculated, the resonant frequency f_R is obtained by applying equation 1, taking the two masses of CLT and the plaster as well as the spring (defined by s') of the insulation material into account. Based on f_R, calculation of the insulated element is carried out according to the simplified equation 5.

$$R_w = -30\ \lg f_R + 110\ \ in\ dB \qquad (5)$$

Figure 3 shows airborne sound measurements of CLT plates with ETICS and the result of the calculation model relating to the resonant frequency f_R.

5.3. Accuracy of the model

Described prediction model for R_w is based on a semiempirical approach with a limited amount of reliable measurements. Thus, it should be improved and extended by adding additional measurements and refining equation 5. Nevertheless, accuracy of the model, considering a standard deviation σ of 1,6 and maximum deviations of +2,0 and -2,6 dB (figure 4), seem to be within common precision of building acoustical applications [16].

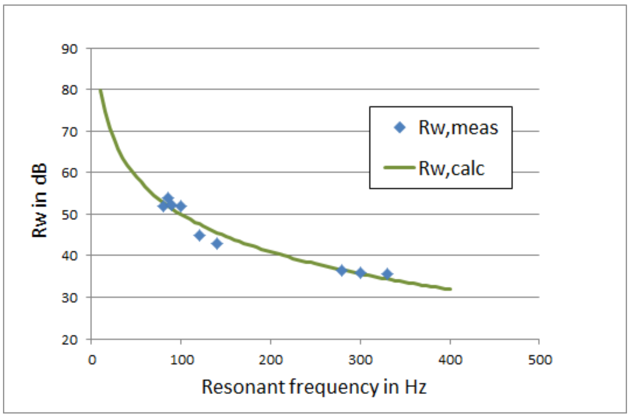

Fig.3. Measurement and calculation of weighted sound reduction iondex R_w of CLT with ETICS

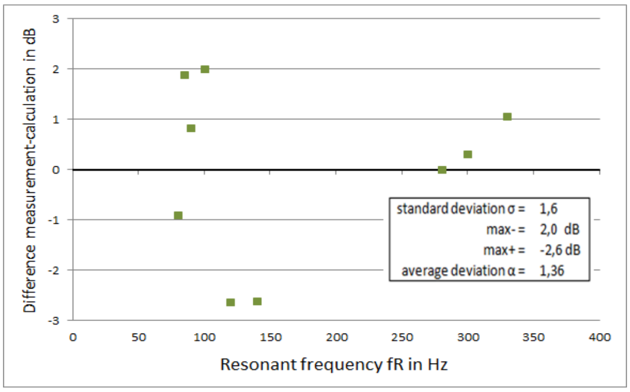

Fig.4. Difference between measurement and calculation according to the prediction model

5.4. Explanatory notes

This chapter addresses some additional aspects like boundary conditions, spectrum adaptation terms and inner gypsum board layers, when the prediction model at hand is applied.

As already mentioned above, sound insulation varies with mounting conditions of the ETICS. For this model, 100 % glue (applied with a toothed spatula) and anchors, covered with insulation material, is assumed, since this (according to the opinion of producers and practitioners) seems to be the typical fixing technique. Non covered anchors lead to a reduction of R_w of 1 dB. Application of the ETICS without anchors does not affect the result in a significant way (compared to the covered situation).

It was also investigated, if including mass of the insulation material into the model has an impact on the accuracy. But no significant evidence for this assumption could be found.

Since traffic noise is the main impact source of an exterior wall, it is necessary to take a closer look at the spectrum adaptation terms for traffic – C_{tr} and $C_{tr,50\text{-}5000}$ – according to ISO 717-1 [18] as well. For the CLT plate, inclusion of C_{tr} or $C_{tr,50\text{-}5000}$ only reduces results between 2 and 4 dB. Application of ETICS on one hand always leads to a significant improvement of R_w, but on the other hand sound reduction index spectrum usually is worsen in the lower frequency range. This locically leads to lower results for R_w+C_{tr} (lowest value for C_{tr} = - 9 dB) and particularely for R_w+$C_{tr,50\text{-}5000}$ (lowest value for $C_{tr,50\text{-}5000}$ = - 23 dB). As shown in figure 5, reduction is related to the improvement of the specific insulation material - the higher the improvement (e.g. with hemp), the higher the reduction in the lower frequency range as well.

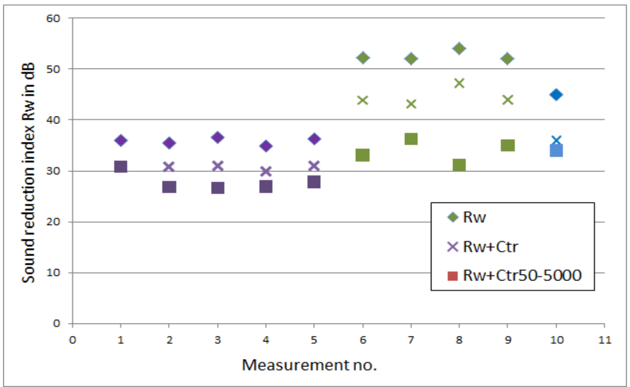

Fig.5. Measurement results of CLT with ETICS R_w (rhomb), R_w+C_{tr} (x) and R_w+$C_{tr,50\text{-}5000}$ (square); polystyrene (purple), hemp (green), mineral wool (blue)

Not all inhabitants prefer wooden surfaces in their interior space. Therefore, on the inner side, CLT is often covered with gypsum boards, which allow for painting and wallpaper. The impact of one or two interior gypsum layers has been investigated as well in this survey. It could be shown, that one additional layer of 12,5 mm gypsum board (standard type) leads to the improvement of + 1 dB, a second layer to another + 1 dB (2 dB in total). These values can be used as default values for the prediction model. In case, R_w of the exterior wall is very low, like polystyrene insulation with a thin plaster layer, a 15 mm gypsum board can lead to an improvement of R_w of + 2 dB.

5.5. Critical remarks to acoustic measurements of CLT plates

Several laboratory measurement results, provided by Stora Enso served as a basis for the development of the single number value prediction model of CLT plates. Since deviation of single number values was remarkable, also the spectrum results of the sound reduction index were compared. Figure 6 shows spectra for the sound reduction index R of three-layer CLT plates, each of them with a thickness of 100 mm and identical thickness of the single layers (30 mm / 40 mm / 30 mm). The figure shows results from different laboratories and different plates, but also different results from the same plates in the same laboratories. This leads to the assumption that acoustic measurement results vary between laboratories for the same CLT plate, but within the same laboratory as well.

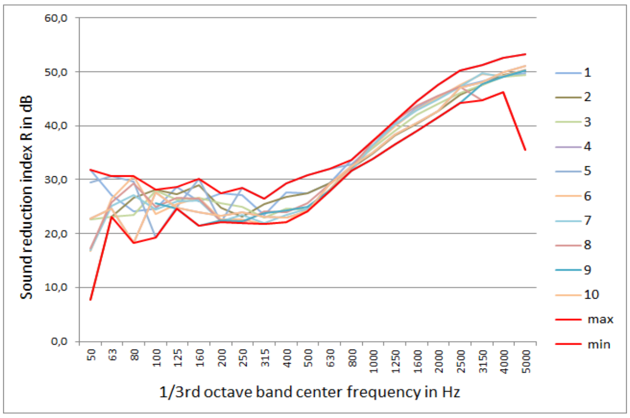

Fig.6. Measurement results for sound reduction index R of three-layer CLT plates 100 mm. Minimum and maximum values in red, measurements from 1 to 10

Weighted sound reduction index of presented measurements vary between 32 and 36 dB. Reasons for this apparent diversity can be found in the dimensions of the plate itself, but mainly in the differences between the transmission suites and the mounting conditions. Thus, it could be shown, that a tight connection of the test specimen to the structure of the test facility increases sound reduction index significantly. Thorsson et al. [19] discovered these differences as well, when the supporting structure of a CLT plate is changed. It is already mentioned in EN ISO 10140-5 [20] that mounting conditions can affect measurement results of sound reduction index and that the mass ratio of the test specimen and the surrounded structure should be taken into consideration. Thus, a minimum loss factor η is recommended for heavy structures (m > 150 kg/m²), but for lightweight structures no special requirements have to be taken into account according to [20]. CLT in dimensions which are commonly used for wall structures with ETICS (60 to 140 mm) have masses from 26 to 62 kg/m² and hence, way below the recommendation of [20]. Nevertheless, measurement results show the impact of mounting conditions on acoustic behavior of "acoustically lightweight" CLT plates and the need for further investigation on this topic, in order to find a reasonable relation to the usual loss factors of these construction types in situ and recommended mounting conditions in laboratories.

6. CONCLUSIONS

A semiempirical prediction model for weighted sound reduction index R_w of CLT and CLT with ETICS has been developed. Basis was a comprehensive database of airborne sound measurements, provided by Stora Enso. Starting with the calculation of the basic CLT element (by developing a “mass law for CLT”), the resonant frequency of the system, including the masses of CLT and plaster and the dynamic behaviour of the insulation material, is determined. Finally the equation for R_w, derived from measurement results, is applied. A satisfying accuracy has been demonstrated.
Generally, weighted airborne sound insulation of CLT always seems to be improved by adding additional layers like ETICS. Significant parameters are dynamic behaviour of the insulation material and mass of the plaster applied. Nevertheless, although improvement can be very high for R_w, considering $C_{tr,50\text{-}5000}$ reduces results significantly for all insulation materials. Particularly for polystyrene, resulting $R_w+C_{tr,50\text{-}5000}$ can be lower than the same parameter for the single CLT plate itself. This should be considered during design stage.
It was mentioned, that air borne sound measurements of CLT plates in laboratories produce weighted results with differences up to 4 dB. Reasons for these diverging performances have been discussed in the paper and lead to the conclusion of the need for guidance of mounting conditions of CLT plates in transmission suites in order to harmonise results of laboratories and to picture the situation on the building site adequately.
An important aspect is the data of the dynamic behaviour of insulation material and its determination by measurement in laboratories. It has to be concluded that producers should provide appropriate data and laboratories are requested to minimize differences of measurement results in order to have the opportunity to improve existing prediction models.
Finally it has to be captured, that the model at hand is developed as an open system which easily can be developed further by taking additional, well documented airborne sound measurements into account. Moreover, additional internal layers have not been considered yet (apart from gypsum board). This should be addressed in further research. Nevertheless, the model seems to be easy to be applied for the practitioner and could be a useful instrument in standards for prediction of acoustic performance of CLT building elements.

7. REFERENCES

[1.] W. Scholl: **Schalldämmung mit Wärmedämm-verbundsystemen**, *Bauphysik* 21, 1999, 20 - 28
[2.] F. Holtz, et al.: **Erarbeitung eines Prognoseverfahrens zur Bestimmung der Schalldämmung von Holzständerwänden auf der Grundlage der Konstruktion und der verwendeten Werkstoffe**, LSW, *Abschlussbericht*, Rosenheim, 2006
[3.] J. Nurzynski: **The effect of additional thermal lining on the acoustic performance of a wall**, *Forum acousticum*, Paris, 2008
[4.] A. Rabold, S. Bacher: **Nachwachsende Rohstoffe für WDVS-Althaussanierung**, *Ift Forschungsbericht*, Rosenheim, 2014
[5.] L. Weber, S. Müller: **Schallschutz bei Wärmedämm-Verbundsystemen**, Fraunhofer IBP, Stuttgart, 2015
[6.] A. Santoni, et al.: **Sound transmission loss of ETICS cladding systems considering the structureborne transmission via the mechanical fixings: Numerical prediction model and experimental evaluation**, *Applied Acoustics* 122, 2017, 88-97
[7.] L. Weber, S. Müller, B. Kaltbeizel: **Einfluss von Wärmedämm-Verbundsystemen auf die Schall-dämmung von Außenwänden**, *Bauphysik* 40 Heft 1, 2018, 19-30
[8.] F. Dolezal, et al.: **Flanking Transmission of Impact Noise at Solid Wood Structures**, *WCTE*, Riva, 2010
[9.] K. Hagberg, et al.: **SEAP – Acosutic Design Tool for Stora Enso Building Solutions**, *ICA*, Buenos Aires, 2016
[10.] N. Kumer: **Software-based calculation of the sound insulation performance of CLT walls**, *Newsletter Stora Enso Building Solutions*, 2017
[11.] D. Urbán, et al.: **Influence of the Dynamic Stiffness of External Thermal Insulation on the Sound Insulation of Walls**, *Euronoise*, Crete, 2018
[12.] EN 29052-1: **Determination of dynamic stiffness -- Part 1: Materials used under floating floors in dwellings**, 1992
[13.] D. Urbán, et al.: **On the Uncertainty of Dynamic Stiffness Measurements,** *DAGA* , Munich, 2018
[14.] EN ISO 12354-1: **Building acoustics. Estimation of acoustic performance of buildings from the per,ormance of elements. Part 1 - Airborne sound insulation between rooms**, 2017
[15.] EN 13986: **Wood-based panels for use in construction. Characteristics, evaluation of conformity and marking**, 2004
[16.] L. Weber, et al.: **Schallschutz bei Wärme-dämmverbundsystemen**, *DAGA*, Hamburg, 2001
[17.] EN ISO 12999-1: **Acoustics. Determination and application of measurement uncertainties in building acoustics. Part 1 - Sound insulation**, 2014
[18.] EN ISO 717-1: **Acoustics. Rating of sound insulation in buildings and of building elements. Airborne sound insulation**, 2013
[19.] P.Thorsson, K. Hagberg, A. Golger: **Measurement Series to Verify the Accuracy of Stora Enso Acoustic Prediction tool – SEAP**, *ICA*, Buenos Aires, 2016
[20.] EN ISO 10140-5: **Acoustics. Laboratory measurement of sound insulation of building elements. Requirements for test facilities**, 2010

8th Congress of the Alps Adria Acoustics Association
Zagreb, Croatia
20 – 21 September 2018

Hrvatsko akustičko društvo
HAD
Acoustical Society of Croatia

The influence of secondary wall details on new descriptors for sound insulation

Neusser Maximilian, Herbert Müllner

maximilian.neusser@acom-research.eu, herbert.muellner@tgm.ac.at

Abstract: *In many scientific publications it has been shown that the influences of secondary wall details of lightweight partitions have a significant impact on the sound reduction index. These influences are distributed over the whole in building acoustics relevant frequency spectrum, whereby a single value evaluation according to EN ISO 717-1 is insufficient. In the context of listening comparisons in an experimental setting, it was examined which derived single number indications best characterize wall constructions in light and solid constructions. The results of the perception experiments and the subsequent analyzes showed a sound insulation index with which lightweight and solid wall constructions can be characterized in a way that is more perceptual and, in a construction neutral way, considering the low frequency range. The presented results offer the possibility of analyzing the influence of the dimension of the screws, the distance between screws, the tightening torque, and the position of the screws on this new sound reduction index. These results are used to redefine and evaluate the influences of secondary wall details. They offer the possibility to optimize lightweight structures and provide measures for increasing manufacturing quality, with reference to a realistic perception of the acoustical performance of wall constructions.*

Key words: building acoustics, sound transmission, psycho acoustics, wall details

1. INTRODUCTION

Light building components, whether from mineral-bound materials or from wood-based materials, are an increasingly prominent part of the built constructions. In addition to this development, the current international discussion of the expansion of the descriptors to describe the building acoustic performance is a challenge for planners and industry. International standards define single-number quantities that are commonly used to rate airborne sound insulation of constructions. Recent psychoacoustic evidence suggests revising the actual standard procedure for rating sound reduction indices to get more reliable correlations between these ratings and the residents' perceived sound insulation quality in dwellings [6]. Many different approaches for rating the sound reduction index were introduced in a draft for revising the EN ISO 717 standard [7]. The goal of this research is to evaluate the influence of secondary wall details on these new single number quantities (SNQ). The two main parameters effecting the sound transmission loss are the screw spacing and the screw torque. The effect of the screw distance in lightweight constructions has already been investigated in several studies. [10] These results show that there is a direct correlation between sound transmission loss and screw spacing. Systematically increasing sound reduction indices of the examined gypsum board wall construction were measured with increasing screw spacings. In addition to the parameter of the screw distance, the screw tightening torque and its influence on the sound insulation and the vibration energy transmission between the stud and the plate were investigated. This influence is a far more unilluminated subject than that of the screw distance. In [2,3] it is shown that the sound insulation of lightweight constructions is significantly influenced by the tightening torque of the screws. The quantification of these influences and the effect on these SNQs, offer the possibility to optimize lightweight structures and provide measures for increasing manufacturing quality, with reference to a realistic perception of the acoustical performance of wall constructions.

2. METTHOD AND THEORY

For the characterization of the illustrated influence of the screw distance and the screw tightening torque, investigations were carried out based on the construction in Figure 17. The second section describes the used reference spectra that have served to calculate the descriptors of the airborne sound transmission loss.

1.1 Test specimens

The construction consists of two 12.5mm gypsum fiberboards and 100x60x1,250mm wooden studs which were screwed together. The distance between the structural axes is 66cm. Choosing gypsum fiberboards allows for the modelling of one as an isotropic material, thus promising an easy numeric handling than a classic gypsum plasterboard.

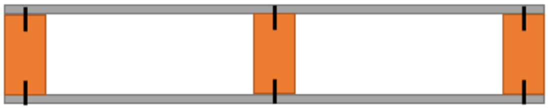

Fig.1. Schematic representation of the investigated construction type (12.5mm gypsum fiberboard, 160x60mm wooden stud, 12.5mm gypsum fiberboard)

Table 1 shows the variety of screw spacings and screw torques included in the investigation. At a screw torque of 1Nm the screw is fairly touching the gypsum board. With 5Nm screw torque the screw is almost driven through the gypsum board. This torque range concludes the whole possible spectrum. The screw spacing starts at 1400mm which means that only 4 screws, each in one corner, holds the gypsum board in place. It is reduced in bisecting steps to 43.75mm.

Variant Number	Screw spacing in mm	Screw torque in Nm
1	1400	5
2		1
3	700	5
4		1
5	350	5
6		1
7	175	5
8	87.5	5
9	43.75	5

Table 1. Overview about the investigated specimen variations in screw spacing and screw torque

1.2 Single number quantities rating

The Suitability of a reference spectrum for rating sound insulation depends on how well its shape matches average spectra of actual noises generated in dwellings. [9] The current research results deliver different approaches for calculating these reference spectrums. [1,4,5,6,7,8,9] Different examples of these spectra are used to rate the frequency depended airborne sound insulation of the investigated building components. The resulting SNQs are compared and the influence of the screw spacing, and the screw torque are quantified. The following section delivers a short overview about the used reference spectra to calculate the SNQs according to formula 1.

$$R_{source} = 10 \cdot lg \left(\frac{\sum_i 10^{\frac{L_{i,source}}{10}}}{\sum_i 10^{\frac{L_{i,source}-R_i}{10}}} \right) \tag{1}$$

All recent studies have shown that the frequency range below 100 Hz is essential for a good correlation between a deposit value and human perception. [4] Therefore, the range from 50 to 5000 Hz was considered in all cases

1.2.1 L_{opt}

The objective in the development of a new spectrum for rating the airborne sound insulation quality of building components was to determine an optimized single number quantity which predicts well subjective loudness of neighbor noise. Experimental Data from [1] of subjective ratings for six different living sounds was used for the optimization process. The subjects listened to filtered stimuli to represent nine different wall constructions. The optimized single number rating R_{opt} agrees better with the perceived sound insulation than any of the standardized single number quantities [1].

1.2.2 L_{living}

This spectrum is intended for situations in which general living sounds predominate. These could include all types of sounds commonly heard in homes. The same spectrum is referred to $C_{50\text{-}5000}$. This spectrum is the same shape as the A-weighting spectrum with some very minor adjustments in the higher frequencies.

1.2.3 L_{modMR}

The reference Spectrum L_{modMR} was developed in the RISE project "PapaBuild" and the "Akustik Center Austria" Coin project [5,6]. This reference is focused to represent equal loudness and annoyance perceptions from different sound sources filtered by a light-weight gypsum board wall, and a heavy-weight lime sand brick wall. The $R_w+C_{50\text{-}5000}$ was the same rating for both walls. The loudness perceptions and annoyance levels were found by listening tests and questionnaires. The resulting single number quantity R_{modMR} brings the overestimation of the importance of the low frequency spectrum for low sound levels into focus.

1.2.4 $L_{Traffic}$

The Spectrum adjustment values C and Ctr were introduced in ISO 717-1:1996 to consider the different spectra of noise sources. This spectrum is intended for use with traffic noise as main sound source.

1.2.5 $L_{Living,85\%}$

Lliving,85% is proposed as a new reference spectrum in the draft [7] for the revision of EN ISO 717. The frequency dependent spectrum weights represent the 85th percentile values of all in the draft described spectra. Compared with the other spectra's in Fig 2, the shape of its spectrum is like that of L_{Living}.

1.2.6 L+

Based on a study of noise spectra in residential buildings of many different types of sound sources the reference spectrum L+ was introduced in [8]. It considerates the the revised equal loudness contours described in ISO 226:2003. It includes values from 50 to 5000 Hz and was proposed in [5].

1.2.7 R_w

The SNQ R_w is based on the single number rating method according to EN ISO 717-1:2013. Among all other SNQs the resulting rating doesn't include the third-octave band values of the sound reduction index between 50 and 100 Hz. Instead of using formula 1 it compares the resulting measurement curve of the sound reduction index to a reference curve.

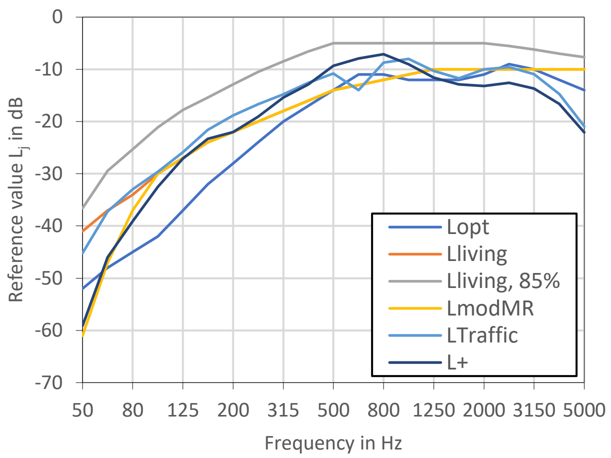

Fig.2. Frequency depended reference spectra for single number ratings

3. RESULTS AND ANALYSIS

The results in figure 3 show a strong dependence of the sound transmission loss of the double wall on the screw spacing over the whole relevant frequency spectrum. The carried-out difference assumes values up to 18 dB in some frequency bands. This phenomenon is mainly due to the reduced coupling between the stander and the plate and to the increasing dynamic stiffness with increasing number of screws and increasing bolt torque of the construction.

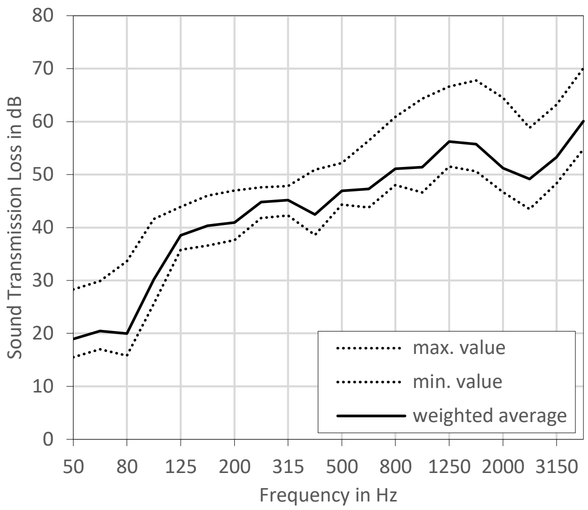

Fig.3. Sound Transmission Loss of a gypsum double wall with different screw spacings and screw torque

Figure 4 shows the sound transmission loss of the investigated gypsum board double wall with varying screw spacing with equal screw torque. The in Figure 4 presented frequency dependent transmission loss curves show a high dependence on the screw spacing over the whole frequency spectrum. In relation with Figure 4 when the half bending wave length is less than the screw spacing the screw joints acts as independent excitation points for the plate. Below this frequency the whole stud acts as a continuous line exciter and the improvement of the sound reduction by the higher screw spacing is reduced. At 250 Hz the curves describing the difference between the reference and the other specimens shows almost no influence of the screw spacing. The overall trend is that a higher screw spacing improves the sound transmission loss.

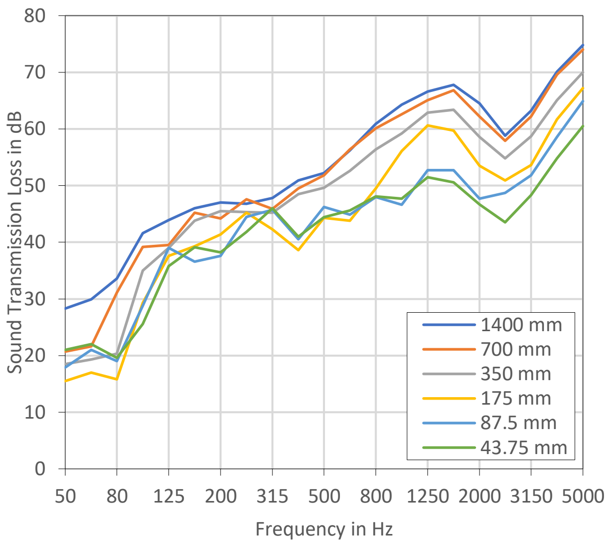

Fig.4. Sound transmission loss of a gypsum double wall with different screw spacings

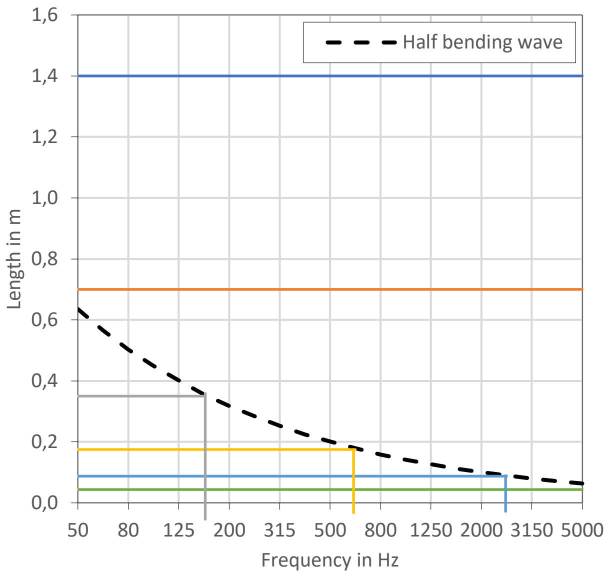

Fig.5. Sound transmission loss of a gypsum double wall with different screw spacings

Figure 6 shows the difference in the sound transmission loss of the investigated gypsum double wall with varying screw torque at different screw spacing. The screw torque shows an effect on the sound transmission loss above the mass spring mass resonance frequency. The difference in screw torque causes values of the ΔSTL up to 4 dB. Figure 2 shows the increasing effect of influencing the sound transmission with screw torque with a decreasing screw spacing. Due to the high measurement insecurity and the small specimens size the result below 100 Hz must be confirmed by measurements with larger specimen sizes. For a detailed presentation on the described effects it is referred to [3] and [2].

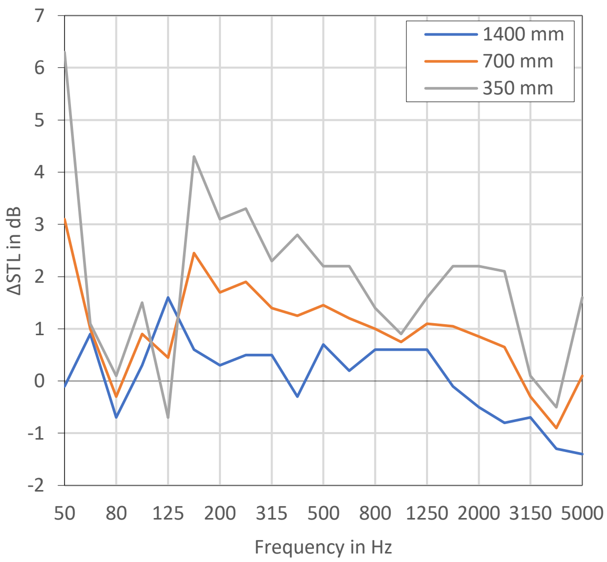

Fig.6. Difference in the sound transmission loss of a gypsum double wall between 5Nm and 1Nm screw torque with different screw spacings

Figure 7 shows the difference in the single number quantities with the 1400 mm screw spacing as reference which were calculated with the reference spectra from figure 2. The resulting SNQs have based on their reference spectrum a different sensitivity to the change of screw spacing. At those screw spacing with highest difference in figure 5 there are two groups of SNQS noticeable. The difference between those two groups are up to 3dB.

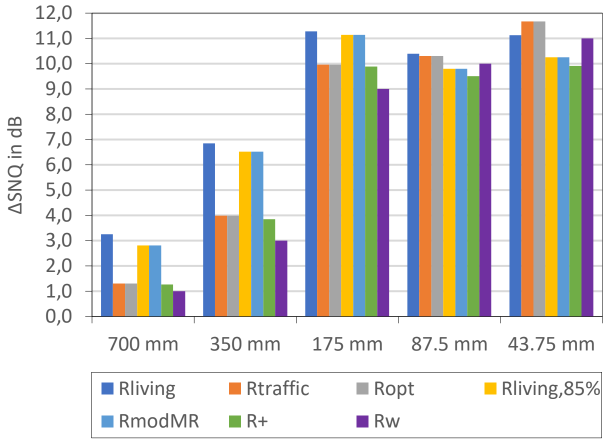

Fig.7. Difference in the single number rating quantities of the specimen variants with different screw spacings (reference 1400 mm spacing)

Figure 8 shows the difference in the resulting single number quantities when changing the screw torque from 5Nm to 1Nm at different screw spacings. The R_{modMR} descriptor showed over all screw spacing variants the highest response. The reference spectrum L_{modMR} provides significant high values in the mid to high frequency range, where the impact on the sound transmission loss of the screw spacing is considerable high. Including the values of the sound transmission loss curves below 100 Hz results only in the 1400 mm variant in a considerable difference between R_w and the other SNQs.

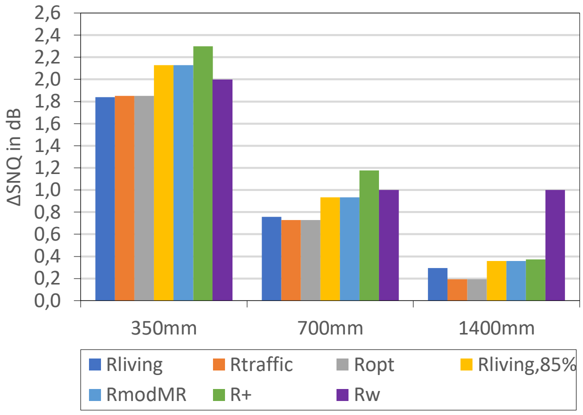

Fig.8. Difference in the single number rated sound transmission loss of a gypsum double wall between 5Nm and 1Nm screw torque with different screw spacings

4. CONCLUSION

Secondary wall details have a high impact on the sound transmission loss of light weight building constructions. The measurements show that the rated sound transmission loss increases up to 10dB, with the loosening of the screws or with a smaller number of screws. The evaluation of the results shows that the different standardized SNQs and alternative descriptors for airborne sound isolation are varying sensitive to the change of secondary wall details. Caused by the different shapes of the reference curves over the frequency range, the sensitivity to the parameters, screw spacing and screw torque, showed varying impact on the calculated SNQs. The differences in the impact of secondary wall parameters on the evaluated descriptors are up to 3dB.

5. FUTURE WORK

The presented results are used to develop listening tests to quantify the importance of the showed impact of secondary wall details on the different SNQs. This quantification helps to determine which future construction rules for light weight building constructions must be designed to reduce the consequence of bad workmanship on the acoustic comfort of building occupants.

6. ACKNOWLEDGMENTS

This research was supported by the results and the members of the RISE project “PapaBuild” and the “Akustik Center Austria” Coin project.

7. REFERENCES

[1.] P. Virjonen, V. Hongisto, D. Oliva: **Optimized single-number quantity for rating the airborne sound insulation of constructions: Living sounds**, The Journal of the Acoustical Society of America 140(6), 2016, 4428-4436

[2.] N.B. Roozen, H. Muellner, L. Labelle, M. Rychtarikova, C. Glorieux: **Influence of panel fastening on the acoustic performance of light-weight building elements: study by sound transmission and laser scanning vibrometry**, Journal of Sound and Vibration, 2015

[3.] M. Neusser, **Analyse des Einflusses von Verbindungsmitteln auf das Schalldämmmaß von leichten Trennwandkonstruktionen durch realitätsnahe Modellierung von Schraub- und Klebeverbindungen,** Phd Thesis, Vienna, 2017

[4.] W.Scholl, **ISO 717-Neues Beurteilungsystem für die Schalldämmung in Gebäuden,** 4. HolzBauSpezial Akustik & Brandschutz, 2013

[5.] H. Müllner et al.: **Final Report - COIN-Projekt „Akustik Center Austria“**, Vienna, 2018

[6.] M. Rychtáriková, H. Muellner, V. Chmelík, B. Roozen, D. Urbán, D. Garcia, C. Glorieux: **Perceived Loudness of Neighbour Sounds Heard Through Heavy and Light-Weight Walls with Equal Rw + $C_{50-5000}$**, Acta Acustica united with Acustica, January 2016

[7.] J. Seidel: **Derivation of a living noise reference spectrum to be proposed for ISO 16717-1**, ISO 16717 committee document, n101, 2012

[8.] W. Scholl, J. Lang, V. Wittstock **Revision of ISO 717: Future single-number quantities for sound insulation in buildings**, AIA-DAGA, 2013, Merano

[9.] D. Masovic´, D. Sumarac Pavlovic´, M. Mijic: **On the suitability of ISO 16717-1 reference spectra for rating airborne sound insulation**, J. Acoust. Soc. Am. 134 (5), November 2013

[10.] Craik, Smith: **Sound transmission through double leaf lightweight partitions. Part I: Airborne sound,** Applied Acoustics, Vol 61, 2000

THE DISCUSSION ON FACADES' SOUND INSULATION IN SLOVAKIA

Daniel Urbán[1,2], N.B. Roozen[3,4], Monika Rychtáriková[5,6]

[1] Czech Technical University in Prague, Faculty of Electrical Engineering, Department of Physics, 166 27 Prague, Czech Republic.
[2] Faculty of Civil Engineering, Slovak University of Technology in Bratislava, Radlinského 11, 810 05 Bratislava, Slovakia.
[3] KU Leuven, Laboratory of Acoustics, Department of Physics and Astronomy, Celestijnenlaan 200D 3001 Leuven, Belgium.
[4] A&Z Acoustics s.r.o., Repašského 2, 84102 Bratislava, Slovakia.
[5] KU Leuven, Faculty of Architecture, Hoogstraat 51, 9000 Gent, Belgium.
[6] STU Bratislava, Department of Architecture, Radlinského 11, 81101 Bratislava.

Abstract:
Standard energy retrofitting of buildings in Slovakia has over the last decades led to an increase of thermal insulation of the building envelope. In order to provide more benefits to building users, considering also other, non-energetic aspects, an increased interest can be seen on the improvement of indoor acoustic comfort.
Our everyday experience shows, that when it comes to the assessment of the quality of building façades, many shortcoming can be seen in the design, realisation and even in legislation. Decisions on criteria and requirements in building acoustics and thus also on requirements on the building envelope, are based on the recommendation of World Health Organisation that uses large scale studies on noise effects on health. Standards typically suggest minimum sound insulation properties of the building elements for exposure to exterior noise.
The most typical examples of the standard energy retrofitting of buildings in Slovakia, involve dwelling houses (usually massive façades with External Thermal Insulation Composite System ETICS), administrative buildings (light-weight façades – single leaf or double leaf) and industrial buildings (insulation of noise generated inside buildings).
This contribution is listing the weak points and crucial parts of façades' design, typical for Slovak architecture.

Key words: sound insulation, façades, building acoustics

1. INTRODUCTION

The main function of partition constructions, especially façades, is to protect the building users (inhabitants, employees etc). The usual goal is to achieve thermal, light, humidity and acoustic comfort in the interior's buildings (in other words to fulfil hygienic requirements). In case of industrial buildings, we are often designing façades to protect also the external environment against a sound propagation from noise generated by machines located inside industrial objects. Nowadays, it is relatively easy to get all the important information on façades sound insulation requirements from national legislation and standards [1].
Target requirements are closely related to the maximum acceptable noise level values in the environment (interior and exterior as well). All criteria are slightly following the recommendations of the World Health Organization (WHO). WHO recommends acceptable maximum noise levels in relation to the human activity [2,3]. Partition structures' sound insulation requirements, their Qualitative evaluation and the way of measurement partially differs depending on country [4].

In Slovakia, depending on the building technology development and cultural and society changes we are dealing with, a diverse spectrum of façade constructions exists. Whether dealing with historic or modern façades, they can be divided as lightweight or massive façades, single or multilayer (two or more layers), ventilated or unventilated, mounted, sandwich, brick or monolithic façades.
Each façade type has its own specifics and justification within the design. Façades' system complexity makes the system less predictable from building acoustics point of view, whether due to resonances in the façade and its

elements, as well as the way of its anchoring and acoustic details design solutions.
In this paper, we will present an overview of the most common façade systems in Slovakia and address their acoustic weaknesses.
Gradually, we will present the influence of external thermal insulation composite system (ETICS) on the decrease of sound insulation of massive façades, we will outline the issue of transparent lightweight cladding, especially of transparent single layer façades and double transparent naturally ventilated façades.

1. EXTERNAL THERMAL INSULATION COMPOSITE SYSTEMS (ETICS)

In connection with the global trend of energy savings, in Slovakia we are adding thermal insulation on façades since eighties of 20th century. After years, the thermal insulation thickness gradually increased from 40mm up to 200 to 300mm on new façades at present times. Although thermal insulation significantly improves the enveloping constructions thermal insulation properties and reduces the buildings' energy needs, in specific cases it reduces the sound insulation of the structures. In Slovakia, the most widely used thermal insulation systems are the external thermal insulation composite systems (ETICS), where the thermal insulation layer is made of polystyrene, mineral wool or glass wool. Thermally insulated wall behaves as a mass spring system, where the thermal insulation (e.g. Mineral Wool) acts as a spring in the system.
Nowadays, we are able to predict at what frequency the ETICS will resonate [5-12]. Publication [8] showed that, the influence on the sound insulation due to ETICS can vary from -8dB to +19dB. Current practice, based on extensive research of Weber et al. [6], is to predict the influence of ETICS on façades sound insulation by means of the relationships given in the standard ISO 12354-1.
Another prediction model to estimate the effect on the sound reduction improvement index ΔR was given by Urban et al. [14] (Eq. 1).

$$\Delta R_{f_0<f<f_c} = 20log\left(m\frac{f}{\frac{\rho_0 \cdot c}{\pi}} - 2\right) + 10log\left(\frac{f}{f_c} - 1\right) + 10log(\eta) \quad (1)$$

where η is the structural loss factor of the wall without ETICS, m is the mass of plaster ρ_0 is the density of air, f denotes the frequency (Hz) and f_c is the theoretical coincidence frequency of the plaster layer of the ETICS. Santoni et al. [15] developed a model that takes the influence of anchors, as commonly used in ETICS, into account. Furthermore, Urban et al. studied a theoretical relation of thermal insulation material choice influence on the resulting sound insulation spectra [16]. In this study eight different material types were chosen, split up into three groups (see **Table 1.**).

Variable	Mineral Wool	Rigid Foam	EPS
ρ(kg/m^3)	53,1 to 112,8	35,8	13,6 to 14,8
d (m)	0,13 to 0,15	0,08	0,11 to 0,15
s (MN/m^3)	4,4 to 10,6	57,7	33,0 to 42,0
ΔR(dB)	2 to 11	-6	-4 to -3
ΔC (dB)	-1 to -9	-4	-4 to -3
ΔC_{tr}(dB)	-4 to -14	-4	-5 to -4

Table 1. Theoretical influence of ETICS on the sound reduction improvement index.

2. LIGHTWEIGHT TRANSPARENT FACADES

The most widely used façades used for administrative buildings are lightweight cladding, specially based on a combination of glass and aluminium. They allow architects to create large transparent surfaces with variable dimensions and shapes.

2.1. Single leaf façades

Single layer façades are the most common transparent type of façades. Thanks to the development in building constructions, today we can design façades having a high sound insulation as well as a high thermal insulation. By improving the façades of the transparent parts (glassing), the weakness of façades became the aluminium parts, the details of the joints and the anchoring of the façades [17]. These parts are in many cases spreading sound energy in the construction. Finding the best solution for façades, the construction of the joints of their parts and the design of the inner walls connection while keeping the lowest possible cost becomes an important issue. The problem is the mass of the given type of façades , where the coincidence frequency and the natural resonance frequencies are both in the sound insulation spectrum, while in case of massive walls the structural resonance is usually below 100Hz. Because of this, a massive wall most oftenly has a better R_w. Other problems can be caused by structural-acoustic resonances of hollow aluminium mullions, which are commonly used on in façades constructions [18]. Despite the fact that the area of the mullions is only a fraction of the façade surface in comparison to the glazing parts, its deteriorating influence on façade acoustic properties can be significant. Major complications may also cause an inappropriate solution to the dilation between façade panels.

2. 2. Double transparent naturally ventilated façades

Other type of lightweight façades are double skin naturally ventilated façades (DTF). DFT's were initially designed to improve the thermal insulation properties of façades and to reduce the energy requirements of buildings. Subsequently, they were also being applied to design objects in urban areas with high noise exposure. In this case the exterior layer of façade works as a "buffer or shield". In Slovakia, commonly used DTF types are naturally ventilated with a width of façade cavity between 0.15 and 1.5m. This allows the user to ventilate the façades cavity, which increases their comfort. In general, the positive effect of the outer DTF layer on the sound insulation is about ΔR≈6dB in comparison to a single leaf façade. Significant research in this area has been published in [19], where the author's goal was to supplement the standard EN 12354-3 [20] by a prediction model applicable to a DTF.
An emperical model was published in [21], which is based on insitu and laboratory measurement data. The authors distinguish two ways of ventilation (slit or mesh), and divided the frequency spectrum into three regions:
- The frequency range with sound insulation behaviour dominated by transmission enhancement due to cavity resonances (Eq.2).
- The frequency range with sound insulation behaviour dominated by the transmission of sound via the ventilation slots (Eq.3).
- The frequency range above the coincidence frequency of the external wall (Eq.4).

$$R_{f \le f_0} = R_1 + R_2 - 4 \text{ dB} \tag{2}$$

$$R_{f_0 \to f_{cr}} = R_{f_0} + 6 \; or \; 9 \text{ dB/oct} \tag{3}$$

$$R_{f_{cr} \to f} = R_{max} + 6 \text{ dB} \tag{4}$$

From an acoustic point of view, the standing waves occurring in the façade cavity often constitute the biggest problem. Standing wave resonance, ventilation elements and other resonances (critical and natural) often cause acoustic problems both for single leaf façades and for DTF's. Furthermore, the anchoring, joints and interior construction connection to the façades are very often causing acoustic bridges in the system.

3. CONCLUSION

This article presents an overview of the current issues of façades and their acoustic properties in Slovakia. It presents an overview of various approaches to predicting the acoustic performance of External Thermal Insulation Composite Systems (ETICS). The mass spring mass resonance generated by interaction of the plaster and the thermal insulation layer are the determining parameters that need to be considered during façades´ design. It also recalls the issue of lightweight cladding. It points to their weak spots such as hollow aluminium mullions, aluminium frames, anchoring solutions and joints between façade and interior structures. Also DTFs, despite the indisputably better acoustic properties than simple façades, have their weak spots as a solution of the ventilation elements and the standing waves occurring in the façade cavity. The field that was addressed in this article is wind induced sounds. This phenomenon is becoming more and more important due to the construction of high-rise buildings with high airflow rates. In all these areas, extensive research is under way in Europe with the aim of designing better façade solutions.

3. ACKNOWLEDGMENTS

This work was supported by the European Commission, H2020-MSCA-RISE-2015 project 690970, "PAPABUILD" APVV-16-0126 and VEGA 1/0067/16.

4. REFERENCES

[1.] STN 73 0532 (2013): Acoustics. Rating of sound insulation in buildings and of building elements. Requirements.
[2.] Berglund, B.; Lindvall, T.; Schwela, D.H.; **World Health Organization. Guidelines for Community Noise**; WHO: Geneva, Switzerland, 1999
[3.] Hurtley, Charlotte, ed. **Night noise guidelines for Europe**. WHO Regional Office Europe, 2009
[4.] Rasmussen, B., & Machimbarrena, M. (2014). **Existing Sound Insulation Performance Requirements and Classification Schemes For Housing Across Europe**. In COST Action TU0901 – Building acoustics throughout Europe. Volume 1: Towards a common framework in building acoustics throughout Europe (pp. 31-54). DiScript Preimpresion, S. L..
[5.] Nurzynski, J. **The effect of additional thermal lining on the acoustic performance of a wall**. In Proceedings of the Forum Acusticum 2008, Paris, France, 29 June–4 July 2008.
[6.] Weber, L.; Müller, S. **Schallschutz bei Wärmedämm-Verbundsystemen**; Fraunhofer IRB Verlag: Stuttgart, Germany, 2015.
[7.] Weber, L.; Zhang, Y.; Brandstetter, D. **Influence of Wall Construction on the Acoustical Behaviour of**

ETHICS. In Proceedings of the DAGA 2002, Bochum, Germany, 4–8 March 2002.

[8.] Weber, L.; Buchele, A. **Acoustic Refurbishment of Residential Buildings with Additional Linings and Additional Lining Constructions-Calculation**, Design, and Optimization; Abridged Version of Research Report B-BA 2/2008; Fraunhofer Institute for Building Physics (IBP): Stuttgart, Germany.

[9.] Weber, L. **Effect of ETHICS on the flanking transmission of outer walls**. In Proceedings of the Fortschritte der Akustik-DAGA, Strasbourg, France, 22–25 March 2004.

[10.] Weber, L.; Brandstetter, D. **Einheitliche Schalltechnische Bemessung von Wärmedämm-Verbundsystemen, -Ergänzung des Berechnungsverfahrens**; IBP-Bericht B-BA 4/2005; Fraunhofer IRB Verlag: Stuttgart, Germany, 2002.

[11.] Weber, **L. Einheitliche Schalltechnische Bemessung von Wärmedämm-Verbundsystemen-Ergänzung des Berechnungsverfahrens**; Fraunhofer IRB Verlag: Stuttgart, Germany, 2005.

[12.] Scholl, W. **Schalldämmung mit Wärmedämmverbundsystemen**. Bauphysik 1999, 21, 20–28.

[13.] ISO 12354-1. **Building Acoustics—Estimation of Acoustic Performance of Buildings from the Performance of Elements-Part 1: Airborne Sound Insulation between Rooms**; ISO: Geneva, Switzerland, 2017

[14.] Urbán, D., Roozen, N. B., Muellner, H., Zaťko, P., Niemczanowski, A., Rychtáriková, M., & Glorieux, C. (2018). **Vibrometry Assessment of the External Thermal Composite Insulation Systems Influence on the Façade Airborne Sound Insulation**. Applied Sciences (2076-3417), 8(5).

[15.] Santoni, A.; Bonfiglio, P.; Davy, J.L.; Fausti, P.; Pompoli, F.; Pagnoncelli, L. **Sound transmission loss of ETICS cladding systems considering the structure-borne transmission via the mechanical fixings: Numerical prediction model and experimental evaluation**. Appl. Acoust. 2017, 122, 88–97

[16.] Urbán, D., Zaťko, P., Roozen, N. B., Muellner, H., Glorieux, C., (2018). **Influence of the dynamic stiffness of external thermal insulation on the sound insulation of walls**, Euronoise 2018.

[17.] Bielefeld, H.W., DeGanyar, T. (2018). **Acoustical Performance of Aluminum Framed Façade Systems**, Euronoise 2018.

[18.] Roozen, N.B., Zaťko, P., Urbán, D., Niemczanowski, A., Müllner, H., (2018). **An experimental study into the airborne sound transmission through a partition wall in buildings via structural transmission of window profiles; a case study**, Euronoise 2018.

[19.] M. Blasco, Ch Crispin, **Geventileerde Dubbele Gevels Akoestische Evaluatie In situ en labo metingen, modelisatie en evaluatie van de toepasbaarheid van de bestaande normalisatie**, WTCB, 2004.

[20.] **EN 12354-3 Building acoustics, Estimation of Acoustic Performance of Build- ings from the Performance of Elements. Part 3: Airborne Sound Insulation against Outdoor Sound**, 2002.

[21.] Urbán, D., Roozen, N. B., Zaťko, P., Rychtáriková, M., Tomašovič, P., & Glorieux, C. (2016). **Assessment of sound insulation of naturally ventilated double skin façades**. Building and Environment, 110, 148-160.

THE EFFECT OF POWER SOCKET HOLES ON THE SOUND INSULATION OF WALLS

Beata Mesterhazy*, Attila Balazs Nagy

Laboratory of Building Acoustics, Budapest University of Technology and Economics,
*bmesterhazy@epsz.bme.hu

Abstract: *Besides flanking transmission construction practice also determines the deviation of sound insulation of walls from laboratory results. Lightweight constructions are usually more sensitive to construction details than heavy walls. In this paper we examine the effect of bored power socket holes on the sound insulation of walls.*
We examined sound insulation of a plastered heavy solid brick wall and a lightweight gypsum wall with approximately the same sound reduction index. We measured airborne sound insulation of these walls with adding 1-12 power socket holes in each of them, 6 holes on each side. Effect of increasing number of holes was evaluated both in the frequency domain and as weighted sound reduction index.
Based on a simple approach, we also calculated the resulting sound reduction index of the two walls with the 1-12 power socket holes. Calculation and measurement results were compared and analysed. As a result, a simple method for predicting the effect of power socket holes on sound insulation of both constructions was determined.

Key words: airborne sound insulation, construction errors, holes, prediction, measurement

CDM EXPERIENCES WITH DIFFERENT ISSUES IN BUILDING ACOUSTICS

Zoltán Horváth

CDM Magyarország Kft., horvath.zoltan@cdmkft.hu

Abstract: *3 different areas are addressed in the presentation where the regional office of CDM or other CDM branches have recently gained first-hand experience: a home cinema was not only isolated, but measured before and ofter the installation; valuable lessons are shared from a large number of sports floor projects; and noise reduction of glass wall is increased with a new concept for an open studio.*

Key words: home cinemas, sports floors, facades

8th Congress of the Alps Adria Acoustics Association
Zagreb, Croatia
20 – 21 September 2018

Hrvatsko akustičko društvo
HAD
Acoustical Society of Croatia

AEROACOUSTIC INVESTIGATION OF THE FORWARD-CURVED FAN

Jurij Gostiša*, Jurij Prezelj*, Marko Hočevar*

*University of Ljubljana, Faculty of Mechanical Engineering, Aškerčeva 6, 1000 Ljubljana, Slovenia
corresponding e-mail: jurij.gostisa@fs.uni-lj.si

Abstract: *Forward-curved fans have been extensively used in various industrial and residential HVAC applications. Regarding their favourable characteristic properties, low noise and small size, forward-curved fans have found use in applications with significant requirement for high flow rates at moderate pressures and efficiency not being of primary importance. For such reasons, they are commonly used in large domestic and professional white appliances. Design of the flow channels and fan installation in those is heavily influenced by limited space available, which results in adverse flow aerodynamics.*

The study is focused on the fan's inlet design and its impact on the fan performance characteristics and local flow properties. One of the main reasons for poor efficiency of the forward-curved fan is the flow separation, which starts at the inlet, develops into the blades and then into the volute. Such vortical flow occupies about a third of the rotor width and thus resulting in flow rate and efficiency reduction. Inlet velocity flow field was studied and its correlation to the emitted acoustic pressure. Two inlet configurations were examined, a regular axial and an implementation of radial inlet, found in a domestic tumble dryer. Local measurements of flow velocity using hot wire anemometry and acoustical pressure measurements were performed and thus provided the discussion about the impact of local inlet flow properties on the fan performance characteristics.

Key words: aeroacoustics, aerodynamics, forward-curved fan, hot-wire anemometry

1. INTRODUCTION

Forward-curved (FC) fans are characterised by two distinctive features, large rotor outlet to inlet ratio (about 3:1) and large number of short chorded blades (around 40). Because of its appearance, this type of fan is also called drum-rotor fan (mostly in Europe), squirrel-cage fan (mostly overseas) and Sirocco fan or multivane impeller by Eck [1]. Despite poor efficiencies, FC fans are commonly used in many domestic and industrial applications requiring high flow rates at moderate pressure increase, compact size, low noise emissions and low manufacturing costs. Wide spread of use is probably the reason why many research groups investigated this type of fans. In his work [1] Eck dedicated a separate chapter to FC fans, noticing the flow separation zone at the inlet of the fan and proposing few design guidelines, while pointing out the lack of fundamental knowledge of design and calculations.

Since then, few research groups worked on the field of FC fans and published many papers on the topic. Flow field in the rotor was investigated by Kind [2,3], who pointed out the complexity of flow patterns with substantial axial and circumferential nonuniformity because of separating inlet flow, especially at flow rates below best efficiency point (BEP). Tsutomu [4,5,6,] published a three-part study on blade shape design, flow around the runner blade and volute casing effects. The study is based on numerical and experimental investigation of different rotors and volute casings, from which optimal number of blades, blade angles, volute size and magnifying/circumference angles were obtained.

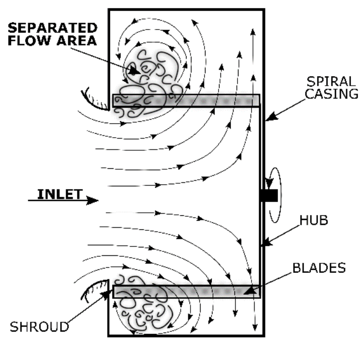

Fig. 1: Flow pattern with distinctive area of flow separation at the inlet of the fan.

A research group from Oveido University in Spain produced continuous research papers [7,8,9] on the topic of aerodynamic and acoustic properties of FC fans, especially double inlet ones used for automotive HVAC systems. They performed a series of numerical and experimental studies, pointing out the effects of volute tongue design on the noise reduction and influence of operating point to highly nonuniform flow through the rotor. Simultaneously a research group from Amirkabir University of Technology, led by Montazerin also performed continuous research on the topic and based on their series of research papers in 2016 published a book [10] on developments in the field. The book covers all major aspects - inlet configuration, rotor and volute design supported by experimental data acquired with LDA measurements and numerical modelling. Furthermore, authors examine noise emissions and contribution of jet-wake-volute interaction to flow characteristics.

In conclusion, extensive work has been done on the topic since 1973, when Eck pointed out the lack of research on the field, but none of that investigates the influence of abrupt inlet configuration design that commonly occurs with fans installed in various appliances. The research, covered in this paper, is focused on the influence of inlet configuration design to local inlet flow field properties and thus performance characteristics of FC fan. A series of experiments were performed to determine fan's performance characteristics, measure inlet flow field with HW anemometry and emitted acoustic pressure fluctuations. Velocities were averaged for each point and presented on a contour graphs for given volume flow rate. Sound pressure signals were presented in a spectrogram as a function of volume flow rate. Furthermore, a novelty approach was used with adopting psychoacoustic metrics to velocity signal analysis.

2. EXPERIMENTAL METHODOLOGY

To determine the performance characteristics of the fan, a measurement apparatus was constructed according to ISO 5801 – installation of category B (free inlet and ducted outlet). This installation was chosen, because it was found to be the most suitable for investigation of inlet flow properties. The apparatus is shown in the Figure 2 and consists the fan section with volute casing (1), orifice for flow rate measurement (2), an auxiliary fan and motorised throttling valve (3). The rotor, used in the study, was taken from a domestic tumble dryer (TD) and is manufactured with injection moulding of polymer material. It has 40 circularly shaped short chorded blades. The outer diameter of the rotor is 155 mm, the inner diameter 115 mm and the width 60 mm. Rotor was driven by Delta ASDA servo drive at precisely 50 Hz. The drive itself also allows measurement of torque on a shaft used to estimate efficiency of the fan. The volute casing was designed according to guidelines for given type and size of rotor, proposed by Montazerin [10]. 4 pressure tapings for measurement of static pressure increase were positioned at the outlet of test section (1), marked with A. Pressure was measured with Endress Hauser Deltabar PMD235 differential pressure transducer. In case of free inlet, low pressure side was not connected (surrounding pressure), while in case of TD inlet configuration, low pressure tapings were mounted on the inlet housing next to the microphone (Fig. 3 – B). Measurement of flow rate was performed according to ISO 5167 with orifice plate installed between two flanges with flange tapings.

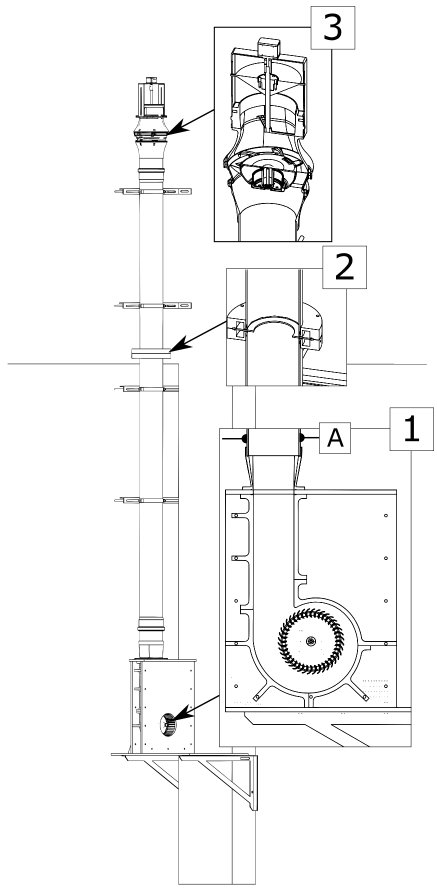

Fig. 2: Measurement apparatus built according to ISO 5801, installation category B, which consists of fan with adjacent spiral casing - 1, orifice – 2, auxiliary fan and throttling valve - 3.

Furthermore, flow velocities were measured with HW anemometer in a plane at the inlet. We used a miniature probe manufactured by Dantec Dynamics, type 55P11 with response of 10 kHz, connected to mini CTA module, type 54T30 of same manufacturer. Probe was calibrated before measurements were performed. Velocity signal was acquired in 144 points on a circular plane next to the inlet. 12 measurement points were distributed on 12 radius lines around the centre of the rotor rotation.

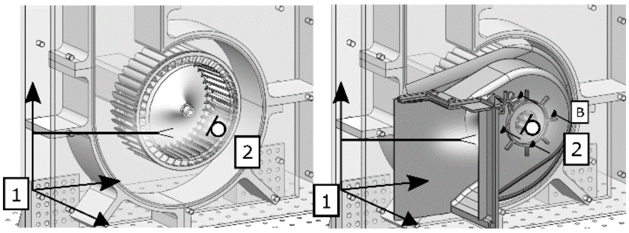

Fig. 3: Hot-wire anemometer probe installed on a 3-axis traversing system – 1 (schematically) and microphone mounted colinearly to the axis of the fan -2.

HW probe was installed on a custom built 3-axis traversing system, which was controlled with Labview code. The probe was positioned in every selected point and then the velocity was acquired for 10 seconds with frequency of 25 kHz using NI9222 module and NI9147 cDAQ chassis. Process was fully automated (except first point needed to be manually positioned in the axis centre) and so very high repeatability achieved.
For sound pressure measurement, a ¼" PCB measurement microphone, type 130A23 was used. Sound signal was acquired with National Instruments cDAQ module, type NI9218 with frequency of 51,2 kHz. Measurement was performed simultaneously with measurement of flow rate while opening the throttling valve. In such way we describe acoustic pressure properties with respect to volume flow rate.
Lately, psychoacoustic metrics became frequently for evaluation of noise emitted by turbomachines [11,12], but we haven't not found a single example of these metrics to be used with non-acoustic signal analysis. Since pressure and velocity fluctuations are strongly related in fluid flows, it would be meaningful to adopt psychoacoustic metrics with velocity signal analysis. With that in mind, we picked Loudness (DIN 45631/A1), Sharpness (DIN 45692), Fluctuation strength and Roughness [13] and with them evaluated velocity signals acquired with HW anemometry.

3. RESULTS AND DISCOUSSION

Results are presented as a comparison of free inlet and tumble dryer inlet configuration in three parts. Firstly, the performance characteristics, following the contour graphs of velocity field and spectrogram of acoustic pressures as a function of volume flow rates and lastly the velocity signals evaluated with psychoacoustic metrics. Average value of each psychoacoustic metric in the inlet area is presented as a contour graph for each inlet configuration at given flow rate. An average value over entire inlet area is calculated for each psychoacoustic metric and presented in a graph as a function of flow rate.

3.1. Performance characteristics

Fans performance characteristics for both inlet configurations are shown in Fig. 4. Both exhibit a distinct unstable area of operation up to about 200 m^3/h, while pressure increase is slightly lower for TD inlet configuration. From there on the operation of the fan is stable for both configurations and second order polynomial curve were interpolated on the measured data.

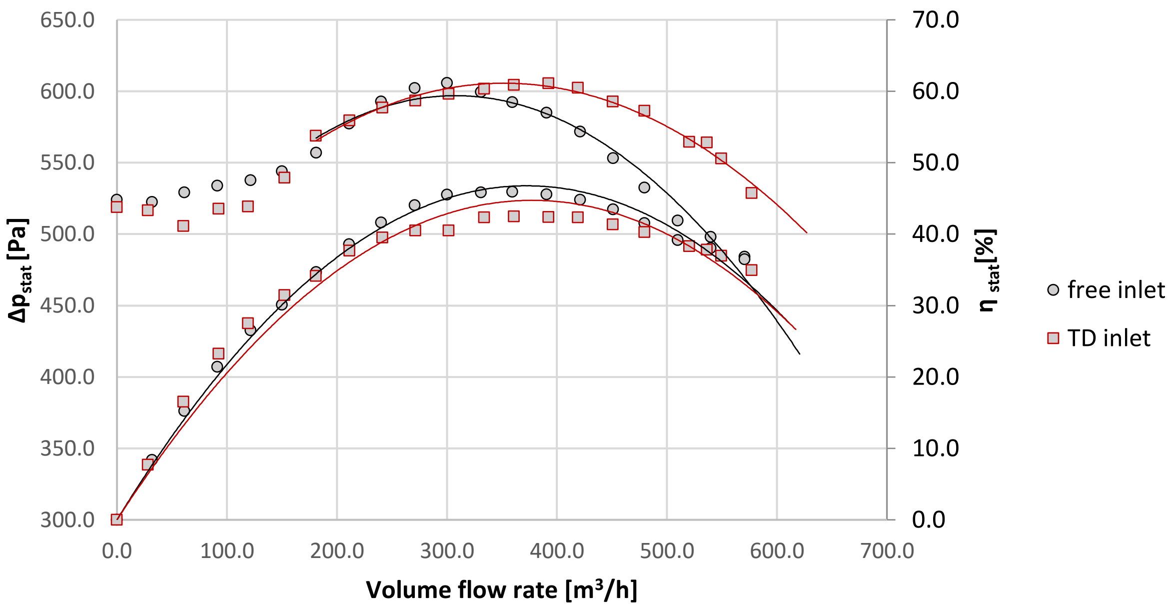

Fig. 4: Performance characteristics of the fan for the case of free inlet and tumble dryer inlet configuration.

The shape of pressure characteristics with TD inlet is elongated and above the pressure characteristics, with free inlet. This could be attributed to the pressure tapings position on the TD inlet housing. Furthermore, while best efficiency point (BEP) for both inlet configurations remains at equal volume flow rate, a slight decrease of efficiency can be noted in the case of TD inlet.

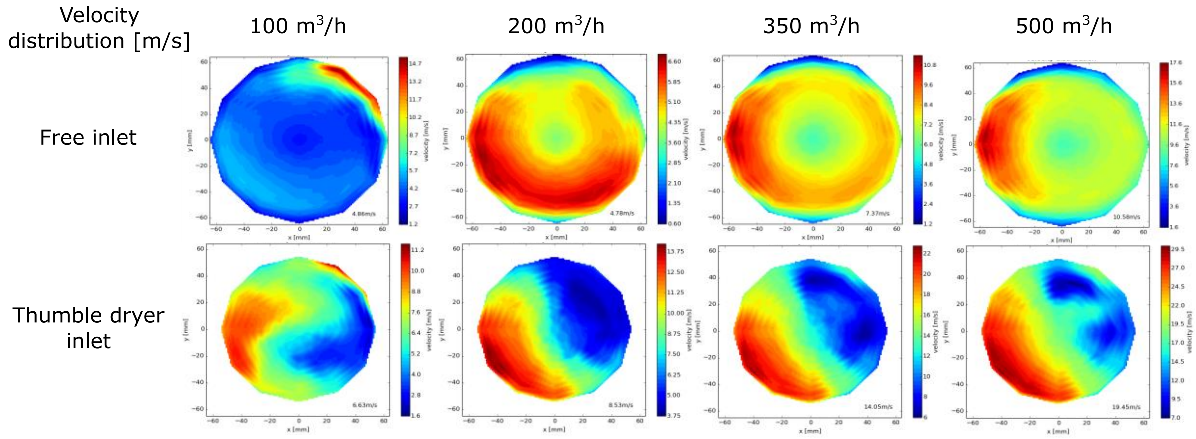

Figure 5: Average velocity distribution at the inlet in case of free intel and TD inlet.

3.2. Velocity distribution and acoustic pressure as a function of flow rate

Velocity distribution was determined by time averaging of the velocity at each measurement point and plotting a contour graph as shown in Fig. 5. In the case of free inlet, velocities are uniformly distributed over the inlet area, with a slight increase in a ring-shaped area around the axis of rotation. At 100 m^3/h an outflow occurs at the top right area of the inlet, just after the volute tongue. The velocity of exiting flow there is much higher compared to the velocity over the rest of the inlet area. That is also the reason, why average velocity at that point exceeds otherwise linear progression of average velocity. Furthermore, a noticeable decrease of velocity occurs at the utmost outer inlet area, since the traversing system was set to acquire the velocity outside of the inlet flow area.

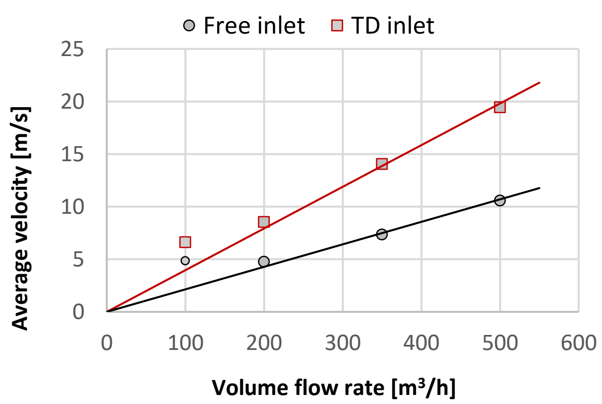

Fig. 6: Velocity averaged over the inlet area graphed as a function of the volume flow rate

While a slight increase of velocity on the low left side is noticeable in the case of free inlet, a pronounced increase occurs in the case of TD inlet. Two areas of high and low velocity are separated with a sharp line. Velocity averaged over the inlet area for the case of TD inlet exceeds the averaged velocity for the case of free inlet at every volume flow rate (Fig. 6). At the 500 m^3/h maximum velocity even exceeds the circumferential velocity of the rotor.

In addition to velocity field, acoustic pressure was investigated. Results are shown in a spectrogram of sound pressure level spectra as a function of volume flow rate (Figs. 7 and 8).

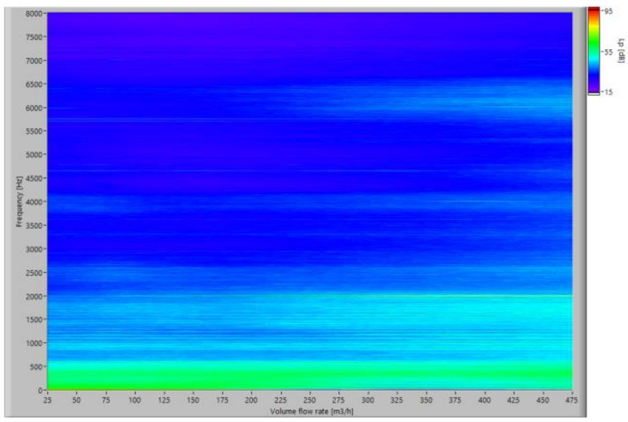

Fig. 7: Spectrogram of sound pressure level as a function of volume flow rate in case of free inlet configuration.

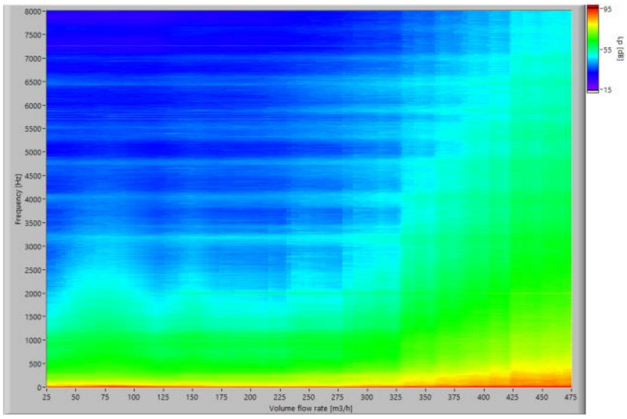

Fig. 8: Spectrogram of sound pressure level as a function of volume flow rate in the case of TD inlet configuration.

Both spectrograms exhibit amplified levels of blade passing frequency (BPF) at 2 kHz with two harmonics, that appear clearly near BEP in the case of free inlet but are masked by broad-band noise in the case of TD inlet. In comparison, the TD inlet configuration broadly exhibits higher levels of pressure fluctuations attributed to strong vorticity occurring at the inlet, which increases with flow rate. Contrary, in the case of free inlet a decrease of pressure fluctuations up to 200 Hz occur in the area near BEP (Fig. 9), due to reduction of large vortices. In that manner we could ascribe the efficiency reduction in BEP to the generation of large vortices.

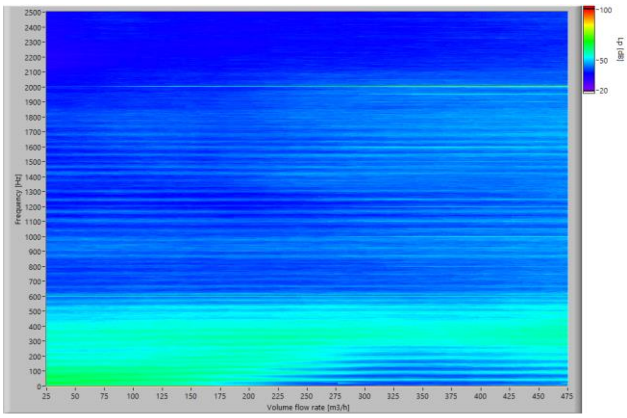

Fig. 9: Pressure fluctuation level decrease near BEP and amplified levels at 50 Hz with its harmonics up to 2kHz.

Narrow-band levels occur over entire volume flow range, at the frequency of 50 Hz (rotational frequency) and its higher harmonics up to 2kHz. These are attributed to the rotor imbalance, which excites the pressure fluctuations with the frequency of rotation.

3.3. Psychoacoustic metrics adopted to velocity signal processing

The goal of psychoacoustic analysis of velocity signals is to relate the aerodynamic phenomena in the inlet area with the inlet configuration type and volume flow rate. Average values of normalised standard deviation and four psychoacoustic metrics (adopted to velocity signal processing) - loudness, sharpness, fluctuation strength and roughness are shown as a function of flow rate in Figure 10. Results are shown as contour graphs of each variable distribution over the inlet area.

Standard deviation of velocity was normalised to maximum velocity at specified flow rate. In the case of free inlet, a distinct area of high standard deviation near volute tongue occurs, a region of high velocity fluctuations that result in emitted noise. This corresponds well with the acoustic pressure measurements (discrete BPF) and findings of Velarde-Suarez [8,9], showing the rotor-volute tongue interaction as one of the dominant sources of aerodynamic noise.

Similar behaviour is noticed with loudness, which also depicts areas of increased levels near volute tongue. In relation to average velocity distribution, we notice high standard deviation and loudness in the areas of lower average velocities.

On the contrary, areas of high sharpness occur in the areas of high average velocity. Sharpness is a hiss like property of sound, dominated by energy at high frequencies, similar to fluctuations of high velocity flow. In that manner, sharpness can be directly related to areas of high velocity.

Velocity fluctuation strength and roughness show similar behaviour. They both indicate loudness modulation, fluctuation strength at frequencies below and roughness at frequencies above 30 Hz. Interestingly, both show almost exact inverse of sharpness distribution. In relation to aerodynamic phenomena, we explain the area of increased fluctuation strength and roughness with presence of large vortices due to the transition between high and low average velocity areas.

Overall, with respect to volume flow rate, a distinct distribution alteration of all analysed metrics occurs between 100, 200 and 350 m^3/h, while results between 350 and 500 m^3/h don't exhibit such variations.

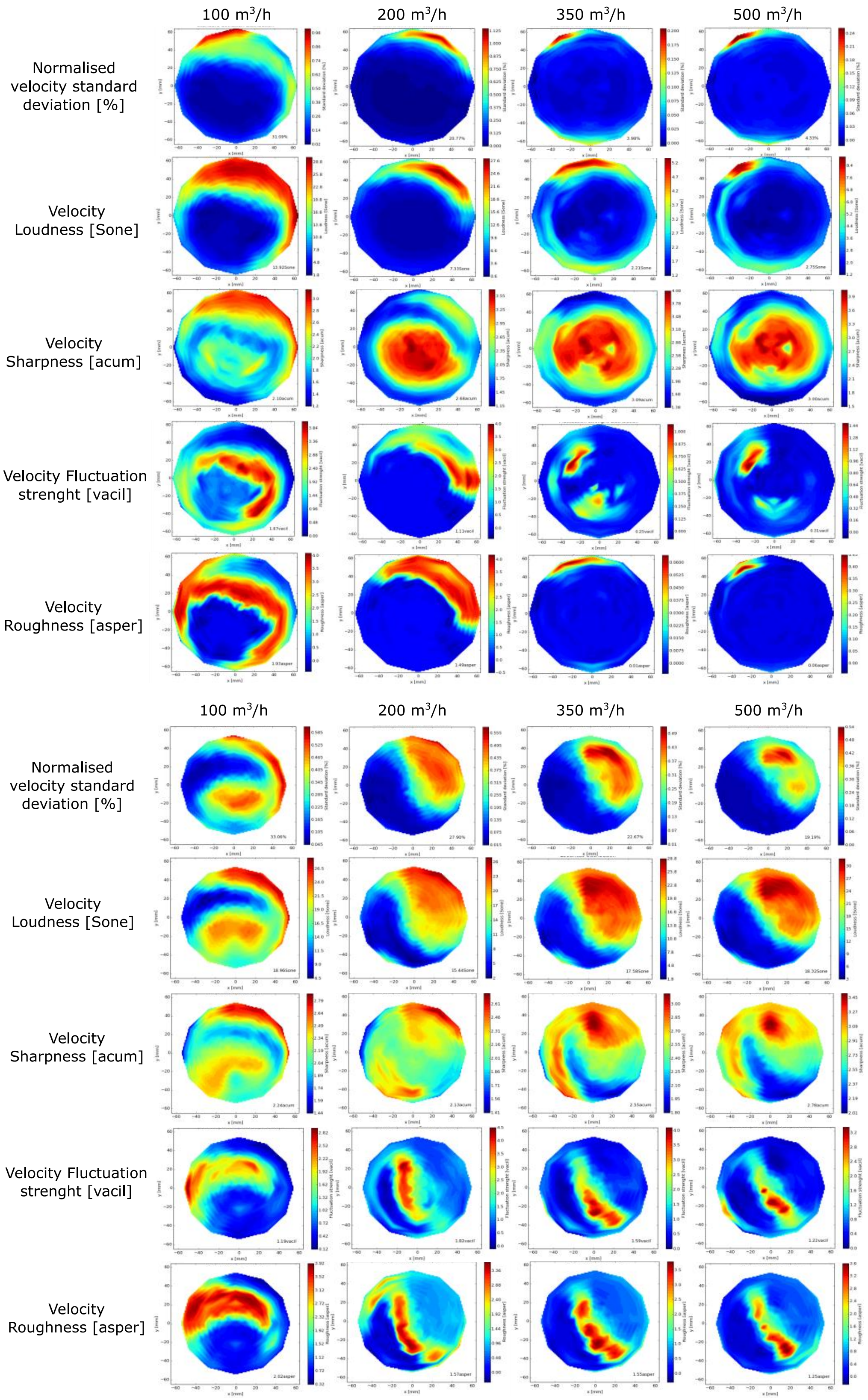

Fig. 10: Normalised velocity standard deviation and psychoacoustic metric levels distribution over the inlet area as a function of flow rate in the case of free inlet (top) and TD inlet (bottom).

Amplitude scales on the contour graphs above are not the same. This is convenient for analysis of metrics distribution but can be misleading when comparing magnitudes. To evaluate relationships among estimators and volume flow rates, each estimator was averaged over entire inlet area and plotted as a function of flow rate (Fig. 11).

Loudness, fluctuation strength and roughness, which were previously coupled with large scale vorticity occurrence, exhibit local minimum at BEP, in the case of free inlet. That progression shows to inlet vorticity having a distinct effect on the inlet losses which result in efficiency decrease at the operation below BEP. On the contrary, sharpness - coupled with high frequency fluctuations, exhibits increase proportional to volume flow rate, for both inlet configurations. That agrees with the idea of sharpness being correlated to high velocity area.

In the case of TD inlet, graphs don't exhibit such distinct pattern. A slight local minimum occurs at 200 m^3/h but does not coincide with the BEP. Fluctuation strength and roughness both decrease with flow rate, but a distinct minimum is not present.

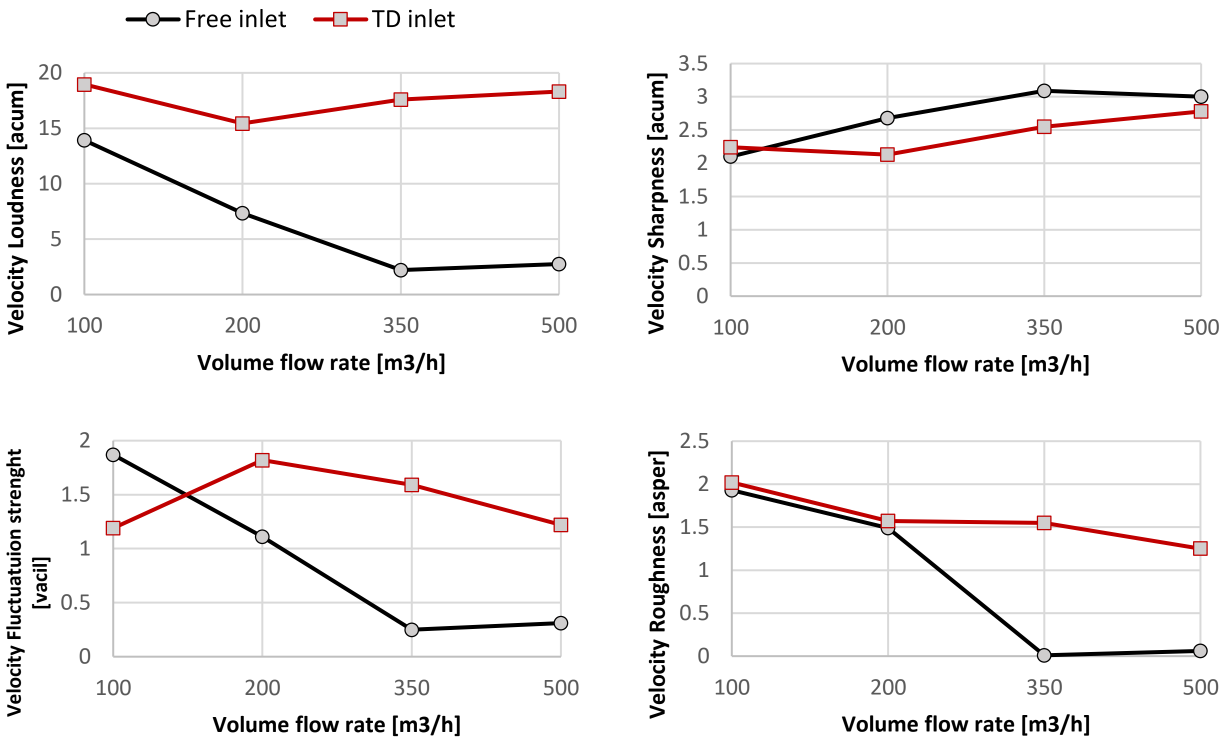

Fig. 11: Psychoacoustic metrics, averaged over entire inlet area and graphed as a function of flow rate in the case of free inlet and TD inlet.

4. CONCLUSION

Aeroacoustic investigation of the forward-curved fan was performed to evaluate the effect of inlet configuration design. Firstly, the performance characteristics for both cases were determined. They don't exhibit any distinct properties except a slight decrease of efficiency in BEP and elongated shape of the pressure characteristics in the case of TD inlet. Furthermore, measurements of local velocities were performed with hot wire anemometer and measurements of acoustic pressure with a measurement microphone. Velocity distribution exhibits uniform, ring shaped contours in the case of free inlet and distinct areas of high and low velocities in the case of TD inlet. Acoustic pressure fluctuations were plotted in a spectrogram as a function of flow rate and exhibit a decrease of low frequencies near BEP, due to reduction of large vortices. Amplified rotational frequency was noticed because of fans imbalance.

A novelty approach with adopting psychoacoustic metrics to velocity signal analysis was used. Loudness, sharpness, fluctuation strength and roughness were found to be useful with interpretation of local aerodynamic properties of fluid flow. Averaged values of loudness, fluctuation strength and roughness exhibit a minimum at best efficiency point, which coincides with vorticity occurrence. On the contrary, sharpness increases proportional to flow rate, which coincides with increase of high frequency fluctuation presence at higher average velocity.

4. REFERENCES

[1.] B. Eck: Fans, 1st English ed., Pergamon Press, Oxford, 1973, 139-155

[2.] R. J. Kind: Prediction of Flow Behavior and Performance of Squirrel-Cage Centrifugal Fans Operating at Medium and High Flow Rates, Journal of Fluids Engineering, 119, 1997

[3.] R. J. Kind, M.G. Tobin: Flow in a Centrifugal Fan of the Squirrel-Cage Type, Journal of Fluids Engineering, 112, 1990

[4.] T. Adachi, N Sugita, et. al.: Study on the Performance of a Sirocco Fan (Optimal blade design), International Journal of Rotating Machinery, 7(6), 2001

[5.] T. Adachi N Sugita, et. al.: Study on the Performance of a Sirocco Fan (Flow Around the Runner Blade), Journal Fluid Thermal Science, 13(3), 2003

[6.] T. Adachi N Sugita, et. al.: Study on the Performance of a Sirocco Fan (Flow Around the Runner Blade), International Journal of Rotating Machinery, 10(5), 2004

[7.] R. Ballesteros-Tajaduraet al.: Numerical model for the unsteady flow features of a squirrel cage fan, Proceedings of the ASME 2009 Fluids Engineering Division Summer Meeting, 2009

[8.] S. Velarde-Suarez et al.: Experimental Study on the Aeroacoustic Behavior of a Forward-Curved Blades Centrifugal Fan, Journal of Fluids Engineering, 121, 1999

[9.] S. Velarde-Suarez et al.: Experimental determination of the tonal noise sources in a centrifugal fan, Proceedings of ASME FEDSM'03, Honolulu, Hawaii, 2003

[10.] N. Montazerin, G. Akbari, M. Mahmoodi: Developments in turbomachinery flow: Forward curved centrifugal fans, Woodhead Publishing in Mechanical Engineering, 2015

[11.] Schneider M, Feldmann C. Psychoacoustic evaluation of fan noise, Fan 2015, Lyon, France, 2015

[12.] J. Prezelj, T. Novaković. Centrifugal fan with inclined blades for vacuum cleaner motor, Applied Acoustics, 2018

[13.] Fastl, Zwicker E. Psychoacoustics – Facts and Models, third edition, Springer-Verlag Berlin, Heidelberg 2007, 325

DEDICATED WAVELET ANALYSIS FOR CRACK IDENTIFICATION IN GEARS

Aleš Belšak, Jurij Prezelj

University of Maribor, Faculty of Mechanical Engineering (ales.belsak@um.si)
University of Ljubljana, Faculty of Mechanical Engineering (jurij.prezelj@fs.uni-lj.si)

Abstract: *Various damages caused to gear units lead to problems and faults in their operation. A crack in the tooth root is one of the least desirable damages as it often causes gear unit operation failure. A test plant was prepared and signals were measured in it. The signals were produced by a faultless gear and other signals were produced by a gear with a crack in the tooth root. Fault detection analysis is based on those signals. Vibrations are monitored to determine whether a crack is present. Significant changes in tooth stiffness are associated with a fatigue crack in the tooth root whereas changes in other dynamic parameters are more common in reference to other faults. A non-stationary signal is analysed on the basis of time frequency analysis tools, e.g. semi hybrid wavelets analysis.*

Key words: gear unit, crack, vibration, wavelet analysis

1. INTRODUCTION

The aim of maintenance is to keep a technical system (gear-unit) in the most suitable working condition, which is done by discovering, diagnosing, foreseeing, preventing and eliminating damages. The purpose of modern maintenance is not only to eliminate failures but also to determine the stage of a potential danger of a sudden failure of system operation. Different signals, condition parameters and other indirect signs help determine incorrect operation, the possibility and location of damages and the possibility of elimination of these damages. The form of damage can be determined on the basis of deviations from the values that are typical of a faultless gear system. This paper represents a continuation of the research presented in [1]. Its objective is to identify a more precise location of a crack.

The elements of a gear unit enable the transmission of rotating movement. A gear unit is a complex dynamic model, nevertheless its movement is usually periodical. Thus, faults and damages are a disturbing quantity or impulse. A disturbance is shown by local and time changes in vibration signals [2,3] and time-frequency changes can be expected [4], which is based on kinematics and operating characteristics [5,6].

2. WAVELET TRANSFORM

The continuous wavelet transform of function $x(t) \in L2(\Re)$ at the time and scale is expressed in the following way [10]:

$$W\ x(u,s) = \int_{-\infty}^{+\infty} x(t) \cdot \frac{1}{\sqrt{s}} \cdot \psi^*\left(\frac{t-u}{s}\right) \cdot dt \tag{1}$$

$$\overline{\psi}_s(t) = \frac{1}{\sqrt{s}} \cdot \psi^*\left(\frac{-t}{s}\right) \tag{2}$$

$$\overline{\Psi}_s(\omega) = \sqrt{s} \cdot \Psi^*(s \cdot \omega) \tag{3}$$

where the transform is presented as the product of convolution; Eq. (2) presents the expression of an average wavelet function and the corresponding Fourier integral transform is shown in Eq. (3).

The function x(t) is multiplied by a group of shifted and scaled wavelet functions in the continuous wavelet transform. Wavelets are locally limited functions and they are applied to analyse the observed function x(t). The continuous wavelet transform is very sensitive to local non-stationarities.

The Morlet wavelet function, a representative of a non-orthogonal wavelet function, is expressed as follows:

$$\psi_{Morlet}(t,\sigma,\eta) = \frac{1}{\sqrt[4]{\pi}} \cdot e^{-\frac{t^2}{2}} \cdot e^{i \cdot \eta \cdot t} \tag{4}$$

Eq. (5) gives a family of wavelet functions, or a shifted u and scaled s Morlet wavelet function:

$$\psi_{Morlet}(t,\sigma,\eta) = \frac{1}{\sqrt{s}} \cdot \frac{1}{\sqrt[4]{\pi}} \cdot e^{-\frac{1}{2}\cdot\left(\frac{t-u}{s}\right)} \cdot e^{i \cdot \eta \cdot \left(\frac{t-u}{s}\right)} \tag{5}$$

There are several types of functions that can be applied as a wavelet basis; their choice depends on the application-related requirements [18–19].
The choice of the Morlet wavelet as the basis function was based on the similarity of formulation with the Gabor transform function investigated in our laboratory. The Morlet wavelet differs from the Gabor transform only in the exponent term, which helps identify the shape of the wavelet.
By using the expression in Eq. (5) it is possible to further transform the time function to the frequency domain as follows:

$$\hat{\psi}_{Morlet}(\omega,\sigma)=\sqrt[4]{\pi}\cdot\sqrt{\frac{2\cdot\pi}{s}}\cdot e^{-i\cdot\omega\cdot u}\cdot e^{-\left(\omega-\frac{\eta}{s}\right)^2\cdot\frac{s^2}{2}} \quad (6)$$

It is possible to decompose the Morlet wavelet, which is a complex wavelet, into two parts: one of them for the real part and the other one for the imaginary part:

$$\psi_{Morlet\ real}(t,\sigma,\eta)=\frac{1}{\sqrt{\pi}}\cdot e^{-\beta^2\cdot\frac{t^2}{2}}\cdot\cos(\omega\cdot t) \quad (7)$$

$$\psi_{Morlet\ imag}(t,\sigma,\eta)=\frac{1}{\sqrt{\pi}}\cdot e^{-\beta^2\cdot\frac{t^2}{2}}\cdot\sin(\omega\cdot t) \quad (8)$$

where β is the shape parameter that balances the time resolution and the frequency resolution.
Only the real part of the Morlet wavelet is usually applied. It is a cosine signal that decays exponentially on the left and right side; its function shape resembles an impulse, which is the reason why the Morlet wavelet is used a lot in mechanical fault diagnostic applications.
Based on the mother wavelet, a daughter Morlet wavelet is obtained by time translation and scale dilation:

$$\psi_{Morlet}(t,\sigma,\eta)=\frac{1}{\sqrt{\pi}}\cdot e^{-\beta^2\cdot\frac{t(t-u)^2}{2\cdot s^2}}\cdot\cos\left(\frac{\pi\cdot(t-u)}{s}\right) \quad (9)$$

where s is the scale parameter for dilation and u for time translation. A daughter Morlet wavelet that closely matches the shape of a mechanical impulse can be constructed by selecting parameters s and u.
Firstly, it is necessary to identify the location and shape of the frequency band that corresponds the impulses. Then it is possible to determine the impulses by filtering. Scale s and parameter β are used to control the location and shape of the daughter Morlet wavelet. By optimising the two parameters for a daughter wavelet, an adaptive wavelet filter can be built. Several researchers addressed the issue of choosing the mother wavelet that adapts best to the signal to be isolated [20, 22, 23]. Optimal wavelet reconstruction is not necessary, whereas optimal daughter wavelet is required. Wang is interested in differences between single- and double-sided Morlet wavelets [21]. Their frequency spectra are quite different. As a real impulse is usually non-symmetric, the right-hand side of Morlet wavelet was chosen for the basis. Such wavelets are supposed to be most appropriate to match the behaviour of hidden impulses.
It is possible to use the fourth standardized moment or Kurtosis to identify faults due to its sensitivity to sharp variant structures, such as impulses.
The fourth standardized moment is determined as shown below:

$$\gamma_2=\frac{\mu_4}{\sigma^4} \quad (10)$$

where μ4 inidicates the fourth moment about the mean and σ indicates the standard deviation. Kurtosis is often determined as the fourth cumulant divided by the square of the second cumulant, which is equal to the fourth moment around the mean divided by the square of the variance of the probability distribution minus 3:

$$\gamma_2=\frac{\kappa_4}{\kappa_2^2}=\frac{\mu_4}{\sigma^4}-3 \quad (11)$$

This is called excess kurtosis. The "minus 3" above is often considered a correction, which makes the kurtosis of the normal distribution equal to zero. As the cumulant is applied, if Y is the sum of n independent random variables, all with the same distribution as X:

$$\gamma_2[Y]=\frac{\gamma_2[X]}{n} \quad (12)$$

If kurtosis was defined as μ4 / σ4, the equation would be more complex. In relation to a sample of n values, the sample kurtosis is as follows:

$$\gamma_2==\frac{\frac{1}{n}\sum_{i=1}^{n}(x_i-\bar{x})^4}{\left(\frac{1}{n}\sum_{i=1}^{n}(x_i-\bar{x})^2\right)^2}-3 \quad (13)$$

xi is the i-th value, and $\bar{x}$ is the sample mean.
The kurtosis increases with the impulse in signals. This means that the kurtosis can be used as a performance criterion of a Morlet wavelet.
The appropriate wavelet can be obtained in the following way:
1. The parameters s and β are modified to produce different daughter wavelets.
2. The kurtosis is calculated for each daughter wavelet.

3. It is very appropriate to use parameters s and β that correspond to the largest kurtosis to determine hidden impulses.

3. WAVELET DE-NOISING

Donoho [12] was the first to use the wavelet threshold de-noising method, the objective of which is to remove independent and identically distributed Gaussian noise. A signal series $x(t)=x_1(t), x_2(t) \ldots x_n(t)$, obtained with a sensor, consists of impulses and noise. It is possible to express x(t) as shown below:

$$x(t) = p(t) + n(t) \tag{14}$$

where $p(t)=p_1(t), p_2(t) \ldots pn(t)$ indicates the impulses to be determined, whereas $n(t)=n_1(t), n_2(t) \ldots n_n(t)$ indicate the noise with mean zero and standard deviation.

Prior information on the impulse probability density function is considered in relation to a specific threshold rule, which is based on the maximum likelihood estimation method. In compliance with this rule, the noise is not necessarily independent and identically distributed Gaussian but it is necessary to know in advance the probability density function of the impulse to be determined.

Hyvarinen introduced the so-called ‘‘sparse code shrinkage’’ method; this method makes it possible to estimate non-Gaussian data under noisy conditions. It is based on the maximum likelihood estimation principle [16].

When it comes to a very sparse probability density function, Hyvarinen [16] used the following function to represent a sparse distribution:

$$p(s) = \frac{(\alpha+2)\cdot(0.5\cdot\alpha\cdot(\alpha+1))^{0.5\cdot\alpha+1}}{2\cdot d\cdot\left(\sqrt{0.5\cdot\alpha(\alpha+1)}+\left|\frac{s}{d}\right|\right)^{\alpha+3}} \tag{15}$$

where d is the standard deviation of the impulse to be isolated, and α is the parameter that controls the sparseness of the probability density function.

For an impulse, for which the probability density function can be represented by Eq. (10), Hyvarinen applied the sparse shrinkage threshold rule [16]:

$$g(u) = sign(u)\max\left(\begin{array}{c} 0\ ,\ 0.5\cdot(|u|-a\cdot d)+0.5\cdot \\ \sqrt{(|u|-a\cdot d)^2-4\cdot\sigma^2\cdot(\alpha+3)} \end{array}\right) \tag{16}$$

where $\sigma = \sqrt{0.5\cdot\alpha\cdot(\alpha+1)}$ denotes the standard deviation of the noise.

As a Morlet wavelet and an impulse are similar, a wavelet transform is adopted. In order to the this, the following steps are performed:

1. The Morlet wavelet with appropriate shape is applied to carry out a wavelet transform for the signal series x(t). Eq. (1) is applied to acquire the wavelet coefficients.
2. The threshold rule from Eq. (16) is applied to shrink the wavelet coefficients.
3. The inverse transform of the shrunken wavelet coefficients is carried out. The result represents an approximation to the impulse to be isolated. W x(u,s) are the reconstructed coefficients. Then, the following equation [10] is applied to purify the signal:

$$x(t) = \frac{1}{C_\psi}\cdot\int_{-\infty}^{+\infty}\int_{-\infty}^{+\infty} W\ x(u,s)\cdot\frac{1}{\sqrt{s}}\cdot\psi\left(\frac{t-u}{s}\right)\cdot du\cdot\frac{ds}{s^2} \tag{17}$$

4. PRACTICAL EXAMPLE

All the measurements were performed in the test plant of the Laboratory for Construction Validation of the Faculty of Mechanical Engineering, University of Maribor.

A single stage gear unit was used. A helical gear unit with straight teeth was integrated into the gear unit [11]. The pinion had 19, whereas the wheel had 34 teeth. Each gear unit had a carburised spur gear pair of module 4 mm. Tests were carried out under constant loads. Accelerometers were fixed on the housings to measure vibrations. The presented results are for a nominal pinion torque of 30 Nm and nominal pinion speed of 1200 rpm (20 Hz). This is a very typical load condition for this type of gear units in industrial applications.

A ground gear pair was a standard gear pair; the teeth quality was 6. It had a crack that was 4.5 mm long and located in a tooth root of a pinion. Measurements were performed under the operating conditions normally related with this type of a gear unit. The measurement process and preparations for analysis are described in detail in [11].

The Morlet wavelet function is used to represent normalised and square values of amplitudes of wavelet coefficients. The connection between the scale and frequency is established, and, consequently, the representation is carried out in a time-frequency domain. This is very appropriate for technical diagnostics. It is namely much simpler to establish adequate characteristics in time-frequency domain (frequency scalogram) than in time-scale domain (scalogram). Based on normalization, the transform matches the Parseval characteristic of energy preservation. This means that the energy of wavelet transform equals the energy of the original signal in time domain.

The continuous wavelet transform with the following parameters: η = 6 and σ = 1 was applied for analysis. The representation of the frequency scalogram is presented in the form of wavelet coefficients or their square values. For analysis, a part of the signal representing one whole rotation of the gear (of a pinion with a crack) and taking 50 ms, was appled.

It is evident from the frequency scalogram that no particularities that would indicate local changes can be observed when it comes to the faultless gear; this applies for a normal representation (**Fig. 1.**) of wavelet coefficients. In relation to normal representation of wavelet coefficients (Fig. 1), the resolution is much better in the lower frequency area, where the reaction of each single tooth at the frequency of 380 Hz is expressed.

When it comes to the signal produced by a gear with a crack, a local small change can be observed in wavelet coefficients, at 11 ms, in frequency scalograms with normal representation (**Fig. 2.**)

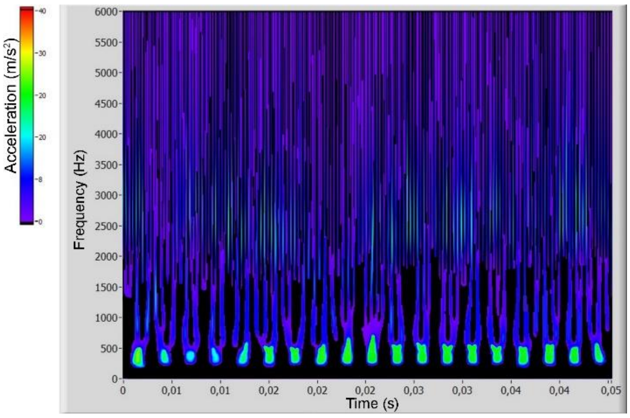

Fig. 1. Frequency scalogram of wavelet coefficient of the reference gear unit

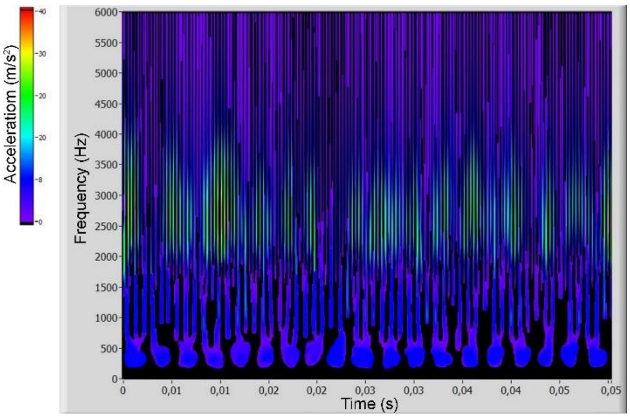

Fig. 2. Frequency scalogram of wavelet coefficient of the gear unit with a gear with a crack in a tooth root

The Morlet wavelet was applied to acquire the adaptive wavelet filter. **Fig. 3** shows the graph of the scale, β and kurtosis relationship. The kurtosis is very sensitive to value β. Let parameter β vary from 0.1 to 5 with a step size of 0.02, and the scale from 1 to 40 with a step size of 0.04. The largest kurtosis value of 5.5 is obtained at β=0.95 and the scale that equals 30, as shown in **Fig. 3**. The Morlet wavelet is appled as a de-noising method. It is possible to use Eq. (15) with α=0.07 to approximate the impulse probability density function. As the noise deviation estimator, MAD/0.793 is applied for each scale. Measured signals of vibrations of a faultless gear and of vibrations of a gear with a crack in the tooth root are presented in **Fig. 4 and 5**. The de-noising signals of a faultless gear are shown in **Fig. 6**. It is possible to observe that no impulses exist in the signals, whereas **Fig. 7** shows the results of filtering with the optimized wavelet filter for signals of a gear with a crack; in these signals impulses at 11 ms can be noted also after the noise has been removed.

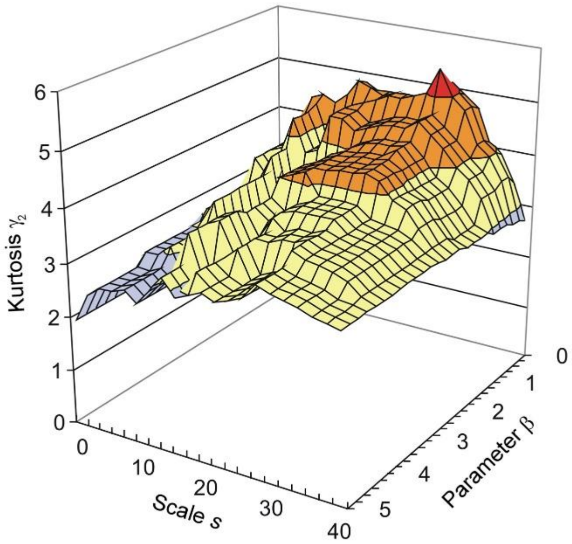

Fig. 3. Graph of the scale, β and kurtosis distribution

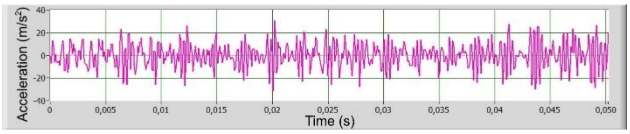

Fig. 4. Measured signal of vibrations of a faultless gear unit

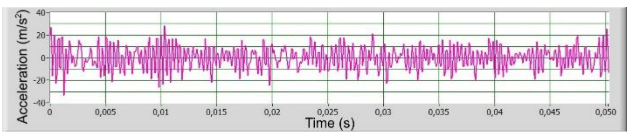

Fig. 5. Measured signal of vibrations of a gear with a pinion with a crack

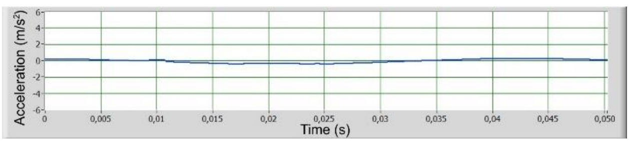

Fig. 6. With Morlet wavelet de-noised signal of vibrations of a faultless gear unit

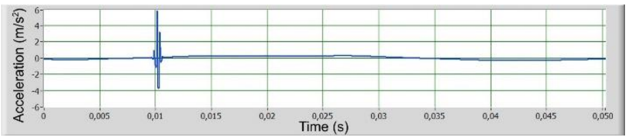

Fig. 7. With Morlet wavelet de-noised signal of vibrations of a gear with a pinion with a crack

4. CONCLUSION

Based on the adaptive wavelet transform it is possible to determine changes and the presence of a damage at the level of an individual tooth. Adaptive wavelet de-noising methods are of much help when determining local changes in gears. Optimised wavelets with Kurtosis match impulses very well. Consequently, the wavelet transform can be used to determine impulses hidden in noise signals. The maximum likelihood estimation threshold rule and prior information on the probability density function of the signals to be determined are applied in relation to this method. This method is applied for extraction of impulses from practical engineering signals and the results are very good.

5. REFERENCES

[1] Belsak A, Flasker J. **Detecting cracks in the tooth root of gears**. Engineering Failure Analysis 2014; 14(8). p. 1466–1475

[2] Adewusi S, AI-Bedoor B. **Wavelet analysis of vibration signals of an overhang rotor with a propagating transverse crack.** Journal of Sound and Vibration 2001; 246(5). p. 777–793.

[3] Bruce AG, Donoho DL et al. **Smoothing and Robust Wavelet Analysis**, Proceedings in Computational Statistics, 11th Symposium, Vienna: 1994. p. 531–547.

[4] James I Taylor. **The Vibration Analysis Handbook**. Vibration Consultans; 1994.

[5] Smith J Derrek. **Gear Noise and Vibration**. New York: Marcel Dekker; 1999.

[6] Victor C Chen, Hao Ling. **Time-Frequency Transforms**. Boston: Artech Hause Publishers; 2002.

[7] Fladrin P. **Time-Frequency/Time-Scale Analysis**. San Diego: Academic Press; 1999.

[8] Mertins A. **Signal Analysis**. New York: John Wiley & Sons Inc; 1999.

[9] Qian S, Chen D. **Joint Time-Frequency Analysis**. Upper Saddle River: Prentice Hall; 1996

[10] Mallat S. **A Wavelet Tour of Signal Processing**. San Diego: Academic Press; 1999.

[11] Belsak A. **Time-Frequency Analysis of the Condition of Gear Units** (Abstract in English). Doctoral Thesis, University of Maribor, Faculty of Mechanical Enginerinng: 2006.

[12] Donoho D L. **De-noising by Soft-Thresholding**. IEEE Trans. Inf. Theory 1995; 41(3). p. 613– 627.

[13] Donoho D L, Johnstone I M. **Ideal Spatial Adaptation by Wavelet Shrinkage.** Biometrika 1994, 81(3). p. 425–455.

[14] Fan J Q, Hall P, Martin M A, Patil P. **On Local Smoothing of Nonparametric Curve Estimators**. J. Am. Stat. Assoc 1996, 91. p. 258–266.

[15] Donoho D L, Johnstone I M. **Adapting to Unknown Smoothness via Wavelet Shrinkage**. J. Am. Stat. Assoc. 1995, 90. p. 1200–1224.

[16] Hyvarinen A. Sparse Code Shrinkage: **Denoising of Nongaussian Data by Maximum Likelihood Estimation**. Neural Comput. 1999, 11(7). p. 1739–1768.

TORSIONAL VIBRATION ANALYSIS OF MULTI-PLATE CLUTCHES FOR VEHICLES

Aleš Belšak, Mario Hirz

University of Maribor, Faculty of Mechanical Engineering (ales.belsak@um.si)
Graz University of Technology, Institute of Automotive Engineering (mario.hirz@tugraz.at)

Abstract: *Multi-plate clutches used for automotive drivetrains have the following advantages over conventional single plate clutches: a higher torque transmission potential and lower actuation forces. Only slightly more space is required for installation. The transmittable torque of multi-plate clutches depends primarily on the number of friction and steel plates. Due to the friction in the guide-ways, the axial forces are reduced from one plate to another. This results in a lowered total torque transmission potential and dynamic behaviour. Consequently, the torsional vibration signature for typical operating conditions is different. Based on time-frequency analysis of vibrations and noise of a non-stationary process, it is possible to determine whether the clutch operation is appropriate.*

Key words: Multi-plate clutch, friction, vibration, time-frequency analysis

1. INTRODUCTION

Friction clutches are used in different kinds of vehicles to fulfil different purposes. They transmit torque from the input to the output shaft in a controlled way in compliance with specific demands, under the influence of actual driving conditions. The torque is transmitted by friction between compressed plates with special friction linings. By means of different friction linings and materials, a suitable friction combination is established with the desired behaviour, particularly regarding the coefficient of friction, noise vibration and harshness (NVH) and wear. Multi-plate clutches are frequently used to enhance the greatest transmitable torque with the installation space being increased as little as possible.
The design of a conventional multi-plate clutch is presented in

Figure **1**. Torque is transmitted by friction between the individual external (steel) and internal (friction) plates, when the clutch is compressed. The external plates, guided in the outer plate carrier, can slide axially but are restrained against rotation to the outer plate carrier. The internal plates are guided in the inner plate carrier and can also slide axially; they are, however, restrained against rotation to the inner plate carrier. When closing the pressure plate (operating piston), the clutch pack is pressed together. In this exemplary application a hydraulic actuation is used to put load on the piston, however, also mechanical, pneumatic, and electromagnetical actuations are present. The piston is pushed back by a return spring when the load is taken away; the clutch opens. [1]

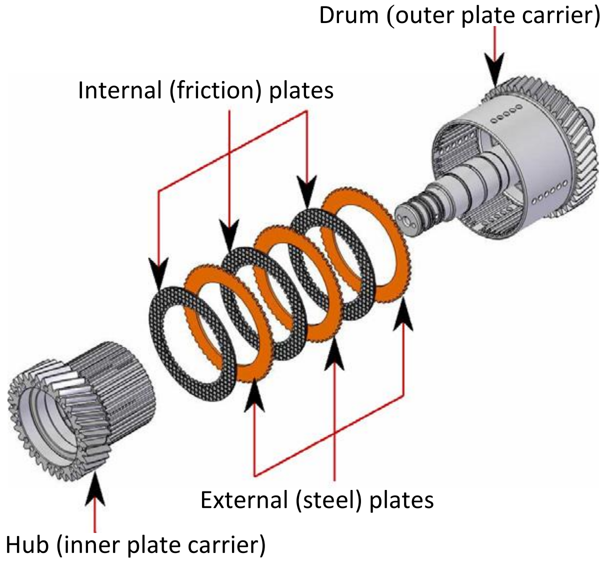

Figure 1: Design of a conventional multi-plate clutch [2]

Without considering the phenomena, such as axial force losses, in a very rough initial estimation, the transmitable torque of a multi-plate clutch can be calculated by multiplying the axial force by the coefficient of friction between the plates, the number of friction surfaces and the mean friction radius. In case of an assumed equal pressure and constant coefficient of friction distribution,

the mean friction radius depends on the inner and outer radius of the friction linings only.
Multi-plate clutches are conventionally realized as wet clutches, where oil is pumped into the clutch package for cooling as well as to improve NVH and wear behaviour of the linings. [3] One main disadvantage of this type of clutches includes the relative high drag losses induced by the oil, especially when the clutch is open. In order to reduce these losses, dry clutches that work without oil, can be used. [4, 5] As dry friction clutches normally have higher coefficients of friction, their torque transmission potential is higher than in conventional wet clutches. Consequently, in dry clutches either the axial force, the number of friction surfaces or the radial expansion can be reduced in order to reach the same torque transmission potential. In contrast to wet clutches, the development of dry clutch technologies provides very special challenges regarding thermal behaviour, NVH and wear. [6, 7] Many researchers have studied the behavior of interaction friction and vibration of the clutch system. [8, 9, 10] For the NHV signature of a clutch, the analysis of torsional vibration is very interesting. [11, 12]

2. TIME-FREQUENCY ANALYSIS OF SIGNAL

Reliability of operation and adequate quality of operation of clutch are negatively influenced primarily by the presence of defect in clutch, this is followed by wear and tear of plates and excentricity caused by backlash in hausing, and errors when assembling and manufacturing the clutch. The condition of clutch is usually monitored on the basis of measured vibrations and torque moment. Deviations from reference values are usually identified on the basis of a frequency spectrum. A clutch is a complex mechanical system with changeable dynamic reactions; as a result it is not possible to define modifications of a frequency component in time, and the approach based on time-frequency methods is more appropriate.
Frequency analysis is often used in diagnostics; however, good results are obtained almost only when periodical processes without any local changes are in question. In concern to classical frequency analysis, time description of vibration is transformed into frequency description, and changes within a signal are averaged within the entire time period observed. As local changes are actually lost in the average of the entire function of vibration, it is very difficult or sometimes impossible to identify local changes.
Above-mentioned deficiencies can be eliminated by time-frequency analysis. Namely, the appearance or disappearance of individual frequency components in a spectrogram indicates local changes that deviate from the global periodical oscillation. In this way, a signal is presented simultaneously in time and frequency.
In relation to technical diagnostics, individual frequency components in signals often appear only occasionally. It is not possible to establish when certain frequencies appear in the spectrum by means of classical frequency analysis of such signals. On the basis of time-frequency analysis it is possible to describe in what way frequency components of non-stationary signals change with time and to define their intensity levels.
Fourier, adaptive and wavelet transforms and Gabor expansion are representatives of various time-frequency algorithms. The basic idea of all linear transforms is to perform comparison with elementary function determined in advance. By means of various elementary functions, different signal presentations can be acquired.
Elementary functions of windowed Fourier and wavelet transforms are based on a time interval that is limited in concern to time; this is where they differ from Fourier transform (elementary functions not limited in relation to time). The resolution of frequency axis, used for window Fourier and wavelet transforms, includes not only frequency data but also time data.
By means of frequency modulation, different resolutions of frequency axis are obtained in relation to windowed Fourier transform, and different resolutions of frequency axis by means of time scaling are obtained in relation to wavelet transform. If the width and the height of the wavelet function are changed, this has direct impact upon time-frequency distribution of the wavelet function. By changing the time scale it is possible to obtain different resolutions of frequency axis.

3. ADAPTIVE METHOD AND TORQUE OSCILATION ANALYSIS

A clutch, which comprises elements making transmission of rotating movement possible, is a complex dynamic model; despite of that, its movement is usually periodical. Faults and damages represent a disturbing quantity or impulse. The disturbance is indicated by local and time changes in vibration signals; consequently, time-frequency changes can be expected . This idea is based on kinematics, dynamic and operating characteristics.
Qian [13] enhanced and concluded adaptive transform of a signal to a large extent although many authors had been developing algorithms without interference parts that reduce usability of individual transforms as opposed to Cohen's class. [14]
Adaptive transform of a signal $x(t)$ is expressed in the following way:

$$x(t) = \sum_{p} B_p \cdot h_p(t) \tag{1}$$

where analysis coefficients are defined using the following equations

$$B_p = \langle x, h_p \rangle \tag{2}$$

whereby similarity between the measured signal *x(t)* and elementary functions $h_p(t)$ of transform is expressed.
The original signal represents the starting point with parameter values $p=0$ and $x_0(t)=x(t)$. In the set of desired elementary functions, $h_0(t)$ is searched for that is most similar to $x_0(t)$ in the following sense

$$\left|B_p\right|^2 = \max_{h_p} \left|\left\langle x_p(t), h_p(t)\right\rangle\right|^2 \tag{3}$$

for $p = 0$. The next step is related to the calculation of the remaining $x_1(t)$

$$x_{p+1}(t) = x_p(t) - B_p \cdot h_p(t) \tag{4}$$

Without giving up the generalisation idea, $h_p(t)$ is to have a unit of energy representation of a signal. Therefore

$$\left\|h_p(t)\right\|^2 = 1 \tag{5}$$

The energy contained in the remaining signal is calculated as

$$\left\|x_{p+1}(t)\right\|^2 = \left\|x_p(t)\right\|^2 - \left|B_p\right|^2 \tag{6}$$

The equation (4) is repeated to find $h_1(t)$ that would suit best $x_1(t)$, etc. In each step one elementary function $h_p(t)$ that suits best $x_p(t)$ is found. The goal of adaptive signal representation is primarily to find a set of elementary functions $\{h_p(t)\}$ that are most similar to time-frequency structure of a signal, and at the same time satisfy equations (1) and (2).

If equation (5) is expressed as

$$\left\|x_p(t)\right\|^2 = \left\|x_{p+1}(t)\right\|^2 + \left|B_p\right|^2 \tag{7}$$

it indicates that the remaining energy of a signal at p-th level can be determined on the basis of $p + 1$ level and the rest B_p. If this process continues, the following result is obtained

$$\left\|x(t)\right\|^2 = \sum_{p=0}^{\infty} \left|B_p\right|^2 \tag{8}$$

The equation is related to energy conservation and is similar to Parseval's relation in the Fourier transform.
The result of using Wigner-Ville distribution for both sides of the equation (1), and organising equations into two groups is as follows:

$$\begin{aligned} P_{WV}\, x(t,\omega) = & \sum_p B_p^2 \cdot P_{WV}\, h_p(t,\omega) \\ & + \sum_{p \neq q} B_p \cdot B_q * P_{WV}\left(h_p, h_q\right)(t,\omega) \end{aligned} \tag{9}$$

The first group represents elementary signal components, and the second one cross interference terms. On the basis of the relation described in (8) and the given value of energy conservation, it is clear that

$$\frac{1}{2 \cdot \pi} \cdot \iint \sum_{p \neq q} B_p \cdot B_q * P_{WV}\left(h_p, h_q\right)(t,\omega) = 0 \tag{10}$$

This is why a new time-dependent adaptive spectrum can be defined as

$$P_{ADT}(t,\omega) = \sum_p \left|B_p\right|^2 \cdot P_{WV}\, h_p(t,\omega) \tag{11}$$

Calculating adaptive spectrogram begins in a wide time range of a measured signal. Then the reduction of this range is required, depending on what are the wished for results. In view of the fact that Fourier integral is included in the elementary operations of searching for a suitable elementary function, the described calculation process is very effective. The accuracy of approximation depends primarily on the size of time-frequency interval. The narrower the intervals, the better the accuracy of representation – which is, however, related to increased time of calculation. This means that a compromise between the accuracy of approximation and the efficiency must be established

4. TEST BENCH INVESTIGATIONS

A specific test plant at the Institute of Automotive Engineering at Graz University of Technology has been used to perform all the measurements. A more detailed description of the clutch can be found in [1].
To determine the presence of torque oscilations, adaptive transform was used. In relation to adaptive spectrogram, frequency transform (PSD) representation for signal decomposition was used. The features of elementary functions are restricted and, therefore, adaptive spectrogram has a fine adaptive time-frequency resolution. Time-frequency resolution of the transform is adapted to signal characteristics. Gauss function (impulse) and linear chirp with Gauss window can be applied as an elementary function. If linear chirps composing a signal are the consequence of a linear change in the rotational frequency of a clutch, it is possible to use an adaptive spectrogram to determine in what ways a possible frequency modulation is reflected in the time-frequency

domain. A possible presence of non-linear frequency modulation may be a problem: a spectrogram may include a certain level of distortion. Adaptive representation is namely approaching non-linear modulation in the form of a linear combination of chirps with linear frequency modulation. This makes the time required for transform calculation increase, along with the larger amount of data and the number of cycles required to search for an adequate elementary function.

The signal of measured values (torque) was 2 s long and composed of, on an average, 12500 measuring points. The clutch under test represents a dry application with five steel and four friction plates. For comparison, adaptive spectrograms related to frequeny transform are given, with the length of the window being 780 points, which is 13% more that the length of the period of one rotation of a clutch. The adaptive spectrogram requires at least 15 times longer calculation time than the the Fourier transform. On the other hand, the resolution of the adaptive transform is, on an average, three times better.

The spectrogram evaluation can be based on an average spectrogram representing an amplitude spectrum of an adaptive transform of a measured signal and by observing pulsating frequencies of individual frequency components. Torque time signal is present in Fig. 2. and 3. The difference is observed between the clutch that was run in and the clutch that was not run in. In the Frequeny specter in Fig. 4. there are additional frequency components in 170Hz, but without information about pulsation. In Fig. 5. the dominant frequency component is at 400Hz. Considering that the amplidude scale is different in the representation of the two clutch status (not run in / run in), it is visible, that the behavior of a dry clutch changes considerable after the running-in phase.

Monitoring the increase or decrease (complete disappearance) in appropriate frequency components is of special interest. This is typical of the frequency of about 170Hz and 400Hz. This phenomenon is expressed only in the adaptive spectrogram (Fig. 6 and 7.).

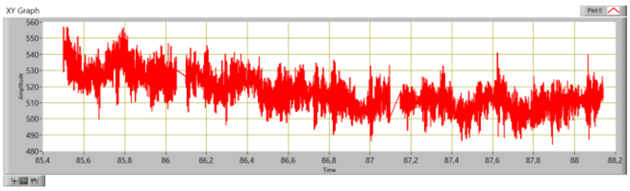

Fig. 2. Time signal of Torque; clutch was not run in

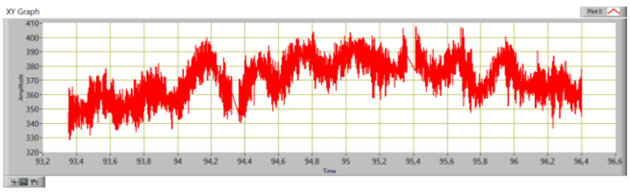

Fig. 3. Time signal of Torque; clutch was run in

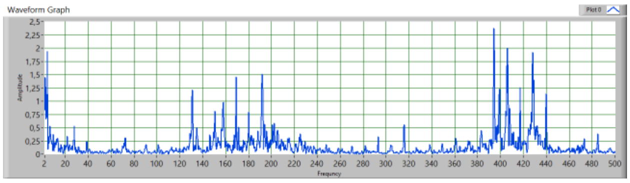

Fig. 4. Frequency specter; clutch was not run in

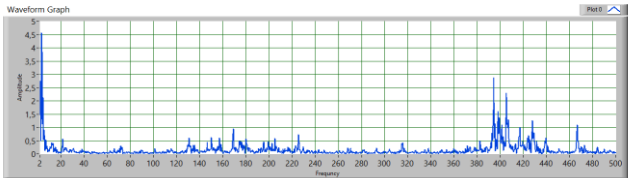

Fig. 5. Frequency specter; clutch was run in

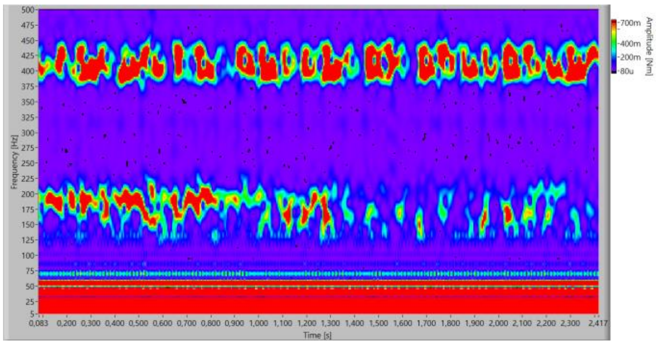

Fig. 6. Time freqency Adaptive spectrogram; clutch was not run in

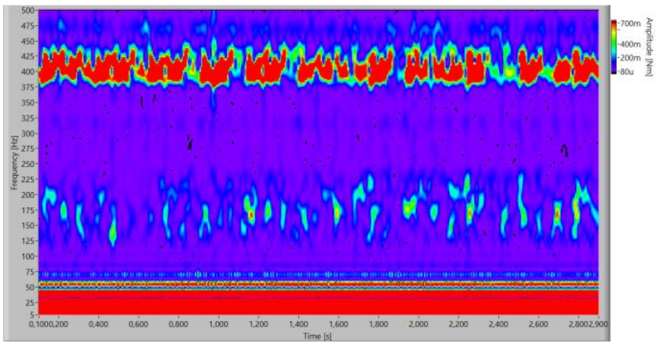

Fig. 7. Time freqency Adaptive spectrogram; clutch was run in

5. CONCLUSION

In this paper torsional vibration analysis is presented for a dry clutch. The methods described can improve development processes and thus increase the safety of operation and, consequently, the reliability of monitoring operational capabilities.

In this way, it is possible to monitor life cycle of a clutch in a more reliable way by using appropriate spectrogram

samples and a clear presentation of the pulsation of individual frequency components, which, along wih the average spectrum, represent a criterion for evaluating the condition of a clutch. Adaptive time-frequency representation makes, above all, a reliable prediction possible; the representation is namely clearer, without increased dissemination of signal energy into the surroundings.
Thus, in relation to life cycle design, it is possible to monitor the actual condition and vital component parts, which can influence the operational capability in a considerable way, by means of an adequate method or criterion.

6. REFERENCES

[1.] C. Gradwohl, A. Belšak, M. Hirz : **Dynamic simulation of multi-plate clutches for automotive applications**. ASim17-10, 2017, 1-17
[2.] A. P. Ompusunggu, P. Sas, H. Van Brussel: **Modeling and simulation of the engagement dynamics of a wet friction clutch system subjected to degradation: An application to condition monitoring and prognostics**, Mechatronics, 23, 2013, 700–712
[3.] P. J. Dolcini, C. Canudas, B. H. Béchart: **Dry Clutch Control for Automotive Applications**, Springer-Verlag London Limited 2010
[4.] W. C. Orthwein: **Clutches and Brakes**, Marcel Dekker, 2004
[5.] T. Butlin, J. Woodhouse: **Sensitivity studies of friction-induced vibration**, Int. J. Vehicle Design, Vol. 51, Nos. 1/2, 2009, 111-129
[6.] V. L. Popov: **Contact Mechanics and Friction**, Springer-Verlag Berlin Heidelberg, 2010
[7.] C. Gang: **Handbook of friction-vibrations interactions**, Woodhead Publishing, 2014
[8.] V. P. Sergienko , S. N. Bukharov: **Noise and Vibration in Friction Systems**, Springer International Publishing Switzerland, 2015
[9.] H. Ouyang, J. E. Motterhead: **Unstable travelling waves in the friction-induced vibrations of disc**, Journal of Sound and Vibration 248(4), 2001, 768-779
[10.] S. L. Qiao, R. A. Ibrahm, **Stohastic dynamic of system with freiction-induced vibration**, Journal of Sound and Vibration 223(1), 1999, 115-140
[11.] D. Centea, H. Rahnejat, M.T. Menday: **Non-linear multi-body dynamic analysis for the study of clutch torsional vibrations (judder)**, Applied Mathematical Modelling 25, 2001, 177-192
[12.] D. Chengwu,S. Rajendra: **Forced vibrations of a torsional oscillator with Coulomb friction under aperiodically varying normal load**, Journal of Sound and Vibration, 325, 2009, 499–506
[13.] S. Qian, D. Chen: **Joint Time-Frequency Analysis**, Prentice Hall, 1996
[14.] A. Mertins: **Signal Analysis**, John Wiley & Sons Inc., New York, 1999

8th Congress of the Alps Adria Acoustics Association
Zagreb, Croatia
20 – 21 September 2018

Hrvatsko akustičko društvo
HAD
Acoustical Society of Croatia

RELEVANCE OF EMPIRICAL MODE DECOMPOSITION FOR FETAL HEARTBEAT DETECTION ON SMARTPHONE DEVICES

Ivan Vican[1], Gordan Kreković[2], Kristian Jambrošić[1]

[1]University of Zagreb, Faculty of Electrical Engineering and Computing, Unska 3, 10000 Zagreb, Croatia;
[2]Visage Technologies, Ivana Lučića 2a, 10000 Zagreb, Croatia
ivan.vican@fer.hr, gordank@gmail.com, kristian.jambrosic@fer.hr

Abstract: *Fetal phonocardiography is a re-emerging method for extracting fetal heartbeat signals with a strong potential to be used as an easily accessible system in prenatal monitoring, especially if employed in conjunction with widespread electronic hardware. Since smartphone devices are going through rapid development of their processing power, sensory capabilities and network connectivity, they are becoming a powerful yet underutilized biomedical tool. Within this study we propose novel features for automatic fetal heartbeat detection based on intrinsic mode functions (IMF) gained through empirical mode decomposition. In order to show that more accurate detection can be achieved with IMF-based features added to the conventional set of audio features, we assessed feature relevance and usefulness using ranking and selection techniques. The results suggest that IMF-based features are relevant for the classification task and can improve prediction accuracy by 3.28%.*

Key words: *phonocardiography; fetal heartbeat; feature extraction; feature ranking; feature selection; machine learning; prenatal care*

1. INTRODUCTION

Fetal heart rate (FHR) monitoring is an important technique in prenatal care that serves as a mechanism with the task of providing information regarding the fetus' health. If any clinical complications are to arise, the fetal monitoring system should obtain prompt diagnosis and notify appropriate intervention [1, 2]. Several techniques can be used non-invasively: fetal electrocardiography (FECG), photo-plethysmography (PPG), Doppler ultrasound, cardiotocography (CTG), fetal magnetocardiography (FMCG) and phonoc-ardiography (FPCG). While all of the latter methods exhibit their advantages and drawbacks [3], Doppler ultrasound has remained the most widespread method of extracting the fetal heart rate, both professionally (e.g. clinics) and non-professionally (e.g. expecting moms at home). Although the correlation between the ultrasonic energy and the fetal health issues has never been proven, there is a number of studies in which some concerns regarding the influence of long-term ultrasound exposure on animals have been raised [4, 5]. A method alternative to ultrasound, fetal electrocardiography, exhibits poor signal-to-noise ratio and requires multiple leads in the non-invasive configuration [6, 7].

Since all of the aforementioned approaches and technologies have their own set of problems and disadvantages, the question whether fetal heartbeat sensing could be made more approachable, especially in the context of preventive and/or personalized healthcare still remains. With over 1.5 billion units sold in 2017 alone, a number of sensors embedded into the smartphone systems has been increasing, with some of them having potential as tools for biomedical data extraction [8, 9]. Since HD audio and teleconferencing demands of the digital era have increased the sensitivity, frequency range and signal-to-noise ratio of smartphone microphones drastically [10], more effort should be taken to assess the feasibility of fetal phonocardiography as a new approach in personalized prenatal care.

The aim of this research is to assess whether fetal heartbeat classification based on audio features can be improved by utilizing empirical mode decomposition (EMD). The signal is decomposed into intrinsic mode functions (IMFs), which can be observed as the "simpler" modes of oscillation of the original signal and thus used for extraction of important data possibly hidden in the noisy original signal. Although another research [11] has used EMD for feature extraction, there are several points on which this paper aims to expand: elaboration of IMF-based feature ranking and selection, comparison between different IMF-based features, and comparison between IMF-based features and audio features.

2. FETAL HEART SIGNAL ANALYSIS

2.1. Fetal heart signal

The spectral content of the mechanical vibrations resulting from fetal heart movement have been extensively studied [12, 13]. Two distinct heart sounds produced by the fetal heart (systolic and diastolic), labeled as S1 and S2, have frequency ranges of 20-40 and 50-70 Hz, respectively [14]. The heart rate of healthy fetus is usually between 120 and 180 bpm (depending on the week of gestation), with rate accelerations and decelerations taking place through specific time intervals [15]. There are several sound sources inside the uterus that interfere with the fetal heart sound, particularly those associated with circulation, respiration and gastrointestinal activity of mother [16, 17].

Another problem is the impedance matching between the sensor and the abdomen skin [18] that further decreases the signal-to-noise ratio of the received fetal heart sound. However, thanks to known parameters of the fetal heartbeat (e.g. spectral content, periodicity, beat frequency), one could extract relevant information by using a number of adaptive algorithms.

2.2. Empirical mode decomposition

As a fundamental part of the Hilbert-Huang transform [19, 20], EMD (methodology given in Figure 1) decomposes the signal into intrinsic mode functions, thus having the ability to break complicated biological signals into a set of functions that provide insight into different modes of oscillation.

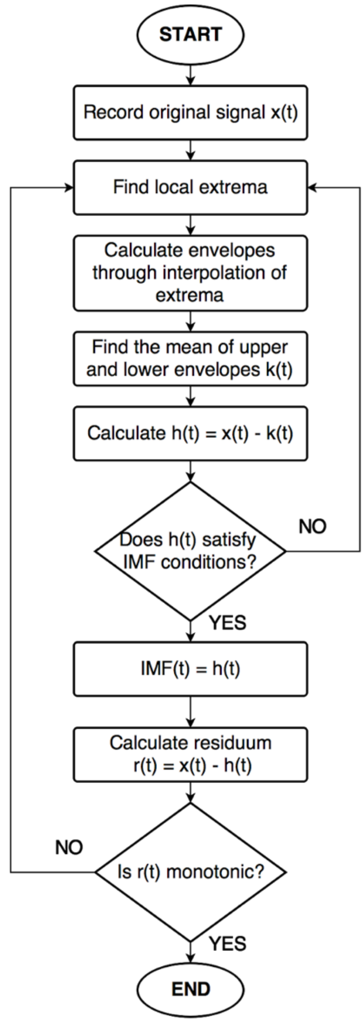

Fig.1. EMD Flowchart

A number of papers regarding the usage of EMD in fetal heartbeat signal extraction have been published [21, 22], supporting the concept of IMF use in meaningful signal

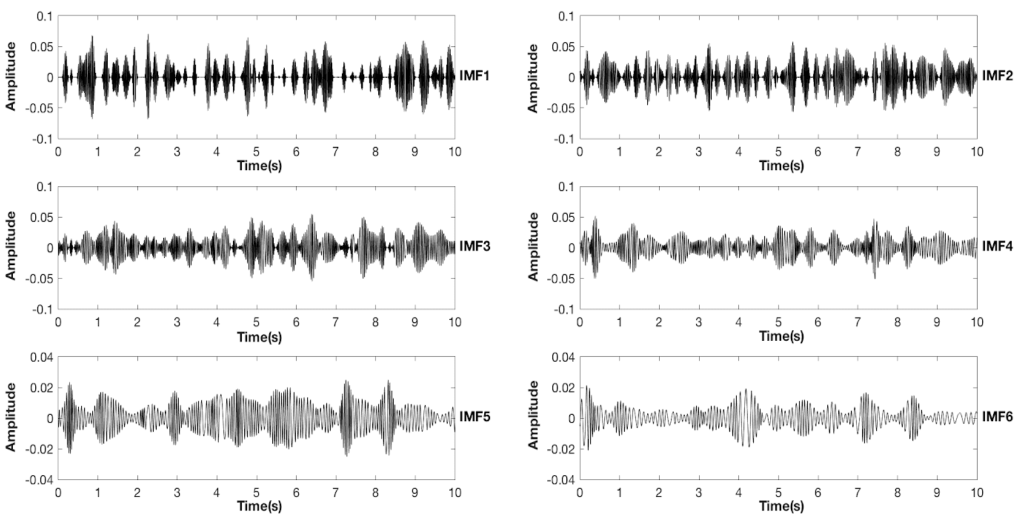

Fig.2. Intrinsic mode functions of the original signal (first 6 IMFs)

analysis. IMFs have to match two criteria, which render the sifting process of EMD data-dependent:

1. The number of extrema and zero-crossings has to differ by 1 at most.
2. The mean value of local maxima and minima envelopes has to be 0.

It should be noted that complying with the aforementioned conditions can take a lot of computational power, therefore alternative criteria were proposed [19]. Figure 2 shows an example of first 6 IMFs extracted through EMD utilization on the fetal heartbeat signal. The resulting signals exhibit much clearer modes of oscillation and enable the extrapolation of the relevant data needed for signal classification. Problems with choosing the relevant IMF from the set and elimination of mode mixing can be mitigated by using the expanded decomposition methodology, known as the ensemble empirical mode decomposition [23]. Also, real-time implementations of the method should be explored further, especially the connection between the computational power of the smartphone, window sizes and their corresponding overlapping factors [21]. A number of other FPCG analysis methods have been proposed in literature that can serve as an alternative to EMD, with different characteristics: Hilbert transform [24], Wavelet transform [25], Matching pursuit [26] and Multibeat autocorrelation [27].

3. METHODOLOGY

As IMFs calculated on fetal phonocardiographic signals contain information about fetal heartbeats [21, 22], statistical features extracted from IMFs could be useful for automatic heartbeat detection. The aim hereof is to analyze IMF-based features in terms of their relevance and usefulness in comparison to audio features that are considered to be conventional features for taxonomic sound classification. The main question of this research was whether IMF-based features could improve performance of automatic heartbeat classification based on audio features.

Audio features are quantitative descriptors of sound characteristics calculated from original or transformed audio signals. They can be useful in measuring perceptual similarities between sounds and in taxonomic sound classification [28, 29, 30], such as zero-crossing rate, spectral centroid, spectral skewness, loudness and so on. Since the process of fetal phonocardiography produces audio signal as a result, audio features are a conventional choice as input variables for a heartbeat classifier. A comparison with IMF-based features can, therefore, indicate applicability of both types of features for the given problem.

In order to show relevance and usefulness of IMF-based features, we prepared a dataset of labeled audio segments and applied several methods for feature ranking and feature selection.

3.1. Dataset preparation

Three recordings taken with iPhone 6S (sampling frequency of 48 kHz) were used as dataset, all recorded on different pregnant women in different weeks of gestation (25th, 30th and 35th week, respectively). The accumulated length of all three recordings were 125 seconds with a total of 270 heartbeats, assessed by two independent experts with experience in FPCG signal analysis and labeling. Once the temporal positions of the beats were labeled, the windows containing heartbeats were extracted from the recordings, each having a length of 300 ms in order to avoid temporal overlap with adjacent heartbeats but still contain substantial length. The remaining data in the original signals (windows between the heartbeats) were also extracted and labeled as signals containing no fetal heart sound information. By labeling distinct heartbeats instead of longer intervals, better temporal resolution can be achieved. The ability to localize heartbeats in time can have many applications, e.g. in calculating fetal heart rate or making a robust, noise free visualization.

Raw recording windows were first filtered through an 8th order Butterworth filter with a cut-off frequency of 250 Hz. A total of 270 audio features containing statistical descriptors (e.g. arithmetic mean, slope, standard deviation) of signal characteristics, such as dynamics, spectrum and fluctuation was extracted by using MIR Toolbox in Matlab [31].

IMF-based features were extracted from the raw recordings windows filtered in the same manner as the recordings prepared for audio feature extraction and resampled to 4.8 kHz, which increased the speed of the empirical mode decomposition without inducing any negative effect on the heartbeat spectrum. IMF-based features were extracted by utilizing basic statistical analysis with 18 descriptors from the first 10 IMFs calculated on signal windows, making a total of 180 features. Statistical features calculated from IMFs were as follows: mean, standard deviation, minimal and maximal values, 5 different percentiles, interquartile range, RMS, crest, coefficient of variation, kurtosis, skewness, number of peaks, one-lag autocorrelation, and zero-cross rate.

3.2. Feature ranking and selection

The purpose of feature ranking methods is sorting of features based on their relevance for predicting the output class. Data set with known class labels is used for calculating feature relevance. Ranking methods are independent of predictors [32] and serve for filtering features in a pre-processing step or as a baseline approach [33, 34, 35]. Within this research we used univariate ranking based on mutual information between each feature and the class label [36]. Since this measure contains quantity of information that a feature shares with the class label, it is commonly employed for univariate feature ranking.

Although feature ranks indicate relative relevance, when combined with other features, they do not necessarily correspond with usefulness. That is to say, relevant features may be redundant and therefore not useful in the optimal subset of features [32, 37]. Therefore, besides the univariate analysis, we also tested importance of IMF-based features using embedded feature selection methods and wrappers. The former ones perform feature selection as an inherent part of the training process with some specific machine learning algorithms, while the latter ones use the underlying algorithm as a black box for validating the relative usefulness of feature subsets [36].

Within this research we opted for a random forest ensemble [38]. After discussing feature ranks, we separately trained the classifier with audio features, IMF-based features, and a combination of all said features in order to show improvements in classification accuracy when IMF-based features are added. As a final step, we employed a wrapper method. More specifically, we used recursive feature elimination with 5-fold cross-validation wrapped around the random forest classifier [39] in order to find a subset of features resulting with the highest validation score.

The aim of this approach is to robustly assess importance of IMF-based features in comparison to conventional audio features and in combination with them using multiple feature ranking and selection methods.

4. RESULTS

4.1. Mutual information

According to feature ranking based on mutual information, six of top ten features and fifteen of top twenty features are calculated from IMFs. The first five most relevant features in decreasing order of relevancy were: (1) mean of the low-energy rate (i.e. the percentage of frames with energy that is less than the average energy of the analysed block), (2) RMS of the 3rd IMF, (3) 10th percentile of the 10th IMF, (4) standard deviation of the 7th IMF, and (5) zero-cross mean. Figure 3 shows mutual information of top 20 features.

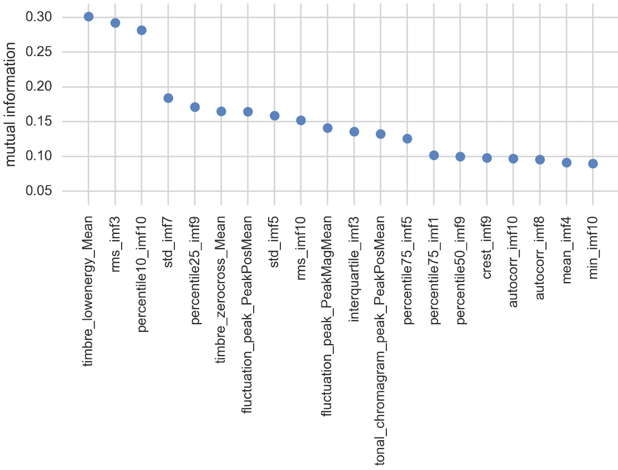

Fig.3. Top 20 features obtained by univariate ranking

4.2. Relevances based on a predictive model

In order to test usefulness of features in the classification task, we used the dataset to train a random forest with 100 trees. According to the random forest, seven of top ten and fourteen of top twenty features are calculated from IMFs. The first five most relevant features in decreasing order of importance are: (1) RMS of the third IMF, (2) 10th percentile of the 10th IMF, (3) standard deviation of the 7th IMF, (4) 25th percentile of the 9th IMF, and (5) mean peak position, which is the only audio feature in top five. Figure 4 shows feature importances obtained using a random forest.

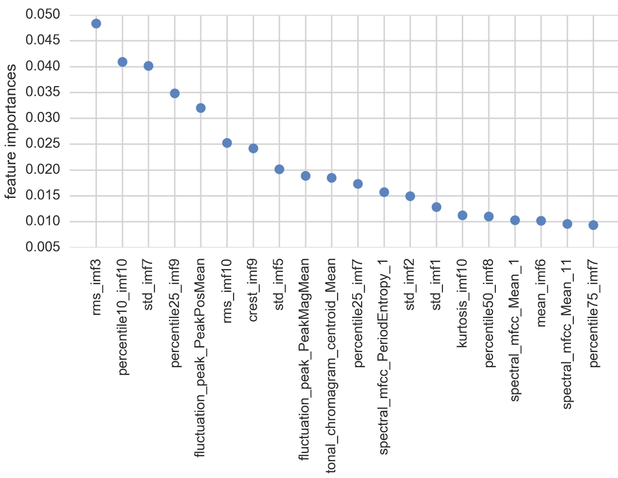

Fig.4. Top 20 features obtained by the inherent learning algorithm of the random forest classifier

In addition to extracting feature importances from the predictive model, we used five-fold cross-validation to assess predictive accuracy of classifiers trained only with audio features, only with IMF-based features, and all feature combined without feature elimination. The prediction accuracies of the random forest were 90.86% for audio features, 93.21% for IMF-based features, and 95.78% for all features. These results suggest that IMF-features improved prediction accuracy of the random forest.

4.3. Recursive feature elimination with cross-validation

The purpose of recursive feature elimination with cross-validation is to find subsets of features leading to the highest predictive accuracy for the employed classifier. The result for the random forest ensemble with 100 trees contained twenty four selected features, among which fourteen were IMF-based features. Assessed by five-fold cross-validation, the accuracy improved from 95.78% for all features to 97.21% for the selected features.

The same procedure of recursive feature elimination was performed separately on audio features and IMF-features in order to compare prediction accuracies. The random forest ensemble trained only on audio features reached the accuracy of 93.93% for top 7 features, while the same classifier trained only on the IMF-based features reached 95.08%. That means that adding IMF-based features to the set of conventional audio features improved the predictive accuracy of the random forest by 3.28%, more accurately from 93.93% to 97.21%.

The predictive accuracy as a function of feature subset cardinality for all three runs of the recursive feature elimination is shown in Figure 5.

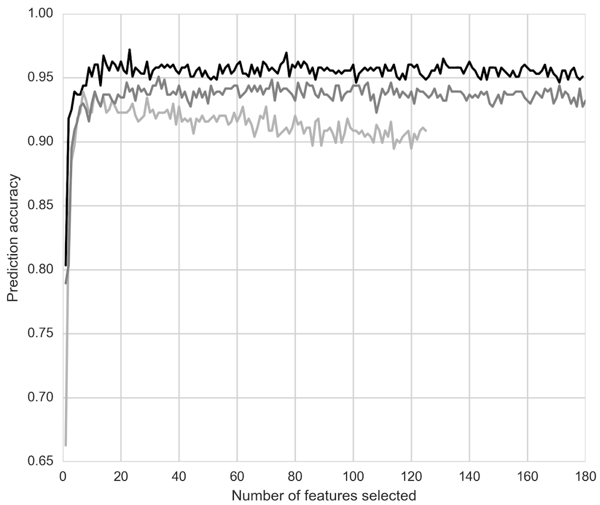

Fig.5. Dependency of prediction accuracy on the number of selected features for random forest. The lightest line represents only audio features, the darker line represents only IMF-based features, while the darkest line refers to all features combined (subsets up to 180 features were shown to improve visibility in the chart)

5. CONCLUSIONS

Fetal phonocardiography is a completely non-invasive method for surveillance of fetal health that can be conveniently implemented as a smartphone application. Since heartbeats are muffled in noise, extraction of useful information from the captured audio signal is not a trivial task. Machine learning algorithms seem to be a valid approach to heartbeat detection in FPCG signals.

In this research we showed that IMF-based features are relevant for such detection, as they can improve the detection using a random forest ensemble when added to the set of conventional audio features.

This study serves as an initial step of designing a fetal heartbeat classifier. After demonstrating the relevance and usefulness of audio and IMF-based features, the next steps will be to select a prediction model, tune its parameters, and validate the results. Those steps will be a part of the future work.

6. REFERENCES

[1.] R.G. Kennedy: **Electronic fetal heart rate monitoring: retrospective reflections on a twentieth-century technology**, J R Soc Med, 91(5), 1998, 244-250

[2.] C. Di Maria, C. Liu, D. Zheng, A. Murray, P. Langley: **Extracting fetal heart beats from maternal abdominal recordings: selection of the optimal principal components**, Physiol Meas, 35(8), 2014, 1649-64

[3.] R.J. Oweis, E.W. Abdulhay, A.M. Alhaddad et al: **Non-invasive fetal heart monitoring techniques**, Biomed Sci Eng, 2(3), 2014, 53-67

[4.] E.S.B.C. Ang, V. Gluncic, A. Duque et al: **Prenatal exposure to ultrasound waves impacts neuronal migration in mice**, Proc Natl Acad Sci USA, 103(34), 2006, 12903-10

[5.] M.E. Schneider-Kolsky, Z. Ayobi, P. Lombardo et al: **Ultrasound exposure of the foetal chick brain: effects on learning and memory**, Int J Dev Neurosci, 27(7), 2009, 677-83

[6.] Z.L. Zhang, Z. Yi: **Extraction of temporally correlated sources with its application to non-invasive fetal electrocardiogram extraction**, Neurocomputing, 69(9), 2009, 894-899

[7.] A. Quinn, A. Weir, U. Shahani et al: **Antenatal fetal magnetocardiography: a new method for fetal surveillance?**, Br J Obstetr Gynecol, 101(10), 1994, 866-70

[8.] S.K. Vashist, E.M. Schneider, J.H.T. Luong: **Commercial smartphone-based devices and smart applications for personalized healthcare monitoring and management**, Diagnostics, 4(3), 2014, 104-28

[9.] H. Ceylan Koydemir, A. Ozcan: **Smartphones Democratize Advanced Biomedical Instruments and Foster Innovation**, Clin Pharmacol Ther, 104(1), 2018, 38-41

[10.] F. Lamonaca, G. Polimeni, K. Barbe, D. Grimaldi: **Health parameters monitoring by smartphone for quality of life improvement**, Measurement, 73, 2015, 82-94

[11.] N. Krupa, M. Ali, E. Zahedi et al: **Antepartum fetal heart rate feature extraction and classification using empirical mode decomposition and support vector machine**, Biomed Eng Online, 10(6), 2011

[12.] F. Kovacs, N. Kersner, K. Kadar, G. Hosszu: **Computer method for perinatal screening of cardiac murmur using fetal phonocardiography**, Comput Biol Med, 39(12), 2009, 1130-36

[13.] P.C. Adithya, R. Sankar, W.A. Moreno, S. Hart: **Trends in fetal monitoring through phonocardiography: Challenges and future directions**, Biomed Signal Proces, 33, 2017, 289-305

[14.] V.S. Chourasia, A.K. Tiwari, R. Gangopadhyay: **A novel approach for phonocardiographic signals processing to make possible fetal heart rate evaluations**, Digit Signal Process, 30, 2014, 165-83

[15.] L.K. Hornberger, D.J. Sahn: **Rhythm abnormalities of the fetus**, Heart, 93(10), 2007, 1294-300

[16.] K.J. Gerhardt, R.M. Abrams, C.C. Oliver: **Sound environment of the fetal sheep**, Am J Obstet Gynecol, 162(1), 1990, 282-7

[17.] D. Querleu, X. Renard, F. Versyp et al: **Fetal hearing**, Eur J Obstet Gyn R B, 28(3), 1988, 191-212

[18.] D.G. Talbert, W.L. Davies, F. Johnson et al: **Wide bandwidth fetal phonography using a sensor matched to the compliance of the mother's abdominal wall**, IEEE Trans Biomed Eng, 33(2), 1986, 175-81

[19.] N.E. Huang, Z. Shen, S.R. Long et al: **The empirical mode decomposition and the Hilbert spectrum for nonlinear and nonstationary time series analysis**, P Roy Soc Lond A Mat, 454(1971), 1998, 903-95

[20.] N.E. Huang, N.O. Attoh-Okine: **The Hilbert-Huang transform in engineering**, CRC Taylor & Francis, 2005

[21.] A. Eftekhar, C. Toumazou, E.M. Drakakis: **Empirical mode decomposition: real-time implementation and applications**, J Signal Process Syst, 73(1), 2013, 43-58

[22.] C.D. Papadaniil, L.J. Hadjileontiadis: **Efficient heart sound segmentation and extraction using ensemble empirical mode decomposition and kurtosis features**, IEEE J Biomed Health Inform, 18(4), 2013, 1138-52

[23.] Z. Wu, N.E. Huang: **Ensemble empirical mode decomposition: a noise-assisted data analysis method**, Adv Adapt Data Anal, 1(1), 2009, 1-41

[24.] S. Sun, Z. Jiang, H. Wang, Y. Fang: **Automatic moment segmentation and peak detection analysis of heart sound pattern via short-time modified Hilbert transform**, Comput Methods Programs Biomed, 114(3), 2014, 219-30

[25.] V.S. Chourasia, A.K. Tiwari: **Design methodology of a new wavelet basis function for fetal phonocardiographic signals**, Scientific World J, 2013, 2013

[26.] M. Akay, E. Mulder: **Examining fetal heart-rate variability using matching pursuits**, IEEE Eng Med Biol, 15(5), 1996, 64-7

[27.] F. Kovacs, C. Horvath, A.T. Balogh, G. Hosszu: **Extended noninvasive fetal monitoring by detailed analysis of data measured with phonocardiography**, IEEE Trans Biomed Eng, 58(1), 2011, 64-70

[28.] P. Herrera-Boyer, G. Peeters, S. Dubnov: **Automatic classification of musical instrument sounds**, Journal of New Music Research, vol. 32, no. 1, 2003, 3-21

[29.] J. J. Burred, A. Lerch: **Hierarchical automatic audio signal classification**, Journal of the Audio Engineering Society, 52(8), 2004, 724-39

[30.] K. D. Martin, Y. E. Kim: **Musical instrument identification: A pattern recognition approach**, J Acoust Soc Am, 104, 1998

[31.] O. Lartillot, P. Toiviainen: **A Matlab toolbox for musical feature extraction from audio**, International Conference on Digital Audio Effects, Bordeaux, 2007

[32.] R. Kohavi, G. John: **Wrappers for feature selection**, Artificial Intelligence, 97(1-2), 1997, 273–324

[33.] R. Caruana, V. de Sa: **Benefitting from the variables that variable selection discards**, JMLR, 3, 2003, 1245–64

[34.] R. Bekkerman, R. El-Yaniv, N. Tishby, Y. Winter: **Distributional word clusters vs. words for text categorization**, Journal of Machine Learning Research, 3, 2003, 1183–208

[35.] J. Weston, A. Elisseff, B. Schoelkopf, M. Tipping: **Use of the zero norm with linear models and kernel methods**, Journal of Machine Learning Research, 3, 2003, 1439–61

[36.] I. Guyon, A. Elisseeff: **An Introduction to Variable and Feature Selection**, Journal of Machine Learning Research, 3, 2003, 1157-82

[37.] A. Blum, P. Langley: **Selection of relevant features and examples in machine learning**, Artificial Intelligence, 97(1-2), 1997, 245–71

[38.] R. Genuer, J-M Poggi, C. Tuleau-Malot: **Variable selection using Random Forests**, Pattern Recognition Letters, 31(14), 2010, 2225-36

[39.] G. Brown, A. Pocock, M.-J. Zhao, M. Luján: **Conditional likelihood maximisation: a unifying framework for information theoretic feature selection**, The Journal of Machine Learning Research 13, 2012, 27–66

8th Congress of the Alps Adria Acoustics Association
Zagreb, Croatia
20 – 21 September 2018

PSYCHOACOUSTIC APPROACH FOR DETECTION OF CAVITATION IN A CENTRIFUGAL PUMP

Jure Murovec*, Jurij Prezelj, Luka Čurović and Tadej Novaković

Faculty of Mechanical Engineering, University of Ljubljana, Aškerčeva 6, 1000 Ljubljana, Slovenia
(jure.murovec@fs.uni-lj.si)

Abstract: *Cavitation in kinetic pumps causes deterioration of the hydraulic performance and damage of the pump by pitting and material erosion. It can appear within the entire range of operating conditions, producing structure vibration and noise. Emmited sound can be utilized as a useful source of information. Detection of cavitation in operation of a kinetic pump based on psychoacoustic metrics is presented in this paper. Proper manipulation and processing of a sound signal leads to extraction of multiple signal descriptors, that can determine the operation point of a centrifugal pump. Presented method can detect the onset of cavitation and is independent of sound pressure level. Its robustness makes it suitable for application in an industrial environment.*

Key words: Cavitation, Centrifugal pumps, Noise, Psychoacoustics, Signal descriptors

1. INTRODUCTION

1.1. Centrifugal pump

Centrifugal pumps are the second most common types of rotating machinery in industry, trailing only electrical motors. Every pump manufacturer supplies characteristic curves which demostrate causality between pump head, power, discharge capacities and operating efficiency. They provide an insigth to pump's performance under given conditions. The ideal operating point for a pump is known as the best efficiency point (BEP), where the pump's capacity and head pressure combine to provide maximum efficiency. Operating outside of the BEP can cause increased wear, reducing operational lifespan while performing with decreased efficiency. There are 13 typical failures of pumps, cavitation being one of the most common, [1].
After the pump is manufactured it is put through performance and net positive suction head (NPSH) tests in order to determine the 3% drop in head, where severe cavitation occurs. The NPSH can be expressed as the difference between the suction head and the liquids vapour head. The purpose is to compare inlet condition of the system with the inlet requirement of the pump. Cavitation causes a drop in pump's efficiency and degradation of the mechanical integrity of the pump. It must be stressed that cavitation starts to occur before the 3% drop in head.

1.2. Cavitation

Cavitation in centrifugal pumps occurs when the absolute static pressure at some point within a pump falls below the saturated vapour pressure of the fluid at the prevailing temperature conditions. Vapor bubbles created by the liquid move through the pump and turn to liquid unexpectedly at a place with higher pressure. Violent collapse or implosion of the bubbles occurs which results in a tremendous increase in pressure, similar to a localized miniature hammer blows, [2]. During the cavitation, pump's surface is being blasted with bursting bubbles, leading to undesirable effects: detorioration of the hydraulic performance of the pump (total delivery head, capacity and efficiency), possible pitting and material erosion in the vicinity of the bubble implosions and vibration of the pump walls, excited by the pressure and flow pulsations, emitting undesirable, hissing noise. In a case of fully developed cavitation within pump there is no flow and the pumping process is stopped.
In attempt to avoid cavitation, pump manufacturers take the high and low capacities of the system into account, resulting in pumps that are designed for operating in the range of 90–110% of their best efficiency point (BEP). Still, the majority of centrifugal pumps are forced to operate outside of this region, [3].
Cavitation can appear within the entire range of operation conditions and because of its harmful effects, its detection and prevention within centrifugal pumps is one of the

most frequently discussed topics and the subject of numerous studies and almost all books, [1,4 - 8].

1.3. Detection of cavitation

Even though it is found to be one of the most frequent faults appearing in centrifugal pumps, cavitation is usually undetectable upon inception. Its existance during normal operation of the pump is generally not identified until its effects have done considerable damage to the pump, [1,9]. To this day, detection of the onset of cavitation remains a great challenge. Different methods have been studied in order to predict and investigate cavitation within pumps during operation:

1. Determination of the net positive suction head (NPSH) by a 3% drop in the total delivery head at the constant flow rate, according to the ISO 3555 standard, [10].
2. Visualisation of the flow through an impeller eye. This method is less appropriate for small pumps and for the flow rates far prom the BEP, as it is most suitable for high-powered pumps, [11 - 13].
3. Paint erosion testing is performed by painting the impeller blades and shrouds and observing of the cavitation erosion by evident removal of the paint, [14, 15].
4. Another method is based on measurement of the static pressure within the flow or on the volute-casing wall [16, 17]. With this method the onset of the cavitation cores is determined indirectly by comparison of the measured static pressure and the vapour pressure at the given temperature of the flow or by the spectral analysis of the vortex patterns and pressure signal using the so called wavelet analysis, [18].
5. Measuring the vibration of the structure, by mounting a transducer in the pump inlet near the impeller blades, or as close as possible to the place of implosion bubbles. The measured signal may be contaminated and corrupted by background noise, such as that of aero-dynamical, mechanical and electromagnetic origins, which attenuate or amplify the measured signal, [19 - 21].
6. A number of studies have been presented about monitoring of cavitation with ultrasound. According to available research, the amplitude of the received ultrasonic signal can also be affected by the turbulent flow, therefore, accurately recognizing the cavitation, especially during its inception stage is difficult, [22 - 24].
7. A method based on measurement of sound pressure in audible range. Some studies have connected descrete frequency tones of cavitation, but as a function of the pump's geometry and material used, [25, 26]. Industrial scale tests were preformed by Neil et al. and Alfayez et al. to determine the ability to detect cavitation ussing acoustic emission, [27,28]. In this case, sensors would have to be attached on the pump from the factory, thus cannot be used on a pump that has an unknown condition. Overall, this method has limited evidence of its effectiveness for a wide range of industrial environments. Lack of robustness and sensitivity to surrounding noise from the environment continues to hinder the use and development of cavitation detection with acoustic emission.

Methods using expert systems based on decision algorhytms tend to be system specific and complex to set up, [29 - 31]. Care must be given to not overtrain or under-fit the data, as taking the newly over-trained decision tree and presenting it with data from an unseen pump may result in poor results. Wang et al. who utilised wavelet analysis, rough sets, and partially linearised neural networks, achieved reasonable accuracy, as the system was able to detect cavitation in 85.1 % certainty, [32]. Classification can be based on statistical features of a vibration signal, as well as a few other measurable quantities, such as flow rate, discharge pressure and temperature.

Although there has been an amazing progress in the study on modelling cavitation in hydraulic machinery, further improvement is still necessary, [33]. In an effort to predict the behaviour of the cavitationg state, models attempt to include all factors involved in the process of cavitation. Inaccuracies arise as a result of nonlinearities of cavitation as well as being insensitive to the operation point, [34 - 36]). Obtaining many parameters is necessary to fine tune the model in order to achieve accurate results. However, this is proven to be a difficult task, which leads us to assumption and thus creating inaccurate models. At this point in time, numerical simulation can only roughly reproduce the phenomenon of cavitation, [37].

After reviewing the accessible literature, we can safely say, that using acoustic emission for detection of cavitation is the most inexpensive method available. It does not require any special equipment and is non evasive for the pump. Operating with a microphone, a sound card and a computer should be relatively straightforward. Accuracy of detection based on total or descrete frequency sound pressure level can be crippled by background noise, making this method almost unusable in tough industrial conditions. However, human hearing is able to identify the process of cavitation quite clearly, which means we can assume that enough information is carried by an acoustic signal. We only need to properly process and extract it and for this reason we have to resort to an area of acoustics known as psychoacoustics.

1.4. Psychoacoustic approach

Psychoacoustics is the science of human perception of sound. It studies the relationship between sensory perception (psychology) and physical variables (physics). Equations were developed to calculate a set of metrics to objectively describe the complex human perception of sound quality, [38]. Loudness N (DIN 45631/A1), tonality T (DIN 45681) and sharpness S (DIN 45692) have already been standardized.

Regarding mechanical engineering, psyhoacoustics are already widely accepted as important approach for the design and manufacturing of products to attract and retain customers [39 - 42]. This is especially true in the automotive industry, as car manufacturers have realized that the produced sound could also serve as a desired acoustic signal, giving the driver feedback about the functioning of the car, [43 - 47]. Gradually, psychoacoustic technique has been spreading to other industrial areas, from car door closing sound quality, design of centrifugal fans for vacuum cleaners, end-of line inspection, gear fault diagnosis, to a concept for general decetion of machine faults, [48 - 52].

Psychoacoustics, a new evolving technique could be one of the solutions to accurately detect cavitation in a centrifugal pump, by extracting psychoacoustic metrics which are based on science of human hearing. Such method would offer using multiple metrics to characterize all stages of cavitation while retaining all the advantages of classical detection using acoustic emission, making it more roboust to surrounding noise, easy to implement and operate in an industrial environment. A method for detection of cavitation in a centrifugal pump using audible sound is presented in this paper. Besides typical psychoacustic metrics, some other simple descriptors of signals were applied. A microphone was used for recording the emitted sound while cavitation was determined by a 3% drop in the total delivery head at multiple flow rates.

2. METHODS AND EXPERIMENTS

2.1. Centrifugal pump setup

The performance and cavitation characteristics, as well as the noise characteristics were measured on a special test stand in a closed loop, according to the valid ISO 3555 standard, [10]. The pump took fluid from a closed vessel in which the pressure level was varied by changing the air pressure above the liquid level using a vacuum pump.

To detect the onset of the cavitation of the pump, the total delivery head is measured at a constant flow rate, with available varying NPSH conditions. At the same time, the sound emission was measured by a microphone placed at a distance of 0.1 m from the pump casing, as seen in Figure 1. Since the NPSH values vary with flow rates, the procedure was repeated for different flow rates. The centrifugal pump used in the experiment had 6 semi-open impeller blades, a 160 mm diameter, head of 32 m while the speed was 2900 min^{-1}. The measuring microphone was a ½ inch Brüel & Kjær 4155 paired with a Brüel & Kjær wide range measuring amplifier type 2636, connected to the computer's soundcard. Labview software served for capturing of the sound, processesing and extracting the data.

Fig. 1. Placement of the measurement microphone near the centrifugal pump used in the experiment.

2.2. Parameters

The parameters for calculation of the 3% drop in head and waveform metrics/descriptors are shown in Table 1.

Table 1. Parameters and corresponding settings used in the experiment.

Parameter	Setting
Flow rate	7 l/s, 7.5 l/s, 7,8 l/s, 8 l/s, 8.4 l/s
Number of operating points for each flow rate	9 to 10
Length of each sound recording	10 s
Alterations done to the recording prior to the metric/desriptor extraction	Normalization and offset correction
Metric extraction time constant	125 ms

For each operation point a 10 s recording was made, bringing the total to 47 recordings. Time constant of 125 ms provided us with 80 metric/descriptor values per operation point. Normalization of the sound signal eliminated the sound pressure level out of the equation, consequently discarding Fluctuation strength, making the detection of cavitation depend solely on shape and characteristics of the waveform.

2.2. Psychoacoustic metrics and signal descriptors

Besides the recorded sound, derivative and log dt/dp of the captured signal were used as an input for the calculation and extraction of psychoacoustic metrics and some other descriptors (Figure 2): Loudnes, Roughness, Sharpness, Tonality, Crest factor, Zero Crossing, RSD of Extrema Amplitude and standard statistic parameters

(STD, Skewness, Kurtosis). Mean value and standard deviation of each metric were calculated.

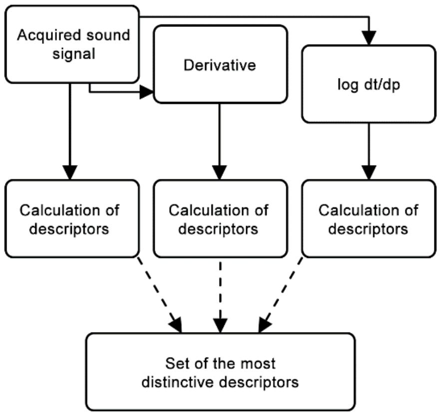

Fig. 2. Inputs for the calculation of psychoacoustic metrics and other descriptors.

For numerical differentiation of the recorded sound signal, the simplest method of Newton's difference quotient was used as seen in Eq. (1), where h represents one sample.

$$f'(x) = \frac{f(x+h) - f(x)}{h} \qquad (1)$$

Eq. (2) describes the second input signal calculated from the recorded sound, labeled with log dt/dp.

$$g(x) = \log \frac{h}{(f(x+h) - f(x) + c)^2} \qquad (2)$$

2.3.1. Loudness

Loudness is a term referring to the human perception of sound level, [38]. The definition of loudness states that 1 sone corresponds to a 1 kHz tone at 40 dB. The loudness scale quantifies loudness to the human ear. Loudness represents the dominant feature for the evaluation of sound quality. To calculate it, specific loudness has to be determined, as given in Eq. (3).

$$N' = 0{,}08 \left(\frac{E_{TQ}}{E_0} \right)^{0{,}23} \left[\left(0{,}5 + 0{,}5 \frac{E}{E_{TQ}} \right)^{0{,}23} - 1 \right] \left[\frac{sone}{Bark} \right] \qquad (3)$$

In this equation, E_{TQ} is the excitation at threshold in quiet and E_0 is the excitation that corresponds to the reference intensity $I_0 = 10^{-12}$ W/m^2. The specific loudness reaches asymptotically the value N´ = 0 for small values of E. Loudness N is then the integral of the specific loudness over the critical-band rate z in [Bark], or in mathematical expression:

$$N = \int_0^{24Bark} N'dz \quad [sone] \qquad (4)$$

2.3.2. Roughness

Roughness correlates to how noticeable or annoying a sound is as heard by the human ear, [38]. More specifically, roughness is a hearing sensation related to loudness modulations at frequencies too high to be discerned separately, such as modulation frequencies greater than 30 Hz. The roughness R in [asper] of any sound can be calculated using the following equations:

$$R = 0{,}3 \frac{f_{mod}}{kHz} \int_0^{24Bark} \frac{\Delta L_E(z)}{dB/Bark} dz \quad [asper] \qquad (5)$$

$$\Delta L_E(z) = 20 \log \left(\frac{N_{max}}{N_{min}} \right) \quad [dB] \qquad (6)$$

In Eq. (6), N_{max} and N_{min} are the maximum and minimum specific loudness in the current critical band.

2.3.3. Sharpness

Sharpness corresponds to the sensation of a sharp, painful, high-frequency sound and it represents the comparison of the amount of high frequency energy to the total energy, [38]. It is calculated as a weighted area of loudness, similar to an area moment calculation, as shown in Eq. (7).

$$S = 0{,}11 \frac{\int_0^{24Bark} N'g(z) z dz}{\int_0^{24Bark} N'dz} \quad [acum] \qquad (7)$$

In Eq. (7), $g(z)$ is the weighting function that has a unitary value of 1 below 3 kHz and non-linearly increases from 3 kHz to 20 kHz, where it has a value of four. For high values of sharpness, significant spectral components at high frequencies are necessary.

2.3.4. Tonality

Tonality represents the auditory perception character related to the pitch strength of sounds. There are many models for calculating tonality; in this paper, the Aures model is used [53].

$$T = c \left(\sum_{i=1}^{n} \left[q_1'(\Delta z_i) q_2'(f_i) q_3'(\Delta Li) \right] \right)^{\frac{0{,}29}{2}} \left(1 - \frac{N_{Gr}}{N} \right)^{0{,}79} [tu] \qquad (8)$$

$$q_1(\Delta z_i) = \frac{0{,}13}{\Delta z + 0{,}13} \tag{9}$$

$$q_2(f_i) = \left(\sqrt{1 + 0{,}2\left(\frac{f}{700} + \frac{700}{f} \right)^2} \right)^{-0{,}29} \tag{10}$$

$$q_1(\Delta L_i) = \left(1 - e^{\frac{-\Delta L}{15}} \right)^{0{,}29} \tag{11}$$

Tonality is used to determine whether a sound consists mainly of tonal components or broadband noise, [38].

2.3.5. Crest factor

Crest factor shows the ratio of peak values to the effective value of a waveform. It indicates how extreme the peaks are.

$$C = \frac{|x_{peak}|}{x_{rms}} \tag{12}$$

2.3.6. Other signal descriptors

Zero crossing represents a point where the sign of a signal changes. This occurs when the waveform is intercepted by the x axis (zero value on the y axis). Additionaly, relative standard deviation of extrema amplitudes was observed, together with typical measures of data characterization: Kurtosis, skewness and standard deviation.

3. RESULTS

3.1. Determination of NPSH critical value

In this section, results of the experiment are presented. Firstly, we determined the NPSH critical values for all five flow rates, as seen in Figure 3. Only the most distinctive signal descriptors were chosen and are displayed in following sections. Plus signs represent points of a 3% drop in total delivery head. Nine operation points were observed for each flow rate, except for flow rates of 7 and 7.5 l/s, where we had ten.

3.2 Primary signal

Results of descriptors extracted from the primary signal are shown in Figures 4 and 5. Almost all metrics provided encouraging results, some of them being exeptional. It has to be pointed out, that the signal was normalized prior to the calculation of all metrics, thus absolute metric values must be ignored.

Most of the presented metrics regarding the recorded signal clarly show a drastic change in their mean value once the cavitation is fully developed. Sharpness stands out as the least significant descriptor, although its value slightly increases before fully developed cavitation occurs. Tonality also seems to indicate the onset of cavitation. Zero crossing has the most constant rise in mean value, while the standard deviation is quite stable thorugh all operation points. As we can see, great differences are present in standard deviation of practicly all metrics at later operation points, which could hint to the unstable and unpredictable/random nature of cavitation in a centrifugal pump.

3.2. Primary signal

Signal derivative, serving as a high pass filter, proved to be a great input for calcuation of descriptors. Two that stood out the most are shown in Figure 5. Sharpness steadily rises by each operation point while number of zero crossings increases early, when the 3% drop in total delivery head is still several operation points away.

3.3. Signal derivative

Signal derivative, serving as a high pass filter, proved to be a great input for calcuation of descriptors. Two that stood out the most are shown in Figure 5. Sharpness steadily rises by each operation point while number of zero crossings increases early, when the 3% drop in total delivery head is still several operation points away.

3.4. Log dt/dp

Loudness of log dt/dp shows a constant drop for all flow rates right before the onset of cavitation, as seen in Figure 7. At the same time, crest factor spikes significantly and then returns down to the values of the initial operation points.

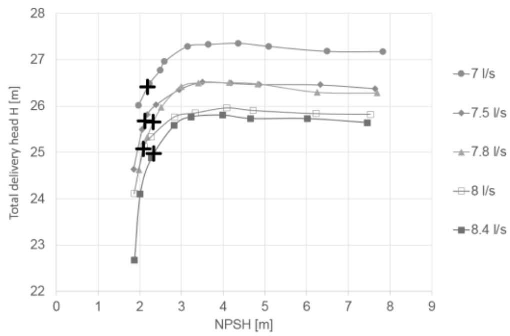

Fig. 3. Determination of NPSH critical value for all flow rates for the pump.

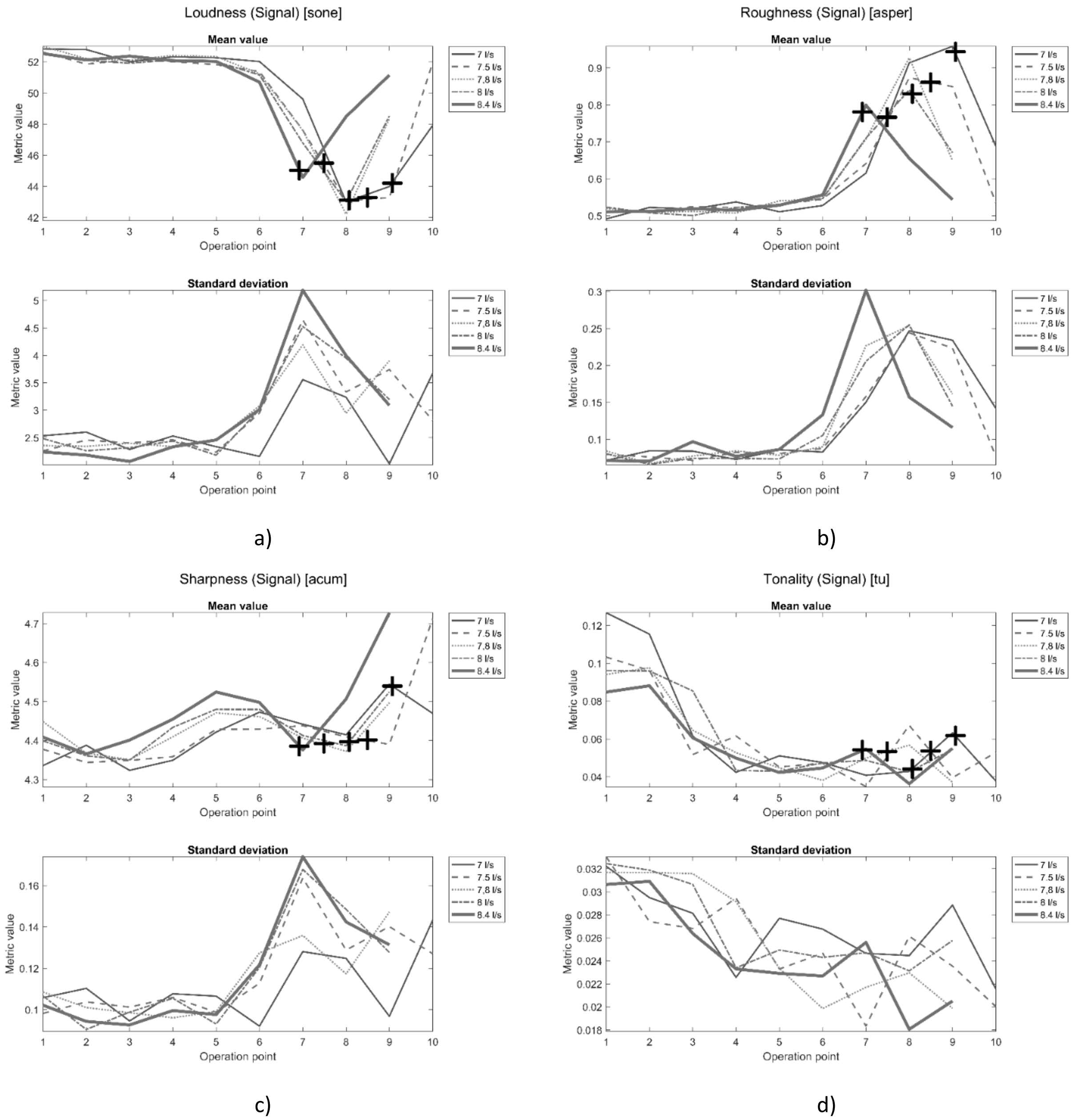

Fig. 4. Four psychoacoustic metrics as a function of operation point calculated directly from the recorded signal are shown: a) Loudnes, b) Roughness, c) Sharpness and d) Tonality. Plus signs represent approximate points of a 3% drop in total delivery head.

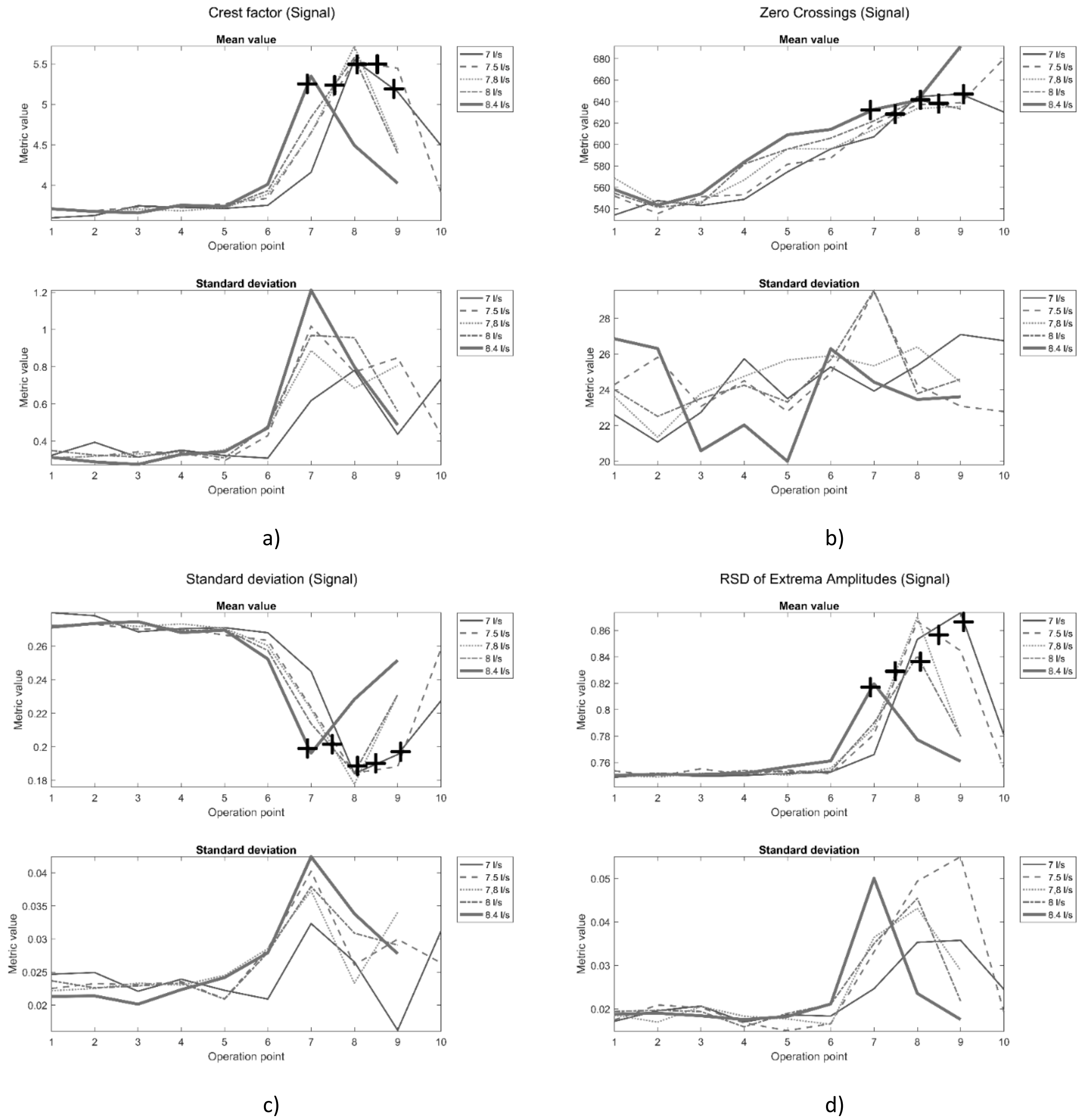

Fig. 5. Four signal descriptors as a function of operation point calculated directly from the recorded signal are shown: a) Crest factor, b) Zero crossing, c) Standard deviation and d) Relative standard deviation of extrema amplitudes. Plus signs represent approximate points of a 3% drop in total delivery head.

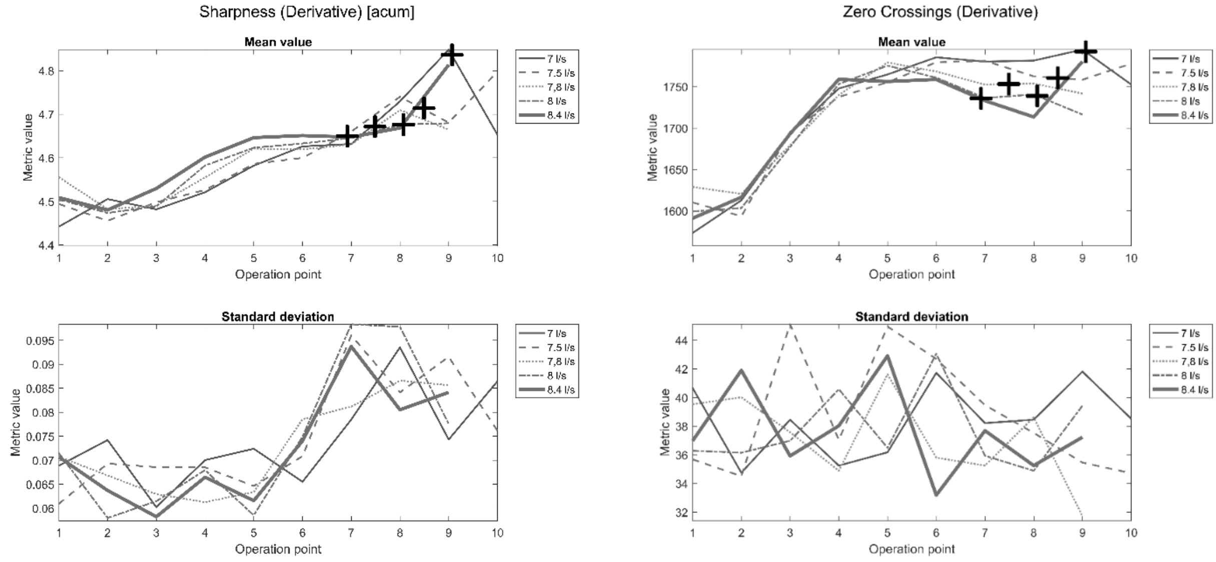

a) b)

Fig. 6. Two descriptors as a function of operation point calculated from the derivative of the recorded signal are shown: a) Sharpness and b) Zero crossing. Plus signs represent approximate points of a 3% drop in total delivery head.

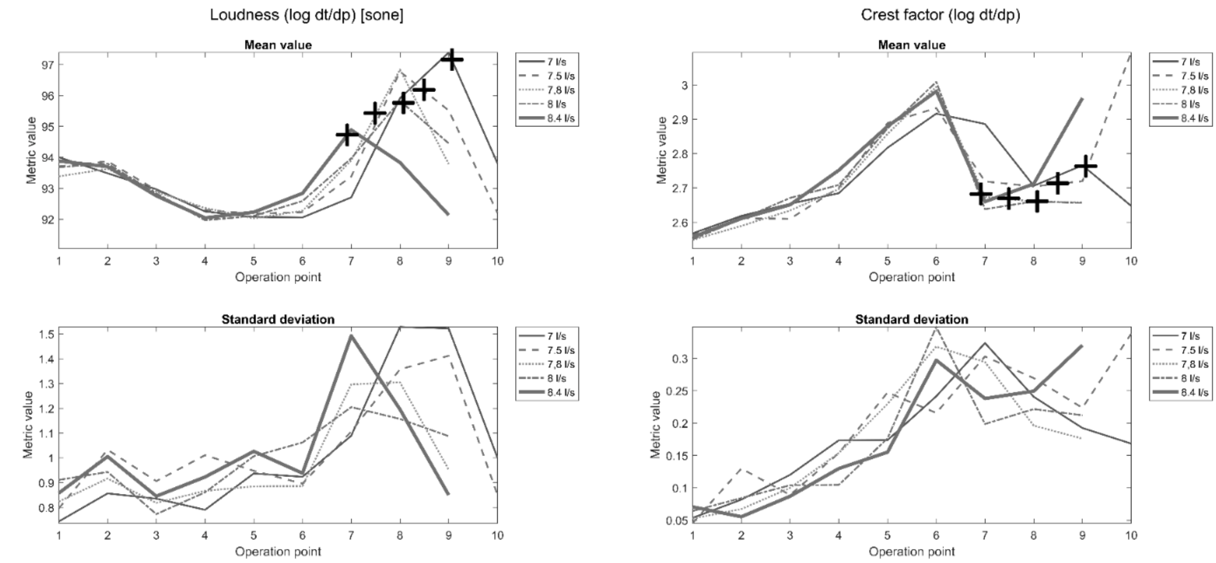

a) b)

Fig. 7. Two descriptors as a function of operation point calculated with Eq. (2) to represent log dt/dp of the recorded signal are shown: a) Loudness and b) Crest factor. Plus signs represent approximate points of a 3% drop in total delivery head.

4. DISCUSSION

All in all, ten different metrics per input signal (primary, derivative and log dt/dp) were used. Time constant of 125 ms provided us with 80 metric/descriptor values for each operation point for five distinctive flow rates.
As seen in Figures 3 to 7, almost all chosen metrics showed exceptional results and many of them clearly distingushing cavitating state from non-cavitationg state. Crest factor (Figure 5 a) being one of them, reaching its mean value of 5 and above when a 3% drop in total delivery head occurs. Inflated values of standard deviation can not be neglected, instead they can serve as another indicator of a chaotic cavitational state. Standard deviation of signal's values (Figure 5 c) shows a significant drop, which can be described with many impulses from the hissing sound, which are not present in early operation points for all flow rates. Loudness (Figure 4 a) presents similar results with even larger disipation of values. Roughness (Figure 5 b) and Relative standard deviation of extrema amplitudes (Figure 5 d) are comparable to Crest factor.
While metrics mentioned above can absolutely be used for recognizing fully developed cavitation, they are not suitable for detecting its onset. For this purpose, Zero Crossing of signal derivative (Figure 6 b) stands out the most, as its value rapidly increases from operation point 2 to 4. It then holds its value throughout full development of cavitation and at the same time the standard deviation remains constant. Loudness of log dt/dp (Figure 7 a) indicates that its value dips right before fully developed cavitation. Tonality (Figure 5 d), Sharpness (Figure 5 c) and Crest factor of log dt/dp (Figure 7 b) also provide some insight about the onset of cavitation and operation point of the centrifugal pump, although the standard deviations of their mean values are not negligible.
Values of Sharpness of signal derivative (Figure 6 a) and Zero Crossings (Figure 5 b) steadily rise throught all operation points of the centrifugal pump. While they could be used to single handedly predict onset of cavitation and its full development, their change in mean value is not big enough compared to their standard deviation. Generally, a high standard deviation is present for all metric values which correspond to operation points that are in vicinity of a full developed cavitation and needs to be addressed. The reason lies in the hissing sound, which provides a lot of spikes in the aquired signal that have a big influence on normalization of the data values. This can be avoided, but in order for the metrics to be completely uncorrelated to the total sound pressure level, the normalization is necessary. On the other hand, standard deviation of mean values could be used as another indicator of unstable conditions within the pump that indicate towards cavitationg state. They can also be minimised with a longer time constant and/or moving average, thus resulting in lower disipiancy of all psychoacoustic metrics and signal desriptors.
A simple source of information as a sound signal proved to carry enough information for detection of onset cavitation in a centrifugal pump. Combining multiple metrics can lead to identification of individual operation point. Within the results provided in this paper, we can see that manipulation of a input signal in a form of a derivative and log dt/dp can reveal new information that might not be noticed right away. A trivial descriptor of zero crossings is a clear example. When applied directly to a recorded signal, it can detect the 3% drop in total delivery head, but comes up short when observing the onset of cavitation. Zero crossings of signal derivative does the opposite. Unable to clearly indicate a fully developed cavitation in the centrifugal pump, it can predict its beginning in the early stages.
A warning system for real-time detection of cavitation in a centrifugal pump can be designed based on presented psychoacoustic metrics and some other descriptors, calculated from a sound signal. An example of a simple decision algorithm of three output values (not cavitating/onset of cavitation/fully developed cavitation) is shown in Table 2. It can be designed and used to indicate the operating point of a centrifugal pump. Shading of individual cells indicates the weighthing factor, darker color corresponding to importance.
This set up serves as demonstration and it would need to be more thoroughly tested and calibrated. However, we can see the simplicity of such warning system which can be done with a single microphone and a computer with a sound card or even a smartphone. A more sophisticated approach can be used, building a decision algorihm on a neural network, enabling an even bigger set of metrics for identification of cavitation in a centrifgual pump.

Table 2. Example of six metric that are suitable to distinguish three different conditions within centrifugal pump.

	Not cavitating	**Onset of cavitation**	**Fully developed cavitation**
Loudness (Signal) [sone]	if value > 50	if value > 50	if 47 > value
Loudness (log dt/dp) [sone]	if 94.5 > value > 93	if 93 > value	if value > 94.5
Crest factor (Signal)	if value > 4	if value > 4	if 5 > value
Crest factor (log dt/dp)	if 2.7 > value	if value > 2.8	if 2.8 > value > 2.6
Zero Crossings (Signal)	if 580 > value	if 620 > value > 580	if value > 620
Zero Crossings (Derivative)	if value > 1700	if value > 1700	if value > 1700

5. CONCLUSION

Results presented in this paper are promising and demonstrate a new way of monitoring of cavitation in a centrifugal pump. Using multiple metrics of a sound signal to characterize all stages of cavitation could prove to be extremely useful. They retain all the advantages of classical detection using acoustic emission by being cheap, easy to implement and operate, while simultaneously making it more roboust to background noise, thus suitable for an industrial environment. Sound signal proved to carry more than enough information if processed and manipulated correctly. With implementation of derivative and log dt/dp, a completely different behaviour of metrics has been achieved: Zero Crossings, Loudness, Sharpness and Crest factor, serving as the most obvious examples. Resourceful processing of sound signals can lead to alternative interpretation of well known psychoacoustic metrics and other signal descriptors that can surpass detection of cavitation by human hearing.

As seen in all figures presented in this paper, standard deviation of results is quite large and should be addressed. Improvement of calculation of metrics in terms of a longer time constant, application of averaging should be the next step, to provide more reliable results. A set up in a noisy, industrial-like environment could determine the actual robustness of such system. Additional tests should be performed on different pumps and experimental cavitation setups. The stage of cavitation could be determined with visualisation with see-through components instead of relying on the total delivery head drop. It is safe to assume, that such system for detection of cavitation on a centrifugal pump can be translated to different areas, for the purpose of process control and fault detection, where a sound signal is present. Modest computational power needed for calculation of psychoacoustic metrics and other presented signal descriptors opens the possibility of developing a smartphone application.

5. REFERENCES

[1.] McKee, K. K., et al. "A review of machinery diagnostics and prognostics implemented on a centrifugal pump, *Engineering Asset Management 2011*. Springer, London, 2014. 593-614.

[2.] Karassik, Igor, and J. Terry McGuire, eds. *Centrifugal pumps*. Springer Science & Business Media, 2012.

[3.] Forsthoffer, William E. *Forsthoffer's best practice handbook for rotating machinery*. Elsevier, 2011.

[4.] Nelik, Lev. *Centrifugal & Rotary Pumps: Fundamentals With Applications*. CRC Press, 1999.

[5.] Shengcai, Li, ed. *Cavitation of hydraulic machinery*. Vol. 1. World Scientific, 2000.

[6.] Grist, Edward. Cavitation and the centrifugal pump: a guide for pump users. CRC press, 1998.

[7.] Al-Hashmi, S., et al. "Cavitation detection of a centrifugal pump using instantanous angular speed." *ASME 7th Biennial Conference on Engineering Systems Design and Analysis*. American Society of Mechanical Engineers, 2004.

[8.] Lobanoff, Val S., and Robert R. Ross. *Centrifugal pumps: design and application*. Elsevier, 2013.

[9.] McKee, Kristoffer K., et al. "A vibration cavitation sensitivity parameter based on spectral and statistical methods." *Expert systems with applications* 42.1 (2015): 67-78.

[10.] ISO 3555. Centrifugal, mixed flow and axial pumps – code for acceptance tests – class B; 1977(E).

[11.] Japikse, David, William D. Marscher, and Raymond B. Furst. "Centrifugal pump design and performance." *Wilder, VT: Concepts ETI, Inc, 1997.* (1997).

[12.] Balasubramanian, Ravi, Eugene Sabini, and Simon Bradshaw. "Influence of impeller leading edge profiles on cavitation and suction performance." *Proceedings of the 27th International Pump Users Symposium*. Turbomachinery Laboratory, Texas A&M University, 2011.

[13.] Hosien, M. A., and S. M. Selim. "RETRACTED ARTICLE: Experimental study of cavitation criterion in centrifugal pumps." *Journal of visualization* 16.2 (2013): 99-110.

[14.] Gülich, Johann Friedrich. Centrifugal pumps. Berlin: Springer, 2008.

[15.] Fukaya, Masashi, Yoshiaki Tamura, and Yoichiro Matsumoto. "Prediction of cavitation intensity and erosion area in centrifugal pump by using cavitating flow simulation with bubble flow model." Journal of Fluid Science and Technology 5.2 (2010): 305-316.

[16.] Newland, D. E. "An introduction to random vibrations, spectral and wavelet analysis. 1993." Essex, England: Longman Scientific & Technical.

[17.] Coutier-Delgosha, O., et al. "Experimental and numerical studies in a centrifugal pump with two-dimensional curved blades in cavitating condition." *Journal of Fluids Engineering* 125.6 (2003): 970-978.

[18.] Tsujimoto, Yoshinobu, et al. "Observations of oscillating cavitation of an inducer." *Journal of fluids Engineering* 119.4 (1997): 775-781.

[19.] Escaler, Xavier, et al. "Detection of cavitation in hydraulic turbines." *Mechanical systems and signal processing* 20.4 (2006): 983-1007.

[20.] Escaler, Xavier, et al. "Vibration cavitation detection using onboard measurements." Fifth International Symposium on Cavitation, Osaka, Japan. 2003.

[21.] Sinha, Jyoti K., and A. Rama Rao. "Vibration based diagnosis of a centrifugal pump." Structural Health Monitoring 5.4 (2006): 325-332.

[22.] McNulty, P. J., and I. S. Pearsall. "Cavitation inception in pumps." *Journal of fluids engineering* 104.1 (1982): 99-104.

[23.] Barkhoudarian, Sarkis. "Ultrasonic cavitation detection system." U.S. Patent No. 5,235,524. 10 Aug. 1993.

[24.] Yan, Zhaoli, et al. "Fluid cavitation detection method with phase demodulation of ultrasonic signal." *Applied Acoustics* 87 (2015): 198-204.

[25.] Černetič, Jan, Jurij Prezelj, and Mirko Čudina. "Use of noise and vibration signal for detection and monitoring of cavitation in kinetic pumps." The Journal of the Acoustical Society of America 123.5 (2008): 3316-3316.

[26.] Čudina, Mirko, and Jurij Prezelj. "Detection of cavitation in operation of kinetic pumps. Use of discrete frequency tone in audible spectra." *Applied Acoustics* 70.4 (2009): 540-546.

[27.] Neill, G. D., et al. "Detection of incipient cavitation in pumps using acoustic emission." Proceedings of the Institution of Mechanical Engineers, Part E: Journal of process mechanical engineering 211.4 (1997): 267-277.

[28.] Alfayez, L., David Mba, and G. Dyson. "The application of acoustic emission for detecting incipient cavitation and the best efficiency point of a 60 kW centrifugal pump: case study." Ndt & E International 38.5 (2005): 354-358.

[29.] Azadeh, Ali, V. Ebrahimipour, and P. Bavar. "A fuzzy inference system for pump failure diagnosis to improve maintenance process: The case of a petrochemical industry." *Expert Systems with Applications* 37.1 (2010): 627-639.

[30.] Sakthivel, N. R., V. Sugumaran, and Binoy B. Nair. "Comparison of decision tree-fuzzy and rough set-fuzzy methods for fault categorization of mono-block centrifugal pump." Mechanical systems and signal processing 24.6 (2010): 1887-1906.

[31.] Yang, Bo-Suk, Dong-Soo Lim, and Andy Chit Chiow Tan. "VIBEX: an expert system for vibration fault diagnosis of rotating machinery using decision tree and decision table." *Expert Systems with Applications* 28.4 (2005): 735-742.

[32.] Wang, Huaqing, and Peng Chen. "Intelligent diagnosis method for a centrifugal pump using features of vibration signals." *Neural Computing and Applications* 18.4 (2009): 397-405.

[33.] Shah, S. R., et al. "CFD for centrifugal pumps: a review of the state-of-the-art." Procedia Engineering 51 (2013): 715-720.

[34.] Hofmann, M., et al. "Experimental and numerical studies on a centrifugal pump with 2D-curved blades in cavitating condition." *http://resolver. caltech. edu/cav2001: sessionB7. 005* (2001).

[35.] Kallesoe, Carsten Skovmose, Vincent Cocquempot, and Roozbeh Izadi-Zamanabadi. "Model based fault detection in a centrifugal pump application." IEEE transactions on control systems technology 14.2 (2006): 204-215.

[36.] Kallesoe, Carsten Skovmose, et al. "Model based fault diagnosis in a centrifugal pump application using structural analysis." Control Applications, 2004. Proceedings of the 2004 IEEE International Conference on. Vol. 2. IEEE, 2004.

[37.] Luo, Xian-wu, J. I. Bin, and Yoshinobu Tsujimoto. "A review of cavitation in hydraulic machinery." Journal of Hydrodynamics, Ser. B 28.3 (2016): 335-358.

[38.] Zwicker, Eberhard, and Hugo Fastl. *Psychoacoustics: Facts and models*. Vol. 22. Springer Science & Business Media, 2013.

[39.] Pietila, Glenn, and Teik C. Lim. "Intelligent systems approaches to product sound quality evaluations–A review." *Applied Acoustics* 73.10 (2012): 987-1002.

[40.] Schneider, Marc, and Carolin Feldmann. "Psychoacoustic evaluation of fan noise." *Proc. of Fan 2015* (2015).

[41.] Di, Guoqing. "An improved psychoacoustic annoyance model based on tonal noises." INTER-NOISE and NOISE-CON Congress and Conference Proceedings. Vol. 253. No. 8. Institute of Noise Control Engineering, 2016.

[42.] Patsouras, Christine, et al. "Psychoacoustic evaluation of tonal components in view of sound quality design for high-speed train interior noise." Acoustical Science and Technology 23.2 (2002): 113-116.

[43.] Bodden, Markus, Ralf Heinrichs, and Angela Linow. "Sound quality evaluation of interior vehicle noise using an efficient psychoacoustic method." Proc. of the 3rd European Conference on Noise Control-Euronoise. Vol. 98. S, 1998.

[44.] Miśkiewicz, Andrzej, and Tomasz Letowski. "Psychoacoustics in the automotive industry." Acta Acustica united with Acustica 85.5 (1999): 646-649.

[45.] Paulraj, Murugesa Pandiyan, Sazali Yaacob, and Allan Melvin Andrew. "Vehicle noise comfort level indication: A psychoacoustic approach." Signal Processing and Its Applications (CSPA), 2010 6th International Colloquium on. IEEE, 2010.

[46.] Brecher, Christan, et al. "Benefit of psychoacoustic analyzing methods for gear noise investigation." Gear Technology 28.5 (2011).

[47.] Duvigneau, Fabian, et al. "Engine Sound Weighting using a Psychoacoustic Criterion based on Auralized Numerical Simulations." 10th European Congress and Exposition on Noise Control Engineering-EuroNoise, Maastricht, ISSN. 2015.

[48.] Parizet Etienne, Erald Guyader, and Valery Nosulenko. "Analysis of car door closing sound quality." Applied Acoustics 69.1 (2008): 12-22.

[49.] Prezelj Jurij and Novaković Tadej. "Centrifugal fan with inclined blades for vacuum cleaner motor." Applied Acoustics 140 (2018): 13-23.

[50.] Cook, Valerie G. Caryer, and Ahad Ali. "End-of-line inspection for annoying noises in automobiles: Trends and perspectives." Applied Acoustics 73.3 (2012): 265-275.

[51.] Kane, P. V., and A. B. Andhare. "Application of psychoacoustics for gear fault diagnosis using artificial neural network." Journal of Low Frequency Noise, Vibration and Active Control 35.3 (2016): 207-220.

[52.] Potocnik, P., Edvard Govekar, and Igor Grabec. "Application of psychoacoustic filtering for machine fault detection." International Journal of Materials and Product Technology 27.3-4 (2006): 229-237.

[53.] Aures W. Sensory Euphony as a Function of Psychoacoustic Sensations, Acustica, 58 (1985), pp. 282–290.

8th Congress of the Alps Adria Acoustics Association
Zagreb, Croatia
20 – 21 September 2018

Monitoring of production cell, based on noise and vibration signals A case study

Tomaž Berlec, Jurij Prezelj, Luka Čurovič, Janez Kušar

University of Ljubljana, Faculty of mechanical engineering (jurij.prezelj@fs.uni-lj.si)

Abstract: *Monitoring of automated production line is usually based on sensors within the production cells, containing a multitude of assembly processes. Sensors for tracking the production process typically provide only digital output, thus they are not able to detect and evaluate environmental conditions during the assembly. In some cases a control of machined parts is included in such cell to provide high reliability of parts geometrical accuracy, before being built into the assembly. This is especially important for high end optical products and electronics with moving parts.*

A system for monitoring of noise and vibration was installed into the production cell containing 7 operations, including an optical measurement of the radar deflector roundness to check its quality before being installed. Production was often interrupted by larger than expected number of unacceptable radar deflectors. Sound and vibration signals were analyzed in order to find the cause for unexpected behavior of measurement procedure. It was found out that noise and vibration signals contain sufficient information for monitoring the measurement process. Signal features were extracted to clearly identify the time lag to be the cause of the false-fault identification.

Additionally, noise and vibration conditions during the assembly process of the product can be integrated into its serial number in order to track its performance during its life time. Such information can lead to optimization of assembly conditions.

Key words: Production line, Production monitoring, noise and vibration, Audible noise as a signal of production process

1. INTRODUCTION

On-line process monitoring, performed by measurements, is crucial for product quality and process stability in manufacturing. Reliability in measurements is a necessary requirement for all quality-oriented organizations looking to efficiently control manufacturing processes. In fact, Six Sigma methodology, which is one of the most important methodologies for controlling and improving process and product quality, considers the assessment of measurement systems as one of its main objectives for success, [1]. Metrology should be understood as an integral part of the production process which must be optimized as a whole.

Monitoring the dimensions and the geometry of all assembly parts and semi-finished products, before they are assembled into the final product, is especially important when the product itself is a measuring device. Measuring system can be integrated into the assembly cell, before final assembly of the product, as depicted in Fig.1. Location of an accelerometer and a microphone used for monitoring of the whole process is depicted in Fig.1.

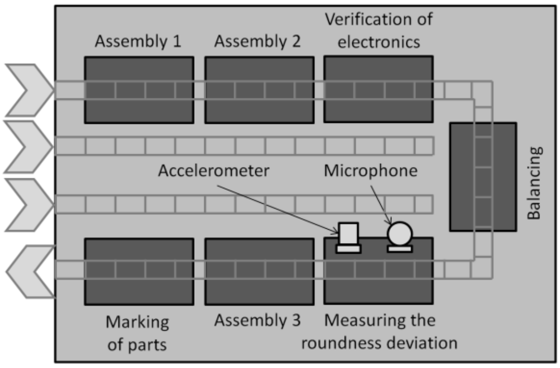

Fig.1. Assembly cell

In our case it was especially important to check the roundness of the radar deflector before being installed. Roundness of a part on a certain section is satisfactory when a point exists in this section from which all the points of the periphery are halfway, this point being the center of the circle. When the section is not totally circular, the part is considered to be out of roundness and this is specified as the difference in distance between the outlying points and the center. In Fig. 2, the degree of deviation of the roundness is the value r_2-r_1, that is, the difference between the maximum and minimum radii. If a part is manufactured by plastic die casting, the resulting profile is imminent of an irregular type, (see Fig. 2); this will affect the durability and operation of the product, [5].

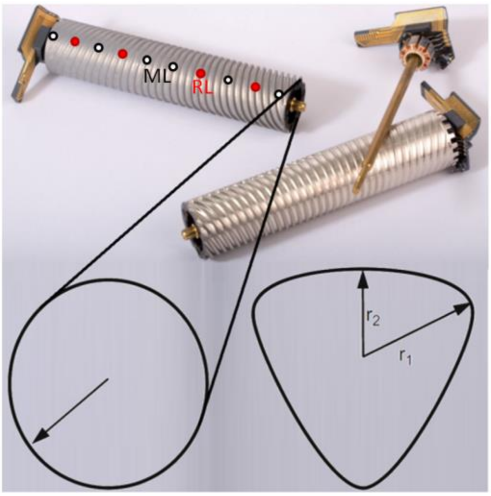

Fig.2. Radar deflector and definition of roundness

Measurement of the roundness is performed via an optical system, detecting the edge of the shadow produced by a laser illuminating the part from one side. The problem occurs if the accepted tolerances, approved by the customer are very tight and are only 10 times the resolution of the optical system. Furthermore, the measured part (radar deflector with electric motor) is lifted from the pallet to an elevated position where it is being measured. The measured part is clamped and lifted to the reference position. At the same time the optical measuring device is lowered to the reference position. At the reference position the radar deflector, whose roundness is being measured, rotates with the aid of its own electric motor. The optical device Keyence independently performs measurements at 10 positions along the rotor marked with ML in Fig.2. Measurement results at 4 reference positions along the rotor, marked with RL in Fig.2, are used for further verification.. The difference between maximum and minimum value should be within the tolerance specified by the customer. If the measurement is not successful, the measurement is performed again. If the measurement fails for the second time, the part is marked as inadequate and is eliminated from the subsequent production steps. However, the decision rules whether the part is acceptable for further manufacturing process, should consider the measuring equipment metrological characteristics — the uncertainty of measurement, [1].

The measurement itself is carried out on the production line, within the assembly cell. The optical measuring system is in close vicinity to different mechanical and pneumatic actuators which are sources of vibration. Through structural and other elements, these vibrations can be transferred to the optical measuring device and to the measured part, thus affecting the measurement itself.

Due to high resolution of optics (0,001 mm), due to a complex procedure of part manipulation and due to a high percentage of part inadequacy (r_2-r_1 > 0,1 mm), it was impossible to determine whether the high level of part inadequacy originates from deviations due to the measuring procedure or it is consequence of the delivered batch full of inadequate parts. Excessive deviation of roundness measurements on the same part, leads to a conclusion that the quality of the rotor cannot be evaluated with such a system. On the 26.07.2018, 919 parts were checked. 18 of them were false unsuitable and 28 were unsuitable. On the 27.07.2018, 1343 pieces were checked. 101 of them was false unsuitable and 77 were unsuitable.

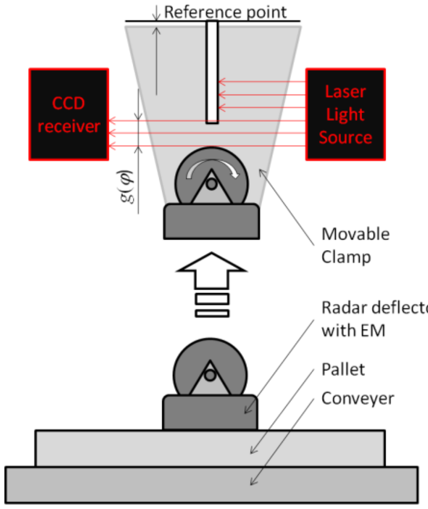

Fig.3. Measuring system for roundness deviation of radar deflector within the assembly cell

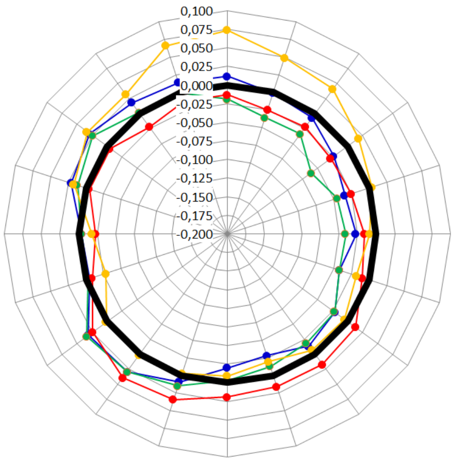

Fig.4. An example of measurement results of roundness deviation (colored curves) at four RL in respect to the perfect roundness, (black curve). Units are in mm

When measurement results influence the decision algorithm for assessment of parts to be or not to be within the specifications, it is necessary to identify the sources of measurement uncertainty, and if appropriate include them into the decision algorithm. This paper presents an example of monitoring the control of the manufacturing process.

1.1 SIGNAL FEATURES SELECTION

In order to monitor the control of manufacturing processes, various sensor signals, such as force, acceleration, temperature, pressure and acoustic emission, can be recorded to gather the information about the process and decision algorithm. Due to the large volume of raw data, in the form of signals sampled with 50 kHz and 24 bit resolution, feature extraction is often carried out to reduce the amount of data. Efficient application dependent features can be extracted when expert knowledge about the controlled processes is available. Whereas, if a lack of expert knowledge is encountered, some general data-driven dimensionality reduction techniques can help, [2]. When a new production process is initialized, a complete understanding of the process is not available. Consequently, signal features without a good physical understanding may be irrelevant or redundant. Under such circumstance, feature selection is commonly applied to pick a minimally sized subset of features for monitoring. By removing a large number of irrelevant and redundant features, feature selection is able to help avoid over fitting, improve model performance, provide more efficient and cost-effective process monitoring, and acquire better insights into the underlying processes that generated the data, [2]. Optical measurement system is subjected to vibrations, and due to the relative long path of light beam from the laser to CCD sensor, including reflection on the mirror, vibrations were the main suspect for the overlooked source of uncertainty. Time signal of vibration amplitude (vibration level chart) provides information about the ongoing process and can be used as a feature for assessing assembly process, [3]. Sound was recorded with the purpose to identify unexpected noise events, which might be correlated to unacceptable measurements. Audible sound proved to be a source of abounded information for monitoring many different processes like pump cavitation [6], GMAW welding [7], Milling [4], grinding [5], and some attempts have been already made to use sound for monitoring the entire production line as a whole, [4].
Sound and vibration signals provide a large number of different features for further analysis. For the purpose of monitoring the events in the assembly cell sound and vibration signals features were selected and recorded with 125 millisecond resolution, among them:

1. Sound pressure level
2. Zero crossing of sound signal
3. Crest factor of sound signal
4. Roughness of sound signal
5. Sharpness of sound signal
6. Tonality of sound signal
7. 1/3 octave spectrum of sound signal
8. Vibration level
9. Zero crossing of vibration signal
10. Crest factor of vibration signal
11. Human weighted vibration level
12. Tonality of vibration signal
13. 1/3 octave spectrum of vibration signal

Besides obvious reason for observing vibration features, each sound feature was selected with a purpose. Tonality for example was selected to check if during the measurements some squeaking occurs from the motor or from the assembly line.

2. EXPERIMENTAL SETUP

Sensor for vibration was mounted on the optical measuring device. The sensor was attached to its surface using wax provided by the producer of accelerometer. Microphone was positioned to a close vicinity of measured part in order to pick up at least some information from the noise generated by its electric motor. Microphone picked up signals from all devices and machines within the assembly cell. Analog signals from sensors were connected to A/D converter with 50 kHz sampling frequency and 24 bit resolution. Program code for feature extraction in real time was written in LabView environment. Only values of signal features were recorded in real time, in order to maintain manageable amount of information for 64 hours, which is for eight 8h long work shifts. Selected features were calculated from 125 milliseconds long signal intervals with no overlapping. In this way we were able to obtain data for two different time scales; long time scale for observation of the assembly process during eight shifts, depicted in Fig.5. and short time scale for observation of a single event during measurement of roundness, depicted in Fig.6.
To observe vibration levels during optical measurements of roundness, the measurement range for vibrations was set for low levels, making vibration measuring system very sensitive. However, gripping the measured part and transporting it into measurement location generated high levels of vibrations, overloading the AD converter during few measurements.

3. RESULTS

Long-term measurements of vibration acceleration were carried between Tuesday 26.7.2017 and Thursday 28.7.2017. During the measurements, the entire production line was in operation. The assembly started with production in the third shift, and was operating six shifts. During the first two shifts the assembly cell was not operational, enabling a good background data for determination of baseline for all the sound and vibration features.

Results of long term measurements of the eight features of sound and vibration are presented in Fig.5. All signals features clearly indicate the difference between the operation and non-operation of the assembly cell. Signal to noise ratio provided by selected features differs. In general we can see that sound signal features do not provide as high signal to noise ratio as vibration signal features. However, sound signal detected unclassified events, starting during the seventh shift and lasting to the end of the eight shifts. Features of the sound signal changed on the large time scale during the seventh working shift. Values of zero crossing decreased, values of roughness increased. Background of the noise level at 4 kHz band increased, yet amplitude remained the same. Vibration signal shows no indication for unclassified events and remains unchanged during all shifts, although the vibration features exhibit the highest signal to noise ratio. Human response to vibrations as a signal feature has the highest signal to noise ratio.

Results for shorter time scale of observation are presented in Fig. 6 for the same features of sound and vibration signal as in Fig.5. Signals of sound features do not provide clear information about the ongoing individual event, because information is hidden in the background noise from a many other noise generating process within the assembly cell. Zero crossing and sharpness are the only two sound features indicating towards impulses marking individual measuring event. Vibration signal and its features however provide excellent insight into the measuring event. We can see that in a short time scale signal to noise ratio of all vibration features is sufficient for information extraction.

Vibration level chart, with time constant T = 125 msec is presented in Fig.7. We see that the timing of the vibrations is uniform and repeats itself. Four typical forms of pulses can be identified in Fig.6. They can be associated with following operation: A) the descent of the optical device, B) the start of the rotation of the rotor, C) the end of the rotation, D) the lifting of the optical device. Vibrations level vary between 45 dB at a time when the measurement is not performed (background level) and 100 dB, which is associated with the rise of the Keyence device. The accelerometer was not calibrated, therefore only the relative values of the vibration acceleration are displayed.

Signal of the Human Weighted Level of vibrations (HWL) in shorter time scale of 3 minutes is presented in Fig. 8. In the y axis, the values of the HWL indicator are displayed, and on the x axis the time in seconds. The image shows a length of cca. 80 seconds. We see that the pulses are more pronounced and shape of the sequence is repeating. Vibration feature HWL was therefore used in the analysis for analysis of measurement duration. This time, the most pronounced impulse is to indicate the descent and rise of the Keyence measuring device during the measurement of the roundness.

3.1 DURATION OF VIBRATIONS

One of the objectives of presented study was to answer the question if it is possible to explain the deviation of roundness measurement results, performed on the optical measuring device, with the help of long-term sound and vibration measurements. Therefore a data base of measured sound and vibration features was compared to results of quality assessment based on automatic decision algorithm, which takes into account only the value of r_2-r_1. If the feature of roundness r_2-r_1 extracted from optical measurements of a part meets QA criteria, then this part is evaluated as OK, otherwise the part is marked as NOK.

During the measurements, it was found that the level of vibration is related to the rotational speed of the radar deflector during the measurement. The relationship between the duration of the measurement and the rotor with the NOK tag was investigated. Duration of the roundness measurement was determined indirectly from the feature signal of the Human Weighted Level, as shown in the Fig.7. Human Weighted Level (HWL) signal is presented in Fig.7 by the red curve, together with vibration level presented by the black curve. Values of the HWL indicator are displayed on the right y axis, values of vibration level are displayed on the left y axis, and on the x axis the time is given in seconds. The signal shows a length of approximately 70 seconds.

The duration Tm of optical measurement is depicted in Fig. 7. The duration of optical measurement differs for each part. It was also noted that measurement duration on the optical device is not always the same as shown in the Fig.8., where two processes are basically carried out. In most cases, the duration of the measurement is approximately 4.2 s for a larger group of measurements. A group of measurements with shorter durations, of only about 2.2 s or about half of the base time was also identified.

Fig.5. Signals of eight different features, based on recorded sound and vibration signals, for a period of 64 hours, with a purpose to monitor the production conditions in an assembly cell

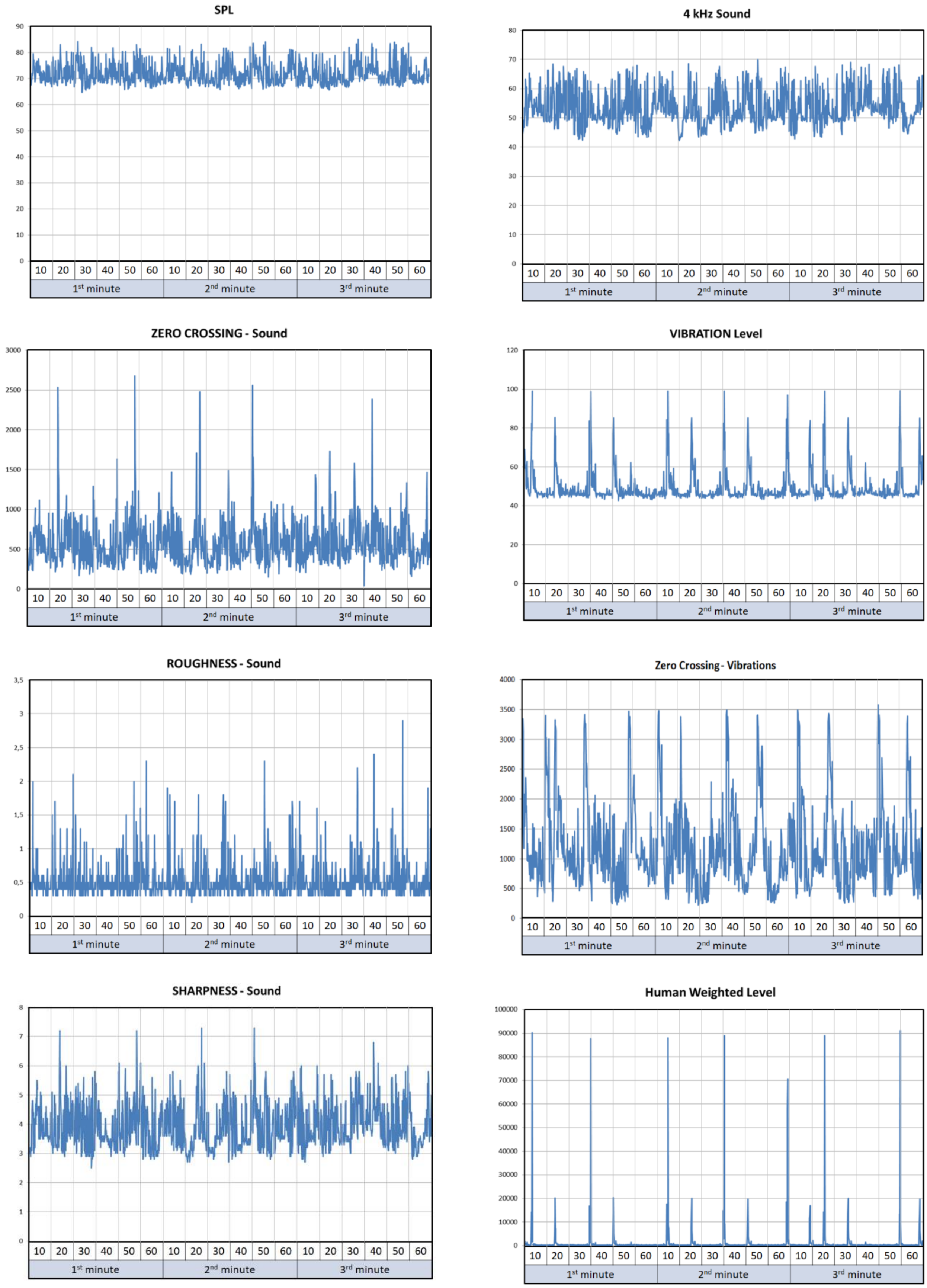

Fig.6. Signals of eight different features, based on recorded sound and vibration signals, for a period of 3 minutes, with a purpose to monitor the conditions on the optical measuring device in the assembly cell during one single cycle

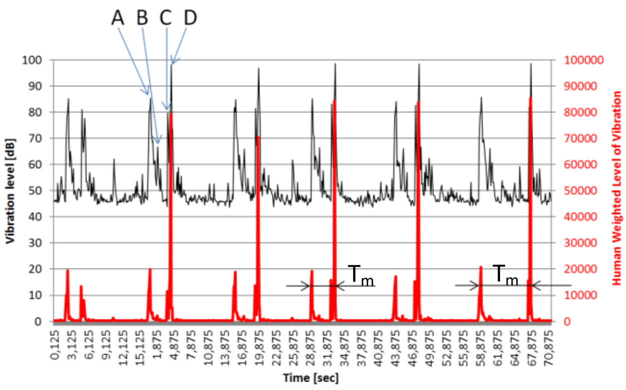

Fig. 7. Vibration level and HWL with defined duration of roundness measurement using optical device Keyence

Duration of the optical measurement determined from Human Weighted Level (HWL) signal during assembly is depicted in Figs. 8. and 9. The y axis shows the duration time Tm in seconds, and on the x axis, the absolute time in seconds. Results of measurement duration can be classified into three groups; typical duration of 4 seconds, shorter duration of 2.4 seconds and randomly prolonged measurement duration up to 18 seconds.

Duration time of optical measurements, based on extraction from HWL, from 26.7.2017, which were run between 0:0 and 14:09 hours are depicted in Fig.8. From Fig.8 it can be observed that optical measurements performed in shorter interval with shorter duration in (Tm of about 2.2 s) occur only in the second half of the day. Optical measurements which indicated an inadequate result, classifying the part as inappropriate for further assembly are marked with red dots in Figs. 8 and 9. Interestingly enough, all parts classified as inappropriate were measured during shorter optical measurement interval.

Duration time of optical measurements, based on extraction from HWL, from 27.7.2017, which were run between 5:53 and 14:09 hours are depicted in Fig.9. Similar distribution of optical measurement time can be observed confirming results from the previous day.

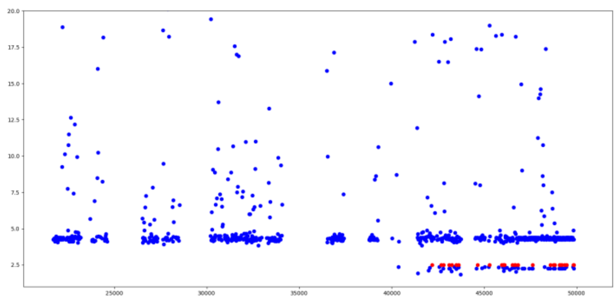

Fig.8. Optical measurement duration of roundness during the assembly process at 26.7.2017

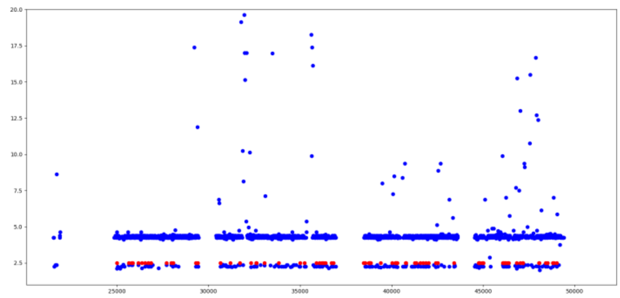

Fig. 9. Optical measurement duration of roundness during the assembly process at 26.7.2017

3.2 AVERAGED VALUE OF VIBRATION AMPLITUDE

Average vibration levels during measurement of roundness feature, with the optical device, on 26.7.2017 are depicted in Fig.10. Due to the shorter measurement time and approximately the same vibration amplitude, the time integrated levels increased by about 3 dB, as depicted in Fig.10. The level of vibration acceleration increases from 73-74 dB to 76-77 dB. Average vibration levels at the time of the measurement with the Keyence device on 27.7.2017. Due to the shorter measurement time, the vibration level is also increased by about 3 dB, similar to that found in the previous diagram.

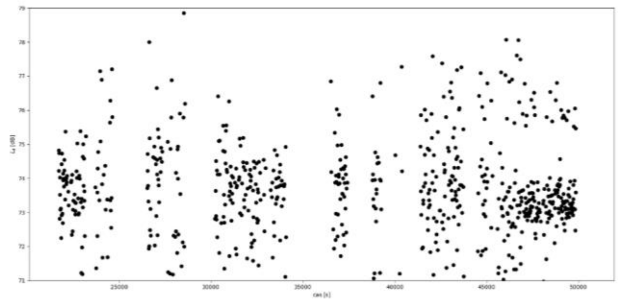

Fig. 10. Vibration level distribution during 26.7.2017

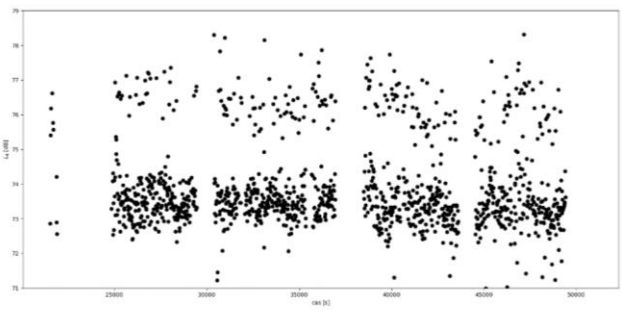

Fig.11. Vibration level distribution during 27.7.2017

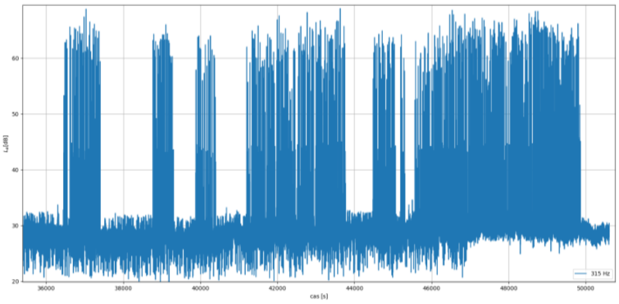

Fig.12. Vibration level at 1/3 315 Hz octave band.

4. CONCLUSIONS

If measurement of dimensions and geometry are included into the automated production, with the purpose to classify semi products as OK and NOK, then all sources of uncertainty should be identified. Recording of sound and vibration signals, and evaluating numerous sound and vibration signal features, resulted in an unexpected identification of source of roundness measurement uncertainty.

The vibration levels caused by the operation of the machines in the vicinity of the optical measuring apparatus were detected and measured. Vibrations originate from production line and are associated with the operation of the optical device. The measurement of roundness is related to the duration of the measurement and consequently to the level of vibration. In this case shorter vibration times also mean a higher effective RMS value during the measurement. Additional gripping and positioning of the measured part to the measurement location adds to the measurement uncertainty.

The analysis shows that the inadequate measurement is entirely related to the shortening of the timing of the measurements. Conversely, it does not always apply. The deviation of the average values of vibrations is considerable. The analysis of the measurement times shows great deviations and, consequently, a large spread. Basically, two processes or two measuring times are detected, which is reflected in the bimodal distribution of both measurement times and the vibration sizes.

Sound signal caries more information about the surrounding and therefore background events can be correlated to possible disturbance in assembly line. Vibration signal carries less information, but consequently provides better signal to noise ratio for a given apparatus under observation.

7. REFERENCES

[1] M.Villeta, et.al., Integrating the continuous improvement of measurement systems into the statistical quality control of manufacturing processes: A novel link, CIRP Annals - Manufacturing Technology, Vol. 61, 2012, pp. 507–510

[2] C.Shao, et.al., Feature Selection for Manufacturing Process Monitoring Using Cross-Validation, Proceedings of NAMRI/SME, Vol. 41, 2013

[3] A.Martini, M.Troncossi, Upgrade of an automated line for plastic cap manufacture based on experimental vibration analysis, Case Studies in Mechanical Systems and Signal Processing, Vol.3, 2016, pp. 28–33

[4] S.Astapov, et.al., Industrial process monitoring by multi-channel acoustic signal analysis, 14th Biennial Baltic Electronic IEEE (BEC) conference 2014,

[5] M.C.Carnero, et.al., Statistical quality control through overall vibration analysis, Mechanical Systems and Signal Processing, Vol. 24, 2010, pp.1138–1160

[6] M.Čudina, J.Prezelj, Detection of cavitation in operation of kinetic pumps: use of discrete frequency tone in audible spectra, Applied acoustics, Vol. 70, issue 4, 2009, pp. 540-546

[7] M.Čudina, et.al., Use of audible sound for on-line monitoring of gas metal arc welding process, Metalurgija, Vol. 47, issue 2, 2008, pp. 81-85.

8th Congress of the Alps Adria Acoustics Association
Zagreb, Croatia
20 – 21 September 2018

Hrvatsko akustičko društvo
HAD
Acoustical Society of Croatia

DESIGN, MODELING AND IMPLEMENTATION OF THE GUITAR AUDIO INTERFACE

Tin Obradović, Siniša Fajt, Vladimir Olujić

University of Zagreb, Faculty of Electrical Engineering and Computing,
Unska 3, 10000 Zagreb, Croatia
tin.obradovic@gmail.com

Abstract: *In this paper, design, modeling and implementation of the fully functional guitar audio interface are described. Initially, the features of the guitar pickup are analyzed. Design and modeling of the audio interface circuitry are then performed based on the results of the analysis. The model is further optimized and implemented. Control measurements are performed on the implemented circuit. Finally, the overall functionality of the audio interface is tested using a simple audio processing application.*

Key words: guitar audio interface, guitar pickup measurements, electronic circuit design, real time audio processing

1. INTRODUCTION

An electric guitar is a well-known and widespread musical instrument. Its shape, dimensions together with its simplicity make it practical for use and transportation. For these reasons, as well as many others, the electric guitar, after all this time, still competes with modern electronic musical instruments and regularly, even some of the old models come into fashion again. One thing is certain, if it wasn't for electric guitar, the majority of music genres and songs that we recognize today wouldn't have existed.

However, original (unprocessed) sound of an electric guitar could be characterized as dry, silent and without much character. For this reason, to the sound of electric guitar, different forms of processing, modification and amplification are regularly applied, in order to obtain the sound of the desired characteristics. Initially, the circuits that performed these functions were solely analog.

As the music, as well as its genres, developed following the advances of the technology, a need for more sophisticated and complicated processing methods has arisen, requirements of which were increasingly difficult to meet using the existing analog electronic systems.

Finally, the introduction and development of digital systems and technology enabled the final breakthrough into a new and yet unexplored domain that offered countless new features and possibilities.

However, the signal that comes from an electric guitar, as well as the audio signals that human ear can correctly interpret are analog signals, as well as the world around us. The overall incompatibility of those two systems in some fundamental characteristics comes into play. In order to enable the implementation of the digital audio processing applications in the surrounding analog world, an interface must be introduced which will provide the proper conversion between the two domains.

That is the main cause of existence and the fundamental task of the audio interface – to interconnect the two domains and therefore enable digital audio processing within the real world and in real time.

For that reason, the main goal of this paper is the implementation of the flexible, practical, reliable and standardized audio interface. Audio interface which is high performance, small in size and specialized to enable an expansion to the compatible digital system with the purpose of providing high quality processing of the guitar audio signal – guitar audio interface.

2. CHARACTERISTICS OF THE GUITAR AUDIO INTERFACE

The fundamental task of the audio interface is to enable the high-quality analog-to-digital (A/D) and digital-to-analog (D/A) conversion, while following, respecting and optimizing certain requirements and specifications given below.

The audio interface provides the adjustment and regulation of the input analog signal, digitizing it and preparing it for the digital processing. It also converts the received digitally processed signal back to analog, further adjusting its parameters before sending it to the output.

The guitar audio interface is further specialized for receiving the guitar audio signal at its input, and feeding its output audio signals into a typical guitar amplifier.
However, other audio signal sources can also be connected to it, as long as they are within the specifications of commercial and professional audio equipment (voltage: -10 dBu or +4 dBu, impedance up to 100 kΩ) [1]

2.1. The structure of the guitar audio interface

The circuitry of the audio interface can be broken down into two main sections: analog and digital. The purpose of the analog circuitry is to establish the regulation of the voltage levels, spectral content and impedance matching between the inputs and the outputs of the audio interface and on-board A/D and D/A converters. The purpose of the digital circuitry is to enable the communication between the audio interface and the compatible digital system (digital signal processor, DSP).
The conceptual block diagram of the guitar audio interface is shown in Fig.1. The audio interface has two input and two output channels, so it enables stereo audio capabilities. The signal from an electric guitar is fed to either of the two inputs; it passes through the protection circuitry and preamplifiers with filters. After that, the signal is digitized in A/D converters and digital audio samples are sent to the compatible processor using the I2S (Inter-IC Sound) protocol.
At the same time, audio samples that are already processed are fed to D/A converters, then further into output amplifiers with filtering, through output protection circuitry and to the outputs of the guitar audio interface. The outputs are usually connected to a guitar amplifier.

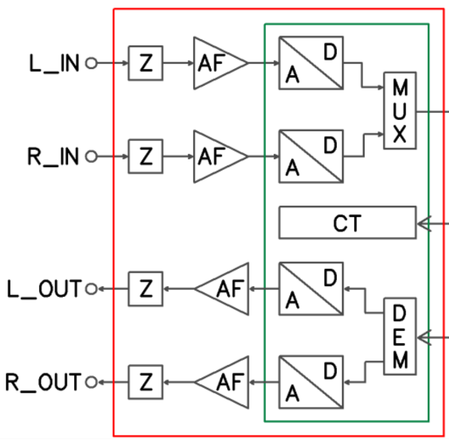

Fig.1. Block diagram of the audio interface

The core component of the audio interface is the codec integrated circuit (elements combined under the green rectangle on Fig.1). The codec combines A/D and D/A converters along with the control circuitry on a single chip.
One of the main reasons for the implementation of the circuitry surrounding the codec is the fact that the codec itself can't be (neither is it intended to be) connected directly to the inputs and outputs of the audio interface. Codec's connection is established via the special adjustment circuit assembly consisted of the protective circuitry, amplifiers and filters.
According to the requirements, a codec with satisfactory performance is chosen. However, whether the performance of the codec, as listed by its manufacturer, will be achievable, depends solely on how the circuitry surrounding the codec is designed and implemented.
Therefore, it is of utmost importance to design and implement the surrounding circuitry that will not (at least not significantly) degrade the performance of the codec.

2.2. Requirements for the guitar audio interface

In order to begin with the modeling of the audio interface, and furthermore, to be able to determine the successfulness of its implementation once it is implemented, the main requirements for the audio interface must be set.
The underlying concept, from which all the requirements listed below are derived, is: whenever and to whatever extent possible, the audio interface must never be the weakest link in the signal transfer and processing chain, considering the parameters of interest.
The guitar audio interface needs to:

- enable the utilization of the standard audio sampling frequencies and quantization resolutions: for CD quality (44.1 kHz and 16 bit quantization) and for studio quality (48 or 96 kHz with 16 or 24 bit quantization)
- adequately filter the signal in order to prevent aliasing or out-of-band noise issues. The filters used should also negligibly affect the spectral characteristics of the in band signal (20 Hz to 20 kHz), in the same time attenuating the out of band spectral components as much as possible.
- adapt the input and output impedances, voltage levels as well as the reference voltage potentials in order to provide compatibility according to the specifications of the typical audio equipment that will be used along with the audio interface.
- provide the dynamic range equal or greater than that of the 16 bit audio track (96 dB)
- implement the overvoltage and/or short circuit protection of its inputs and outputs as well as the prevention of the other critical failure states, which could cause the damage to the sensitive circuitry of the audio interface

- implement the noise and interference protection sourcing either from the audio interface itself or from its environment
- exhibit negligible harmonic distortion (< 0.1%) over the specified operating voltage range
- ensure the digital audio data exchange, according to standardized protocols
- ensure the basic manageability for the main aspects of its functionality via a digital interface
- exhibit minimal input-to-output latency, so it can be used in the real-time audio processing applications
- be reliable during operation and exhibit low power consumption

On top of all of the given requirements, it will be demanded that the guitar audio interface meets all of them, using the lowest possible component count, total cost and physical dimensions of the final circuit.

3. DESIGN AND MODELING OF THE GUITAR AUDIO INTERFACE

The goal of modeling is to develop the model of the audio interface circuitry which optimally fulfils the specified requirements, in the same time being close enough to reality, that its implementation doesn't pose too big of a step.
The modeling of the guitar audio interface circuitry begins with the selection of the most important, main component: audio codec. All the surrounding circuitry will be modeled according to the parameters of the audio codec.
The codec chosen for this particular audio interface is the *PCM3060* from Texas Instruments, mainly because of its appropriate specifications, availability and relatively reasonable price compared to the available performance. The codec uses sigma-delta modulation with adequate filtering to achieve high quality conversion between the analog and digital domain. It features two input and two output channels, with many features that are controllable via the digital interface. [2]

Codec *PCM3060*		
Parameter	**Value**	**Unit**
Analog power supply voltage	+5	V
Digital power supply voltage	+3.3	V
Full scale input voltage (ADC)	3	V_{pp}
Input impedance	10	kΩ
Output voltage (DAC)	4	V_{pp}
Load impedance	10	kΩ

Table 1. Important parameters of the audio codec

The most important part of the circuitry surrounding the codec are the active filters. Those active filters are implemented using the operational amplifiers. The operational amplifiers chosen for this particular design are *LME49720*.
The parameters of the codec *PCM3060* that are of most importance for the design and modeling of the audio interface circuitry are listed in Table 1. [2]
The parameters of the operational amplifiers *LME49720* that are of most importance for the design and modeling of the audio interface circuitry are listed in Table 2. [3]

Operational amplifier *LME49720*		
Parameter	**Value**	**Unit**
Power supply voltage	5 - 36	V
Output voltage swing (at 5 V supply)	3	V
Differential input impedance	30	kΩ
Open loop voltage gain	140	dB
Gain bandwidth product	55	MHz
Output impedance	13	Ω

Table 2. Important parameters of the op. amplifier

3.1. Measurements of the guitar pickup

On its input, the guitar audio interface receives the signal from the electric guitar pickup. Guitar pickup is a transducer that converts the mechanical oscillations of the guitar strings into an analog electrical signal. In order to properly model the input circuitry of the audio interface, it is necessary to identify the main characteristics of that signal, and therefore to explore and determine the main parameters of the guitar pickup as its source.
Although there are multiple types of the guitar pickup concerning the sole mechanism and physical nature of the conversion, the most common type of the guitar pickup is a magnetic/inductive pickup, which uses magnetic induction to perform the conversion. Inductive pickups can be made as a single coil type or double coil (Humbucker) type. [4]
The inductive pickup consists of the multilayer, high inductance coil wound around a stack of magnets. The magnets form the magnetic field around the coil and guitar strings. The guitar strings are made out of ferromagnetic material (usually steel) so when the string oscillates, it disturbs the surrounding magnetic field according to its movement. The disturbance in the magnetic field induces the electricity in the coil, i.e. generates the output signal. [4] [5]
The coil is made out of very thin enameled copper wire of great length, which forms many turns and layers. Therefore, other than the dominant inductance (L) property, this coil exhibits the resistance (R) and capacitance (C) properties, which in this case cannot be ignored.

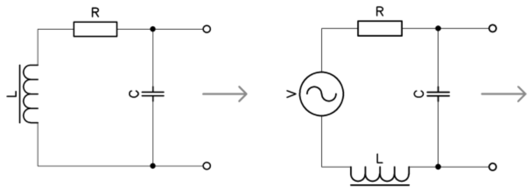

Fig.2. Electrical schematic of a guitar pickup

Fig.2 shows the schematics of the more accurate electrical model of a guitar pickup, as the passive dipole (on the left), as well as the signal generator (on the right). [4]
In order to correctly model the guitar pickup, its RLC parameters must be determined through measurements. The measurements are conducted and the resulting gain and phase frequency characteristic are given in Fig.3 (green line). From the parameters determined through the analysis of the results, namely: lower and upper corner frequencies and the gain in the frequency band between them, RLC parameters of the pickup are calculated. The obtained RLC parameters are then verified and confirmed by computer simulation (red line in Fig.3).

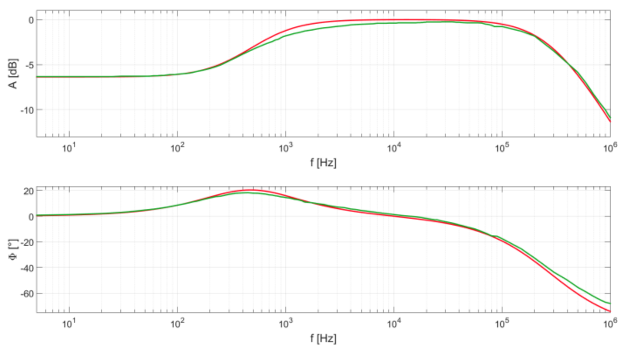

Fig. 3. Frequency characteristics of the guitar pickup

The other significant parameter of the guitar pickup that needs to be determined is the maximal voltage swing that can be reached on its output connectors, while the strings are strummed with maximal force, of course, within reason. It can be measured using an oscilloscope connected to the pickup output connections, while the strings are strummed with maximal force.
Using the described measurements, the parameters of the guitar pickup listed in Table 3 are obtained.

Parameter	Value	Unit
Resistance, R	4700	Ω
Inductance, L	2.4	H
Capacitance, C	125	pF
Maximal output voltage swing	3.2	V

Table 3. Parameters of the guitar pickup

3.2. Modeling and simulation of the input circuitry

The input circuitry has multiple purposes. It needs to enable the appropriate impedance matching, amplification and filtering in order to adjust and regulate the parameters of the original guitar pickup signal and thus prepare it for A/D conversion.
After the main parameters of the guitar pickup are determined and knowing the most important parameters of the audio codec and operational amplifiers, the successful modeling and design of the input circuitry can be undertaken.
Using the operational amplifier, the active band pass filter is designed. The resulting circuit schematic is given in Fig.4. The circuit schematic can be broken down into few sections/sub-circuits. The first part consists of the inductor L_p, resistor R_p and capacitor C_p which represent the electrical model of the guitar pickup, as explained before.

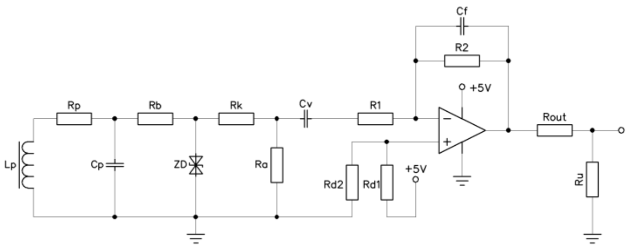

Fig. 4. Schematic of the input circuit

The second part consists of resistors R_b, R_k, R_a and Zener diode ZD. It ensures the impedance matching between the input impedance of the input circuitry and the impedance of the pickup, contributes to the regulation of the voltage gain in the pass-band, as well as the overvoltage protection. The resistors R_b and R_k also limit the current through the Zener diode thus protecting it. Simple but effective overvoltage protection of the input is crucial because the circuitry of the audio interface is very sensitive to overvoltage.
The third part is the band pass active filter. It performs several tasks: it ensures the proper voltage range and reference at the input of the A/D converter, filters the signal removing the DC component from it and attenuating the unwanted frequency components (below 20 Hz and above 20 kHz), therefore preventing frequency aliasing issues and out-of-band noise propagation.
The coupling capacitor C_v eliminates the DC component and sets the lower corner frequency of the filter. DC component elimination is crucial because the signal from the guitar pickup is referenced to 0 V (ground) and operational amplifier and input of the A/D converter are referenced to (+2.5 V). The resistor R_1 increases the input resistance, therefore improving the impedance matching. Resistor R_2 determines the voltage gain factor, and along with the capacitor C_f determines the upper

corner frequency of the filter. Resistor R_{out} limits the current between the output of the operational amplifier and the input of the A/D converter.

Resistors R_{d1} and R_{d2} represent the voltage divider implemented within the codec integrated circuit, used to provide the stable voltage reference for A/D conversion. The resistor R_u represents the input impedance of the A/D converter.

The gain frequency characteristics of the input filter, considering the case when an ideal voltage signal source is connected to it, must be constant within the audible frequency band. Therefore, the upper and lower corner frequencies (-3 dB points) have to be beyond and below the limits of the audible frequency band. All the out-of-band frequency components are unwanted and need to be well attenuated.

Before the simulation of the input circuitry design is conducted, a brief mathematical analysis and modeling is undertaken in order to approximately determine the values of the components which will provide a starting point for the further optimization.

The mathematical analysis is also used to simplify and enhance the understanding of the operation of the circuit and the ways in which particular component values influence its functionality. For that reason, the mathematical analysis of the whole circuit at once for the whole range of frequencies would be too complicated. Therefore, the analysis will be broken down into three distinct cases.

Firstly, the operation of the circuit at low frequencies is considered. At low frequencies, the capacitor C_f can be represented as open circuit due to its high impedance.

The transfer function in the Laplace domain of the configuration just described is given by equation (1), where $R_{\mathrm{IN}} = R_{\mathrm{B}} + R_{\mathrm{K}} + R_1$.

$$A_{\mathrm{BPF}}(s) = \frac{R_2 R_{\mathrm{U}}}{R_{\mathrm{OUT}} + R_{\mathrm{U}}} \cdot \frac{s C_{\mathrm{V}}}{s R_{\mathrm{IN}} C_{\mathrm{V}} + 1} \tag{1}$$

From equation (1), it is evident that the values of the resistors R_b, R_k and R_1 along with the capacitor C_v will define the lower corner frequency of the filter, according to equation (2).

$$f_{\mathrm{c}} = \frac{1}{2\pi R_{\mathrm{IN}} C_{\mathrm{V}}} \tag{2}$$

After further refinement of the equation (1) in the complex frequency domain, the condition given by equation (3) is obtained. Using that condition, the lower corner frequency of the filter can be set to the value required to set the drop of its gain by k dB at angular frequency ω.

$$\tau_{\mathrm{d}} = R_{\mathrm{IN}} C_{\mathrm{V}} = \frac{1}{\omega\sqrt{1 - 10^{-\frac{k}{20}}}} \tag{3}$$

In this particular case, it is demanded that the gain drops by 0.5 dB at 16 Hz, compared to the gain at middle frequencies. Since the value of the capacitor C_v is chosen to be 4.7 µF, according to equation (3) the value of the input resistance must be 8948 Ω. The lower corner frequency will then be around 4 Hz.

Next case that is considered is operation of the circuit at middle frequencies, where the impedance of the capacitor C_v is low enough that it can be represented as short circuit, and impedance of the capacitor C_f is still high enough to be considered open circuit. The transfer function of that configuration is given by equation (4).

$$A_{\mathrm{BPF}} = \frac{R_2 R_{\mathrm{U}}}{R_{\mathrm{IN}}(R_{\mathrm{OUT}} + R_{\mathrm{U}})} \tag{4}$$

It is evident that the gain at the middle frequencies is frequency invariant and is defined only by the values of resistors. The gain of the filter at middle frequencies must be set to such value that it provides the adaptation of the maximal voltage level of the guitar pickup ($V_{\mathrm{P,MAX}}$) to A/D converters full-scale input voltage swing ($V_{\mathrm{ADC,MAX}}$). The condition given by equation (5) must be met.

$$\frac{R_2 R_{\mathrm{U}}}{(R_{\mathrm{P}} + R_{\mathrm{IN}}) \cdot (R_{\mathrm{OUT}} + R_{\mathrm{U}})} = \frac{V_{\mathrm{ADC,MAX}}}{V_{\mathrm{P,MAX}}} \tag{5}$$

Following the condition (3) the value of the resistor R_2 is determined to be $R_2 = 18769\ \Omega$.

Finally, the operation of the circuit at high frequencies is considered. At high frequencies the capacitor C_v can be represented as short circuit due to its low impedance and only the dominant influence of the capacitor C_f on the frequency characteristics is considered.

The transfer function of the described configuration is given by the equation (6).

$$A_{BPF}(s) = \frac{R_2 R_{\mathrm{U}}}{R_{\mathrm{IN}}(R_{\mathrm{OUT}} + R_{\mathrm{U}})} \cdot \frac{1}{s R_2 C_{\mathrm{F}} + 1} \tag{6}$$

Therefore, the values of the resistor R_2 and capacitor C_f define the upper corner frequency of the filter, according to equation (7).

$$f_{\mathrm{c}} = \frac{1}{2\pi R_2 C_{\mathrm{F}}} \tag{7}$$

The upper corner frequency of the filter will be set to 48 kHz according to the recommendations given in the datasheet of the codec *PCM3060*. Therefore the value of

the capacitor C_V, obtained using the equation (7) is $C_V = 177\ pF$.
Fig.5 shows the final schematic of the input circuitry. The values of the components are selected to match the commercially available values which fall close to those calculated above. After a few iterations of the simulation and smaller corrections, the final values of the components (also shown in Fig.5) have been obtained.

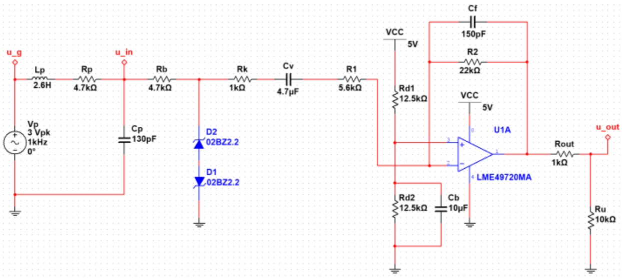

Fig. 5. Final input circuit schematic

Fig.6. shows the gain and phase frequency characteristics of the input circuitry, obtained by simulation. The red curve shows the frequency characteristics of the filter alone, the blue curve shows the frequency characteristics of the guitar pickup, and the green curve shows the frequency characteristics of the whole system: guitar pickup with the active filter.

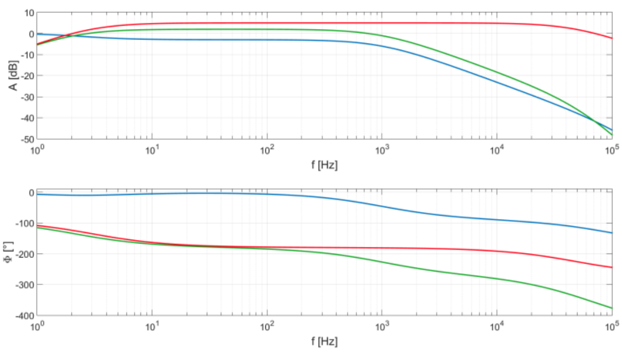

Fig. 6. Input circuit simulation results

The simulation results show that the gain for the in-band signal is A = 4.95 dB, lower corner frequency is f_{lc} = 3 Hz and upper corner frequency is f_{uc} = 48 kHz. If the influence of the guitar pickup at the input of the filter is considered, than the gain for the in-band signal is A = 1.94 dB, lower corner frequency is then f_{lc} = 2.1 Hz and upper corner frequency is f_{uc} = 987 Hz.
The results of the computer simulation match the results obtained by the mathematical analysis and therefore meet the requirements. The design of the input circuitry is ready for implementation.

3.3. Modeling and simulation of the output circuitry

The purpose of the output circuitry is to enable the regulation and filtering between the output of the D/A converter and the output of the audio interface. It is required to regulate the voltage levels as well as the impedances of the input and output, in the same time removing the unwanted frequencies by filtering.
Reviewing the typical input stages of the guitar amplifiers as well as effect units shows that the typical input impedance of those circuits is between 4 kΩ to 100 kΩ, with the typical voltage levels between 240 mV (-10 dBu) to 1.2 V (+4 dBu). [1]
The MFB filter topology is selected to be used as a starting point for the design of the output circuitry. The voltage gain of the MFB filter is given by equation (8). [6]

$$A_V = -\frac{R_1}{R_3} \tag{8}$$

Following the recommendations given by the manufacturer, in order to maintain the quality of the D/A converters output signal, it should not be loaded with impedance lower than 10 kΩ. Therefore, resistance of the resistor R_3 is selected to be 10 kΩ.
Maximal voltage swing at the D/A converter's output of the codec *PCM3060* is 4 V. Maximal voltage swing at the output of the audio interface is required to be 2.25 V. The required gain is then equal to 0.5625. Therefore, the value of the resistor R_1 is equal to 5600 Ω.
The upper corner frequency of the MFB filter is given by equation (9) and the quality factor by equation (10). [6]

$$f_c = \frac{1}{2\pi \cdot \sqrt{R_1 R_2 C_1 C_2}} \tag{9}$$

$$Q = \frac{\sqrt{\frac{C_1}{C_2}}}{\sqrt{\frac{R_1}{R_2}} + \sqrt{\frac{R_2}{R_1}} + \frac{\sqrt{R_1 R_2}}{R_3}} \tag{10}$$

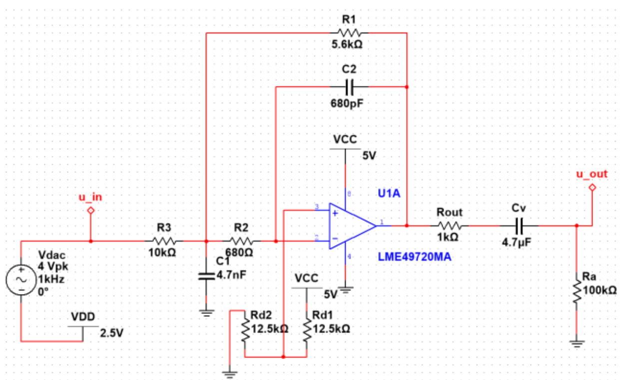

Fig. 7. Final output circuit schematic

The values of the rest of the components are calculated using these two equations. The upper corner frequency is set to be 48 kHz, and quality factor to be 0.707.
The final circuit design is shown in Fig.7.

The frequency characteristics obtained by computer simulation of the circuit given in Fig.7. are shown in Fig.8. The simulation results show that the gain for the in-band signal is A = -5.31 dB and upper corner frequency is fg = 48 kHz.

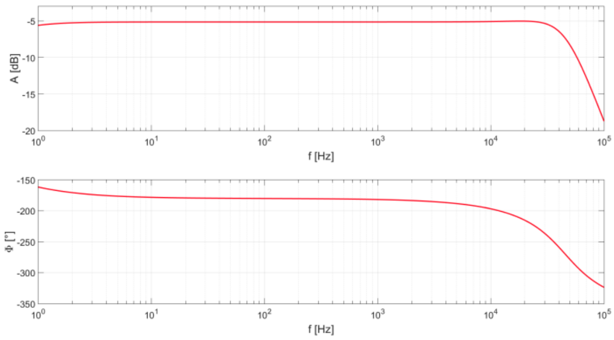

Fig. 8. Output circuit simulation results

The results of the computer simulation match the results obtained by the mathematical analysis and therefore meet the requirements. The design of the output circuitry is ready for implementation as well.

3.4. Modeling of the power supply

The electronic components, of which the audio interface circuitry is consisted, have a very narrow tolerance range for the voltage level on their power supply pins. For that reason, use of the precise voltage regulators is essential. The right voltage regulator is selected according to the required voltage rating and power capabilities.
The maximal power consumption values for the input and output circuits are also obtained by computer simulation. According to the simulation, the maximal power consumption of the input circuit equals 4 mW and the maximal power consumption of the output circuit equals 7.4 mW.
The expected maximal power consumption of the codec *PCM3060*, according to the specifications given by the manufacturer, is around 180 mW. The sum of all these power consumption values gives the total maximal expected power consumption of the audio interface which is estimated to be around 200 mW.
According to this calculation, two voltage regulators *LM1117* are selected, the first with the rated voltage of 5 V, for the analog section of the circuit, and the other with the rated voltage of 3.3 V, for digital section.

4. IMPLEMENTATION OF THE GUITAR AUDIO INTERFACE

The theoretical analysis and modeling, as well as the computer simulation have set the foundation for the successful implementation and realization of the guitar audio interface.
The implementation itself, however, requires the utilization of the particular set of the theoretical as well as experimental rules which transfer the modeled design, in the form of the electrical schematic with the corresponding set of parameters, into the final realization of the circuit with the functionality according to specifications, on a circuit board.

4.1. Design of the printed circuit board

The audio interface represents the barrier between the analog and digital domain, meaning that its printed circuit board contains the traces that carry the digital signals with their characteristics (short rise time, high frequencies, high voltage range, high tolerance towards interference and noise) as well as the analog signals with their characteristics (lower frequencies, low voltage range, low tolerance towards interference and noise).
In order to prevent the interference between analog and digital sections of the circuitry which would cause deterioration of the performance of the audio interface, the digital and analog sections are physically separated to a sufficient distance. The individual input and output audio channels are also separated from one another to an acceptable distance to avoid unwanted interference between them.
The lengths of the traces are also considered. The digital traces are made to be as short as possible, connecting the codecs digital pins directly to the on-board connector. The analog traces are also made to be as short as possible and also their length between the channels as similar as possible.
The power supply traces are routed on the bottom side of the board. There are four main power supply traces (+5 V_{cc}, +3.3 V_{dd}, GND, V_{in}) and one for the reference voltage for A/D and D/A conversion (+2.5 V). To avoid the voltage disturbances during the operation of the audio interface circuitry, blocking capacitors are used, positioned under every integrated circuit on the PCB.
In order to eliminate the electromagnetic interference and noise coming from the environment, the connector pads for the electromagnetic shield surrounding the analog section of the circuitry are made.
Fig.9 shows the final design of the PCB, made according to the directives given above. The top layer of the PCB is shown on the left side and the bottom layer is shown on the right side. The dimensions of the PCB are 44 mm x 46 mm.

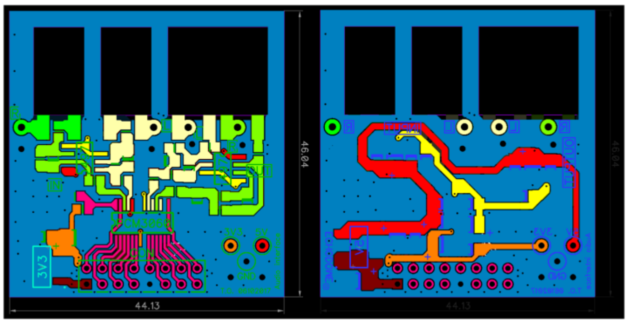

Fig. 9. Final PCB design

4.2. Fabrication of the PCB

Since the PCB is designed with precise and fine details, its manual fabrication would be inefficient and excessively demanding (expensive). Therefore, the PCB design is manufactured in specialized factory procedure. The final result is the finished PCB board, shown in Fig.10.

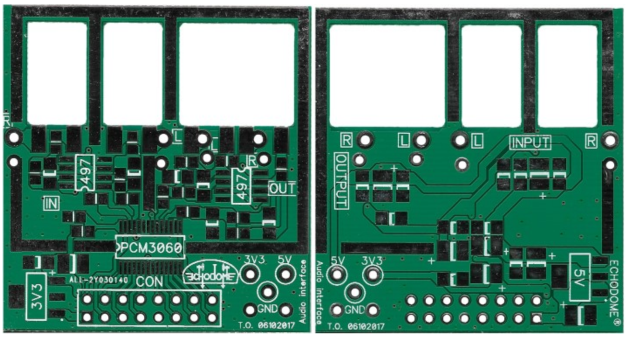

Fig. 10. Manufactured PCB board

4.3. Assembly of the electronic components

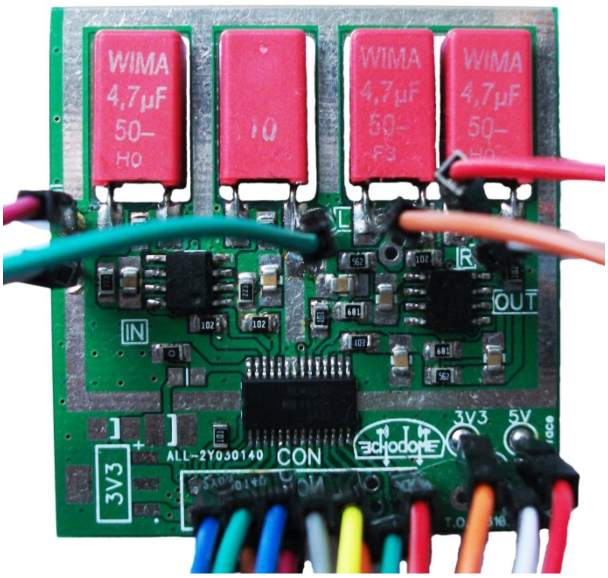

Fig. 11. Assembled audio interface

On the surface of the PCB, electronic components are manually soldered. For the evaluation and testing purposes, the connectors and cables are added as well. Fig.11 shows the assembled audio interface circuit board along with the connectors used for control and evaluation purposes.

4.4. Assembly of the digital audio processing system

For the control, evaluation and demonstration purposes, the complete digital audio processing system needs to be assembled.

The digital system which is going to control the guitar audio interface and exchange data with it is the microcontroller (MCU) *STM32F407*, based on the *ARM 32-bit Cortex M4* architecture, chosen for its suitable characteristics and I2S and I2C (Inter-Integrated Circuit) communication protocols implemented on-board.

Fig.12 shows the audio interface board, microcontroller *STM32F407* board, connectors for guitar and amplifier and power supply connector assembled on a breadboard, forming the digital audio processing system.

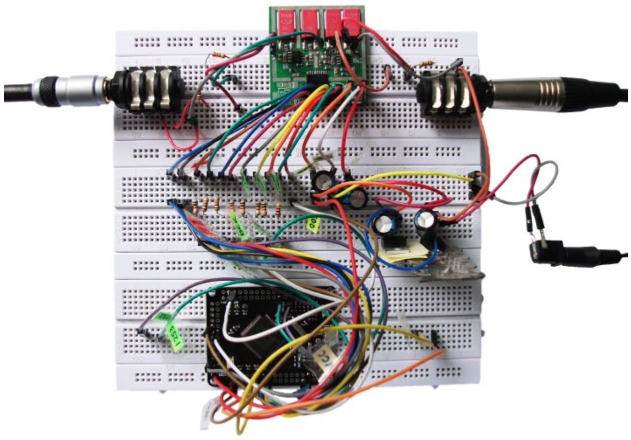

Fig. 12. Assembled digital audio processing system

The microcontroller is programmed to establish the communication with the codec *PCM3060*, to change and control codecs settings via the I2C bus and exchange digital audio samples via the I2S bus. The microcontroller is also programmed to implement a basic real-time audio processing application - *delay* effect, for demonstration purposes.

The assembled digital audio processing system is prepared for evaluation and control measurement.

5. MEASUREMENTS OF THE GUITAR AUDIO INTERFACE

In order to determine whether the requirements set at the beginning are fulfilled and to what extent, the control measurements are conducted.

5.1. Measurements of the frequency characteristics

The frequency characteristics of the measured circuit are obtained as follows: using the signal generator, at the input of the circuit, pure sine wave signal with the constant amplitude and fixed frequency is applied. Using the oscilloscope, the amplitudes of the signal at the output of the circuit $V_{m,out}$, as well as its input $V_{m,in}$ are determined. The voltage gain A of the circuit, for that particular frequency is calculated using the equation (11). [7]

$$A[\mathrm{dB}] = 20 \log\left(\frac{V_{\mathrm{m,out}}}{V_{\mathrm{m,in}}}\right) \tag{11}$$

From the delay time t_d between the input and output at a fixed (known) frequency f, the phase difference φ can be calculated using the equation (12).

$$\varphi = 360 \cdot t_d f \tag{12}$$

This procedure is then repeated for every frequency within a chosen set. The results are then plotted to give the gain and phase frequency characteristics of the measured circuitry.
The frequency characteristics of the input circuitry obtained using the procedure described above are shown in the Fig.13. The red line represents the frequency characteristics of the left input channel, and the green one represents the frequency characteristics of the right input channel.

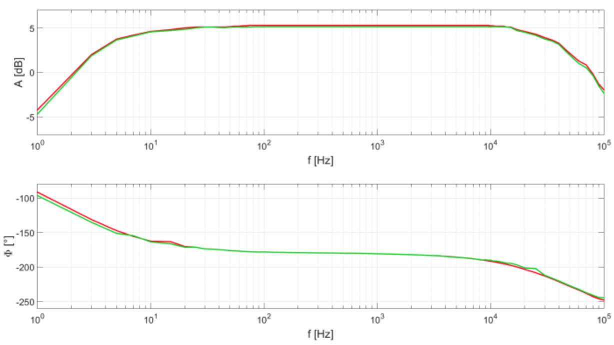

Fig. 13. Input circuit measurement results

Parameter	Value	Unit
Pass band voltage gain	5.25	dB
Lower corner frequency	4	Hz
Upper corner frequency	48	kHz
Gain deviation (20 Hz – 20 kHz)	0.6	dB
Phase deviation (20 Hz – 20 kHz)	32	°
Gain deviation (80 Hz – 10 kHz)	0.03	dB
Phase deviation (80 Hz – 10 kHz)	11.5	°

Table 4. Measured input circuit parameters

The parameters of the input circuitry that can be determined from the frequency characteristics, averaged for both channels are given in Table 4.
The measurement results confirm the results obtained by the computer simulation and therefore meet the requirements. The input circuitry of the guitar audio interface is successfully implemented and realized.
The frequency characteristics of the output circuitry are shown in Fig.14. The red line represents the frequency characteristics of the left output channel, while the green line represents the frequency characteristics of the right output channel.

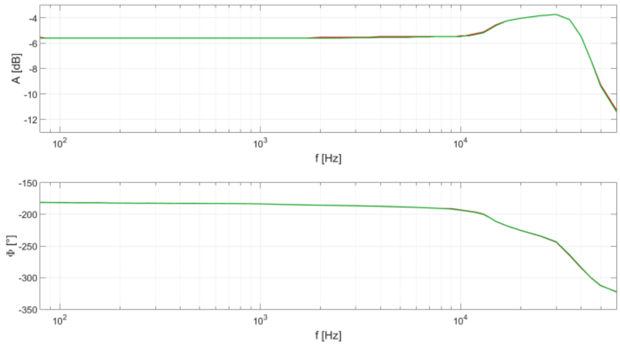

Fig. 14. Output circuitry measurement results

The parameters of the output circuitry, determined from the frequency characteristics, averaged for both channels are given in Table 5.

Parameter	Value	Unit
Pass band voltage gain	-5.8	dB
Upper corner frequency	47.6	kHz
Gain deviation (20 Hz – 20 kHz)	0.98	dB
Phase deviation (20 Hz – 20 kHz)	52	°
Gain deviation (80 Hz – 10 kHz)	0.12	dB
Phase deviation (80 Hz – 10 kHz)	8.3	°

Table 5. Measured output circuit parameters

The measurement results confirm the results obtained by the computer simulation and therefore meet the requirements. The output circuitry of the guitar audio interface is also successfully implemented and realized.
In order to determine to what extent the audio interface preserves the gain and phase relationships in the original signal along the whole path from input to output, the frequency characteristics of the whole signal path through the audio interface is obtained.
The test sine signal is fed to the input of the interface, and the oscilloscope probe is connected to its output. The gain frequency characteristic of this measurement setup is shown in Fig.15. The red line represents the frequency characteristics of the left channel, and the green one the frequency characteristics of the right

channel. The measurements are conducted with the sampling frequency set to 48 kHz.

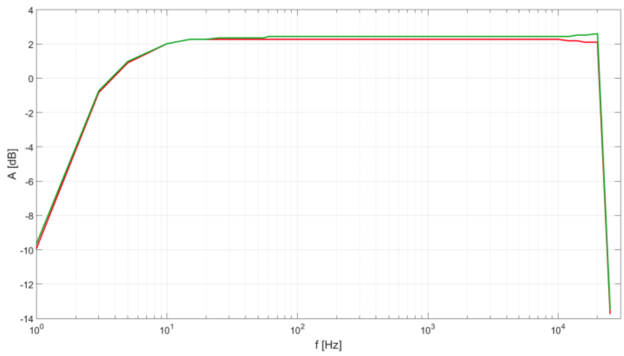

Fig. 15. Input-output measurement results

From the determined frequency characteristics, the parameters of the whole signal path, given in Table 6 are determined.

Parameter	Value	Unit
Pass band voltage gain	2.36	dB
Lower corner frequency	3	Hz
Upper corner frequency	21	kHz
Gain deviation (20 Hz – 20 kHz)	0	dB
Gain deviation (80 Hz – 10 kHz)	0	dB
Gain deviation between channels	0.12	dB

Table 6. Measured input-output parameters

The measurement results show that the frequency characteristics are close to ideal ones: they are flat/constant within the whole audible frequency band, and exhibit a rapid gain drop outside of that band. Therefore, they meet the requirements.

5.2. Measurements of the harmonic distortion

The harmonic distortion measurements are conducted using the frequency analyzer and a pure sine wave generator. The pure sine wave of 1 kHz is fed to the input of the audio interface. The signal goes through the whole path through the audio interface and from the output is then fed to the frequency analyzer. The measurements are conducted for each channel separately.
In the spectrum obtained by the frequency analyzer, the main frequency component as well as its harmonics can be identified. The amplitudes of the harmonic components and main component are determined. According the formula given by equation (13) the THD factor is calculated. [8]

$$THD = \frac{\sqrt{{V_2}^2 + {V_3}^2 + {V_4}^2 + \cdots}}{\sqrt{{V_1}^2 + {V_2}^2 + {V_3}^2 + {V_4}^2 + \cdots}} \cdot 100\% \qquad (13)$$

For different voltage levels of the input sinusoidal signal, different values of the THD factor are obtained. In Fig.16 the relationship between the input signal level and measured THD factor value are given for left (blue line) and right (green line) channel.

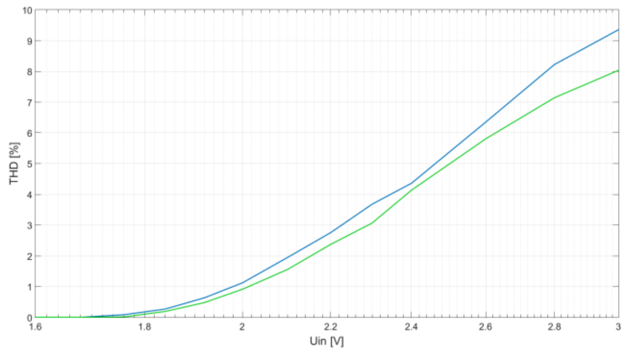

Fig. 16. THD factor measurement results

The results show that, for an input voltage within the line level voltage range (<1.2 V, <+4 dBu) the expected THD factor along the whole signal path through the audio interface is less than 0.003 %.

5.3. Measurements of the dynamic range

The dynamic range of the A/D converter is limited by the maximum input voltage range (3 V_{pp} for the codec *PCM3060*) on one end, and by the existence of a certain level of intrinsic noise on the other end. Since at 24 bit conversion the quantization voltage level is much smaller than the residual noise voltage level, a certain number of bits in encoded signal will be saturated by noise and effectively couldn't be used to carry useful audio information. Thus, the number of bits that will encode a useful signal is 24 - b_n, where b_n is the number of bits saturated by noise.
If the output communication on the I2S bus is intercepted and displayed in oscillogram, the number of bits saturated by noise can be determined. While this measurement is conducted, the respectable inputs of the audio interface are shorted to ground.
The measurement results show that the lower 7 bits (of 24) are saturated by noise, which means that the upper 17 bits are able to encode the useful signal. Therefore, the input dynamic range of the audio interface is calculated by equation (14)

$$DIN_{\mathrm{ADC}} = 20 \log\left(\frac{2^{24}}{2^7}\right) = 102.4 \ \ \mathrm{dB} \qquad (14)$$

The dynamic range of the output of the audio interface is limited by the maximum output voltage range (2.25 V_{pp} in this case) from the upper end, and by the typical residual noise voltage level from the lower end.

However, due to the lack of the more advanced measurement equipment capable of achieving the required precision, the residual noise voltage level at the output of the audio interface couldn't be explicitly determined. Still, using the measurement results made during the THD measurements (section 5.2) the residual noise level can be estimated using the following analysis. The frequency analyzer plots the spectrum of the signal obtained at the output of the audio interface. In that spectrum, the main frequency component and its harmonics can be identified, as explained in the previous section. Other than that, the residual noise spectrum can also be observed. That residual noise originates from the frequency analyzer itself and represents one of the factors that constrain its measurement accuracy. The level of that residual noise doesn't exceed -95 dBV. Therefore, the level of the residual noise originating from the outputs of the audio interface falls somewhere below -95 dBV. Although it cannot be explicitly determined, it is estimated using the following calculation:

$$DIN_{\mathrm{DAC}} = 20\log(2.25) + 95 \approx 102 \ \ \mathrm{dB} \qquad (15)$$

5.4. Measurements of the power consumption

Another one of the important parameters, especially if the audio interface is to be used within the battery powered systems, is its power consumption during operation. The power consumption is determined by measuring the current that the audio interface circuitry draws from the power supply multiplied by the fixed voltage (+5 V) of the power supply.
The power consumption is measured for few operating setups or scenarios. The results are given in Table 7.

Setup	Power [mW]
audio interface in power saving mode, MCU in power saving mode	74.5
audio interface in power saving mode, MCU active	288.5
audio interface active (sampling frequency 48 kHz), MCU active	437
audio interface active (sampling frequency 96 kHz), MCU active	483

Table 7. Power consumption measurement results

Since the power consumption of the whole digital audio processing system is considered here, the power consumption of the audio interface alone is lower than the values given in the Table 7 and is estimated to be around 250 mW. That value is a bit higher than the one obtained by simulation, but the difference is not significant.

5.5. Measurements of the input-output latency

For the real-time audio processing applications, it is crucial that the audio interface itself has a negligible contribution to the final latency of the whole system.
The measurement is conducted as follows: an impulse signal is fed at the input of the audio interface and the time required for a response to reach the output is measured.
When the 48 kHz sampling frequency is used, the measured latency equals 740 µs (equal for both channels), and if the 96 kHz sampling frequency is used, the measured latency equals 370 µs. The measurements are conducted using the 24 bit quantization.

5.6. Subjective listening test

After performing the objective measurements of the most important parameters of the guitar audio interface, a subjective listening test is performed in order to determine whether the difference between the original sound of the electric guitar and the one transmitted through the whole audio interface signal path can be perceived.
To facilitate the comparison, both signals are brought to a switch that can directly commute between them. The signal is then fed to the headphone amplifier and is listened to by headphones. Other than the guitar audio signal, the same procedure is also performed for the (stereo) music signal.
Throughout the listening test (at 48 kHz sampling frequency and 16 bit quantization) no audible difference in audio quality between the original audio content and the one transmitted through the audio interface was perceived. The frequency content is identical and there is no audible noise and interference or any other form of degradation of sound quality.

5.7. The analysis of the measurement results

The frequency characteristics measurement results show that the circuitry of the audio interface exhibits negligible amplitude and phase deviations over the whole audible frequency band, while properly attenuating the out-of band frequencies. That can be observed especially if the input-output frequency characteristics are considered. That means that the audio interface preserves the spectral characteristics of the original signal along its whole path.
According to the results, both channels have very similar parameters, making the audio interface suitable and optimized for stereo audio signal applications.
The THD factor measurement results show that for the line level signals (-10 dBu or 4 dBu) the audio interface exhibits imperceptible harmonic distortion over the whole signal path from input to output.

The power consumption measurement results show that the audio interface can also be used in battery powered systems (using the battery of acceptable size) since its maximal power consumption is estimated at 250 mW, and furthermore, with the utilization of the smart power management (putting parts of the codec circuitry into stand-by mode, if not used) it is possible to significantly decrease this power consumption value.
The input-output latency measurement results show that the audio interface negligibly contributes to the total acceptable latency of the digital audio processing system, and therefore can be used within the real time audio processing applications.
The results of the measurements altogether have generally even exceeded the expectations. Moreover, according to the evaluation criteria used by the *Rightmark* software, the prototype of the audio interface developed here would get an excellent rating and could be put within the class of the semi-professional or even professional grade audio interfaces (used as a part of professional high performance sound cards and studio equipment). By subjective listening test, such results are further confirmed.

6. CONCLUSION

The processing of the electric guitar audio signal is necessary in order to improve its certain imperfections as well as to enable musicians or audio engineers to shape it, adapt it and make it specific, according to their personal preferences. The digital audio signal processing provides great flexibility and countless possibilities. The audio interface bridges the gap between the analog and digital domains, enabling the digital audio signal processing within the surrounding analog world.
Using the set of simple mathematical tools and models, the results of the computer-supported simulations as well as the experimental results and practical knowledge, the guitar audio interface is, as confirmed by the measurement results, successfully implemented and realized while all of the requirements and specifications are met and even exceeded.
After the fully functional guitar audio interface is implemented and realized, the further development should be focused on the software implementation of the audio processing tools on a compatible processor.

7. REFERENCES

[1] Kyttälä, T: **Solid-State Guitar Amplifiers**, www.thatraymond.com/downloads/solidstate_guitar_amplifiers_teemu_kyttala_v1.0.pdf, 2008.
[2] **PCM3060 – 24-bit, 96/192-kHz Asynchronous Stereo Audio Codec**, http://www.tij.co.jp/jp/lit/ds/symlink-/pcm3060.pdf, *Texas Instruments Inc.*, 2008.
[3] **LME49720 – Dual High Performance, High Fidelity Audio Operational Amplifier,** http://www.ti.com/lit-/ds/symlink/lme49720.pdf, *Texas Instruments Inc.*, 2016.
[4] Lähdevaara, J: **The Science of Electric Guitars and Guitar Electronics**, http://guitarscience.net/papers-/guibook.pdf, 2014.
[5] Rossing, T. D: **The Science of String Instruments**, *Springer*, Stanford, CA, 2010.
[6] Steffes, M: **Design Methodology for MFB Filters in ADC Interface Applications**, http://www.ti.com/lit-/an/sboa114/sboa114.pdf, *Texas Instruments Inc.*, 2006.
[7] Cabot, R. C: **Fundamentals of Modern Audio Measurement**, *Journal of the Audio Engineering Society*, NY, 1999.
[8] Temme, S: **Audio Distortion Measurements**, *Bruel & Kjaer*, 1992.
[9] Zölzer, U: **DAFX – Digital Audio Effects**, *John Wiley & Sons*, England, 2002.

NONLINEAR RESPONSE OF LOUDSPEAKERS

Tilen Mramor *, Danijel Svenšek*, Belšak Aleš**, Jurij Prezelj***

* Faculty of Mathematics and Physics, University of Ljubljana
**Faculty of mechanical engineering, University of Maribor
*** Faculty of mechanical engineering, University of Ljubljana

Abstract: *Electromechanical systems are predisposed to non-linear distortions. Small-radii loudspeaker drivers and broadband loudspeaker drivers are particularly sensitive to this effect, while they need to achieve long linear excursions to provide sufficient dynamic range. Non-linear distortions are traditionally observed with methods which have been developed for identification and quantification of different sources of nonlinear distortions within the electro-mechanical system. Standardized methods are based on typical test signals like sinus sweep, and on loudspeaker response analysis, based on digital signal processing focused towards frequency domain, (Fourier and inverse Fourier transformation). In available literature only few studies have been found where nonlinear distortions are studied simply in time domain. However, even if analyses have been performed in time domain, only standardized test signals were used. Therefore we decided to develop a new test signal forcing the operation of the loudspeaker into nonlinear regime. Such approach enables fast identification of nonlinear distortions from signals in time domain and also makes it possible to find the nonlinear convolution operator responsible for harmonic distortions. To prove this system to be applicative, tests have been performed on three different loudspeakers. Designing a quality loudspeaker that will be less affected by nonlinear distortions is difficult, time consuming and expensive, this is why the proposed method has potential to become a quicker and cheaper alternative.*

Keywords: nonlinear distortion, loudspeaker design, nonlinear convolution, nonlinear operator, time domain

1. INTRODUCTION

Analysing electromechanical systems is becoming increasingly important, particularly when application demands from system specific performance which introduces nonlinearities. A single linear model does not precisely match these systems. Nonlinearity is usually determined from additional measured responses of the system at different levels of input signal, [1, 2].

Measurements of acoustic systems are affected by noise and by nonlinearity, among others. While measurement noise may be reduced by increasing the length of the excitation signal and by averaging the outputs from several excitations, the nonlinearity remains an inherent problem of these techniques and is difficult to be characterised accurately.

A number of approaches to nonlinear observations are available in the technical literature, Kemp and Primack compared two such methods for nonlinear system identification; Diagonal Volterra model and Exponential sine sweep, [3]. Both processes are time consuming and demand automatized measurement equipment and data analysis. Other methods, which are used for identification of nonlinear distortions within the electromechanical system, demand sophisticated equipment and extensive signal processing. Therefore we decided to approach the process of evaluating the effects of nonlinearity in electromechanical systems with a new, faster and simplified method for numerical modeling of nonlinearity.

All loudspeakers are prone to nonlinear distortions especially small and full-range loudspeakers. Full-range loudspeakers were selected because they are widely used in products but rarely studied in literature, which is why developing a better loudspeaker should be a relevant solution to improve the global quality of the system. Despite the technological process improving, low-cost loudspeakers used in multimedia devices are still highly nonlinear [4].

Most loudspeaker systems are consisted of amplifier, cabinet, crossover and loudspeaker unit. The main source of nonlinearity is the loudspeaker unit. The loudspeaker nonlinearities depend on displacement of the coil x (Fig.1) and on the electrical current in the voice coil, [4]. x_{lin} depicts the limit within the loudspeaker works as a linear system. x_{max} depicts the maximum displacement within the loudspeaker is working, and x_{damage} is the limit after which the loudspeaker is damaged. Sources of nonlinearity are directly related to the geometry and material properties of the internal components such as motor suspension, cone and enclosure, [2]. Nonlinearities, which produce distortion, can be classified into three categories. The first type corresponds to the motor nonlinearities, second type corresponds to the suspension nonlinearities, and the third type corresponds to the acoustical nonlinearities. The last source of nonlinearity is not described here since these nonlinearities are directly produced only if sound pressure level exceeds 130 dB. This is not possible with small full-range loudspeaker, [5].

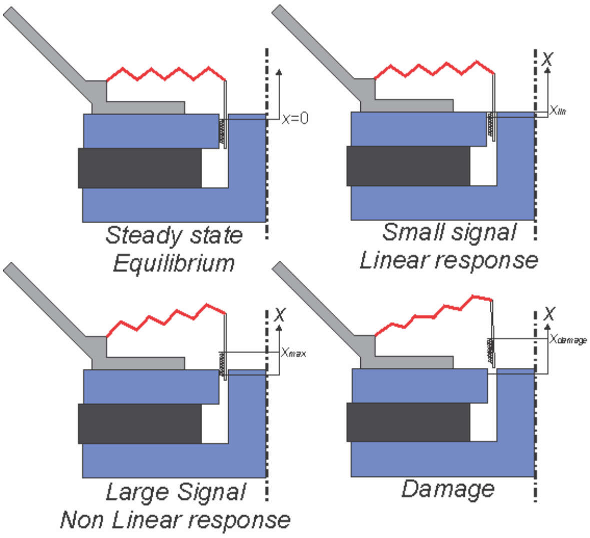

Fig. 1. Working range of loudspeaker

1.1. The motor system

Correlation between force factor Bl, which is integral of the flux density B versus voice coil wire length l; and the displacement x(t) of the voice coil are a major sources of nonlinearities, [2]. It can be observed by comparing the level ratio of different harmonics; odd harmonics are much more affected by this source of nonlinearity than the even harmonics, [4]. The force factor Bl depends on the geometry of the coil-gap configuration and the flux density field generated by magnet. Therefore, the force factor depends on the voice coil position. For small displacements the force factor value is almost constant, because the same number of windings is in the gap. The magnetic field induction B is the superposition of two fields. First field is created by the permanent magnet and is time independent. This field crosses through the yoke pieces but only 30 % serves to move the coil, [5]. The second field is created by the voice coil and is time dependent.
Klippel proposed to model the force factor by using a 2nd order polynomial, [2];

$$Bl(x) = Bl_0 + Bl_1 x + Bl_2 x^2 \quad (1)$$

The force factor depends on the displacement x of the voice coil, and this variation is not symmetrical relative to the equilibrium position. The model that was developed for this dependence can be found by using a 4th order polynomial function, [6].

1.2 Voice coil inductance

The coil self-inductance depends on the moving part position. This dependence generates a reluctant force which is given by, [5]:

$$F_{rel}(t) = \frac{1}{2} i(t)^2 \frac{dL_e(x)}{dx} \quad (2)$$

We see that when the inductance L_e does not depend on the voice coil position x, the reluctant force $F_{rel}(t)$ equals zero. This is actually one of the assumptions of the Small signal model using lumped parameters. If the coil is in free air above the gap the inductance is much lower than when operating the coil below the gap where the surrounding material is steel which decreases the magnetic resistance, [2].

1.3 Eddy currents

The electrical conductivity of the iron is high enough to let the eddy currents appear in the iron yoke pieces of the motor. Vanderkooy proposed a model which takes this phenomenon into account. The interaction between the eddy currents and the current in the coil generates a drag force F_{drag} which can be written as follows, [7]:

$$F_{drag} = \mu(i,x) \frac{dx(t)^{1,7}}{dt} \quad (3)$$

Where μ (i,x) can be defined as the sensitivity of the drag force, according to the eddy currents. Force therefore depends on the input current, and on the position of the voice coil within the magnetic field.

1.4 The suspension system

The suspension system (Fig. 2) in any speaker is comprised of two elements, the surround and the spider. The surround is usually made of rubber, foam or treated linen. The surround helps keep the cone centered, provides a damped termination for the cone edge and provides portion of the restoring force that keeps the coil in the gap. The spider is mostly made of rubber, impregnated fabric or molded plastic.

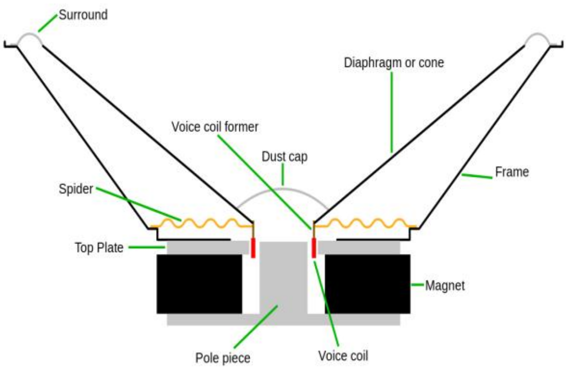

Fig. 2. Loudspeaker driver cross-section depicting the suspension system

The small signal model using lumped parameters describes a suspension as an ideal spring, but an actual suspension always shows nonlinear behaviour. In consequence, its compliance C_{ms} depends on the movement amplitude and the induced damping parameter depends greatly on both; the amplitude and frequency. More generally, many authors use the mechanical stiffness k which is defined by:

$$k=\frac{1}{C_{ms}} \tag{4}$$

Like the force factor Bl, k can be written in terms of the 2nd order polynomial function.

$$k(x)=k_0+k_1x+k_2x^2 \tag{5}$$

Such model has been used by Klippel [2], to model the nonlinear behaviour of both; the surround, and the spider. However, such model cannot take into account the effect of the hysteretic response of elastomers.

2. MODELING THE NONLINEARITY

Sources of nonlinearity in the loudspeaker usually reduce its response at higher amplitudes. Level of such reduction depends on the loudspeaker construction and on the amplitude of the driving signal. The problem of finding a good and simple nonlinear model structure is a complex issue. There are numerous available numerical models for describing the nonlinearity of the loudspeakers, but two most common are the Hammerstein model and the Volterra series.

2.1 Volterra series

A Volterra series characterizes time-invariant nonlinear system with a straightforward filter structure, in which the system (input–output equation) is rendered as a polynomial series. Due to the advantage that Volterra series expansion is a linear combination of nonlinear functions of the input signal, adaptive Volterra filters are well suited for the modeling of nonlinear systems and for using the nonlinear system identification algorithms, such as the least-mean-square (LMS) algorithm and the recursive least-square (RLS) algorithm. Assume $x(n)$ and $y(n)$ represent the input and output signals, respectively. The polynomial series based Volterra series is given by the following expression, [8].

$$\begin{aligned} y(n)=&h_0+\sum_{m_1=0}^{\infty} h_1(m_1)x(n-m_1) + \\ &\sum_{m_1=0}^{\infty}\sum_{m_2=0}^{\infty} h_2(m_1,m_2)x(n-m_1)x(n-m_2)+\cdots+ \\ &+\sum_{m_1=0}^{\infty}\sum_{m_2=0}^{\infty}\cdots\sum_{m_p=0}^{\infty} h_p(m_1,m_2,\ldots,m_p)x(n-m_1)x(n-m_2)\ldots x(n-m_p) \end{aligned} \tag{6}$$

Where $h_p(m_1, m_2, \ldots, m_p)$ is defined as the p-th order Volterra kernel, and h_0 is a constant value, which can be ignored in the adaptive filtering. Actually, h_p can be regarded as impulse response for different types / rates of nonlinearities. Matrix $h_p(m_1, m_2, \ldots, m_p)$ is assumed to be symmetric.

Volterra series simulation and measurement are showing in [11] a suitable way to characterize the nonlinear behaviour of the electromechanical system. Experimental comparison showed that the Volterra model can effectively and accurately predict the sound pressures and harmonic distortions within the bandwidth of the training signal, [8]. Volterra models can be seen as a generalization of the simple convolution operator used for linear systems. Such models represent exactly any nonlinear analytical system, and approximate any nonlinear system with a fading memory. Measurement methods were already developed to identify the first two or three terms of the Volterra series. These experimental methods are time consuming because they require many measurements. Moreover the difficult physical interpretation of the different terms of the Volterra series limits its use, [10].

2.2 Hammerstein model

Mathematical relation between the input x(t) and the output y(t) of a Hammerstein model is given by,

$$y(t)=\sum_{n=1}^{N} h_n * x^n(t) \tag{7}$$

where * denotes the convolution. In this model, each impulse response $h_n(t)$ is convolved with the input signal $x(t)$, elevated to its n-th power and the output y(t) is the sum of these convolutions. The first impulse response h_1 represents the linear response of the system. The other impulse responses h_2, h_3 … h_N model the nonlinearities, [9]. The family of impulse responses is referred to as the Kernels of the model. Any cascade of Hammerstein models is fully represented by its Kernels. It can easily be shown that cascades of Hammerstein models correspond to Volterra models having diagonal Kernels in the temporal domain. This nonlinear model is thus referred to in literature as a diagonal l Volterra model, but also as a cascade of Hammerstein models, [9].

2.3 Proposed simplified model of nonlinearity

Dominant sources of loudspeaker nonlinearity reduce the loudspeaker's response at higher amplitudes. Level of the response reduction depends on the construction of the loudspeaker driver and on the amplitude of the driving signal. By using a trigonometric function, we get a much more straightforward approach to describing sources of nonlinearities, than describing it with polynomial. Influence of nonlinear magnetic flux, with weak smooth nonlinear characteristics, can be described by Eq.8, [12], as depicted in Fig. 3 for different rates of nonlinearity.

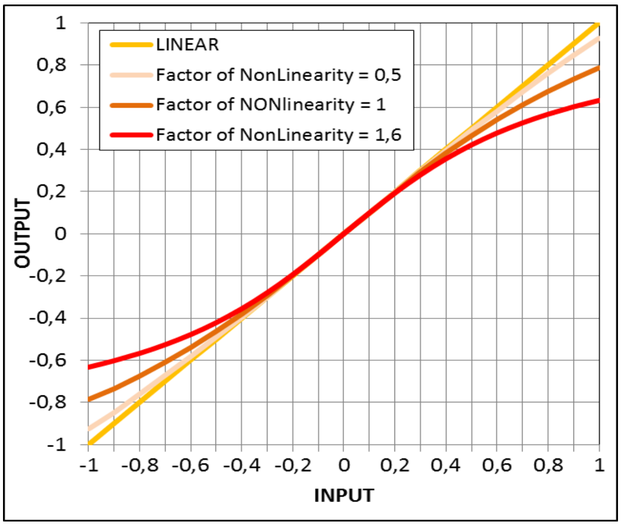

Fig. 3. Nonlinear response can be described by a simple trigonometric function [12]

$$N\{s(t)\} = \frac{arctan(k_{nonlin}s(t))}{k_{nonlin}} \tag{8}$$

Nonlinear operator $N\{s(t)\}$ can be applied in the equation to different positions; they are presented in the Table 1.

Operator N at:	Equation
INPUT	$y_N(t) = h(n) * N\{x(t)\}$
OUTPUT	$y_N(t) = N\{y(t)\} = N\{h(n) * x(t)\}$
CONVOLUTION	$y_N(t) = \sum_{n=1}^{T_0} [N\{h(n) * x(t-n)\}]$

Table 1. Application of nonlinear operator N

Each position of the nonlinear operator $N\{s(t)\}$ provides a different result, as depicted with the set of resulting numerical equations given in Table 2.

Operator N at:	Equation
INPUT	$y(t) = \sum_{n=1}^{N} k_0(n) \frac{k_{nonlin} arctan(x(t-n))}{k_{nonlin}}$
OUTPUT	$y(t) = \frac{\arctan(k_{nonlin} * \sum_n^N x(t-n)\, k_0(n))}{k_{nonlin}}$
CONVOLUTION	$y(t) = \sum_{n=1}^{N} \frac{\arctan(k_{nonlin} x(t-n) k_0(n))}{k_{nonlin}}$

Table 2. Numerical calculations for modeling

In order to be able to compare simulation in time domain, with measured impulse response, a new test signal was developed. The main idea of the new test signal was to speed up the process of measurements and to enable the visual perception of the nonlinearity effect directly in time domain.

2.4 Proposed test signal

Proposed test signal is combined from two functions Fig. 4; form the harmonic function representing the carrier signal with subsonic frequency and from the Kronecker delta function, which is usually defined on a finite domain. Kronecker delta is a function of two variables that take values from 1 to 0 and is referred to as an impulse. Impulses are used for the basic identification of system response. When it is the input to a discrete-time signal processing element, the output is called the impulse response of the element. Its representation in frequency domain is theoretically similar to random signal / white noise. To harmonically move the loudspeaker motor from linear into the nonlinear working range, frequency of the harmonic function was set to 7 Hz, which is well below the working range of any full-range loudspeaker. While the amplitude of the subsonic signal linearly decreases, the amplitude of the impulses remains the same relative to the baseline of the carrier signal, as depicted in Fig. 4.

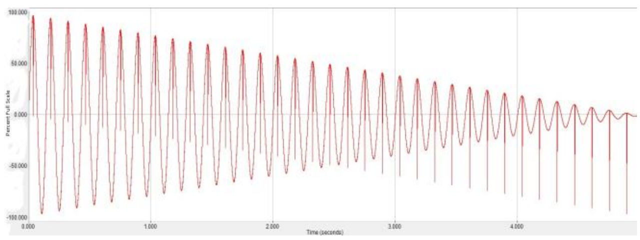

Fig. 4. Proposed test signal

When a loudspeaker is excited by a proposed signal with low amplitude, it can be considered as a linear system, even if this is not entirely true due to the dependence on electrical current. As presented in Fig. 1, the nonlinearity needs to be taken into account only for excitation signals with higher amplitudes, when the loudspeaker coil starts to perform large strokes. It is therefore necessary to take into account the rate of displacement over time to correctly model the loudspeaker nonlinearity, [4]. Proposed signal does exactly that. It enables fast and simple measurements of the nonlinearity effect at different levels of the crucial part of the input signal which causes the nonlinear response.

3. MEASUREMENT SETUP

Measurements were performed in the anechoic chamber, (Fig. 5) with a volume of 36 m3. The signal from the measurement microphone B&K type 4940 was amplified with the measurement amplifier B&K type 2636 and sampled with A/D converter set to 100 kHz sampling rate and 16 bit resolution. The Behringer power amplifier, which provided 1000 W (RMS), was used for driving the loudspeakers. Acoustic measurements were performed with a microphone and loudspeakers at a fixed position. The proposed test signal was reproduced three times at each amplification level.

The proposed test signal was used to evaluate one woofer loudspeaker with an effective piston area of 137 cm^2 and two full-range loudspeakers with an effective piston area of 31 cm^2 and 38,5 cm^2. Three signals were measured; sound pressure signal, voltage on the loudspeaker and the electric current. The electric current was measured via voltage drop across four resistors connected together in parallel producing equivalent resistance of 0,55 Ohm. During the measurements, the amplification was set to deliver a specific RMS value of electric current on all three tested loudspeakers, based on their RMS value.

Fig. 5. Measurement setup in anechoic chamber

4. MEASUREMENTS RESULTS

Full-range or woofer loudspeaker cannot produce sound pressure at the subsonic frequency of the carrier signal at 7 Hz. Full-range loudspeaker cannot reproduce such a low frequency due to small dimension and too low excursion of loudspeaker membrane, even woofer whose dimensions are bigger was struggling with excursion. Although the membrane was actually moving accordingly with the signal during the experiment no sound with such a low frequency was generated. In our experiment loudspeakers were therefore actually working as high pass filters. While loudspeakers were able to reproduce impulses, they completely filtered out the subsonic component of the test signal. However, this subsonic component of the test signal has significant influence on the performance of the loudspeaker.

At the start of the test signal, the energy of the subsonic part dominates within the RMS value. At the end of the signal only impulses remain within the test signal and RMS value of the signal depends only on the amplitude of impulses. If the loudspeaker is excited with low levels of the proposed signal, then the subsonic part of the signal does not push the loudspeaker motor outside the linear part of the driver motor. At increased level of the signal, the subsonic part of the signal pushes the coil outside the linear part of the driver motor and the superimposed impulse response is adequately altered, according to the effect of nonlinearity. When the amplitude of the subsonic part of the signal is decreased, the coil is working within the linear part of the driver motor, and the impulse response adequately returns to the linear response fig. 6.

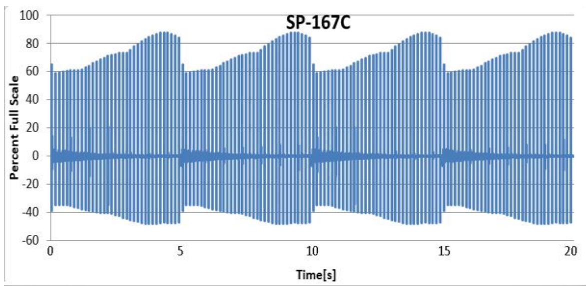

Fig. 6. Response of the loudspeaker SP-167C to the test signal presented in Fig. 4

A comparison between the impulse responses of the woofer and full-range loudspeakers when working in linear range and in nonlinear range are presented in Fig. 7, 8 and 9. In all three figures, the linear impulse response is presented with thin orange line and impulse response with nonlinear behaviour is depicted by a thin blue line.

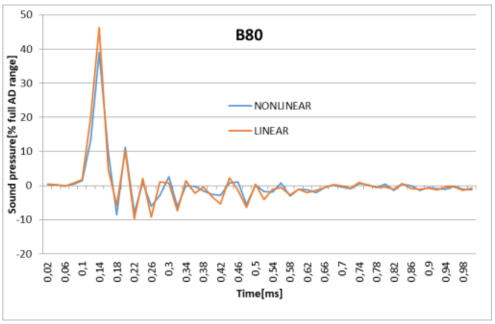

Fig. 7. Comparison between two different measured impulse response of full-range loudspeaker B80; linear- orange line, nonlinear-blue line

In all cases we can see that high amplitude of subsonic part of the signal (nonlinear part) reduces the amplitude of the impulse response.

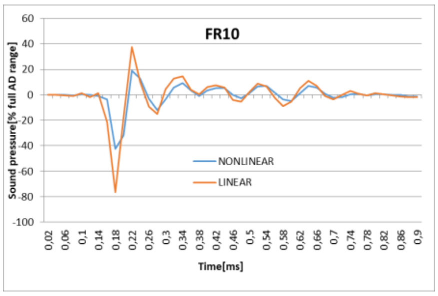

Fig. 8. Comparison between two different measured impuls response of full-range loudspeaker FR10; linear- orange line, nonlinear-blue line

We can observe the effect of nonlinearity in impulse response of the loudspeakers from the first peak up to the linear part differently. The effect of nonlinearity in impulse response occurs differently based on the type of loudspeaker. Loudspeaker B80 started operating in linear regime after two peaks, on the other hand nonlinear impulse response of FR10 and woofer SP-167C is more affected by the subsonic signal component as nonlinear impulse response of B80.

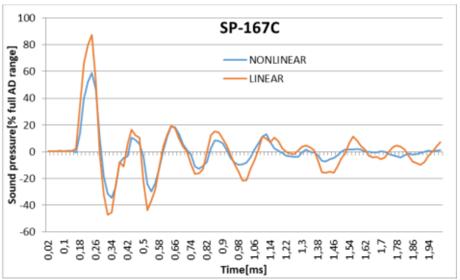

Fig. 9. Comparison between two different measured impulse response of woofer loudspeaker SP-167C; linear- orange line, nonlinear-blue line

5. EXPERIMENTAL RESULTS

Linear and nonlinear impulse response spectra of three different loudspeakers B80, FR10 and SP-167C are presented in Fig. 10. Frequency domain is generally used for description of loudspeaker performance, even though that description in frequency domain is only a transformation from the time domain. Presented spectra are from a single impulse. Nonlinearity caused by the subsonic part of the signal has strong effect in frequency range from 100 Hz and up to 10 kHz.

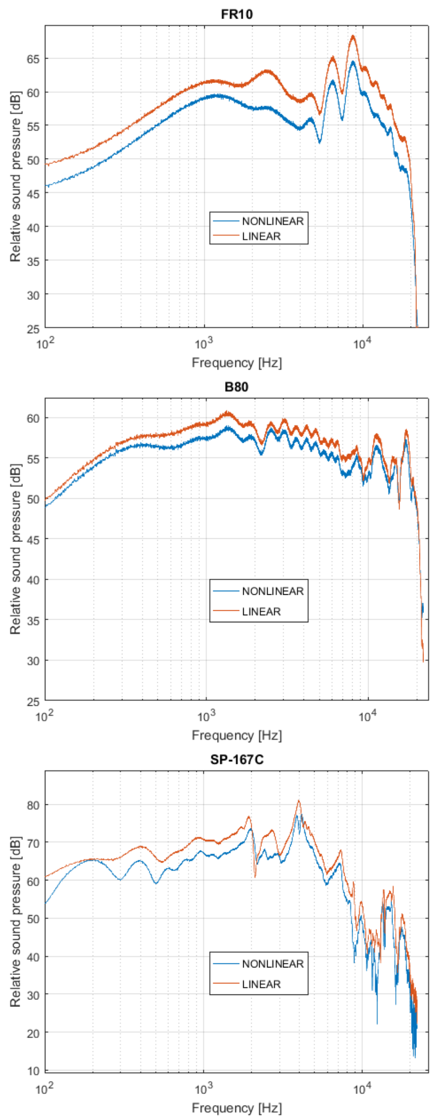

Fig. 10. Measured effect of nonlinearity using proposed test signal for loudspeaker FR10, B80 and SP-167C

From all presented results we can conclude that the new proposed test signal enables lucid observations of loudspeaker deviation from linearity already in time domain. Consequently, a quantification of nonlinearity can be easily performed directly from the measured sound pressure signals.

6. CONCLUSIONS

In this paper, a different identification of nonlinear distortions was presented. We developed a new test signal, which is forcing the operation of the loudspeaker into nonlinear regime. Quick and lucid comparison of loudspeaker drivers and their nonlinearity rate can be performed already in time domain without any need for additional signal processing. A simple nonlinear operator is introduced into the convolution integral, for the purpose of simulating the nonlinear response.

6. REFERENCES

[1] Shoichiro Saito, Akira Nakagawa, and Yoichi Haneda, Dynamic impulse response model for nonlinear acoustic system and its application to acoustic echo canceller, 2009 IEEE Workshop on Applications of Signal Processing to Audio and Acoustics October 18-21, 2009, New Paltz, NY

[2] W. Klippel, Tutorial "Loudspeaker Nonlinearities-Causes, Parameters, Sysmptoms", J. Audio Eng. Soc. Vol. 54, Number 10, pp. 901-939 (2006 Oct.).

[3] Jonathan Kemp, Harel Primack, Impulse response measurements of Nonlinear systems: Properties of existing techniques and wide noise sequences, J.Audio Eng. Soc., Vol. 59, No. 12, pp. 953-963, 2011 December

[4] E. Sturtzer, G. Pillonnet a, G. Lemarquand b, N. Abouchi a, Comparison between voltage and current driving methods of a micro-speaker, Applied Acoustics 73 (2012) 1087–1098

[5] R. Ravaud, G. Lemarquand, T. Roussel, Time-varying nonlinear modeling of electrodynamic loudspeakers, Applied Acoustics 70 (2009) 450–458

[6] B. Merit, G. Lemarquand *, V. Lemarquand, Performances and design of ironless loudspeaker motor structures, Applied Acoustics 71 (2010) 546–555

[7] J. Vanderkooy, W.R. Datars, Nonlinear effects in the de Haas-van Alphen effect, Physics Letters A, Volume 25, Issue 3, 14 August 1967, Pages 258–259

[8] Wei Ji, Woon Seng Gan, Identification of a parametric loudspeaker system using an adaptive Volterra filter, Applied Acoustics 73 (2012) 1251–1262

[9] Marc Rebillat, Romain Hennequin, Etienne Corteel, Brian F.G.Katz, Identification of cascade of Hammerstein models for the description of nonlinearities in vibrating devices, Journal of Sound and Vibration, 330, (2011), pp.1018–1038

[10] Marc Rebillat, Romain Hennequin, Etienne Corteel, Brian F.G.Katz, Identification of cascade of Hammerstein models for the description of nonlinearities in vibrating devices, Journal of Sound and Vibration, 330, (2011), pp.1018–1038

[11] M. J. Reed, M.O.Hawksford, Practical systems modelling using of nonlinear the Volterra audio series, AES 100th convention, 1996, May 11-14, Copenhagen

[12] L. Půst, Nonlinear effects on the rotor driven by a motor with limited power, Applied and Computational Mechanics 1 (2007), pp. 603 – 612

8th Congress of the Alps Adria Acoustics Association
Zagreb, Croatia
20 – 21 September 2018

Hrvatsko akustičko društvo
HAD
Acoustical Society of Croatia

PHYSIOLOGY OF MONAURAL AND BINAURAL MEASUREMENTS OF INFRASOUND

Name(s) of the author(s): Matej Tomc, Aleš Magajne, Gregor Geršak, Samo Beguš

Affiliation (E-mail address): University of Ljubljana, Faculty of electrical engineering, Tržaška 25, 1000 Ljubljana, Slovenija (mt8907@student.uni-lj.si)

Abstract: *A method for measuring human physiological responses to low-frequency and infrasonic pure-tones is presented. The method allows for binaural and monaural measurements, allowing direct comparison of the responses. To avoid subjective perception-based responses of the test persons' physiological measurements were performed by means of a multiparameter system for autonomous nervous system observation. To determine the discomfort levels in test persons, focusing on comparing the binaural and monaural methods, skin temperature, skin conductance and heart rate were measured. The goal of this study was to design and build a measuring system for evaluation of monaural versus binaural measurements using test person's physiology.*

Key words: Infrasound, physiology, binaural, monaural

1. INTRODUCTION

1.1. Infrasound

The term infrasound in used to denote sounds in the sub 20 Hz frequency range. A common misconception is that sounds under 20 Hz are inaudible for humans, hence the word infra, meaning under. However, this is not true. Humans are able to hear sounds down to a few Hertz in frequency given that the amplitudes of these sounds are high enough. Studies have shown that human ear sensitivity is highly dependent on sound frequency. In the infrasound range, this manifests as a need for increasingly higher amplitudes to reach the hearing threshold the lower the sound frequency. The equal-loudness-level contours also get compressed in infrasound frequency range resulting in high changes in perceived loudness despite relatively small changes in sound pressure level [1]. Sounds in the infrasound frequency range also gradually lose their tonal properties and begin to feel discontinuous.[2]

The most common sources of infrasound are thunders, earthquakes, volcanic eruptions and sea waves as well as traffic, aviation, wind turbines and air conditioning [3]. Changes in our lifestyle have resulted in an increase of man-made infrasound sources that are present in our everyday lives. These changes have an impact on the quality of our day-to-day life as well as posing as a potential health hazard [4-10].

1.2. Monaural and binaural hearing

In infrasound frequency range, a large portion of the sensation of full body exposure to sound does not originate from the hearing organ, but rather the vibrations that are felt all over the body. However, the primary and most important sensory organ for detecting infrasound are still ears [15]. Therefore an insert earphone is, while not the best reproduction of real life exposure to infrasound, still an adequate way of producing infrasound and has been a favoured way of producing stimuli for test including infrasound in recent years [11-14].

When using insert earphones a choice of having earphones for both or only one ear is presented. It is commonly accepted that listening to sounds with both ears as opposed to only one gives the person a binaural advantage. The reported binaural thresholds are typically around 3 dB lower than their monaural counterparts. This idea is generally accepted when it comes to normal frequency range, there are differentiating opinions when it comes to infrasound range. While some studies have reported binaural advantage in this range [15, 16], others have found none [13, 17].

1.3. Modern methods in measurements of effects of infrasound on humans

This research is a part of European Metrology Programme for Innovation and Research (EMPIR) project titled Metrology for modern hearing assessment and protecting public health from emerging noise sources, also known as

Ears II for short. The project has two focuses. Firstly, it focuses on further development of ear simulators for adults, children and neonates, following up the already concluded Ears I project. The second focus area is improvement in understanding of human response to infrasound and ultrasound, including assessment methods for potential health risks [10].

Fig.1. Ears II project logo

The EMPIR initiative is co-funded by the European Union's Horizon 2020 research and innovation programme and the EMPIR Participating States

Fig.2. Logo of European Metrology Programme for Innovation and Research (right)

To reach proper understanding of human hearing in infrasound and ultrasound frequency range as well as the effects of these sounds on our health, an interdisciplinary approach is necessary combining audiology, neuroscience and physiology. Technologies such as EEG and fMRI are being combined with traditional audiological methods. These methods are necessary, as differences between human subjective perception of sounds and their physiological response that is based on autonomic nervous response have been found. [19]

2. MONAURAL AND BINAURAL SYSTEM FOR MEASURING EFFECTS OF INFRASOUND

2.1. Measuring set-up

The measuring system was set up at Faculty of Electrical Engineering, University of Ljubljana. To study the effects in a controlled environment, the faculty's anechoic chamber was used [18].

Fig.3. Anechoic chamber at Faculty of Electrical Engineering, University of Ljubljana

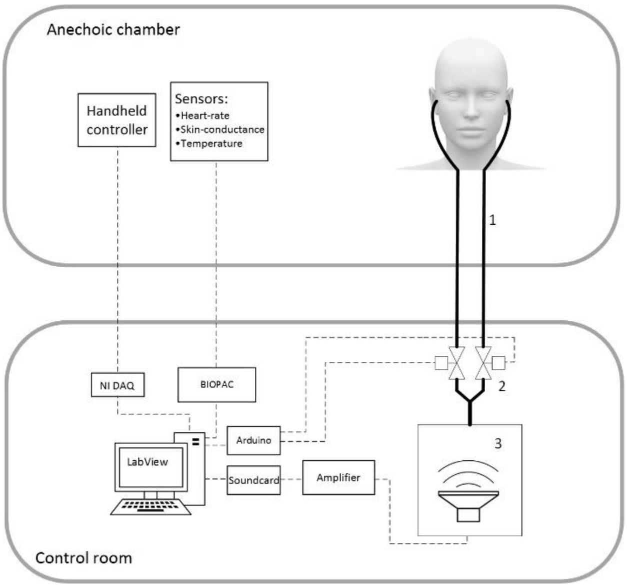

Fig.4. Measuring set-up: 1) Stethoscope headpiece, connected to silicone tubes, 2) Valves, 3) Loudspeaker

To produce pure tones in infrasound frequency range, a loudspeaker with very low harmonic distortion was needed. If the harmonic distortion was too high, there was a danger of test subjects hearing higher harmonic components of the sound, while the sound at original frequency might even remain inaudible. This can happen very easily due to the previously discussed differences in hearing sensitivity at very low frequencies. A suitable loudspeaker was provided by Physikalisch-Technische Bundesanstalt, Braunschweig, Germany, that developed this sound source specifically for the Ears II project [10].
To connect the sound source with an earphone, a silicone hose was used. The short hose led to a Y-splitter. Two hoses were connected to the ends of the splitter and were then through the valves led into the anechoic chamber, where they were connected to the stethoscope headpiece.

Hoses with different lengths, materials and diameters were tested. In the end, a pair of eight meters long Polyvinyl chloride hoses with inner diameter of 4 mm and outer diameter of 6 mm was used. Compared to a softer silicone hose of the same diameter and a polyvinyl chloride hose of a much bigger diameter, the chosen one had a better frequency response as well as the fact that it conducted the least noise from outside the anechoic chamber.

The valves used were manual and were opened and shut using an Arduino controlled servomotor. This meant that the opening and closing of the valves was relatively slow, eliminating the audible pops that would be otherwise produced by shutting solenoid valves. As shown in Figure 5, the valves were effective enough at stopping the sound, so we can confidently say that when the valve of one airway was open and the other closed, the listening experience can be considered monaural. Note that there is no need for the frequency response in Figure 5 to be flat, as the only generated sounds will be pure tones at preprogrammed frequencies.

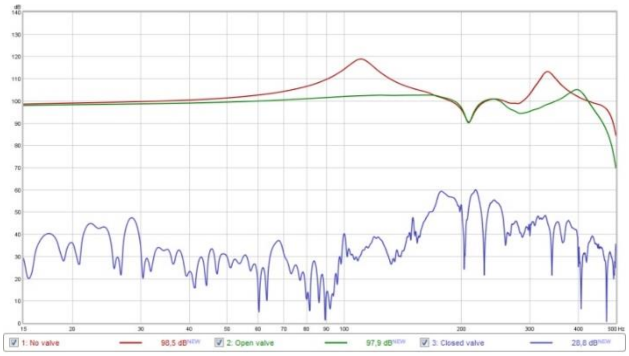

Fig.5. Frequency responses: Blue: closed valve, Green: opened valve, Purple: No valve

In place of traditional earphones, a headpiece of a stethoscope was used. The tubing of stethoscope was removed and the headpiece was connected to the sound carrying hoses.

In the first part of the experiment, some user input is required, so test persons were given a handheld controller that consisted of a rotating potentiometer and a pushbutton.

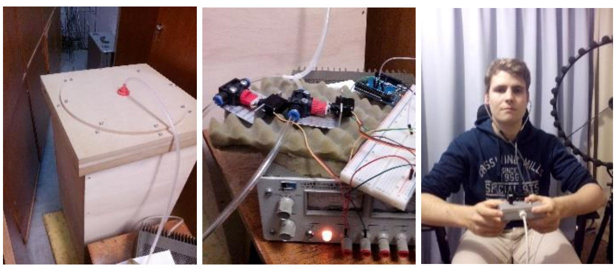

Fig.6. Loudspeaker (left), Y-splitter and valves (middle), a person holding the controller and wearing the earphones

In front of a test person, a screen that displayed the instructions was placed.

For measuring physiological responses of test persons, Biopac MP150 module was used as a data acquisition device. To measure skin conductance and hear-rate modules EDA100C and PPG100C were used respectively. Measurements of skin temperature with SKT100C module were also planned, but were later dropped due to a malfunction of the temperature measuring system.

National Instruments DAQ 2344XX module was used to send trigger signals from the main computer to Biopac and to read values from the handheld controller.

The bulk of the programming was done in LabVIEW 2014, where all audio generation was done. Control of the Arduino that handled the valves was also handled in LabVIEW as well as the handheld controller and the screen. The Biopac MP150 module's software was however incompatible with the main computer's operating system, so the AcqKnowledge 4.1 software was run on another machine. The AcqKnowldege software was also used for the majority of data analysis.

2.2. Test protocol

The test consisted of three parts with first and third part being the same. Research participants were requested to keep the earphones inserted throughout the whole experiment. In the first part, participants were asked to determine their amplitude threshold. The sounds played were pure tone pulses at 125 Hz. Using the handheld controller, the participants adjusted the amplitude of the signal using the potentiometer and confirmed their threshold choice with the pushbutton. The thresholds were determined for both ears three times as well as three times for each ear. Using this data, a better ear was chosen. The ear considered better was the one for which a lower average threshold was determined.

The third part of the experiment was identical to the first one. The purpose of that was to make sure no threshold shifts occurred during the experiment.

The middle part of the experiment was preprogrammed and did not require any user input. It was also the part when the physiological measurements were done. To keep the participant appropriately engaged in the experiment, a relaxing video of a beach scene was played on the screen. This was done to prevent the person's thoughts wandering off resulting in unwanted changes in their physiology.

Following the first part of the experiment, 90 seconds time window of inactivity was included to allow the participants physiology to stabilize. The latter part of this inactivity period was also used to acquire the baseline physiology value of each participant. After that six series of sound pulses were played.

Each series was played with a unique pair of parameters applied to it. The first parameter was frequency, which could assume the values of 8 Hz (infrasound, far from

normal frequency range), 16 Hz (infrasound near normal frequency range) and 125 Hz (in normal frequency range, clearly audible). The second parameter determined the position of the valves meaning the difference between hearing the sounds with both the ears or just the better ear. The six series were not always played in the same order as the Latin square design was used to change up the order with every participant.
Each of the six series was constructed in the same way, barring the aforementioned two parameters. Each series started with a turn of the valves, which produced a quiet humming sound, followed by 30 seconds of silence. This pause was needed to eliminate the reaction to the sound produced by the valves from affecting the physiological results as well as giving time for the physiology to stabilize after the stimuli that had just ended. Following the pause there was a sound signal. The sinusoidal pure sound signal followed the envelope shown in Figure 7. The pulses gradually gradually got louder until they reached the full amplitude. The tested amplitudes were selected in such a manner that the theoretical threshold was crossed in the rising section and the full amplitude signal was theoretically audible. The gradual rise was included for the purpose of reducing the effect of surprise of suddenly hearing a sound at a high amplitude from the physiological response.

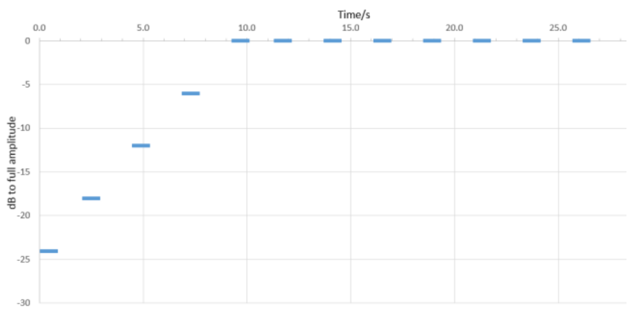

Fig.7. The pulses gradually rise in amplitude.

The signal consisted of pulses of approximately one second of sound followed by one second of silence. Rising the amplitude from zero to the desired value in an instant proved to produce a popping sound side effect, therefore a 0.1-second long linear ramp was added to the beginning and end of each pulse. That successfully eliminated that side effect.
During the second part of the experiment, the physiological data was acquired. Immediately after the testing was concluded, every participant was interviewed in an informal manner. In the free interview, the participants were asked to describe their thoughts and feelings during the experiment, as feelings such as boredom, sleepiness or some other unrelated discomfort could result in faulty experiment data.

2.3. Test persons

Fifteen students (5 women and 10 men) volunteered for the study. None of the participants had ever been diagnosed with any hearing problem.

2.4. Data analysis

The physiological data was first manually reviewed. Moving artefacts were filtered out and the outliers were removed. In 30 % of the signals the heart rate values and especially standard deviation of heart rate was corrupted and discarded because of motion artefacts.
Mean value and standard deviation of skin conductance level (SCL) and heart rate (HR) as well as number and amplitude of skin conductance responses were calculated for the 90 seconds baseline and the duration of each series of sounds. Number of SCR pulses (pulses in skin conductance signal, with amplitudes exceeding 0.02 µS and representing a measure of subject's momentary arousal) and sum of the mean SCR pulse amplitudes were calculated.
Normality was checked using Shapiro-Wilk test and the independent samples equal variances T test was used to compare effects of the monaural and binaural hearing to the subject's physiology. Statistical significance was assumed at $p \leq 0.05$.

2.5. Results

An increase in SCL values and standard deviation of SCL is associated with increase in psychological arousal of the subject. Increased number and amplitude of SCR pulses is also deemed a result of psychological arousal. The same stands for an increase in value of HR and standard deviation of HR (representing heart rate variability).
In short, an increase in aforementioned parameters would suggest a higher level of discomfort and annoyance of a participant. For example, if higher SCL values were measured in monaurally played series of sounds compared to binaurally played series of sounds of the same amplitude and frequency, that would indicate an increase in the participant's discomfort level.

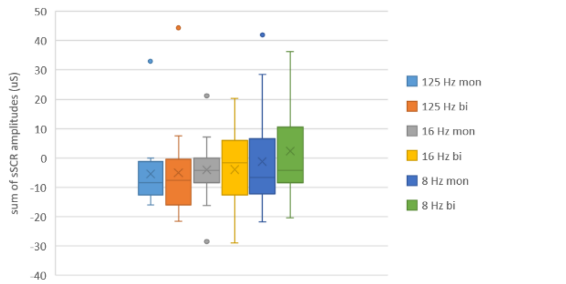

Fig.8. Comparison of sums of SCR amplitudes for different frequencies for monaural and binaural hearing

Physiology	Sound frequency	t value	df	p
SCL	125 Hz	1.186038	28	0.245574
	16 Hz	0.187703	28	0.852463
	8 Hz	0.991527	28	0.32992
stdSCl	125 Hz	0.830926	28	0.413045
	16 Hz	1.189663	28	0.244169
	8 Hz	1.237406	28	0.226213
SCR	125 Hz	0.213857	28	0.832208
	16 Hz	1.187777	28	0.444169
	8 Hz	0.855287	28	0.399652
SCRampl	125 Hz	0.080528	28	0.93639
	16 Hz	0.023826	28	0.98116
	8 Hz	0.586761	28	0.562066
avgHR	125 Hz	0.479043	26	0.635913
	16 Hz	0.159985	26	0.874129
	8 Hz	0.4146	26	0.681835
stdHR	125 Hz	0.084415	28	0.933327
	16 Hz	0.530837	28	0.599718
	8 Hz	0.133207	28	0.894983

Table 1. Comparison of physiological paramteres during monaural and binaural hearing

As seen in table 1 and figure 8, no statistically significant differences between monaural and binaural hearing were found for any of the physiology parameters

3. CONCLUSION

A measuring system for measuring human physiological responses to low-frequency and infrasonic pure-tones was built. The system allows for monaural and binaural testing, as well as a comparison between the two.

When comparing the monaural and binaural measurements in our study, no significant statistical difference in the physiological responses between the monaural and binaural measurement methods was observed.

This leads us to believe that both monaural and binaural are suitable methods when measuring human responses to infrasound. Furthermore, when being interviewed, some participants reported the inability to determine the sound source. Many participants found either 8 Hz or 16 Hz or even both frequencies to be discomforting. The reported discomfort had sometimes also shown itself in the physiological data, but not always. None of them noted that a binaural or monaural experience was particularly better or worse.

4. REFERENCES

[1.] Moller H, Pedersen C S.: **Hearing at low and infrasonic frequencies**, *Noise Health* 2004;6:37-57

[2.] Yeowart N.S., Bryan M.E., Tempest W. (1967): **The monaural M.A.P. threshold of hearing at frequencies from 1.5 to 100 c/s**, *J. Sound Vib*., Vol. 6(3), 335-342

[3.] B. Berglund, P. Hassmén, in R. F. S. Job: **Sources and effects of low-frequency noise**, *J. Acoust. Soc.* Vol. 99, No. 5,pages 2985–3002, May 1996.

[4.] Leventhall H G.: **Low frequency noise and annoyance,** *Noise Health* 2004;6:59-72

[5.] EEA European Environment Agency: **Noise in Europe 2014**, Copenhagen, 2014, ISBN 978-92-9213-505-8.

[6.] Krahé, D. Schreckenberg, F. Ebner, C. Eulitz, U. Möhler: **Machbarkeitsstudie zur Wirkung von Infraschall, Umweltbundesamt**, Dessau, 2014, Online available via http://www.umweltbundesamt.de/publikationen/machbarkeitsstudie-zu-wirkungen-von-infraschall.

[7.] HPA Health Protection Agency (UK) 2010: **Health effects of exposure to ultrasound and infrasound (RCE-14) – Report of the independent Advisory Group on Non-ionising Radiation**. ISBN 978-0-85951-662-4. Online available via the website of the Health Protection Agency http://www.hpa.org.uk/

[8.] Salt, A. N. & Lichtenhan, J. T.: **How Does Wind Turbine Noise Affect People?,** *Acoustics Today*, 2014, 10, 20 – 27.

[9.] Kaczmarska A., Łuczak A.: **A Study of Annoyance Caused by LowFrequency Noise During Mental Work**, *International Journal of Occupational Safety and Ergonomics (JOSE)* 2007, Vol. 13, No. 2, 117–125

[10.] Ears ll: The Project. Online avalible via: https://www.ears-project.eu/ears2-project.html. [23.5.2018].

[11.] Weichenberger M, Bauer M, Kühler R, Hensel J, Forlim CG, Ihlenfeld A, et al. (2017): **Altered cortical and subcortical connectivity due to infrasound administered near the hearing threshold – Evidence from fMRI**. PLoS ONE 12(4): e0174420.

[12.] Weichenberger M, Kühler R, Bauer M, Hensel J, Brühl R, Ihlenfeld A, Ittermann B, Gallinat J, Koch C, Sander T, Kühn S.: **Brief bursts of infrasound may improve cognitive function--An fMRI study** Hearing research 328, 87-93 (2015)

[13.] Robert Kühler, Thomas Fedtke and Johannes Hensel: **Infrasonic and low-frequency insert earphone hearing threshold**, *J Acoust Soc Am* 137(4), 2015

[14.] Martin Bauer, Tilmann Sander-Thömmes, Albrecht Ihlenfeld, Simone Kühn, Robert Kühler and Christian Koch: **Investigation of perception at infrasound frequencies by functional magnetic resonance imaging (fMRI) and magnetoencephalography**

(MEG), *Congress on Sound and Vibration*, ICSV 22 (2015)

[15.] Yeowart N.S., Evans M.J. (1974): **Thresholds of audibility for very low-frequency pure tones**, *J. Acoust. Soc. Am.*, Vol. 55(4), 814-818

[16.] Anderson C.M.B., Whittle L.S. (1971): **Physiological noise and the missing 6 dB**, *Acustica*, Vol. 24, 261-272

[17.] Sivian L.J., White S.D. (1933), On minimum audible sound fields, J. Acoust. Soc. Am., Vol. 4, 288

[18.] Rosana Černelič, **Merjenje akustičnih karakteristik gluhe sobe in snemalnega studia**, diplomsko delo, Univerza v Ljubljani, Fakulteta za elektrotehniko, Ljubljana: 2015.

[19.] Carol L. Mackersie, Imola X. MacPhee, and Emily W. Heldt: **Effects of Hearing Loss on Heart Rate Variability and Skin Conductance Measured During Sentence Recognition in Noise**, *Ear Hear*, 2015 Jan;36(1):145-5

8th Congress of the Alps Adria Acoustics Association
Zagreb, Croatia
20 – 21 September 2018

Hrvatsko akustičko društvo
HAD
Acoustical Society of Croatia

EVALUATION OF COMMERCIAL SOFTWARE FOR CALCULATING AND REPORTING MEASUREMENTS IN ACOUSTICS

Biljana Tanatarec

Centar za mjerenja u okolišu d.o.o. (btanatarec@cmo.hr)

Abstract: *Sound measuring systems mainly consist of microphone, electronic amplifier, frequency weighting possibilities and software for data acquisition and analysis. Sometimes commercial software does not fulfil its intended use described in technical documentation. Evaluation of commercial software available today on the market and used for acoustic measurements will be described in this paper through three case studies. Root cause analysis has shown that commercial software does not always follow the changes given in new editions of different standards. Also, changes of commercial software made by manufacturer are not always efficiently checked and verified before the software is placed on the market. A part of the problem related with maladjusted commercial software is from manufacturers' use of outdated hardware.*

Key words: sound measuring system software, evaluation of commercial software

1. INTRODUCTION

When ordering a measuring device you are expecting that all parts of the device are working properly as it was declared in manufacturer's documentation. The user of newly bought equipment may check hardware and connectors to see if they work. But what is the situation with software? User of a measuring device usually is not software expert and he does not have the knowledge of software codes and programming language or he is not able to make changes or to adjust software included in complete package of measuring system. The user can only assume that something is wrong. Three real life situation examples on using different software will be described in this paper. Some advices and precautionary measures of what to do when one finds himself in similar situations will also be given.

2. THREE CASE STUDIES

2.1. 1st Case Study – Software is not compatible with new International Standard

A company bought a complete set of equipment to measure airborne and impact sound insulation within buildings and of building elements. This measuring system has been compatible with international standards series ISO 140, *Acoustics -- Measurement of sound insulation in buildings and of building elements*. In 2014 four standards from that series ISO 140-4:1998, ISO 140-5:1998, ISO 140-7:1998 and ISO 140-14:2004 were withdrawn and replaced with ISO 16283-1:2014, *Acoustics -- Field measurement of sound insulation in buildings and of building elements -- Part 1: Airborne sound insulation* [1.]. Later, in year 2017 ISO issued amendment to aforesaid international standard ISO 16283-1:2014/Amd1:2017 [2.]. In year 2015 ISO issued ISO 16283-2:2015 *Acoustics -- Field measurement of sound insulation in buildings and of building elements – Part 2: Impact sound insulation* [3.].

Manufacturer of equipment used for impact sound insulation measurements has issued a new upgrade of software so that it could be compatible with international ISO 16283-2:2015 standard. This upgrade has been included as an option in drop-down menu of built in software of sound level meter where one can choose available international or national standard on which the measurements and calculations are based upon.

In June 2016, more than half a year after ISO 16283-2:2015 was issued, during the laboratory preparation process for building acoustics measurements and testing of a new software, head of a laboratory noticed that software ordered and paid for did not work properly when in drop-down menu option ISO 16283-2 was selected. But the software worked well when option for obsolete ISO 140 was selected. Head of laboratory wrote to manufacturer on one of his contact addresses and quickly received an answer with a request to send documentation which supports his findings. After measurement examples, detailed description of a problem and photo documentation were sent to manufacturer, in a week the answer was received. Manufacturers' officer stated that they received some other complaints on the same mater and that they will solve the problem as soon as possible. In a few months a new upgrade of improved software was released and it worked impeccably at least until new upgrade was released. This leads to the second problem user encountered.

2.2. 2nd Case Study – Software worked well before an Official Update and not at all after installation

In the beginning of year 2018 manufacturer decided to release new enhanced upgrade of software with various bug fixes and his decision was not based on new standard issues regarding building acoustics. After user installed a new release of software for calculating and reporting measurements of impact sound insulation it did not work again. This happened more than 2 years after ISO 16283-2:2015 standard was released. Once again, user contacted manufacturer and described what the problem was. While manufacturer is still fixing that problem, a new edition of international standard ISO 16283-2:2018 *Acoustics -- Field measurement of sound insulation in buildings and of building elements – Part 2: Impact sound insulation* [4.] was published in May 2018 and it withdraws and replaces ISO 16283-2:2015 standard. It remains to see when the user will actually be able to utilize the software and equipment for its intended use.

2.3. 3rd Case Study – Obsolete Hardware Connection

Noise dosimeter is a device used for measurements of cumulative sound pressure levels over a period of time to help assess noise exposure of a person. Noise dosimeter consists of sound level meter and microphone in a small robust housing which can be mounted on the shoulder of the worker who is working in noisy working environments.

Problem arose when measurer tried to transfer collected data on a portable computer. Measurer used purchased commercial software for post processing and calculation of personal noise exposure. With aforesaid software, measurer should be able to connect dosimeter to a PC using infra-red light and transport all data collected. However, since the infra-red to USB cable imitates a serial RS 232 connection via software, measurer had not been able to identify the right COM port that was assigned to that cable. Measurer tried many times over and over again to identify the right serial port which could be used for transportation of data. He had not succeeded. Although, a connection from PC to dosimeter was established (because time and date from PC was transferred), the connection vice versa failed and data from dosimeter could not be submitted to further statistical calculations. The only way to read data from the device is to check screen of dosimeter and see a few selected and already calculated noise parameters only for the one most recent measurement. And that kind of data is completely useless, since analysis of working day of a person that wore a noise dosimeter was impossible. When a new measurement starts it is impossible to read data from previous measurement.

3. LEGAL STATUS OF RELATIONSHIP MANUFACTURER-USER

Does manufacturer have any obligations to his customer ones the equipment and software is bought? Answer to this question may be found in two international standards which describe a process on putting products on the market:

1. ISO/IEC 17050-1:2004, *Conformity assessment — Supplier's declaration of conformity — Part 1: General requirements* [5.] In publicly available introduction of this standard is written: "This part of ISO/IEC 17050 has been developed with the objective of providing general requirements for a supplier's declaration of conformity. It addresses one of the three types of attestation of conformity, namely attestation undertaken by the first party (e.g. the supplier of a product). Other types are second-party attestation (e.g. where a user issues an attestation for the product the user is using) or third-party attestation. Each of these three types is used in the market in order to increase confidence in the conformity of an object. This part of ISO/IEC 17050 specifies requirements applicable when the individual or organization responsible for fulfilment of specified requirements (supplier) provides a declaration that a product (including service), process, management system, person or body is in conformity with specified requirements, which can include normative documents such as standards, guides, technical specifications, laws and regulations. Such a declaration of conformity can also make reference to the results of assessments by one or more first, second or third parties. Such references are not to be interpreted as reducing the responsibility of the supplier in any way. These general requirements are applicable to all sectors. However, these requirements might need to be supplemented for specific purposes, for example for use in connection with regulations. A supplier's declaration of conformity of a product (including service), process, management system, person or body to specified requirements can be substantiated by supporting documentation under the responsibility of the supplier. In cases where this is desirable, or necessary, reference is made to ISO/IEC 17050-2".

2. ISO/IEC 17050-2:2004, *Conformity assessment — Supplier's declaration of conformity — Part 2: Supporting documentation* [6.]. In publicly available introduction of this standard is written: "A supplier's declaration of

conformity is a form of attestation of conformity to meet demands from the market and regulators for confidence. The acceptance of a supplier’s declaration of conformity could be enhanced by retaining documented information on which the supplier bases the declaration and making this documentation available upon request. This part of ISO/IEC 17050 specifies requirements for the documentation to support a supplier’s declaration of conformity. Besides enhancing confidence in the supplier's declaration of conformity, such documentation may assist relevant authorities in their surveillance activities. Conformity of a product (including service), process, management system, person or body to specified requirements, which can include normative documents such as standards, guides, technical specifications, laws and regulations, may need to be rigorously substantiated under the responsibility of the supplier, irrespective of the industry sector involved.”

Both international standards are accepted in European standardization by two European organizations for standardization, CEN and CENELEC, and they make a part of possible citations or references in legislative documents throughout the whole Europe. All organizations which supply goods or services and the competent authorities to ensure that products made available on the market conform to the requirements given in applicable standards.

3. CONCLUSION

A problem always occurs when a new measuring device is not working properly as it was described in manufacturers´ documentation. In first case study, manufacturers´ implementation of requirements given in the new ISO 16283-2 standard was and is very slow and it ultimately leads to customer dissatisfaction. Additional problem occurs when newly upgraded software, which initially worked, is not working anymore. Also, another problem occurs when a measuring device was advertised as consistent with a new ISO standard, which obviously it was not. User is not in possession of original software codes or any other tool to check its rightfulness. He can only detect problem, communicate with manufacturer and wait for its solution. Aforementioned cases give us a warning that quality control and even quality system of manufacturer is not always as customer would expect. Those cases may be sources of customer complaints and they may ultimately lead to downgraded manufacturers´ position in the market.

The third case was a strange one. Why manufacturer thought that imitation of a serial RS-232 connection via software is necessary, customer could not comprehend. A serial RS-232 connection is very old and outdated solution, not used in new devices and even younger users do not have any knowledge of it. Not to mention that transferring data became much more complicated, assuming it works at all. Better and recent solutions about data transfer to avoid imitation of serial ports are welcomed.

4. REFERENCES

[1.] International Standard ISO 16283-1:2014, ***Acoustics -- Field measurement of sound insulation in buildings and of building elements -- Part 1: Airborne sound insulation,*** International Organization for Standardization (ISO), Geneva, 2014

[2.] International Standard ISO 16283-1:2014/Amd1: 2017, ***Acoustics -- Field measurement of sound insulation in buildings and of building elements -- Part 1: Airborne sound insulation – Amendment 1,*** International Organization for Standardization (ISO), Geneva, 2017

[3.] International Standard ISO 16283-2:2015 ***Acoustics -- Field measurement of sound insulation in buildings and of building elements – Part 2: Impact sound insulation,*** International Organization for Standardization (ISO), Geneva, 2015

[4.] International Standard ISO 16283-2:2018, ***Acoustics -- Field measurement of sound insulation in buildings and of building elements -- Part 2: Impact sound insulation,*** International Organization for Standardization (ISO), Geneva, 2018

[5.] International Standard ISO/IEC 17050-1:2004, ***Conformity assessment -- Supplier's declaration of conformity — Part 1: General requirements,*** International Organization for Standardization (ISO), Geneva, 2004

[6.] International Standard ISO/IEC 17050-2:2004, ***Conformity assessment -- Supplier's declaration of conformity — Part 2: Supporting documentation,*** International Organization for Standardization (ISO), Geneva, 2004

Hrvatsko akustičko društvo
Acoustical Society of Croatia

MEASUREMENT UNCERTAINTY IN THE FIELD OF ENVIRONMENTAL NOISE AND BUILDING ACOUSTIC MEASUREMENTS: EXPERIENCE FROM INTERLABORATORY COMPARISONS

Antonio Petošić[1], Petar Franček[1], Mario Štrbac[1], Peter Zaťko[2], Daniel Urbán[3], Daniel Szabó[4]

[1] University of Zagreb, Faculty of Electrical Engineering and Computing, Unska 3, 10 000 Zagreb
[2] A&Z Acoustics s.r.o., Repašského 2, 84102 Bratislava, Slovakia (antonio.petosic@fer.hr)
[3] Department of Physics, FEE, CTU Prague, Technicka 2, 166 27 Prague, Czech Republic
[4] Slovak University of Technology in Bratislava, Department of Building Construction, Radlinského 11, 81368 Bratislava, Slovakia

Abstract: *In this paper the problem of measurement uncertainty in acoustic measurements has been discussed regarding the results of interlaboratory comparison (ILC). The measurement results of ILC in the field of environmental noise and in the field of sound insulation measurements (airborne and impact) have been examined regarding the proposed methods for calculation standard deviations in repeatability and reproducibility conditions. In the field of environmental noise measurements, of point sound source, the measurement results (19 laboratories) precision and accuracy are discussed regarding the microphone positions (on the reflection plane and close to the reflection plane). The results for expanded measurement uncertainty calculations, obtained following instructions from old ISO 1996-2:2007 and new ISO 1996-2017 are compared and discussed. In the field of building acoustic measurements the measured parameters of airborne and impact sound insulation (31 laboratories, 5 independent measurements) are compared regarding the obtained mean values and measurement uncertainties by removing outliers and finding standarddeviations in repeatability and reproducibility conditions according to ISO 5725-2 and ISO 12999-1:2014 and by approach described in GUM adopted for input parameters in each individual measurement and calculating overall standard uncertainty. In addition, the possibility to measure airborne sound insulation parameters by using acoustic camera has been considered regarding averaging the large number of measurement microphone positions in source and receiving room and finding measurement uncertainties for sound pressure levels and reverberation times in large number of measurement positions.*

Key words: environmental noise parameters, building acoustic measurements, expanded measurement uncertainties calculations for each independent measurement and by using ILC results.

1. INTRODUCTION

The accreditation procedure according to ISO 17025:2017 for laboratories which are doing acoustic measurements (in the field of environmental noise, sound insulation measurements) is tedious task [1]. They have to verify and validate they own procedures according relevant international standards which can be changed every few years. Quality control is the main motive of individual laboratories to cooperate in the ILC but it can be used to make detail analysis of all individual results of laboratories included in environmental noise and sound insulation parameters measurements [2]. All of these laboratories certify the environmental noise parameters of the noise sources (industrial and small workshop sites, road, rail and air traffic), and sound insulation performance of different building elements for external customers. In addition to measurements, the calculation procedures like estimating the environmental noise by knowing sound power of sound sources determined according to ISO 3744:2010 [3] or estimating the sound insulation parameters of building structures according ISO 12354-1,2,3:2017 [4-6] can also be in the field of accreditation.

1.1. Measurement of environmental noise parameters

The environmental noise measurements are conducted now in accordance to the ISO 1996-2:2017 [7]. The special attention has to be provided regarding measurement accuracy and precision due to influence of measurement equipment, procedures and people who are conducting the measurements and making reports.

The main influence on measurement accuracy and uncertainty according to the new ISO 1996-2:2017 [7] standard are different regimes of sound source working and meteorological conditions when noise levels are measured at longer distances from the source in some particular part of the year.

The interlaboratory comparison has been organized in 2015. by Croatian Acoustic Society for 19 labs which have accreditation according ISO 17025:2005 in the field of environmental noise measurements. They usually measure the environmental noise parameters defined in ISO 1996-1:2016 [8] ($L_{A,eq}$, $L_{1,}L_{95}$, $L_{C,peak}$) from the new sound source in the environment with some residual noise at short distances without significant influence of meteorological conditions (wind speed and direction).

In this paper the measurement results of 19 labs are presented with obtained measurement uncertainty for each individual lab and overall uncertainty obtained for ILC comparison without outliers. The measurement uncertainties for considered measurement situation (small distances) are compared with calculations described in old ISO 1996-2:2007 [9] and new ISO 1996-2:2017 standard [7]. The overall measurement uncertainty is discussed and compared with each individual lab measurement uncertainty. The results for background noise and noise source are presented for two different measurement positions (in front of the reflecting surface and on the reflecting surface).

1.2. Measuring building acoustic parameters

In the field of building acoustics the sound insulation parameters are measured according ISO 16283-1:2014 [10], ISO 16283-2:2016[11] and ISO 16283-3:2016 [12] standards with measurement uncertainty calculated from ISO 12999-1:2014 standard [13]. Each one of lab (31 participants) performed five independent measurements of airborne sound insulation parameters (sound reduction index, standardized sound level difference, in repeatability condition by changing microphone positions when sound pressure levels and reverberation times are measured in each individual measurement) on the measurement object (lightweight partition) according IS0 16283-1:2014 and during measurement of impact sound insulation parameters of floating floor (normalized and standardized impact sound pressure levels) according to [11].

There are two different approaches in measurement uncertainty calculations described in [13]. The first calculation method for measurement uncertainty is based on standard deviations in reproducibility conditions determined from several interlaboratory comparisons according to the ISO 5725-2:1994 [14].

The second approach is based on measurement uncertainty calculations for each individual measurement of sound insulation parameters [15]. In this approach described in [15] the standard deviations and measurement uncertainty are determined from all measured parameters (sound pressure levels in the source and receiving room, reverberation time, the influence of instruments' measurement uncertainty is taken into account).

The problem with single-number values for sound insulation parameters and their uncertainties determined according to ISO 717-1:2013 [16,17] and ISO 717-2:2013 are described in [18, 19]. There is a big problem to find correlation coefficients for different types of testing objects (separating walls) between one-third octave bands in the frequency range of interest (50 Hz-5000 Hz) for determination of weighted sound insulation parameters uncertainties.

In this work the results of 31 laboratories are presented with their individual measurement uncertainty determined as standard deviations in repeatability conditions. Also overall measurement uncertainty from all measurement results without outliers has been determined according to [13].

2. THEORETICAL BACKGROUND FOR UNCERTAINTY CALCULATIONS

In agreement with modern statistical methods, the concepts of standard deviations in repeatability and reproducibility conditions have been used to state the precision of the measurements carried out according to a testing methods.

2.1. General statistics

Assuming a measurand Y is going to be determined from N measurements of independent variables X_1, X_2, X_3,.., X_N, then Y will be a function of those quantities which can be written with equation (1).

$$y=f(X_1,X_2,X_3,..X_k....X_N) \tag{1}$$

The values x_1, x_2, x_3,.., x_n are estimates of the input quantities X_1, X_2, X_3,.., X_N, as a consequence each estimate, x_i, will have an uncertainty associated, $u(x_i)$, which is expressed from experimental standard deviation given with eq. 2 [7].

$$\sigma = s(x_i) = \sqrt{\frac{1}{N-1} \cdot \sum_{k=1}^{n} (x_i - \bar{X})^2} \tag{2}$$

Standard measurement uncertainty is in general statistics defined as experimental standard deviation of mean value of each measured parameter by using eq. (3). The standard deviation of mean value is given by the standard deviation of the observations divided by the square root of the number of observations.

$$u(x_i) = \frac{s(x_i)}{\sqrt{N}} \quad (3)$$

The equation (3) for experimental standard deviation in repeatability conditions is valid if the difference between measured values (expressed in dB) are small. In the general case the more correct equation is given by using eq (4) when measured quantities are converted to relative numbers and vice verse [7]:

$$u(x_i) = 10 \cdot log_{10}\left(10^{0,1 \cdot L_k} + S(x_i)\right) - L_k \quad (4)$$

where L_k is energy averaged sound pressure level of N_m independent measurements in the meteorological and emission window according to eq. 5 [7].

$$L_k = 10 \cdot log_{10}\left(\frac{1}{N_m} \cdot \sum_{i=1}^{N_m} 10^{0.1 \cdot L_i}\right) \quad (5)$$

This equation is valid only if each of the independent measurements last equal time. If the independent measurements last non-equal in time then additional time weighting should be used when calculating averaged value. $S(x_i)$ is obtained with eq. (2) converting the measurands in dB into relative numbers according to the eq (6).

$$S(x_i) = \sqrt{\frac{1}{n-1} \cdot \sum_{k=1}^{n} \left(10^{\frac{L_i}{10}} - 10^{\frac{L_k}{10}}\right)^2} \quad (6)$$

$u(x_i)$ is the standard measurement uncertainty for each individual measurand. The overall measurement uncertainty is given for the case if there is no correlation with eq.(7).

$$u = \sqrt{\sum_{i=1}^{N} \left(\frac{\partial f}{\partial x_i}\right)^2 \cdot u^2(x_i)} \quad (7)$$

If the measured variables are correlated then the equation is a little bit complicates and is given with eq. (8).

$$u = \sqrt{\sum_{i=1}^{N} \left(\frac{\partial f}{\partial x_i}\right)^2 \cdot u^2(x_i) + 2\sum_{i=1}^{N-1} \sum_{j=i+1}^{N} \frac{\partial f}{\partial x_i} \cdot \frac{\partial f}{\partial x_j} \cdot u(x_i, x_j)}$$

(8)

There is a big problem to find correlation coefficient $r(x_i,x_j)$ between individual measurands defined with eq. (9).

$$r(x_i, x_j) = \frac{u(x_i,x_j)}{u(x_i) \cdot u(x_j)} \quad (9)$$

If the estimates x_i and x_j are independent, $r(x_i, x_j) = 0$, and a change in one does not imply an expected change in the other.

It should be noted that in new ISO 1996-2:2017 and old ISO 1996-2:2008 the measurement uncertainty in repeatability conditions is defined with equation (7) by assuming sensitivity coefficients of 1.

There is also interesting research about the influence on logarithmic values on the PDF functions for A-weighted equivalent continuous sound pressure levels for the traffic noise [20]. It is shown that PDF function with logarithmic values is asymmetric around mean value (arithmetic or logarithmic) so special attention should be aimed in detection of outliers assuming apriori normal distribution of measurands. The similar is observed when impact sound insulation parameters are measured and distributions for normalized and standardized sound pressure levels at different frequencies are shown in [21].

2.2. Detection of outliers in ILC

The results of several independent measurements are averaged and the mean value of interest is checked with Grubb's statistics and standard deviations should be checked with Cochran's statistics [14].

Cochran's test is used to check if there are cell standard deviations of several (n≥5) independent measurements exceptionally large and would inflate the estimate of the repeatability standard deviation if retained.

Grubb's test is used to check if there are means in laboratory results that are exceptionally high or low and would inflate the estimate of the reproducibility standard deviation if retained.

The treatment of outliers is dealt with in clause 7 of ISO 5725-2 [14], particularly in clauses 7.1 to 7.3. An outlier can be considered as a result which is sufficiently different from all other results to warrant further investigation. When carrying out the outlier tests, it should be understood that outliers should not be discarded or rejected purely from a statistical point of view.

After Cochran's test has been carried out, the tabulated mean values for each particular level of interest are arranged where results with bad standard deviations are removed from calculations. Several Grubbs' tests are then carried out.

Firstly, the test is carried out to establish whether the highest or lowest mean value can be identified as a single outlier. If an outlier is indicated, it is discarded and the test is repeated for the other extreme value. For a particular level of interest, Grubbs' test for one outlier enables the calculation of the quotient of the difference between the suspect value and the mean of all the values for that level, and the standard deviation of all values. This ratio is then compared with computed or tabulated (critical) ratio values at 95 % and 99 % confidence levels.

In the environmental noise parameters measurements' analysis, the measurement uncertainty (not standard deviation) for equivalent A-weighted value under repeatability conditions (the same operator with same instrument makes the several measurements **at the same position**) have been compared, together with expanded measurement uncertainty of each individual lab (which was approximately the same ±3,6 dBA for each laboratory). In addition the measurement uncertainty calculation according the new standard ISO 1996-2:2017 on the same measurement situation is calculated.

In the building acoustics parameters measurements the five independent measurement have been done under repeatability conditions (the same operator, the same equipment, the different positions of microphone in the source and receiving rooms). The standard deviations and means value of each individual lab are tested by using Cohran and Grubbs statistics according ISO 5725-2:1994 and overall mean and measurement uncertainty has been found as well as the individual measurement uncertainty of each lab participated into interlaboratory comparisons.

It should be noted that repeatability conditions are not defined in the same way for environmental noise parameters measurements (at the same measurement position according ISO 1996-2:2008, ISO 1996-2:2017) and different positions when sound pressure levels for building acoustics parameters determination are measured.

It should be also noted that standard uncertainty of the measurement results for environmental noise parameters (*L'*-parameter measured form source with residual noise, L_{res}-residual noise measurement result) and for sound insulation parameters is defined in different ways. Measurement uncertainty for building acoustics parameters determined by verification of labs' own procedure is defined as standard deviation *s* (eq. 2), not as experimental standard deviation of mean as *u* (eq. 3.) for environmental noise parameter results.

2.3. Environmental noise parameters measurement uncertainty calculations

In the environmental noise parameters measurement uncertainty calculations, it is assumed that there are no correlation between parameters and overall uncertainty budget depends on sound source itself, other sources which cause background noise, propagation path uncertainty due to different meteorological conditions and measurement chain at the receiver point and also the measurement position (free field, close to the reflection surface and on the reflection surface). The functional equation L=f(L',L_{res}) between measurand L' (under the influence of residual noise) and estimated value noise level from the source L during the specified conditions for which a measured value is wanted is derived according eq. (10).

$$L = L' + \delta_{slm} + \delta_{sou} + \delta_{met} + \delta_{loc} + \delta_{res} \quad (10)$$

where δ_{slm} is the error due to the measurement chain (sound level meter in the simplest case),

δ_{sou} is the error due to deviations from the ideal operating conditions of the source,

δ_{met} is the error due to meteorological conditions and ground conditions deviating from the ideal conditions, this is changeable part so that is the reason why the measurements are divided in meteorological classes.

δ_{loc} is the error due to the selection of receiver position and δ_{res} is the error due to residual noise. Each source of error is function of each several other sources of error. The clear derivation is only for measured value under the influence of residual noise given in eq. (11-14).

It is assumed that intensity of two sources (residual noise and sound source) is the same as SPL in the far field (which is usually not true for low frequencies in spectrum) but for equivalent levels it is true assumption as well as assumption that these two noise sources are not correlated. The derivation for the influence of residual noise on the true value is given with eq. (11-16).

$$I = I' - I_{res} \quad / \cdot \frac{1}{I_0}, \frac{I}{I_0} = \frac{I'}{I_0} - \frac{I_{res}}{I_0} \quad (11)$$

$$10 \cdot log_{10}\left(\frac{I}{I_0}\right) = 10 \cdot log_{10}\left(\frac{I'}{I_0} - \frac{I_{res}}{I_0}\right) \quad (12)$$

$$L \ = 10 \cdot log_{10}\left(\frac{I}{I_0}\right), L' = 10 \cdot log_{10}\left(\frac{I'}{I_0}\right), \quad (13)$$

$$L_{res} = 10 \cdot log_{10}\left(\frac{I_{res}}{I_0}\right) \quad (14)$$

$$L = 10 \cdot log_{10}\left(10^{\frac{L'}{10}} - 10^{\frac{L_{res}}{10}}\right) = 10 \cdot log_{10}\left(10^{\frac{L'}{10}}(1 - 10^{\frac{L_{res}-L'}{10}})\right) \quad (15)$$

$$L = 10 \cdot log_{10}\left(10^{\frac{L'}{10}}\right) + 10 \cdot log_{10}(1 - 10^{-0,1\cdot(L'-L_{res})})$$

$$L = L' + 10 \cdot log_{10}(1 - 10^{-0,1\cdot(L'-L_{res})}) \quad (16)$$

The sensitivity coefficients for each parameter are given with equation (17) and (18).

$$c_{L'} = \frac{\partial L}{\partial L'} = \frac{1}{1-10^{-0,1\cdot(L'-L_{res})}} \quad (17)$$

$$c_{L_{res}} = \frac{\partial L}{\partial L_{res}} = \frac{-10^{0,1(L'-L_{res})}}{1-10^{-0,1\cdot(L'-L_{res})}} \quad (18)$$

The overall uncertainty will be expressed as an expanded uncertainty *U*. This quantity will, with a statement of confidence, define an interval where the measurand Y will be. This will be obtained by multiplying the combined standard uncertainty by a numerical factor, known as the coverage factor, k given with equation (19).

$$U = k \cdot u \quad (19)$$

A coverage factor of 2 is normally used, which corresponds to a coverage probability of 95% for environmental noise measurements and coverage factor k=1 with one side coverage probability of 84%.

The measurement uncertainty budget in the new ISO 1996-2:2017 standard is rather complicated even for simple situation and in the case compared to the old standard for A-weighted continuous equivalent sound pressure level. The measurement uncertainty in old standard ISO 1996-2:2007 is given by eq. (20) for A-weighted equivalent sound pressure level.

$$u = \sqrt{1^2 + X^2 + Y^2 + Z^2} \quad (20)$$

Where 1 dB(A) is measurement uncertainty because of instruments (1 class), it can be different operator, different equipment, same measurement place.

X- measurement uncertainty due to under repeatability conditions. It should be determined from at least 3 and preferably 5 measurements under repeatability conditions (the same measurement procedure, the same instruments, the same operator, the same place) and at a position where variations in meteorological conditions have little influence on the results;

Y- this value will vary depending upon the measurement distance and the prevailing meteorology. A method using a simplified meteorological window is provided in Annex A of the Standard ISO 1996-2:2006 (in this case $Y = \sigma_m$). For long-term measurements different weather categories will have to be dealt with separately and then combined together. For short-term measurements variations in ground conditions will be small. However, for long-term measurements, these variations may add considerably to the measurement uncertainty.

Z- The value will vary depending on the difference between measured total values and the residual sound.

This component of measurement uncertainty is derived in [22] assuming that there is no difference in residual noise when measurement of the source noise ($L_{res,\ during}$) and when there is no noise from the source ($L_{res.after}$) is given with eq. (21).

$$L = 10 \cdot log_{10}\left((10^{\frac{L}{10}} + 10^{\frac{L,res,during}{10}} - 10^{\frac{L_{res,after}}{10}}\right) \quad (21)$$

The total measurement uncertainty due to influence of the residual noise is given by equation (22).

$$Z = \sqrt{2} \cdot u_{res} \cdot 10^{0,1 \cdot (L_{res,after} - L\ \ )} \quad (22)$$

When several measurements are done averaged values for residual noise and corrected noise levels from the source are included in equation (22). The laboratories usually measure the overall level with the source turned on and then turn off the source and measure residual noise several times after. They usually don't do turning on and off the source because this is not possible in practical situations.

The measurement uncertainties for all labs in repeatability conditions for A-weighted equivalent continuous sound pressure level have been calculated in this way for each individual lab where only a small difference in X and Z contribution and two other contributions (instrumentation, meteorological influence) same has been done for overall results. The similar calculation for considered situation is repeated according to the recommendations in the new ISO 1996-2:2017 standard.

The quantities and uncertainty budget are given for simple situation according ISO 1996-2:2017 are given in **Table 1.** The measurement uncertainty due to instruments (Class 1) is reduced on 0,5 dB(A) and sensitivity coefficient for source and sound level meter are added. There are other factors having influence on the measurement uncertainty (meteorological conditions, location of measurement position).

Table 1. a) Uncertainty budget according new ISO 1996-2:2017 [7]

Quantity	Estimate (dB)	Standard uncertainty u (dB)	Sensitivity coefficient
$L' + \vartheta_{slm}$	L'	0,5	$\frac{1}{1 - 10^{-0,1 \cdot (L' - L_{res})}}$
ϑ_{sou}	0	u_{sou}	1
ϑ_{met}	0	u_{met}	1
ϑ_{loc}	0-6	u_{loc}	1
$L_{res} + \vartheta_{res}$	L_{res}	u_{res}	$\frac{-10^{0,1(L' - L_{res})}}{1 - 10^{-0,1 \cdot (L' - L_{res})}}$

ϑ- are input quantities to allow for any uncertainty from assumed operating condition of the source, assumed meteorological conditions and residual noise.

In the standard [7] it is not clearly written that *u* are standard deviation of mean value and not standard deviation value. The standard deviation of mean value is obtained by dividing standard deviation with number of observations.

2.4. Building acoustics parameters measurement uncertainty

The measurement uncertainty calculations for building acoustic parameters are defined in standard ISO 12999-1:2014 by using standard deviations in reproducibility conditions determined experimentally from different interlaboratory comparisons. The laboratory verifies their own measurement procedure by doing measurements in repeatability conditions (with changed positions of microphones and comparing their results with standard deviations in repeatability conditions from ISO 12999-1:2014 or those obtained from ILC).

In this paper the obtained uncertainties are compared by using GUM and ISO 5725-2 approaches.

In the GUM approach the measurement uncertainty is calculated for each individual measurement (by knowing uncertainties of each variable included in calculations [15]).

In agreement with ISO 5725-2, the concepts of standard deviations in repeatability and reproducibility conditions have been used to state the precision of the measurements carried out according to a test method.

Standard deviations in repeatability conditions (s_r) shows the closeness of agreement between mutually independent test results obtained with the same method on identical test material in the same laboratory with the same equipment by the same operator within short time intervals.

Standard deviations in reproducibility conditions (s_R) shows the closeness of agreement between test results obtained with the same method on identical test material in different laboratories with different operators by using different equipment. The determination of the standard deviations in repeatability and reproducibility conditions of a test method obtained by an interlaboratory comparison, taking into account the procedures given in international standards ISO 12999-1:2014 and ISO 5725:1994. Tentative values of sr and s_R are given in ISO 12999:1-2014 [13]. The s_r and s_R values may also be used to verify the proper operation of test procedures of a laboratory which has not taken part in the comparison.

3. MEASUREMENT SITUATIONS AND PARAMETERS

3.1. Environmental noise parameters

The point source was located on h_s=3m and receiver position (h_r=1,5 m) was chosen on the façade and in front of the façade with distance from the source of 25 m. The ground between source and receiver was grass and equation (11) [7] for critical distance where meteorological conditions does not have influence on measurement results and uncertainty was satisfied.

The measured parameters were:

L_{Aeq} (dB(A)) – A-weighted equivalent sound pressure level (corrected to free field conditions) when the source is turned on and off

L_{95} (dB(A)) – time and A-weighted value exceeded in 95% of considered time interval

L_1 (dB(A)) - time and A-weighted value exceeded in 1% of considered time interval;

$L_{C,peak}$ (dB(C)) – C-weighted peak sound pressure level;

A-weighted one-third octave band levels when the source is turned on;

L_{res} (dB(A)) – equivalent level of residual noise;

A-weighted one-third octave band levels when the source is turned on.

In the results shown here, we have compared in details parameters at the two different positions with probability density functions and measurement uncertainties.

Fig. 3.1. Measurement situation for environmental noise parameters and windows settings where labs choose their measurement positions

3.2. Building acoustics parameters

In the ILC the lightweight partition made of 20 mm chip floor slab between two rooms, for the airborne sound insulation measurements and timbre floor for impact sound insulation. In the ILC-s, not only acoustic insulation parameters (R'-apparent sound reduction index, D_{nT}-standardized level difference and L'_n-normalized impact sound pressure levels, L'_{nT}-standardized impact sound pressure levels) are compared, but also the geometrical parameters of rooms (volumes without furniture and area of the considered partition). Reverberation times in the receiving room are also compared because acoustic insulation parameters depend on them [10-12].

3.2.1. Airborne sound insulation parameters

There are two parameters used for expression of the airborne sound insulation: the standardized level difference $D_{n,T}$ between rooms or the apparent sound reduction index R' of the separating element as a function of frequency, whichever is appropriate. The each lab in this ILC-s determined all parameters but sound reduction has been considered more in details. Sound reduction index R' which depends on the area of measured element (S), and on the equivalent absorption area A which is calculated from geometrical dimensions (volume of the receiving room) and measured reverberation time in the receiving room.

The standardized level difference is given with eq. (23) which includes the difference in the energy-average sound pressure levels between the source and receiving rooms:

$$D_{nT} = D + 10 \cdot log\frac{T}{T_0} \qquad (23)$$

T_0- is the reference reverberation time; for dwellings, T_0 = 0,5 s. T is the reverberation time in the receiving room.
The sound reduction index is given by eq. (24) [10]:

$$R' = D + 10 \cdot log_{10}(\frac{S}{A}) \qquad (24)$$

The equivalent absorption area A of the receiving room is given by eq. (25):

$$A = 0{,}161 \cdot \frac{V}{A} \qquad (25)$$

where V is the receiving room volume (m^3) with the furniture excluded because it has influence on the reverberation time T [10-12].

3.2.2. Impact sound insulation parameters

The impact sound insulation can be expressed with two parameters: the normalized impact sound pressure level (L'_n) and the standardized impact sound pressure level ($L'_{n,T}$) as a function of frequency. Normalized impact sound pressure level (L'_n), given with eq. (3), is impact sound pressure level in the receiving room L'_i (averaged in time and space) increased by a correction term, which is given in dB, being ten times common logarithm of the ratio of the measured equivalent absorption area A of the receiving room eq. (26) to the reference absorption area A_0 = 10 m^2.

$$L'_n = L'_i + 10 \cdot log\frac{A}{A_0} \qquad (26)$$

Standardized impact sound pressure level, $L'_{n,T}$, is the impact sound pressure level L_i reduced by a correction term which is given in dB, being ten times common logarithm of the ratio of the measured reverberation time T of the receiving room to the reference reverberation time T_0 = 0.5 s [12]:

$$L'_{n,T} = L'_i - 10 \cdot log\frac{T}{T_0} \qquad (27)$$

The measurement setups for airborne and impact sound insulation parameters are shown in **Fig 3.2.**

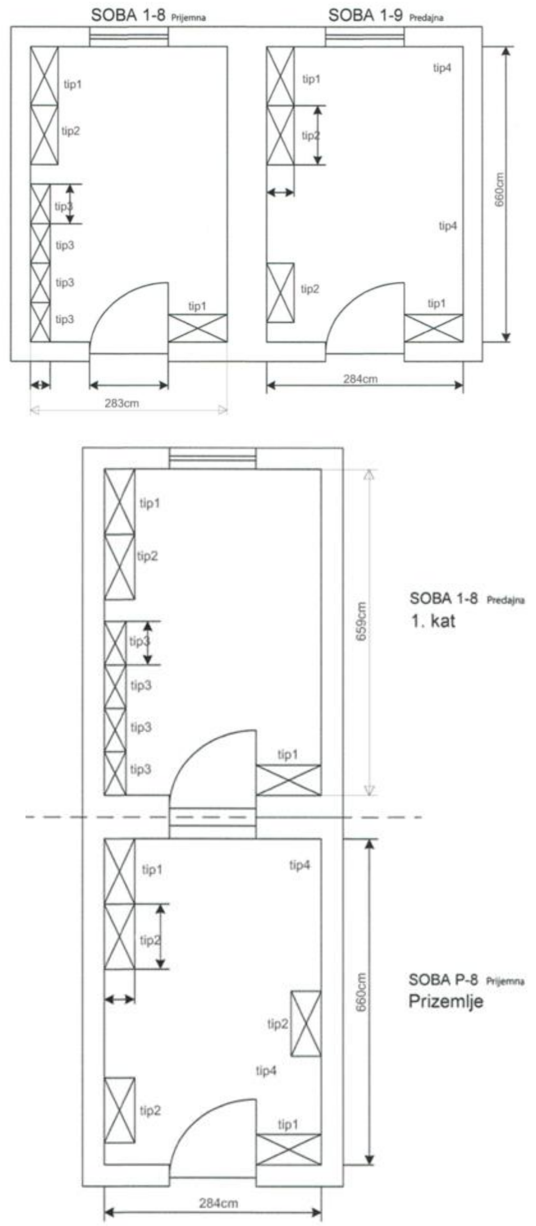

Fig 3.2. The transmitting and receiving room in the considered situation for a) airborne and b) sound insulation parameters measurements

The measurement of sound pressure levels with sound level meter is restricted only in few positions depending on the rooms' size and we tried to increase the number of measurement positions by using acoustic camera with 80 microphones and averaging the sound pressure levels in 80*5 positions in source and receiving rooms (**Fig 3.3**). The .wav files form all microphones were recorded and imported in MATLAB where analysis for finding equivalent sound pressure levels for 15 s recordings (broadband and in one-third octave bands) has been done by using Audio System toolbox.

Fig 3.3. Measurement SPL and reverberation time with acoustic camera in large number of positions

4. MEASUREMENT RESULTS

4.1 Environmental noise parameters

There were a big problems in detecting a penalty due to tonal component in spectrum appeared due to standing wave in the window setting shown in **Fig 3.1.** The tonal component has been reported from 4 labs on the position directly on the facade and for 2 labs for the position in front of the facade.

There were no tonal components in the sound source signal which was pink noise emitted from loudspeaker.

The results for rated A-equivalent noise parameters when the source is on and off at two different positions are shown in **Fig 4.1.** The averaged results of all labs (without excluded outliers) are shown in Table 4.1.

a) Residual noise- the source is turned off

Label	$L_{A,eq}$ (dBA)	L_{95} (dBA)	L_1 (dBA)	$L_{Z,eq}$ (dB)	$L_{A,max}$ (dBA)	$L_{A,min}$ (dBA)	$L_{Z,max}$ (dB)	$L_{Z,min}$ (dB)
AVG-pos1	38,7	35,2	45,2	59,1	50,7	34,3	70,0	53,1
u1-pos1	0,4	0,5	0,6	0,4	0,9	0,6	1,1	0,5
AVG-pos2	38,9	35,6	44,8	60,5	50,6	34,8	72,0	54,0
u2-pos2	0,4	0,5	0,6	0,5	1,0	0,6	1,1	0,5
Difference Mean (p1-p2)	-0,2	-0,3	0,4	-1,3	0,1	-0,6	-2,0	-0,9

b) Environmental noise parameters when the source is turned on

Label	AVG pos1	u-pos1	AVG-pos2	u-pos2	Difference of mean (pos1-Pos2)
L_{Aeq} (dBA)	58,1	0,2	59,0	0,2	-0,9
L_{Req} (dBA)	58,1	0,2	59,0	0,2	-0,9
L_{95} (dBA)	57,6	0,2	58,3	0,2	-0,7
L_1 (dBA)	59,5	0,5	60,0	0,2	-0,4
$L_{C,peak}$(dBC)	80,0	0,7	79,4	0,5	0,5
L_{Zeq} (dB)	64,7	0,3	65,6	0,3	-0,9
L_{ceq} (dBC)	64,3	0,2	64,3	0,2	-0,1
$L_{A,max}$ (dBA)	59,7	0,3	61,3	0,4	-1,5
$L_{A,min}$ (dBA)	57,1	0,2	58,0	0,2	-1,0
$L_{Z,max}$(dB)	71,5	0,8	73,4	1,3	-1,9
$L_{Z,min}$(dB)	62,2	0,2	62,7	0,2	-0,5

Table 4.1. Compared environmental noise parameters levels at two different postions (pos 1 on the facade and pos 2 in front of the facade)

The comparison between A-weigted spectral values at two different positions are shown in **Fig 4.1.**

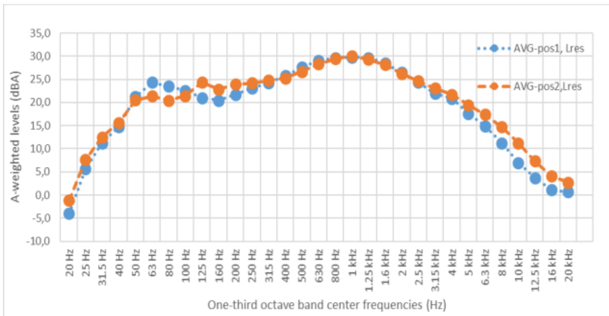

a)

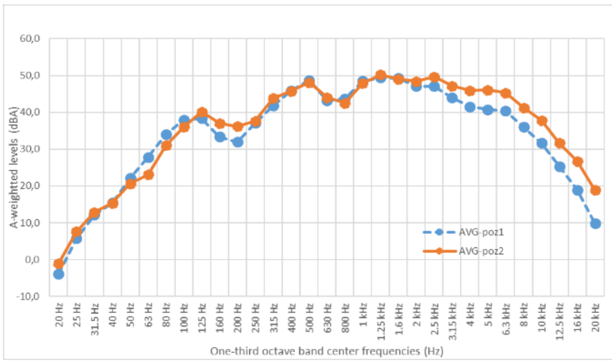

b)

Fig. 4.1. Difference between A-weighted spectral values for two different positions for a) residual noise and b) source noise

The laboratories have chosen different time intervals and different numbers of measurements (from 5 min up to 30 minutes from 3 measurements up to 5 measurement intervals).

The overall results for position 1 with expanded measurement uncertainties of each lab are shown in **Fig 4.2.** It is evident that each lab reported almost the same expanded measurement uncertainty (±3,6 dB(A)) calculated by using eq. (20). The average value of all labs is marked with red (58,1 dB(A)).

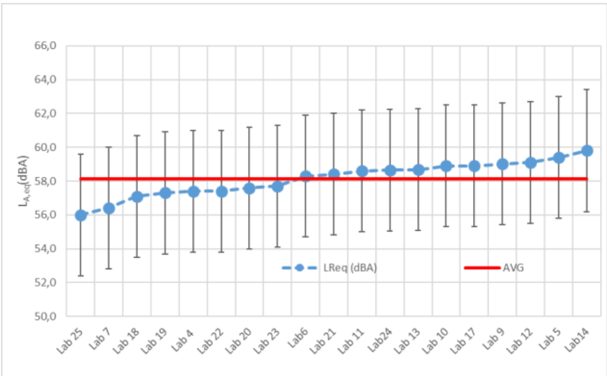

Fig. 4.2. The average value (arithmetic) and expanded measurement uncertainty of all labs

In addition, PDF functions of rated values $L_{A,eq}$ are shown in **Fig 4.3** for residual noise and source noise at two different positions. Several different distributions were tested especially at position 1 where results show strong asymmetric behaviour.

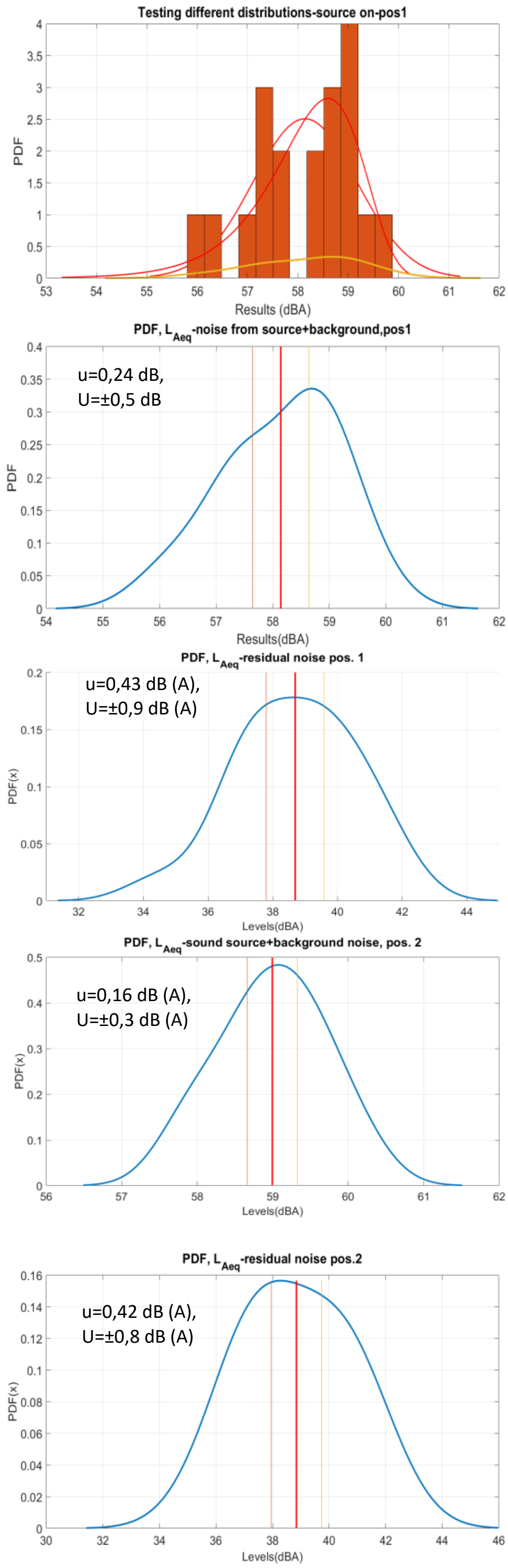

Fig. 4.3. PDF functions of measured $L_{A,eq}$ mean values with standard deviations for different measurement positions

It is visible that for residual noise and source noise the PDF function of A-weighted equivalent noise level is symmetrical around mean value. For source noise, the PDF function is asymmetrical at position 1 on the facade.

There is also difference for the mean determined by assuming arithmetic and logarithmic average from all valid results. Also, the standard deviations (u) are significantly different and the results are shown in **Table 4.2.**

Table 4.2 Comparison between means and expanded uncertainties obtained with different ways of calculation (arithmetic and logarithmic)

Situation/Parameter	Arithmetic mean (dBA)	U_k (dBA)	Logarithmic mean (dBA)	U_k (dBA)	Max PDF (dBA)
Residual noise-pos1	38,7	0,9	39,1	1,5	38,8
Source -pos1	58,1	0,5	58,3	1,4	58,7
Residual noise-pos2	38,9	0,9	39,2	1,5	38,3
Source -pos2	59,0	0,3	59,1	1,4	59,1

4.2. Sound insulation parameters

The measurement uncertainty from one individual measurement of each parameters is rather complicated because includes all parameters with their functional dependence.

For standardized level difference (D_{nT}) the derivation of the measurement uncertainty by knowing measurement uncertainties and sensitivity coefficients from all parameters which enter in the equation for calculation is given in reference [15] and we have derived the equation (28) for *R*'.

$$u(R') = \sqrt{(c_{L1}\cdot u(L_1))^2 + \left(c_{L2}\cdot u(L_2)\right)^2 + (c_{Lres}\cdot u(L_{res}))^2 + (c_S\cdot u(S))^2 + (c_A\cdot u(A))^2 + (c_{inst}\cdot u(L_{inst}))^2} \quad (28)$$

Where *c* are sensitivity coefficients and *u* are standard uncertainties from all variables in equation for *R*' (levels in source and receiving rooms, reverberation time, residual noise uncertainty, surface of the wall, equivalent absorption area, instrumentation). In this approach it is assumed that these parameters are not correlated so simplified form eq. (7) is used.

Different problems in calculations due to large number of parameters like converting dB onto Pa are considered in [15].

We have derived the equations for sound reduction index (*R*') and estimated measurement uncertainties when measurements are done for two loudspeaker positions and calculation of sound reduction index are done for each loudspeaker position (R'_1 and R'_2).

The averaged value of airborne sound insulation for measurement results for two loudspeaker positions is given with eq. (29).

$$R' = -10\cdot\log\left(\frac{1}{2}\cdot\left(10^{\frac{R_1}{10}} + 10^{\frac{R_2}{10}}\right)\right) \quad (29)$$

The measurement uncertainty *u*(*R'*) from known measurement uncertainties from results for two different loudspeaker positions is given by using eq. (30).

$$u(R') = \sqrt{(c_{R1}\cdot u(R_1))^2 + \left(c_{R2}\cdot u(R_2)\right)^2} \quad (30)$$

This calculation for each individual source position should be repeated for all sound insulation parameters according new ISO 16283-1,2,3 standards.

The main problem is to find uncertainty for sound pressure when continuous moving microphone is used because there is only one measurement result for one loudspeaker position.

All input parameters for calculation of standardized level difference ($D_{n,T}$) apparent sound reduction index (*R*') (surface of the wall, reverberation time, level difference) have been analysed by using Grubbs and Cochran statistics having purpose to find outliers. The results for surface of the wall, volume of receiving room and reverberation time in receiving room obtained in ILC (mean value and standard deviation) without outliers are shown in **Fig 4.4** in situation when airborne sound insulation is measured. The problem with geometrical parameters measurements is that not all labs have measured the geometry parameters 5 times so only averaged result is shown. The results for apparent sound reduction index in one third octave bands are shown in **Figure 4.5.**

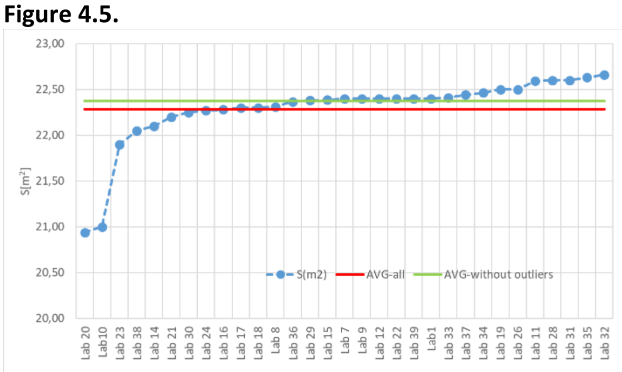

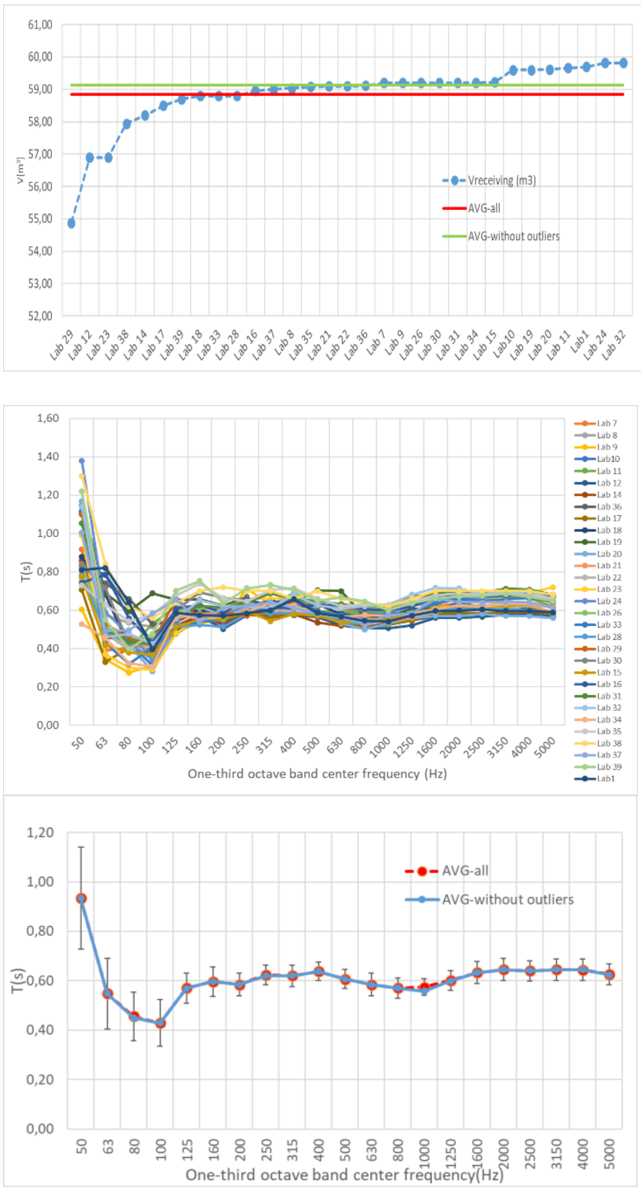

Fig. 4.4. Measurement results of all labs, surface, volume of receiving room, all results for reverberation time and mean value of reverberation time in one-third octave bands and standard deviations (with and without outliers).

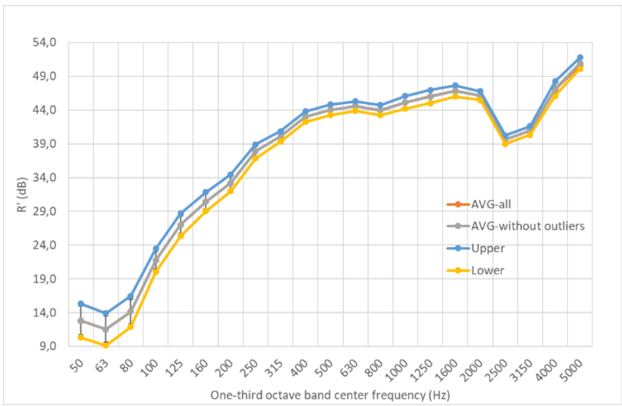

Fig. 4.5. Mean value of sound reduction index in one-third octave bands and standard deviations with upper and down curve of sound reduction index calculated from obtained standard deviations in repeatability conditions of MLU results

The single number values for each lab (averaged 5 independent measurements) with measurement uncertainties obtained by using no correlation and full correlation assumptions between five independent measurements are shown in **Fig 4.6.** The basic difference that averaged value form 5 independent measurement results can be determined by averaging 5 single number values or averaging the one-third octave bands values and finding mean value by moving reference curve.

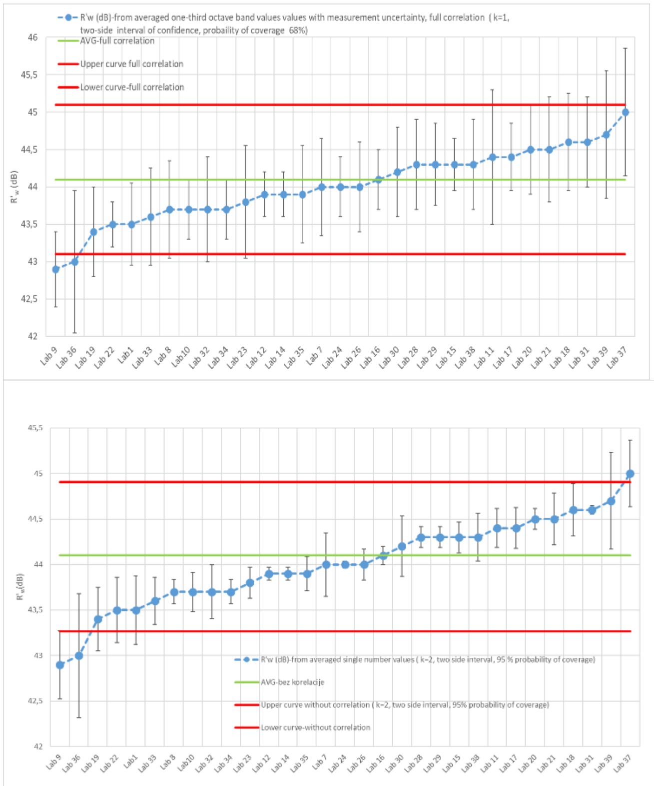

Fig. 4.6. Single number values for sound reduction index and measurement uncertainties under two different assumptions (no correlation and full correlation between 5 independent measurements)

It is visible that some labs have larger measurement uncertainty when no correlation assumption is considered compared to the situation when full correlation is assumed.

The same procedure is repeated for impact sound insulation parameters and the results for normalized impact sound pressure levels in one-third octave bands is shown in **Fig 4.7.**

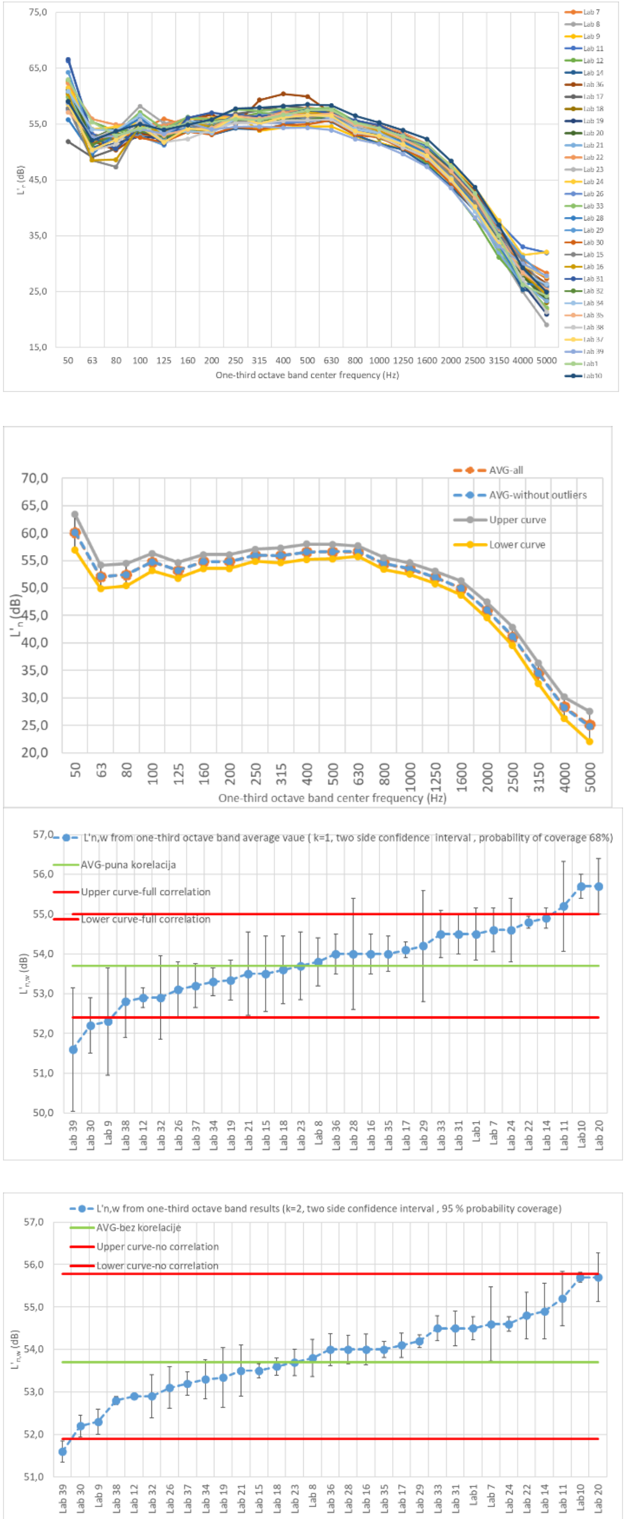

Fig. 4.7. Results for normalized impact sound pressure levels in one-third octave bands and single number values with measurement uncertainties assuming full correlation and no correlation between one-third octave bands' results

The comparison for calculations of measurement uncertainties in one third octave bands with tentative values given in ISO 12999-1:2014, standard deviations from repeatability conditions obtained in MLU and from individual measurement of one lab for sound reduction index in another situation (not in ILC) are shown in **Fig 4.8.** The approach with averaging overall sound pressure level and for each loudspeaker position are considered.

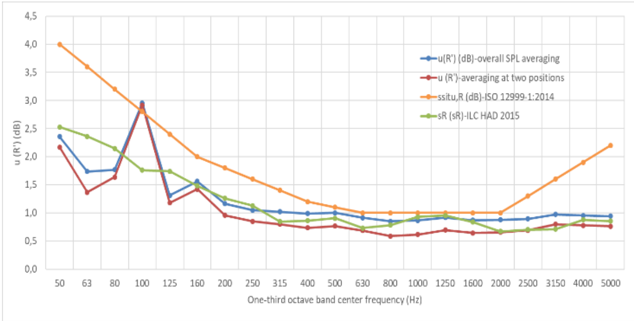

Fig. 4.8. Comparison between different way for obtaining measurement uncertainties (from independent measurement) and by using standard deviations in reproducibility conditions

The same calculations will be provided in the future for each individual measurement of each lab and for overall results of ILC in the future.

4.3. Comparison between acoustic camera and classical sound level meter measurement results

Having purpose to test standard deviations between multiple measurement positions the measurement of sound pressure level in receiving and transmitting room has been done with acoustic camera with 80 microphones at 5 positions. The standard deviations from all measurement results in each octave bands are given in **Fig 4.9** a) for sound pressure levels and for reverberation times.

The averaged results for sound pressure levels in the source room and receiving room for two loudspeaker position are shown in **Fig 4.9.**

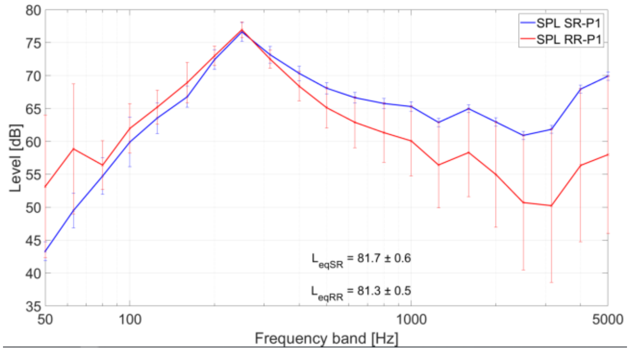

a)

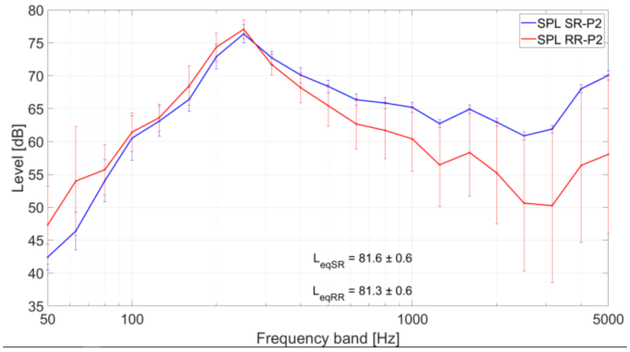

b)

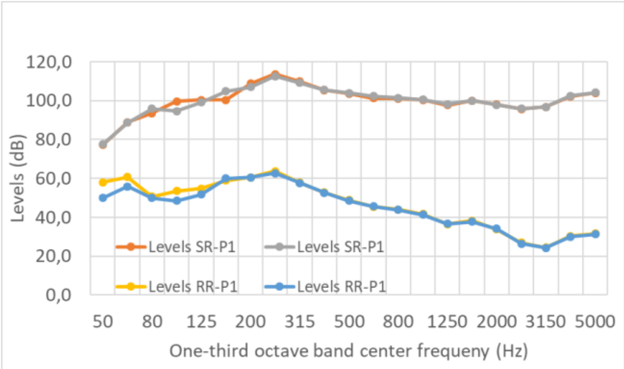

c)

Fig. 4.9. Averaged results for sound pressure levels from 80 microphones at five camera positions for (a) first and (b) second loudspeaker position in source and receiving rooms and for sound level meter averaged results in one-third octave bands

The same is repeated for reverberation times at large number of measurement positions.

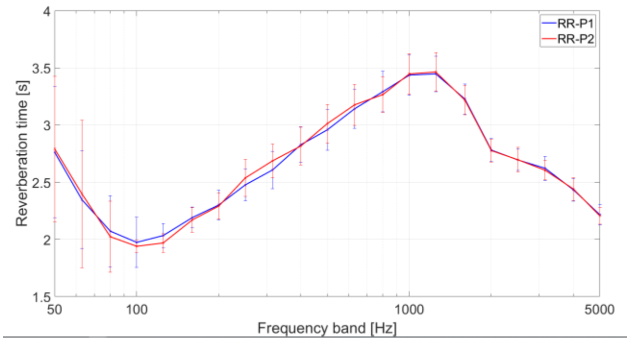

a)

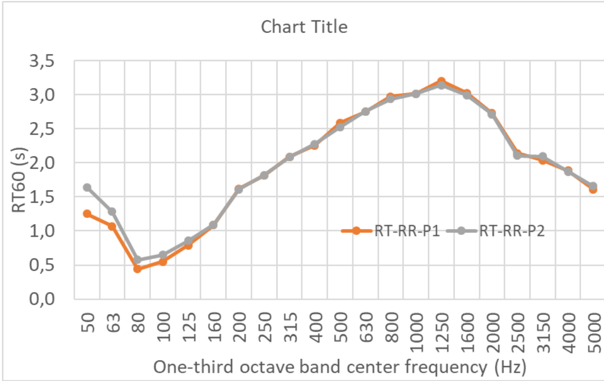

Fig 4.10. The averaged results for reverberation times with standard deviations at two loudspeaker positions in the receiving rooms (a) acoustic camera and b) sound level meter

The standard deviations obtained per loudspeaker positions with acoustic camera and sound level meter are compared in **Table 4.3.**

Band [Hz]	Camera $S_{SPL\ SR-P1}$	SLM $S_{SPL\ SR-P1}$	Camera $S_{SPL\ SR-P2}$	SLM $S_{SPL\ SR-P2}$	Camera $S_{SPL\ RR-P1}$	SLM $S_{SPL\ RR-P1}$	Camera $S_{SPL\ RR-P2}$	SLM $S_{SPL\ RR-P2}$
50	1.5	1,9	2.0	2,9	10.8	7,8	5.9	6,2
63	2.6	2,9	2.8	4,5	9.9	4,4	8.3	3,4
80	2.8	3,0	3.2	4,7	3.7	4,1	3.8	3,5
100	3.8	4,2	3.4	3,1	3.8	1,9	2.9	1,2
125	2.3	5,4	2.3	1,2	2.6	3,3	2.1	0,5
160	1.6	2,3	1.8	2,8	3.1	2,6	3.0	1,3
200	1.5	1,8	1.9	1,4	1.5	0,8	2.1	1,6
250	1.4	2,5	1.4	2,3	1.2	1,0	1.4	1,2
315	1.3	1,0	1.0	0,5	1.4	0,9	1.6	1,0
400	1.1	0,3	1.2	1,1	2.2	0,7	2.3	0,9
500	0.8	0,5	0.9	0,8	3.1	0,7	3.1	0,6
630	0.8	0,5	0.8	0,9	3.8	0,3	3.8	0,7
800	0.8	0,7	0.8	0,6	4.5	0,6	4.3	0,3
1000	0.7	0,5	0.8	0,6	5.3	0,5	4.9	0,4
1250	0.6	0,4	0.6	0,7	6.5	0,2	6.3	0,1
1600	0.6	0,5	0.6	0,4	6.7	0,5	6.7	0,2
2000	0.6	0,4	0.6	0,4	8.0	0,2	7.8	0,4
2500	0.6	0,5	0.6	0,4	10.2	0,3	10.3	0,2
3150	0.6	0,5	0.6	0,5	11.6	0,3	11.7	0,2
4000	0.6	0,4	0.6	0,6	11.6	0,4	11.7	0,1
5000	0.6	0,6	0.7	1,0	12.0	0,3	12.1	0,2

a)

Band [Hz]	Camera S_{RT-P1}	SLM S_{RT-P2}	Camera S_{RT-P2}	SLM S_{RT-P2}
50	0.6	0,4	0.6	0,3
63	0.4	0,5	0.6	0,2

80	0.3	0,1	0.3	0,1
100	0.2	0,1	0.1	0,1
125	0.1	0,1	0.1	0,1
160	0.1	0,1	0.1	0,1
200	0.1	0,1	0.1	0,2
250	0.1	0,1	0.2	0,2
315	0.2	0,1	0.1	0,1
400	0.2	0,1	0.2	0,2
500	0.2	0,1	0.2	0,1
630	0.2	0,1	0.2	0,1
800	0.2	0,1	0.2	0,1
1000	0.2	0,1	0.2	0,1
1250	0.2	0,1	0.2	0,1
1600	0.1	0,1	0.1	0,1
2000	0.1	0,1	0.1	0,1
2500	0.1	0,0	0.1	0,0
3150	0.1	0,1	0.1	0,0
4000	0.1	0,0	0.1	0,0
5000	0.1	0,1	0.1	0,0

b)

Table 4.3. Comparison between standard deviations obtained with acoustic camera and sound level meter for each loudspeaker position in source and receiving rooms for levels and reverberation times.

It is evident that results for levels (absolute values) and their standard deviations are not comparable between acoustic camera and sound level meter especially in receiving room because sensitivity of microphones has been changed due to lower level of sound signal in the receiving room.

5. DISSCUSION AND CONCLUSION

5.1. Results for environmental noise parameters

It is visible that for equivalent A-weighted value parameters (all valid results in MLU obtained by using Grubbs statistics) that the PDF function for rating level at position 1 (on the façade) is asymmetric around maximum value of PDF. The logarithmic and arithmetic mean in that case have different values (>0,5 dB(A)) which can slightly underestimated mean value if results of al labs are considered.

If the measurement uncertainty is taken into assessment with limit values (according to maximum increase of level for 1 dB(A)) into account for this situation measurement uncertainty doesn't not give any wrong decision rule. But for example, if residual noise level is much closer to the level of noise when the source ins on than the measurement uncertainty have significant influence of assessment and decision rule according to the new ISO 17025:2017 standard. If the limit value for example was mean value of overall results, when high uncertainties obtained by using calculation according to the ISO 1996-2:2007 (**Fig 4.2**) or ISO 1996-2:2017 are taken into account all labs would give negative assessment of measured value due to asymmetric PDF function and very large expanded measurement uncertainties obtained by suggested calculations in old and new ISO 1996-2 standard.

For example, if we consider the 19 results of labs as independent results the example of measurement uncertainty of overall ILC results are compared in **Table 5.1.**

Quantity	Estimate	Standard Uncertainty	Sensitivity Coefficient	Uncertainty Contribution
$L_{A,eq}$	58,3	0,5	1,0	0,5
ϱ_{slm}	0,0			0,0
ϱ_{sou}	0,0	0,2	1,0	0,2
ϱ_{met}	0,0	2,0	1,0	2,0
ϱ_{loc}		0,0	0,0	0,0
ϱ_{res}		0,4	0,0	0,0
$L_{A,eq,res}$	39,1			
$u=sqrt(u_1^2+u_2^2+..)$				2,1
$L_{A,eq,\ corrected}$	58,2		Expanded k=2	4,2

Table 5.1. Measurement uncertainties calculations for all ILC results (19) according to ISO 1996-2:2017 for position 1

It is visible that due to influence of meteorological conditions measurement uncertainty is higher when new standard ISO 1996-2:2017 recommendations are used in calculations.

5.3. Results for sound insulation

It is noticeable that also for sound insulation parameters there can be different approach in measurement uncertainty calculations.

When PDF functions for sound insulation parameters measured from 31 laboratories are considered (apparent sound insulation index and normalized sound pressure levels) the PDF distribution is almost symmetrical around mean value and obtained measurement uncertainty is much lower compared to the situations when standard deviations in repeatability conditions are used for calculations of measurement uncertainties. The PDF function and overall measurement uncertainty from all ILC results when observing *R'* parameter is given in **Fig 5.1a)** and for L'_n in **Fig 5.1b).**

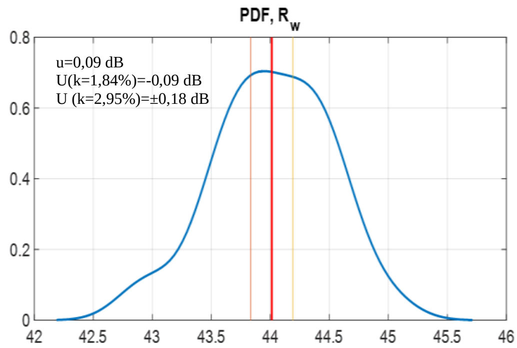

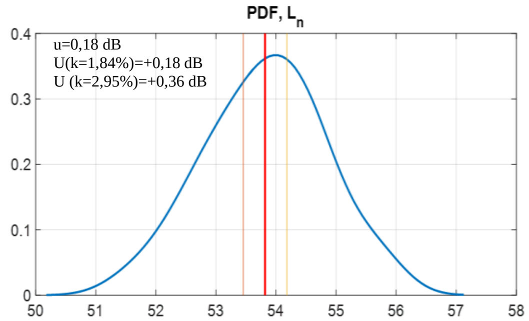

Fig.5.1.a) PDF function for *R'* and b) for L'_n with measurement uncertainty (standard deviation in repeatability conditions) calculated assuming normal distribution of single number values

The comparison between obtained measurement uncertainties for these two parameters measured in ILC (averaged 31 results with 5 independent measurements) assuming standard deviation in repeatability conditions given in ISO 12999-1:2014 standard and those obtained in this ILC are shown in **Table 5.2.**

Parameter	Standard deviations in reproducibility conditions from ILC	Standard deviations in reproducibility conditions from standard ISO 12999-1:2014
R'_w	-1,0	-1,5
R'_w+C	-1,0	-1,8
R'_w+C_{tr}	-1,5	-2,3
$R'_w+C_{50\text{-}5000}$	-1,5	-2,8
$R'_w+C_{tr,50\text{-}5000}$	-2,0	-3,5

Parameter	Standard deviations in reproducibility conditions from ILC	Standard deviations in reproducibility conditions from standard ISO 12999-1:2014
$L'_{n,w}$:	+1,3	+1,3
$L'_{n,w}+C_i$	+0,8	+0,8
$L'_{n,w}+C_{i,50\text{-}2500}$	+1,3	+1,3

Table 5.2. Measurement uncertainty for overall ILC results assuming different standard deviations in reproducibility conditions (sound reduction index and normalized impact sound pressure level)

There is some difference between measurement uncertainties obtained from one individual measurement compared to the standard deviations.

There is also visible, that there is no significant difference between results for standard deviations obtained by using acoustic camera with large number of microphones and classical sound level meter at 5 different positions.

6. ACKNOWLEDGEMENT

Part of this research is funded by PAPA BUILD project during Antonio's stay in Bratislava, Slovakia. RISE project "PapaBuild" Advanced physical-acoustic and psycho-acoustic diagnostic methods for innovation in building acoustics (in short "PapaBuild") has received funding from the European Union's Horizon 2020 research and innovation Programme under the Marie Skłodowska-Curie grant-agreement No 690970 [23].

7. REFERENCES

[1.] ISO 17025:2017, **General requirements for the competence of testing and calibration laboratories**

[2.] ISO/IEC 17043:2010, **Conformity assessment -- General requirements for proficiency testing**.

[3.] ISO 3744:2010, **Acoustics -- Determination of sound power levels and sound energy levels of noise sources using sound pressure -- Engineering methods for an essentially free field over a reflecting plane.**

[4.] ISO 12354-1:2017, **Building acoustics -- Estimation of acoustic performance of buildings from the performance of elements -- Part 1: Airborne sound insulation between rooms.**

[5.] ISO 12354-2:2017, **Building acoustics -Estimation of acoustic performance of buildings from the performance of elements -- Part 2: Impact sound insulation between rooms.**

[6.] ISO 12354-3:2017, **Building acoustics -Estimation of acoustic performance of buildings from the performance of elements - Part 3: Airborne sound insulation against outdoor sound.**

[7.] ISO 1996-2:2017, **Acoustics - Description, measurement and assessment of environmental noise -- Part 2: Determination of sound pressure levels.**

[8.] ISO 1996-1:2016, **Acoustics -- Description, measurement and assessment of environmental**

noise -- Part 1: Basic quantities and assessment procedures.

[9.] ISO 1996-2:2007, **Acoustics -- Description, measurement and assessment of environmental noise -- Part 2: Determination of environmental noise levels.**

[10.] ISO 16283-1:2014, **Acoustics -- Field measurement of sound insulation in buildings and of building elements -- Part 1: Airborne sound insulation.**

[11.] ISO 16283-2:2015**, Acoustics -- Field measurement of sound insulation in buildings and of building elements -- Part 2: Impact sound insulation.**

[12.] ISO 16283-3:2016, **Acoustics -- Field measurement of sound insulation in buildings and of building elements -- Part 3: Façade sound insulation.**

[13.] ISO 12999-1:2014, **ISO 12999-1 Acoustics. Determination and application of measurement uncertainties in building acoustics – Part 1: Sound insulation,** Geneva (Switzerland): International Organization for Standardization; 2010.

[14.] ISO 5725-2: 1994, **Accuracy (trueness and precision) of measure-ment methods and results – Part 2: Basic method for the determination of repeatability and reproducibility of a standard measurement method**.

[15.] María Machimbarrena, Carolina Rodrigues A. Monteiro, Stefano Pedersoli, Reine Johansson, Sean Smith: **Uncertainty determination of in situ airborne sound insulation measurements**, Applied Acoustics 89 (2015) 199–210

[16.] ISO 717-1:2013 Acoustics: **Rating of sound insulation in buildings and of building elements – Part 1: Airborne sound insulation**, Geneva (Switzerland): International Organization for Standardization; 2010.

[17.] ISO 717-2:2013 Acoustics, **Rating of sound insulation in buildings and of building elements – Part 2: Impact sound insulation**, Geneva (Switzerland): International Organization for Standardization; 2010.

[18.] Carolina Monteiro, Marcel Borin, María Machimbarrena, Mariana Shimote: **AIRBORNE SOUND INSULATION: A STUDY ON THE COR-RELATION BETWEEN 1/3 OCTAVE BAND VALUES AND ITS IMPACT ON THE RESULTING SNQ UNCERTAINTY** , 24 th International Congress on sound and vibration, London ,2017.

[19.] Carolina Monteiro, Marcel Borin, Reine Johansson, María Machimbarrena: **Individual uncertainty calculations of sound insulation measurements: a proposal of compromise values for 1/3 octave bands correlation coefficients**, EURONOISE 2018.

[20.] Bartosz Przysucha: **Uncertainty Analysis in Acoustic Investigations**, COMPUTER SCIENCE & ENGINEERING 2013" (CSE-2013), 21–23 NOVEMBER 2013, LVIV, UKRAINE.

[21.] ERIK BACKMAN HENRIK LUNDGREN: **Measurement and evaluation uncertainties of impact sound insulation: An investigation of light weight structures**, Master of Science Thesis in the Master Degree Sound and Vibrations, CHALMERS UNIVERSITY OF TECHNOLOGY Gothenburg, Sweden, 2010 Master´s Thesis 2010: 136

[22.] Momir Praščević, Dragan Cvetković, Darko Mihajlov: **THE UNCERTAINTY SOURCES IN ENVIRONMENTAL NOISE MEASUREMENTS AND THE UNCERTAINTY ESTIMATION**, FACTA UNIVERSITATIS Series: Mechanical Engineering Vol. 9, No 2, 2011, pp. 183 – 192.

[23.] https://www.papabuild.eu/

8th Congress of the Alps Adria Acoustics Association
Zagreb, Croatia
20 – 21 September 2018

ACOUSTIC PERFORMANCE OF LARGE PARALLEL BAFFLED SILNCERS BY USING IN-SITU MEASUREMENT METHOD

Antonio Petošić, Sanja Grubeša, Petar Franček, Slobodan Šodolović

University of Zagreb, Faculty of Electrical Engineering and Computing, Unska 3, 10 000 Zagreb
(antonio.petosic@fer.hr)

Abstract: *In this research, acoustic parameters of six different configurations of parallel baffled silencers have been compared by using in-situ measurement method according to ISO-11820:1996 standard. The geometrical (length, thickness and distance between baffles) and absorption parameters of baffles have been changed (full absorption and half-absorption surface) and their influence on the silencer performance in channel without and with flow have been measured. Transmission and insertion loss acoustic parameters in octave frequency bands from 63 Hz up to 16 kHz are determined in the in-istu measurement setup with influence of the reflections from baffles at inlet side and opening at outlet side. Also, analytical expressions (Piening and trapezoidal equation) for one parallel baffled silencer's configuration have been compared with measurement values on octave bands of interest. The sound pressure distribution between baffles has been also measured and it is evident that there SPL change at the beginning is much larger compared to the value at the end of silencer.*

Key words: parallel baffled silencers, insertion and transmission loss, artificial and real sound source, sound pressure distribution inside the baffles.

1. INTRODUCTION

The performance of large industrial baffled silencer is very important for reducing the environmental noise from large industrial plants. Their performance is measured by using international standards describing in-situ measurement conditions [1] and laboratory conditions [2]. The performance of the silencer can be modelled by using empirical equations which rarely include all effects having influence on their performance [3, 4, 5] or more precise numerical methods [6]. Regarding the experimental, analytical and numerical methods to determine the acoustic properties of parallel baffled silencers there is no direct comparison of the acoustical performance between same silencers with different length, thickness of baffles and distance between baffles. There is also no available data about performance of silencers regarding the increase of the length or putting small gap between baffles in the direction of sound propagation through the climatization channel.

Comparing the in-situ and laboratory setups for measurements, we have decided to use less complicated in-situ measurement setup [1] as closest to the real operating conditions when these types of silencers are installed at the outlet of climatization chamber.

In addition to the measurements of parameters with artificial and real sound source we have measured the sound pressure distributions between baffles.

2. THEORETICAL BACKGROUND

The acoustical parameters measured are Insertion Loss (IL) and Transmission Loss (TL) for sound power levels. Insertion loss for sound pressure level is defined as sound pressure difference on the receiving side (point or small surface to avoid influence of non-diffuse sound field) of measurement setup when silencer is not installed and when the silencer is installed. The insertion loss for sound pressure level is defined with eq. 1 [1,2].

$$D_{ips} = L_{pII} - L_{pI} \tag{1}$$

where L_{pII} save raged sound pressure level without silencer and L_{pI} is averaged sound pressure level with silencer.

The insertion loss for sound power level (*IL*, D_{is}) is the same as calculated insertion loss for the sound pressure level because the measurement surface for calculating sound power from sound pressure (intensity) is the same (outlet channel or surface after opening).

TL is defined as reduction of the sound power through the test object as difference of sound power level before and after the silencer (in inlet and outlet duct for this measurement setup) [1].

The transmission loss of sound pressure level is defined as difference of the averaged pressure levels measured at the source side ($\overline{L}_{p2}$ - in channel) and on the measurement surface on the receiving side ($\overline{L}_{p1}$ –in room, without diffuse field in our situations) (eq. 2)

$$D_{ts} = L_{p2} - L_{p1} \tag{2}$$

Transmission loss (*TL*) for sound power level is determined from sound pressure levels and by knowing the surface where the sound pressure levels are averaged (sound pressure levels are transformed into intensity and intensity into acoustic power). The additional correction terms (K_1, K_2) in some cases should be added to calculations due to corrections for different type of sound fields and influence of the reflections at silencer entrance and outlet of the channel due to reflections(eq. 3) [1].

$$D_{ts} = L_{w2} - L_{w1} \tag{3}$$

The sound power level at receiver side is calculated by using eq. 4.

$$L_{w1} = \bar{L}_{p1} + 10 \cdot \lg \frac{S_1}{S_0} + K_1 \tag{4}$$

The sound power level at source side is calculated by using eq. 5.

$$L_{w2} = \bar{L}_{p2} + 10 \cdot \lg \frac{S_2}{S_0} + K_2 \tag{5}$$

where S_1 is surface on the receiving side and S_2 is the surface on the transmission side. The sound power levels are determined from averaged sound pressure levels assuming that sound intensity and pressure are connected via measurement surface and using plane wave relation for fundamental propagation mode. This cause some errors in estimation of parameters because this approximation is valid under cut-off frequency.

3. MATERIALS AND MEASUREMENT SETUPS

First all parameters of baffles have been considered and then the measurement setup is analyzed.

3.1 Parameters of baffles

The geometrical parameters having influence on the silencers performance are length (500 mm, 1400mm, 2000 mm), thickness of baffles (100 mm, 200 mm, 300 mm) and space between baffles (50 mm, 75 mm, 100 mm). In addition of changing geometrical parameters the reflective sheet (2 mm thickness) is added on the half of the absorptive side.

The baffles can have two total absorptive sides (full absorption-A) and partially reflective sides (half of the surfaces on the two side-opposite orientation).

The acoustic parameters (absorption coefficient) of mineral rock wool (thickness 50 mm and density 50 kg/m^3) which fills the baffles are given in **Table 1**.

f [Hz]	125	250	500	1000	2000	4000
α-50 mm	0,2	0,6	0,95	1,0	1,0	0,95

Table 1. Absorption coefficient of mineral glass wool

3.2 Measurement setups

Broadband pink noise is generated with artificial sound source (without flow) for all configurations and with real source in some silencer configurations (uniaxial fan with flow speed of 2,3 m/s in duct) and sound pressure levels (SPL) are measured at inlet duct in front of the silencer), in the duct after silencer (receiving side 2) and in room without diffuse field (receiving side 1), behind the installed silencer in channel as proposed in ISO 11820:1996 [1] for in-situ operating conditions. There are number of possible situations (but due to restrictions the chosen measurement setup is shown in **Fig 1**. The width and height of the empty channel where baffles are located are L_x=1325 mm and L_y=1025 mm.

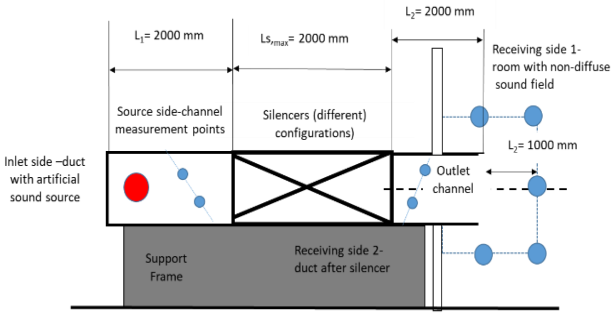

Fig. 1. Measurement setup according ISO 11820:1996 chosen for the considered situation

3.3 Possible effects on the measurement results in in-situ conditions

The source side closed channel was chosen to simulate in-situ conditions with real source in the air handling unit and parallel baffled silencer behind the source. The appropriate length is chosen to scale down the resonance frequencies of empty channel below the frequency range of interest.

A resonance frequency of closed channel at one end as shown in **Fig. 1** is defined with eq. 6, were *c* is speed of sound in air *c*=343 m/s at room temperature, *L* is the total length of the channel and is n is an odd number (1, 3, 5...) representing the resonance mode of interest.

$$f_n = n \cdot \frac{c}{4L} \tag{6}$$

The several resonance frequencies of measurement system for empty channel closed at one end are shown in **Table 2**.

n	1	3	5	7	9
f_n [Hz]	14,3	42,9	71,5	100,1	128,7

Table 2. The resonant frequencies of empty channel closed at one end

4. MEASUREMENT RESULTS

The results for different configurations are compared and discussed here in this paper.Firstly, we show the results obtained for measurement configuration with absorptive baffles and we have compared the IL parameters for the same configuration (L=500 and 2000 mm, s=50 mm, d=100 mm).

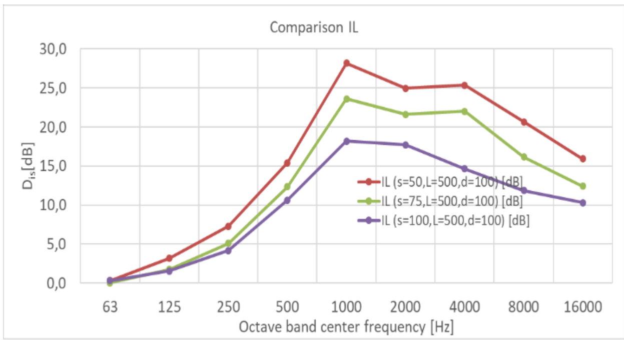

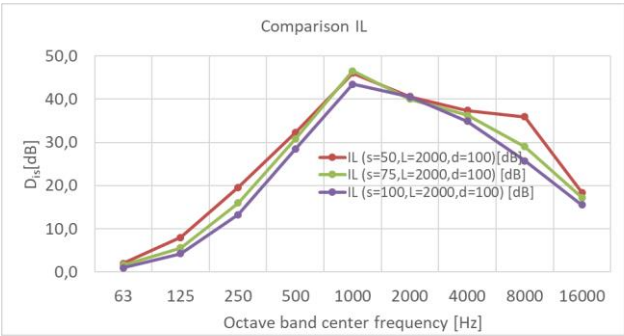

Fig. 2. Comparison between IL parameter for absorptive baffles with given thickness *d*, space *s* and length *L*.

It is evident that TL and IL parameters are not the same as in laboratory configurations due to reflections from baffles and anechoic termination having influence on the results when TL parameter is considered (**Fig. 3.**).

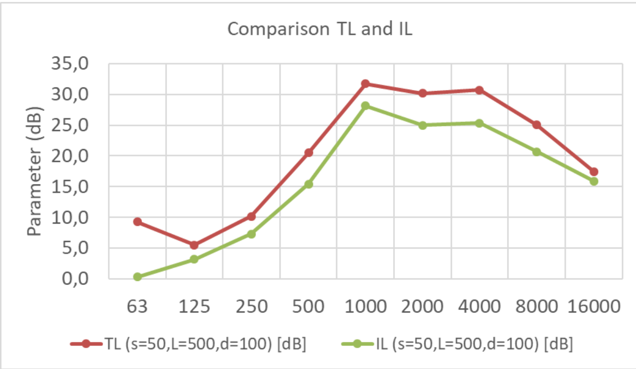

Fig 3. Comparison between TL and IL parameter for the same configuration

This can be avoided by using laboratory setup [2] when additional elements are used in measurement channel (modal filter and anechoic termination).

4.2. Comparison between full absorptive and semi reflective baffles

The comparison in performance between in IL parameter for full absorptive and semi-reflective baffles is shown in **Fig. 4**.

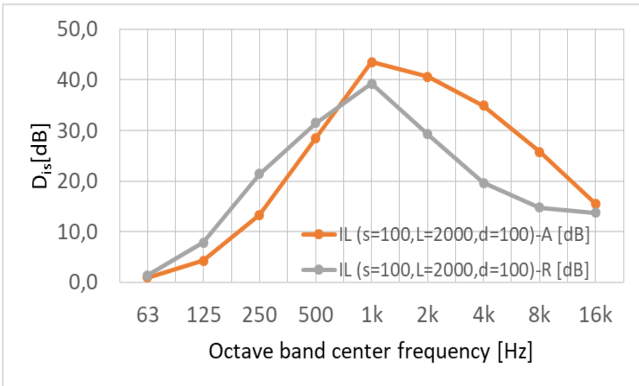

Fig.4. Comparison between absorptive and semi-reflective baffles performance

4.3 Comparison between artificial and real sound source

Additional measurements of IL parameter have been done when the artificial sound source and real sound source (axial fan) giving the flow between baffles of 12 m/s. The results are shown in **Fig. 5.**

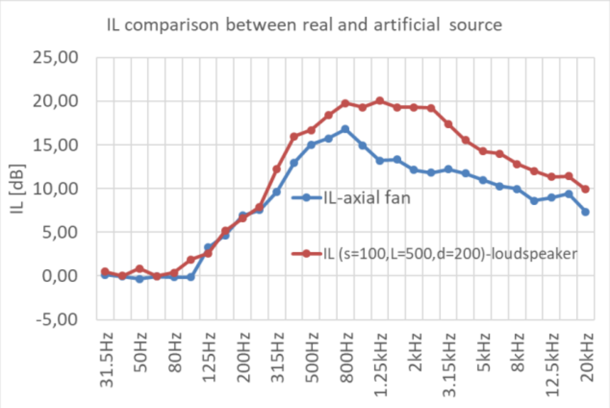

Fig. 5. The comparison in performance when artificial and real sound source are used in measurements.

4.4. Comparison in performance when space between baffles is added in the direction of propagation

The long baffles with L=2000 mm are replaced with two shorter baffles with L=1000 mm with some spacing 110 mm between baffles and the difference in performance for IL (D_{is}) parameter is shown in **Fig. 6.**

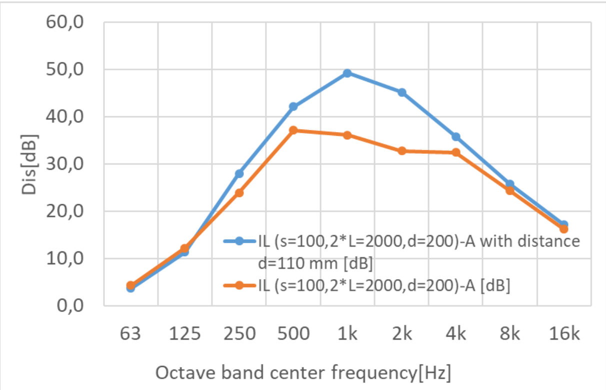

Fig. 6. Comparison of the silencer performance when baffles with L=2000 mm are replaced with two shorter baffles in direction of propagation

4.4. Comparison between measurement and calculation results

The comparison between theoretical calculations according Piening and trapezoidal equation [3,7] and measurement results for one configuration are shown in **Fig. 7**.

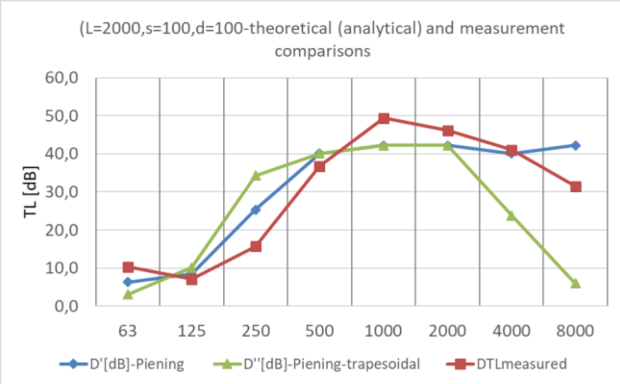

Fig. 7. Comparison between analytical and measurement results for one configuration**.**

The analytical equations use assumption that absorption in baffles linearly depend with length which is not obtained in measurements of SPL level between the baffles. The results for SPL distribution between baffles (L=2000, s=200, d=300) vs. distance from the beginning are shown in **Fig. 8.**

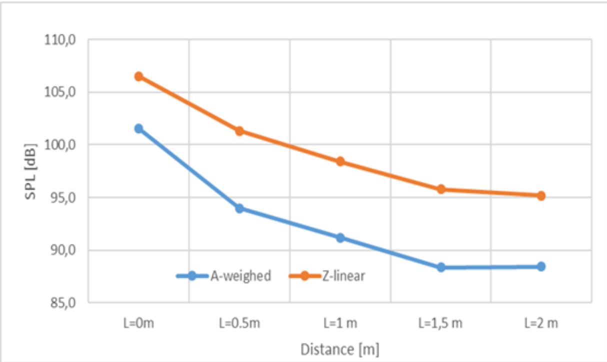

Fig. 8. SPL distribution between central baffles (broadband and A-weighted).

4.5 Measurement uncertainty

The measurement uncertainty for this measurement method (coverage factor k=2, two side interval of conformity, 95 % confidence level for two-sided test) for octave bands of interest are given in **Table 3**. The standard deviations in repeatability conditions are determined by repeating measurements for one configuration. Measurement uncertainties are compared with those in reproducibility conditions given in ISO 3744:2010 Standard [8].

Octave-band centre frequency [Hz]	One-third-octave band centre frequency [Hz]	Standard deviation of repeatability – from measurements [dB]	Standard deviation of reproducibility in ISO 3744:2010 [dB]
31,5	25-40	1,6	-
63	50-80	1,5	5
125	100-160	1,6	3
250	200-315	1,6	2
500	400-630	1,5	1,5
1000	800-1250	1,5	1,5
2000	1600-2500	1,5	1,5
4000	3150-5000	1,5	1,5
8000	6000-10000	1,8	2,5
16000	12500-20000	2,0	2,5
A-weighted		1,4	1,5
Z-linear		1,2	-

Table 3. Measurement uncertainties obtained by repeating measurements

5. CONCLUSION

It is evident that TL is higher few dBs in each octave band of interest due to reflections from baffles on inlet side (increased pressure level at inlet side for different configurations) and reflection from open end of the duct so the difference between sound pressure (power) is larger.

It is also evident , when baffles are longer then influence of space between baffles does not play significant role in silencer performance. The TL parameter is higher at lower frequencies because resonance effects appear at inlet side due to reflection from baffles with small spacing between them.

The semi-reflective baffles are heavier when they are longer so the performance is better at lower frequencies compared with absorptive baffles.

When real source is considered the parameters of silencer are lower at higher frequencies because self-noise appears at higher frequencies and it has significant influence on the performance [9].

The analytical calculation methods by using Piening and trapesiodal formula do not give satisfactory results because analytical equations assume linear dependence of TL vs. length of silencer which is evidently not obtained with measurements. When SPL distribution between baffles is measured it is evident that at the beginning of the baffled channel the SPL gradient is much higher than at the end of baffled part of silencer.

In the future research the laboratory measurement setup will be used having purpose to reduce influence of reflections on measurement results and also pressure drop will be measured having purpose to estimate

6. REFERENCES

[1.] EN ISO 11820:1996, **Acoustics- measurement of silencers in situ**;

[2.] ISO 7235-2003, EN ISO 7235:2009, **Acoustics -- Laboratory measurement procedures for ducted silencers and air-terminal units -- Insertion loss, flow noise and total pressure loss**

[3.] H. V. Fuchs: **Schallabsorber und Schalldämpfer**, book, springer Verlag, 2010.

[4.] M.L. Munjal: **Acoustics of Ducts and Mufflers**, 2nd Edition, 2014.

[5.] David A. Bies, Colin H. Hansen: **Engineering Noise Control: Theory and Practice**, Fourth Edition, 2009.

[6.] R. Binois, E. Perrey-Debain, N. Dauchez, Benoit Nennig, J.-M. Ville, et al.: **On the efficiency of parallel baffle-type silencers in rectangular ducts: prediction and measurement**, Acta Acustica united with Acustica, Hirzel Verlag, 2015, 101, pp.520-530.

[7.] Prof. Dr.-Ing. Helmut V. Fuchs: **Grundlagen der SchalldämpferauslegungTeil 1: Vereinfachte Formeln für sichere Dimensionierung**, IKZ-FACHPLANER Heft12/2007.

[8.] ISO 3744:2010, Acoustics, **Determination of sound power levels and sound energy levels of noise sources using sound pressure -- Engineering methods for an essentially free field over a reflecting plane**.

[9.] VDI 2081:2001, Blatt1, Blatt2, **Noise generation and noise reduction in air conditioning systems**;

8th Congress of the Alps Adria Acoustics Association
Zagreb, Croatia
20 – 21 September 2018

Hrvatsko akustičko društvo
HAD
Acoustical Society of Croatia

MODELLING COLLISION PROBLEMS IN MODEL-BASED SOUND SYNTHESIS OF STRING INSTRUMENTS

Bence SZAKSZ[a] and Péter FIALA[b]

[a] Affiliation 1: Faculty of Mechanical Engineerning, Budapest University of Technology and Economics, Műegyetem rkp. 3-9, 1111 Budapest, HUNGARY, e-mail: szaksz.bence@gmail.com
[b] Affiliation 2: Faculty of Electrical Engineering and Informatics, Budapest University of Technology and Economics, Magyar tudósok körútja 2, 1117 Budapest, HUNGARY

Abstract: *The aim of this paper is to simulate string vibrations in the presence of an obstacle in both directions perpendicular to the string. The rigid obstacle is suspended through a spring – damper system. Penalty method is used to solve the problem of nonlinear interaction between the string and the obstacle. In the simulation, schemes based on modal superposition and spatial discretization are combined. Based on these the paper introduces a finite differential scheme that, in the case of free vibrations, gives a perfect result regardless of the time step size, but it is also appropriate to consider nonlinear interactions. One possible application of this simulation is the modelling of the "slide" guitar technique. In this case, the string is released from an initial shape that forms due to the static equilibrium with the nonlinear contact force. Finite element method is used to determine this initial shape. The energy level of the numerical simulation is examined as well. The paper gives a minimum sampling frequency above which the whole system will be stable.*

Key words: numerical methods, 3D string vibration, collision, sound synthesis

1. INTRODUCTION

The physical background of collisions has been investigated for a long time. Hertz wrote the earliest publication in 1881 in this topic [1]. One of the most obvious problems is the string-obstacle interaction, which was the subject of many publications.
The interaction between an ideal string and a rigid obstacle was solved analytically in the second half of the 20th century [2,3]. Later, with the spread of computers, the numerical approach to the problem opened new possibilities. It was easier to take into account the string stiffness and the nonlinearity of the collision.
There are two ways to model the vibrations in a string. One possibility is the spatial and temporal discretization of the equation of motion [4]. The spatial discretization can be made by final difference or finite element method. For the temporal discretization, time-stepping schemes are applicable that are based on finite differences. The advantage of the time-stepping methods is that they can model nonlinear processes. Some numerical methods are using digital waveguides to simulate the discretized system [5,6,7].
The other possibility is the modal superposition [8,9]. The free vibration of the string can be modelled with this method nearly without errors in the case of sufficient number of modelled modes. The disadvantage of this method is that it is not applicable for nonlinear problems since it is based on superposition.
The discretization schemes and the modal superposition can be combined as well. This method was used in [10,11] where the nonlinear collision of a string with a fixed obstacle was modelled.
This paper uses the combined scheme to model the interaction between a string and an obstacle, which is suspended through a spring-damper system. After describing the method the energy balance is examined. One possible application of this simulation is the modelling of the slide guitar. It is examined as well how the scheme can describe the slide guitar. In this case, the string is released from an initial shape that forms due to the static equilibrium with the nonlinear contact force. The paper uses finite element method to determine this initial shape. Finally, the simulation results are examined in Section 3.

2. MODELLING THE COLLISION OF A STRING WITH AN OBSTACLE

2.1. Continuous model

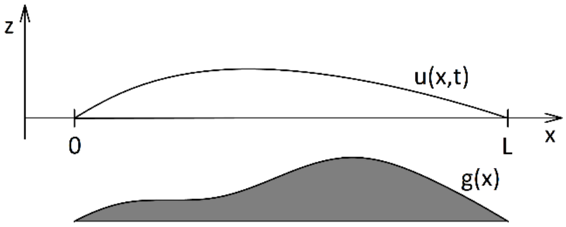

Fig.1. Vibration of a string in the presence of a g(x) obstacle

A stiff string with length L [m], mass per unit length μ [kg/m], Young modulus E [Pa], and second moment of inertia I [m^4] is considered. It is stretched in x-direction with tension T [N]. The lateral displacement of the string is denoted with $u(x,t)$ in z-direction and with $v(x,t)$ in y-direction. The string is vibrating in the presence of an obstacle $g(x,t)$. The force per unit length coming from the interaction with the obstacle is denoted with $f(x,t)$ [N/m] in the z-direction and with $f_f(x,t)$ [N/m] in the y-direction. The equation of motion with these notations is:

$$\mu\ddot{u}(x,t) - Tu''(x,t) + EIu''''(x,t) = f(x,t) \qquad (1)$$

$$\mu\ddot{v}(x,t) - Tv''(x,t) + EIv''''(x,t) = f_f(x,t) \qquad (2)$$

In these partial differential equations dot denotes time derivative and prime stand for spatial derivatives. Boundary conditions are also needed to solve the equations. Because of the pinned ends the boundary conditions are ($\forall t \in \mathrm{R}^+$):

$$\mathrm{u}(0,\mathrm{t}) = \mathrm{u}(\mathrm{L},\mathrm{t}) = 0 \ \text{ and } \ u''(0,t) = u''(L,t) = 0 \quad (3)$$

$$\mathrm{v}(0,\mathrm{t}) = \mathrm{v}(\mathrm{L},\mathrm{t}) = 0 \ \text{ and } \ v''(0,t) = v''(L,t) = 0 \quad (4)$$

The interaction force f(x,t) is calculated by using a penalty method [10,11]. The string can penetrate the obstacle but that is 'punished' with larger reaction force, that is nonzero only if the string penetrates the obstacle (u(x,t) < g(x,t)), in this case the force increases nonlinearly.

$$\mathrm{f}(\mathrm{x},\mathrm{t},\mathrm{u}) = \mathrm{f}\big(\eta(\mathrm{x},\mathrm{t},\mathrm{u})\big) = \mathrm{K}[\eta(\mathrm{x},\mathrm{t},\mathrm{u})]_+^{\alpha} \qquad (5)$$

where η(x,t,u)=g(x)-u(x,t) is the penetration, K is the stiffness of the contact and α is the exponent that describes the nonlinearity. The force is zero if η is negative, this is indicated with the $[.]_+$ notation, which represents the positive part of the argument: $[\mathrm{x}]_+ = \frac{x+|x|}{2}$.

The force can be represented as the derivative of a potential ($\psi(\eta)$) according to the penetration: $\mathrm{f} = \frac{d\psi}{d\eta}$.

$$\psi(\eta(\mathrm{x},\mathrm{t},\mathrm{u})) = \frac{\mathrm{K}}{\alpha+1}[\eta(\mathrm{x},\mathrm{t},\mathrm{u})]_+^{\alpha+1} \qquad (6)$$

The contact force in the y-direction is described with Coulomb friction, which is the function of the relative velocity of two bodies. This force is acting only if the string is in interaction with the obstacle, and therefore the horizontal motion of the string is coupled with its vertical motion. Eq. (7) describes the formula of the friction force.

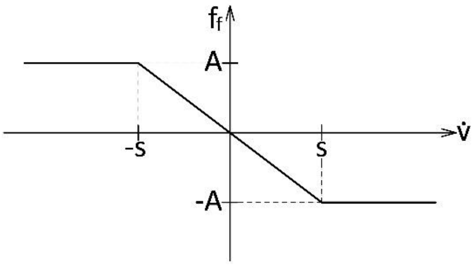

Fig.2. The Coulomb friction

$$f_f(\dot{v}) = A\begin{cases} 1 & if \ \ \dot{v} < s \ \ and \ \ u < g \\ \dot{v}/s & if \ \ |\dot{v}| < s \ \ and \ \ u < g \\ -1 & if \ \ \dot{v} < s \ \ and \ \ u < g \\ 0 & if \ \ u < g \end{cases} \qquad (7)$$

2.2. Modal description including losses

The motion of the string can be described with the modal superposition, but there is a need for discretization. Using the first N_m modes the displacement can be approximated as:

$$\hat{u}(\mathrm{x},\mathrm{t}) = \sum_{j=1}^{\mathrm{N}_m} q_j(t)\phi_j(x) \qquad (8)$$

where $q_j(t)$ refers to the j-th modal amplitude and $\phi_j(x) = \sqrt{\frac{2}{L}}\sin\left(\frac{j\pi}{L}x\right)$ is the j-th normalized mode. Substituting this expression in Eq. (1) and adding losses, the following equation can be obtained:

$$\mu(\ddot{\boldsymbol{q}}(t) + 2\Upsilon\dot{\boldsymbol{q}}(t) + \boldsymbol{\Omega}^2\boldsymbol{q}(t)) = \boldsymbol{F}(t) \qquad (9)$$

where $\boldsymbol{F}(t)$ represents the generalized force vector, which contains the interaction force projected onto the modes, $\boldsymbol{q}(t) = [q_1(t), q_2(t), \ldots\, q_{\mathrm{N}_m}(t)]^T$ is the vector of the modal coordinates, Υ and $\boldsymbol{\Omega}$ are diagonal matrices with $\Upsilon_{jj} = \sigma_j \geq 0$ which represent the j-th damping coefficient, and $\Omega_{jj} = \omega_j$ which is the j-th natural frequency. The damping coefficient σ_j is the inverse of the quality factor (Q_j).

$$\sigma_j = \mathrm{Q}_j^{-1} = \mathrm{Q}_{j,air}^{-1} + \mathrm{Q}_{j,ve}^{-1} + \mathrm{Q}_{j,te}^{-1} \tag{10}$$

In the model, three types of loss are considered that belong to the string. The losses are coming from the air resistance ($\mathrm{Q}_{j,air}^{-1}$) and from the unideal material properties of the string like the viscoelasticity ($\mathrm{Q}_{j,ve}^{-1}$)and the thermoelasticity ($\mathrm{Q}_{j,te}^{-1}$) [10].

$$\mathrm{Q}_{j,air}^{-1} = \frac{R}{\mu\omega_j}, \;\; \mathrm{R} = 2\pi\eta_{air} + \pi d\sqrt{2\eta_{air}\rho_{air}\omega_j} \tag{11}$$

$$\mathrm{Q}_{j,ve}^{-1} = \frac{\mu EI\delta_{ve}}{T^2}{\omega_j}^2 \tag{12}$$

where η_{air} refers to the dynamic viscosity and ρ_{air} to the density of the air. The viscoelastic loss angle and the thermoelastic quality factor can be approximated from measurements, $\delta_{ve} = 4.5 \cdot 10^{-3}$ and $Q_{j,te}^{-1} = 2.03 \cdot 10^{-4}$. Another loss type is the dissipation during the interaction between the string and the obstacle. The contact force reduces according to the dissipated energy [10].

$$f(\mathrm{x,t,u}) = \frac{d\psi(\mathrm{x,t,u})}{d\eta(\mathrm{x,t,u})} + \frac{d\eta(\mathrm{x,t,u})}{dt}\mathrm{K}\beta[\eta(\mathrm{x,t,u})]_+^{\alpha} \tag{13}$$

The coefficient $\beta \geq 0$ influences the amount of the dissipation. According to this formula the contact force is larger at increasing penetration than at decreasing penetration, so the collision is dissipative.

2.3. Numerical scheme

The modal solution has to be combined with the finite difference method in order to be able to simulate the nonlinear interaction between the string and the obstacle. Dividing the string into *N* pieces leads to *N*+1 nodes. The displacement of the first and last node is zero therefore the displacement should be calculated and stored only at the internal nodes (*i*=1, 2, …, *N*-1). The displacement at a certain point of the string can be calculated by discretizing Eq. (8).

$$u(\mathrm{x}_i,\mathrm{t}) = \mathrm{u}_i(\mathrm{t}) = \sum_{j=1}^{\mathrm{N}-1} q_j(t)\phi_j(\mathrm{x}_i) \tag{14}$$

In this expression, the same number of modes is used as the number of internal nodes. Eq. (14) can be reformulated in a matrix form, where $\boldsymbol{S}$ is a symmetric matrix with the entries $S_{ij} = \sqrt{\frac{2}{L}}sin\left(\frac{j\pi i}{N}\right) = \phi_j(x_i)$.

$$\boldsymbol{u} = \boldsymbol{Sq} \tag{15}$$

The matrix $\boldsymbol{S}$ is invertible since it is square and it is containing the orthonormal modes. Therefore, the vector of the modal coordinates can be calculated from the displacement vector $\boldsymbol{u}$.
The analytical solution of Eq. (9) is known [10] and gives the following difference scheme:

$$\frac{\mu}{\Delta t^2}\left(\boldsymbol{q^{n+1}} - \boldsymbol{Cq^n} + \boldsymbol{\widetilde{C}q^{n-1}}\right) = \boldsymbol{F^n} \tag{16}$$

where

$$\mathrm{C}_{ii} = e^{-\sigma_i\Delta t}\left(e^{\sqrt{{\sigma_i}^2-{\omega_i}^2}\Delta t} + e^{-\sqrt{{\sigma_i}^2-{\omega_i}^2}\Delta t}\right) \tag{17}$$

$$\widetilde{\mathrm{C}}_{ii} = e^{-2\sigma_i\Delta t} \tag{18}$$

In Eq. (16) the superscript *'n'* refers to the actual, *'n+1'* to the subsequent and *'n-1'* to the previous value of the variable. The excitation is known as a function of the displacement ($\boldsymbol{f^n}$) thus Eq. (16) should be premultiplied by $\boldsymbol{S}$ and combined with Eq. (15) to get a formula, which is applicable in a simulation.

$$\frac{\mu}{\Delta t^2}\left(\boldsymbol{u^{n+1}} - \boldsymbol{Du^n} + \boldsymbol{\widetilde{D}u^{n-1}}\right) = \boldsymbol{f}^n \tag{19}$$

where:

$$\boldsymbol{D} = \boldsymbol{SCS^{-1}} \text{ and } \boldsymbol{\widetilde{D}} = \boldsymbol{S\widetilde{C}S^{-1}} \tag{20}$$

This formula gives an almost perfect result, regardless of the time step size, in the case of free vibrations, but it is also appropriate to consider nonlinear interactions.
The discretized equation of motion in the *y*-direction is similar to the one in *z*-direction.

$$\frac{\mu}{\Delta t^2}\left(\boldsymbol{v^{n+1}} - \boldsymbol{Dv^n} + \boldsymbol{\widetilde{D}v^{n-1}}\right) = \boldsymbol{f_f}^n(\boldsymbol{\xi}^n) \tag{21}$$

where $\boldsymbol{\xi}^n = \frac{\boldsymbol{v}^{n+1}-\boldsymbol{v}^{n-1}}{2\Delta t}$ is the horizontal velocity. After expressing $\boldsymbol{v}^{n+1}$ from the definition of $\boldsymbol{\xi}^n$ the only unknown will be the velocity and so the equation will be solvable.

$$\boldsymbol{v^{n-1}} - \boldsymbol{Dv^n} + \boldsymbol{\widetilde{D}v^{n-1}} + 2\Delta t\boldsymbol{\xi}^n - \frac{\Delta t^2}{\mu}\boldsymbol{f}^n(\boldsymbol{\xi}^n) = \boldsymbol{0} \tag{22}$$

2.4. Collision with a mass-spring-damper system

In this section the collision with a rigid obstacle, which is suspended through a spring–damper system, is examined (Fig.3.).

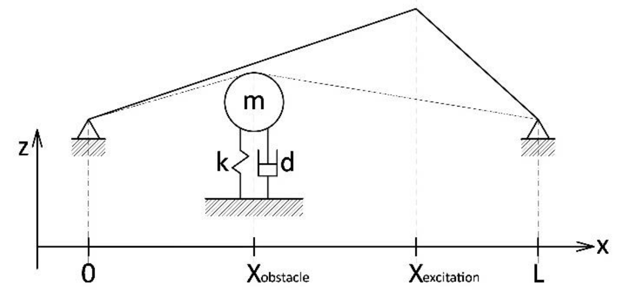

Fig.3. Modelling the obstacle as a mass-spring-damper system

Eq. (23) is Newton's 2nd law for the rigid body.

$$-\int f(\mathrm{x},\mathrm{t})dx - kg(\mathrm{t}) - d\dot{g}(\mathrm{t}) = m\ddot{g}(\mathrm{t}) \qquad (23)$$

Where g refers to the displacement of the body in z-direction, k [N/m] is the stiffness of the spring, d [Ns/m] is the damping factor, m [kg] is the mass of the body and f(x,t) [N/m] refers to the contact force per unit length that is already used in Eq. (1) and Eq. (5). To be able to use in a numerical simulation, Eq. (23) should be discretized with respect to time and space. Using the finite difference method it will turn to the following expression.

$$-\sum_{i=1}^{N-1} f_i^n \Delta x = kg^n + d\delta_{t\cdot}g^n + m\,\delta_{tt}g^n \qquad (24)$$

with the difference operators $\delta_{t\cdot}g^n = \frac{g^{n+1} - g^{n-1}}{2\Delta t}$ and $\delta_{tt}g^n = \frac{g^{n+1} - 2g^n + g^{n-1}}{\Delta t^2}$. The body is able to move only in the z-direction, therefore the position of its surface can be described with its geometry $\boldsymbol{g}_{geom}$ and its vertical displacement g^n.

$$\boldsymbol{g}_{surf}{}^n = \boldsymbol{g}_{geom} + g^n \cdot \mathbf{1} \qquad (25)$$

Where $\mathbf{1}$ is a $(N-1) \times 1$ vector containing only ones. The penetration $\boldsymbol{\eta}^n$ depends on these new parameters.

$$\boldsymbol{\eta}^n = \boldsymbol{g}_{surf}{}^n - \mathbf{u}^n = \boldsymbol{g}_{geom} + g^n \cdot \mathbf{1} - \mathbf{u}^n \qquad (26)$$

The motion of the string and the body can be coupled by multiplying Eq. (24) with $\mathbf{1}$ and combining with Eq. (26) and Eq. (19). After simplifications one will get a system of nonlinear equations where the only unknown variable is $\boldsymbol{r} = \boldsymbol{\eta}^{n+1} - \boldsymbol{\eta}^{n-1}$.

$$\mathbf{0} = \frac{\Delta t^2}{\mu}\boldsymbol{f} + [\boldsymbol{P}\boldsymbol{f}dx + \boldsymbol{e}] \cdot \frac{1}{\frac{m}{\Delta t^2} + \frac{d}{2\Delta t}} + \boldsymbol{a} + \boldsymbol{b} + \boldsymbol{r} \qquad (27)$$

where $\boldsymbol{P}$ is a $(N-1) \times (N-1)$ matrix containing only ones, that summarizes the entries of the force vector and multiplies those with $\mathbf{1}$ too. The entries of the contact force vector $\boldsymbol{f}$ are:

$$f_i(r_i, a_i) = \frac{\psi(r_i + a_i) - \psi(a_i)}{r_i} + \frac{1}{2\Delta t} r_i K \beta [\eta_i{}^n]_+^\alpha \qquad (28)$$

and

$$\boldsymbol{a} = \boldsymbol{\eta}^{n-1} \qquad (29)$$

$$\boldsymbol{b} = \boldsymbol{D}\boldsymbol{u}^{\boldsymbol{n}} - \widetilde{\boldsymbol{D}}\boldsymbol{u}^{\boldsymbol{n-1}} - \boldsymbol{g}_{geom} \qquad (30)$$

$$\begin{aligned} \boldsymbol{e} &= \left(\mathbf{u}^n + \boldsymbol{\eta}^n - \boldsymbol{g}_{geom}\right)\left(k - \frac{2m}{\Delta t^2}\right) \\ &+ \left(\mathbf{u}^{n-1} + \boldsymbol{\eta}^{n-1} - \boldsymbol{g}_{geom}\right)\left(\frac{m}{\Delta t^2} - \frac{d}{2\Delta t}\right) \end{aligned} \qquad (31)$$

If there is no interaction then the body and the string are moving separately and their motion is described with linear equations. In the case of the nonlinear contact, the solution of Eq. (27) can be obtained with Newton-Raphson method. After calculating $\boldsymbol{r}$ one gets the displacement of the body and the string by substituting back into Eq. (26) and Eq. (24).

2.5. Stability of the numerical method

One of the most important properties of a numerical scheme is its stability. This section examines the stability limitations of the method described in section 2.4.
Rewriting the equation of motion of the string (Eq. (16)) the energy types are easier to recognize.

$$\left(\breve{\boldsymbol{C}}_1 \delta_{tt}\boldsymbol{q}^{\boldsymbol{n}} + \breve{\boldsymbol{C}}_2 \boldsymbol{q}^{\boldsymbol{n}} + \delta_{t\cdot}\breve{\boldsymbol{C}}_3 \boldsymbol{q}^{\boldsymbol{n}}\right) = \boldsymbol{F}^n \qquad (32)$$

with the coefficient matrices:

$$\breve{\boldsymbol{C}}_{1,ii} = \frac{1 + \tilde{\mathrm{C}}_{ii}}{2} \qquad (33)$$

$$\breve{\boldsymbol{C}}_{2,ii} = \frac{1 - \mathrm{C}_{ii} + \tilde{\mathrm{C}}_{ii}}{\Delta t^2} \qquad (34)$$

$$\breve{\boldsymbol{C}}_{3,ii} = \frac{1 - \tilde{\mathrm{C}}_{ii}}{\Delta t} \qquad (35)$$

Multiplying with the matrix $\boldsymbol{S}$ and using the new parameters $\breve{\boldsymbol{D}}_1 = \boldsymbol{S}\breve{\boldsymbol{C}}_1\boldsymbol{S}^{-1}$, $\breve{\boldsymbol{D}}_2 = \boldsymbol{S}\breve{\boldsymbol{C}}_2\boldsymbol{S}^{-1}$ and $\breve{\boldsymbol{D}}_3 = \boldsymbol{S}\breve{\boldsymbol{C}}_3\boldsymbol{S}^{-1}$ Eq. (32) becomes:

$$\mu\left(\breve{\boldsymbol{D}}_1 \delta_{tt}\boldsymbol{u}^n + \breve{\boldsymbol{D}}_2 \boldsymbol{u}^n + \breve{\boldsymbol{D}}_3 \delta_{t\cdot}\boldsymbol{u}^n\right) = \boldsymbol{f}^n \qquad (36)$$

Defining the scalar product of two vectors as $\langle \boldsymbol{u}, \boldsymbol{v} \rangle = \Delta x \sum_{i=1}^{N-1} u_i v_i$ and multiplying Eq. (36) with the string velocity ($\delta_{t\cdot}\boldsymbol{u}^n$) leads to the time derivative of the energy.

$$\frac{\mu}{2}\langle\breve{\boldsymbol{D}}_1\delta_{t+}\boldsymbol{u}^n,\delta_{t+}\boldsymbol{u}^n\rangle+\frac{\mu}{2}\langle\breve{\boldsymbol{D}}_2\boldsymbol{u}^n,\boldsymbol{u}^{n+1}\rangle \\ +\mu\langle\breve{\boldsymbol{D}}_3\delta_{t\cdot}\boldsymbol{u}^n,\delta_{t\cdot}\boldsymbol{u}^n\rangle=\langle\boldsymbol{f}^n,\delta_{t\cdot}\boldsymbol{u}^n\rangle \tag{37}$$

The energies belonging to the obstacle are calculable in a similar way. Multiplying the equation of motion of the body with its velocity ($\delta_{t\cdot}g^n$) leads to the time derivative of the energy balance.

$$m\cdot\delta_{tt}g^n\delta_{t\cdot}g^n+k\cdot g^n\delta_{t\cdot}g^n+d\cdot\delta_{t\cdot}g^n\delta_{t\cdot}g^n \\ =-\delta_{t\cdot}g^n\sum_{i=1}^{N-1}f_i^n\Delta x \tag{38}$$

Adding Eq. (37) and Eq. (38) results the energy:

$$H^{n+1/2}=H_{string}^{n+1/2}+H_{obstacle}^{n+1/2}+H_{contact}^{n+1/2} \tag{39}$$

where

$$H_{string}^{n+1/2}=\frac{\mu}{2}\langle\breve{\boldsymbol{D}}_1\delta_{t+}\boldsymbol{u}^n,\delta_{t+}\boldsymbol{u}^n\rangle+\frac{\mu}{2}\langle\breve{\boldsymbol{D}}_2\boldsymbol{u}^n,\boldsymbol{u}^{n+1}\rangle \tag{40}$$

$$H_{obstacle}^{n+1/2}=\frac{m}{2}\cdot\delta_{t+}g^n\delta_{t+}g^n+\frac{k}{2}\cdot g^ng^{n+1} \tag{41}$$

$$H_{contact}^{n+1/2}=\langle\boldsymbol{\psi}^{n+1/2},\boldsymbol{1}\rangle \tag{42}$$

and the dissipation:

$$\delta_{t-}H^{n+1/2}=-\mu\langle\breve{\boldsymbol{D}}_3\delta_{t\cdot}\boldsymbol{u}^n,\delta_{t\cdot}\boldsymbol{u}^n\rangle-d\cdot(\delta_{t\cdot}g^n)^2 \\ -\langle\delta_{t\cdot}\boldsymbol{u}^n,\delta_{t\cdot}\boldsymbol{u}^nK\beta[\boldsymbol{\eta}]_+^\alpha\rangle \tag{43}$$

with the difference operators $\delta_{t+}u^n=\frac{u^{n+1}-u^n}{\Delta t}$ and $\delta_{t-}u^n=\frac{u^n-u^{n-1}}{\Delta t}$. $\breve{\boldsymbol{D}}_3$ is positive semidefinite [10] and $d,\beta\geq 0$, so the time derivative of the energy balance of the whole system is negative, thus the system is stable if the total energy is positive for all time steps. If Eq. (40), Eq. (41) and Eq. (42) are all positive, then this is true. Eq. (42) is positive because of the definition of the potential. It can be seen that Eq. (40) is also positive [10] and Eq. (42) has a lower limit :

$$H_{obstacle}^{n+1/2}\geq(\delta_{t+}g^n)^2\left(\frac{m}{2}-\frac{\Delta t^2}{4}\frac{k}{2}\right) \tag{44}$$

Thus choosing the time step size to $\Delta t<2\sqrt{\frac{m}{k}}$ results a stable system. This corresponds to π-times the eigenfrequency of the spring-mass system.

Moving the obstacle in *x*-direction does not need any external energy in a continuous system, because there are no forces acting in this direction, but the simulation will not always be stable. Numerically it can be done by moving the geometry of the obstacle and recalculating at the node points of the string. In this case Eq. (42) will change to the following expression which can be negative:

$$H_{contact}^n=\frac{\Delta x}{2}\cdot\sum_{i=1}^{N-1}(\psi_i^{n+1}-\psi_i^{n-1}) \\ \cdot\left(1-\frac{geom_i^{n+1}-geom_i^{n-1}}{\eta_i^{n+1}-\eta_i^{n-1}}\right) \tag{45}$$

2.6. Calculation of an initial shape with FEM

In the case of the slide guitar technique, the string is released from an initial shape that forms due to the static equilibrium with the nonlinear contact force. One way to calculate this shape is using the finite element method.

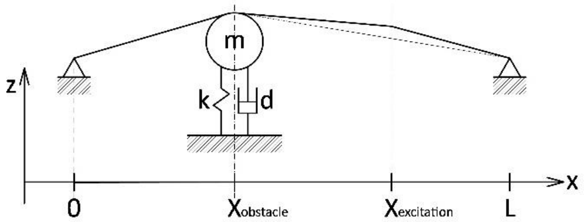

Fig.4 The shape of the string at the moment of the plucking

In this section the position of the obstacle is considered to be fixed. The initial compression of the string, belonging to this position, will be calculated after knowing the contact force at the static equilibrium. Determination of the initial shape is based on the boundary value problem that comes from Eq. (1) and Eq. (3), with $\ddot{u}(x,t_0)=0$.

$$-Tu''(x)+EIu''''(x)=f(x) \tag{46}$$

$$\mathrm{u}(0)=\mathrm{u}(\mathrm{L})=0\ \text{ and }\ u''(0)=u''(L)=0 \tag{47}$$

The solution is defined as the superposition of the basis functions $\phi_j(x)$.

$$u(x)\approx\sum_{j=1}^{n}\phi_j(x)q_j \tag{48}$$

Applying the Galerkin method leads to the expression:

$$EI\int_{x=0}^{L}\phi_i(x)u''''(x)\,dx-T\int_{x=0}^{L}\phi_i(x)u''(x)\,dx \\ =\int_{x=0}^{L}\phi_i(x)f(x)dx \tag{49}$$

After partial integration, utilizing the boundary conditions and substituting Eq. (48), Eq. (49) can be written in a matrix form.

$$(\boldsymbol{K}_1 + \boldsymbol{K}_2)\boldsymbol{q} = \boldsymbol{f} \tag{50}$$

with

$$K_{1,ij} = EI\left(\int_{x=0}^{L} \phi_i''(x)\phi_j''(x)\,dx + [\phi_i \cdot u''']_0^L\right) \tag{51}$$

$$K_{2,ij} = T\left(\int_{x=0}^{L} \phi_i'(x)\phi_j'(x)\,dx - [\phi_i \cdot u']_0^L\right) \tag{52}$$

$$K_{2,ij} = T\left(\int_{x=0}^{L} \phi_i'(x)\phi_j'(x)\,dx - [\phi_i \cdot u']_0^L\right) \tag{53}$$

$$f_i = \int_{x=0}^{L} \phi_i(x) f(x) dx \tag{54}$$

Here $\boldsymbol{K}_1$ and $\boldsymbol{K}_2$ are the stiffness matrices of the system, $\boldsymbol{q}$ contains the coefficients of the basis functions and $\boldsymbol{f}$ is the vector of the excitation. Eq. (50) can be solved by using third order basis functions for a known excitation. But the interaction force is nonlinear, therefore the initial shape can be determined only iteratively, which is arranged with Newton Raphson method. An error function is defined as:

$$\boldsymbol{r}(\boldsymbol{q}) = (\boldsymbol{K}_1 + \boldsymbol{K}_2)\boldsymbol{q} - \boldsymbol{f} \tag{55}$$

and the square of its norm should be minimized. But the nodes at the ends of the string and at the excitation can not move, the iteration may move only the unconstrained nodes (uDOF). Let $\boldsymbol{R}(\boldsymbol{q})$ be the derivative of the error function according to $\boldsymbol{q}$.

$$\boldsymbol{R}(\boldsymbol{q}) = (\boldsymbol{K}_1 + \boldsymbol{K}_2) - diag(\boldsymbol{f}') \tag{56}$$

$$\boldsymbol{q}_{uDOF}^{n+1} = \boldsymbol{q}_{uDOF}^{n} - {\boldsymbol{R}_{uDOF}^{n}}^{-1}\boldsymbol{r}_{uDOF}^{n} \tag{57}$$

Here prime is used for the derivative according to $\boldsymbol{q}$. If the Newton-Raphson method is used in this way then the solution can converge quite quickly and accurately.

3. SIMULATION

In this section, the simulation results are examined in the case of different parameter settings.
First the string is excited next to a standing obstacle and its motion is observed both in the vertical and in the horizontal plane. The vibration is examined both at the excited and at the non-excited sides of the string in the case of different stiffness parameters. The energy balance is investigated as well. In section 3.4. the effect of different obstacle parameters is compared. Finally the string vibration and its energy balance is examined when the obstacle is moving in the *x*-direction.

3.1. Parameter setting

The standard parameters that are used in the simulations, if there is no other value mentioned, are corresponding to a ‘g’ guitar string.

d [mm]	μ [kg/m]	L [m]	B [-]	T [N]
0.457	1.30e-3	0.650	1.18e-4	84.6

Table 1. String parameters

For the calculation of losses, it is necessary to know the density and the viscosity of the air and to define the thermoelastic loss and the viscoelastic loss angle.

$\rho_{air}\ [kg/m^3]$	$\eta_{air}\ [Ns/m^2]$	$Q_{te}^{-1}\ [-]$	δ_{ve} [-]
1.20	1.80e-5	2.03e-4	4.50e-3

Table 2. Loss parameters

The excitation is at ¾ string length and the obstacle is at 0.3 L. The shape of the body is choosen to a cylinder with the radius $R_{cyl.}$ The used parameters of the obstacle and those of the interaction are:

$R_{cyl}\ [m]$	$m\ [kg]$	$k\ [N/m]$	$d\ [Ns/m]$
2.40e-2	0.04	5e4	5e2

Table 3. Obstacle parameters

$K\left[\frac{N}{m^{\alpha+1}}\right]$	α [-]	$s\ [m/s]$	$A\ [N]$
1e13	1.5	1e-5	0.03

Table 4. Contact parameters

The sampling frequency (Fs) of the simulation was chosen to thousand times the first eigenfrequency of the ‘g’ string, so to 196 [kHz]. In order to not to use undersampled modes, the modes with higher eigenfrequencies than Fs/6 were filtered out.

3.2. Vertical vibration

In this section, the vertical vibration and its energy balance is examined.
The simulation was run with three different string stiffnesses (Fig.5.). The scheme calculates with viscoelastic losses as well. Therefore, the higher the stiffness, the faster the energy of the system decreases. The string is less flexible in the case of higher stiffness, which can be seen on the figure as well.

Increasing stiffness means increasing inharmonicity, thus the eigenfrequencies of the string will be shifted up.

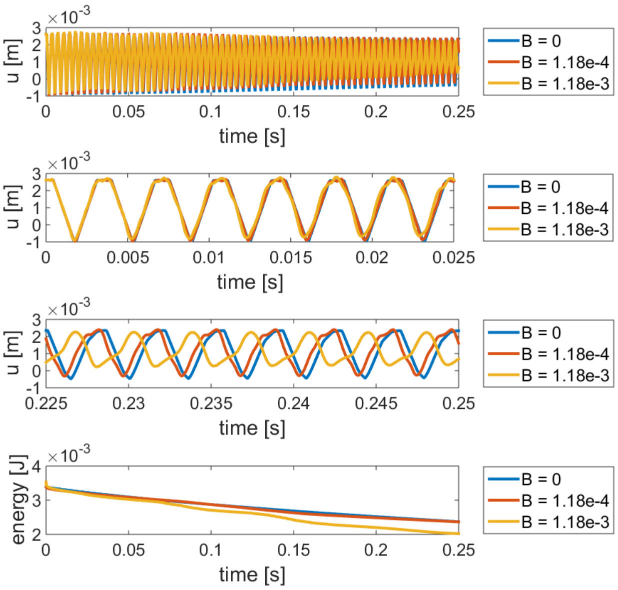

Fig.5. Comparing the effect of different string stiffnesses. Vertical vibration is observed on the excited side of the string

Table 5. compares the analytically calculated eigenfrequencies with those derived from the numerical simulation. The eigenfrequencies are almost the same, that means, that the obstacle (with these parameters) is behaving like a pinned end.

B = 0		*B = 1.18e-4*		*B = 1.18e-3*	
Num. [Hz]	Anal. [Hz]	Num. [Hz]	Anal. [Hz]	Num. [Hz]	Anal. [Hz]
280.4	280.3	280.8	280.3	282.2	280.5
561.1	560.7	562.0	560.8	565.9	562.0
839.8	841.0	842.2	841.4	848.3	845.4
1121.8	1121.3	1122.6	1122.4	1132.3	1131.9
1402.9	1401.7	1404.5	1403.7	1417.7	1422.2

Table 5. Eigenfrequencies in the case of different string stiffness values

Fig.6. shows the motion of that side of the string which was not plucked. In the beginning it performs forced vibration under the action of the other side, after 0.1 second it turns to the eigenfrequency of the examined side. Increasing the string stiffness cause stronger coupling between the two side, therefore the amplitude of the vibration will be larger.

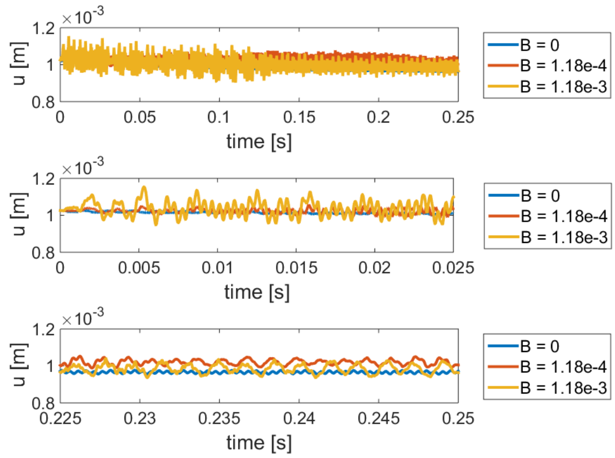

Fig.6. Comparing the effect of different string stiffnesses. Vertical vibration is observed on the not excited side of the string

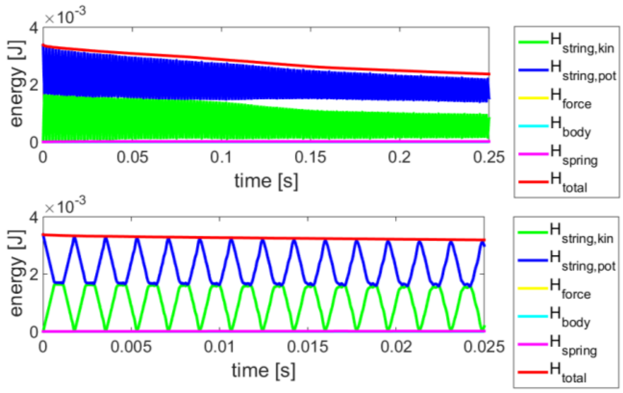

Fig.7. The energies belonging to the vertical motion of the system

Fig.7. presents the different energy types of the system. As it can be seen, the string stores the main part of the energy. Its kinetic energy starts from zero because the string was released with zero initial velocity. Because of the obstacle, the equilibrium position of the string is not in the u = 0 plane, therefore its potential energy is shifted up. Both the kinetic and the potential energy is changing periodically in time on the frequency of the excited side. Because of the built in dissipations the total energy of the system is decreasing.

3.3. Horizontal vibration

The horizontal vibration is similar to the vertical vibration, but the dissipation is much larger in the horizontal case. The string is vibrating on its original frequency (196 Hz) which belongs to its total length. But because of the Coulomb friction, the horizontal vibration of the string will be negligible within 0.1 seconds independently of the stiffness of the string.

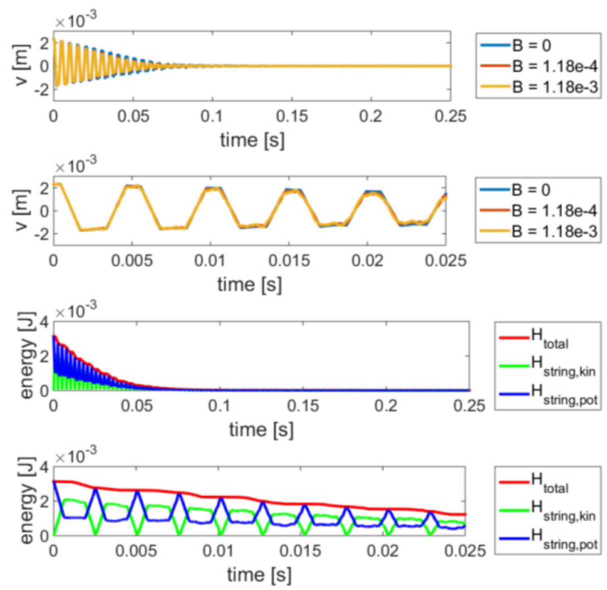

Fig.8. Comparing the effect of different string stiffnesses, and the change of the stored energy (B = 1.18e-4) belonging to the horizontal vibration.

3.4. Changing the parameters of the obstacle

It is interesting to examine the effect of changing the parameters of the spring-mass-damper system.
Fig.9. shows the changing of the energies in the case of different obstacle parameters. The red line belongs to a parameter setting which means already an overdamped mass-spring-damper system. In the case of smaller damping coefficient the obstacle is underdamped (Fig.10.) and the total energy decreases less. However, using large *d* value leads to barely moving body and the dissipation will be smaller.
The initial equilibrium state requires the same contact force, therefore the compression of the spring will be different in the case of different stiffness values. Thus the spring and also the system have larger initial total energy if the stiffness is smaller, but the dissipation will be smaller by increasing the stiffness.
Increasing the mass of the obstacle leads to lower velocity of the body therefore to less dissipation through the damper.
The displacement of the body in the case of these parameter settings, except *k* = 500 [N/m], is smaller than 50 μm which means that it can be considered as a pinned end.

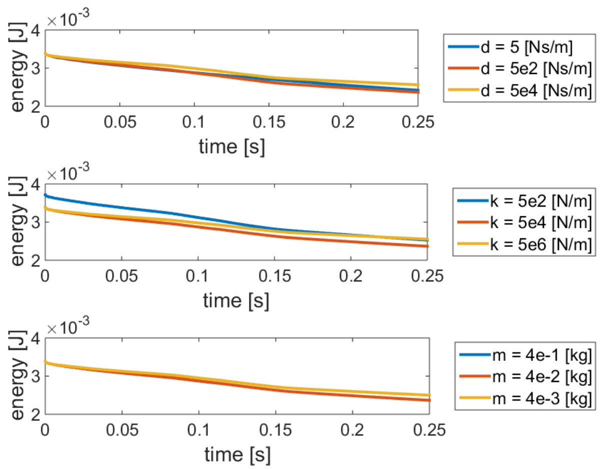

Fig.9. Comparing the effect of different parameters on the stored energy belonging to the vertical vibration.

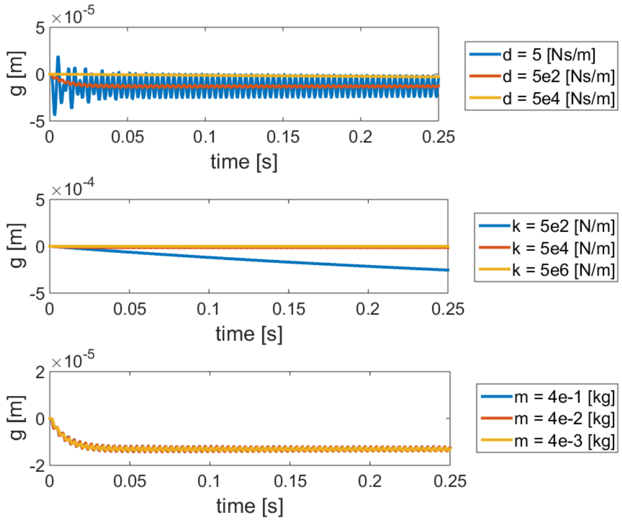

Fig.10. Comparing the effect of different parameters on the motion of the body.

The validity of the sampling frequency limit (Eq. (44)) was also examined. Choosing the stiffness to $k = 6.4 \cdot 10^9 \left[\frac{N}{m}\right]$ results a spring-mass system with 400 kHz eigenfrequency which is larger than twice the sampling frequency. The simulation seems to be stable during the first period but after that the body starts to oscillate on the sampling frequency and the system will be unstable. Under the critical stiffness the simulation is stable.

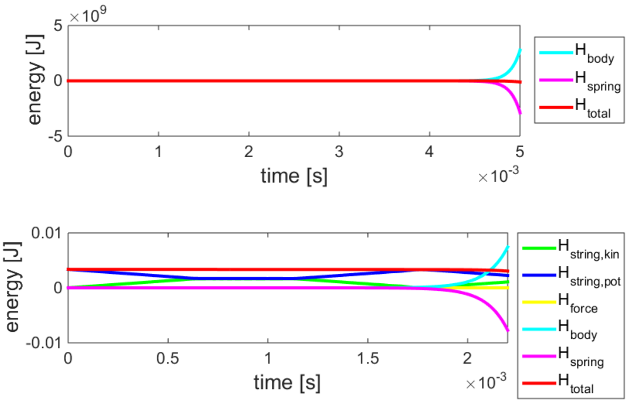

Fig.11. The change of the stored energy when the eigenfrequency of the spring-mass system is too high compared to the sampling frequency.

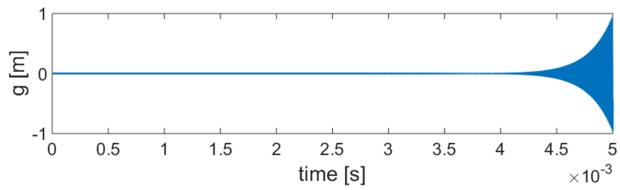

Fig.12. The motion of the body when the eigenfrequency of the spring-mass system is too high compared to the sampling frequency

3.5. Moving obstacle

The slide guitar is based on moving an object along the string without lifting it. This section presents simulation results in the case of a moving obstacle.
The obstacle has a constant velocity thus the free length of the string decreases linearly with respect to the time. This causes hyperbolic change in the eigenfrequencies (Fig.13.) which are corresponding to the analytical values.

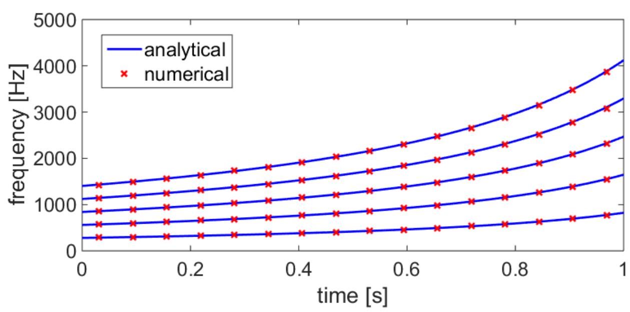

Fig.13. The change of the eigenfrequencies of the excited side of the string in the case of moving obstacle

The total energy of the system decreases and after a while it becomes negative. It is what Eq. (45) predicted. However the energy of the string, the body and the spring is still positive.

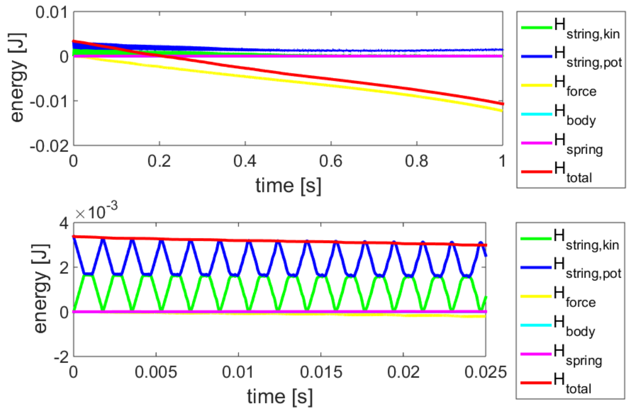

Fig.14. The change of the energy balance belonging to the vertical motion of the string in the case of moving obstacle

The motion of the obstacle does not have large effect on the horizontal vibration of the string. The only effect is that when the obstacle is close to one end of the string then the contact surface is larger. So there are more contact points where the friction can act and the dissipation will be stronger. The vertical vibration of the string will be negligible within 0.1 seconds independently of the stiffness of the string like in section 3.3.

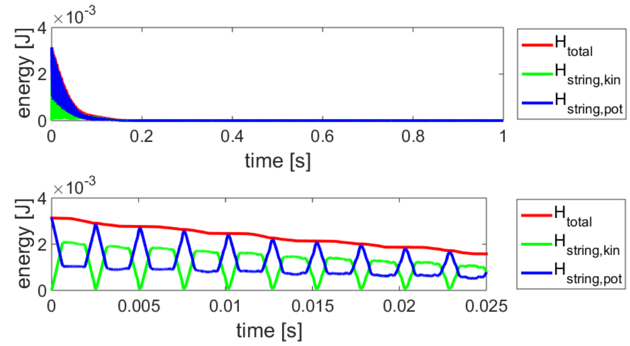

Fig.15. The change of the energy balance belonging to the horizontal motion of the string in the case of moving obstacle

4. CONCLUSION

In this study, string vibrations were examined in the presence of an obstacle in both directions perpendicular to the string. The obstacle was chosen as a rigid body suspended through a spring-damper system. Nonlinear contact force was considered between the string and the obstacle which was implemented as a penalty method. In the simulation, schemes based on modal superposition and spatial discretization were combined. The introduced finite differential scheme gives an almost perfect result regardless from the time step size in the case of free vibrations, but it is also appropriate to consider nonlinear interactions.

During the simulations the string was released from an initial shape that forms due to the static equilibrium with the nonlinear contact force. This shape was determined using the finite element method. The energy balance of the numerical simulation was examined as well. The paper gives a minimum sampling frequency above which the whole system will be stable. However in the case of moving obstacle, which would correspond to the slide guitar, the total energy becomes negative. The eigenfrequencies, which were obtained from the simulation, are corresponding to the free length and to the stiffness of the string.

This work might be compared with measurements, which could be made in three different way: based on optics [12], based on electromagnetic field [13], or with laser Doppler vibrometer. The model might be extended with more realistic excitation [14], and with the coupling between more strings [15].

4. REFERENCES

[1.] H. Hertz: **On the contact of elastic solids**, *J. für die Reine und Angewandte Math*, 29, 1881, 156-171.

[2.] H.Cabannes: **Motion of a string vibrating against a rigid fixed obstacle**, *Mathematical Modelling*, 8, 1987, 364-365.

[3.] H. Cabannes, H. Neunzert: **Periodic motions of a string vibrating against a fixed point-mass obstacle**: *II, Mathematical Methods int he Applied Sciences*, 6, 1984, 55-67.

[4.] S. Bilbao: **Numerical sound synthesis: Finite Difference Schemes and Simulation in Musical Acoustics**, Wiley, Chichester, (2009)

[5.] G. Evangelista, F. Eckerholm: **Player-instrument interaction models for digital waveguide synthesis of guitar: touch and collisions.** IEEE Trans Audio Speech Language Process, 18(4), 2010, 822–32.

[6.] G. Evangelista, F. Eckerholm: **Structurally passive element for modeling guitar pluck action,** 13th *International Conference on Digital Audio Effects*, 2010

[7.] D. Kartofelev, A. Stulov, H. - M. Lehtonen, V. Välimäki: **Modeling a vibrating string terminated against a bridge with arbitrary geometry**, *Stockholm Music Acoustics Conference*, 2013

[8.] C. P. Vyasarayani, S. Birkett, J. McPhee: **Modeling the dynamics of a vibrating string with a finite distributed unilateral constraint: application to the sitar**, *Journal of Acoustical Society of America* 125(6), 2009, 3673–3682.

[9.] A. K. Mandal, P. Wahi: **Natural frequencies, modeshapes and modal interactions for strings vibrating against an obstacle: relevance to sitar and veena**, *Journal of Sound and Vibration,* 338, 2015, 42–59.

[10.] C. Issanchou, S. Bilbao, J. Le Carrou, C. Touzé, O. Doaré: **A modal-based approach to the nonlinear vibration of strings against a unilateral obstacle: Simulations and experiments in the pointwise case**, *Journal of Sound and Vibration*, 393, 2017, 229-251.

[11.] C. Issanchou, J. Le Carrou, C. Touzé, B. Fabre, O. Doaré: **String/frets contacts in the electric bass sound: Simulations and experiments**, *Applied Acoustics*, 129, 2018, 217-228.

[12.] J. Le Carrou, D. Chadefaux, L. Seydoux, B. Fabre: **A low-cost high-precision measurement method of string motion,** *Journal of Sound and Vibration,* 333, 2014, 3881-3888

[13.] J. Pakarinen, M. Karjalainen: **An apparatus for measuring string vibration using electric field sensing**, 2003, Stockholm

[14.] D. Chadefaux, J. Le Carrou, B. Fabre: **A model of harp plucking**, Acoustical Society of America, 133(4), 2013, 2444-2455

[15.] V. Debut, J. Antunes, M. Marques, M. Carvalho: **Physics-based modeling techniques of a twelve-string Portuguese guitar: A non-linear time-domain computational approach for the multiple-strings/bridge/soundboard coupled dynamics,** Applied Acoustics, 108, 2016, 3-18

8th Congress of the Alps Adria Acoustics Association
Zagreb, Croatia
20 – 21 September 2018

Hrvatsko akustičko društvo
HAD
Acoustical Society of Croatia

GRANULAR SOUND SYNTHESIS

Nikola Kudrna[1], Kristian Jambrošić[2]

University of Zagreb, Faculty or Electrical Engineering and Computing, Unska 3, Zagreb, Croatia
([1]nikola.kudrna@fer.hr, [2]kristian.jambrosic@fer.hr)

Abstract: *Today, granular sound synthesis is a purely digital synthesis that processes or builds sound from small audio segments called sound grains. Because of its complexity, granular synthesis is rarely implemented in hardware, and is used exclusively by plug-ins in the digital audio workstation software. In the Ableton Live, a software for DAW, granular synthesis is intuitively implemented with a free plug-in called Argotlunar. The varied parameters in plug-in can be grain envelope, grain length, spacing between grains, grain frequency content, number of grains in the default period of time and many more.*

Key words: sound, synthesis, granular synthesis, grains, Haas effect, DAW

1. INTRODUCTION

1.1. Types of sound syntheses

With the producer's music education, sound knowledge and with the possibilities offered by computer synthesis, countless different sounds can be created: songs, effects for movies and virtual reality, etc. Sound synthesis is a creative process of creating or producing sound. There are analogue and digital syntheses.
Analogue synthesizers create sound with three main analogue modules: VCO (Voltage Controlled Oscillator), VCA (Voltage Controlled Amplifier) and VCF (Voltage Controlled Filter), and types of analogue syntheses are additive and subtractive.
Digital syntheses have far more possilbities and are more creative. The most widespread digital syntheses are FM, additive, subtractive, wavetable, S&S (Samples & Synthesis), physical modelling and sample replay sound synthesis.
Additive synthesis is based on adding frequency components to the original sound, while subtractive synthesis works in the opposite way – by removing frequency components with filters. FM synthesis works the same way as FM radio. On the main carrier signal, which is in the audible frequency range, producer modulates another signal of different frequency. In wavetable synthesis the producer can select more than one waveform, work on them with filters and switch between them in real time. Sample replay and S&S are based on working with more or less complex sound samples, and physical modelling uses mathematical functions to describe an entire music instrument.

1.2. Granular synthesis

Allowing producers to create sound from absolutely nothing, granular synthesis is currently one of the most creative syntheses in the music production world. It builds sound from small audio segments called sound grains, Figure 1. Their length extends from 5 to 100 ms, but most commonly from 20 to 50 ms as the resolution of human hearing temporal sensitivity is in that interval. Hence, if small enough, the gap between two grains is audible.
This can be compared with eye resolution. The movie projector shoots a certain number of images per second on the screen, but a human eye cannot process the changes that are so fast, it simply sees a moving picture.

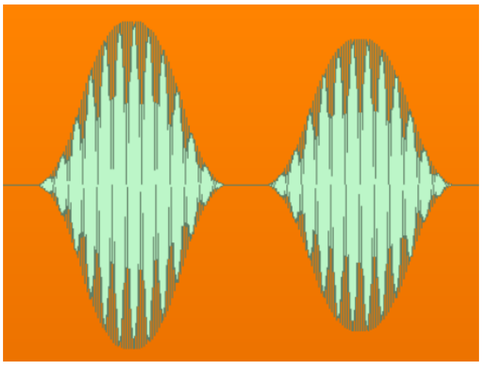

Fig.1. Two sound grains

The following persons are highly respected for their contribution in the development of granular synthesis: Greek musical theorist and engineer Iannis Xenakis, British-Hungarian engineer, physicist and Nobel prize winner Dennis Gabor and American programmer and the composer of electronic music Curtis Roads, who composed many tracks just using granular synthesis. His first experimental composition made with granular synthesis dates back to 1975.

2. GRAIN PARAMETERS AND HAAS' EFFECT

The main parameters varied by producers who implement granular synthesis in their productions are grain length, grain envelope, panorama (pan, stereo effect), density of grains, spacing between grains, repetition rate and grain frequency content.

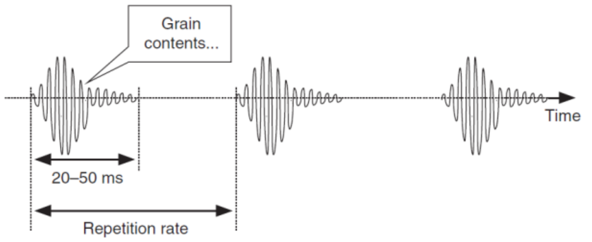

Fig.2. Grain parameters [1]

Grain length and spacing between grains are parameters that can be used for describing Haas effect, Figure 2. For a simple sine sound wave pulse shorter than 40 ms, human ear cannot recognize it as a tone with certain frequency, but as a short pulse. This does not have to be true for complex sounds, because Haas effect is frequency dependent.
Frequency contents of grains can be varied by low pass, high pass, bandpass and notch filters in the form of simple graphic equalizers.
Grain envelope is another important parameter. In most cases envelope of each grain begins and ends with an amplitude zero. If the grain envelope is sharp at the beginning or ending of a grain, it creates higher frequencies in spectrum and it sounds like a pulse or a kick. A series of such grains sound like a pulse wave or tooth saw wave. If the envelope's beginning and end are at amplitude zero, then the series of grains sounds constant and smooth. Figure 3. shows how a sound grain is produced.

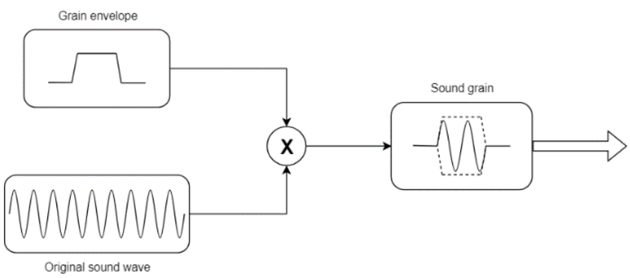

Fig.3. Production of sound grain

2.1. ADSR envelope

ADSR stands for Attack – Decay – Sustain – Release and it describes the four stages of one of the most used envelopes in sound synthesis, Figure 4. It can be used as an envelope of grains in granular synthesis. Attack is a short time in which the amplitude increases from zero to maximum of the envelope. Decay is the time in which the amplitude is slightly declining, and most commonly is as short as the Attack time. Sustain is in most cases the longest part of an ADSR envelope in which amplitude remains the same after Decay. Release is the ending of the envelope and its amplitude is declining from the Sustain level to zero. Release can be described as the reverberation. [2]

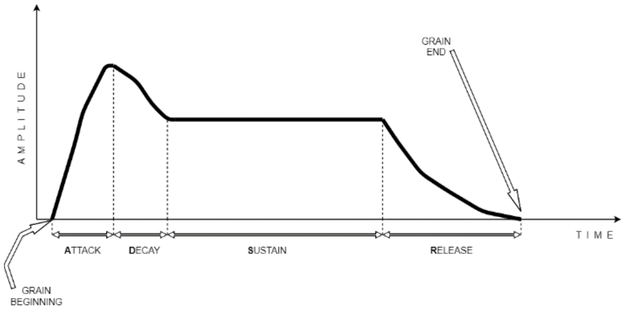

Fig.4. ADSR envelope

3. GRANULAR SYNTHESIS IN ABLETON LIVE

Ableton Live is a software used with digital audio workstations (DAW), and it is one of the most used software in modern electronic music production. It has implementations for Windows and Mac OS. If a producer has adequate audio hardware, he can use Ableton Live not only for producing and mastering, but even for DJ-ing.
Ableton has a very intuitive interface and is easy to work with. Its interface can be shown as a session view (all the instruments and effects used in the project) or as an arrangement view (project timeline), Figure 5.

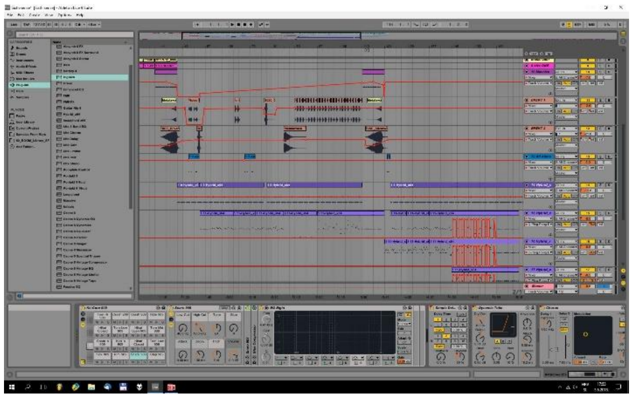

Fig.5. Ableton Live in arrangement view

To use granular synthesis, the producer must have an adequate plug-in. Argotlunar is a free VST plugin that is easy to work with and has a very intuitive interface. It implements granular synthesis by just using potentiometers and sliders, Figure 6. [3]

Fig.6. Argotlunar's interface

Parameters that can be changed in the shown examples are grain length (Dur), spacing between grains (IOT) and frequency contents of grains (Gliss nad Trans). The granular synthesis is going to be implemented on a 220 Hz sine wave and on pink noise.

3.1. Variation of grain length on sine wave

Variation of grain length is interesting to be observed in time and frequency domain. The constant parameter in this example is spacing between grains (IOT), which is 50 ms. Grain length is changing linearly from 200 ms to 5 ms, Figure 7. This is determined on Ableton's timeline where the parameter sweep was specified on observed section (sine wave, 220 Hz) and then defined to change linearly on certain effect, in this case, grain length (Dur) in Argotlunar. In the beginning of audio file, the grains are long enough for the human ear to recognize them as 220 Hz tone. However, as time elapses, the grains are becoming shorter and human ear cannot recognize them as a tone anymore, but as a pulse. This is how Haas effect works on simple sounds[5, 6].

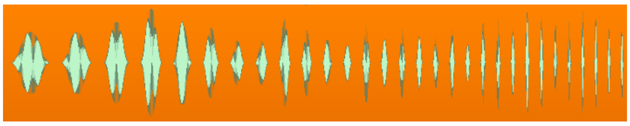

Fig.7. Linear variation of grain lenght in time domain – 220 Hz sine wave

The beginning of the audio file in frequency domain looks logical, Figure 8. The component at 220 Hz is dominant, and a higher harmonic is present as well with a much smaller amplitude (440 Hz). The frequency spectrum of the end of the audio file is wider, because Fourier analysis states that if a signal is very short in time domain, it is wide in frequency domain, Figure 9.

Fig.8. The beginning of audio file in frequency domain

Fig.9. The end of audio file in frequency domain

3.2. Variation of grain length on pink noise

Similar to the previous example, this one observes the variation on grain length, but this time with pink noise. The constant parameter is again spacing between grains (IOT) and its value is 1 ms, which is a minimum in Argotlunar plug-in. The grain length is varied linearly with a parameter sweep in Ableton's timeline from 400 ms to just 5 ms, which is also the minimum in Argotlunar plug-in, Figure 10.

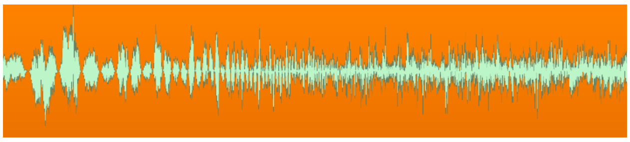

Fig.10. Linear variation of grain length in time domain – pink noise

In the frequency spectra of the end of the audio file in this example, one specific frequency stands out. That is the frequency of repeating grains with 5 ms grain length and 1 ms spacing between grains:

$$T_{generated} = Dur + IOT = 5\ ms + 1\ ms = 6\ ms \tag{1}$$

$$f_{generated} = 1 / T_{generated} = 1 / 6\ ms = 166.67\ Hz \qquad (2)$$

This frequency enters the hearing frequencies range (20 Hz – 20 kHz) as it is shown on the frequency spectrum in Figure 11.

Fig.11. The end of audio file in frequency domain – 167Hz stands out of the pink noise

3.3. Variation of spacing between grains on sine wave

This example can also show how the Haas effect works. The constant parameter is now grain length (Dur) and it is set to 50 ms. The spacing between grains is varied linearly with a parameter sweep in Ableton's timeline from 350 ms to 5 ms, Figure 12.

When spacing between the grains drops below 40 ms, human ear cannot recognize it anymore as a gap because it is too short. This is also because of the Haas effect.

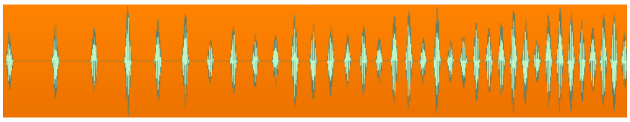

Fig.12. Variation of spacing between grains on sine wave in time domain

The frequency that is generated in the end of the audio file because of the grain repetition does not enter the hearing frequency range (20Hz – 20kHz):

$$T_{generated} = Dur + IOT = 50\ ms + 5\ ms = 55\ ms \qquad (3)$$

$$f_{generated} = 1 / T_{generated} = 1 / 55\ ms = 18.2\ Hz \qquad (4)$$

Hence, the frequency domain does not change and it is not shown in the example.

3.4. Variation in frequency content of grains (Trans, Gliss)

Trans is a parameter that changes the central frequency of the grain, and Gliss changes it linearly from the beginning to the end of the grain – *glissando*.

In the first part of example, parameter Trans is varied linearly with parameter sweep in Ableton's timeline from default central frequency (220Hz) to the maximum of the potentiometer (higher central frequency), Figure 13.

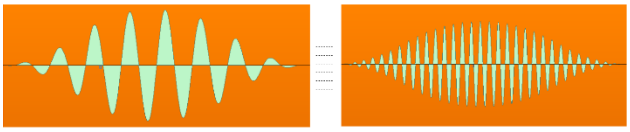

Fig.13. Variation of parameter Trans in time domain – the first and the last grain in audio file

It is important to highlight that the grains in Figure 13. are about equally long.

The second part of this example shows how parameter Gliss is varied. The potentiometer is linearly varied from the default state (central frequency at the beginning and the end of the grain is the same – 220Hz) to the maximum state (the *glissando* is at maximum – the frequency is changing upwards from the beginning to the end of the grain), Figure 14.

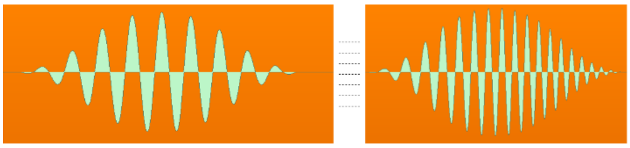

Fig.14. Variation of parameter Gliss in time domain – the first and the last grain in audio file

The grains in Figure 14. are again equally long.

The beginning and the end of each grain in figure 14 is the same, but the end of the last grain is at much higher frequency than the one at the beginning of the grain.

The spectrum of the last grain in the audio file shows the *glissando* effect very well, Figure 15 and 16.

Fig.15. Spectrum of the first grain in audio file of this example – the central frequency at 220 Hz and small amount of higher harmonic

Fig.16. Spectrum of the last grain in audio file of this example – the frequency content of a grain is wider than the one at the figure 15

4. CONCLUSION

The audio examples presented in this article are just the tip of and iceberg on what granular synthesis can offer. It is very creative, and can build interesting sounds. Besides creativity, granular synthesis can be very useful in revealing psychoacoustic effects such as Haas effect.
As the development of electronic music goes on, along with the bigger market for new creative and innovative sounds that can be used in the modern music production, the granular synthesis is used more and more often.
With some time invested, each music producer can implement granular synthesis with many free or commercial plug-ins on his or her digital audio workstation software.

5. REFERENCES

[1.] Martin Russ: ***Sound Synthesis and Sampling***, Elsevier, 3rd edition, 2009
[2.] Rick Snoman: ***Dance Music Manual – Tools, Toys and Techniques***, Focal Press, 3rd edition, 2014
[3.] Argotlunar plug-in: http://mourednik.github.io/argotlunar/
[4.] Hugo Fastl and Eberhard Zwicker: ***Psychoacoustics: Facts and Models***, Springer, 2006
[5.] Brian C. J. Moore: ***An Introduction to the Psychology of Hearing***, Brill, 6th edition, 2013

8th Congress of the Alps Adria Acoustics Association
Zagreb, Croatia
20 – 21 September 2018

Hrvatsko akustičko društvo
HAD
Acoustical Society of Croatia

RAIN NOISE SOUND INTENSITY TESTING – LONDON 2012 OLYMPICS INTERNATIONAL BROADCASTING CENTER CASE STUDY

Konca Saher

Interior Arch. and Env. Design, Kadir Has University, Istanbul, Turkey
(konca.saher@khas.edu.tr)

Abstract: *Thin sheet metal roof claddings are widely used in large span buildings due to their lightweight properties, speed and ease of installation and durability. However, metal sheet roofs have low sound insulation performance, especially against the impact noise from the rain. In this article, rain noise from the metal roofing of the International Broadcasting Centre (IBC) studios in London 2012 Olympic Village is investigated. An additional roof layer on top of the existing roof construction was proposed to improve the existing metal roof build-up against potential rain noise intrusion and to be able to meet internal ambient noise level performance standards. Four different additional layer of roof build-ups were proposed with various cuspate thicknesses and geotextile filters. Tests were conducted in Sound Research Laboratories (SRL) at Sudbury, Suffolk, to determine the Rain Generated Impact Sound Transmission of these build-ups. The measurements of the sound intensity levels caused by artificial heavy rainfall on four types of roof build-ups allowed performance comparison of products and estimation of the sound pressure levels in the room due to rainfall on the roof, thereby the most suitable roof construction was chosen.*

Key words: rain noise testing, metal roofs, sound intensity testing

1. INTRODUCTION

This article examines the process of choosing the appropriate roof construction against the rain noise intrusion in the roof of the International Broadcasting Centre at the London 2012 Olympic Park during London 2012 Olympic and Paralympic Games. International Broadcasting Centre is a steel frame structure which is of 275-meter length, 50-meter width and 30-meter height and designed to be the media centre of the Olympic Games by hosting more than 20.000 media members, photographers, and journalists. The building which has the largest floor area in the Olympic Park, has a flat metal roof system consisting of sheets laid on the lining profile and the construction of the designed system was completed in the early 2012. Flat roof systems have advantages over other roof systems such as cost, ease of application and flexibility in design. However, in the structures where flat metal roof systems are used, especially structures such as broadcasting studios where sound insulation is extra important, the noise intrusion by rainfall should be taken into account from the beginning of the design. Thus, it is ensured that recommended internal ambient noise levels for broadcasting studios are not exceeded.

In the year 2012, when this work was done, there was no regulation or performance criteria for broadcast studios related to rain impact noise. In the absence of guidance levels for maximum allowable sound pressure levels due to rain noise in the standards, it was proposed that the reverberant sound pressure level in the studios should not exceed the internal ambient noise level of 35 dBA (LAeq) within the studio areas. This level was the recommended internal ambient noise level within the broadcasting studios by Olympic Broadcasting Services.

In this article, firstly noise monitoring results are evaluated in order to understand how rain impact noise of the existing flat metal roof effects the internal ambient noise levels in the existing studios. Noise monitoring results show that the existing flat metal roof cannot provide the interior ambient noise level of 35 dBA (LAeq) within the studios determined by Olympic Broadcasting Services. To improve the existing metal roof build-up against potential rain noise intrusion and to be able to meet LAeq performance standards, it was proposed to install an additional layer formed from a cuspate and geotextile filter on top of the existing roof construction. Four different additional layer of roof build-ups with various cuspate thicknesses and geotextile filter were proposed. The sound levels caused by artificially created rainfall were measured in four different types of roof systems, the performances of the different systems were compared and the most suitable roof constructions were recommended.

2. NOISE MONITORING AND RECOMMENDED ROOF STRUCTURES

Rainfall recordings were made in the International Broadcasting Centre to determine how rainfall effected the internal ambient noise level within the studios for existing metal roof conditions. Particularly in the case of severe or heavy rainfall, the determination of the internal ambient noise levels will play a role in determining the sound attenuation values required for the roof layers that are to be recommended.

Continuous background noise monitoring was carried out from Friday 18th November 2011 until Wednesday 21st December 2011. The sound level meter was set-up within a typical studio which was also relatively a quiet studio in terms of noise from road traffic. The monitoring equipment operated continually 24 hours a day for the whole duration of the survey. Measurements were 5 minutes in duration during the day and night time period. The daily background noise measurement results were compared with rainfall monitoring station data in order to match the noise levels with rainfall rates and times.

Noise monitoring results show that the lowest ambient noise levels in the studio is between 25 dBA and 33 dBA for the night time zone (between 23: 00-7: 00) when there was no rain recorded. The noise levels rise during rainfall, from a minimum of 3dB increase during light rain (0.5mm/hr) to a maximum increase of 20dB during intense rainfall (4.8mm/hr). It was observed that the peaks at the measured noise levels correspond to the peaks at the precipitation rate. The highest rain noise measured is around 50 dBA within the studio. (Table 1)

Table 1. The highest rain noise measured within the broadcasting studios

	Frequency							
	63	125	250	500	1000	2000	4000	LAeq
Highest Rain Noise Measured	51.6	50.9	45.9	45.5	45.8	40.5	41.5	49.8

The rain noise monitoring results indicate that indoor ambient noise levels, based on the most severe rainfall, are 15 dB above the indoor ambient noise level criteria set by the Olympic Broadcasting Services, which is an unacceptable indoor ambient noise level value for broadcast studios. Therefore, in order to improve the roof performance, four types of roof layer constructions are proposed which will be applied directly on top of the existing roof.

The existing roof on the International Broadcasting Centre building was a metal sheet roof system built up with rockwool insulation. Data on the acoustic performance of the roof structure provided by the manufacturer indicates a 44 dB Rw overall performance for the roof.

To improve the noise attenuation afforded by the existing roof build-up against rain noise, an additional element formed from a cuspate and geotextile filter on top of the existing roof construction was proposed. Four different types of extra roof layers were proposed which are detailed below and shown in Figure 1.

1. Roof layer 1: Formed from a 12 mm cuspate (extruded from polyethylene sheet) and geotextile filter bonded to the stud face.
2. Roof layer 2: Formed from a 25 mm cuspate (extruded from polyethylene sheet) and geotextile filter bonded to the stud face.
3. Roof layer 3: Formed from a 25 mm cuspate (extruded from polyethylene sheet) and fully wrapped in geotextile.
4. Roof Layer 4: Formed from a 25 mm cuspate (extruded from polyethylene sheet) and fully wrapped in geotextile plus 15mm high performance non woven geotextile on top.

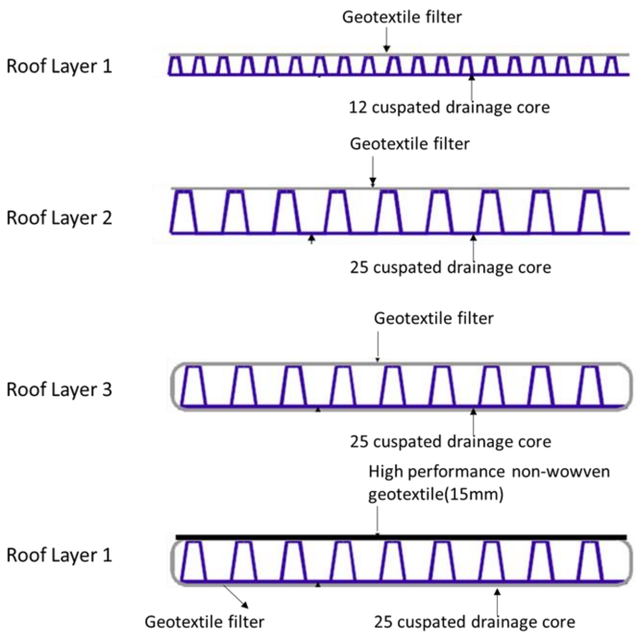

Fig.1. Proposed additional roof layers

3. RAIN NOISE TESTING RESULTS

The measurements were made on 2nd April 2012, Monday at Sound Research Laboratories (SRL), Suffolk, United Kingdom. The measurement of rain noise radiated by a roof element is quoted in terms of the sound intensity level LI in dB re 10^{-12} W/m^2. This was measured directly beneath the roof element using a sound intensity probe. The measurement of sound intensity of each roof layer was made in accordance with BS EN ISO 15186-1: 2003[1] and ISO/CD 140-18 [2]. The schematic diagram of the measurement set-up is shown in Figure 2.

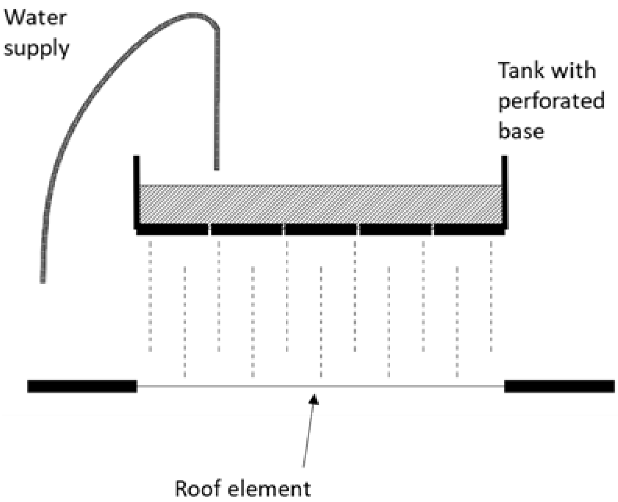

Fig.2. Schematic diagram of measurement set-up.

The rain noise standard describes two types of artificial rainfall that can be used: intense and heavy. In this project, heavy rainfall was used for the comparison of proposed roof constructions. However, it should also be noted that heavy rainfall (a rainfall rate of 40mm/h) has a return period of ~50 years, therefore, the calculations shown here are therefore done for the absolute worst case.

The sound intensity levels caused by each roof layer was measured separately. Roof construction details and test numbers are shown in detail in Table 2. It shoulde be noted that the base roof at the laboratory was not the same as the existing International Broadcasting Centre roof, however, the relative sound insulation improvement from the base roof was calculated for each proposed roof layer.

Table 2. Test numbers and construction details of the roofing.

Test Number	Sample Description	Construction Details
1	*Base Roof*	Tin Roof
2	*Base Roof+Roof Layer 1*	Formed from a 12 mm cuspate (extruded from polyethylene sheet) and geotextile filter bonded to the stud face.
3	*Base Roof+ Roof Layer 2*	Formed from a 25 mm cuspate (extruded from polyethylene sheet) and geotextile filter bonded to the stud face.
4	*Base Roof+ Roof Layer 3*	Formed from a 25 mm cuspate (extruded from polyethylene sheet) and fully wrapped in geotextile.
5	*Base Roof+ Roof Layer 4*	Formed from a 25 mm cuspate (extruded from polyethylene sheet) and fully wrapped in geotextile plus 15mm high performance non woven geotextile on top

The sound intensity level difference from the base roof for each proposed roof layer was calculated in each frequency band. (Table 3) These values have been used to calculate the likely internal ambient noise levels inside the International Broadcasting Centre studios for each roof construction and compared with the highest measured noise levels inside the studio during the rain monitoring (49.8 dBA).

Table 3. Calculation of Internal Ambient Noise Levels for each Roof Construction

Sound intensity level difference from the base roof									
Test No	Sample Description	Frequency							
		63	125	250	500	1000	2000	4000	
2	Base Roof+Roof Layer 1	3.1	7.1	5.6	9.3	16.2	21.3	26.3	
3	Base Roof+ Roof Layer 2	4.0	7.3	4.9	10.2	16.4	24.2	30.7	
4	Base Roof+ Roof Layer 3	4.4	7.0	5.3	10.5	18.1	30.0	38.3	
5	Base Roof+ Roof Layer 4	10.6	11.0	14.0	24.6	30.4	41.0	48.1	
Improvement of Internal ambient noise levels									
Test No	Sample Description	Frequency							
		63	125	250	500	1000	2000	4000	LA eq
	Highest Rain Noise Measured	51.6	50.9	45.9	45.5	45.8	40.5	41.5	49.8
2	Base Roof+ Roof Layer 1	48.5	43.8	40.3	36.2	29.6	19.2	15.2	37.2
3	Base Roof+ Roof Layer 2	47.6	43.6	41.0	35.3	29.4	16.3	10.8	37.0
4	Base Roof+ Roof Layer 3	47.2	43.9	40.6	35.0	27.7	10.5	3.2	36.5
5	Base Roof+ Roof Layer 4	41.0	39.9	31.9	20.9	15.4	-0.5	-6.6	27.6

The results indicate that the calculated internal ambient noise levels for Test no 2, 3 and 4 are slightly over (1-2 dBA) Olympic Broadcasting Service's internal ambient noise level criteria of 35 dBA. However, calculated internal ambient noise level for Test no 5 is around 27 dBA and well below of 35 dBA and therefore should satisfy Olympic Broadcasting Service's requirement for rain noise. However, it was predicted that the application of a suspended ceiling would improve the performance of the studios against rain impact noise and the roof structures in Test no 2, 3 and 4 are very likely to satisfy the internal ambient noise level performance of 35dBA,recommended by Olympic Broadcasting Services.

4. CONCLUSION

In this article, the process of determining the appropriate roof construction against the possible rain noise from the International Broadcasting Centre studios in the London 2012 Olympic Village has been examined. In order to improve the performance of the existing metal roof against possible rainfalls and to meet the internal LAeq performance standards, four different roof layers with different thicknesses of polyethylene membrane and geotextile filter combinations were proposed over the existing roof construction. Tests of the proposed systems were carried out in Sound Research Laboratories (SRL), Suffolk, Sudbury, and the rain impact noise of the measured roof systems was determined. Sound intensity levels caused by artificially created heavy rainfall in four different types of roof systems were measured and values were used to calculate the likely internal ambient noise levels. Thus, the performances of the four different roof layers and materials used were compared.

The results show that the first three recommended additional roof layers under heavy rainfall conditions would provide internal ambient noise levels of slightly above the 35 dBA, which is the recommended internal ambient noise level by the Olympic Broadcasting Service for broadcasting studios. However, it was predicted that the performance of the roof structures would improve with the application of a suspended ceiling and the resulting internal ambient noise levels would satisfy the Olympic Broadcasting Service's performance criteria.

4. REFERENCES

[1.] International Standards Organization. Acoustics – Measurement of sound insulation in buildings and of building elements – Part 18: Laboratory measurement of sound generated by rainfall on building elements. International Standard ISO/CD 140-18 (ISO TC43/SC2 N 0751 13 January 2004).
[2.] International Standards Organization. Acoustics – Measurement of sound insulation in buildings and of building elements – Part 18: Laboratory measurement of sound generated by rainfall on building elements. International Standard ISO/CD 140-18 (ISO TC43/SC2 N 0751 13 January 2004).

NOISE PROTECTION IN INDUSTRIAL BUILDINGS: ARCHITECTURAL DESIGN STRATEGIES

Ezgi DADAŞ and Füsun DEMIREL

E-mail address: ezgidadas@gazi.edu.tr

Abstract: *Noise is an important type of environmental pollution that adversely affects people's hearing health and disrupts work performance. The noise exposed in the work environment is a major problem affecting millions of workers across the world. In this study, it is aimed to improve the conditions of the acoustic comfort in the work environment and to reduce the noise at the source which is spread around the environment. In line with this target, acceptable noise levels for work environments, the effects of excessive noise in the workplace and noise control techniques were analyzed. The necessary amount of noise control may be applied at the source, at the receiver, or in the transmission path between the source and the receiver. Architectural design strategies for noise control in industrial buildings includes; vibration isolation, enclosures to confine the noise, barriers to prevent the noise, surface damping and acoustic absorption on interior surfaces. Related strategies have been researched to cope with the ongoing noise problem with the progress of technology and industrial activities.*

Key words: industrial noise, noise reduction, occupational health, noise control

1. INTRODUCTION

Noise is one of the most common health risks in an industrial production environment. As a result of technological developments in industrial facilities, mechanical equipment varies, making noise sources diversified over time. These noises are usually complex. It occurs with the contribution of many different sources. In general, noise sources in industrial buildings can be collected in three main headings as noise caused by workers' social activities, noise caused by the production activity that is the main function of facilities, and noise caused by structural technical support elements and their installation.

In almost all workshops, there is a level of noise that will often pass the danger threshold in terms of health. Due to constant and intense exposure to noise, the cardiovascular and psychomotor system, especially the hearing system of the employees are negatively affected. This situation also leads to accidents in the business. The adverse effects of the noise on employee health and safety should be demonstrated, and the development of preventive measures must be carried out in each workplace in a multidisciplinary understanding.

Noise control includes all precautions that can be taken to protect people against the harmful effects of the noise. These precautions can be technical and managerial content. Measures such as limiting the daily working times of employees working at high noise levels, regulating the working hours of noisy machines that do not work continuously, and handling noise as a parameter in production processes are some related administrative measures. Industrial noise control with technical content is architectural decisions and engineering applications. The measures for noise taken during the design of machines and processes are carried out by engineering applications.

In the present study, the noise resulting from production action is discussed. The noise measures taken during the design phase of machines and processes, which are covered by engineering applications, are excluded from this research.

2. EFFECTS OF NOISE ON WORKING LIFE

Although economic development in society is a positive result of industrialization, the environmental pollution has a negative impact on the whole society. The development of technology and industrialization brings the environmental and worker health problems. Noise, which is one of these problems, has an important impact on human health. The most important effect of noise is that high-intensity noise destroys the hearing sense. The sound intensity that the inner ear and its formations can compensate is limited. Noise or sound that exceeds this limit is damaging the hearing sense. The anatomical and physiological structures that protect the inner ear cannot prevent this damage completely.

Temporary threshold shift: As a result of changes in the chemical balance of the cells in the inner ear caused by high-intensity noise, the hearing is temporarily impaired. Hearing loss occurs primarily at 4000-6800 Hz, then the hearing threshold is considered to increase up to 500, 1000 and 2000 Hz.

Permanent threshold Shift: If the noise is continuous, irreversible impairments occur in the inner ear cells that cannot rest, and hearing loss gain a permanent character. The sound that is generally described as acoustic trauma, especially in the highest frequency of hearing levels, around 4000 Hz, has the most impact on the ear. At 4000 Hz, the temporary shift is not noticed because it does not prevent the understandability of speech at first. However, speech becomes incomprehensible, especially in noisy areas as the loss continues to spread at medium frequencies [1].

For many years it has been accepted that noise only causes problems related to the auditory system. The effect of noise on human health and human behavior reaches more serious dimensions day by day. Other than hearing loss, it causes many physiological, psychological effects, and effects on work performance. The human ear hears the sounds from 20 to 200 Hz. The sound below this value is called infrasonic sound and the sound above it is called ultrasonic sound. Even if these sounds are not heard by people, they can cause various effects such as nausea, headaches, and restlessness.

Research has shown the effect of noise on the veins that feed the brain. The vessels extending to the brain are enlarged before the noise, and headaches occur after constant exposure to noise. When exposed to noise, red blood cells are collected in small blood vessels, and the veins are contracted with spasm. Thus, noise causes the blood to thicken and coagulate and can pose a risk for heart attack. Due to the decrease in the number of leukocytes as a result of noise, a decrease in general body resistance occurs. The loud noise causes blood vessel pressure due to vasospasm. This leads to the growth of muscle fibers in the flat muscles, the formation of narrow spaces in small veins, and the increase in resistance to blood flow. As a result, hypertension occurs. In cases where noise limit values are exceeded, fatigue and mental activity slow down. It is necessary to make a greater effort to be able to avoid distractions, to prolong the perception time, and to gather attention again. Work accidents can occur because of sudden noises and no audible alarms [2].

Recommended limits of noise levels for the number of hours exposed by OSHA (Occupational Safety and Health Administration)[3].

Number of hours exposed	Sound level dBA
8	90
4	95
2	100
1	105
0.5	110

Table 1. Recommended noise exposure limits

3. INTERNATIONAL REGULATIONS ON NOISE EXPOSURE IN INDUSTRIAL PLANTS

One of the environmental health problems that the World Health Organization (WHO) defines as "a physical, mental and social well-being of man" is noise. Noise has emerged as one of the results of the industrialization process in developed countries. Noise levels recommended by WHO for production volumes are 65-70 dB [4].

According to the directive of the European Parliament and Council numbered 2003/10/EC and dated 6/2/2003; the minimum health and safety measures to be taken against the risks associated with the noise exposure of employees were determined. When designing production processes and selecting machines, taking into consideration the noise factor, regular maintenance of all technical equipment, regulation of working times and breaks in consideration of noise exposure, and necessary precautions to be taken for air and solid-borne noises are mentioned. Personal precautions must be taken when these precautions are not adequate. The minimum and highest exposure values are determined by the exposure limits.

- exposure limit values: LEX,8h = 87 dB(A);
- upper exposure action values: LEX,8h 85 dB(A);
- lower exposure action values: LEX,8h = 80 dB(A).

The effect of noise reduction on hearing protectors is taken into account when assessing the noise exposure of employees, and the effect of the protectors on hearing is not taken into account for the exposure values. If the exposure of workers to noise exceeds the lower exposure value, employers must supply their hearing protectors in the production environment. If the upper exposure value is exceeded, the hearing protectors must be used by employees. Employers are obliged to supervise the use of protectors. The weekly noise exposure determined by the required measurements should not exceed the exposure value of the 87 dBA, if it exceeds, the employer is responsible for determining the reasons and taking the necessary precautions [5].

3.1. Architectural Design Strategies for Noise Control in Industrial Buildings

In cases where high-level noise is foreseen in the production space, if the layout of the different functional building sections is in the design phase of the building, the decisions and measures taken during the architectural design process are decisive for the protection of employers from noise. Measures to reduce the noise level should be taken in a planned manner starting from the first phase of the design of the industrial structure. The design process should be modeled in the virtual environment using an acoustic simulation program to predict the auditory environment in the production area and take the necessary precautions at the design stage and evaluated according to the appropriate acoustic criteria for noise control. In this process, the variables related to the design should be evaluated together with the acoustic requirements, and different design options should be tested in the modeling of the design. Noise mapping technique is frequently used to monitor and control noise in production volumes. Noise map shows the changes in the ambient sound pressure according to the physical environmental conditions on a plan. Noise maps allow people to check if the limit values are exceeded. The number of workers exposed to high noise can be determined. The areas at risk can be identified, and a simple representation can indicate the extent to which employees will be exposed to noise during the process.

During the design process of the industrial structure, the basic decisions about planning the land layout should be evaluated for noise. If possible, social and managerial functional areas should be planned separately from the production volume.

When designing the workplace layout;

- Enough distances between machines should be left to ensure that operators are not affected by the noise of other machines,
- High-level noise generating devices should be planned, if possible, away from the walls and corners both in a horizontal and vertical way,
- Vibration amplitude should be planned to allow machines capable of stimulating the structure of the building to fit on the floor, and if it is not planned on the floor, it should not be positioned in the middle of the floor plate.
- Single noise sources that are not directly related to production, such as a transformer, generator, should be planned behind natural or artificial obstacles as possible [6].

By using enclosures, thus noise generating machines are isolated from the environment. It is created by the enclosure of all machines or part of them without hindrance to the production flow [7]. Commonly used enclosures consist of a hard outer casing, an inner sound barrier and an inner sound absorbing layer. Nowadays, standard modular enclosures designed and manufactured for this purpose are used. In cases where the enclosure walls are not insulated with flexible materials, the vibrations make the enclosure wall a source of the noise. Partial enclosures are used in conditions where high-frequency noise generating production flows such as pressing and riveting that are not suitable for continuous enclosures.

The retention of the sound can be achieved by **using the barrier** between the source and the receiver. It is effective in conditions where the reflected sound level in the production volume is low. Barriers are more efficient in reducing noise at high frequencies. To control reflections, absorbent materials should be used on the faces of obstacles facing the source and on the ceiling. At high frequencies, noise reduction is more effective than at low frequencies [7].

By increasing the **surface absorbency properties** of the production volume, noise reduction can be achieved for workers outside the critical distance limit to the machine. The sound attenuation provided by increased absorbing is always limited. Absorbent materials are applied to ceilings, but if it is not possible due to lighting or factors such as a crane, suspended absorbers in the form of the panel can be used. These are mineral woolly felt compressed between perforated sheet metal [6].

Reducing the transmission of impact sounds to the structure is achieved by changing the transmission path between the vibration source and the emissive surface. This change can be achieved in different ways, such as the application of floating flooring, the application of flexible equipment that reduces the transition of vibration, the creation of interruption in the structure. Insulating pads, elastomers, steel-based devices, and pneumatic devices are used when applying flexible materials.

The noise should be considered while designing the building shell in situations where there are noise sensitive structures in the environment, and it should be designed to provide sufficient loss of sound transmission. The roofs made of lightweight elements may be especially insufficient for noise insulation. As an environmental noise source, industrial plants are a problem that is studied for a long while and mentioned in the legislation.

4. CONCLUSION AND RECOMENDATIONS

Industrial structures are most conspicuous work environments where noise must be monitored because noise levels are high and because they employ an important working population throughout the world. Today, after the industrial structure has become running, the necessary noise measurements are made and improvement projects are put into practice. Therefore, the required noise reduction is not achieved or need non-economic changes. Thanks to the development of technology in our age, necessary strategies can be simulated by using acoustic simulation programs in the process of designing industrial structures. Noise maps are a common way to do this. Noise maps allow people to check if the limit values are exceeded, to determine the areas at risk, and to predict how much noise the employees will be exposed to during the process. However, there is no standard for mapping noise in working environments. Comprehensive standards and regulations should be developed in this regard.

4. REFERENCES

[1.] R. Toprak, N. Aktürk : ***Harmful Effects of Noise,*** *Journal of Turkish Hygyenist and Biologists*, 61(1), 2004, 49-58

[2.]E. Belgin, M. Çalışkan: N***egative Effects of Noise on Human Health***, *Noise in Working Life and Protection of the Hearing,* Ankara, 2004

[3.] Occupational Safety and Health Standards https://www.osha.gov/pls/oshaweb/owadisp.show_document?p_table=STANDARDS&p_id=9736

[4.] M. Concha-Barrientos, D. Campbell-Lendrum, K. Steenland, ***Occupational Noise,*** *WHO Publication*, Geneva, 2003

[5.] Directive 2003/10/EC of the European Parliament and Council, 2003

[6.]M. N. Ilgürel : ***The Noise in the Architecture of Industrial Buildings for use as a Design Criterion***, Master Thesis, Yildiz Technical University, İstanbul, 2003.

[7.]P. P . Narang (1995) ***Noise Control Strategies for Occupational Safety and Better Working Environments***, *International Journal of Occupational Safety and Ergonomics*, 1:4, 311-329.

8th Congress of the Alps Adria Acoustics Association
Zagreb, Croatia
20 – 21 September 2018

Hrvatsko akustičko društvo
HAD
Acoustical Society of Croatia

BAD PRACTICE OF ONE ACOUSTICAL EXPERT OPINION

Ferdinand Deželak

Institute of Occupational Safety (Ferdo.Dezelak@zvd.si)

Abstract: *In this paper a bad practice at a particular district court is briefly highlighted. Here one court expert witness was appointed by this court in order to solve some audiometric and acoustic problems concerning a plaintiff's hearing loss as a result of a firecracker explosion. This explosion took place very close to his right ear with a* $L_{C\,peak}$ *at around 150 dBC. However, due to incorrect metrics used, the expert estimated this level to be 124 dB only, failing to reach the correct result by approximately 26 dBC. On this basis, he concluded that no hearing damage could be possible as a result of this explosion. Apart from using the incorrect metric, he also confused some important acoustic quantities and facts, resulting in even more cardinal errors. Due to a lack of fundamental expertise regarding high impulse noise and its propagation, he was unable to recognize the importance of its amplitude and spectral content in respect to hearing damage. He further confused reflection, refraction, diffraction and many other factors, which all resulted in quite misleading expert opinion and its conclusion.*

Key words: firecracker noise, high impulse noise, expert opinion, hearing damage, peak level, audiometry

1. INTRODUCTION

In this article, a presentation is made of bad work practices at the District Court of Ljubljana. Situations where some Slovenian courts select experts who lack necessary knowledge and experience are not rare. Consequently, such expert opinions can be quite wrong, including those in the field of acoustics and audiometry. In this paper one of such cases which is related to a set of other poorly guided procedures at this court is highlighted.

It all started when a powerful firecracker exploded approximately 4 to 5 metres from the right ear of the victim. This loud explosion resulted in hearing impairment, so the victim was compelled to submit a prosecution at the District Court against the perpetrator. However, the judges at this court were not interested in finding a fair and legal solution as they symphatised with the perpetrator. Therefore, the process of this court was far from being fair and professional.

The first judge, F.K., presiding over this case was generally not be of high moral character and has been engaged in some activities which were quite incompatible with his position as an independent and impartial judge of a full-time office and with his general judicial function. Although he was suspended after four years of work on this case, another judge of this court, A.B., continued applying this bad practice, especially in the field of acoustics and audiology, which were a crucial elements of this case. So, the second judge appointed a court expert, A.G., (who was even not a member of the court experts society) in order to solve questions concerning this explosion and its consequences to hearing impairment. However, this expert was not only in a biased position but was also unfamiliar with fundamental acoustic and audiometric facts, so he was not able to provide the correct answers to the plaintiff and the court. As a result of even more deficient expertise, the new judge proclaimed almost all acoustic and medical questions as unimportant and irrelevant. On the other hand, she permanently intervened and discussed these professional questions, although she did not understand them. It comes as no surprise then that most citizens do not trust such a judicial system.

In this article, the author primarily focused on the incorrect position of this expert and the misleading aspects of his opinion, pointing to further bad practice in this district court and resulting in quiet wrong conclusions.

2. LEGISLATIVE REQUIREMENTS

The use of fireworks and firecrackers is strictly limited in most of the European countries. According to Slovenian legislation, although the use of certain categories of fireworks is permitted, even these can only be set on between December 26th and January 2th and even then only at appropriate locations [1]. Unfortunately, some people still violate these legislative requirements. In many cases, police actions mitigated these problems by taking appropriate measures, especially of a preventive character. On the other hand, some problematic cases, where personal injuries are involved for instance, were regularly entrusted to the courts, where it is expected a right and fair solution to be found. Often however, successful police actions are entirely revoked as a result of corruption and erroneous court decisions. This paper describes one such case which was quiet unprofessional and of a highly corruptive nature. It is being processed in the District Court of Ljubljana where it has already been ongoing for almost 7 years and has resulted in high costs without any effect.

On April 10th 2012 one person threw a firecracker which exploded close to the right ear of the plaintiff. This explosion was unpredicted and unexpected, so the plaintiff's ears were totally unprotected and were exposed to a high-impulse sound pressure level exceeding 150 dBC. Independent audiometric tests showed that this resulted in hearing impairment with the plaintiff losing approximately 7% of his hearing. However the first judge, who started processing this case, ignored these audiometric tests completely together with the most valid evidence. Due to corruption revealed, this judge was consequently suspended. However, this has not improved the situation. After five years his successor adopted a similar corruptive practice. She decided to appoint an expert in order to resolve some professional questions on acoustics and audiology. Apart from her biased position, she selected the expert with an unprofessional expertise and experience. This resulted in quite unprofessional work by this expert, including his poorly planned measurements, erroneous calculations and quite incorrect conclusions, and also not forgetting the high costs involved for his work. Despite additional examination, he was unable to give correct answers to the most important questions.

3. A BASIC REQUIREMENTS FOR THE AUDIOMETRIC TEST ROOM

In order to obtain a reliable measure of hearing ability and its loss, many factors must be considered. For this purpose some tests are usually performed in specially designed audiometric test rooms. One of the most important requirements, in order to avoid masking the test signal by ambient noise in such a test room, is that the levels of the ambient noise shall not exceed certain values. The standards ISO 8253 [2,3] provide threshold levels, which indicate the maximum ambient sound pressure levels which are still permissible when other minimum hearing threshold levels are to be measured. It sets out procedures for determining hearing threshold levels by pure tone air conduction and bone conduction audiometry.

Ambient sound pressure levels in an audiometric test room shall not exceed the values specified in table 2 of the standard ISO 8253 – 2 [2]. The test subject and the tester shall be neither disturbed nor distracted by non-related events nor by people in the vicinity.

For this reason, permissible ambient noise for threshold determinations in an audiometric test room shall not exceed certain values in order to avoid masking the test tones. These values are specified as maximum permissible ambient sound pressure levels in one-third octave bands for the lowest hearing threshold level. So, to satisfy ambient noise requirements, it will be necessary in many circumstances to use a sound-isolating booth. Furthermore, a calibration interval of not more than one year is recommended.

4. SOME PHYSICAL CHARACTERISTICS OF FIRECRACKER NOISE

A firecracker usually consists of a cylinder-form tube, filled with an explosive, producing a loud noise when it explodes. In such explosions a definite amount of chemical energy is partially converted into electromagnetic energy (heat and light), and partly into mechanical energy as a shockwave. The physical characteristics of such explosions depend on the type of firecracker and its composition, primary on the size, weight and encapsulation of the explosive used which present the most important emission factors. Apart from emission, a considerable role in sound overpressure formation at the point of reception is played by the distance and presence of different objects that influence reflections, diffractions etc.

Firecracker explosions belong to a group of high impulsive noises which are particularly hazardous for hearing impairment. The firecracker explosion produces a transient sound signal which is manifested as an impulse noise with sharp rising time (more than some 100 dB/s) and of short duration.

It is true, that the noise from a gunshot, especially from some larger calibers, can be even noisier. However, it is important to note that shooters, bystanders and other personel exposed to such noise usually tend strictly to apply hearing protection devices. On the other hand, when fireworks are used, such protection is almost never applied. This is especially true for persons not using firecrackers and during the time when their use is strictly prohibited.

4.1. Types of impulsive noise due to firecracker explosions

A firecracker explosion outdoors, in an open space without any reflective obstacles, produces a non-reverberant A-type impulse noise with a single spike-form overpressure which can be approximated as a Friedlander impulse as shown in Fig. 1*a*. On the other hand, a firecracker explosion indoors or in a semi-open space results in a reverberating effect and are usually described as a B- or C-type impulse, Fig. 1*b* and *c* [4].

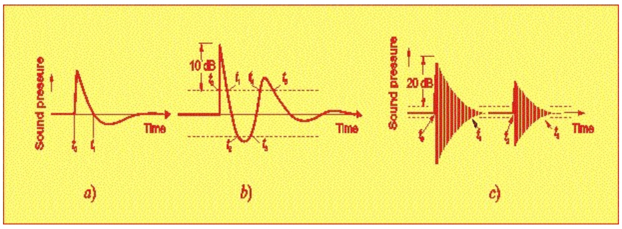

Fig. 1. Sound pressure levels of different types of impulse noise in time domain; *a*) A-duration (t_1-t_o), *b*) C-duration (t_1-t_o)+(t_3-t_2)+(t_5-t_4), and *c*) B-duration (t_1-t_o)+(t_3-t_2)

The main characteristics of these types of impulse noise can be described by using three basic parameters: rising time, impulse duration and peak overpressure. These parameters depend on the source, i.e., firecracker used.

The duration of A-type impulse (also called A-duration) is determined as the time required for the main wave to reach its unweighted peak sound pressure and return to baseline, (t_1-t_o). This is the time taken for the overpressure to fall for the first time to zero value at t_1 in Fig. 1*a*. In the case of ideal waves, it is equal to the positive phase duration used in blast physics. With B-duration, the total time required for the peak of a pulse level exceeding the criteria -20 dB, is depicted in Fig. 1c. The corresponding level is therefore about two-thirds of the peak pressure value. C-duration is determined as the time required for the envelope of the unweighted peak sound pressure to decay by 10 dB (Fig. 1b). If the path lengths involved are short enough, the reflections may interfere with the original pulse producing a complex pressure time history.

The A-type impulse can be described as a combination of linear function for the rising part and exponential function during its decay [5], (fig. 2):

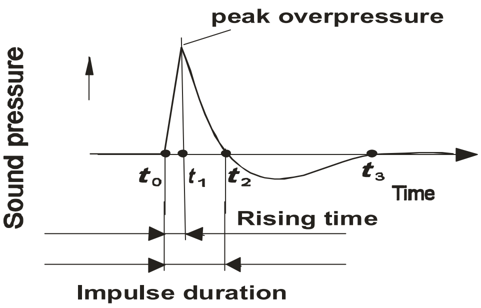

Figure 2: The Friedlander wave as a firecracker explosion in time domain

$$p(t) = p_r(t) + p_p(t) \qquad (1)$$

where

$$p_r(t) = p_{peak}\left(\frac{t - t_o}{t_1 - t_o}\right) \quad for \quad t_o \le t \le t_1 \qquad (2a)$$

and

$$p_p(t) = p_{peak}\left(1 - \frac{t - t_1}{t_2 - t_1}\right) e^{-\frac{t - t_1}{t_2 - t_1}} \quad for \quad t \ge t_1 \qquad (2b)$$

Here p_{peak} is the overpressure amplitude and t_2 is the ime taken for the overpressure to fall to zero value for the first time.

The A-type of impulse has a form of the Friedlander pulse occurring as a result of a near instantaneous release of energy from a point source in a free field without any reflecting surfaces. Such a pulse is comprised of a rapid rise from ambient levels to a peak pressure followed by a relatively slow decay to ambient levels and, finally, a rarefied period before recovery to ambient pressure again.

The peak value of sound overpressure is the maximum absolute value of the instantaneous sound pressure in Pa. The rise time is the time interval between the start of an impulse and the time when the peak value is attained. In practice this is taken as the time to rise from 10% to 90% of its maximum absolute value of the sound pressure. Duration is the time interval between the start of an impulse and the time when an impulse decays to a zero value.

All of these parameters (peak level, rise time and duration) depend on the type of firecracker and its characteristics, especially the containment (mass or charge weight and type of explosive used), encapsulation, the size of firecracker, its geometric characteristics and its design. These variants of the Friedlander pulse can be mostly characterized in terms of a peak decay time or a band pressure decay time.

Typical firecracker explosions outdoors, at a distance of some metres, produces a peak sound pressure level highly exceeding levels as adopted for hearing protection. The region of non-linear acoustics starts above 150 dBC. A typical firecracker exploding outdoors produces high sound pressure levels [6,7], at distances of around 5m, peak overpressure levels is between 145 and 160 dBC. The spectral distribution of energy in such an impulse is controlled by the A-duration and the rise time.

Where there are reflective surfaces, such as the ground or walls, additional pulse components can exist (see Fig. 1*b* and *c*). Reflecting surfaces produce secondary reflected waves. These reflections can interefere with the original pulse, producing a complex temporal pattern. The time interval between the primary and secondary waves depends on the relative distances between the reflecting surfaces and the receiver. The peak and spectrum of the reflected components depend on the impedance characteristics of the reflecting surface.

5. EFFECTS OF FIRECRACKER NOISE TO HEARING DAMAGE

When a firecracker explodes, it produces ear-splitting sounds which may be amusing to the user, but on the other hand, this is generally recognized as a source of danger noise pollution in the environment. This can further shift the hearing threshold or even produce deafness. Many impulse noises from firecrackers are so intense that a single unexpected impulse incident to unprotected ears can result in severe and permanent hearing loss, even when the impulse is very short and contains relative little energy.

Impulse noise from firecracker explosions creates several particular hazards to the human auditory system. First, the high peak levels associated with firecrackers may damage the cochlea by causing rapid mechanical failure and injury. A series of rapidly occurring impulses can be partially attenuated by the acoustic reflex, a reflexive contraction of the middle-ear muscles, while isolated impulses reach the cochlea before activation of the acoustic reflex. It is very important however, that contraction of the middle ear muscles can occur prior to occurrence of the impulse noise if such a noise had been warned prior by another loud signal. Price refers to the human reaction to such an unexpected and expected sounds as the unwarned response and warned response [8, 16]. Thus, the expected occurrence of a noise impulse is much safer for the hearing organ (warned response) than the unexpected event (unwarned response - as was the case during the plaintiff's exposure to the firecracker explosion). This difference in human reaction may be caused not only by the anticipatory contraction of the middle ear muscles but also by lower general physiological stress within the auditory system. For example, an extreme unwarned response (the startle response) is characterized by vasoconstriction and sudden increase in blood pressure that can affect the biochemistry of the organ of Corti. Thus, single intense and unexpected explosions may result in large cochlear lesions and significant hearing loss. This damage is termed "acoustic trauma" and hearing at most frequencies may be affected. Additional symptoms include a sense of "fullness" in the ears, e.g. speech sounding muffled and a ringing in the ears (i.e. tinnitus). Although a certain amount of hearing recovery takes place after an acoustic trauma episode, the individual is often left with severe, permanent hearing loss. So an additional 7% hearing loss of the plaintiff was undoubtedly the result of the firecracker explosion close to his right ear.

Exposure to noise levels greater than 140 dB can cause permanent hearing damage. Almost all firecrackers create noise with C peak level of over the 140-dB level at a distance of a few metres. In locations where the reverberation is present , sounds can bounce off walls and other structures, making noises louder and increasing the risk of hearing loss.

Exposure to the sound of a firecracker can result in permanent hearing loss, meaning the exposed person will have trouble discerning consonant sounds such as "t", "k", "s," "sh," or "p" and other high-pitched sounds. In such case it is also difficult to understand speech on social occasions, especially when many people are speaking simultaneously [9]. Such people may also suffer from ringing in their ears, i.e. tinnitus. This ringing, as with hearing loss, can be permanent.

It is true that exposed people can prevent hearing loss by using appropriate protective hearing devices, such as earmuffs or earplugs. Of course, this holds true only when such exposure is expected in advance. For this reason the additional importance of differences between expected and unexpected impulses must be taken into consideration.

High impulse noise, especially when a firecracker explosions are involved, has a different effect on the ear than normal noise as the protective mechanisms of the ear are less effective for a very short noise. A 1.5 ms noise at 150 dB can damage the ear permanently to some degree even though its equivalent energy level wouldn't be significant.

6. DESCRIPTION OF PROCEDURES UNDERTAKEN BY THE EXPERT

6.1. Erroneous medical investigations

The expert, A.G., invited the plaintiff who was exposed to the firecracker explosion, to undertake some audiometric tests. During these tests however, the plaintiff had many problems recognizing the audiometric signals. There was no significant sound absorption in the test room, and audiometric test signals were difficult to recognise due to the high level of background noise. A loud conversation between other clients and employees was clearly heard from adjacent areas, so the plaintiff did not have the opportunity to recognise the audio signals clearly. He was disturbed and distracted by non-related events and by people in the vicinity. After the plaintiff pointed out this issue, the expert tried to mitigate this problem by simply sending her nurse to the adjacent rooms in order to quieten these loud and disturbing conversations. In this way the expert performed the audiometric tests under very unsatisfactory and unconventional conditions.

The expert did not describe the compliance with standards of the audiometric room in which he performed these auditory tests. He also failed to state whether the maximum permitted ambient sound pressure level, Lmax, was not exceeded in this test room. Also, he did not answer whether the ambient sound pressure levels were ever measured and compared with the maximum permitted levels of ambient sound pressure levels; for example Lmax according to ISO 8253-2 at a starting frequency of 125 Hz and a zero level of 10 dB. Furthermore, he did not state what kind of walls the test room in which he carried out these audiometric investigations had, neither their sound insulation properties at individual frequency bands. Finally, he also failed to provide information on the sound absorption characteristics of this room.

6.2. Incorrect procedures and calculations

The informations used by the expert were totally defective in order to draw any trustworthy conclusions. Instead of professional access, he operated with quite irrelevant data, like the description of the plaintiff's oral cavity colour, his tongue frenulum, his throat and the throat mucous [10]. Not only are such informations unnecessary for this kind of testimony from an expert but, by doing so, he also revealed sensitive personal data concerning the plaintiff. From existing medical documentation he fully revealed quantitative data about the plaintiff's blood sugar, blood pressure, triglycerides and cholesterol levels. On the other hand, he completely omitted to correlate these values with eventual plaintiff's hearing damage. These data were not required and were totally unnecessary as part of an expert's testimony, neither did the expert use them in any part of his testimony.

6.3. Wrong metrics used

According to the Directive 2013/29/EU [11], fireworks are categorized into four categories F1 to F4. So fireworks which present a low hazard and low noise level and which are intended for outdoor use in confined areas belong to category F2; and fireworks which present a medium hazard and are intended for outdoor use in large open spaces and whose noise level is not harmful to human health belong to category F3. For category F2, the safety distance for fireworks is set to be at least 8m away. For category F3, fireworks must be ignited at least 15 m away and the maximum noise level at these distances must not exceed 120 dB (A, imp), or an equivalent noise level determined by another appropriate measuring method, at the safety distance.

It is obvious that there is not an arbitrary 120 dB limit (without any dynamics and weighting) as the expert used it, resulting in his quiet wrong results. First, It is ridiculous what the expert did with this value! He used a point source model with reference 120 dB (A, imp) at a distance of 8m and calculated what the sound pressure level at 5m (the distance of the firecracker explosion to the plaintiff's ear in the expert's opinion) should be and obtained 124.08 dB. Secondly, neglecting the true limit of 120 dB (A, imp), he simply ignored dynamics and frequency weighting and compared this value with hearing damage limit directly. Then he drew the conclusion that this is even less than 130 dB, so according to such reasoning, the plaintiff was not exposed to any risk to his hearing at all [10]. It is quite clear (except to the expert, A.G.) that decibels, measured with the dynamics impulse and weighted with filter A, are not identical with peak level decibels weighted with filter C. This difference is of crucial importance since the limits of a noise when assessing any risk to hearing is expressed as $L_{C\ peak}$, that is using the peak value and weighted with filter C [12]. Obviously, the expert does not distinguish between these basic acoustic descriptors, denoted by $L_{AI\ max}$ and $L_{C\ peak}$. The difference between these two indicators is enormous and in the vast majority of cases, including this one, affects the result decisively. During the examination the expert insisted, that these are all "audiologic decibels", without any further explanation, convincing the judge which disabled any further questions.

The difference between the $L_{C,\ peak}$ and $L_{AI,\ max}$ indicators is about 26 dB in the actual case of the firecracker explosion. This means that a maximum noise level of 124.08 dB(A, Imp) corresponds to a much higher level of $L_{C,\ peak}$, which exceeded 150 dBC at the location of the plaintiff's most exposed ear.

Here the expert made a cardinal mistake which was probably due to a lack of understanding the most important issues and fundamentals of acoustics. Misunderstanding these decibel units, he tried to calculate the sound pressure level at a distance of 5m for the F2 category firework and obtained 124.08 dB [10]. He did not explain which kind of decibels he had in mind. Based on this incorrect noise descriptor, he simply concluded that being 5 metres from such a firecracker explosion, the sound pressure level due to this firecracker explosion did not reach the limit value (130 dB) at which hearing loss could occur. He did not transform these metrics to the C-weighted level. Furthermore, he did not explain (and obviously even did not understand) which time dynamic he used for the limit value. In his confusion he simply denied any possibility of hearing loss or tinnitus, since, in his opinion, the plaintiff had not been exposed to a impulse noise of 130 dB or more. Of course, his conclusion was absolutely wrong, based on his incorrect calculation and the totally wrong use of the descriptors and their units. It can be easily proved that in this case the $L_{C\ peak}$ level exceeded 150 dBC.

According to Slovenian and European regulations, the cornerstone of hearing protection criteria against high impulse sounds is a maximum permitted level, $L_{C\ peak}$. This stipulates that there is a risk of hearing loss above 135 dBC with respect to the reference pressure of 20 µPa. This corresponds to a sound pressure level of ppeak = 112 Pa. This means that at the time of the firecracker explosion, the plaintiff was exposed to at least 32x (over thirty times) greater energy level than is permitted which, of course, resulted in acute hearing impairment. For impulse dynamics, the time constant, or the rise time is 35 ms during its increase [15]. The time constant is defined by the IEC standards. It also denotes the time needed to reduce the amplitude of an exponentially decreasing signal by a factor of 1 / e = 0.3679...

The expert, A. G., was not familiar with these decisive facts and obviously confused the L_{Peak} with an alternative descriptor L_{Imax}, which led to enormous errors. The peak detector L_{Peak} on a sound level meter must have a response of less than 100 µs (100 microseconds). L_{Peak} is usualy measured in combination with C or unweighted (flat) network. This is one of the most important reasons why the interpretations of the expert, A.G., are completely wrong.

Even using a rough comparison of the time constant for the impulse dynamics and the peak response time, an approximate ratio of 350: 1 is evident, which corresponds to the logarithmic ratio of about 25 dB. Additionally, the difference between the C weighted and A weighted filters also makes a certain contribution to this difference. It is well known that C weighted levels are generally higher than A weighted ones, with the exception in one part of the high frequency audible region. However, since the spectrum of the firecracker explosions is shifted towards higher frequencies, this contribution is much less than the contribution due to different time constants.

It is quite clear that the expert, A.G., confused peak level L_{peak} with the maximal level $L_{I,\ max}$. Peak is, by the IEC definition, the greatest absolute instantaneous sound pressure during a given time interval.

Additionally the expert here underestimated the risk impairment as well by using the Pyrat firecracker of the F2 category, although most probably a type of Megatron firecracker of the F3 category was used in this case, whose peak levels greatly exceed 155 dBC at a distance of 5m.

6.4 .Confusion about sound wave phenomena

The expert considered the unevenness of the walls and the corners of the surrounding houses where, according to his opinion, the air waves were refracted [10]. There were obviously no air waves in question, but rather sound waves. Even worse, he completely confused the effects of reflection and refraction with diffraction and scattering. The expert obviously does not distinguish between these terms.

6.5. Confusion about low and high frequency content of an explosion

According to his biased position, the expert was looking for some unrealistic facts in trying to explain the plaintiff's hearing loss. He namely declared that the plaintiff may have suffered hearing impairment during his military service in the artillery more than 35 years previously. Without any evidence he guessed that he was certainly repeatedly exposed to strong impulse noise and loss of hearing which consequently would, in his opinion, result in the formation of a tinnitus [10]. These are again speculative and false statements, without any evidence, and also contrary to the theory of high-energy impulse noise.

The plaintiff emphasized that he was actually in the artillery, but in the computing units far away from artillery operations. Additionally, during his servicing, only artillery firing simulations were performed, so he was never exposed to real artillery gunfire himself. Even if he were, his hearing damage would be completely different. Namely, the sound impulse bursts of the fireworks is quite different from that produced by artillery fire with a frequency spectrum that is markedly shifted towards higher frequencies, as proven below.

When launching artillery missiles, one has to deal with substantially larger masses of explosives, exceeding thousands of times the mass of firecracker explosives. For this reason, the duration of artillery explosions is considerably longer than that of firecrackers, resulting in lower frequency components.

In figure 2 the time dependence of sound overpressure is shown which is an approximation of sound impulses resulting from firecracker explosions and heavy weapon operations.

Here the rising time is very short, so only the exponential function during the decay (eq. 2b) of the Friedlander impulse is of practical importance. In the time domain, the sound pressure of the Friedlander pulse $p_F(t)$ can be written in the form

$$p_F(t) = p_{peak}\left(1 - \frac{t - t_1}{t_2 - t_1}\right) e^{-\frac{t - t_1}{t_2 - t_1}} \qquad (3)$$

where p_{peak} is the maximum peak sound pressure

The time domain can be transformed into a frequency domain by using the Fourier transform $P_F(\omega)$ [5]:

$$P_F(\omega) = \int_{-\infty}^{\infty} p_F(t) e^{-i\omega t} dt = \frac{i\omega t_p^2}{(1 + i\omega t_p)^2} \qquad (4)$$

where $\omega = 2\pi f$ is the circular frequency.

Next, we find the effective value of $p_F(rms)$.

$$P_F(rms) = \sqrt{\frac{1}{T_P}\int_0^T p^2{}_F(t)\, dt} = \sqrt{\frac{1}{T_P}\left(e^{-2T/t_p}\left(-\frac{T_P^2}{2t_p} + \frac{T_P}{2} - \frac{t_p}{4}\right) + \frac{t_p}{4}\right)} \qquad (5)$$

Whereby the T_P is selected as a point on the time axis in which the pressure $p_F(t)$ is asymptotically approximated to 1% of the baseline value, which is approximately $T_P = t_r + 6t_p$. Here T_P denotes the time required for such an approximation where the time of rising is t_r and t_p is the time of the decreasing Friedlander pulse to zero.

In this way the frequency spectrum of the pulse or its energy distribution is obtained.The amplitude spectrum is given by the following equation [5]

$$|P_F(\omega)| = \frac{\omega t_p^2}{(1 + \omega^2 t_p^2)} \qquad (6)$$

Looking for the extreme value of this function, yields

$$\frac{d\,|P_F(\omega)|}{d\omega} = \frac{t_p^2 - \omega^2 t_p^4}{(1 + \omega^2 t_p^2)^2} = 0 \qquad (7)$$

from which it follows $\omega = 2\pi f_F = \frac{1}{t_p}$, or $f_F = 1/2\pi t_p$.

It is evident that the spectrum reaches the maximum amplitude at the frequency $f_F = 1/2\pi t_p$, and the maximum value of the amplitude spectrum is $|P(\omega)|_{max} = t_p/2$. Therefore, there is a significant difference between the duration of these two different explosions. For example, a firecracker produces an impulse with an A duration of about 1ms and a peak in the spectrum at about 2000 Hz. At launching an artillery shell, it has a duration of about ten times longer so the maximum spectrum level is shifted to lower frequencies by one decade , which is around 200 Hz (figure 3 and 4)

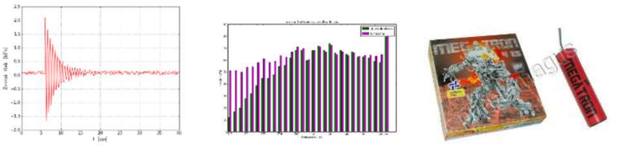

a) b) c)

Figure 3: time diagram of sound pressure a) and shape of its spectrum b) due to the firecracker explosion c) shifted to high frequencies [13].

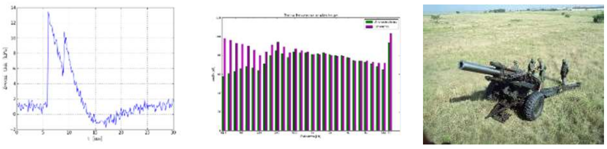

a) b) c)

Figure 4: time diagram of sound pressure a) and spectral shape b) due to the firing of a howitzer c) – the spectrum is shifted to low frequencies [13]

Thus the sounds produced by large-caliber weapons have acoustic energy predominantly concentrated in the low frequency range (below 400 Hz) while the spectral content of sounds produced by firecrackers extends higher, around 1500 – 2500 Hz.

Also, a comparison of these physical facts and the plaintiff's hearing loss characteristics shows that his hearing impairment cannot be the result of artillery fire noise as the plaintiff had already explained that he had never been exposed to it. Also, medical evidence proved that the damage to hearing had increased by 7% between the two audiometric tests, in less than 2 years apart, soon after the firecracker explosion; on the other hand, this firecracker accident occurred more than 30 years after the plaintiff had completed his military service in the artillery. Furthermore, the default assumption of the expert, A.G., that all soldiers and other personnel in artillery are exposed to artillery noise is ridiculous; similar to saying that all workers employed in court are judges or all workers employed in health care are doctors. Using such a set of incomplete and mainly erroneous information, the expert tried to speculate throughout his testimony. On the other hand, by ignoring the most important data and lacking even the most fundamental theoretical knowledge he was unable to prove his claims of course.

6.6. Confusion and misunderstanding of occupational noise exposure

The expert further assumed that the plaintiff was occasionally exposed to high levels of noise at his workplace. He further speculated that the protective hearing devices were not sufficient as the noise was also transmitted through the cranial path to the inner ear [10]. However he did not provide any evidence about the propagation of the sound energy transferred to the inner ear through the bones of the skull against airborne transmission. Although he tried to explain hearing loss in this way, he did not give any estimate of how much of the sound energy was transferred to the inner ear through the bones of the skull against airborne transmission. These expert statements are thus again baseless. The use of earplugs and earmuffs (especially when combined) successfully protects or reduces the exposure of auditory organs to noise levels by up to 40 dB. Only when even higher reductions are required it is necessary to reduce the transmission to the inner ear by the cranial path as well. Neither the plaintiff nor the vast majority of workers have need to take any of such precautions so far. The applicant suggested the expert to describe one practical case where, according to his experience, such or a similar problem arose in his practice, but no answers have been forthcoming so far.

The expert further insisted that during recreational shoting and, at some workplaces, strong vibrations are transferred through the bones to the inner ear. However, he was again unable to clarify what he meant by “strong vibrations”, even not in which units these vibrations are expressed.

6.7. Deficient expertise regarding asymmetric exposure during sport shooting

The expert further speculated on information regarding the plaintiff’s involvement in some sport shooting activities without any professional background [10].

For this reason a few words about sport shooting activities should be mentioned first. Here, the expert also misinterpreted the information about the plaintiff’s involvement in sports shooting. The applicant was actually engaged in some occasional sports shooting activities. However, there are some facts in relation to shooting itself that must be elucidated. During sport shooting activities, there is namely a pronounced asymmetry in the impairment risk to both ears [14]. During shooting, the right part of a shooter head rests slightly on the right shoulder and the left ear is directed against the barrel that is on the side of the explosion (Fig 5). Consequently, the left ear is much more exposed to the resulting sound impulse burst than the right ear. On the other hand, the right ear is located in the shadow of the head, which protects it, particularly at high frequencies. The ear that is tucked into the shoulder thus sustains lower dB levels than the ear that is exposed to the muzzle of the gun, so the left ear sustains higher levels of damage than the right ear in right handed shooters. When shooting right-handed (as in the case of the plaintiff) the shooter’s left ear is facing forward and thus receives more of the muzzle blast than the right ear which is more backward facing. On the other hand, the plaintiff, as with most shooters, uses correctly fitting personal hearing devices for ear protection to both ears.

Fig 5: the usual position of head during shoting

This fact is indisputably confirmed by a number of investigations and statistics regarding hearing damage of shooters, especially hunters who rarely use personal protective equipment. Such asymmetry in noise exposure applies practically to all shooters (except to left-handed ones, who mostly use customised firearms especially adapted for them). A very similar phenomenon occurs with many professional musicians as well, especially violinists and string players; they also lean the right ear against the shoulder, so their left ear is significantly more exposed to sound energy as well. It was consequently proved that the left ear predominantly experienced more hearing loss during sport shooting activities than the right. Hearing loss amongst rifle shooters also tend to be asymmetrical, however here the left ear is closer to the barrel and tends to be more impaired as it is closer to the explosion whereas the right ear is protected by the head [14]. A further asymmetry was postulated due to the explosion of the firecracker being close to the plaintiff’s right ear during the absence of personal protective devices, exposing his right ear to the noise of the firecracker.

Even the expert, A. G., confirmed that the plaintiff’s right ear is significantly more damaged than the left one. This assertion additionally confirms the fact that the plaintiff was unable to obtain such hearing damage as a result of some shooting activities, but as a result of a powerful and unexpected firecracker explosion which occurred in the immediate vicinity of his right ear.

7. CONCLUSION

Almost all expert conclusions are completely wrong as a result of the substantial errors in his calculations and the incorrect application and misunderstanding of the metrics used. Furthermore, the expert disregarded many physical laws and facts, such as differences in the spectral characteristics of small (firecrackers) and large explosions (artillery shells). He neglected the sound exposure asymmetry characteristics of the left and right ear during sport shooting and the efficiency of personal protective equipment used etc.

In the case of any excessive noise, or even on a suspicion of excessive noise, the plaintiff always used personal protective equipment to protect his hearing; if necessary even additional protection, by which the noise emission levels in the ears were reduced by up to 40 dB. This is also his duty, as he provides a professional service in this field, such as noise assessment and its control. So it is quite clear that different occupational and recreational types of noise to which the plaintiff was subjected to through his duties presented no risk of damage to his hearing. The emission levels of sound energy released during occasional bursts and similar noisy events which he received during his workshift were consequently approximately ten thousand times lower than that which the plaintiff's inner ear received during the firecracker explosion. On the other hand, the plaintiff found himself in a quiet different situation on April 10, 2012, as he was been completely surprised by an unexpected firecracker explosion. So he did not have any chance to take the appropriate preventive measures or to use any other form of protection for his health.

The expert argued that the plaintiff would have sought medical help if he suffered hearing impairment due to a firecracker explosion. He did not explain, however, whether such a failure in his hearing, caused by a firecracker, would even be curable. According to another independent expert, hearing impairment of between 7 and 12%, caused by a firecracker explosion, cannot be rectified.

In the existing expert testimony, there are a number of significant errors, many of them of a fundamental nature, which had a decisive influence on the final results and its conclusions. The expert performed audiometric tests under extremely unfavourable conditions; he paid no attention to the fundamentals of acoustics and audiology, nor to the human perception and reaction to sound. He misinterpreted the acoustic characteristics of firecracker explosions with artillery and sports firearms. The expert did not take into account the basic acoustic characteristics of such different groups of bursts. The most fatal error he made, however, was the confusion between different metrics he employed in the evaluation of high-impulse noise. He simply confused the descriptor $L_{AI,\,max}$ and $L_{C,\,peak}$, which differs by approx. 26 dB for firecracker explosions. This additional confusion in metrics resulted in fatal error of the peak level by 26 dBC. This difference was even a little higher, as the firecracker applied in his calculation was of a third, rather than of a second, category (Megatron or Extreme instead of Pirate, with which the expert based his calculations). In this way, the expert's conclusion regarding the exposure to 124 dB peak level instead of a much higher value of over 150 dB was totally wrong of course. It is ridiculous that some judges still have faith in such erroneous data and conclusions.

8. REFERENCES

[1.] Zakon o eksplozivih in pirotehničnih izdelkih, O.J. RS, 35/2008
[2.] EN ISO 8253 Acoustics- Audiometric test methods- Part 1: Basic pure tone air and bone conduction threshold audiometry
[3.] EN ISO 8253 Acoustics- Audiometric test methods- Part 2: Sound field audiometry with pure tone and narrow-band test signals
[4.] ISO 10843: Acoustics - Methods for the description and physical measurement of single impulses or series of impulses
[5.] R. P. Hamernik, K. D. Hsueh: Impulse noise: Some definitions, physical acoustics and other considerations; JASA 90(1), July 1991, 189-196
[6.] N. Kapoor, A. P. Singh: Firecracker noise and its auditory implications, Proceedings of the Tenth International Congress on Sound and Vibration, Stockholm, 2-6 July 2003, 5063-5070.
[7.] O. V. Mohanan & M. Singh: Characterisation of sound pressure levels produced by crackers; Applied acoustics, Vol. 58, December 1999, 443-449
[8.] G.Richard Price: Impulse noise hazard: From theoretical understanding to engineering solutions; Noise Control Engineering Journal 60 (3), May - June 2012, 301-312
[9.] Non – binding guide to good practice for the application of directive 2003/10/EC Noise at Work; Chapter 7: Hearing damage and health surveillance, European Commission Directorate-General for Employment, Social Affairs and Equal Opportunities, December 2007, 112 - 119
[10.] Anton Gros: Expert witness opinion n° II P 1669/2015, District Court of Ljubljana, 14. August 2017, 1 - 10
[11.] Directive 2013/29/EU of the European parliament and of the council of 12 june 2013 on the harmonisation of the laws of the member states relating to the making available on the market of pyrotechnic articles
[12.] Directive 2003/10/EC on the minimum health and safety requirements regarding the exposure of workers to the risks arising from physical agents (noise)
[13.] Military noise environment Hearing Protection – Needs, Technologies and Performance, NATO Technical report by Task Group HFM – 147, November 2010, chapter 3
[14.] P. Rasmussen, G. Flamme, M. Stewart, D. Meinke. J.

Lankford: Measuring recreational firearm noise, Sound & Vibration, August 2009
[15.] IEC 61672 – 1, Electroacoustics – Sound level meters, Part 1: Specifications
[16.] G. R. Price: Predicting Mechanical Damage to the Organ of Corti, Hearing Research, Vol 226, April 2007, 5 - 13

Measurement-based methods for separating wheel and track contributions to rolling noise and new methods for pass-by noise certification

Gerald Schleinzer [a], David Thompson [b], Ines Lopez Arteaga [c], Michael Dittrich [d], Erwin Jansen [d], Antoine Malkoun [e], Egoitz Iturritxa [f], Matthias Stangl [g]

a. Siemens Mobility GmbH, Eggenberger Straße 31, 8020 Graz, Austria
b. Institute of Sound and Vibration Research, University of Southampton, Southampton SO17 1BJ, UK
c. KTH Royal Institute of Technology, The Marcus Wallenberg Laboratory for Sound and Vibration Research, Teknikringen 8, SE-100 44 Stockholm, Sweden
d. TNO, PO Box 96864, 2509 JG Den Haag, The Netherlands
e. Alstom Transport, 6 rue de Strasbourg, 67110 Reichshoffen, France
f. CAF, Technology Division, R&D Department, J.M. Iturrioz 26, 20200 Beasain, Spain
g. DB Systemtechnik, Völckerstraße 5, 80939 München, Germany

Abstract: A pass-by measurement of a train is one part of the homologation of a train in the EU. The measured noise contains different sources such as traction noise, noise from auxiliary equipment, aerodynamic noise and rolling noise. With the current method it is not possible to distinguish the vehicle and track part of the noise. Further reductions of limit values may not be achieved on current TSI tracks and more stringent requirements for measurement tracks carry the risk that such tracks are not available on a customer's network. Therefore there is a need for the future to separate noise into its different components and further to find a method to transpose the rolling noise part to a virtual reference track. The method needs to be easy but with sufficient accuracy and robust in homologation situations. In this study some existing and new methods for noise separation are under investigation. Most of the methods can assess the track component of noise with acceptable accuracy. However, the wheel noise component could only be estimated using three methods and unfortunately these did not give reliable results in the current tests. The paper contains in the first part a shorted summary of earlier publications [12] [14] and focuses in the second part on a partial transposition to a virtual reference track with only knowledge of the total and the rail part of rolling noise.

Key words: Railway pass-by noise, certification, TSI, noise separation, transposition, virtual reference track

1. INTRODUCTION

Different noise sources on a train form the total noise. These are traction noise, rolling noise, noise from auxiliary equipment and aerodynamic noise at high speeds. Over a wide speed range rolling noise is the most important source and is radiated by vibrating rails and wheels where the excitation comes from the wheel and rail acoustical roughness [1]. A high level of roughness together with low damping of wheel and rail leads to high levels of rolling noise. For any noise reduction measures it is important to know if the noise and which frequency part of it are mainly coming from the vehicle or from the track. The noisier component will always mask reductions of the second noisy component. Therefore the current standards try at least to limit the influence of the rail noise on pass-by measurements.

At the moment ISO 3095 [2] defines the track properties of a reference track. This track need to be used in certification tests for the Technical Specification for Interoperability (TSI) Noise [3]. The TSI sets the noise limit values under certain operating conditions. The reference track is mainly defined by an upper limit of the rail roughness and a lower limit of the track decay rate (TDR). Both were chosen on the one hand to minimise the influence of the track on the measurement but on the other hand also to make it not too difficult to find a reference track in each European country. So neither the rail roughness nor the track radiation can be completely neglected. Hence the measurement results are not representing only the vehicle noise. The current measurement also does not allow to separate wheel and track noise.

The work presented assesses existing and new methods for rolling noise separation. A series of pass-by measurements have been carried out between Munich and Augsburg including the measurement of the track properties so that the different methods could be compared under well defined conditions.

Six methods are able to estimate the track noise where three methods are intended to estimate the vehicle noise. Different partners carried out the measurements and the results where compared without further adjustments or tuning. Additionall data of recent TSI measurements [15] were collected to show typical average rail roughness and track decay rates of measurement tracks. Such average values could be used to define a virtual reference track.

1. OVERVIEW OF WHEEL/RAIL SEPARATION

The goal of separation is to reveal the different contributions to the measured noise. Figure 1 shows the various sources contributing to the noise during a train pass-by. The noise emission is defined as averaged sound pressure level at 7.5 m from the track centreline over the transit time of the train, as defined in the ISO standard [3].

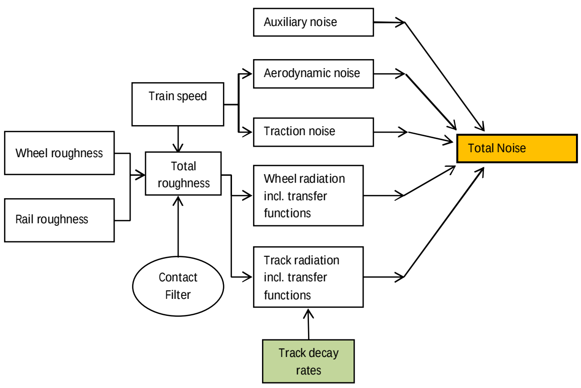

Fig.1. Vehicle and track contributions to pass-by noise including rolling noise and other sources, including the excitation mechanism of rolling noise.

3. MEASUREMENT CAMPAIGN

Field tests have been carried out between Munich and Augsburg on the normal operational track to test the various separation methods. A test train including the "Schallmesswagen" of DB was used for the measurements, Figure 2. The wheels of the coaches were of type BA093 and almost new. The coaches were all disc-braked to give smooth wheels and one bogie of the middle coach remained unbraked to ensure constant wheel roughness during the tests. The locomotive was far enough away from the test section (red) so the only sources of noise on the train were from rolling noise (wheels and track).

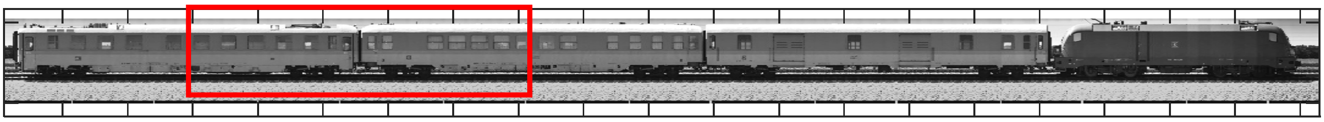

Fig.2. Test train with three coaches used for the study.

4. REFERENCE RESULTS

In order to assess the accuracy of the separation methods a set of reference results has been created. These were made with a TWINS model [4] together with measured rail vibration. Figure 3 shows an example of the contributions of wheel, rail vertical and lateral vibration to the overall noise spectrum.

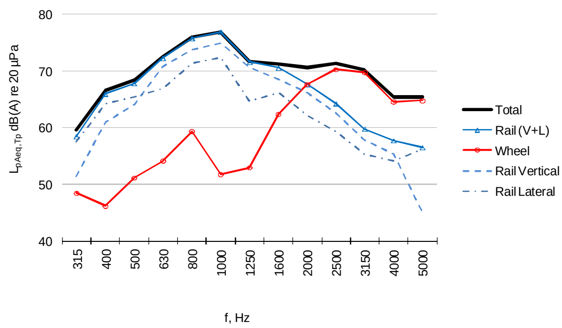

Fig.3. Separation according to reference results. Example at 80 km/h.

5. SEPARATION METHODS IN BRIEF

A detailed overview about the different methods can be found in [14] and in the public deliverable D7.4 of the Roll2Rail project [12].

5.1. WSE - wave signature extraction

One of the new methods is based on wave signature extraction (WSE) using a near-field microphone array which has been developed as part of this work. Further details are given in Zea et al. [8, 9]. The method has some similarities to the SWEAM method [10]. The main idea of WSE is to estimate the track contribution by means of wavenumber-domain filters, which are designed according to the radiation properties of the rail. The accuracy of the WSE method is largely dependent on the filter design. Sources of error can be associated with the estimation of the wavenumbers when using data before and after the pass-by. The method doesn't need any additional measurements before the actual pass-by.

5.2. Beamforming

Another method was proposed using beamforming for wheel/rail source separation, based on the fact that the radiation from the rail is not like a point source but rather occurs under an angle to the normal with at least 10° [7]. Thus by limiting the focus angle of the array within a small range, ±10° to the normal, the sound radiation from waves propagating along the rail should be suppressed and only the radiation from the wheel (and the sleepers) should remain. During the field tests, the microphone array stud at 7.5 m from the nearest rail (8.25 m from the track centre), and the centre of the array was at 1.51 m above the top of the railhead. The expected frequency range of results is 500 Hz to 5000 Hz. The results from the beamforming method indicate that it didn't suppress the rail noise as expected. However beamforming was the only method in this project which could identify the wheel component in a direct way.

5.3. ATPA Advanced transfer path analysis

Transfer Path Analysis is a well known method for assessing different noise paths towards a given destination. The Advanced Transfer Path Analysis (ATPA) method is an enhanced experimental method for obtaining the noise contributions [11]. The objective of the method is to obtain the decomposition of the sound pressure PM at a target location as the sum of N noise contributions. These contributions are obtained as the product of the operating vibration signal ak with a given the so-called Direct Transfer Function (DTF). The so-called 'Global Transfer Functions' (GTF) correspond to the physical transfer functions measured when performing impact testing with excitation at one subsystem. Both DTFs and GTFs are characteristics of the physical system and do not depend on operating conditions. However, GTFs can be measured experimentally, but not DTFs. The ATPA needs a static test before the pass-by test to measure these GTFs. This needs extensive instrumentation and is very time consuming. A simplification of these tests is required.

5.4. MISO method

At the end of the project the so called "MISO method" as described in [6] was added to the comparison and has been applied using the data of the ATPA method. A trigger signal was reconstructed from the rail vibration. The microphone position at 2.8 m from the nearest rail is further away than intended in the original implementation of the method (1.0 m from the nearest rail). Since the purpose of the close microphone is to measure only track noise in a section between the bogies of a coach the wheels may have contaminated the pure track noise in this study. The MISO method does not need the knowledge of the acoustical track characteristics and the setup is rather simple.

5.5. Methods based on pass-by analysis (PBA)

Already for a long time the pass-by analysis (PBA) method [5] is on the market. It can be used to determine the total transfer function and combined effective roughness for each test run. Separation could also be achieved if the vehicle transfer function LHpR,veh(f) is measured using static tests. In our case for frequencies below 2 kHz it was assumed that the track is dominant, and the wheel transfer function was set 7 dB lower than the total transfer function. The track transfer function adapted to 1 dB below the total. For frequencies of 2 kHz and above, the wheel was assumed to be dominant, and the transfer functions were set the other way round. A second option used a previous static wheel transfer function measurement of a 730 mm diameter reference vehicle from the STAIRRS project [13]. The accuracy of the method depends on the availability of reasonable distribution function which split total noise into a track and a wheel part. Mixed traffic on a railway line may provide sufficient data to obtain theese functions. The applied methods are basically inexpensive and practical to use.

5.6. Track Transfer Functions from TWINS

As part of the reference result also the Track Transfer Functions from TWINS were pointed out and used as a method on its own. The measurement of rail vibrations with accelerometers is rather easy and the calculated transfer funtions (TF) convert the spectrum of the vertical and lateral rail acceleration directly into an estimate of the vertical and lateral part of the pass-by noise. It needs to be investigated how much these transfer functions differ from test site to test site. The method is also not jet validated for slab tracks.

6. ACCURACY ASSESSMENT

In the following only an overview about the deviations from the reference results is given. More details are shown in [14]. It is found that most of the methods can obtain the track component of noise with acceptable accuracy. However, beside from the TWINS model, the wheel noise component could only be estimated directly using three methods and unfortunately these did not give satisfactory results in the current tests. Table 1 shows mean and maximum deviations from the reference results for overall noise levels and for 1/3rd octave bands.

Table 1. Accuracy assessment of separation methods

Method	PBA with distribution function	PBA with static wheel transfer function	Beamforming with rail radiation models	WSE	ATPA	MISO	Track Transfer Functions from TWINS
Accuracy=root of mean quadratic deviation (max. deviation) in dB							
Wheel							
Overall level	2.2 (2.9)	2.8 (2.9)	3.8 (5.2)	n/a	n/a	n/a	n/a
1/3 octave band	8.6 (19.2)	6.2 (12.6)	10.8 (23.3)	n/a	n/a	n/a	n/a
Rail/Track							
Overall level	0.7 (0.9)	1.3 (1.9)	0.4 (0.8)	1.9 (3.1)	0.5 (0.7)	1.1 (1.6)	0.4 (0.8)
1/3 octave band	1.9 (4.3)	7.7 (17.4)	1.5 (4.1)	2.0 (4.9)	2.9 (9.6)	3.7 (9.4)	1.5 (4.1)

7. DEFINITION OF A VIRTUAL REFERENCE TRACK – TYPICAL ISO MEASUREMENT TRACK

A virtual reference track could be a solution to allow pass-by tests on non-compliant tracks, to make pass-by test on different ISO-tracks more comparable, to reduce the uncertainty during certification and to stimulate low-noise solutions on vehicles. This means that the influence of the different measurement tracks should be omitted as much as possible. There is also the wish that silent vehicles should clearly show up in pass-by certification test and low-noise measures at the vehicle should lead to lower measurement results. A discussion about this quickly leads to the question on which track a vehicle should be tested. Should it be a "normal" operational track, a bad track or a rather good track? A bad track mainly means high rail roughness and high rail noise radiation whereas a good track means low rail roughness and low rail radiation (high Track Decay Rates). We certainly might wish that noise reduction measures at the vehicle should show positive effects wherever the vehicle is running. The mechanisms of rolling noise generation clearly show that the latter is impossible. A noisy track will always mask silent vehicles. On the other hand low-noise rail traffic is not necessarily needed in the entire rail network. Focusing on hot spots is a better economic approach. So, silent tracks where needed in combination with low-noise vehicles are the best solution. Testing a vehicle on a low noise track makes low-noise solutions visible and will therefore stimulate low noise solutions. The big obstacle is that a simple tightening of the ISO requirements for the measurement track could make it impossible to find one. Therefore a virtual reference track with appropriate characteristics is a possible solution. As a starting point, which is coherent with the current TSI noise limits, a typical average measurement track from recent certification tests can be taken [15].

8. PARTIAL TRANSPOSITION TO A VIRTUAL REFERENCE TRACK

As a result of this study we saw that it seems easier to assess the rail noise part during pass-by rather than the other vehicle noise components. Hence at least a partial transposition with only knowledge of the total noise and its track part should be taken into account. The idea is based on the fact the the track decay rates influence the vertical and lateral rail noise radiation as shown in the following equations:

$$\Delta L_{Rail,V} = -10\log_{10}\left(\frac{TDR_{V,STD}}{TDR_V}\right) \quad (1)$$

$$\Delta L_{Rail,L} = -10\log_{10}\left(\frac{TDR_{L,STD}}{TDR_L}\right) \quad (2)$$

where $TDR_{V,STD}$ and $TDR_{L,STD}$ are then the track decay rates of a virtual reference track where TDR_V and TDR_L are the track decay rates of the measurement track.

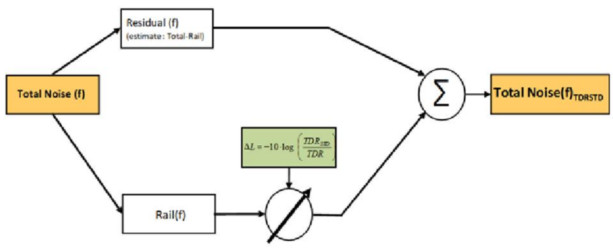

Fig.4. Partial transposition to a virtual reference track

According to the transposition scheme shown in figure 4, the rail noise is first separated from the other sources (sleepers and vehicle). Due to the problems when calculating level differences the residual part is not intended to give an estimate of the vehicle noise, simply the residual that is not to be adjusted. The rail part is then modified to allow for the differences in track decay rates between the measurement track and the virtual track and is finally recomposed with the residual to give an estimate of the overall pass-by level on the virtual track.

Track decay rates from recent certification tests (typical average ISO-compliant measurement track, table 2, fig. 5 and 6) are proposed to define the virtual reference track in order to remain compliant with the current TSI limit values.

frequency Hz	$TDR_{V,STD}$ dB/m	$TDR_{L,STD}$ dB/m
250	7.50	3.38
315	10.38	1.97
400	11.86	1.25
500	13.29	1.28
630	9.33	1.94
800	9.96	1.21
1000	4.64	0.66
1250	8.58	0.46
1500	5.02	1.05
2000	1.78	1.10
2500	1.62	1.56
3150	1.82	2.61
4000	2.85	3.23
5000	5.21	1.37

Table 2. Track decay rates of a typical average ISO measurement track [15]

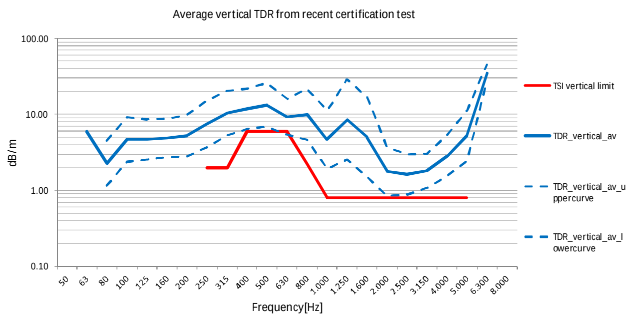

Fig.5. Average rail vertical TDR from recent certification tests [15]

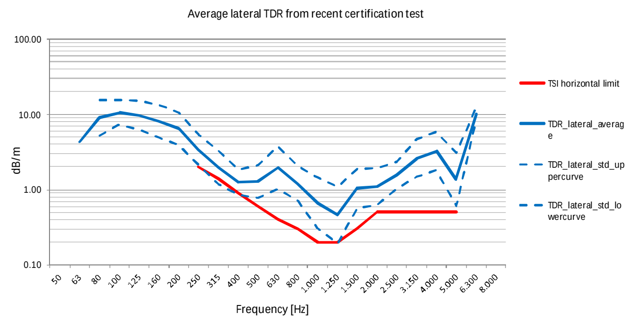

Fig.6. Average rail lateral TDR from recent certification tests [15]

The method in figure 4 would remove the uncertainties arising from differing track decay rates which can be much higher than the uncertainties due to rail roughness. Figure 5 and 6 show the mean values and the standard deviation of the TDRs. Such a method would even make measurements possible where ISO compliant tracks are not available e.g. where the use of a slab track cannot be omitted. The possible success of such a method very much relies on the accuracy of rail noise assessment and if the rail noise assessment is simple and robust enough for a certification test. Only if a sufficient accuracy for the complete transposition method can be achieved and the method was validated then it is ready to be introduced in a new standard. Some methods for noise separation are promising. But still there is a lack of experience with those methods and the accuracies may need to be enhanced. Further research work about this subject is planned. A further step would be to take also rail roughness into account for transposition. This is in detail even more complicated.

9. CONCLUSIONS

A series of pass-by measurements have been performed to assess different existing and new methods for rolling noise separation. A set of reference values has been calculated with a TWINS model including measured rail vibration data. The reference results allowed an accuracy assessment of the methods. Six methods were able to estimate the track component of noise where three methods could estimate the wheel noise. The estimation of the track component gave acceptable accuracy with about 0.5-2 dB deviation from the reference results. The estimation of the wheel noise did unfortunately show too high deviations. For implementation in a practical situation, for example as part of a new vehicle testing procedure, the cost and practicality of the methods has to be considered. Some details about this can be found in reference [12]. A partial transposition method to a virtual reference track was presented. Such a method would remove the uncertainties arising from differing track decay rates and would increase the comparability and reproducibility of measurement results. Such a method would also allow to measure on tracks which do not comply with ISO 3095. Mean values of track decay rates from recent certification test were proposed to define a virtual reference track. The choice of such a virtual reference track would stimulate low noise vehicle solutions.

Acknowledgements

The work described in this paper has been carried out as part of the Roll2Rail project, which has been financially supported by the European Union's Horizon 2020 grant, agreement No. 636032. The authors are grateful to the staff of Deutsche Bahn without whom the field tests would not have been possible, to the many colleagues who assisted in the tests and for the leadership of former colleagues Siv Leth, Ulf Orrenius, Adam Mirza and Léo Baures.

4. REFERENCES

[1.] D. Thompson, Railway Noise and Vibration: Mechanisms, Modelling and Means of Control, 1st ed. Elsevier, 2009.

[2.] ISO 3095:2013. Acoustics – Railway applications – Measurement of noise emitted by railbound vehicles, International Standards Organization, Geneva, 2013.

[3.] Commission Regulation (EU) No 1304/2014 of 26 November 2014 on the technical specification for interoperability relating to the subsystem ‘rolling stock — noise’, Official Journal of the European Union, L356/421-437, 2014.

[4.] D.J. Thompson, B. Hemsworth, N. Vincent, Experimental validation of the TWINS prediction program, part 1: method. Journal of Sound and Vibration 191, 123-135, 1996.

[5.] M.H.A. Janssens, M.G. Dittrich, F.G. de Beer, C.J.C. Jones, Railway noise measurement method for pass-by noise, total effective roughness, transfer functions and track spatial decay, Journal of Sound and Vibration 293 (2006) 1007–1028.

[6.] F. Létourneaux – STAIRRS Report - D11 Part 5 - MISO: A measurement method to separate noise emission of railway vehicles and tracks, November 2003

[7.] T. Kitagawa, D.J. Thompson. The horizontal directivity of noise radiated by a rail and implications for the use of microphone arrays. Journal of Sound and Vibration 329(2), 202-220, 2010.

[8.] E. Zea, L. Manzari, I. Lopez Arteaga, G. Squicciarini, D. Thompson. Separation of track contribution to pass-by noise by near-field array techniques. Proceedings of the 22nd International Congress on Acoustics, Buenos Aires, 2016.

[9.] E. Zea, L. Manzari, G. Squicciarini, L. Feng, D. Thompson, I. Lopez Arteaga. Wavenumber–domain separation of rail contribution to pass-by noise. Journal of Sound and Vibration 409, 24-42, 2017.

[10.] B. Faure, O. Chiello, M.-A. Pallas, C. Servière. Characterisation of the acoustic field radiated by a rail with a microphone array: The SWEAM method. Journal of Sound and Vibration 346, 165-190, 2015.

[11.] F.X. Magrans, Method of measuring transmission path, Journal of Sound and Vibration, 74(3), 321-330, 1981.

[12.] D. Thompson, G. Squicciarini, J. Wändell, I. Lopez Arteaga, E. Zea Marcano, A. Malkoun, E. Iturritxa, A. Guiral, I. Gutiérrez, G. Schleinzer, M. Stangl, B. Martin Lopez, C. Chaufour, Roll2Rail Deliverable D7.4 – Assessment and validation of source separation methods, April 2017.

[13.] H.W. Jansen, F.G. de Beer, M.G. Dittrich: Validation measurements for level 2 measurements with indirect roughness, TNO report DGT-RPT-020078, STAIRRS deliverable, report STR23TR150702TNO2, July 2002.

[14.] D. Thompson, G. Squicciarini, J. Zhang, I. Lopez Arteaga. E. Zea, M. Dittrich, E. Jansen, K. Arcas, E. Cierco, F.X. Magrans, A. Malkoun, E. Iturritxa, A. Guiral, M. Stangl, G. Schleinzer, B. Martin Lopez, C. Chaufour, J. Wändell: Assessment of measurement-based methods for separating wheel and track contributions to railway rolling noise, Applied Acoustics 140 (2018) 48-62.

[15.] D. Thompson, G. Squicciarini, J. Wändell, I. Lopez Arteaga, E. Zea Marcano, A. Malkoun, E. Iturritxa, A. Guiral, I. Gutiérrez, G. Schleinzer, M. Stangl, B. Martin Lopez, C. Chaufour, Roll2Rail Deliverable D7.1 – Specification of desired capability of separation methods and track quality, February 2016.

Experimental Assessment of Aerodynamic Noise on an Airfoil Surface

David Fujs, Tino Bucak, Davor Franjković

Faculty of Transport and Traffic Sciences, University of Zagreb, Vukelićeva ul. 4, Zagreb, Croatia
david.fujs380@gmail.com

Abstract: *This paper describes the aerodynamic noise measurement method on an airfoil surface in laboratory conditions with non-standard equipment. The experiment and the measurements were performed in closed subsonic wind tunnel at the Aerodynamic Laboratory of Faculty of Transport and Traffic Sciences, University of Zagreb. To complete the measurement set, a charge amplifier and 3D printed airfoil model with six simple piezoelectric sensors were designed. The sensors were used for the airfoil surface noise assessment at different angles of attack and air stream velocities in the tunnel. After relayed through 6-way selector switch, the signal from each sensor under various conditions was suitably conditioned by the charge amplifier and recorded on PC for post-process data analysis. The paper gives the results of FFT analysis and offers discussion about observed correlations between absolute value of angle of attack and low frequency noise levels and spectra, especially prominent while gradually approaching critical angle of attack, the point where stalling of the airfoil occurs.*

Key words: aerodynamic noise, acoustics, piezoelectric transducers, sensors, condition amplifiers, airfoil NACA 2421, experimental measurements, FFT analysis

1. INTRODUCTION

While the role of aircraft noise measurements is becoming more significant in the industry, measuring methods are continuously being created, improved and implemented. Since aircraft is a complex noise source, such progress is needed for better understanding of aeroacoustics and noise control, as for research and development of new technologies and solutions in aircraft industry.

The idea behind the work described in this paper was to target and analyze the aerodynamic noise on an airfoil surface as a specific noise source area generated by an airstream within the closed subsonic wind tunnel. The wind tunnel and other elements of the measurement set which were designed and built for the experiment are described in the following chapter. Since a wind tunnel itself is a noise source as well, particular corrections for measured data were made, which are also described in the paper. The differences in spectral features of an airfoil surface noise between different flight regimes were identified and are shown in the results section. Possible cause and the nature of the noise characteristics are discussed afterwards. Applications and possible improvements are described in the conclusion of the paper. [1]

2. MEASUREMENT SET

The experiment was performed in the Aerodynamic Laboratory of Faculty of Transport and Traffic Sciences, University of Zagreb. The scheme of a closed subsonic wind tunnel used for the experiment is shown in the Fig. 1.

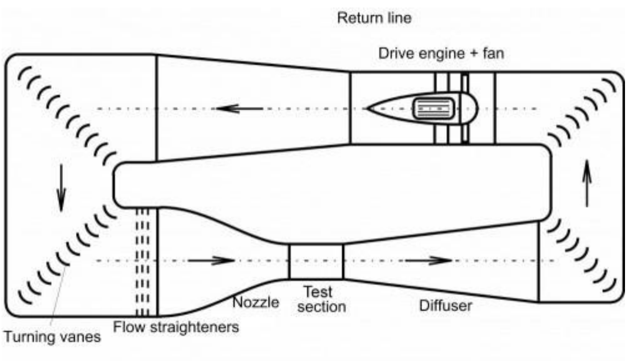

Fig. 1. Closed subsonic wind tunnel AT1 arrangement [2]

The wind tunnel AT1 is driven by an asynchronous motor and a fan. Airspeed is controlled by frequency as an independent variable. Maximum frequency is 50 Hz, at which the engine rotates at 2900 RPM. [3]

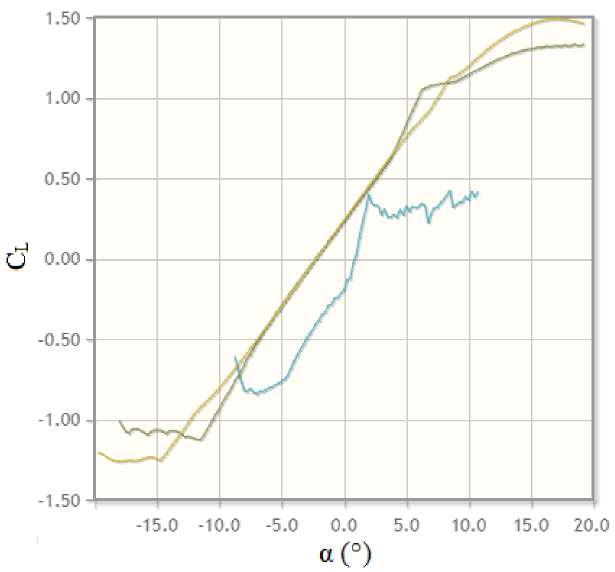

Fig. 2. C_L / α diagram (NACA 2421) [4]

In the tunnel, it is possible to achieve airspeeds of Reynolds numbers around Re = 10^6.

NACA 2421 model was chosen for the experiment. C_L / α diagram for NACA 2421 is shown in the Fig. 2. The diagram in the Fig. 2. represents C_L / α values for three different Reynolds numbers:

- Re = 50 000 (blue)
- Re = 200 000 (green)
- Re = 1 000 000 (brown)

The model was designed to fit the test section of the wind tunnel AT1. 3D printer was used to print the model. The axles and the spacing wheels were connected to the airfoil for mounting purposes. The model is shown in the Fig. 3.

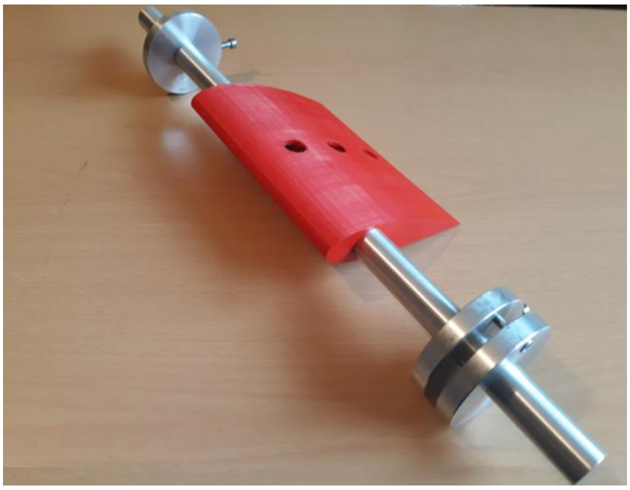

Fig. 3. Airfoil model with mounting elements

To complete the airfoil construction, six piezoelectric sensors were fixed to the model with their respective wires going through the left axis as shown in the Fig. 4.

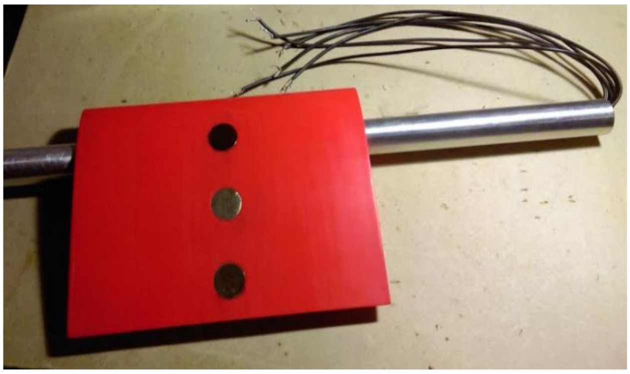

Fig. 4. Piezoelectric sensors on the lower surface of an airfoil

For purposes of conditioning the signal from the sensors, a charge amplifier was built with low noise dual op-amp IC. The amplifier has two different channels, one for airfoil sensors and the other for control (reference) sensor). The amplifier is shown in the Fig. 5. [1]

Fig. 4. Dual-channel charge amplifier

3. MEASUREMENTS

The airfoil was mounted in the test section of the subsonic wind tunnel. Signals from the sensors were relayed through a 6-way selector switch to the charge amplifier and recorded on a PC. Headphones and oscilloscope were used for signal monitoring , before and during each recording. Airspeed was determined by reading the scale on a manometer which was connected to pitot-static tube in the tunnel. Angular scale was written on outer spacing disk of the model. Since airfoil model was designed so that it can rotate around its lateral axis, it was possible to set specific angle of attack for each measurement. The whole measurement set is shown in the Fig. 5.

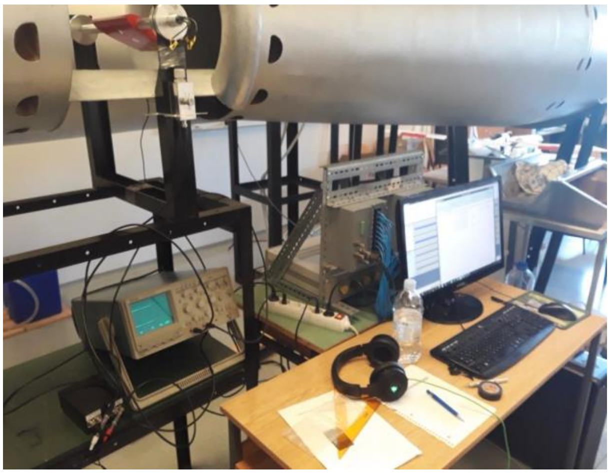

Fig. 5. Measurement set during experimental recording in the wind tunnel

The signal from each sensor was recorded together with a signal from the control sensor, the latter being mounted in the lower part of the test section. By using dual channel amplifier, signals from airfoil and control sensors were conditioned separately and recorded as a "stereo" signal on a computer. Control sensor was used as a reference in analysis, since the wind tunnel itself generates significant noise. Also, control sensor was near the model and it was influenced by the angular position of the airfoil. For those reasons, reference data of the control sensor was determined by generating average noise level values from each individual airfoil sensor recording at airspeed that was measured and at neutral angle of attack. By using this method, influence of the airstream caused by airfoil position on a control sensor and its recordings was minimized.
Before post-process, recordings were edited. The right channel which contained the original control sensor signal was switched by average signal generated in a manner described above.

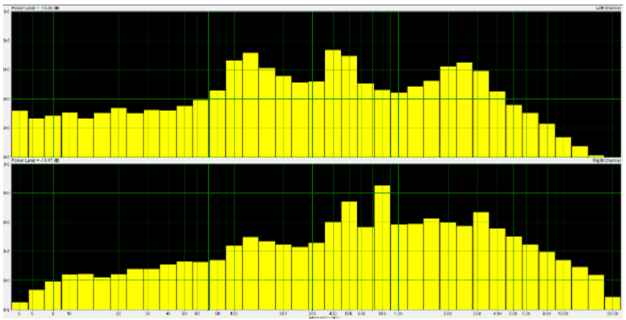

Fig. 6. Edited signal data split in two channels by FFT analysis software

Noise data from recordings was analyzed in 1/3 octave spectra during FFT post-processing. and organized according to different angles of attack and airspeeds. The transfer function was used for calculating relative sound pressure level and spectra, i.e., the difference between the left (airfoil sensor signals) and right (average values of the control sensor signal) channel. One example of data representation in FFT software is shown in the Fig. 6. The upper graph shows airfoil sensor signal, while lower shows average control sensor signal. The values are presented as relative sound pressure values in 1/3 octave.
The process was then repeated for each case (individual airfoil sensor at specific angle of attack and airspeed). [1]

4. RESULTS

Individual measurements were grouped into graphical representation of data. The results show significant correlations.
In first example, it was possible to group individual sensors data at a single airspeed (60 knots) and to show correlation between relative sound pressure level for each sensor and the angle of attack. The results of specific example are shown in the Fig. 7.

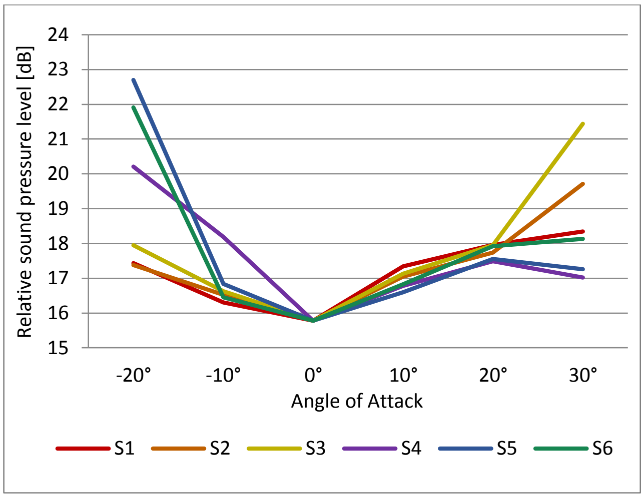

Fig. 7. The impact of the angle of attack on the noise level on an airfoil surface at 60 knots

Sensors on the upper surface (S1, S2, S3) and lower surface (S4, S5, S6) are numbered according to their position on the airfoil, from leading edge to trailing edge of the airfoil. Thus, S1 represents the sensor on the upper surface closest to the leading edge, while S6 represents the sensor on the lower surface closest to the trailing edge. The graph in the Fig 7. shows gradual increase in relative sound pressure level at the airfoil surface as the angle of attack increases or decreases beyond neutral position. Also, at negative angles the increase in sound pressure level is more significant at lower sensors, while at positive angle the increase is more significant at upper sensors. Data suggests that sensors which were on the surface, where separation of the airstream would occur at more significant angles of attack, detected higher sound pressure level than those which were on the other surface of the airfoil and which are exposed to incoming airflow from the tunnel. This pattern can be seen at both positive and negative angles of attack. Furthermore, noise buildups are most prominent between -20 and -10 degrees for lower surface and between 20 and 30 degrees for upper surface. If compared with Fig. 2, this coincides with stalling angles of the airfoil when the airstream deflection occurs and the turbulent airflow is present in the vicinity of the sensors. Overall, the noise measurements show noticeable correlations between data from sensors and aerodynamic features of the airfoil. An additional method of representing airfoil surface noise is by showing frequency spectra of measured data between different angles of attack at constant airspeed for each sensor. By plotting relative sound pressure level over frequency spectra it is possible to examine airfoil surface noise in greater detail.

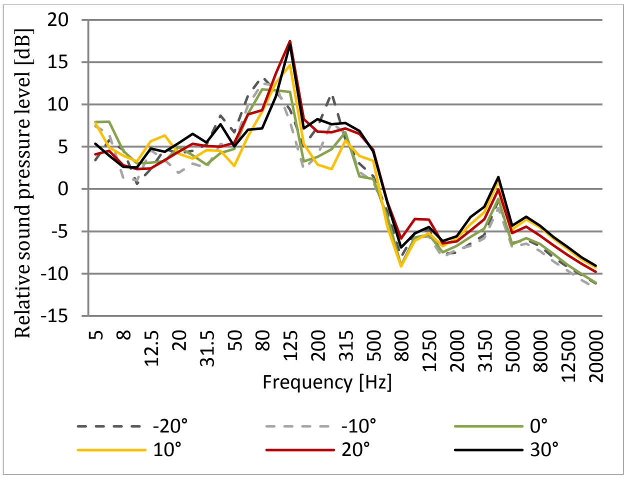

Fig. 8. Relative sound pressure level in 1/3 octave spectrum measured at sensor S1 at 40 knots

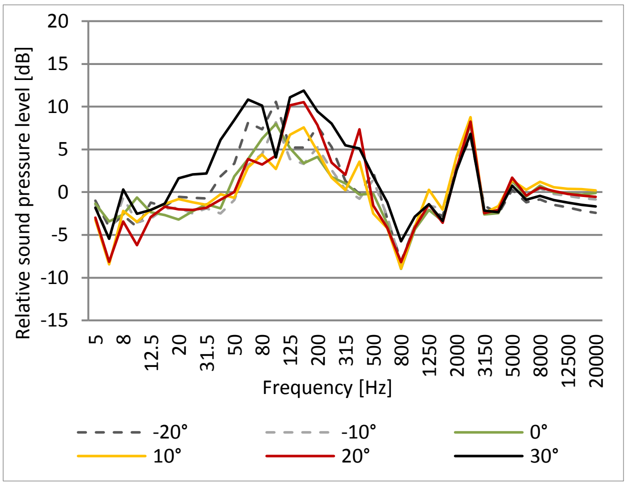

Fig. 9. Relative sound pressure level in 1/3 octave spectrum measured at sensor S2 at 40 knots

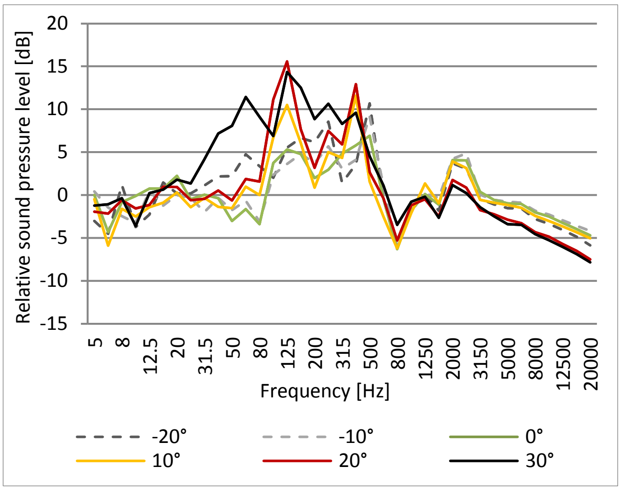

Fig. 10. Relative sound pressure level in 1/3 octave spectrum measured at sensor S3 at 40 knots

Measured relative sound pressure level in 1/3 octave spectrum for different angles of attack at the airstream velocity of 40 knots is shown in the figures 8, 9 and 10 for sensors S1, S2 and S3, respectively. By comparing data from different sensors, it is possible to detect changes in the airflow behavior on the airfoil surface in respect to sensor positions and various angles of attack. On the upper surface, the sensor S1 (Fig. 8.) measured small differences in relative sound pressure level between various angles of attack. On the other hand, sensors S2 and S3 show significant increase in low-frequency noise levels at greater angles of attack. As mentioned before, this behavior could be explained by taking aerodynamic properties of the airfoil into account. Sensor S1 is closest to the leading edge and it is positioned in the airfoil surface area where separation of the airstream, in terms of increasing angle of attack, occurs later compared to sensors S2 and S3, which are positioned more downstream.

Since measurement set used in the experiment was manually built and lacks necessary calibration, it is obviously subject to possible errors and imperfections. Some of them can be seen in the Figures 8. to 10. as significant peaks of increased SPL value from AC mains hum harmonics and imperfect grounding. [1]

5. CONCLUSION

The results of the experiment offer an insight into airstream behavior on the airfoil surface and the ability to detect its nature by noise measurements. The method shows the possibility of assessing airfoil surface noise in terms of aerodynamic behavior of the airfoil at different angles of attack and airspeeds. Since a single airfoil was used in the assessment, the data is limited, but it also offers a possibility to expand measurements to other airfoil models and to introduce cross-analysis of the data between different airfoils to the measurement process. Such comparison between various airfoils could confirm the applicability of the method in different areas even further.

This method can be used for academic purposes at universities, as a demonstration of aerodynamic and aeroacoustic features of an airfoil in an airstream. Also, the idea of measuring airfoil surface noise in terms of aerodynamic behavior of an airfoil could be implemented in the development of the stall detection system, which could be used whether in laboratories for more thorough research, or even be installed on an aircraft for inflight tests.

6. REFERENCES

[1.] D. Fujs: **Experimental Assessment of Aerodynamic Noise Characteristics on an Airfoil Model** (Master thesis), *Faculty of Transport and Traffic Sciences, University of Zagreb*, *2018 (in Croatian)*

[2.] D. Franjković, A. Domitrović**: Podzvučni aerodinamički tunel za školske namjene (Subsonic Wind-tunnel for Educational Purposes)**, *Suvremeni promet, No. 3-4, Vol. 21, Zagreb, 2001 (pp 223-230, in Croatian)*

[3.] K. Krajček Nikolić: **Katalog laboratorijske opreme 2014. (Laboratory Equipment Catalogue 2014),** *Faculty of Transport and Traffic Sciences, University of Zagreb; 2014*

[4.] http://www.airfoiltools.com *(accessed March/2018)*

EXTERNAL NOISE ANALYSIS OF SUPERSONIC FIGHTER AIRCRAFT MIG-21 UMD

Dominik Jerinić[1], Marko Maradin[1], Tino Bucak[2]

[1]Ministry of Defense, Croatian Air Force, King Petar Krešimir 4 Square, 10000 Zagreb, Republic of Croatia (dominik.jerinic01@gmail.com)
[2]University of Zagreb, Faculty of Transport and Traffic Sciences, Vukelićeva 4, 10000 Zagreb, Republic of Croatia

Abstract: *This paper contains overview and analysis of supersonic fighter's MiG-21 UMD external noise parameters measured during typical aircraft engine power settings in static i.e. on-ground conditions: idle power, maximum continuous power, 1st afterburner stage and 2nd afterburner stage. The research aims to evaluate the noise impact on ground staff while handling supersonic fighter on the tarmac. Assessed data show noise levels well above recommended under all aircraft engine regimes.*

Key words: aircraft noise, supersonic fighter, Mig-21

1. INTRODUCTION

During aircraft ground operations, airmen outside of an aircraft are subjected to high levels of vibration, exhaust gases and aircraft noise. The latter two are also the main environmental adverse parameters of air traffic [1]. In this paper, noise impact on airmen is presented in relation to different engine regimes which are used during ground and air operations. Different engine regimes produce different noise levels that affect human nervous system and concentration [2].

2. AIRCRAFT AS A SOURCE OF NOISE

During flight operations, several noise sources contribute in overall aircraft noise image, while being strongly dependent on flight regime [1]. The engines (i.e. powerplant) prevail as the dominant noise sources and they are primarily taken into account in this study. In general, the more power the engine(s) produces, the higher the noise level is. Consequently, the minimum noise level is produced during minimum power setting, which is used for engine warm-up and/or certain ground checks, while the highest noise level is achieved in maximum engine power setting which can be even higher than 100% of nominal one. This power setting is used during take-off and/or some tactical maneuvering. Fig. 1 shows noise level footprint for two different frequencies during certain aircraft approach.

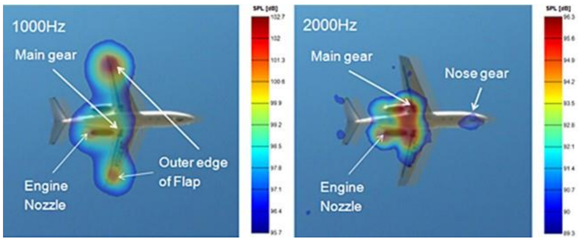

Fig. 1. Noise spreading into environment [3]

During the years, fuselage and engine constructors were trying to reduce aircraft noise impact on civil population and environment. Looking backward for 50-60 years, noise levels are reduced by approx. 25 dB or 80% [3]. The noise can be commonly reduced in three ways: at the source, along the propagation path(s) or implementing passive protections at the observer position. Fig. 2. shows the progress in noise reduction during the last six decades.

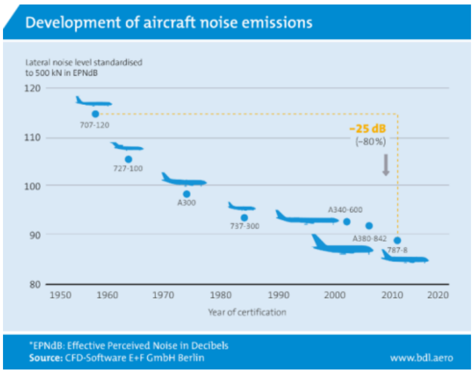

Fig. 2. Noise levels reduction [4]

3. MEASUREMENT OF EXTERNAL NOISE OF SUPERSONIC FIGHTER MIG-21 UMD

3.1. Characteristics of MiG-21 aircraft

MiG-21 UMD is a supersonic fighter, single engine two-seater made by Russian engineers Mikoyan and Gurevich during 1960s. It's made of aluminum/magnesium alloy with steel reinforcements and fiberglass. Delta wings and conventional tail allows supersonic flight. MiG-21 UM was upgraded to MiG-21 UMD in 2003. for Croatian Air Force and it's in operational use until today. Table 1 shows some tactical-operational characteristics of MiG-21 UMD aircraft.

Table 1. Technical-operational characteristics of MiG-21 UMD aircraft

Description	Value
Seat number	2
Engine	Tumansky R-13-300
Maximum Thrust	41,55 (without afterburner) 64,73 (with afterburner)
Length (with pitot-tube)	15,76 m
Wing span	7,15 m
Height	4,10 m
Wing area	23 m^2
Basic empty mass	5730 kg (with crew)
Take-off mass (with two R-3S)	8000 kg
Maximum take-off mass	8500-9500 kg
Maximum speed at mean sea level	1300 km/h (1,06 Ma)
Maximum speed at 12000 m	2150 km/h (2,02 Ma)
Maximum rate of climb	6400 m/min
Maximum celling	15250 m (theoretically 18000 m)
Maximum range	1100 km
Maximum fuel capacity with additional tanks	3090 litres

Croatian Air Force MiG-21 UMD aircraft is presented on Fig. 3.

Fig. 3. Croatian Air Force MiG-21 UMD [5]

3.2. Measurement method and equipment

External noise measurement of MiG-21 UMD was completed in static (on-ground) conditions with parking brake engaged, using Class 1 Sound Analyzer. The measurement of polar characteristic was performed around the airplane in 45° step at minimum engine power (in further text: IDLE) and at distance of approx. 3 m (Fig. 4). The noise level at 180° position was not measured due to safety reasons. Second measurement was executed at 270° position while following engine regimes: IDLE, maximum continuous power (in further text: MCP), 1st stage afterburner (in further text: 1A) and 2nd stage afterburner (in further text: 2A) at the same distance.

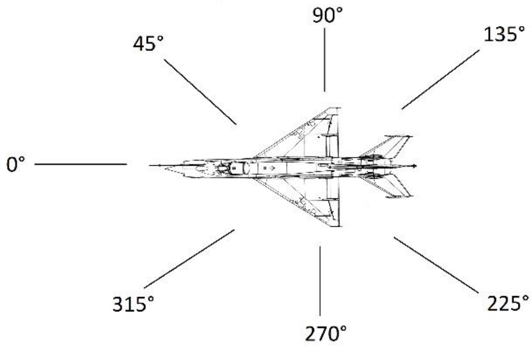

Fig. 4. Positions of external noise measurement

3.3. The results and analysis

Following figures and tables shows noise values LA_{eq} expressed in dBA. Table 2 represents noise values of first measurement according to positions previously mentioned.

Position	LAeq (dBA)
0°	111,7
045°	107,2
090°	101,6
135°	99,7
180°	/
225°	100,3
270°	97,3
315°	101,7

Table 2. Measurement results of MiG-21 UMD external noise at different positions

Results from Table 2 are graphically shown in Fig. 5.

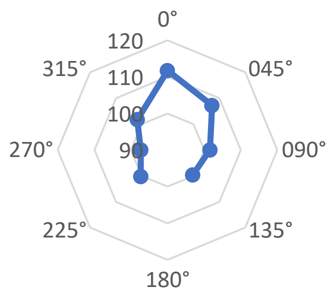

Fig. 5. Polar characteristic of MiG-21 UMD external noise

The highest noise level of 111,7 dBA was measured at position 0°, at which the intake noise generally prevails. The lowest noise level is achieved at 270° position. It is expected that at 180° position the highest noise levels occur due to high temperature and speed of exhaust jet stream, but, again, mandatory rear-end safety clearance hindered the measurement at that specific point. As mentioned before, second measurement was performed at 270° position for different engine power setting regimes. These results are presented in Table 2 and Fig. 6.

Table 2. Measurement results of MiG-21 external noise level at position 270°

Engine regimes	LAeq (dBA)
IDLE	101,1
MCP	116,8
1A	121,6
2A	119,1

The minimum noise level of 101,1 dBA was, as expected, measured during IDLE power setting. The highest noise level of 121,6 dBA was measured during engine regime 1A with maximum afterburner.

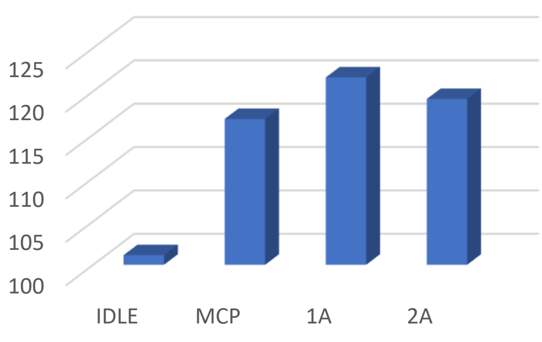

Fig. 6. MiG-21 UMD external noise level in different engine regimes

4. CONCLUSION

During the past six decades, aircraft noise in general was gradually reduced by 80% or 25 dBA. In aircraft operations, the highest noise impact on pilots and ground technicians is generated by aircraft engine. Engine regime or power setting strongly defines the noise characteristics. Exposure to high noise levels can lead to hearing problem in airmen, both pilots and aircraft technicians. Maximum recommended level is set to 90 dBA for acceptable acoustical comfort, which is also highly time-dependent [1]. The minimum recorded value of noise level during MiG-21 UMD engine running was 97,3 dBA which already exceeds the recommendation. The maximum measured noise level was 121,6 dBA during maximum engine power 1A regime. This value is more than 35% higher than recommended and above threshold of pain which rises concerns and should be taken seriously. However, for more detailed results about noise impact on environment and civil population, i.e. ground footprint, the measurements should be done during air operations over the airport using specific procedures for take-off and landing, which is planned in near future.

REFERENCES

[1] D. Jerinić, M. Maradin, T. Bucak: ***Interior noise analysis of supersonic fighter aircraft MiG-21 UMD***, *7th International Ergonomics Conference – ERGONOMICS 2018,* Zadar, 2018

[2] J. Ivošević, T. Bucak, P. Andraši: ***Effects of interior noise on pilot performance***, *Applied Acoustics,* Vol 139, 2018

[3] K. Yamamoto, Y. Yokokawa: ***Development of technology for investigating noise sources on passenger aircraft***, *JAXA,* Tokyo, 2011

[4] Development of noise level (image), *Available from:* https://www.google.hr/imgres?imgurl=http%3A%2F%2Fwww.bdl.aero%2Fmedia%2Ffiler_public%2F0f%2F63%2F0f63c957-068b-44c2-8215-51ace1830361%2Fdevelopment-of-aircraft-noise-emissions.png&imgrefurl=http%3A%2F%2Fwww.bdl.aero%2Fen%2Fbdl-reports-en%2Faircraft-noise-report%2F&docid=KnA12o6MV7XHkM&tbnid=VZ-tKZemFhp4CM%3A&vet=10ahUKEwi_h9alnPzSAhVE0xQKHbJXCPMQMwgiKAkwCQ..i&w=3000&h=2340&bih=770&biw=1600&q=aircraft%20noise&ved=0ahUKEwi_h9alnPzSAhVE0xQKHbJXCPMQMwgiKAkwCQ&iact=mrc&uact=8#h=2340&imgrc=VZ-tKZemFhp4CM:&vet=10ahUKEwi_h9alnPzSAhVE0xQKHbJXCPMQMwgiKAkwCQ..i&w=3000 *Accessed: 2017-10-01*

[5] MiG-21 UMD aircraft of the Croatian Air Force, *Available from:* https://upload.wikimedia.org/wikipedia/commons/thumb/3/35/Croatian_Air_Force_Mikoyan-Gurevich_MiG-21UMD_Lofting-1.jpg/1200px-Croatian_Air_Force_Mikoyan-Gurevich_MiG-21UMD_Lofting-1.jpg *Accessed: 2017-11-09*

8th Congress of the Alps Adria Acoustics Association
Zagreb, Croatia
20 – 21 September 2018

ACOUSTICS OF CONTEMPORARY CHURCHES IN CROATIA

Kristian Jambrošić[1], Marko Horvat[2]

University of Zagreb, Faculty or Electrical Engineering and Computing, Unska 3, Zagreb, Croatia
([1]kristian.jambrosic@fer.hr, [2]marko.horvat@fer.hr)

Abstract: *There is a significant time gap, spanning from the end of World War 2 to the early 1990s, during which almost no houses of worship, including catholic churches, were built in Croatia. Building technology and building materials have changed drastically during this period. As a result, modern-day churches have significantly different acoustical characteristics compared to churches of similar size built a century ago or earlier. Moreover, the architects of today deliberately deviate from tradition, when it comes to visual appearance of both the interior and the exterior of these buildings. The choice of new shapes and materials in the design process is reflected in acoustical properties of these spaces as well. Unfortunately, the acoustics of modern houses of worship often proves to be inferior to the one found in traditionally designed ones. The paper shows the comparison of basic acoustical parameters measured in 28 modern-day catholic churches in Croatia. Case studies made in order to achieve acceptable intelligibility in the interior of these churches through suitable acoustic treatment are listed and described as well. In some cases, a sound reinforcement system was designed to further improve the intelligibility of the spoken word. The collected data is compared to the one obtained for older churches that were built at least 100 years ago.*

Key words: worship space acoustics, reverberation time, speech intelligibility, sound reinforcement systems

1. INTRODUCTION

Acoustics of worship spaces has been a popular topic of research among acousticians ever since acoustics had been recognized as a scientific field. There are at least two reasons for that. First, worship spaces in general are usually large or very large in terms of their floor plan surface area and their volume. As such, they can be considered as acoustically difficult spaces to design because large volumes inherently lead to long reverberation and consequent problems with speech intelligibility. Second, all religions put a strong emphasis on the spoken word in religious celebrations, making it an essential part of the liturgical process. Therefore, adequate intelligibility of speech is crucial in worship spaces. Yet, large spaces often exhibit quite the opposite acoustical behaviour [1-2].

Christianity has been the dominant religion throughout Croatian history, Catholicism in particular. Churches have been built since the start of the known Croatian history in this region of Europe in the 7th century A.D. Nowadays, the range of churches that can be found in Croatia spans from the earliest period to contemporary buildings. However, not all of them are in mint condition. Most of them are used on a daily basis for liturgy and other ceremonies. Good acoustic conditions with adequate speech intelligibility is crucial in these spaces [3-6].

The motivation for writing this paper is the extensive work done by the authors in the area of church acoustics, particularly the contemporary churches. It was observed that the designers of contemporary churches tend to ignore the demands put on the acoustics of such spaces, resulting in acoustical conditions that are worse than the ones found in old churches. The paper shows general differences in acoustic behaviour between old, modern and contemporary churches. Acoustic measurements either done by the authors or by other researchers [7] are used for comparison of basic acoustic parameters of churches belonging to one of the three categories, also taking into account the volume of these spaces.

There are many acoustic parameters connected to the field of room acoustics. Many of them are used for evaluation of the acoustic quality of closed spaces. There is a particularly huge number of parameters for evaluating the acoustics of concert halls, with new parameters being proposed by researchers in this field.

Nevertheless, the first impression about the acoustics of a space is its natural reverberation and the matching objective parameters are the reverberation time (T_{30}), and similarly the early decay time (EDT). For this reason, reverberation time is still the first and most important room acoustic parameter that is used for describing the acoustics of rooms and spaces, and churches are no exception to this rule.

For all said reasons, this paper presents the reverberation time of churches as the main parameter for the evaluation of their acoustic quality. Longer reverberation times in churches lead to lower speech intelligibility. Therefore, reverberation time can be used as a good measure to estimate the overall acoustic comfort of the churches. Since there is always a central, large volume with more or less no obstacles hanging from the ceiling, the overall acoustic comfort is thus mostly influenced by the overall reverberation time, especially for people sitting or standing in the central part of a church. Sound reinforcement systems installed in churches can help improve the speech intelligibility. Naturally, favourable natural acoustic conditions in a closed space put less demand on the loudspeakers used in these systems.

2. THE DESCRIPTION OF INVESTIGATED CHURCHES

Although the main goal of the paper is to compare contemporary churches build after World War 2 (mostly in the last 30 years) with the older ones, the investigated churches were grouped in three categories. The term “old churches” refers to the ones built up to the year 1900; “modern churches” are the ones built in the first half of the 20th century; “contemporary churches” are those built in the last three decades.

2.1. Old churches - from the 13th century to 1900

Figures 1 – 10 show 10 churches (both their exterior and interior) whose year of completion falls into the stated period. They are listed according to their volume, from smaller to larger. Each caption indicates the name of the church, its location, the year of completion, its ID number according to Table 1, and its inner volume.
These churches have been included due to availability of the room acoustics data, although they are perhaps not the most representative ones for the stated period. Some of these churches are famous and well known in Croatia, such as the cathedral in Zadar (#10), whereas others are only known locally. What is important is that all these churches are still used in liturgy, thus their acoustics is very important and influencing their functionality.

Fig.1. Saint George, Belec (1350), #1, 390 m^3.

Fig.2. Saint Martin, Belec Martinščina (1300), #2, 450 m^3.

Fig.3. Mother of God of the Hill, Lobor (1680), #3, 1150 m^3.

Fig.4. Saint Mary of Snow, Belec (1743), #4, 1440 m^3.

Fig.5. Saint Anna, Lobor (1830), #5, 2450 m^3.

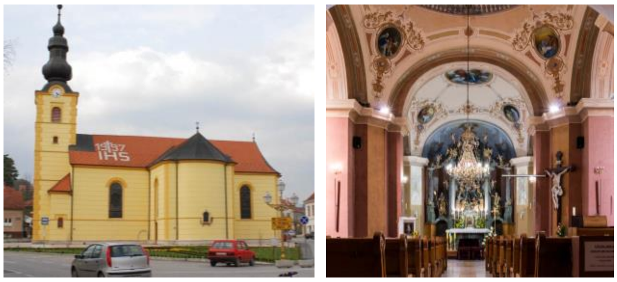

Fig.6. Assumption of the Blessed Virgin Mary, Zlatar (1762), #6, 2900 m^3.

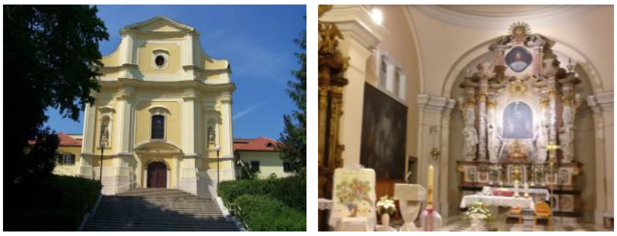

Fig.7. Saint Francis of Ksaver, Zagreb (1752), #7, 3500 m^3.

Fig.8. Saint Catherine, Zagreb (1632), #8, 5000 m^3.

Fig.9. Saint Peter, Zagreb (1770), #9, 6200 m^3.

Fig.10. Saint Anastasia Cathedral, Zadar (1285), #10, 11500 m^3.

2.2. Modern churches - from 1900 to 1940

The group of modern churches is represented by five buildings that were built in the first 4 decades of the 20th century, and are shown in Figure 11 - 15. They stand out regarding their year of completion and were grouped in a separate group, because the newest church from the group of old ones was completed in 1830, and the oldest church from the contemporary group was finished in 1985. All the churches in this group are somewhat larger than the old churches, as indicated in the captions of the figures and in Table 1.

Fig.11. Our Lady of Health, Split (1937), #11, 6200 m^3.

Fig.12. Saint Mary Helper, Zagreb (1940), #12, 7000 m^3.

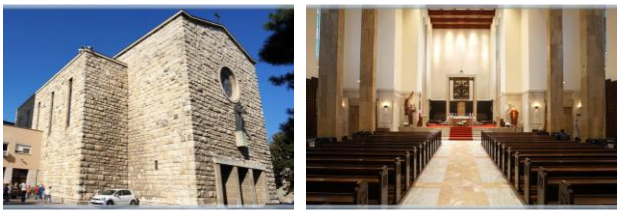

Fig.13. Saint Antoine, Zagreb (1934), #13, 10100 m^3.

Fig.14. Saint Blaise, Zagreb (1915), #14, 12785 m^3.

Fig.15. Basilica of the Sacred Heart of Jesus, Zagreb (1902), #15, 13000 m^3.

2.3. Contemporary churches - from 1985 onward

The group of contemporary churches includes 13 buildings built from 1985 up to date, shown in Figures 16 – 28. There is a rather obvious gap of 45 years between 1940 and 1985, during which almost no churches were built in Croatia due to political reasons.
The churches in this group present an opportunity to look into possible differences in the acoustics of the recent era compared to older buildings, and to determine whether these differences are significant or not.

Fig.16. Blessed Virgin Mary Nativity church, Zagreb (1990), #16, 2600 m^3.

Fig.17. Saint Andrew Apostle, Split (2012), #17, 3020 m^3.

Fig.18. Rise of the Holly Cross church, Lukarišće (2012), #18, 3600 m^3.

Fig.19. Our Lady's church, Bibinje (1985), #19, 3940 m^3.

Fig.20. Holy Redeemer church, Split (2011), #20, 5200 m^3.

Fig.21. Virgin Mary Mother of God, Zagreb (2004), #21, 5840 m^3.

Fig.22. Croatian Martyrs Church, Udbina (2011), #22, 6035 m^3.

Fig.23. Blessed Augustin Kažotić, Zagreb (2011), #23, 7000 m^3.

Fig.24. Immaculate Heart of Mary, Zagreb (1995), #24, 7500 m^3.

Fig.25. Christ the Good Shepherd, Mostar (2015), #25, 7700 m^3.

Fig.26. Sanctuary of the Holy Mother of Freedom, Zagreb (2000), #26, 9400 m^3.

Fig.27. Our Lady of the Big Croatian Baptism Pledge, Knin (2014), #27, 10100 m^3.

Fig.28. Basilica of Our Lady of the Island, Solin (2018), #28, 13680 m^3.

3. ACOUSTIC MEASUREMENTS AND RESULTS

As stated before, the only acoustic parameter available for all 28 buildings is the average reverberation time in octave bands. An overview of its values is given in Table 1. Beside the average reverberation time (average of measured values in octave bands 500 Hz and 1000 Hz), the bass ratio (BR) is shown as well.

3.1. Frequency dependent reverberation time

It might be interesting to see what the frequency dependent reverberation time looks like for all churches, especially within the three groups (old, modern and contemporary). For this reason, the reverberation times for all churches are shown in Figures 29 - 32. All reverberation time values are normalized by dividing them with the average values (taken from octave bands at 500 and 1000 Hz) shown in Table 1.

#	Name of the church	Location	Built in year	Basic building style	V (m^3)	Before renovation		After renovation	
						T_{30}(s)	BR	T_{30} (s)	BR
1	Saint George	Belec	1350	Romanesque / Gothic	390	1,09	1,04		
2	Saint Martin	Martinščina	1300	Gothic	450	1,38	1,38		
3	Mother of God of the Hill	Lobor	1680	Gothic / Baroque	1150	2,58	1,18		
4	Saint Mary of Snow	Belec	1743	Baroque	1440	1,70	1,02		
5	Saint Anna	Lobor	1830	Baroque / Classicism	2450	3,11	1,31		
6	Assumpt. of the Blessed Virgin Mary	Zlatar	1762	Baroque	2900	2,92	1,15		
7	Saint Francis of Ksaver	Zagreb	1752	Baroque	3500	3,68	1,14		
8	Saint Catherine	Zagreb	1632	Baroque	5000	3,53	0,93		
9	Saint Peter	Zagreb	1770	Baroque	6200	4,56	0,95		
10	Saint Anastasia Cathedral	Zadar	1285	Romanesque	11500	2,80	0,81		
11	Our Lady of Health	Split	1937	Modern	6200	3,47	1,05		
12	Saint Mary Helper	Zagreb	1940	Modern	7000	4,50	1,01		
13	Saint Antoine	Zagreb	1934	Modern	10100	6,16	0,86		
14	Saint Blaise	Zagreb	1915	Modern	12785	7,98	1,02		
15	Basilica of the Sacred Heart of Jesus	Zagreb	1902	Neo Baroque	13000	5,88	1,01		
16	Blessed Virgin Mary Nativity church	Zagreb	1990	Contemporary	2600	3,66	0,66	1,38	1,01
17	Saint Andrew Apostle	Split	2012	Contemporary	3020	5,58	0,96	2,53	1,00

18	Rise of the Holy Cross church	Lukarišće	2012	Contemporary	3600	6,55	1,35	6,55	1,35
19	Our Lady's church	Bibinje	1985	Contemporary	3940	5,14	0,87	2,43	1,14
20	Holy Redeemer church	Split	2011	Contemporary	5200	5,28	1,05	2,11	1,33
21	Virgin Mary Mother of God	Zagreb	2004	Contemporary	5840	5,65	1,08	1,78	1,08
22	Croatian Martyrs Church	Udbina	2011	Contemporary	6035	8,80	0,90	3,99	1,18
23	Blessed Augustin Kažotić	Zagreb	2011	Contemporary	7000	13,33	0,82	5,55	1,05
24	Immaculate Heart of Mary	Zagreb	1995	Contemporary	7500	3,99	1,12	3,99	1,12
25	Christ the Good Shepherd	Mostar	2015	Contemporary	7700	11,70	1,59	2,25	1,29
26	San. of the Holy Mother of Freedom	Zagreb	2000	Contemporary	9400	2,78	1,09	2,78	1,09
27	Our Lady of the Big Croatian Baptism Pledge	Knin	2014	Contemporary	10100	13,30	1,29	3,30	1,06
28	Basilica of Our Lady of the Island	Solin	2018	Contemporary	13680	8,13	1,12	3,48	1,33

Table 1. The overview of the investigated churches. For contemporary churches, the acoustical situation before and after renovation is shown (in some cases only simulation, and in other acoustic measurements). Single-number reverberation time is given as an average in octave bands of 500 Hz and 1000 Hz.

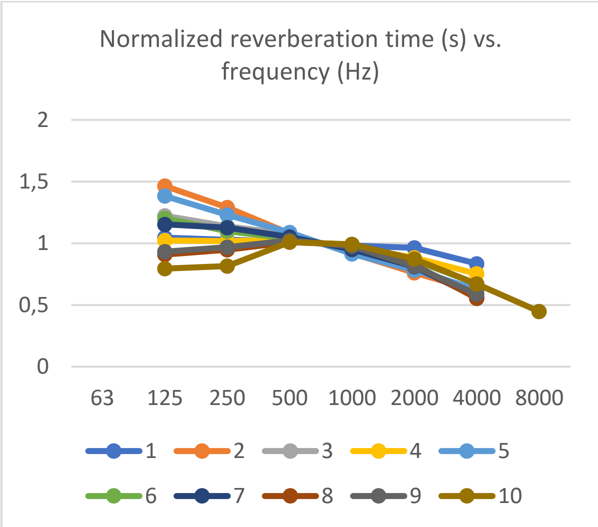

Fig.29. Normalized reverberation time for old churches.

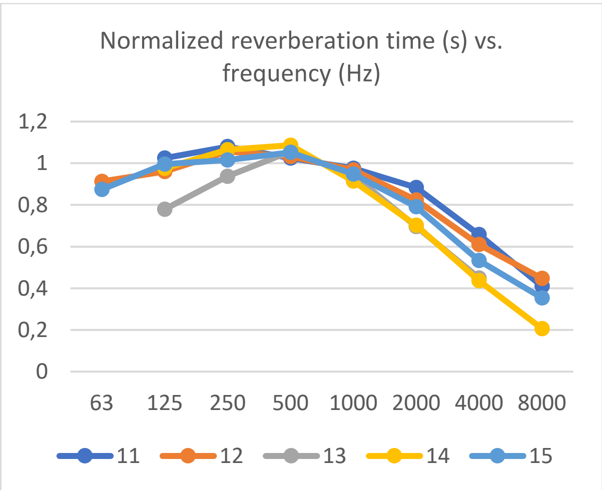

Fig.30. Normalized reverberation time for modern churches.

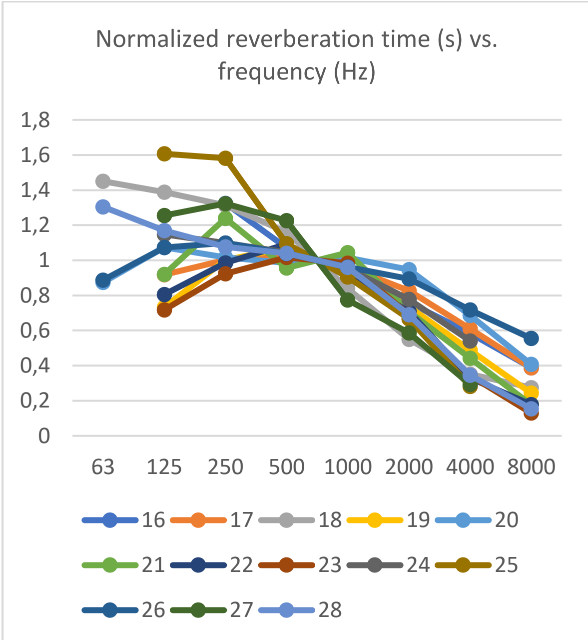

Fig.31. Normalized reverberation time for contemporary churches before renovation.

The normalized frequency-dependent reverberation times show some interesting findings. First, old churches have a rather great variability in the low frequency region (below 500 Hz), but at medium and high frequencies they behave very similar. This is no big surprise since these churches are quite different in age, and the greatest difference is in the roof type - some have wooden roofs (thus having a substantially lower reverberation time), and some have stone or brick roofs/ceilings.
Modern churches, on the other hand, were built inside 30-40 years, and they are very much alike regarding the used building materials and interior outfit. Thus, the

normalized frequency-dependent reverberation times are shaped almost identically for all five measured churches.
Finally, the normalized frequency-dependent reverberation times obtained for contemporary churches show a large variability, especially at low frequencies. The reason is for that is clear - the choice of materials used for interior design nowadays is large. In this group, we can find churches with largest measured bass ratios, as is clearly indicated in Figure 31. After acoustic renovation of some of these churches, the normalized frequency-dependent reverberation times become more uniform, showing less variability in the low frequency region, as shown in Figure 32. This is an obvious goal of acoustic renovation in contemporary churches.

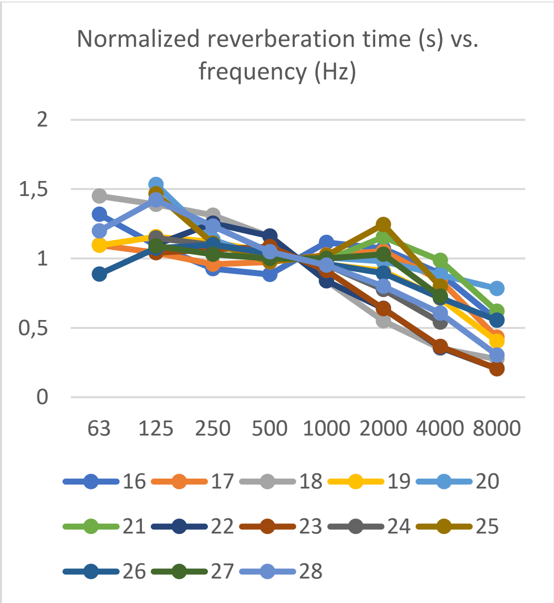

Fig.32. Normalized reverberation time for contemporary churches after renovation.

3.2. Average reverberation time vs. volume

Another possibility of comparing churches from different eras is by comparing their average reverberation time shown in Table 1, depending on their inner volume. These graphs are shown in Figure 33. The red line presents the group of old churches, with the corresponding linear regression line in the same colour. The green lines represent the group of modern churches in the same fashion. The blue lines represent all contemporary churches before acoustic renovation, regardless of whether they need it or not. The yellow lines present only the contemporary churches that are in need of some kind of acoustic treatment. Finally, the purple line shows contemporary churches after acoustic renovation, including the ones in which the acoustics issues were addressed properly in the design stage, thus having no need for interventions of any kind.

Some facts are obvious from Figure 33. Reverberation time of old churches tends to have a rather strong linear dependency on the volume. The exception is the largest church (Saint Anastasia Cathedral), in which the reverberation time is disproportionately small with regard to its considerable volume. The investigated modern churches are mostly of larger size, and represent a continuation of the trend already ascertained for old churches. The green curve shows almost a perfect continuation of the red curve. The respective regression lines do not match, but if the largest old church was removed as an outlier, both regression lines would have almost the same slope and are almost a perfect extension of each other. When old and modern churches are investigated together, the resulting data show a very strong linear dependency of the reverberation time on the inner volume. The resulting linear regression line has a high goodness of fit with the associated R^2 = 0.90. This suggests that the acoustic situation in old and modern churches reflects the consistency of the construction techniques used in building and interior finishing of these buildings.
The available data suggests that the acoustic situation in contemporary churches is quite different. Most of them were built without any consideration about the acoustic comfort or speech intelligibility inside. This is clearly indicated with the blue curve in Figure 33, which shows a very large variability. However, it would be fair to say that some of the contemporary churches were designed and built having in mind the acoustics of the building, and, therefore, in these cases there is no need for interventions of any kind. Thus, for the sake of fairness, churches with recognized acoustical problems that needed renovation are grouped and the resulting data is shown with the yellow curve in Figure 33. It is clear that modern construction and interior design of churches, that utilizes primarily hard and reflective materials such as smooth concrete or marble, inevitably leads to problems with acoustics inside such buildings. These problems seem to be much more pronounced than in old and even modern churches of similar size. The data on the after-renovation state in these churches was gathered either only from simulation or by measurements after the renovation was done. The acoustical situation after renovation, shown with the violet curve shows the trend in contemporary acoustic design. In essence, the goal is to attain acoustical conditions in a church that will be better for the intelligibility of the spoken word than the ones found in old churches. On the other hand, controlled reverberation is highly desired, but not at the expense of solemnity that is expected in houses of worship. Therefore, the goal of contemporary acoustic design, as the authors see it, is to compromise between improving the intelligibility of the spoken word as much as possible, while keeping the reverberation time long enough to maintain the overall acoustic impression expected in a church. The obvious outliers in the purple line show the cases where acoustic

renovation could not be applied in the extent it should have been, for technical or financial reasons. However, the data clearly show the intentions and goals of contemporary acoustic design, as viewed and implemented by the authors.

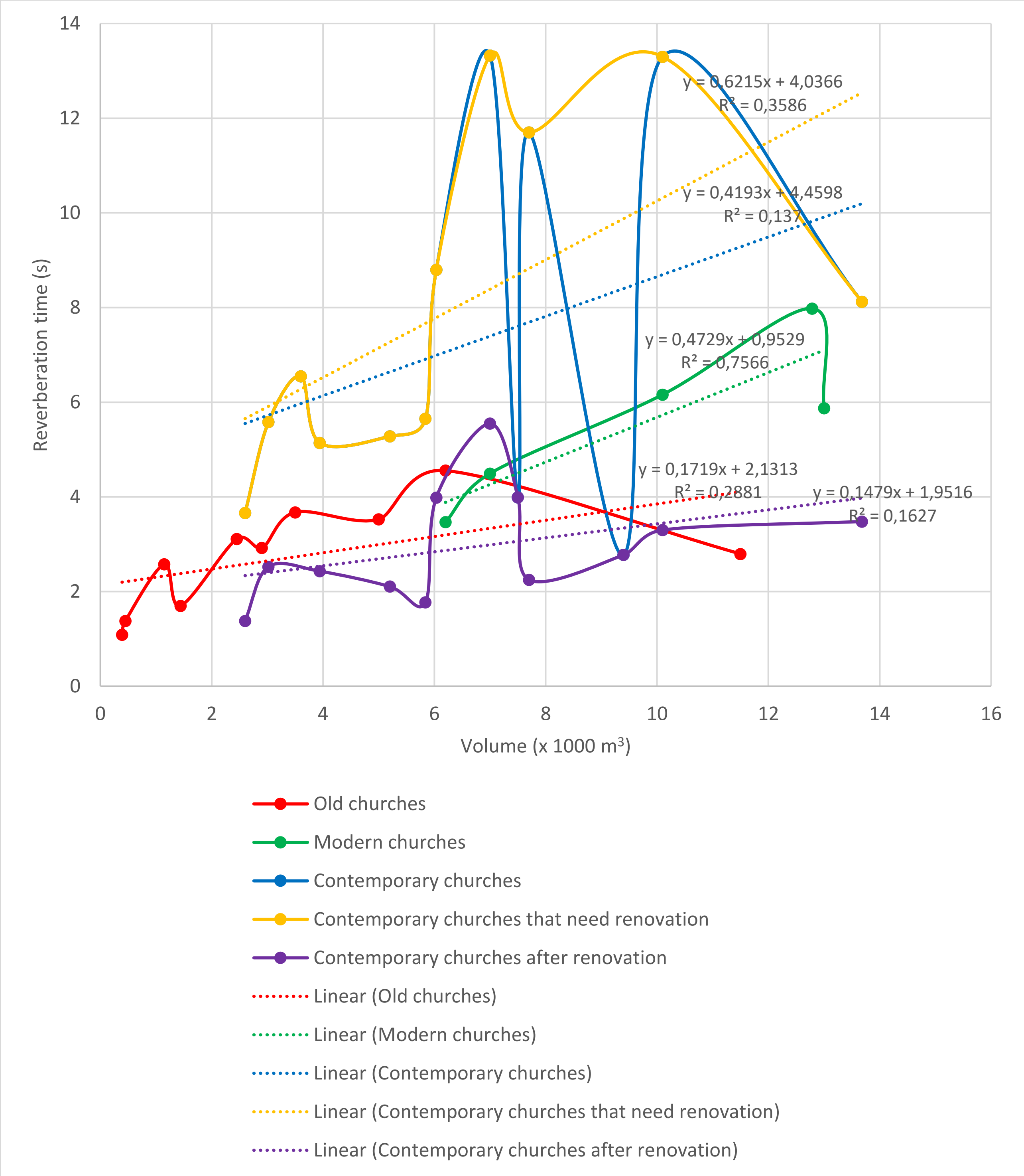

Fig.33. Reverberation time vs. volume for all investigated churches

4. CONCLUSION

In this paper, a simple overview of reverberation times in 28 churches in Croatia of different size and age was shown. The churches were grouped into three groups according to their year of completion: old churches (up to 1900), modern churches (from 1900 to 1940), and contemporary churches (from 1985 to recent buildings). Since they differ significantly in size, the comparison was made with their volume as the independent parameter.
The acoustic situation in old and modern churches shows consistency in construction and interior finishing techniques over the centuries, resulting in a fairly smooth increase in reverberation time with the increase of volume. The reverberation time in larger churches is rather high, but still does not reach values that would be designated as utterly unacceptable.
Contemporary churches show a huge variability in their acoustic characteristics. Changes have occurred in construction techniques and materials, leading to excessive use of hard, reflective materials. Moreover, an acoustic project is hardly ever a part of the building project. As a result, many of them have excessively high reverberation times in their finished state and require a thorough acoustic renovation. Old and modern churches simply do not have examples of particularly bad acoustics, at least not to the extent of the contemporary ones.
Contemporary acoustic design and renovation philosophy has already been applied by the authors in all investigated contemporary churches. It rests on the desire to provide better acoustic conditions in a modern church than the ones found in an old church of similar size by shortening its reverberation. At the same time, the reverberation is to be kept long enough to maintain the required degree of solemnity expected in a house of worship. The data shown in the paper confirms the successful implementation of this design philosophy.

5. REFERENCES

[1.] D. R. Jones: **Sound of Worship - A Handbook of Acoustics and Sound System Design for the Church**, *Focal Press*, Oxford, 2011
[2.] F. Martellotta: **Optimal Reverberation Conditions in Churches**, *International Congress on Acoustics ICA*, Madrid, 2007, 1-6
[3.] R Suarez, J. J. Sendra, A. Alonso: **Acoustics, Liturgy and Architecture in the Early Christian Church. From the domus ecclesiae to the basilica**, *Acta Acustica united with Acustica*, 99, 2013, 292-301
[4.] E. Cirillo, F. Martellotta: **Acoustics and Architecture in Italian Catholic Churches**, *International Symposium on Room Acoustics ISRA*, Seville, 2007, 1-13
[5.] A. Gagliano, F. Nocera, A. Cicero, M. C. Gioia, A. Agrifoglio: **Analysis and acoustic correction of a contemporary Italian church**, *Energy Procedia*, 78, 2015, 1623 - 1628
[6.] D. T. Bradley, E. E. Ryherd, L. M. Ronsse: **Worship Space Acoustics: 3 Decades of Design**, *Springer*, New York, 2016
[7.] J. Vodopija: **Determining acoustical quality of sacral spaces**, Phd Thesis, *University of Zagreb*, 2011
[8.] J. Rio, C. Buono: ***House of Worship Sound Reinforcement***, *Course Technology PTR*, Boston, 2009

8th Congress of the Alps Adria Acoustics Association
Zagreb, Croatia
20 – 21 September 2018

ENHANCEMENT OF BASS FREQUENCY ABSORPTION IN FABRIC-BASED ABSORBERS

Jonas Schira
Head of Acoustics
Gerriets GmbH
Im Kirchenhürstle 5-7

jschira@gerriets.com

Abstract: *Sound absorption in fabrics normally does only cover the middle and high frequencies above 250 Hz. But if installed in front of an enclosed air volume, the absorption capabilities of fabric roll banners below 250 Hz can be boosted significantly. This presentation will present a series of measurements, carried out by the Centre of building physics (ZFB) of the technical University of Stuttgart, which show the enhancement of bass frequency absorption of the fabric roll banners. It will be presented that a fabric absorber, consisting of two layers of fabric, can show an absorption coefficient of α = 0,40 and higher in frequencies below 250 Hz, if this absorber is installed in a wooden enclosure. The measurement data will be compared with the calculated sound absorption of membrane absorbers. A high coincidence between the measurements and the calculated absorption coefficients can be shown. Therefore the theory of a combined absorber, consisting of a porous and at the same time diaphragm absorber, can be deviated. These double layer absorption banners, without the wooden enclosure, have also been installed in both the big and the small concert hall in the Elbphilharmonie. The presentation will be complemented by showing architectural solutions for integrating these kind of fabric roll banners in moden concert halls.*

Key words: low frequency absorption, fabric absorbers, roller banners

1. INTRODUCTION

The key characteristic of a multipurpose hall is to host different kinds of events, from modern ballet to rock concerts. Although the concept of designing a multipurpose hall isn't new, the variety of shows presented is much bigger than in the early days. The first examples of venues equipped for variable and multipurpose use can be found back in the 1920s [1]. One of the important features of these halls is the variable reverberation time to adjust the venue according to the event. These variable reverberation times can also be found in planning standards, such as the German DIN 18041 [2].

To achieve variable reverberation times different methods have been used throughout the last decades, for example the utilization of highly absorbing fabrics. In the concert hall *La Maison Symphonique in Montréal*, for example, over 2000 m² of highly absorbing curtains are installed on motorized tracks to vary the reverberation time. These kind of installation allow the user to quickly change the reverberation time by the push of a button. The disadvantage of those systems is the reduced absorption capability in the low frequencies.

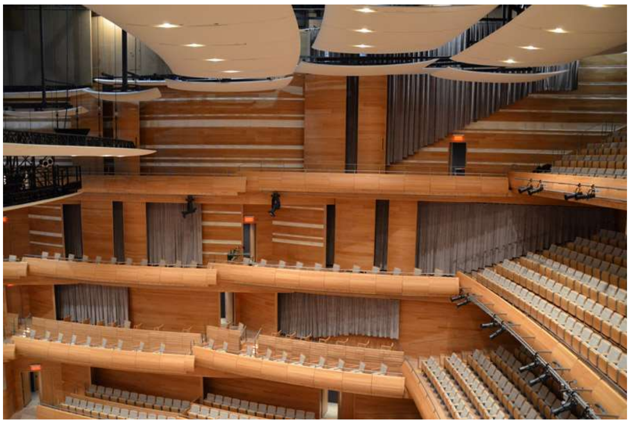

Fig.1. Absorbing curtains in *La Maison Symphonique*, Montréal, Canada Architect: Diamond & Schmitt, Acoustician: Artec Consultants, Inc. / Fisher Dachs Associates

Especially for the purpose of amplified Rock and Pop-music the reverberation time in the lower frequency bands has to be decreased in order to create a suitable reverberation time.3 In contrast, however, an increasingly longer reverberation time in the bass frequencies provides for the impression of "warmth" in classical music.4 This discrepancy results in the need of variable absorption, according to Adelman-Larsen especially in the lower frequency band of 125 Hz. So the challenge for fabric and curtain manufacturers is to find a way to improve the low frequency absorption in these fabric-based absorbers.

During the research and development of retractable textile absorbers a series of measurements has been taken out to determine the best method of installation in order to create the maximum absorption capability in the low frequency bands. These measurements show interesting results on how to increase the absorption coefficients below 250 Hz, so fabric-based absorbers provide a more broadband absorption than previously known.

2. METHOD

To determine the absorption capabilities of fabrics in correlation with their specific installation method, only one type of fabric has been used, a material called Absorber CS by the German manufacturer Gerriets GmbH. This fabric fulfils the following technical specifications:

Material:	100% Trevira CS
Weight:	530 g/m²
Width:	450 cm
Flow Resistance:	RS = 838 Pa s/m (according to DIN EN 29053)
Color:	white

All measurements have been carried out in reverberation chambers according to DIN EN ISO 354 at Müller BBM GmbH in Planegg, Germany, as well as at Centre for Building Physics (Zentrum für Bauphysik ZFB) the Technical College of Stuttgart, Germany.

3. RESULTS

The measurements carried out at the Müller BBM facilities were limited to standard installation methods of curtains, which means the fabric has been attached to ta track in the ceiling, hanging loosely in front of the wall.

1. flat panel of fabric with 100 mm distance to the wall
2. fabric with 100 % fullness (double amount of fabric on the same length) with 100 mm distance to the wall
3. two flat panels of fabric in front of each other, distance of 100mm to the wall of back layer, 190 mm air gap in between the panels

The following results of the ISO 354 measurement could be obtained:

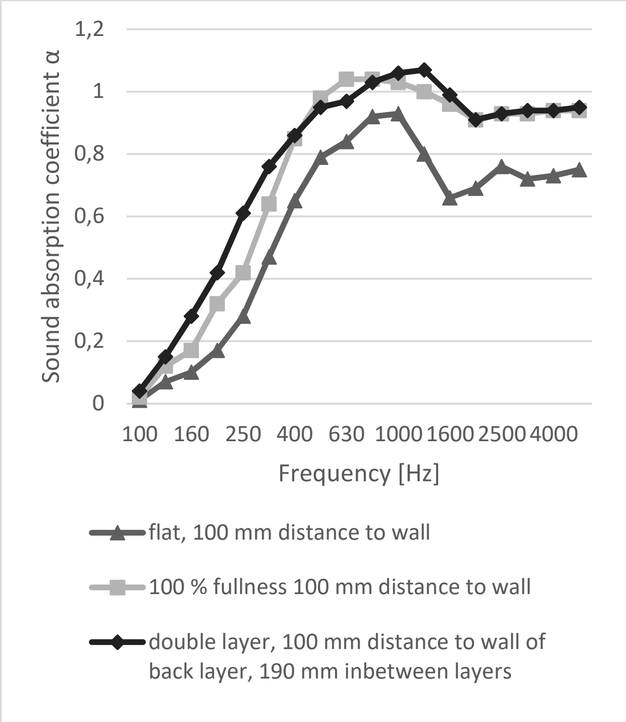

Fig.2. measurement of the absorption coefficient by Müller BBM, test report N° M108538

The following measurements have been carried out at the Centre for Building Physics in Stuttgart. In addition to the standard installation of fabrics the textiles have been mounted in a wooden frame made of 19mm melamin coated chipboards. All measurements in this second test series included setups with two flat panels of Absorber CS in different distances to the wall and with as well as without the wooden enclosure.

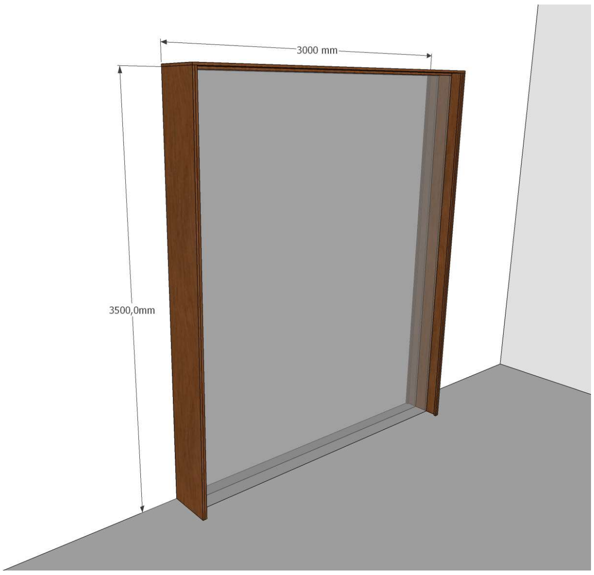

Fig.3a. design of the test setup at ZFB, Stuttgart

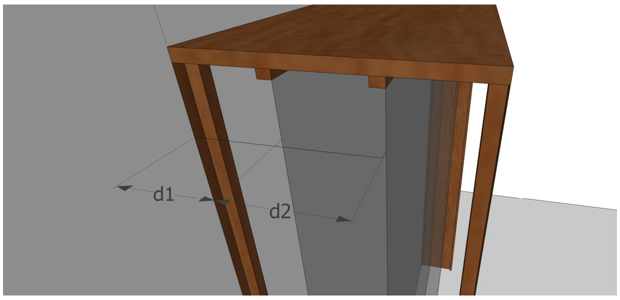

Fig.3b. design of the test setup at ZFB, Stuttgart

The measurements have been carried out with the following distances of the fabric panels:

1. d1 = 100 mm, d2 = 145 mm, no enclosure
2. d1 = 200 mm, d2 = 245 mm, no enclosure
3. d1 = 100 mm, d2 = 145 mm, wooden enclosure
4. d1 = 200 mm, d2 = 245 mm, wooden enclosure

Fig.4. test setup without enclosure at ZFB, Stuttgart

These double leyer fabric constructions can be installed on a roller banner mechanism to create a variable absorbing element. The wooden enclosure simulates a roller banner being installed in a niche in the wall (see fig. 7). Depending on the type of installation an air gap on the sides of the fabric may occur. Therefore a measurement of the two layers of fabric in the wooden enclosure with an air gap of 100 mm on each side has been made.

Fig. 5. test setup with wooden enclosure at ZFB, Stuttgart

The following results of the ISO 354 measurement could be obtained:

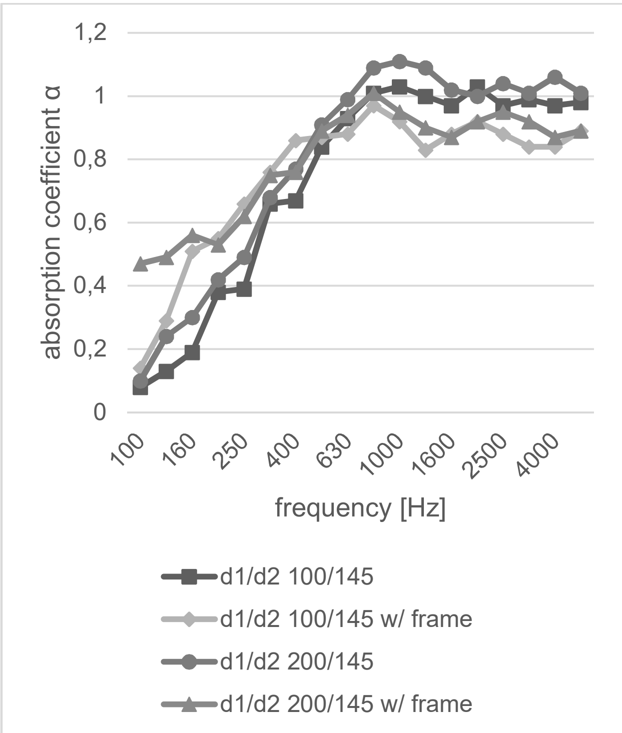

Fig. 6. test results of second measurement series at ZFB, Stuttgart / test report N° B2016-01-II

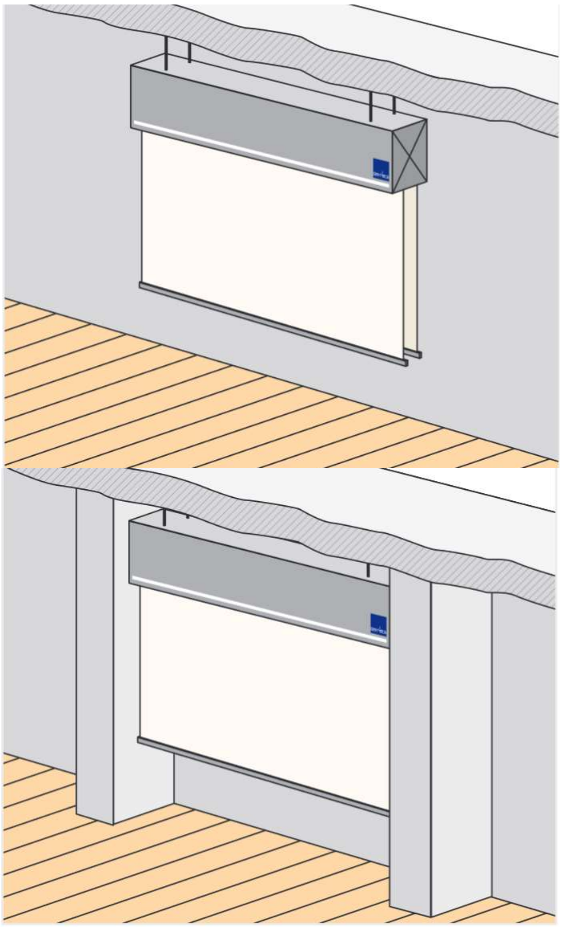

Fig. 7. Roller banners with double layer fabric, freely hanging in front of the wall and installed in a niche

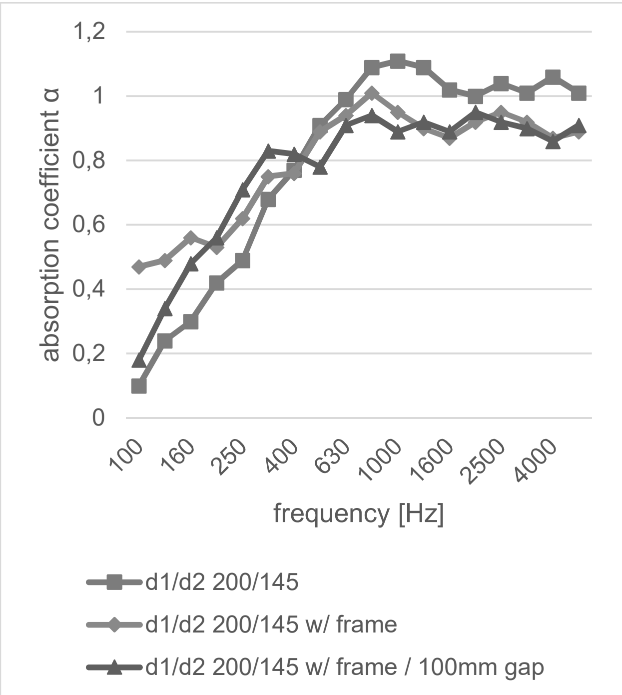

Fig. 8. Measurement of an 100 mm airgap on the left and right side of the fabric, in comparison with the freely hanging and the fully enclosed material, measurement report N° B2017-16-I

In some project acoustic roller banners could be deployed out of the ceiling in the middle of the room. Therefore a further measurement has been carried out with the two layers of fabric with a spacing of 145 mm installed in the middle of the reverberation room.

Fig. 9. Double layer fabric absorber installed in the middle of the room, ISO 354 measurement

The measurement results of this method depend heavily on the surface of the object taken in account to calculate the absorption coefficient. The surface area of the fabrics is 10,71 m², but since both sides are exposed to the room one could also calculate with 21,42 m² of surface area. Both calculation are given in the following test result if this measurement.

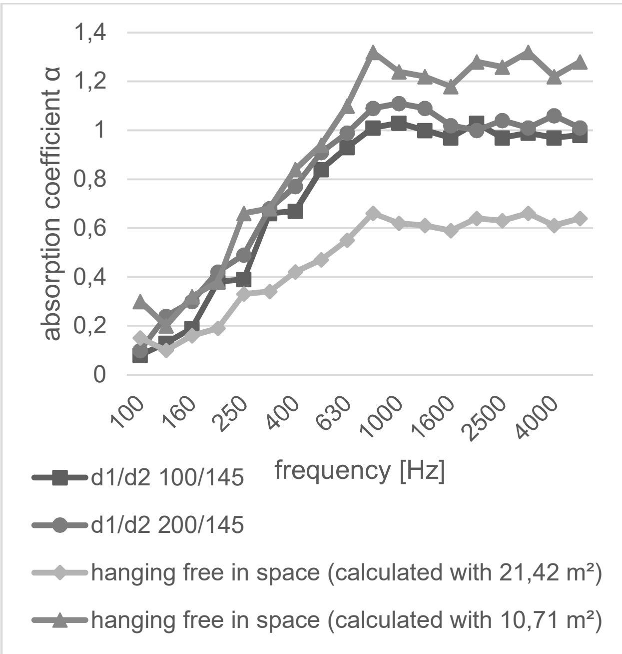

Fig. 10. measurement of freely hanging fabric absorber, absorption coefficient calculated with two different surface areas, measurement report N° B2018-07/01

4. DISCUSSION

The first series of measurements concentrated on the standard installation of fabric absorbers as curtains (see fig. 2). A broadband increase of the sound absorption coefficient can be observed when fullness is added to a curtain, but still the αw in the 125 Hz frequency band is below 0.2, so no significant absorption capability can be noticed. The biggest increase in the lower and low-mid frequencies can be achieved by installing two flat panels of fabric in front of each other with a certain distance in between the fabrics. In order to build a retractable and variable absorbing element these panels have to be attached to a roller banner mechanism.

To further enhance the absorption capability in the bass frequencies the following two measures prove to be effective: increase the distance to the wall of both layers and install the textile panels in a wooden enclosure. Introducing the wooden housing had the greatest effect, shown in figure 11.

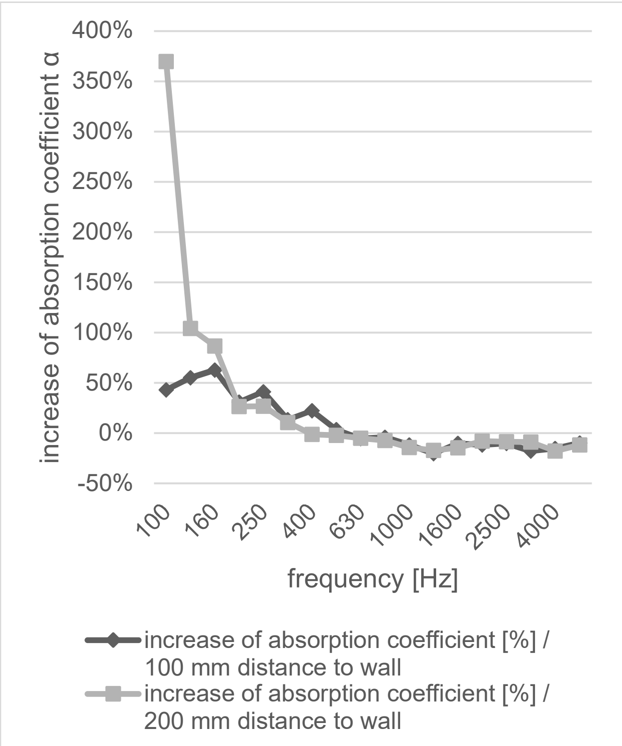

Fig. 11. increase of absorption coefficient by introducing the wooden enclosure in comparison to freely hanging textile

The biggest effect shows an increase of 370 % at 100 Hz when the fabric is installed with a higher distance to the wall, in this case 200 mm instead of 100 mm. This effect can be utilized in building projects when a roller banner is installed in between two columns or in a niche, so the air volume behind the fabric layers gets closed off completely. If there are air gaps due to technical reasons an increase of the bass frequency absorption can still be observed, but not as effectively as with a completely closed system (see fig. 8).

4.1. Theoretical Model

A possible explanation of this effect can be found when combining different models of sound absorption. The absorption coefficient with and without the enclosure of the middle and high frequency above 400 Hz differ less than 10 %, so it can be expected that the porous absorption of the fabric hardly is impaired by the wooden housing. The situation in the lower frequencies is a lot different, as can be seen by the measurements.

By enclosing the layers of fabric in the wooden housing a concluded air volume is created. The front textile layer, although it is not airtight, can be interpreted as a membrane, so a spring-mass-system is created. If the second and inner layer of fabric functions as the dampening of the air volume with a low dampening factor and the thickness of the system is considerably lower than λ/4 of the absorbed frequency bands, than the following formula (1) by Fuchs [5] can be used to calculate the absorption of the system:

$$\alpha = \frac{4r'}{(r'+1)+(Z'_R\,F)^2} \tag{1}$$

The mass of the textiles is 0.48 kg/m². If the absorption of the system is calculated with a low dampening factor for the second layers of fabric of r' = 0.2 the calculated bass frequency absorption of the mass-spring-system shows a high correlation with the increase of the measured absorption coefficients for the enclosed system.

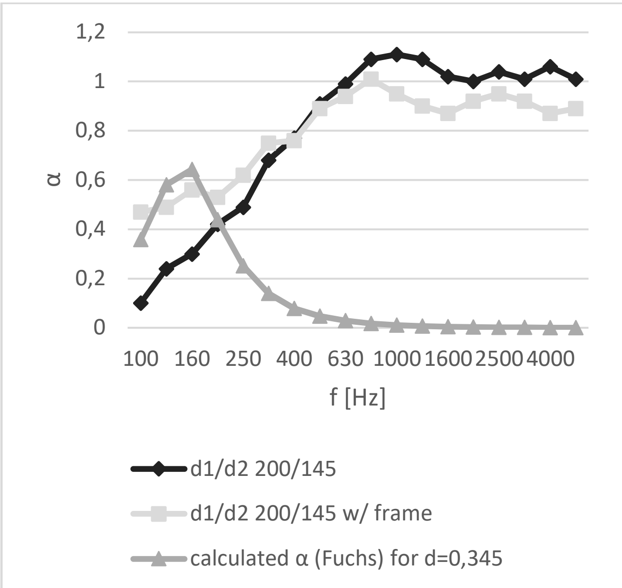

Fig. 13. comparison of measured absorption coefficient and calculated bass absorption of a similar membrane absorber

3. CONCLUSION

One possible conclusion for the enhancement of bass frequencies in fabric-based absorber can be the combination of porous absorption in the middle and high frequency bands and the membrane absorption effect in the lower frequencies when the two layers of fabric are mounted in an enclosure. This opens an interesting opportunity for planners and acousticians to introduce broadband variable absorbers as roller banners, but with a highly increased performance below 250 Hz.

4. REFERENCES

[1.] M. Holden: **Acoustics of Multi-Use Performance Art Centers**, CRC Press (Boca Raton), 2016
[2.] DIN 18041 - **Acoustic quality in rooms – Specifications and instructions for the room acoustic design**, Beuth (Berlin), 2016
[3.] N. W. Adelman-Larsen: **Suitable reverberation times for halls for rock and pop music**, *Journal of the Acoustical Society of America*, 2010
[4.] L. L. Beranek: **Concert Halls and Opera Houses: How They Sound,** Springer (New York), 1996
[5.] H. V. Fuchs: **Schallabsorber und Schalldämpfer**, Springer Verlag, Berlin Heidelberg, 2010

8th Congress of the Alps Adria Acoustics Association
Zagreb, Croatia
20 – 21 September 2018

Hrvatsko akustičko društvo
HAD
Acoustical Society of Croatia

THE APPLICABILITY OF ACOUSTIC DESIGN APPROACHES IN EARLY DESIGN STAGE BY ARCHITECTS

Çiğdem Türk, Nurgün Tamer Bayazıt

turkc@itu.edu.tr

Abstract: *This paper aims to take a fresh look at the applicability of three main acoustic approaches to the early design stage of indoor spaces, which are architectural acoustics, soundscape and aural architecture. The design stage of an indoor space begins with a sense of atmospheric space before the creation of the actual space. Throughout the whole design process, architects endeavor to retain the desired atmosphere of space. In this paper, three main approaches will be analyzed by considering their earliest starting point regardless of their frequency of occurrence. The usability of these approaches and whether they require special acoustic training for architects will also be investigated. Acoustic experts can adopt acoustic design approaches in the preliminary or detailed design stage in accordance with legislation, standards and/or certification requirements in a functional limitation. The lack of knowledge on acoustic outcomes of the desired atmosphere, on the other hand, may result in the creation of negative aural spaces. Understanding the atmospheric intentions of architects and the sense of aural spaces requires a common language based on human-space interaction for both architects and acousticians. The absence of such a language makes spaces rather acoustically-forced quasi-spaces. This review will demonstrate the necessity of understanding the aural component in atmospheric design as a starting point for the acoustic design.*

Key words: Indoor space design stages, acoustic design, architectural acoustics, soundscape design, aural architecture, atmosphere

1. INTRODUCTION

"Is there anyone who has not, at least once, walked in a room and felt the atmosphere?" [1]

A sense of atmospheric space which architects intend to retain throughout the whole design process is the initial design stage of an indoor space. The value of this intention arises from the existing link between the architectural quality and the presence/absence of atmosphere. Vitruvius's "pathos" can be a means of inducing emotion (delight) to architecture, according to Pallasmaa et al. the link that connects architecture to pathos, connects the building to the human spirit, to the enigma of life. [4]. Zumthor explains the quality of good architecture as the ability of the building to move by invoking feelings and he uses the term atmosphere for it [5]. The way we grasp an atmosphere is the direct, simultaneous, total and immediate judgement of the character of space before our intellectual or detailed understanding [2]. On the other hand, how are architects able to create an atmosphere that reflects such a powerful grasp? Böhme says, making atmosphere does not refer to the manipulation of material conditions of things, or other tools like sound and light, because it is not a thing. But rather it is something between things and perceivers [3].
Upon comparing the old architectural entities to those that are contemporary, Pallasmaa [6] concludes that the early architecture made out of mud and clay features haptic and muscular qualities and this evaluation requires the involvement of other senses besides sight. He criticizes contemporary architecture for lacking the sensual quality pertaining to other senses as a result of the hegemony of sight. Rasmussen [7] agrees that we acquire a general impression of the thing we experience but hardly associate it with auditory senses mainly because we do not take into account the use of other senses that played a part in the formation of that impression.
The purpose of this paper is to evaluate the existing acoustical approaches in the early indoor architectural design and to point out the lack of a sound methodology in terms of incorporating acoustics in the initial design stage. This initial design stage is important both for designing an affective auditory component in creating the desired atmosphere and for determining the basic design parameter for the acoustic specialist.

2. THE ABSENCE of AURAL COMPONENT: WHY and WHEREFORES

An article published by Elsen and Heylingen [8] explores how sensory experience is conducted during the early phases of architectural design through an ethnographic observation in an architectural firm and they analyzed 985 graphic components to understand sensory related design intentions of architects. At first glance, the results of the study approved that sight is the dominant sense in architectural design, but it is not the only sense to be found in architectural representations. Free hand sketches are the most common representations used to express sensory experiences with up to five senses. The authors point that CAD tools and scale models are generally well accepted in terms of gaining insights about end-user's experiences; however, the results showed that the number and the intensity of five senses shown in these tools are dramatically decreasing. Since these simulations require detailed visuals of space, these tools can rarely be used in the blurry stages of early design to represent sensory intentions of architects. In collaborative stages of design, CAD tools are used for exchanging architectural design development outcomes. Because 2D or 3D CAD tools lack the sensory potential free sketches possess, there is a danger for the immaterial and formless atmospheric design elements to disappear.

The study by Elsen and Heylingen [8] proves that while sight might be the only sense in architectural representations, hearing is never the sole sense component that is taken into consideration. Whenever hearing is involved, it is merely to compliment sight, the dominant sense, in section sketches.

According to a study carried out in 2014 on architectural education in Turkey [9], the proportion of required classes related to acoustics in undergraduate education is 60%. This ratio is 92% for universities established before 1990, whereas it is 33% for universities established after 2010. Topics pertaining to acoustics are taught as subordinate to other lessons, usually only theoretically, ranging from 1 to 7 weeks. Moreover, students give secondary importance to theoretical courses. Due to limited studio hours and the small number of weekly lessons in the undergraduate curriculum, it is difficult for the students to apply the theoretical background of acoustics to their studio practice with a holistic understanding [10].

A study by Sheridan and Van Lengen proves that this structural problem is not peculiar to Turkey. *“Architecture schools often teach acoustic design as a part of the core curriculum, but to our knowledge, very little exploration has been done in the studio using sound as a generative thesis for design.”* [11]

Based on the previously mentioned studies, there are three main factors regarding why hearing is not a part of the atmospheric design process. The first one is the obvious fact that hearing is often overlooked as one of the components that make up the atmosphere. Another factor that contributes to this problem is that the tools used while developing and representing the designs lack the required emphasis on hearing. The third factor, which precedes and perpetuates the first two, is that architectural education does not embrace the site investigations, experimentations, and workshops that focus on the knowledge and skills pertaining to how hearing could be integrated into the design process.

3. The APPLICABILITY of THREE MAIN ACOUSTIC APPROACHES IN AN EARLY DESIGN STAGE

The studies on sound-related architecture have their origins in Vitruvius's works. The emergence of architectural acoustics began with the new problems encountered as Greek theatres become closed concert and theatre halls in the 17th and 18th centuries. Protecting the liveness of music and rendering speech understandable were the main goals of the architectural acoustics. In the 19th Century, Wallace Clement Sabine formulated the relationship between the texture of the surfaces, the volume and the acoustics of the space. It is seen that analyses such as reverberation time, scale model, ray tracing methods, and subjective parameters began to be used. Today, within the scope of acoustic modelling studies, subjective and objective parameters of the un-built spaces can be analyzed and the acoustic environment can be evaluated at the design stage with auralization tools.

Kang defines "acoustic spaces" as sensitive spaces in terms of speech and listening while non-acoustic spaces include all enclosed spaces other than acoustic spaces. Today, people spend most of their daily lives in non-acoustic spaces. Performance requirements in building regulations designed to protect human health were developed for these non-acoustic space types, which can be considered new in architectural acoustics. However, these performance requirements were specified based on their functions, and there are no determinants beyond background noise and reverberation time for the architectural acoustics. In sustainability scales, assessments are made by analyzing how well these limits are improved. However, we are witnessing that today's indoor spaces are redefined with regard to their functional variety and new usage patterns. This requires a re-examination of the function-based predictions of the architectural acoustics. There are no research sets on which we can analyze the acoustic expectations of people from these new types of spaces, what is more, it is also unknown how an auditory environment can be complementary in the unique architectural context. This requires us to question the origin of the existing standards. Architectural acoustics studies are carried out to reduce the reverberation time and the background noise to the appropriate level which is a process that may start once the concept design is finalized. Since early in the design stage the decisions on material and form have not been made yet, architectural acoustics conditions remain unknown which leaves the acoustician with the restricted position of dealing with the acoustic problems thereby causing the emergence of acoustically-forced spaces. The critique of Sheridan and Van Lengen in this regard is parallel to the above evaluation.

"At present, acoustical engineering is typically applied to architecture in remedial fashion: either to completed buildings or to designs already conceived along different sensory lines." [11]

The term "soundscape", the second approach, was first introduced by the Canadian composer R. M. Shaffer as an antithesis to environmental noise control in 1977. Schaffer and Truax, the pioneers of the soundscape researches, take sound as a resource in relation to its perception and meaning instead of noise or waste. Urban or suburban soundscapes have been explored by searching the relationship between individual sound sources, overall sound environment and pleasantness - unpleasantness from the perspective of perceivers. Many tools have been designed and used (such as sound-walks, blind-walks, interviews, questionnaires, recordings, lab studies, etc. along with sound measurements) to conduct field studies by many disciplines including urban design, psychology, music, and architecture.

Recently, ISO-12913 part-1 (2014) and part-2 (2016) were published to define the general conceptual framework of soundscape and inform about data collection. Based on the definition given in the standard, the soundscape is "an acoustic environment as perceived or experienced and/or understood by a person or people in context" [16]. In addition to that, the framework can be seen as a reference to design customized methodologies. To evaluate the measurable data and its link to perception in an outdoor soundscape, generally, A weighted sound pressure level measurements and main psychoacoustic measurements (loudness, sharpness, roughness, tonality) are conducted. [12, 13, 14, 15, 16]

Despite the great attention to explore outdoor soundscapes, very limited research has been developed for indoor spaces [15]. Kang put forward many complex and interrelated factors to describe a soundscape [17]. When it comes to indoor space perception, the built entity has to be taken into consideration with its acoustic characteristics [14]. Dökmeci [14], like Kang, proposed the given indoor soundscaping framework with three main variables (contextual experience, built entity and sound environment) and nine related factors. Nine factors are divided into twenty-eight sub-factors.

Because the way we grasp an atmosphere is immediate, the evaluation of an atmosphere is judgmental. On the other hand, the perception of soundscape contains cognitive process within its complex structure. Therefore, investigations carried out for indoor spaces, don't contain all the factors that may change the final assessment. To design a soundscape, researchers propose site investigations by conducting soundscape methodologies, but architects and students of architecture cannot explore the existing soundscape to such an extent. Simpler, more useful and quicker tools are urgently needed to characterize soundscapes and to gain an understanding of the design process. Recent urban and suburban soundscape studies are parallel to affect theory which is used to define the atmosphere, and this would be a hope for architects to appropriate soundscape as a powerful design tool to pick both immaterial and formless clues from the indoor or outdoor environments.

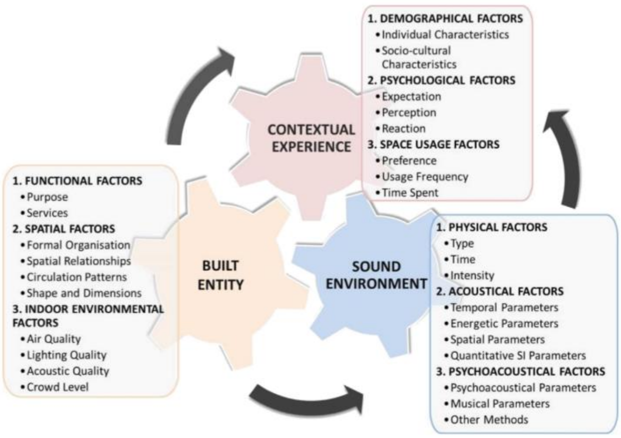

Figure 1. Dökmeci's indoor soundscaping framework [14]

The third approach is aural architecture. Acoustician Barry Blesser and environmental psychologist Ruth-Linda Salter published their book named "Spaces Speak, Are You Listening? Experiencing Aural Architecture" in 2007. In 2009, they made a presentation titled "The Other Half of the Soundscape: Aural Architecture". In the simplest way, their term of aural architecture refers to the creation process of a soundscape. The soundscape is the outcome of an aural architecture designed by an aural architect. To indicate the complexity of a soundscape, Blesser and Salter give an example of noisy restaurants. Restaurants have a cycle between the diners' conversation sounds and the background noise. For acousticians and social scientists, such a restaurant environment is problematic, on the contrary, both physical and cultural acoustics cooperate and arrive at the conclusion that diners might perceive the soundscape as being positive. They also conculuded that there is a need for the system view to truly understand soundscapes. [18]

The aural architect is an artist, a designer and a social engineer who selects specific aural attributes for the space based on the activities to produce sonic events, users' experiences, and interactions with the aim of providing social cohesion. Because they assert that "those who control the soundscape control the world" [18]. Aural architecture is an aspect of real and virtual spaces that produce an emotional, behavioral, and visceral response in inhabitants. Various combinations of spatiality generate aural architecture. They define six types of spatiality:

navigational, social, timbre, musical, aesthetic, and symbolic. [18, 19]

Aural architecture's strong suit is the space itself with its geometry, volume, and materiality which turns the space into a spatial aural texture. Blesser and Salter's aural architecture requires aural embellishments like visual ones. The physical conditions of the acoustics of a space are defined as passive aural embellishments. Intentionally designed active sound sources are active aural embellishments which create acoustic horizons and generate space using digital technologies or natural sources. In the light of recent design attempts of aural architecture, the aural design of these spaces become a sound object of art for musical aesthetics. Fowler summarizes the outcome of the aural architecture approach by saying that "the architecture then of these pavilions served or facilitated the delivery of thematic content that was bound to musical narratives. Thus, the architectonic dimensions and materiality of the pavilions are not in themselves designed to evoke aural architectures". As stated by Blesser and Salter, the internalised auditory experience is an experience of the external auditory environment through sensation (detection), perception (recognition), and effect (meaningfulness). Due to the complexity of the set of these interactions (sensation, perception, and effect), people's aural experience cannot be designed entirely in the early design stage. Another difficulty is that this kind of complexity requires interdisciplinary investigations, and it cannot be performed within one discipline in this design stage. [19]

Despite the increasing attention to the soundscape and aural architecture, these new approaches cannot be used for the early design process for above mentioned similar reasons. Experimental studies carried out in architecture faculties in simplified frameworks show that students who are directed to experience space through sound find their own innovative ways of developing sets of knowledge and skills that can expand their design potential. This necessitates the development of fast, simple and effective experimental pedagogies for space reading that can be used in architectural studio practices.

4. AURAL COMPONENT OF ATMOSPHERE; The MISSING LINK

In the light of the above-mentioned applicability analysis of three main approaches to indoor acoustic design in the early design stage, architects don't have any tools or frameworks to read architectural spaces and to capture the aural component which is embedded in the atmosphere of a space. The aural component should be explored through a judgmental approach in a simplest and immediate way. The language of the approach should be clear and understandable for everyone from architects, to acousticians; form other collaborators to future users. This is the only possible way to exchange the immaterial and formless idea which would be protected through the design stages and to make the aural component an integral part of design praxis in architectural studios.

Examining human-environment relationship through cognition has been a general tendency for years, but currently, affect and emotion studies draw quite an attention from different fields. The cognitive system is used to interpret and make sense of the environment, whereas the affective system is judgmental. Therefore, we can assign positive or negative valence to the environment rapidly and effectively. The term "core-affect" (or mood, affect or feeling) refers to basic mood, simple and primitive feeling, and the core of all emotion-laden occurring events. Basically, it consists of two components; valence (pleasure-displeasure, feeling good-bad) and arousal (sleepy-activated). Core-affect exists in a person and as a part of his/her general reaction to the world. Besides, "affective-quality" exists in a stimulus (space, object, device, etc.) and it is related to the stimulus's capacity to change the core-affect of the perceiver. Affective-quality is perceived through appraisals which consist of two components; pleasantness and eventfulness. [20, 22]

In architecture, if a space has an affective quality, it will move the perceiver's feelings and change his/her core-affect through the intentionally designed atmospheres. Because atmosphere is "in-between" and "in the air" as stated by Brennan, the aural part of an atmosphere cannot be separated from other components but, it can be understood through its presence and absence. In architecture, Küller conducted many site-studies to understand affective qualities of urban and sub-urban environments, but he examined sound in the frame of noise. His indoor studies on affective quality were based on light and color.

The amount of research that uses affective components (vibrancy-pleasantness) is increasing in the field of soundscape: one of these studies was published by Aletta, Kang and Axelsson in 2016. Long since pleasantness has been the important indicator for soundscape evaluations, but vibrancy (or eventfulness) is a new discovery, and they conclude that

"The potential soundscape descriptors identified so far seem to converge towards the two-dimensional soundscape model of perceived affective quality." [13]

Andringa and Bosch who study artificial intelligence and cognitive engineering presented a remarkable paper titled "Core affect and soundscape assessment: Fore-and background soundscape design for life" in 2013. They identify four types of sonic environments (calm, chaotic, eventful, boring) with respect to fore-back ground sounds. In 2018, they developed an application (MoSART) for mobile devices which records real-time soundscapes and analyses the affective character of an environment by means of a quick questionnaire.

Based on the given review, it is possible to conclude that an approach that can be used to create the aural component in the initial design has not yet been established. By developing such an "affective approach", it will be possible to develop architectural practices that determine the atmospheric quality by defining the affective qualities of the space with its auditory dimension. In this way, it is possible to create a common language among architects and acoustic specialists to overcome potential problems.

5. CONCLUSION

Approaches to the acoustic design of indoors can be grouped under three main titles; architectural acoustics, soundscape, aural architecture. Architectural acoustics, the first of these methods, is handled by the acoustical specialist who intervenes to remedy the problems after the design decisions of the non-acoustic space have been made. Architects see this approach as a different area of expertise. Complex and interrelated determinants of soundscape and aural architecture studies require interdisciplinary approaches that architects, alone, cannot perform early on. While the absence of aural components is criticized in the architectural designs, the analyzed situation demonstrates that it is difficult to conduct the aural design in the early period with the mentioned methods. The development of a model that will determine its aural component during the creation of the atmospheric idea is important both for the architects to put their own design on the right footing and for the acoustic specialists to have a reference point. A simpler, quicker and easier tool can create a possibility for multidisciplinary design language In order to exchange ideas.

4. REFERENCES

[1.] T. Brennan: ***The Transmission of Affect***, Cornell University Press, Ithaca, 2004

[2.] J. Pallasmaa: **Space Place and Atmosphere. Emotion and Periperal Perception in Architectural Experience**, *Lebenswelt: Aesthetics and Philosophy of Experience*, 4, 2014, 230-245

[3.] G. Böhme: **The Art of the Stage Set as a Paradigm for an Aesthetics of Atmospheres**, *Ambiences*, 2013, URL: http://journals.openedition.org/ambiances/315

[4.] K. S. Smith, A. C. Smith: ***Building the Architect's Character: Explorations in Traits***, Routledge, New York, 2018

[5.] P. Zumthor: ***Atmospheres: Architectural Environment, Surrounding Objects***, Basel: Birkhäuser, 2006

[6.] J. Pallasmaa: ***The Eyes of the Skin: Architecture and the Senses***, Chichester: Wiley, 2014.

[7.] S. E. Rasmussen: ***Experiencing Architecture,*** Cambridge, Mass: M.I.T. Press, 2012

[8.] C. Elsen, A. Heylingen: **Presentations of Sensory Experiences in the Early Phases of Architectural Design: There is more than meets the Eye**, *J. Design Research*, 12 (4), 2015, 239-259

[9.] O. Çakır, Z. Sevinç, E. İlal: **Türkiyede Mimarlık Eğitiminde Akustik: Güncel Durum**, *1. Ulusal Yapı Fiziği ve Çevre Kontrolü Kongresi*, 2014

[10.] E. E. Türkkan, İ. Basa, M. Gürel: **Interaction Between Design Studio and Curriculum Courses: Bilkent University Case**, *Open House International*, 35(3), 2010, 66-75

[11.] T. Sheridan, K. Van Lenghen: **Hearing Architecture Exploring and Designing the Aural Environment**, *Journal of Architectural Education*, 57(2), 2003, 37-44

[12.] J. Kang: ***Urban Sound Environment***, Taylor & Francis Incorporating Spon, Abingdon, 2007

[13.] F. Aletta, J. Kang, Ö. Axelsson: **Soundscape Descriptors and a Conceptual Framework for Developing Predictive Soundscape Models**, *Landscape and Urban Planning*, 149, 2016, 65-74

[14.] P. N. Dökmeci Yörükoğlu, J. Kang, : **Analyzing Sound Environment and Architectural Characteristics of Libraries Through Indoor Soundscape Framework**, *Archives of Acoustics.* 41(2), 2016, 203-212

[15.] J. Xiao, F. Aletta, **A Soundscape Approach to Exploring Design Strategies for Acoustic Comfort in Modern Public Libraries: a Case Study of the Library of Birmingham**, *Noise Mapp*, 3, 2016, 264-273

[16.] B. Brooks, B. Schulte Fotkamp: **The Soundscape Standard**, *Inter-Noise*, Hamburg, 2016

[17.] M. Zhang, J. Kang: **Towards the Evaluation, Description, and Creation of Soundscapes in Urban Open Spaces**, *Environment and Planning B: Planning and Design.* 34(1), 2007, 68-86.

[18.] B. Blesser, R. Salter: **The Other Half of the Soundscape: Aural Architecture**, *World Federation Acoustic Ecology Conference*, Mexico City, 2009

[19.] M. Fowler: **Sounds in space or space in sounds? Architecture as an auditory construct**, *Architectural Research Quarterly*, 19(1), 2015, 61-72

[20.] J. A. Russell: **Core Affect and the Psychological Construction of Emotion**, *Psychological Review*, 110(1), 2003, 145-172.

[21.] T. C. Andringa, K. A. van den Bosch: **Core Affect and Soundscape Assessment: Fore-and Background Soundscape Design for Life**, *Inter-Noise*, Austria, 2013

[22.] Ping Zhang, Na Li: **The Importance of Affective Quality**, *Communications of the ACM*, 48(9), 2005, 105-108

Ray-tracing semiclassical (RTS) frequency response modeling for local- and extended- reaction boundaries

Rok Prislan, Daniel Svenšek

Department of Physics, Faculty of Mathematics and Physics, University of Ljubljana (rok@prislan.net)

Abstract: *Phased geometrical methods are able to capture interference phenomena and therefore extend the use of geometrical methods to lower frequencies. We have introduced the acoustic ray-tracing semiclassical (RTS) method, which is a frequency domain phased geometrical method, capable of directly reproducing the acoustic Green's function. Previously we had demonstrated that RTS accurately reproduces the lowest modes in a rectangular room with weakly absorbing boundaries (real and frequency-independent impedance). In the presented study we extend the validation of the RTS method to a set of practically relevant boundary conditions. We study two additional boundary conditions: a local-reaction boundary simulating a resonating absorber and an extended-reaction boundary representing a porous layer described within the Delany-Bazley-Miki model backed by a rigid boundary, as well as a combination thereof. The RTS-modeled spatially dependent pressure response is compared to results of the finite element method. The RTS results show systematic agreement for all boundary conditions and disclose some interesting particularities of the method.*

Key words: acoustic modeling, geometrical modeling, phased geometrical methods, semiclassical propagator, Green's function

1. INTRODUCTION

Room acoustics simulations have become a valuable design tool for acousticians to predict room acoustic parameters, model room modal shapes, optimize the positioning of public address systems etc. Notwithstanding their increasingly versatile applicability, these tools should be still used carefully. In fact, it is not in all circumstances that relevant results are obtained and caution as well as thorough understanding of the underlying principles of each modeling technique is required from the user.

An important group of methods are geometrical methods which assume that sound propagates from the source in straight lines, implying that diffraction/scattering effects are not included by definition. Generally, the geometrical modeling techniques are limited to large rooms/sufficiently high frequencies, where the sound field is not significantly shaped by distinct room modes. A special, rather restricted but practically widely used subgroup of these methods are energy methods, which consider solely the propagation of sound energy implying that also interference effects are disregarded. These methods are used in commercial room acoustics simulation engines (e.g., ODEON [1, 2]). The energy methods are complemented by the so-called phased geometrical methods in which phase information is included.

Various implementations of geometrical methods exist and their further differentiation is commonly performed on the basis of their stochastic nature (e.g. the implementation of ray-tracing method by Krokstad et al. [3]), the presence of virtual sources (image source method [4]) or other criteria. Each implementation has its advantages and disadvantages for specific types of problems; for recent reviews cf., e.g., refs. [5-7]. It is troublesome to systematically group and differentiate geometrical methods, which are also combined in a hybrid form as e.g. CARISM [8] and PARISM [9].

Generally, the inclusion of the phase information improves the quality of the results obtained at low frequencies. Suh and Nelson showed [10] that the geometrically modeled impulse response agrees better with the experiment if the phase is included. Marbjerg et al. [9] also showed that the inclusion of angle dependence and phase shifts on reflections of an absorber is important in a phased image source method.

To the best of our knowledge phased geometrical methods had been previously implemented [9,11-20] as image source methods, beam tracing and RTS. The methods were tested to model various acoustic parameters or impulse responses, while the low frequency response, on which we focus, was reproduced only by some of them. Among the mentioned implementations only Aretz et al. [14] makes a strict numerical comparison with FEM for a set of more complex

BCs (Helmholtz resonator, porous absorber) in the frequency range of our interest. The reproduced response is modeled remarkably above the Schröder frequency [22], while it is severely inaccurate below it.

In the previous study [20] we have shown that in a rectangular room with a rather clean BC the lowest room modes can be correctly modeled by the RTS modeling technique. The main focus of the study was firstly to adopt the quantum mechanic semiclassical theory and establish a connection of this thoroughly elaborated concept with acoustic modeling, and secondly to test the behavior of the RTS technique by comparing the modeled G with its analytical solution. Weakly damped locally reacting boundaries were assumed, corresponding to a real frequency- and angle-independent boundary impedance identical for all bounding surfaces.

The aim of the present study is to validate the RTS method in a practically relevant environment, i.e., by using realistic BCs. Besides i) the BC used in the previous study, two additional BCs are implemented: ii) a frequency-dependent local-reaction BC of a resonating absorber and iii) an extended-reaction BC of a porous boundary layer covering a rigid base described within the Delany-Bazley-Miki model [22]. These particular BCs were chosen because they are well known in theoretical acoustics. On equal basis, alternative BC models can be implemented into RTS as long as the reflection coefficient can be formulated.

The results obtained by RTS are compared with FEM which is considered reliable at low frequencies. In a rectangular room with the same proportions as in the previous study [20], the comparison is made for the three BCs applied homogeneously and on top of that, for their more realistic inhomogeneous distribution. The comparison includes the magnitude of the obtained pressure response up to 300 Hz, since at higher frequencies the FEM method would not produce correct results in acceptable time limits for the models under study (tested on a workstation with a 2 GHz processor base frequency). The 300 Hz computation limit also allowed us to focus on the low frequency region up to the Schröder frequency, which for the BCs under study ranges between 160 and 360 Hz.

2. BOUNDARY CONDITIONS

2.1. Specular reflection coefficient

As we are concerned with the behavior of the method at lower frequencies, only specular reflections are considered. Diffuse (stochastic) reflections are not included although they are known to be significant in geometrical modeling techniques [6,23]. A link between the diffuse sound field and its geometrical interpretation was described in ref. [24], together with experimental tests that indicated that the complexity of the room boundaries (which produces diffuse reflections) is relevant only at higher frequencies.

In geometrical modeling techniques, the BC is implemented via the specular reflection coefficient *r* [25], which is the ratio *B/A* of complex sound pressure amplitudes of the reflected wave, $p'(\boldsymbol{r},t)=B\exp[j(\boldsymbol{k}'\cdot\boldsymbol{r}-2\pi ft)]$, and the incident wave,

$$p(\boldsymbol{r},t) = A\exp[j(\boldsymbol{k}\cdot\boldsymbol{r} - 2\pi f t)] \qquad (1)$$

where $|\boldsymbol{k}| = |\boldsymbol{k}'| = k = 2\pi f/c_0$ is the wavenumber, f is the frequency, c_0 the speed of sound in air and j the imaginary unit. Generally, *r* is a complex quantity inducing both a magnitude as well as phase change of the reflected sound wave. As is common to geometrical acoustics we assume reflection coefficients which are valid for a plane wave reflection on an infinite surface. As each sound ray is multiply reflected, its amplitude B_i after the *i*-th reflection is calculated recursively as

$$B_i = \mathrm{r}\ B_{i-1} \qquad (2)$$

with B_0 =1.

The reflection coefficient is completely determined by the impedance *z* of the boundary and the angle of incidence θ of the ray with respect to the boundary normal [25] ,

$$r(\theta) = \frac{\mathrm{z}\cos(\theta) - \mathrm{z}_o}{\mathrm{z}\cos(\theta) + \mathrm{z}_o}, \qquad (3)$$

where $z_o = \rho_o c_o$ is the air impedance and $\rho_o$the density of air $\rho_o = 1.204\ \mathrm{kg/m^3}$ and $\mathrm{c_o} = 343\ \mathrm{m/s}$ is considered throughout this study).

Under the local-reaction assumption the BC includes only the normal velocity component [26] and the impedance is defined by the boundary impedance, which is angle-independent. In contrast, in the case of an extended-reaction boundary, its impedance depends on the frequency and the angle of incidence.

The reflection coefficient is directly related to the (energy) absorption coefficient $\alpha(\theta) = 1 - |r(\theta)|^2$. The half-space solid angle average of $\alpha(\theta)$ is the diffuse sound field absorption coefficient α_{diff}.

The absorption coefficient for all three BCs was chosen to be relatively low, which is a more challenging test case for geometrical methods as many reflections have to be modeled. Furthermore, the structure of the modes in the response, which is of our interest, is finer and more delicate in case of low absorption.

The computational efficiency of the RTS method is not compromised if the impedance z depends on frequency and angle of incidence. In fact, in this study we put this under a direct test and introduce just these dependencies, arising naturally in the implementation of the three different BC described in detail in the following.

2.2. Real-impedance boundary

The BC previously tested with RTS [20], i.e., weakly damped boundaries with a real impedance $z_n = 60\,z_0$, is an example of local reaction and is used also in this study for comparison. The corresponding reflection and absorption coefficients are frequency-independent as also shown in Fig. 1. This BC is not particularly realistic, although rather low and frequency-independent absorption coefficients are in practice measured for massive structures with smooth finishing (e.g., painted concrete walls).

2.3. Resonance absorber

This BC models a resonating sound absorber, characterized by its complex impedance [27]

$$z_m(f) = r_m - j(2\pi f m_S - \rho_0 c_0 \cot(k d_m)) \quad (4)$$

consisting of specific resistance r_m, specific inertance $-j2\pi f m_S$ of the mass per area m_S and specific stiffness $j\rho_0 c_0 \cot(k d_m)$ of the air-filled cavity with depth d_m. For low frequencies ($kd_m \ll 1$), $\cot(kd_m) \approx 1/kd_m$and the impedance is simplified to

$$z_m(f) = r_m - j\frac{2\pi m_S}{f}(f^2 - {f_m}^2) \quad (5)$$

where

$$f_m = \frac{c_0}{2\pi}\sqrt{\frac{\rho_0}{m_S d_m}} \quad (6)$$

is the resonance frequency of the absorber.
The parameters used in the simulation are $m_S = 10\ \mathrm{kg/m^2}$, $d_m = 0.14\ \mathrm{m}$ and $r_m = 15 z_0$ resulting in the resonance frequency of $f_m = 50.6\ \mathrm{Hz}$. In Fig. 1, the corresponding dip in the reflection coefficient and peak in the absorption coefficient can be seen at the resonance frequency. The reflection coefficient used in RTS for this BC is obtained by inserting Eq. (4) into Eq. (3).

2.3. Extended-reaction boundary

A layered structure of the boundary leads to the extended-reaction BC. In our case we use a $d_p = 5\ c\mathrm{m}$ thick layer of porous material covering a perfectly rigid wall.
An empirical model of rigid-frame porous materials was introduced by Delany and Bazley in 1970s [28]. The model was later modified and generalized by Miki [22] and is today known as the Delany-Bazley-Miki model. In our implementation, we follow its recent description by Yasuda et al. [29].

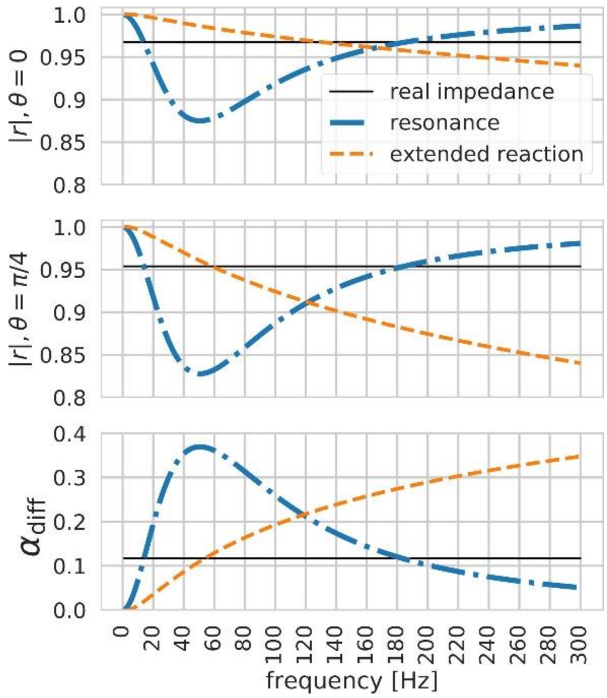

Fig. 1. Absolute values of the reflection coefficients r(θ) for the real impedance, resonance and extended-reaction BCs used in the simulation, for incidence angles θ=0 (top) and θ=π/4 (middle). Bottom: the corresponding diffuse sound fiel absorption coefficient.

In this model, the specific impedance of the bulk porous material z_p and the wavenumber k_p (dispersion relation) are given by

$$\begin{aligned} z_p &= z_0 g_z\left(\frac{f}{\sigma}\right) \\ k_p &= k g_k\left(\frac{f}{\sigma}\right) \end{aligned} \quad (7)$$

where σ $[\mathrm{N}\frac{\mathrm{s}}{\mathrm{m}^4}]$ is the linear specific airflow resistivity and the functions $g_z(x)$ and $g_k(x)$ are

$$\begin{aligned} g_z &= 1 + a_z x^{q_z} - j b_z x^{q_z}, \\ g_k &= 1 + a_k x^{q_k} - j b_k x^{q_k}, \end{aligned} \quad (8)$$

with the constants $a_z = 0.07$, $b_z = -1.07$, $q_z = 0.632$, $a_k = 0.109$, $b_k = -0.160$, $q_k = 0.618$.
The boundary impedance of such an extended-reaction boundary, formed by a rigid wall covered with a layer of the described porous material with thickness d_p, can be shown to be [29]

$$z_e(f,\theta) = -j z_0 g_z\left(\frac{f}{\sigma}\right)\frac{g_k\left(\frac{f}{\sigma}\right)}{\sqrt{{g_k}^2\left(\frac{f}{\sigma}\right) - \sin^2\theta}}\ \mathrm{x}$$
$$\mathrm{x}\ \cot\left[\frac{2\pi f\, d_p}{c_0}\sqrt{{g_k}^2\left(\frac{f}{\sigma}\right) - \sin^2\theta}\right] \quad (9)$$

and depends on the frequency f as well as on the angle of incidence θ. The reflection coefficient used in RTS for this

BC is obtained by inserting Eq. (9) into Eq. (3). To complete the picture, $\sqrt{g_k{}^2\left(\frac{f}{s}\right)-\sin^2\theta/g_k} = \cos\theta'$, where θ' is the (complex) angle of refraction in the porous layer.
The value $\sigma = 500\ \mathrm{N}\frac{\mathrm{s}}{\mathrm{m}^4}$ was used in the simulation, which is relatively low in comparison to typical materials [27]. The rather low value was chosen to contain the diffuse-field absorption coefficient of all BCs in the same range. It can be seen on Fig. 1 that in the considered frequency range the reflection coefficient monotonically decreases while the absorption coefficient monotonically increases with frequency.

3. RTS METHOD

The RTS method resides on the semiclassical approximation of quantum mechanics and in our previous publication [20] we have demonstrated that this concept can be transferred also to acoustics. The link here is the amplitude (Helmholtz) equation, which is identical for the acoustic wave equation and the Schrödinger equation of quantum mechanics. The resulting acoustic RTS method is a frequency domain method, the main advantage of which is that it yields directly the Helmholtz equation Green's function G of the room.
From the technical perspective it is a ray-tracing method, where sound rays are propagated from the source $\boldsymbol{r}_0$ in random directions, upon hitting a boundary they are reflected according to reflection rules, and are in the end summed up in a point (region) of interest. In our case, the rays are emitted in random directions with isotropic probability distribution. At the boundary they are specularly reflected and the pressure amplitude factor changes as defined by Eq. (2), with the reflection coefficient r corresponding to the BC of choice.
The segments of a multiply reflected ray constitute a trajectory. If a trajectory crosses the observation region centered at $\boldsymbol{r}$, it qualifies as a path, i.e., a valid connection between the source and the observation region. The Green's function G is numerically constructed as

$$\mathrm{G}(\boldsymbol{r},\boldsymbol{r}_0,\mathrm{k}) = \frac{1}{\pi R^2 N}\sum_l^L B_{l,i} d_l \exp[jkd_l] \tag{9}$$

where

- N is the total number of sound rays emitted from the point souce at $\boldsymbol{r}_0$,
- R is the radius of the spherical observation region centered at $\boldsymbol{r}$,
- R is the total number of paths l with lengths d_l, that are identified by the simulation. d_l is computed as the sum of lengths of piecewise straight sections of each ray running from the source to the observation region,
- $B_{l,i}$ is the complex amplitude of the sound ray of path l after i-th reflection.

The factord_l represents the density of paths for the three-dimensional case of flat or piecewise flat boundaries, where (de)focusing effects are absent [20].

4. RESULTS AND DISCUSSION

The dimensions of the room are $a \times b \times c = 4.215\ \mathrm{m} \times 3.647\ \mathrm{m} \times 3\ \mathrm{m}$ as in our previous study [20]. There we showed that the method works for any position in the room by computing G_p in 630 simulation points. Nevertheless, to exclude that any conclusions would be based on the particularity of a chosen position, the current simulation was performed for two pairs of source/observation points, Fig. 2, designated as corner and inner positions.

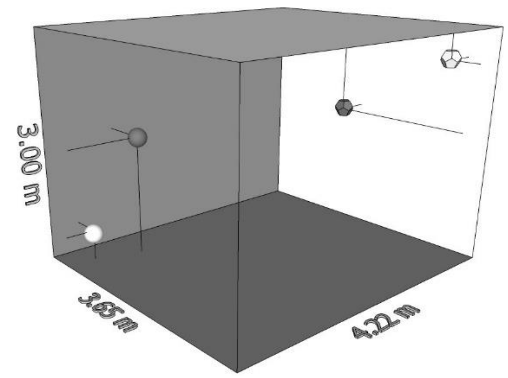

Fig. 2. A sketch of the room with sound sources (dodecahedrons) and observation points (spheres) for the two studied source/observation pairs. The corner positions (white) are situated in diagonally opposite corners 0.402 m away from each wall, while the inner positions (gray) are at $\boldsymbol{r}_0 = (3.6, 1.8, 1.1)\ \mathrm{m}$ and $\mathbf{r} = (1, 0.6, 1.6)\ \mathrm{m}$. In case of the mixed BC, the floor (dark gray) is imposing the real impedance BC, the ceiling and one of the walls (light gray) the extended-reaction BC, while the remaining walls (transparent) are imposing the resonance BC.

The number of modeled reflections per ray was set to $M = 100$, the number of emitted sound rays was $N = 52\,428\,800$ and the size of the observation region was $R = 0.2$ m. The simulation parameters were determined empirically, such that a further increase of M, N, and a decrease of R had no significant influence on the results. Without parallelization, this simulation would be running for approximately 4 days on a single-core processor of a desktop computer (no code optimization). In our case the code was parallelized and was running on a cluster. We however emphasize that practically valuable results are obtained already with drastically less rays and reflections, reducing the computational resources to a fraction.

Four BCs were tested: real impedance, resonance, extended reaction and mixed. In the first three cases the same BC is applied to all boundaries (homogeneous BC), whereas in the mixed case the three BC are distributed as shown in Fig. 2.

The extended BC was implemented in COMSOL by defining a porous material layer covering a perfectly rigid boundary. The porous material is already implemented into COMSOL in form of several poroacustic models. In our case we used the same model (Delany-Bazley-Miki) and flow resistivity as for RTS. Such an implementation into COMSOL means covering a perfectly rigid boundary by a layer of fluid material characterized by Eq. (7). If one first calculates the impedance and then the plane wave reflection coefficient of such boundary, as is done in Eqs. (9) and (3), one gets exactly the reflection coefficient used in RTS. Thus, the RTS and FEM implementations of the extended-reaction BC are equivalent.

The pressure response $G_p = \sqrt{8\pi\rho_0 c_0 P}G$ was calculated with both methods at the same frequencies in 0.05 Hz steps up to 300 Hz. In COMSOL the finite element meshing is done automatically with tetrahedrons and the grid spacing is not fixed. We have additionally set the maximum allowed mesh spacing to 0.34 m, which grants a minimum of approximately 6 mesh points in the studied frequency bands. Empirically, 6-10 mesh points per wavelength are recommended in case of a fixed mesh [30]. An additional verificatory simulation with a much finer mesh did not deliver any observable changes.

In Fig.3, the magnitudes of the pressure responses obtained with RTS and FEM for the four BCs and both positions are presented in dB scale up to 300 Hz. We observe the following.

- In most cases the peaks and dips of G_p coincide well in frequency, level and width. The agreement is remarkable and leads to the conclusion that the RTS method correctly models the Green's function for all studied BCs. The observed peak-to-valley range is larger in comparison to the responses modeled by some other phased geometrical methods [14-16] which are mainly below 30 dB. Nevertheless we stress that it is impossible to make a fair comparison with other results as the peak-to-valley range also depends on the amount of absorption in the room which was different in the mentioned studies.
- A general exception exists for the lowest room modes (the peaks below 70 Hz) the magnitude of which is slightly but systematically underestimated by RTS. This phenomenon was observed and discussed already in the previous study [20] and seems to be an inherent feature of the semiclassical approximation that does not depend on the BC. In comparison with responses obtained by some other phased geometrical methods for the lowest modes e.g. Refs. [12,14,15], this phenomenon is a drawback of the RTS method. The mentioned studies also report improvement when applying spherical reflection coefficients. In this aspect, RTS is different as it is based on plane waves by definition, and thus on plane wave reflection coefficients.
- A noisy behavior (random, stochastic error) of RTS can be observed in frequency zones without prominent peaks and dips of G_p but with a low absorption α_{diff} at the same time. Note such a zone around 250 Hz for the resonance BP ($\alpha_{\mathrm{diff}} \approx 0.08$) in the corner position.
- A noisy behavior of RTS for the extended-reaction BC is observed in the frequency range below 40 Hz, which is due to lack of absorption (there we have $\alpha_{\mathrm{diff}} < 0.05$, Fig. 1) and would disappear if more reflections were modeled. As this noise is present only for very low absorption, it is not perceived as a practical limitation of the RTS method. Similar convergence issues were previously reported by other authors in case of low absorption (see e.g. [16]). It is impossible to generally compare our results with results obtained by other phased geometrical acoustic methods as each was conducted at very different rate of absorption.

For the mixed BC, in the corner position the agreement between both methods is equally good as for the other BCs and no peculiarities are observed. In contrast, in the inner position deviations are severer. In particular the dips between 160 Hz and 250 Hz do not coincide.

If we observed a discrepancy in the response that increases with frequency, it could be related to the error of calculating the propagation length of the paths. As the error is observed only in a limited frequency range this explanation is not plausible. As we also have not observed any improvements by increasing the number of rays, we furthermore conclude that the error is not related to the statistical sensitivity of the method at high frequencies. This phenomenon is interesting as it is not systematic, i.e., it occurs only in one position and in a limited frequency range. Performing a FEM simulation on a finer mesh on one hand, and testing the influence of RTS parameters (number of reflections, number of emitted sound rays, radius of the observation region) on the other did not bring any noteworthy improvement.

At this stage we conclude that this peculiarity should be systematically addressed in further more specific studies - by testing more positions and more variety in the distribution of different BCs.

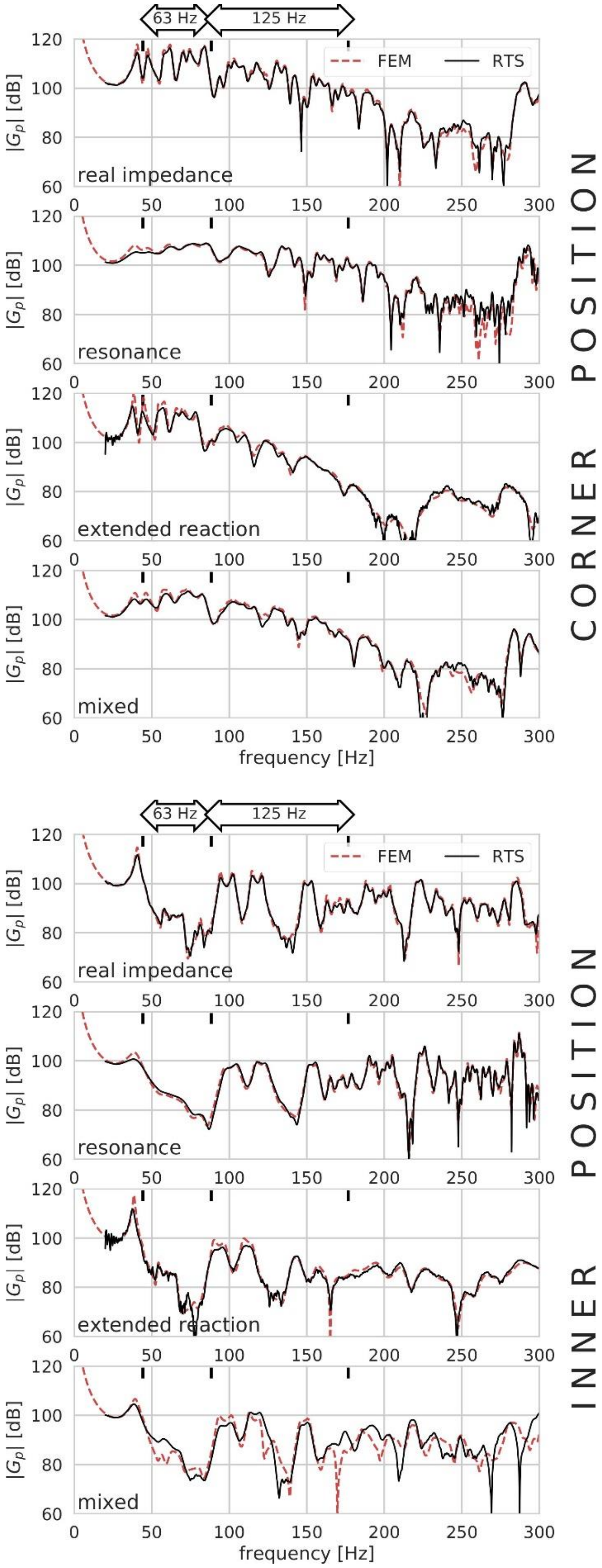

Fig. 3. The absolute value G_p of the pressure response modeled by RTS (sold black) and FEM (dashed red) for the corner (top four graphs) and inner (bottom four graphs) positions and the four BCs as indicated.

5. CONCLUSION

We have performed a stark test of the acoustic RTS (ray-tracing semiclassical) method for a wide selection of realistic boundary conditions, confronting it face-to-face with the results of a full wave FEM method which is considered accurate in the studied lower frequency range.

We have shown that the pressure responses obtained by RTS and FEM agree in their normalization, i.e., there is no scaling uncertainty in the RTS-computed response. Moreover and most importantly, for the majority of the studied cases the peaks and dips of the spatially dependent responses coincide remarkably well in frequency, level and shape. The agreement is systematic for all studied BCs with the exception of the mixed BC in the inner position, where in a limited frequency range the dips in the response do not coincide.

Some further particularities of the RTS method were exposed - the underestimation of the peaks corresponding to the lowest modes and the presence of noise in case of low G_p values as well as for highly reflective boundaries. Generally we can conclude that for the case of the rectangular room and the tested BCs, RTS is an adequate method for modeling the spatially dependent pressure response.

In conclusion, our study validates the RTS method for a set of practically relevant boundary conditions in rectangular rooms, thereby further promoting it for low-frequency geometrical acoustic modeling. Nevertheless, the RTS method was tested objectively and results were compared to competitive phased geometrical methods when possible. Some uncertainties in the case of inhomogeneous BCs were revealed, which should be systematically addressed in the future. Future studies should also validate and characterize the RTS method for general room geometries, including in particular (de-)focusing effects of curved boundaries.

4. REFERENCES

[1.] G. Naylor, **Odeon - another hybrid room acoustical model**, *Appl. Acoust.,* 38(1993).

[2.] B.-I. Dalenbäack, **A new model for room acoustic prediction and auralization**, *Ph.D. thesis,* Chalmers University of Technology (1995).

[3.] A. Krokstad, S. Strom, S. Sørsdal, **Calculating the acoustical room response by the use of a ray tracing technique,** *J. Sound Vibr.,* 8 (1968) 118-125.

[4.] J. B. Allen, D. A. Berkley, **Image method for eciently simulating smallroom acoustics**, *J. Acoust. Soc. Am.,* 65 (1979) 943-950.

[5.] M. Vorländer, **Computer simulations in room acoustics: Concepts and uncertainties**, *J. Acoust. Soc. Am.,* 133 (2013) 1203-1213.
[6.] L. Savioja, U. P. Svensson, **Overview of geometrical room acoustic modeling techniques**, *J. Acoust. Soc. Am*., 138 (2015) 708-730.
[7.] A. Pompei, M. A. Sumbatyan, N. F. Todorov, **Overview of geometrical room acoustic modeling techniques**, *Acoust. Phys*, 55 (2015) 708-730.
[8.] G. I. Koutsouris, J. Brunskog, C.-H. Jeong, F. Jacobsen, **Combination of acoustical radiosity and the image source method**, *J. Acoust. Soc. Am.,* 133(2013) 3963-3974.
[9.] G. Marbjerg, J. Brunskog, C.-H. Jeong, E. Nilsson, **Development and validation of a combined phased acoustical mradiosity and image source model for predicting soundfields in rooms**, *J. Acoust. Soc. Am.,* 138 (2015) 1457-1468.
[10.] J. S. Suh, P. A. Nelson, **Measurement of transient response of rooms and comparison with geometrical acoustic models**, *J. Acoust. Soc. Am.,* 105(1999) 2304-2317.
[11.] M. Vorländer, **Simulation of the transient and steady state sound propagation in rooms using a new combined sound particle - image sourcealgorithm**, *J. Acoust. Soc. Am.,* 86 (1989) 172-177.
[12.] C.-H. Jeong, I. Jeong-Guon, J. Rindel, **An approximate treatment of reaection coecient in the phased beam tracing method for the simulation of enclosed soundfields at medium frequencies**, *Applied Acoustics,* 69 (2008) 601-613.
[13.] S. M. Dance, J. P. Roberts, B. M. Shield, **Computer prediction of sound distribution in enclosed spaces using an interference pressure model**, *Applied Acoustics,* 44 (1995) 53-65.
[14.] M. Aretz, P. Dietrich, M. Vorländer, **Application of the mirror source method for low frequency sound prediction in rectangular rooms**, *Acta Acust. united Ac.,* 100 (2014) 306-319.
[15.] Y. W. Lam, **Issues for computer modelling of room acoustics in non-concert hall settings**, *Acoust. Sci. & Techn.,* 26 (2005) 145-155.
[16.] C.-H. Jeong, J.-G. Ih, **Effects of source and receiver locations in predicting room transfer functions by a phased beam tracing method**, *J. Acoust. Soc. Am.,* 131 (2012) 3864-3875.
[17.] M. A. Boucher, B. Pluymers, W. Desmet, **Interference effects in phased beam tracing using exact half-space solutions**, *J. Acoust. Soc. Am.,* 140(2016) 4204-4212.
[18.] M. Hodgson, A. Wareing, **Comparisons of predicted steady-state levels in rooms with extended- and local-reaction bounding surfaces**, *J. Sound Vib.,* 309 (2008) 167-177.
[19.] A. Wareing, M. Hodgson, **Beam-tracing model for predicting soundfields in rooms with multilayer bounding surfaces,** *J. Acoust. Soc. Am.,* 118 (2005) 2321-2331.
[20.] R. Prislan, G. Veble, D. Svenšsek, **Ray-trace modeling of acoustic green's function based on the semiclassical (eikonal) approximation,** *J. Acoust. Soc. Am.,* 140 (2016) 2695-2702.
[21.] M. Schröder, **Die Statistischen Parameter der Frequenzkurven von Grossen Räumen**, *Acta Acust. united Ac.,* 4 (1954) 594-600.
[22.] Y. Miki, **Acoustical properties of porous materials. generalizations of empirical models**, *J.Acoust.Soc.Jpn.(E),* 97 (1990) 19-24.
[23.] M. Vorländer, **International round robin on room acoustical computer simulations**, *Proceedings of the 15th International Congress on Acoustics,* Trondheim, Norway, 1995, pp. 689-692.
[24.] R. Prislan, J. Brunskog, F. Jacobsen, C.-H. Jeong, **An objective measure for the sensitivity of room impulse response and its link to a difuse soundfield**, *J. Acoust. Soc. Am.*, 136 (2014) 1654-1665.
[25.] H. Kuttruf, ***Acoustics: An Introduction***, Taylor & Francis, New York, NY,USA pp. 99-102, 2007.
[26.] F. Fahy, ***Foundations of Engineering Acoustics***, Elsevier Academic Press,London, UK pp. 156, 2001.
[27.] T. J. Cox, P. D'Antonio, ***Acoustic Absorbers and Di users: Theory, Design and Application***, Taylor & Francis, New York, NY, USA p. 208, 2009.
[28.] M. E. Delany, E. N. Bazley, **Acoustical properties of porous absorbent materials**, *Applied Acoustics*, 3 (1970) 105-116.
[29.] Y. Yasuda, S. Ueno, H. Sekine, **A note on applicability of locally-reacting boundary conditions for delany-bazley type porous material layer backed by rigid wall**, *Acoust. Sci. Tech.,* 36 (2015) 459-462.
[30.] S. Marburg, B. Nolte, ***Computational Acoustics of Noise Propagation in Fluids - Finite and Boundary Element Methods***, Springer-Verlag, Berlin, Heidelberg pp. 310, 2008.

8th Congress of the Alps Adria Acoustics Association
Zagreb, Croatia
20 – 21 September 2018

Hrvatsko akustičko društvo
HAD
Acoustical Society of Croatia

OPTIMAL REVERBERATION TIME

Siniša Fajt, Miljenko Krhen, Fabijan Žunić

University of Zagreb, Faculty of Electrical Engineering and Computing
Unska 3, 10000 Zagreb, Croatia

Abstract: *The necessity of determining the optimum reverberation time in relation to the purpose of the room appears as a problem during the design and modeling of room acoustics. The paper discusses different recommendations for determining the optimum reverberation time, which are analyzed graphically and numerically. Since reverberation time is a frequency-dependent function, the optimal frequency response characteristic is analyzed as well due to the frequency dependence of the absorption coefficient. Based on the so proposed criteria for selecting the optimum reverberation time value and its optimal frequency characteristic, it is possible to adjust the room and building acoustics in order to obtain optimal values of the acoustic quality of room.*

Key words: Reverberation time, Room acoustic, Absorption coefficient, Frequency characteristic

1. INTRODUCTION

Reverberation time is the measure of specific part of sound process called reverberation. Duration of muting to the absolute threshold of hearing depends on multiple factors:

a) Room volume - V, volume defines sound absorption in the air and contribution of direct and reflected sound
b) Room shape - Shape determines number and form of reflective surfaces. That defines trajectory and time interrelation between direct and reflected sound
c) Absorption of walls in the room - alfa(f), This factor determines amplitude contribution of reflected sound and phase ratio depending on whether the wall is solid or soft

Considering the fact human ear can hear reverberation, which is directly related to room characteristics, measure called reverberation time is defined. Reverberation time is defined as the time needed for the sound to be lowered for 60 dB. Therefore, sound pressure (intensity or energy density) needs to decrease for 60 dB. It is important to mention that reverberation time is frequency dependent value because of frequency dependence of the absorption in the air and especially in the walls of the room. According to this, reverberation time can be expressed in three ways:

a) as average reverberation time, while considering it is expressed with average absorption coefficient in the specific frequency range (usually center frequencies)
b) as reverberation time on 1000 Hz, while considering it is expressed with absorption coefficient on 1000 Hz
c) as frequency characteristic of reverberation time, as complete information of reverberation on specific frequency.

Reverberation time theory was developed by Wallace Clement Sabine (1923.)

1.1. Reverberation time - Sabine (a<2)

$$T_r(f)=0.161\cdot\frac{V}{a(f)\cdot S},\ [\mathrm{s}] \qquad (1.1.)$$

This equation gives wrong results if the average absorption coefficient is greater than 0.2 and is only applicable for rooms with long reverberation time.

1.2. Reverberation time – Eyring

As Sabines equation works only for certain rooms, Eyring came up with the formula which helps us calculate reverberation time in rooms with bigger average absorption coefficient.

$$T_r(f)=0.161\cdot\frac{V}{-S\cdot\ln(1-\alpha(f))},\ [\mathrm{s}] \qquad (1.2.)$$

Considering the attenuation caused by air which appears on higher frequencies:

$$T_r(f)=0.161\cdot\frac{V}{4\cdot m(f)\cdot V-S\cdot\ln(1-\alpha(f))},\ [\mathrm{s}] \qquad (1.3.)$$

Where the *m* factor is sound absorption coefficient in the air which depends on relative humidity of the air and frequency.

2. T_{r20}, T_{r25}, T_{r30}, T_{r35}

For the purpose of measurement and estimation of reverberation time in the conditions where 60 dB dynamics cannot be achieved, following parameters were introduced: T_{r20}, T_{r25}, T_{r30}, T_{r35}. These parameters indicate estimation of reverberation time based on decreasing sound levels from -5 to -20 dB, -25 dB, -30 dB or -35 dB extrapolated on the fall of 60 dB.

$$T_r(f)=60\cdot\left(\frac{\Delta L(f)}{\Delta t}\right)^{-1},\ [\mathrm{s}] \qquad (1.4.)$$

Kuttroff has recommended extrapolation area of reverberation time from -5 to 35 dB [1]. Recommended frequencies on which measurement of reverberation time is needed are: 125, 250, 500, 1000, 2000 Hz [2]. For concert halls Jordan had recommended optimal values of reverberation time from 1.4 to 8 seconds [3]. Cremer and Muller had recommended optimal values of reverberation time for concert halls ranging from 1.6 to 2.2 seconds [4]. Beranek had recommended values based on his research ranging from 1.7 to 2 seconds [5]. Bradley, however, recommended reverberation time ranging from 1.2 to 3.4 seconds for the mid frequencies (500 - 1000 Hz) depending on the music genre [6]. Based on various subjective testing of different authors, impact on subjective parameters of room acoustics was determined: Reverberance and Liveness.

3. OPTIMAL REVERBERATION TIME

Optimal reverberation implies following:

- optimal reverberation time considering the volume and purpose of the room
- optimal frequency characteristic of reverberation time
- optimal rise and fall characteristic of sound intensity in the room
- optimal reverberant-to-early sound ratio in the room

3.1. Optimal reverberation time considering the volume and purpose of the room

When it comes to the purpose of the room they can be divided as follows: Rooms designed for speech transmission and rooms designed for music transmission. According to that, proper acoustic parameters of the room intended for speech are defined by speech intelligibility. Dependence of syllable intelligibility on reverberation time was defined by Knudsen as seen on Figure 1.

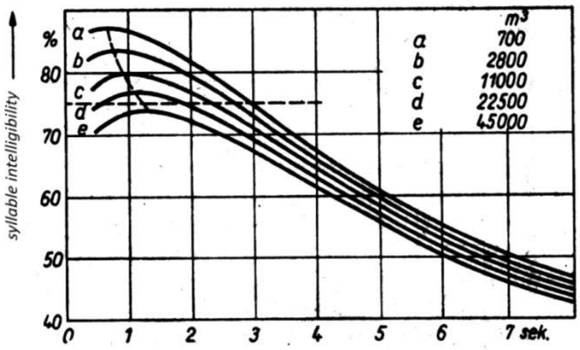

Figure 1. Percentage of syllable intelligibility depending on reverberation time for the rooms with different volumes. As seen in figure, syllable intelligibility of 75% (dashed horizontal line) cannot be achieved in the room indicated by the e) curve.

Therefore, reverberation time in smaller rooms has to be less than one second, and more than one second in larger rooms. For the room of 1100 m^3, Knudsen calculated dependence of syllable intelligibility on reverberation time for different *orators.* That calculation resulted in following cognition: Reverberation time has to be longer for quiet voice. When it comes to loudspeakers, reverberation time strives towards zero, but the fact that the human ear cannot hear reverberation time lower than 0.35 seconds should be considered, as that is its own reverberation time [7]. Optimal reverberation time for speech ranges from 0.7 to 1.4 seconds depending on the volume of the room from 100 m^3 to 50 000 m^3. This can be visible in the Figure 2 which is in accordance with the theoretical optimal reverberation time for speech. Due to the slow membrane response in the ear, sounds that are coming in the time interval lower than 0.1 seconds are received as single sound. If the time constant is bigger than 0.1 seconds sounds are heard individually. While one part of the reflecting sound, coming to the ear 0.1 seconds after direct sound, benefits the loudness, the other part of the sound which comes after 0.1 seconds is blending with the new sound and is considered as noise. Analyses have shown reduction of syllable intelligibility in dependence of noise loudness:

- if the noise is equally loud as useful sound - syllable intelligibility is 60%
- if the noise loudness is 4 phons lower than loudness of useful sound - syllable intelligibility is 85%
- if the noise loudness is 8 phons lower than loudness of useful sound - syllable intelligibility is 94%

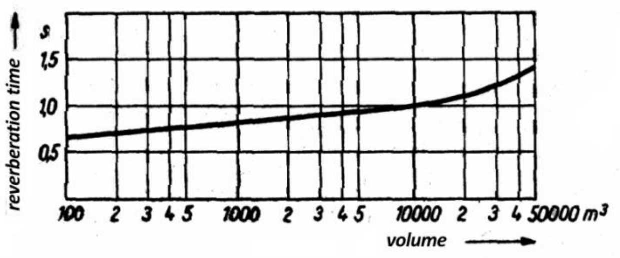

Figure 2. Optimal reverberation time for speech in dependence of room volume

According to that, loudness of unwanted reflected sound should be 4 - 8 phons lower than loudness of useful sound. If that decrease in volume level has to last less than 0.1 seconds, optimal reverberation time in the rooms for speech has to range from 0.75 (0.1*60/8) to 1.5 (0.1*60/4) seconds.

Unlike speech where the main criterion is speech intelligibility, when it comes to music, reverberation is aesthetic problem. In general, there are some factors that affect the amount of reverberation time:

- music taste
- music genre
- orchestra composition
- interpretation of the conductor
- skills of the musicians
- music education (or experience) of the listener, tradition related to the acoustic characteristics of the rooms designed for music listening

Statistical analyses have contributed to the determination of optimal reverberation time in dependence of room volume as shown in figure 3 [7].

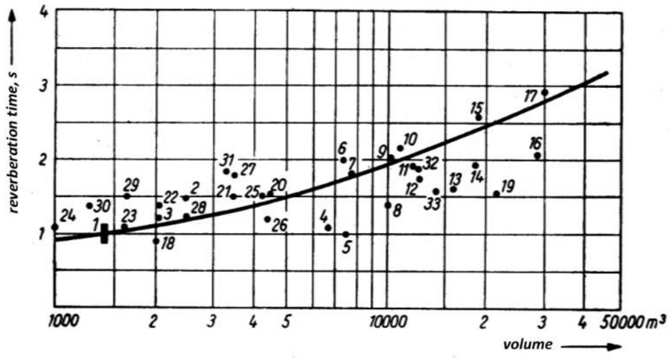

Figure 3. Reverberation time on center frequencies in dependence of room volume of halls acoustically rated as excellent. Charted curve shows reverberation time proportional to third root of volume. Numbers next to dots are referring to halls: 1 - studio number 3 in Danish radio-home (reverberation time variable); 2 - studio number 2 in Danish radio-home; 3 - Altes Gewandhaus, Leipzig; 4 - Beethovensaal, Berlin; 5 - Staatsoper, Berlin; 6 – Gewandhaus, Leipzig; 7 – Halsingborg Concert Hall; 8 – Covent Garden, London; 9 – St. Margaret's, London; 10 – Festspielhaus, Bayreuth; 11 – Big hall in The Gothenburg Concert House; 12 – Queen's Hall, London; 13 – Konzerthaus, Vienna; 14 – Filharmonija, Berlin; 15 – St. Thomas Church, Leipzig; 16 – Eastman Theatre, Rochester; 17 –St. Michael's Church, Hamburg; 18 – Stenhammersalen, Gothenburg; 19 – Salle Pleyel, Paris; 20 – studio number one, Zürich; 21 – studio number one, Geneva; 22 – studio number one, Basel; 23 – studio number one, Lugano; 25 – Kilburn Hall, Rochester; 26 – Test Hall, Cambridge; 27 – Conservatorium, Leipzig; 28 – Aeollian Hall, London; 29 – Holywell Concert, Oxford; 30 – Entrence Hall to Balls Park, Herts; 31 – David Memorial Hall, Uppingham; 32 – Free Trade Hall, Manchester; 33 – Coulston Hall, Bristol.

Specific dependence of reverberation time on room volume can be noticed and calculated by excluding the extreme values that are obvious anomaly. With the following assumptions:

- acoustic quality is defined by the ratio of direct and reflected sound which excludes the fact that the result depends on geometric features of the room
- that ratio is constant for each type of music
- distance from source - receiver (listener) grows proportionally with the length of each hall

it is calculated that the reverberation time is $\sqrt[3]{V}$ [7].

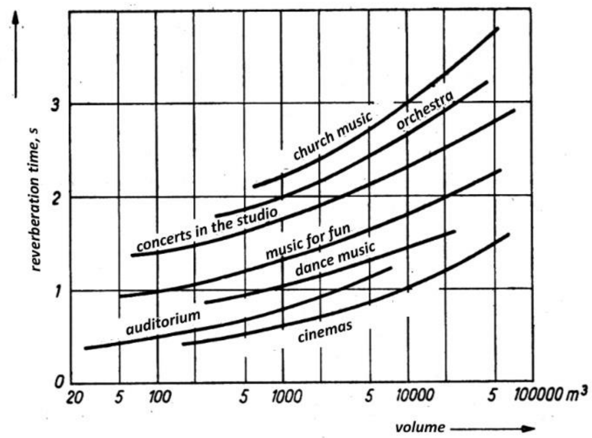

Figure 4. Dependence of optimal reverberation time on volume on center frequencies for different types of music.

According to the shape of the curve, direct impact of volume on optimal reverberation time considering just its purpose can be seen. Considering the volume and purpose of the room from various authors, certain similarity can be noticed by comparing various types of demonstrations of optimal reverberation time. Differences in that comparison are in absolute values and details of elaboration of certain room. More detailed view of optimal reverberation time in dependence of purpose and volume is seen on figure 5. [8].

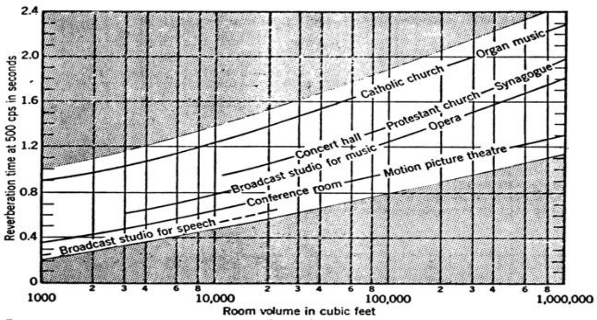

Figure 5. Optimal reverberation time for rooms of different volumes and purposes. (According to Bolt, Beranek and Newmann)

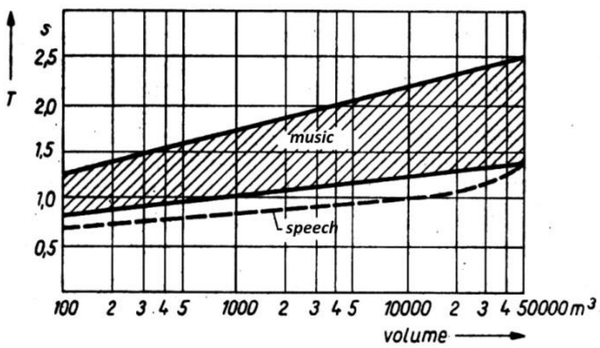

Figure 6. Optimal reverberation time on center frequencies in dependence on volume, according to Knudsen [7].

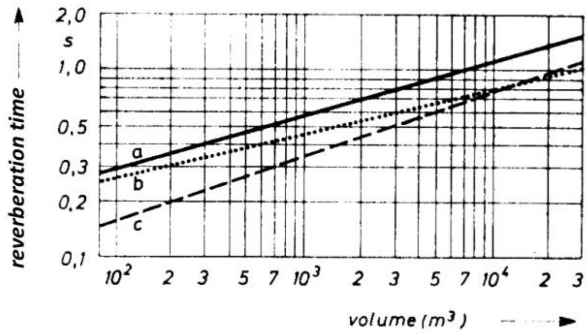

Figure 7. Optimal reverberation time for television studios with maximum reverberation time between 500 and 2000 Hz (Burd, Gilford and Spring, 1966). Curve (a) indicates the longest acceptable reverberation time, curve (c) is the shortest reverberation time that can be achieved under certain conditions.

Matras has discovered following dependence of reverberation time on volume while considering purpose of the room:

- rooms for sacred music: $T_{opt.} = \frac{1}{10} \cdot \sqrt[3]{V}$
- concert halls: $T_{opt.} = \frac{9}{100} \cdot \sqrt[3]{V}$
- theaters and auditoriums: $T_{opt.} = \frac{7.5}{100} \cdot \sqrt[3]{V}$

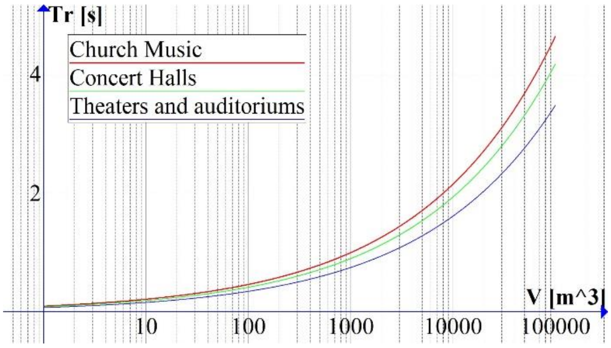

Figure 8. Optimal reverberation time according to Matras

While determining reverberation time for rooms intended for music reproduction, already recorded reverberation should be taken into consideration. In the rooms for reproduction or audio mixing, reverberation should be minimized, so it would not increase already recorded reverberation. In the big halls, such as cinema, problem of equal sound distribution on all seats appears. In the other words, sound is amplified by the reverberation. Because of that, certain amount of reverberation is necessary for reproduction in big halls. Dependence of optimal reverberation time on volume for cinema halls is seen on figure 9. [7].

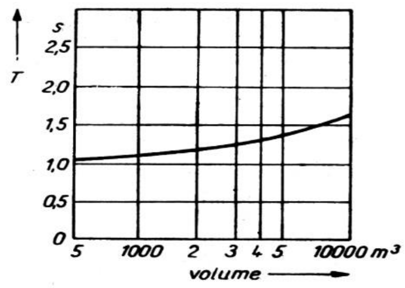

Figure 9. Optimal reverberation time in dependence on volume for cinemas

For calculation of optimal reverberation time following expression can be used [9]:

$$T_{60}=K(0.0118V^{1/3}+0.1070) \qquad (1.5.)$$

where constant K depends on room purpose:
- K=4 – for speech
- K=5 – for orchestral music
- K=6 – for choir and rock music

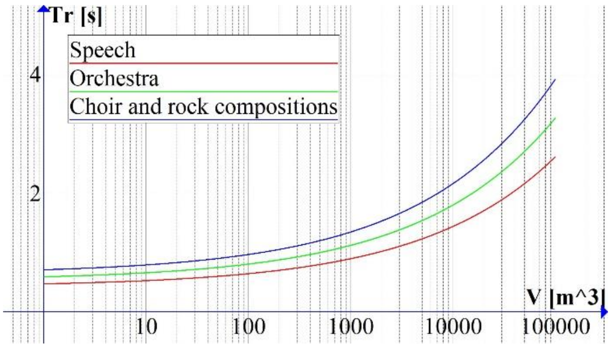

Figure 10. Optimal reverberation time according to Crocker

As recommended, on octave frequencies lower than 250 Hz optimal reverberation time gradually increases. According to demands of Nordic public radio distribution corporations [10] optimal reverberation time for music studios and reference rooms can be calculated with the following formula:

$$T_m = T_0\sqrt{\frac{S}{S_0}} \pm 0.05\,,\ [\mathrm{s}] \qquad (1.6.)$$

where the parameters are:

S_0 = 60 m², T_0 = 0.35 s, S – floor area of the room

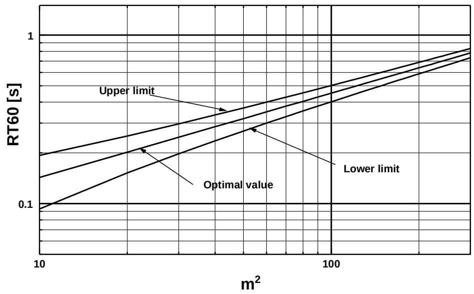

Figure 11. Optimal reverberation time for music studios and reference rooms on the floor area according to demands of Nordic public radio distribution corporations.

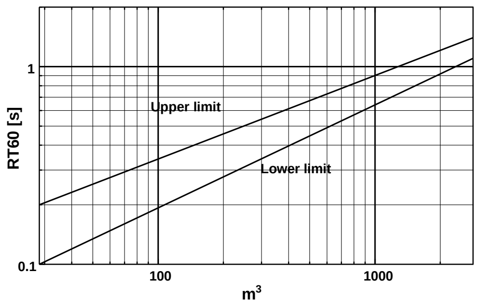

Figure 12. Acceptable upper and lower limits of optimal reverberation time (on 500 Hz) depending on room volume for cinemas according to Dolby demands [11].

4. FREQUENCY CHARACTERISTIC OF REVERBERATION TIME

Optimal reverberation time is usually expressed for center frequencies or for the following frequencies: 500 Hz, or 512 Hz. Various authors because of different technical and acoustic reasons, recommend various frequency characteristic or limits under which that characteristic should be persistent. Figure 13. [7] displays the curves with frequency characteristics of reverberation time based on researches of various authors.

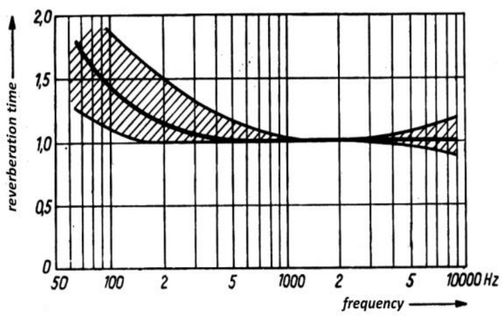

Figure 13. In the drawn area, frequency characteristics are recommended by various authors

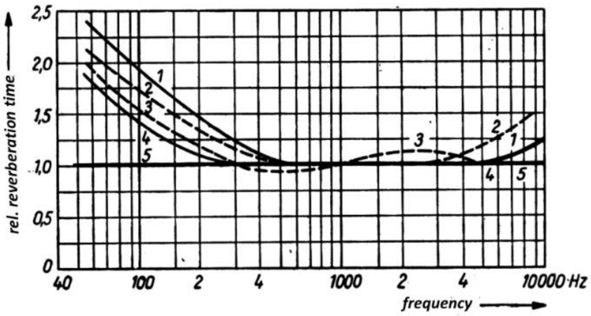

Figure 14. Frequency characteristics of reverberation time according to various authors: 1 – MacNair, 1930.; 2 – Morris and Nixon, 1963.; 3 – Danish radio-home, 1942.; 4 – Rickmann and Heyda, 1940.; 5 – Békésy, 1943.

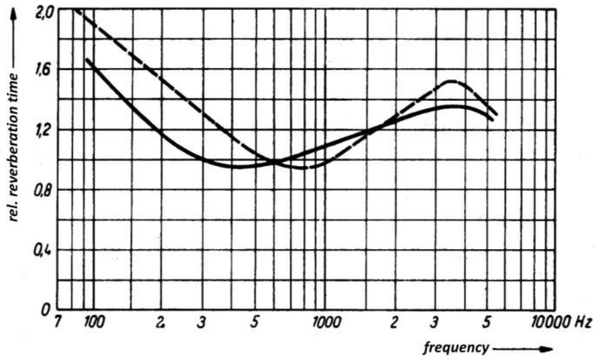

Figure 15. Frequency characteristic of reverberation time in the studio number 3 in Danish radio - home. Solid line represents favorable result, dashed line represents poor result.

It can be noticed that larger reverberation time is needed on low frequencies. Bigger deviation under 500 Hz indicates that reverberation is not critical in that area. In the area from 500 Hz to 2 kHz it can be noticed that even small alterations can have a big impact on acoustic quality. Decreasing of reverberation time above 3 kHz is inevitable and impact of that phenomenon on acoustic quality is not yet discovered. Some studies tend to prove it has good effect on acoustic quality. For frequency characteristic of reverberation time in general it can be stated:

- in small volume speech studios, it is recommended reducing reverberation time on low frequencies
- in studios for entertainment music it is recommended to reduce reverberation time on high frequencies
- in big studios for symphonic music, the rise of frequency characteristic of reverberation time towards lower frequencies should grow proportionally with the size of the hall

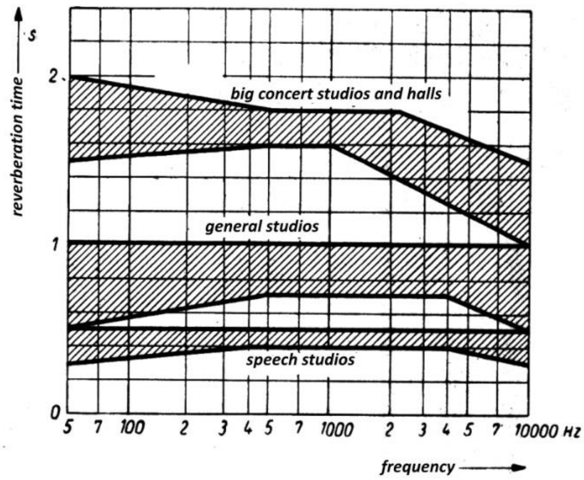

Figure 16. Dependence of reverberation time on frequency according to Beranek

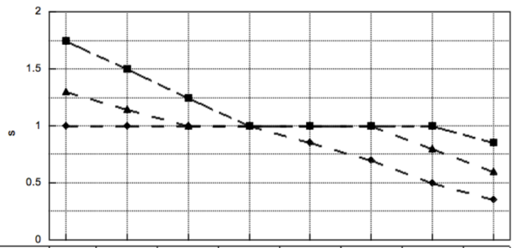

Hz	63	125	250	500	1000	2000	4000	8000
TG	1.75	1.5	1.25	1	1	1	1	0.85
TD	1	1	1	1	0.85	0.7	0.5	0.35
TM	1.3	1.15	1	1	1	1	0.8	0.6

Figure 17. Reverberation time borders for cinemas according to Dolby requirements

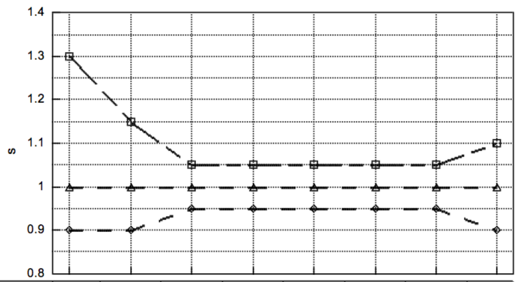

Hz	63	125	250	500	1000	2000	4000	8000
TG	1.3	1.15	1.05	1.05	1.05	1.05	1.05	1.1
TD	0.9	0.9	0.95	0.95	0.95	0.95	0.95	0.9
TM	1	1	1	1	1	1	1	1

Figure 18. Reverberation time borders for music studios according to requirements of Nordic public radio distribution corporations

On figures 17. and 18. following labels were used:

- TG – upper limit
- TD – lower limit
- TM – optimal value

5. CONCLUSION

Various recommendations of optimal reverberation time from different authors while considering the purpose of the room indicates the complexity of its determination. Further standardization based on scientific research containing objective measurement and subjective assessments is necessary. In general, optimal form of frequency characteristic of reverberation time depends on various factors: room volume, music genre, orchestra composition, etc. This paper revealed new insights for the study of optimal reverberation time especially for multimedia presentation rooms and virtual reality in real time.

6. REFERENCES

[1.] H. Kuttroff, “Room Acoustics”, Elsevier Applied Science, London, 1991.

[2.] D. Davis, C. Davis, “Sound System Engineering” 2nd edition, Howard W. Sams & Co., Indianapolis, 1987.

[3.] V. L. Jordan “A Group of Objective Acoustical Criteria for Concert Halls”, Appl. Acoust. 14, 1981.

[4.] L. Cremer and H. A. Muller, preveo T. J. Shultz, “Principles and Applications of Room Acoustics”, Applied Science, London, 1982, Vol 1

[5.] L. L. Beranek, “Concert hall acoustics – 1992.”, J. Acoust. Soc. AM. 92, 1 - 39 ,1992.

[6.] J. S. Bradley, Data from 13 North American Concert Halls, Internal Report No. 688, IRC-CNRC, July 1994.

[7.] T. Jelaković, “Zvuk, sluh, arhitektonska akustika”, Školska knjiga, Zagreb, 1978.

[8.] L. L. Beranek, “Acoustics”, McGraw-Hill Company, New York, Toronto, London, 1954.

[9.] Malcolm J. Crocker, “Encyclopedia of Acoustica”, John Wiley & Sons, Inc., Canada, 1997.

[10.] Tehnical Recommendation from the Nordic Public Broadcasting Corporations, “N 12-A Sound Control Rooms and Listening Rooms”, Second edition, 1992.

[11.] Ioan Allen, “Tehnical Guidelines for Dolby Theatres”, Dolby Labratories Inc, Rev 1.33, 1994.

8th Congress of the Alps Adria Acoustics Association
Zagreb, Croatia
20 – 21 September 2018

AUDIO SIGNAL PROCESSING IN ACOUSTICALLY DIFFERENT ROOMS

Miljenko Krhen, Siniša Fajt, Fabijan Žunić

University of Zagreb, Faculty of Electrical Engineering and Computing
Unska 3, 10000 Zagreb, Croatia

Abstract: *In this article, the influence of different room acoustic treatments on audio signal processing is examined. Impulse response is measured in two different rooms upon which this research is based on. An identical recording was processed in both rooms in the digital audio workstation software AVID Pro Tools. Individual samples and whole recordings were subsequently analyzed in a reference room. After the analysis, a subjective assessment was conducted based on the quality of the recording, followed by a frequency analysis of selected samples from the recording. By adopting the ultimate conclusion on the quality of the recording, the reference room for processing audio signals was simulated in the room acoustics software AFMG EASE.*

Key words: Reverberation time, Measuring impulse response, Signal processing, AVID Pro Tools, AFMG EASE

1. INTRODUCTION

Room acoustics indicates the quality of analog signal transmission in certain environment. Those analog signals contain useful information such as speech (lecture room, church) or music (concert hall, auditorium, studio). Speaking of acoustic characteristics of certain rooms, we can surely declare they are main factor of good transmission and reception of analog signals depending on the purpose of the room. Methods of measurement and projecting rooms with satisfying acoustic parameters are very complicated. The aim of every designer is to accomplish the finest possible transmission between the sound source and the listener. Additionally, the purpose of the room should be taken into consideration. Design of the room for the speech transmission with the focus on the speech intelligibility differs from the design of the room for music editing/listening, which is more complex domain.
Some of the reasons for complexity of designing rooms for music transmission are coverage of almost entire human hearing range (20 kHz), complex signal dynamics, multiple instruments playing at the same time, etc. This is where an issue on how to design a room which satisfies certain acoustic parameters is discussed. When the structure, attributes, form and materials used to build a room are taken into consideration, analyzing and designing a room is very complicated task. As a result of imperfection, which makes music pleasant to listen to, and number of other factors, acoustic parameters can’t be precisely measured and mathematically analyzed. The subjective impression based on proper psycho-acoustic experience has a big role in evaluation of acoustic quality of the room. Objective parameters which determine the acoustic quality of the rooms are: Reverberation Time, Early Decay Time, Room Constant, Hall Radius, Clarity, Center Time, Definition, Reverberant-to-Early Sound Ratio, Support, Relative Level or Strength Index, Tonal Color or Timbre, Temporal Diffusion, Weighted Signal-to Noise Ratio, Speech Transmission Index, Articulation Loss of Consonant, Speech Intelligibility, Useful-to-Detrimental Sound Ratio, Lateral Energy Fraction, Inter-Aural Cross-Correlation Coefficient, Initial Time Delay Gap, Directional Diffusion Index.
This project was focused on measurement of reverberation time and impact of analyzed rooms on subjective evaluation of acoustic quality.

2. MEASUREMENT

For the purpose of determining the better work experience in certain rooms, reverberation time is measured in rooms C-10-13 and C-10-15. Electronic and Acoustic System Evaluation and Response Analysis (EASERA) software was used along with other measuring equipment: Computer, TASCAM USB sound card, Crown XLS1500 class D amplifier, omnidirectional sound source and measuring microphone. Omnidirectional sound source was connected to the output of the amplifier and placed in the middle of the room. Computer was linked to sound card whose output was then linked to amplifier. Measuring microphone was connected to the input of the sound card and placed on the spot where the reverberation time was measured. Following measure signals were used: Continuous variable frequency signal (further referred to as Sweep), continuous signal in which the frequency increases or decreases logarithmically with time (further referred to as Log Sweep), maximum length sequence signal – pseudorandom binary sequence (further referred to as MLS).

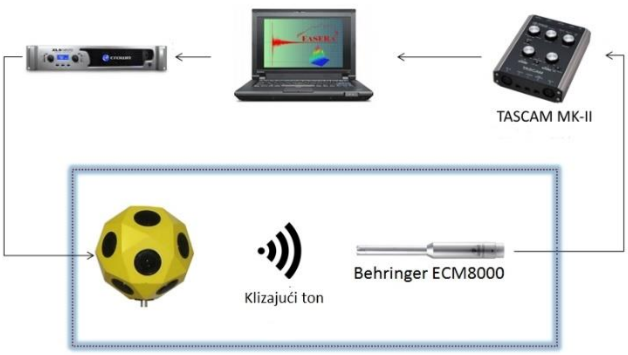

Fig. 1. Principle measurement block scheme

STI	0,485
RaSTI	0,476
Al_{Cons} [%]	12,284

Table 2. STI, RASTI, Al_{Cons} measured with MLS excitement

C_7, dB	C_{50}, dB	C_{80}, dB	C_{35}, dB	D, dB	L_7, dB	L_{50}, dB
- 12,6	- 2,9	- 0,3	- 5	0,34	82,2	90,4
L_{80}, dB	L_{35}, dB	L_{Total}, dB	Center time, ms	ST1, dB	ST2, dB	Arrival time, ms
91,9	88,9	95,1	265	8,3	10	96,65

Table 3. Acoustic quality parameters measured with MLS excitement

2.1. Room acoustic quality parameters for C-10-15

2.1.1. MLS excitement

f, Hz	EDT, s	T10, s	T20, s	T30, s
125	1,97	2,17	2,87	3,82
250	1,33	1,40	1,67	1,67
500	1,64	1,58	1,67	1,51
1000	1,71	1,58	1,55	1,53
2000	1,45	1,59	1,52	1,52
4000	1,38	1,40	1,35	1,46
8000	1,09	0,96	0,99	1,09
250-2k	1,53	1,54	1,60	1,56
500-4k	1,55	1,54	1,52	1,51

Table 1. Reverberation time (1/1 Oct.) measured with MLS excitement

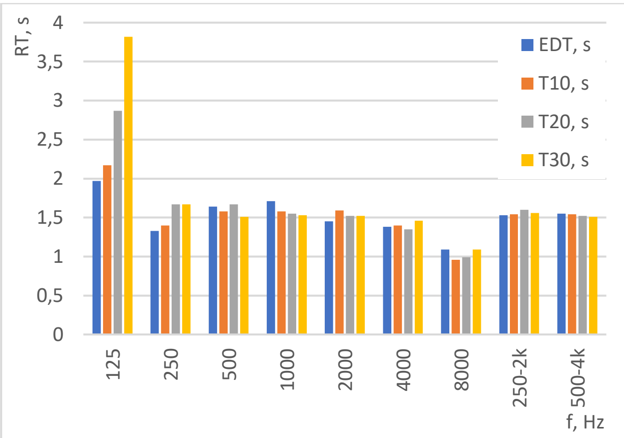

Fig. 2. Graphical representation of reverberation time (1/1 Oct.) measured with MLS excitement

2.1.2. LOG sweep excitement

f, Hz	EDT, s	T10, s	T20, s	T30, s
125	2,19	2,41	2,35	2,33
250	1,42	1,56	1,59	1,57
500	1,51	1,51	1,65	1,58
1000	1,65	1,54	1,55	1,54
2000	1,46	1,61	1,52	1,50
4000	1,42	1,36	1,32	1,30
8000	1,04	1,00	1,00	0,99
250-2k	1,51	1,56	1,58	1,55
500-4k	1,51	1,51	1,51	1,48

Table 4. Reverberation time (1/1 Oct.) measured with LOG sweep excitement

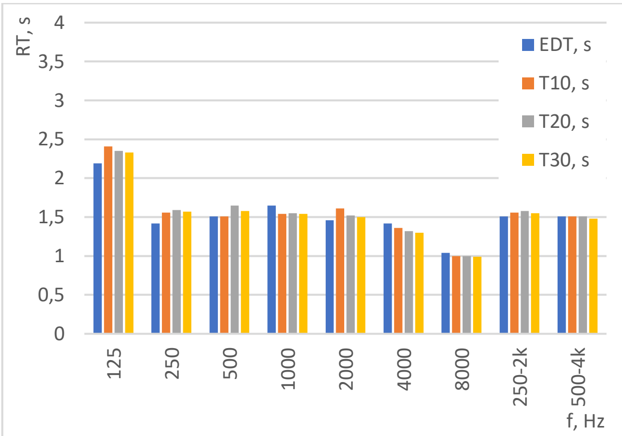

Fig. 3. Graphical representation of reverberation time (1/1 Oct.) measured with LOG sweep excitement

STI	0,493
RaSTI	0,467
Al_{Cons} [%]	11,781

Table 5. STI, RASTI, Al_{Cons} measured with LOG sweep excitement

C_7, dB	C_{50}, dB	C_{80}, dB	C_{35}, dB	D, dB	L_7, dB	L_{50}, dB
-15,3	-4,2	-0,5	-6,8	0,27	83,5	93,3
L_{80}, dB	L_{35}, dB	L_{Total}, dB	Center time, ms	ST1, dB	ST2, dB	Arrival time, ms
95,6	91,3	98,9	128	11,3	13,2	81,94

Table 6. Acoustic quality parameters measured with LOG sweep excitement

2.1.3. Sweep excitement

f, Hz	EDT, s	T10, s	T20, s	T30, s
125	2,3	2,64	2,64	2,42
250	1,35	1,76	2,01	2,14
500	1,49	1,41	1,75	1,62
1000	1,6	1,58	1,61	1,54
2000	1,41	1,61	1,51	1,51
4000	1,42	1,33	1,31	1,33
8000	1,06	0,98	0,96	0,98
250-2k	1,46	1,59	1,72	1,7
500-4k	1,48	1,48	1,54	1,5

Table 7. Reverberation time (1/1 Oct.) measured with sweep excitement

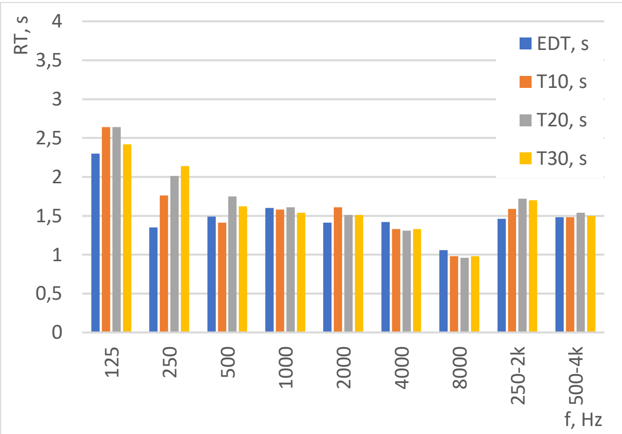

Fig. 4. Graphical representation of reverberation time (1/1 Oct.) measured with sweep excitement

STI	0,479
RaSTI	12,746
Al_{Cons} [%]	0,478

Table 8. STI, RASTI, AlCons measured with sweep excitement

C_7, dB	C_{50}, dB	C_{80}, dB	C_{35}, dB	D, dB	L_7, dB	L_{50}, dB
-21,6	-6,5	-2,1	-9	0,18	77,4	91,6
L_{80}, dB	L_{35}, dB	L_{Total}, dB	Center time, ms	ST1, dB	ST2, dB	Arrival time, ms
94,8	89,5	99	270	16,9	19,2	77,08

Table 9. Acoustic quality parameters measured with sweep excitement

2.2. Room acoustic quality parameters for C-10-13

2.2.1. MLS excitement

f, Hz	EDT, s	T10, s	T20, s	T30, s
125	0,72	0,69	0,54	0,55
250	0,60	0,62	0,55	0,63
500	0,49	0,61	0,56	0,52
1000	0,49	0,45	0,43	0,44
2000	0,39	0,45	0,41	0,40
4000	0,38	0,44	0,43	0,46
8000	0,40	0,37	0,40	0,38
250-2k	0,49	0,53	0,49	0,50
500-4k	0,43	0,49	0,46	0,45

Table 10. Reverberation time (1/1 Oct.) measured with MLS excitement

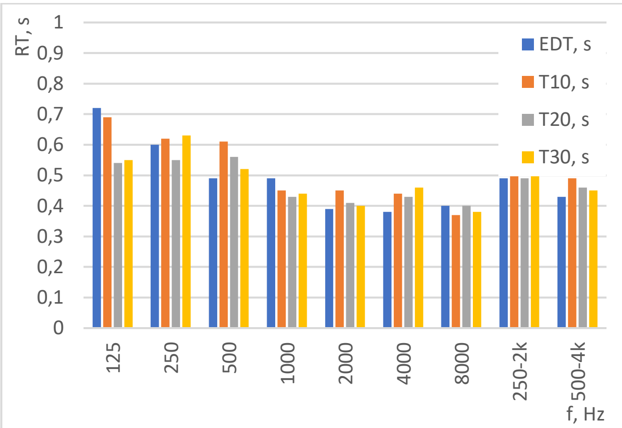

Fig. 5. Graphical representation of reverberation time (1/1 Oct.) measured with MLS excitement

STI	0,689
RaSTI	0,680
Al_{Cons} [%]	4,081

Table 11. STI, RASTI, Al_{Cons} measured with MLS excitement

C_7, dB	C_{50}, dB	C_{80}, dB	C_{35}, dB	D, dB	L_7, dB	L_{50}, dB
- 4,9	4,7	7,7	2,6	0,74	95,5	100,4
L_{80}, dB	L_{35}, dB	L_{Total}, dB	Center time, ms	ST1, dB	ST2, dB	Arrival time, ms
100,9	99,7	101,6	190	2,1	2,6	90,77

Table 12. Acoustic quality parameters measured with MLS excitement

2.2.2. LOG sweep excitement

f, Hz	EDT, s	T10, s	T20, s	T30, s
125	0,69	0,69	0,46	0,56
250	0,50	0,60	0,55	0,55
500	0,50	0,57	0,56	0,55
1000	0,48	0,44	0,46	0,43
2000	0,40	0,44	0,44	0,44
4000	0,38	0,44	0,43	0,46
8000	0,39	0,37	0,41	0,44
250-2k	0,47	0,51	0,50	0,49
500-4k	0,44	0,47	0,47	0,47

Table 13. Reverberation time (1/1 Oct.) measured with LOG sweep excitement

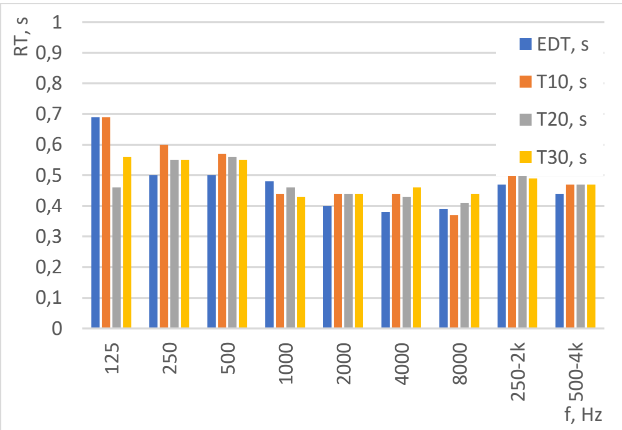

Fig. 6. Graphical representation of reverberation time (1/1 Oct.) measured with LOG sweep excitement

STI	0,762
RaSTI	0,759
Al_{Cons} [%]	2,745

Table 14. STI, RASTI, Al_{Cons} measured with LOG sweep excitement

C_7, dB	C_{50}, dB	C_{80}, dB	C_{35}, dB	D, dB	L_7, dB	L_{50}, dB
- 44	6,1	10,3	3,5	0,801	100,3	105,1
L_{80}, dB	L_{35}, dB	L_{Total}, dB	Center time, ms	ST1, dB	ST2, dB	Arrival time, ms
105,6	104,4	106	31,36	2,1	2,5	93,15

Table 15. Acoustic quality parameters measured with LOG sweep excitement

2.2.3. Sweep excitement

f, Hz	EDT, s	T10, s	T20, s	T30, s
125	0,61	0,72	0,49	0,59
250	0,62	0,60	0,53	0,53
500	0,60	0,55	0,53	0,55
1000	0,60	0,55	0,48	0,47
2000	0,48	0,48	0,44	0,46
4000	0,55	0,45	0,45	0,46
8000	0,51	0,41	0,45	0,44
250-2k	0,57	0,54	0,50	0,50
500-4k	0,56	0,51	0,48	0,48

Table 16. Reverberation time (1/1 Oct.) measured with sweep excitement

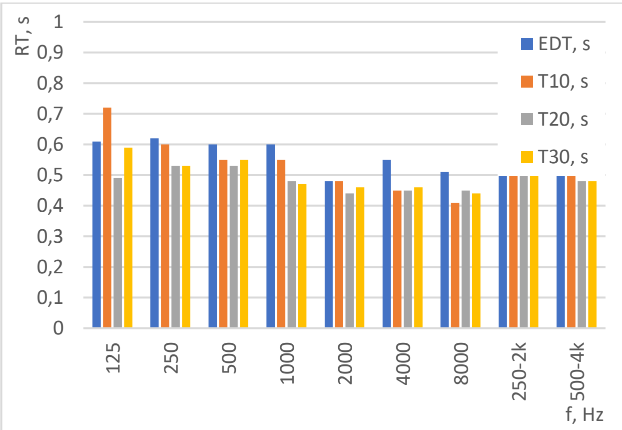

Fig. 7. Graphical representation of reverberation time (1/1 Oct.) measured with sweep excitement

STI	0,705
RaSTI	0,716
Al_{Cons} [%]	3,742

Table 17. STI, RASTI, Al_{Cons} measured with sweep excitement

C_7, dB	C_{50}, dB	C_{80}, dB	C_{35}, dB	D, dB	L_7, dB	L_{50}, dB
-4,9	4,7	7,7	2,6	0,748	95,5	100,4
L_{80}, dB	L_{35}, dB	L_{Total}, dB	Center time, ms	ST1, dB	ST2, dB	Arrival time, ms
100,9	99.7	101.6	190.44	2.1	2.6	90.77

Table 18. Acoustic quality parameters measured with sweep excitement

3. AUDIO SIGNAL PROCESSING SETUP

Audio material with separated audio samples of each instrument was processed in Avid Pro Tools software. Yamaha MSP5 Studio monitors linked to M-Audio Fast Track Pro sound card were used as a reference sound system in both rooms. Monitors were positioned in an equilateral triangle towards the audio engineer to achieve so-called “sweet spot”.

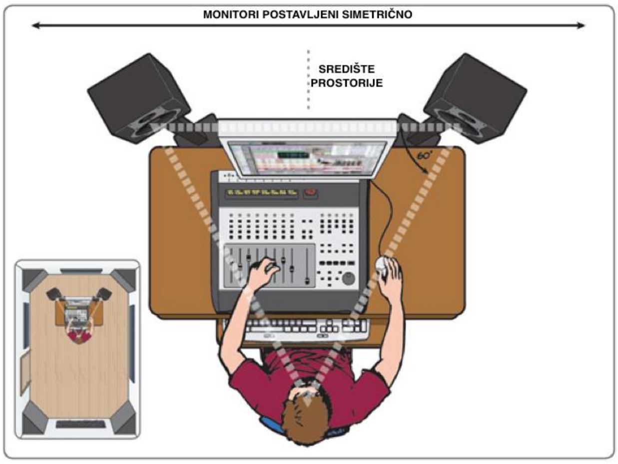

Fig. 8. Audio equipment layout

4. SIGNAL PROCESSING IN ROOM WITH LONG REVERBERATION TIME

First signal processing took place in the room C-10-15 which has longer reverberation time on certain frequencies. Audio equipment was set up as previously described. First step was balancing the loudness of each instrument to create satisfying fusion of instruments. In the next step the tracks containing drums, guitars and percussion were linked to separate busses. This, for example, allows balancing loudness of all instruments that include drums by using only one fader. Afterwards, those busses were linked to one track called “Master”.

Fig. 9. View of all active channels

Audio samples (including master track) were mainly processed in frequency domain by equalizing every sound sample to achieve satisfying sound. Custom settings on compressors and limiters seen in pictures were used to modify dynamic range of audio signals.

However, modifying time spectrum of signal was the most interesting part. Digital reverb and delay effect were used even though the room itself has increased reverberation time. It was expected that there won’t be need of using before mentioned effects in time domain, but they were still used as the natural reverberation was not creating desired effect audio engineer strives for. These characteristics of room resulted in exhausting and tiresome work while mixing and mastering tracks.

Fig. 10. View of graphical interface settings for frequency signal processing

Fig. 11. View of graphical interface settings for dynamic signal processing

Fig. 12. View of graphical interface settings for time signal processing (Echo effect)

Fig. 13. View of graphical interface settings for time signal processing (Delay effect)

5. SIGNAL PROCESSING IN REFERENCE ROOM

Reference room is constructed to meet the audio industry standard for sound listening room.

Setting up the gear and testing audio in reference room significant difference, even in unprocessed audio samples, was noticed compared to the previous room. Considering the fact this room has tuned reverberation time for signal processing and audio mixing, workflow and overall atmosphere was enhanced. Identical equipment was used and active monitors were placed identically as in previous room.

Significant difference was noticed especially in snare drum while rehearsing unprocessed audio samples. Main reason for that is shorter reverberation time on 2.5kHz - 5kHz where its "punch" is manifested, but also shorter reverberation time on lower frequencies whose presence generates additional noise effect. Linking to busses and other software settings were identical as in previous room. Balancing sounds and signal processing, however, was different.

Fig. 14. View of all active channels

Signal processing in frequency domain required usage of different types of filters than previous room.

Fig. 15. View of graphical interface settings for frequency signal processing

As modifying dynamic range of audio signals comes after the processing in frequency domain it can't be compared to any dynamic processing in previous room. Modifying signals in time domain required different approach and those custom settings are seen in figures.

Fig. 16. View of graphical interface settings for time signal processing (Echo effect)

Fig. 17. View of graphical interface settings for time signal processing (Delay effect)

6. FREQUENCY ANALYSIS

Subjective assessment is not quite valid approach to any conclusion. Frequency analysis was generated on selected audio samples in which the most significant difference is noticed after rehearsal of both final mixes in reference room.

Processed audio samples chosen for analysis and comparison are: Snare drum, kick drum along with electric guitar and the complete song. Audacity function "Plot Spectrum" was used for analysis.

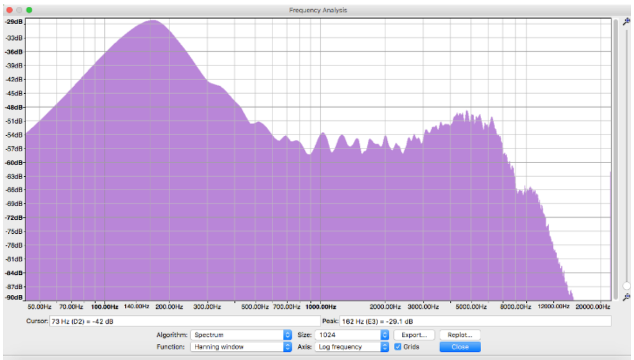

Fig. 18. Frequency spectrum of snare drum – C-10-15

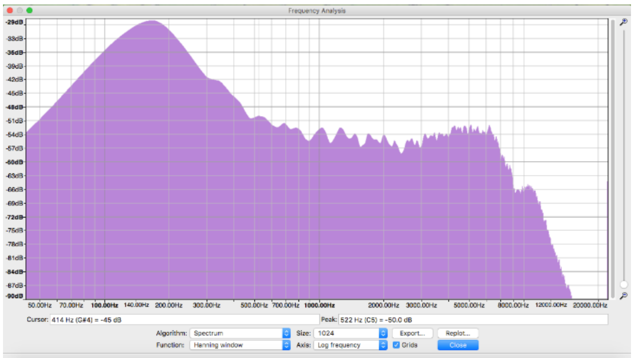

Fig. 19. Frequency spectrum of snare drum – reference room

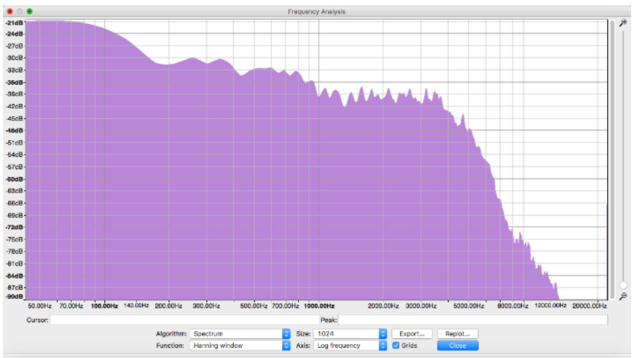

Fig. 20. Frequency spectrum of electric guitar and kick drum – C-10-15

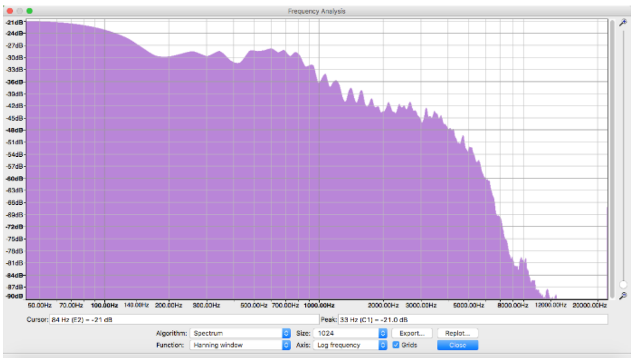

Fig. 21. Frequency spectrum of electric guitar and kick drum – reference room

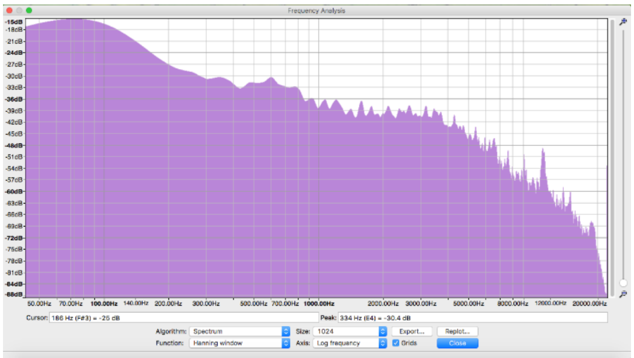

Fig. 22. Frequency spectrum of the entire recording – C-10-15

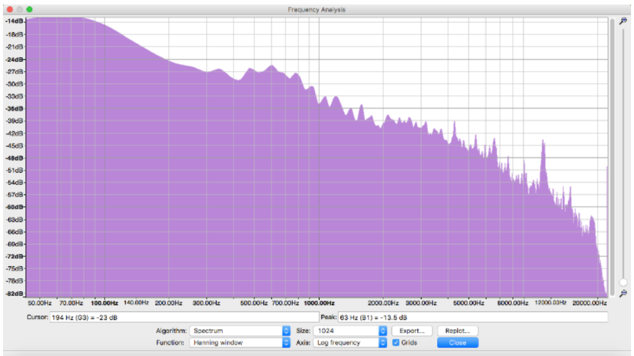

Fig. 23. Frequency spectrum of the entire recording – reference room

7. SIMULATION OF REFERENCE ROOM IN EASE SOFTWARE

Reference room plan drawn in AutoCad was imported to EASE in order to make comparison between measured and simulated reverberation time. Added materials, with following absorption values are used on these surfaces:

1. For wooden wall and blackboard - wooden panel
2. For floor - wooden surface
3. For wall and ceiling - plaster with smooth finish
4. For carpet - standard commercial carpet
5. For doors - standard wooden doors
6. For white and black absorbers - special materials based on the characteristic of ones that are in real room.

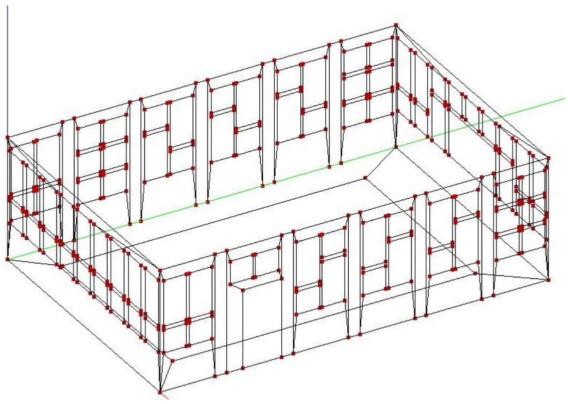

Fig. 24. 3D view of reference room used in computer simulation

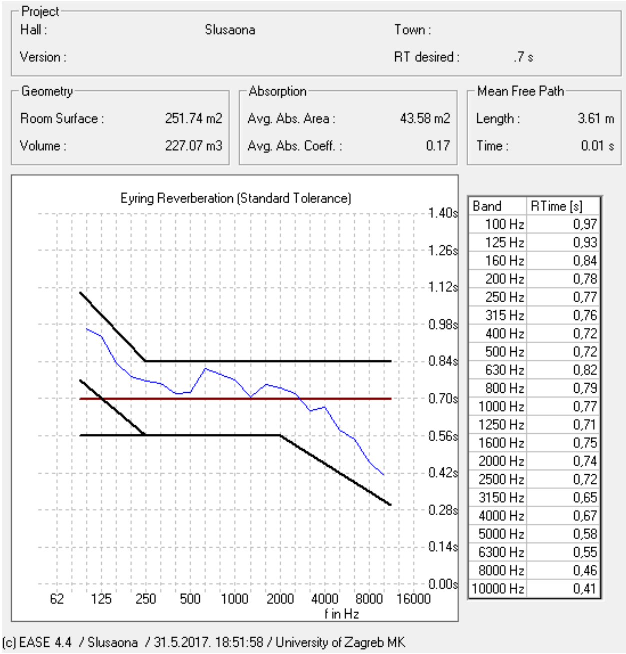

Fig. 25. Simulated reverberation time of reference room

8. CONCLUSION

New "project" was created in AVID Pro Tools in order to compare processed songs. In addition to entire songs, processed audio samples in different rooms which include: Snare drum, bass guitar and snare drum playing at the same time, electric guitar and kick drum playing at the same time were also added to the project. After rehearsal in reference room, the most significant difference in processed audio samples was noticed in before mentioned instruments.

Complete song mixed in reference room contains less noise in added reverb effects and is pleasant to listen, which is the most important factor. Main hypothesis was that because of longer reverberation time in the room C-10-15 there will be no need of adding reverb effects on certain elements while mixing a song. However, natural reverb effect that is present in the room was not giving quite satisfying sound while mixing so digital effects in time domain were added. That song sounded proper, but only in that room. Big difference was noticed in the time domain when rehearsing and comparing that song with the one mixed in reference room. This difference is best manifested in the kick and snare drum samples.

After this subjective assessment, frequency analysis was generated in the purpose of determining differences in frequency spectrum of before mentioned audio samples. Considering the fact that audio samples before processing were identical, similarities in frequency spectrum were expected (seen in figures) as the only differences were in the time domain.

Reference room (C-10-13) proved itself as better option than C-10-15 for audio signal mixing so it has been chosen for simulation in EASE software. Simulated reverberation times reasonably differ from those measured in the real room. This is because the absorption values of the material as well as the space are approximated in the simulation and can't be the same as in the actual room.

All things considered, audio signal processing should be done in the room which has reverberation time similar to the one measured in reference room. It is important to mention that reverberation time is just one of many parameters of acoustic quality of space and it is not the only one that matters when it comes to determining the acoustic quality of certain room.

Associating subjective impressions while mixing a song with objective parameters of acoustic quality of space has led to unexpected results. The findings discovered in this paper have revealed new insights for the study of the correlation between acoustics of the space and processing of the audio signals as well as of the reverberation time phenomena itself.

9. REFERENCES

[1.] Fajt, Siniša. Vrednovanje kvalitete akustički obrađenih prostora, doktorska disertacija, Fakultet elektrotehnike i računarstva, Zagreb, 2000.

[2.] Fajt, Siniša; Krhen, Miljenko; Milković, Marin. Sound Source Influence to the Room Acoustics Quality Measurement, Tehnički vjesnik : znanstveno-stručni časopis tehničkih fakulteta Sveučilišta u Osijeku (1330-3651) 2 (2015)

[3.] Krhen, Miljenko; Fajt, Siniša; Milković, Marin. Principal Component Analysis in Determining the Best Setup for Acoustic Measurements in Sound Control Rooms, Tehnički vjesnik : znanstveno-stručni časopis tehničkih fakulteta Sveučilišta u Osijeku (1330-3651) 5 (2015)

[4.] Everest, F. Alton; Pohlmann, Ken. Master Handbook of Acoustics, 1981.

[5.] Grupa Autora. Music production & Engineering – Vol 1-24, Berklee college, Boston, Massachusetts, 1999

8th Congress of the Alps Adria Acoustics Association
Zagreb, Croatia
20 – 21 September 2018

DEVELOPMENT OF ACOUSTIC PARAMETER CALCULATION TOOL FOR BIM SUPPORTING SOFTWARE PACKAGE

Paulína Šujanová[1], Herbert Müllner[2]

Affiliation (E-mail address): [1]paulina.sujanova@stuba.sk, [2]hmuellner@tgm.ac.at

Abstract: *In the following paper the initial phases of the preparation for computational tool enabling the calculation of acoustic parameters for Building Information Modeling (BIM), supporting architectural design tools will be presented. The goal is to use the opportunities provided by a BIM model and use the 3D model and also information stored to evaluate basic acoustic performance parameters, such as the calculation of the average sound absorption coefficient. Attention is paid to maintaining the interoperability between the model set up and calculation process.*
Firstly the limitations of BIM design tools and current state-of-the art parameter set up will be defined. Secondly, existing tools, fully or partially using BIM provided information, for calculation of acoustic parameters will be described. Their functionality and interoperability with BIM design tools will be defined. The results of the state-of-the art analysis will be used for the benchmarking of the developed tool for acoustic calculations. Thirdly, possible design structures and the expected functionality of the developed tool will be described. Lastly, a mock-up version and current functionality of the developed tool will be presented.

Key words: building information modeling, acoustic parameters, calculation tool

1. Introduction

Building Information Modeling (BIM) is a central information platform to support the integration and analysis of data, wherein all the project data is stored in a single data repository. BIM enables gathering of data for defined elements, storing information about their geometry, position, design, parametric performance and other relevant data necessary for support of construction, fabrication, performance evaluation and procurement activities [1.]. The implementation is supported (mandatory in certain countries) by local authority offices [2.], and the BIM methodologies are being Standardized and also implemented in legislation.
In this paper we will present the constrains of developing a computational tool enabling calculation of acoustic parameters in a BIM supporting modeling platform. The goal was to identify a suitable platform and to use the already available 3D model information, establish a live connection between acoustic calculation and 3D modeling. The tool strives to enable a smoother and dynamic designing process where the necessity of integration of the 3D model into a dedicated third-party acoustic simulation software would be completely omitted, and to enable quick comparison of design variants.

1.1. Limitations of BIM software and selection

BIM modeling in recent years has seen one of the highest increases in the engagement of architecture, engineering and construction (AEC) professionals, and has undergone one of the most promising developments in the industry. BIM modeling supports cooperation of professionals involved in project drafting and realization, and supports the development of sustainable building facilities. The final model is data rich, representing a full virtual 3D model of the developed construction, storing parametric data including dimensions, design, costs, physical properties of elements, description of relationships between objects, as well as life-cycle information. BIM modeling has the potential to minimize the fragmentation of the building design process, enabling inclusive involvement of large groups of stakeholders ranging from design, construction, operation, and maintenance, having beneficial impact on clash detection, cost effectiveness and overall sustainability [3., 4.].
To the identified most often used BIM software packages by architects and civil engineers belong:

- Revit (Autodesk) [5.];
- Bentley Architecture and its products (Bentley) [6.];
- ArchiCAD (Graphisoft) [7.];
- Allplan (Nemetschek) [8.].

Whereas all of the above-mentioned software enable multidisciplinary and collaborative design process to create intelligent structure models in coordination with

other building components, internally all the input data is stored differently, in proprietary data formats. This means all external applications need to be developed in a compliant language (specific to each individual software), otherwise they can not be integrated [9. – 11.].
Data derived from different BIM software can be shared among software applications through Industry Foundation Classes (IFC). IFC is a neutral, non-proprietary open international standard for BIM data [12.].

2. Application model options

An application for calculation of acoustic parameters using the data stored in a BIM model can be developed as:

- a plug-in for a dedicated BIM software platform;
- a plug-in developed in a graphical algorithmic modeling platform extension for a BIM software package;
- as an autonomous software using imported BIM data.
- hybrid solutions

All these options have their own advantages and disadvantages based on the limitation of their functionality, development complexity and interoperability of the interchanged data.

2.1. A plug-in for a dedicated BIM software platform

To extend the core functionality of BIM software, Revit and ArchiCAD allow you to program with a compliant language an extension plug-in, which is than after installation available in Add-Ins External Tools toolbar. The program would have to consist of BIM data extraction module, and calculation module.
This method has following advantages:

- easy to use – the plug-in is fully integrated into the BIM software platform, no need to get to know a new platform;
- the interoperability is looped – changes in architecture can be immediately verified by the tool;
- no need to export and import the created BIM model into a separate platform;

the disadvantages:

- limited functionality – the plug-in is limited by the Application Program Interface (API) provided by the proprietary software developer.
- has to be developed for each BIM software separately, based on each proprietary data format.

This type of the application model is best used for quick evaluation of acoustic performance of an indoor space during the schematic building design stage. It enables to quickly verify the impact of various designs and materials. Also in this application version all the acoustic performance parameters of different materials and constructions are stored within the BIM model. However, until now none of the above mentioned BIM software package does, by default contain acoustic performance data on any element or material.
To the authors knowledge there is no such application yet available for any of the above mentioned BIM software packages.

2.2. A plug-in developed in a graphical algorithmic modeling platform extension for a BIM software package

To develop the plug-in, it is possible to use a graphical scripting platform extension for a BIM software package. This can be for example an application developed in Grasshopper for ArchiCAD [13.] or in Dynamo for Revit [14.].
To the advantages of this solution belongs:

- changes in design will result in changes in simulation – the platforms communicate directly in order to create and manipulate a BIM model in full or in parts through the graphical scripting interface;
- it is not necessary to import the current design into a third-party simulation software;
- the graphical scripting platforms are fully or partially open-source;
- the lightweight scripting interface and the fact that the script is represented visually, no, or minimal programming experiences are required to start.

The disadvantages to be considered:

- the necessity to be familiar with two software platforms;
- for more complex application the graphical representation of the script becomes difficult to manage;
- assigning and storing of acoustic properties is done outside of the BIM software platform.

There is already a plug-in available for acoustics simulation called Pachyderm developed in Grasshopper (by Arthur van der Harten) [15.] and can be used for models created in Rhinoceros or Archicad (uses the geometry data). It enables the use of common geometrical acoustics algorithms. Pachyderm is capable to output data on reverberation time, early decay time, center time, clarity, definition and strength/loudness. No other similar application is available to the authors knowledge.

2.3. An autonomous software using imported BIM data

In this version, relevant data is exported from the BIM model and imported into an autonomous simulation software. This version is the one most commonly used, where a 3D model is imported to a simulation software such as ODEON and EASE [16. – 17.]. The advantages of this model are:

- as a separate simulation engine, the most complex simulations, predictions, visualization and prediction can be enabled;
- if well prepared, the results are the most accurate.

The main disadvantages are:

- most of the available software are only able to import the 3D model geometry, and no parametric performance data can be used from the BIM model;
- the imported geometry has to be altered after import, to make it compatible and fulfill the requirements given by the simulation software;
- material acoustic performance properties have to be added in the simulation software.

Some of the disadvantages could be eliminated if the simulation software would be able to import data in the IFC standard for BIM data. This was enabled only for COMSOL [18.]. The necessary information for acoustic analysis (simulation environment, sound source location, and acoustic absorption coefficient) are extracted from the IFC file through a developed API (application programming interface)

This method has current advantages:

- it enables to quickly import data from BIM model into advanced software for acoustic analysis;

and disadvantages:

- the interoperability is limited, and the streamline of work is only one direction, no feedback loop between architectural design and acoustical analysis (changes in architecture will not be automatically updated in acoustical analysis).

3. Application design

As our goal was to use the already available 3D model and performance data to enable basic acoustic calculations in the environment of a Building Information Modeling (BIM) software platform, we have decided to develop a plug-in for dedicated BIM software platform, in our case for Revit. This was done based on the following assumptions:

- there does not yet exist (to the authors knowledge) an acoustic performance evaluation plugin for Revit, whereas there is already Pachyderm for Rhinoceros and ArchiCAD [15., 19.];
- Revit has a well-developed support infrastructure, and a broad documentation database, which simplifies the software development [9.];
- Revit is the most used BIM authoring software;
- ArchiCAD plugin development is limited to C and C++ programming language, whereas Revit .NET API enables to use any .NET compliant language including VB.NET, C#, C and C++.
- Similar plug-ins such as Pachyderm will serve as a benchmark.

4. Current state of the plug-in development

We have developed a basic application which enables calculation of average sound absorption coefficient of a room.

Currently the development mainly consists on drafting the work flow, whereas the whole functionality would be provided by a downloadable plug in. Until now, this functionality was already provided:

- Application info note, which loads on start up.
- A dedicated application panel, providing all the functionality of the application.
- By button triggered generation of a shared parameter file with predefined acoustic parameters.
- A command for selecting element faces, and extraction of relevant data such as element name, ID, area, material and shared parameter values.
- A command for extracting data, by picking up a room for evaluation. The data includes definition of boundary elements, with their area, element ID, material, and shared parameter values. This selection tool is an enhanced tool based on a room selection tool developed and made available by Jeremy Tammik [20.]. It handles all the special cases which can arise while modeling the boundary elements of a room. Also the broad variety of bounding elements that can be used.

Further it is necessary to:

- Prepare a dedicated task dialog, which will contain a list of selected faces, and enable selection/deselection of further faces. Enable a lookup and adjustment of relevant data. And enable calculation.
- Resolve the Revit native problem of selecting floors and ceilings. Due to the way floors and ceilings are modeled in Revit, the program is not working with actual real areas of ceilings and floors but is counting them based on the area enclosed by the boundary elements such as walls and windows. If for example a room would have stairs, the area provided would only represent the gross floor plan area, not the actual area of the stairs.
- Provide a data set providing sound absorption coefficient values for standard materials and standard wall structures.
- Calculation process.
- Export of results.

Attention will have to be put, for handling room designs with exceptions, and in cases no material description or insufficient data is provided.

3. CONCLUSION

In this paper we have presented the initial phases of preparation and development of a computational tool enabling calculation of acoustic parameters in a BIM supporting modeling platform. The tool strives to enable basic acoustic calculations in the environment of Revit. The goal is to use the already available 3D model, and to establish a live connection between acoustic calculation and 3D modeling. This will enable a smoother and more dynamic design process where the necessity of integration of the 3D model into acoustic simulation software (such as ODEON) would be completely omitted.

4. REFERENCES

[1.] Ch. Eastman, P. Teicholz, R. Sacks, K. Liston: **BIM Handbook: A Guide to Building Information Modeling for Owners, Managers, Designers, Engineers, and Contractors.** New Jersey: John Wiley & Sons, Inc. 2008. ISBN 978-0-470-18528-5.

[2.] Infrastructure and Projects Authority: **Government Construction Strategy 2016-20,** March 2016. Available at: https://www.gov.uk/government/uploads/system/uploads/attachment_data/file/510354/Government_Construction_Strategy_2016-20.pdf

[3.] A. Ghaffariahoseini, J. Tookey, A. Ghaffarianhoseini, N. Naismith, S. Azhar, O. Efimova, K.Raahemifar: **Building Information Modeling (BIM) uptake: Clear benefits, understanding its implementation, risks and challenges,** *Renewable and Sustainable Energy Reviews* 75, 2017, 1046-1053. http://dx.doi.org/10.1016/j.rser.2016.11.083

[4.] M. Reizgevičius, L. Ustinovičius, D. Cibulskiene, V. Kuhut, L. Nazarko: **Promoting Sustainability through Investment in Building Information Modeling (BIM) Technologies: A Design Company Perspective**, Sustainability 10(600), 2018. doi: 10.3390/su10030600

[5.] Autodesk: **Revit: Built for Building Information Modeling.** 2018. Available at: https://www.autodesk.com/products/revit/overview

[6.] Graphisoft: **Archicad.** 2018. Available at: http://www.graphisoft.com/archicad/

[7.] Nemetschek Group: **Allplan.** 2018. Available at: https://www.allplan.com/uk_en/

[8.] A. Malleson: **BIM Survey: Summary of findings**, NBS National BIM Report 2014. RIBA 2014

[9.] Autodesk. **Revit Platform Technologies. Autodesk Developer Network.** 2018. Retrieved September 13, 2018, from https://www.autodesk.com/developer-network/platform-technologies/revit

[10.] Graphisoft. **The Platform for developers.** [online]. 2018. Available from: http://archicadapi.graphisoft.com/ 1.

[11.] Allplan. **Getting started with Allplan API.** [online]. 2018. Available from: http://pythonparts.allplan.com/

[12.] ISO 16739. **Industry Foundation Classes (IFC) for data sharing in the construction and facility management industries.** 2013.

[13.] Graphisoft. **ARCHICAD – Rhinoceros – Grasshopper Connection.** [online]. 2018. Available from: http://www.graphisoft.com/archicad/rhino-grasshopper/

[14.] Autodesk. **Dynamo BIM**. [online]. 2018. Available from: http://dynamobim.org/

[15.] van der Harten, A. Pachyderm **Acoustical Simulation. An Open Source Acoustics Simulation Laboratory.** [online]. 2018. Available from: http://www.perspectivesketch.com/pachyderm/index.php/author

[16.] Odeon. **The Odeon acoustics software | Simulation and measurements**. [online]. 2018. Available from: https://odeon.dk/acoustics_simulation_software/

[17.] EASE. **Software - EASE - Enhanced Acoustic Simulator for Engineers.** [online]. 2018. Available from: http://ease.afmg.eu/

[18.] COMSOL. **COMSOL Multiphysics® Modeling Software.** [online]. 2018. Available from: https://www.comsol.com/

[19.] Autodesk. **Revit Store: Plugins, Add-ons and Extensions for Revit.** [online]. 2018. Available from: https://apps.autodesk.com/RVT/en/Home/Index

[20.] Tammik, J. **The Building Coder: Determining Wall Opening Areas per Room.** [online]. 2016. Available from: http://thebuildingcoder.typepad.com/blog/2016/04/determining-wall-opening-areas-per-room.html#5

8th Congress of the Alps Adria Acoustics Association
Zagreb, Croatia
20 – 21 September 2018

Hrvatsko akustičko društvo
HAD
Acoustical Society of Croatia

ROOM ACOUSTICS CALCULATOR FOR EDUCATIONAL AND DESING PURPOSES

Šubic, N., Kunič, R.

University of Ljubljana, Faculty of Civil and Geodetic Engineering, Chair for Buildings and Constructional Complexes, Jamova cesta 2, 1000 Ljubljana, Slovenia (nika.subic@fgg.uni-lj.si, roman.kunic@fgg.uni-lj.si)

Abstract: *An educational version of an acoustic calculator was designed to enable future civil and architectural engineers an extensive insight into the field of room acoustics and its important role in the design and construction process of a building. In the first section of the program the user defines the parameters of the given space and is throughout the input process assisted by the program with definitions and explanations of the required input data. The user can choose the intended use of the room, number of persons in the room and adjust the quantity of various materials. While inputting the data, the second section of the program generates the results, so that the user can simultaneously observe the effect of the changes made. The end results of the program are values of reverberation time spectrally represented for octave bands between 125 Hz and 4000 Hz, sound absorption coefficients, Schroeder frequencies and room modes for the selected room. Results are given for different states of the room so that the user can compare and study the effect of absorptive materials and people on room's acoustic properties. Additionally separate instructions were made to help with further analysis of results and serve as base of knowledge on the subject of room acoustics.*

Key words: acoustic calculator, reverberation time, room modes, education of building acoustics

1. INTRODUCTION

For an engineer, an extensive knowledge of his main field of work is required, as well as a broad understanding of other fields involved in the common tasks and activities. For civil and architectural engineers room acoustics presents one of the associated fields and its role in the design and construction process of a building therefore should not be overlooked. As it is important to educate the future engineers in the broadest way possible, an acoustical program was designed, which presents the essential concepts of room acoustics.

The program ARTIE (*Analysis of Reverberation Time in Indoor Environments*) was created foremost for educational purposes. It is meant for civil and architectural engineers at the Faculty of civil and geodetic engineering in Ljubljana, Slovenia, as well as other students, whose curriculum includes acoustic design. The program calculates reverberation time in the octave range from 125 Hz to 4000 Hz and room modes for small or medium sized perpendicular rooms (rooms in a shape of a cuboid).

The reverberation time is calculated using Sabine's and Eyring-Norris's equations and the calculated values are compared with the optimal values considering the intended use of the room. In addition, reverberation time in different conditions of the room can be analysed, such as occupied, unoccupied and with added absorption or without. This way it is possible to evaluate the effect of added absorption or people in the room on reverberation time values.

Furthermore, the program performs a three-dimensional calculation of modal frequencies, which affect the acoustic behaviour of the room at low frequencies and determines the critical frequency for the given condition of the room.

ARTIE works in a Microsoft Office Excel environment and is firstly written in Slovenian language. The completed acoustic analysis can be saved in a form of a PDF report consisting of input data, reverberation time analysis and room modes for the specific project.

The main advantages of the program are that it is written in Slovenian language, it follows the national guidelines and the materials used for analysis are non-commercial. In this way, the students can perform an independent analysis of room acoustic parameters in accordance with the current legislation.

2. THEORY

The program stands on the established analytical calculations for room acoustic parameters, presented in the text below.

2.1. Reverberation time

Calculations of the reverberation time are based on modified Sabine's (1) and Ering-Norris's (2) equations:

$$T_{60,S} = \frac{0{,}163 * V}{A + (4mV)} \quad (1)$$

$$T_{60,Ey} = \frac{0{,}163 * V}{-S * \ln(1-\bar{\alpha}) + (4mV)} \quad (2)$$

$T_{60,S}$ presents the reverberation time in seconds calculated with Sabine's equations, *V* is the volume [m^3] of the analysed space, *A* is the equivalent sound absorption area [m^2] and *m* the air attenuation coefficient [m^{-1}]. $T_{60,Ey}$ is the reverberation time [s] calculated using Eyring-Norris's equations, *S* is the sum of all the surfaces in the room [m^2] and $\bar{\alpha}$ is the average absorption coefficient of all the surfaces in the room.

Sabine's equation (1) is the most commonly used equation for analytical calculations of reverberation time and was therefore implemented into the program ARTIE. However, the precision of the results is lowered when analysing rooms with high average absorption coefficient, that is why Eyring-Norris's equation (2) was added to the analysis. *Slovenian national guidelines* [1] advise, that when $\bar{\alpha}$ is greater than 0.20 the use of equation (2) is more appropriate.

2.2. Absorption coefficient

Values of sound absorption coefficients α for different materials are gathered from literature [2] [3] and translated to Slovenian. There are more than 120 materials collected with α values for octave bands from 125 Hz to 4000 Hz. The data is arranged according to the most common use of the material in the room: walls, ceiling, floor, glazing, furniture etc.

2.3. Optimal reverberation times

Values of reverberation time are compared to optimal values regarding the intended use of the room in question, as stated in the German standard *DIN 18041: Acoustic quality in rooms – Specifications and instructions for room acoustic design* [4]. There are five different intended uses specified: music, speech/presentation, education/ presentation, education/communication and sport. In addition to the optimal reverberation times at 500 Hz and 1000 Hz, a tolerance range for the octave range from 125 Hz to 4000 Hz is defined, that allows at least a 20% deviation (Fig. *1*).

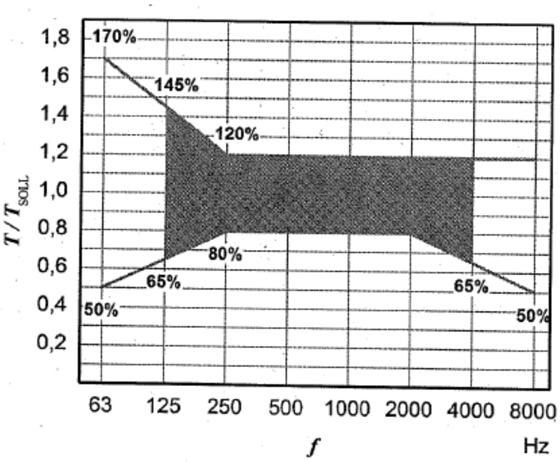

Fig. 1. Tolerance range for optimal reverberation time [4].

2.4. Room modes

For calculation of modal frequencies at which room modes occur, equation (3) was used [5]:

$$f_i = \frac{c}{2}\sqrt{\left(\frac{x}{L}\right)^2 + \left(\frac{y}{W}\right)^2 + \left(\frac{z}{H}\right)^2} \quad (3)$$

Where f_i represents a modal frequency [Hz] (*i = 1, 2, 3, … ∞*), *c = 343 m/s* is the speed of sound, *x, y, z* present the number of half wavelengths between the parallel surfaces (*1, 2, 3, … ∞*) and *L, W, H* are the distances between the reflective surfaces [m] (length, width and height of the space respectively).

The calculated room modes are one-, two- or three-dimensional, depending on the number of surfaces the sound wave reflects of.

2.5. Critical frequency

Generally, the sound field in a room is described as diffuse, however when dealing with lower frequencies, the modal response of the room is dominant and dictates the sound field. The frequency, that presents the boundary between the diffuse behaviour and modal behaviour is called critical frequency or Schroeder frequency and is calculated with equation (4) [5]:

$$f_{critical} = 2102\sqrt{\frac{T_{60}}{V}} \quad (4)$$

Where $f_{critical}$ is the critical frequency [Hz], T_{60} is the average reverberation time of the room [s] and *V* is the volume of the room [m^3].

3. PROGRAM

3.1. Content and layout

The program is designed in Microsoft Office Excel and consist of 6 sheets meant for public use and 6 sheets that run in the background. The user sheets are (with Slovenian translations written in brackets):

(a) INFO (‘info’),
(b) REVERBERATION TIME (‘odmevni cas’),
(c) APPLIED MATERIALS (‘uporabljeni materiali’),
(d) ROOM MODES (‘lastne frekvence’),
(e) ABSORPTION COEFFICIENTS (‘koeficienti absorpcije’) and
(f) PRINT (‘izpis’).

In the background sheets all the calculations are executed, four sheets are used for reverberation time analysis in four different conditions of the room and two sheets are used for modal frequency analysis.

3.2. Organization and user interaction

The program is organized in a way that the user has access only to the input data and results (user sheets) and not the calculation process (background sheets) - all the background sheets are locked and hidden. The cells in the user sheets are also mainly locked, with the exception of certain cells, that are intended for input data such us dimensions of the room and material properties. Unlocked cells have yellow background colour and additional comments with instructions for use. When the input information is incomplete or invalid, the cells with missing information turn red, alerting the user of an error.

The main interaction with the user is done through sheet (b) where most of the input data is added (Fig. *2* – left side). In sheet (b) the dimensions of the room are entered, the reduction of room volume due to furniture and other equipment, relative humidity, number of people in the room, the intended use of the room and all the surface materials in the room along with their area in m^2. Input of surface materials is divided into materials present in the basic condition of the room and additional absorption materials for analysis of the effect of added absorption. The user can choose from more than 120 common materials and add up to 10 new materials into the material library in sheet (e).

Simultaneously to the input process, the sorting of data and calculations of reverberation time are done in the background sheets and the in-between results are

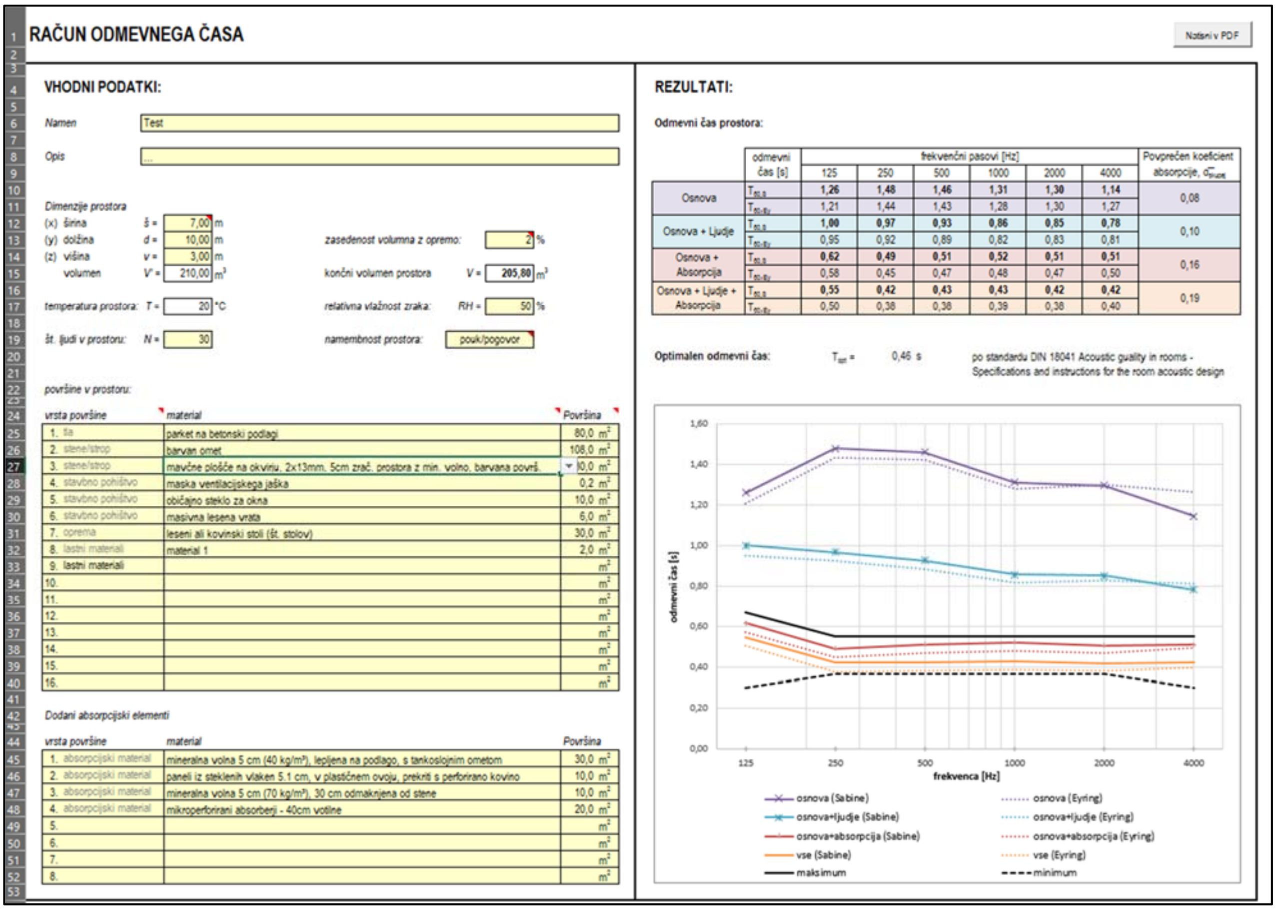

Fig. 2. Sheet (b) REVERBERATION TIME acts as the main interface for the user. The left part is intended for input of information about the given indoor space and the results are presented on the right side.

presented next to the input data (Fig. *2* – right side). This enables the user to see the effect of the changes in input data on the end result. The results are presented in form of a table and graph. For every octave band, the maximum of eight different reverberation times are calculated and compared to the optimal reverberation time and the tolerance range. The reverberation times are calculated by two equations (equation (1) and (2)) and for four different conditions: unoccupied basic room ('Osnova'), occupied basic room ('Osnova + Ljudje'), unoccupied room with added absorption ('Osnova + Absorpcija') and occupied room with added absorption ('Osnova + Ljudje + Absorpcija'). Each condition is plotted in a different colour: purple, blue, red and orange respectively and can be compared with the tolerance range for the specific use of the room, plotted in black colour. A comparison of reverberation time values of different room conditions as well as the difference in the two equations can therefore be made.

In sheet (d) room modes and eight critical frequencies (again for all four conditions and by two equations) are calculated as well as presented graphically. All the modal frequencies up to the critical frequency for the specific room are presented on a graph, as seen in Fig. *3*. For the graphical presentation, the critical frequency calculated by the Sabine's equations for occupied room with added absorption was selected, as it represents the end condition of the given room the most accurately.

A button is placed on the sheet (d) which executed the calculation of the room modes and plotting of the graph. In the background sheets the first 1330 modal frequencies are calculated, which corresponds to the values of *x, y, z* = 0 to 10 (equation (3)). Additionally, the results are organized and the selection of data for the graph is done in the background sheets.

Other three user sheets are completely locked and meant only for overview of data. Sheet (a) has some basic information about the program and a note from the authors, in sheet (c) the user can see the absorption qualities of the selected materials and sheet (f) is an output sheet for producing the final PDF report. All the data that the user has access to in the process of the acoustical analysis is combined in the final report. This includes:

- input data including acoustic properties of the used materials,
- results of reverberation time calculations in the form of a table and graph,
- results of room modes calculations: first 45 modal frequencies, graph and
- critical frequencies.

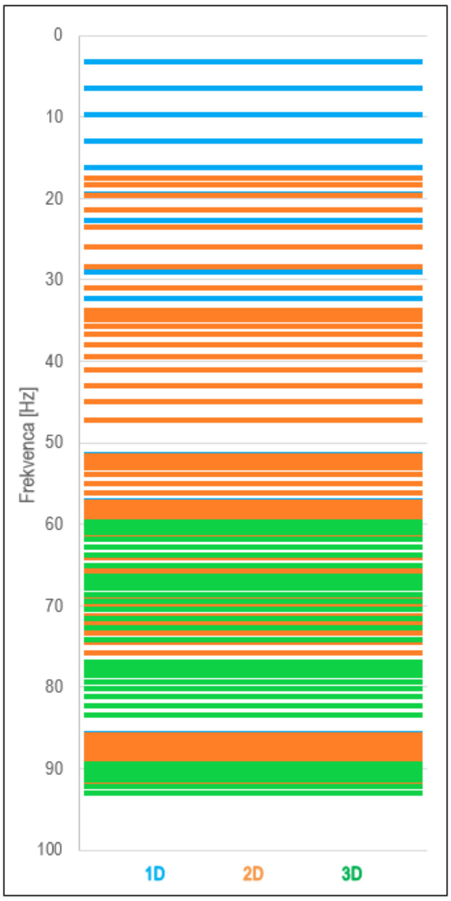

Fig. 3. Modal frequencies up to the critical frequency for the specific room. The one-, two- and three-dimensional modal frequencies are presented in different colours: blue, orange and green respectively.

3.3. Instructions for use

Instructions for use were written as support for the future users – engineering students. The document is comprised of two parts:

- basic theory of sound and room acoustics, and
- description of the program and instructions for use.

The essential room acoustic parameters, as presented in chapter 2 of this article are extensively explained in the first part of the document. Additionally the effect of reverberation time on the sound field in the room and humans perception of sound is described, as well as basic principles of sound absorbers, different types of absorbers and their implementation into spaces.

In the second part, instructions for use of the program are given. The emphasis is on user interaction, how to work with the program and what the user can change, select, and compare. The program is presented by the different sheets the user can interact with.

4. CONCLUSION

The created program presents an important contribution to the educational material on room acoustics at the Faculty of civil and geodetic engineering in Ljubljana. The basic principles of acoustic design of rooms are presented through analytical simulations and supported with extensive user manual containing instructions and basic theory. As it follows the latest national guidelines and is in accordance with the European legislation, it can be used in a wider sense, not only as an educational tool. The presented version of the program will serve as a basis for further improvements and adaptations. After the inclusion of the program in the educational and design process, the next stage of research and development will follow, in order to improve the efficiency and enhance the user experience.

5. REFERENCES

[1] Technical guideline TSG-1-005:2012: Protection against noise in buildings, 2012.
[2] Cox, T. J., D'Antonio, P. Acoustic absorbers and diffusers: theory, design, and application. 2nd edition. Oxon. Taylor & Francis, 2009, 85, 156-174, 440-444.
[3] Bies, D.A., Hansen, C.H., Emgeneering noise and control: theory and practice, 3rd ed. Spon Press, 2003, 303-305.
[4] DIN 18041: 2015; Acoustic quality in rooms – Specifications and instructions for room acoustic design, 2015, 10-12.
[5] Howard, D., Angus, J., Acoustics and Psychoacoustics, Forth Edition, Oxford, Elsevier Ltd., 2009, 334-339.

DIFFUSIVE SURFACE DESIGN GUIDELINES

Louena Shtrepi

Department of Energy, Politecnico di Torino, Corso Duca Degli Abruzzi 24, 10129

Abstract: *More than a decade ago the standard ISO 17497:2004 has proposed the scattering and diffusion coefficients measurement methods, which are useful for the characterization of the most important acoustic properties of the diffusive surfaces. The use of the standard has enabled a more accurate comparison between design solutions and the generation of an increasing database of diffusive materials. However, further work is needed in order to increase designers' awareness through simple design rules and approaches. Acoustic panels need to be optimized based on aesthetic and acoustic constraints in order to meet the requirements of both designers and acousticians. Hence, new strategies in enhancing the efficiency of the design should be investigated. This study aims to give a series of guidelines based on the most effective design aspects investigated through measurements in the past fourteen years of the ISO application. Moreover, an overview of the optimization approaches is presented.*

Key words: diffusers, scattering, design, surface optimization

1. Introduction

The correct use of diffusive surfaces or diffusers plays a key role in the sound field within an enclosed space, since they determine the acoustic quality for the listeners and music players. Diffusers are usually applied to treat first-order reflections, thus often they are used to prevent echoes from the rear wall of concert halls. It is assumed that the best concert halls take benefit not only from the basic room shape but also from the corrugations of the walls [1, 2]. It was shown that also other environments such as classrooms [3] or outdoor spaces [4] are improved acoustically by the use of diffusive surfaces. However, these surfaces need to be further studied from both the design and the acoustic point of view in order to become a useful design element in architectural projects.
Continuous research on diffusive surfaces brought to the introduction of the standard ISO 17497-1:2004 [5], which refers to the measurement of the random-incidence scattering coefficient in diffuse field, and ISO 17947-2:2012 [6], which refers to the measurement of the directional diffusion coefficient in free-field. In this way the comparison between different surface treatments has become easier [7]. The scattering coefficient is defined as the ratio of the non-specularly reflected sound energy to the total reflected energy. While the diffusion coefficient is intended to be a measure of quality of the diffusers, i.e. a measure of the uniformity of the scattered sound (Fig.1). Both these coefficients are frequency dependent single numbers.
The standards have played an important role in extending the database of scattering and diffusion coefficients [8], which are practically relevant for acousticians and practitioners alike as input data for acoustic simulations in the preliminary or verification phase of the project [9].
Beside the measurements of the acoustic scattering, very important has been also the validation of a prediction models. The calculation methods suggested in Embrechts et al. [10] and Embrechts and Billon [11] have been validated by full-scale and scale-model measurements in Schmich-Yamane et al. [12].
The use of numerical data has made possible the optimization and the enhancement of the specifications of the diffuser [13]. The numerical optimization of the diffusers profile has been object of different studies aiming to limit the production costs and absorption characteristics. In this way the shape of the diffusor and the required diffusion could be tailored based on the requirements of the specific case. Cox [14] showed the optimization of Schroeder diffusers through iterative boundary element method (BEM) based simulations. Further, Orlowski [15] showed a curve optimization technique for a diffusor in a new recital hall, and profiles of optimum diffusers were suggested in Takahashi [16].
However, after more than a decade from the standards more effort is needed to bring closer designers and acousticians in order to generate valid solutions from

both aesthetical and acoustic point of view for a larger cases of environments.
This work aims to give simple geometrical guidelines for the diffusers performance optimization based on the literature review. It aims to help to raise the awareness about the potential solutions that might be generated by realizing very complex structures. The focus will be mainly on the maximization of the random-incidence scattering coefficient.

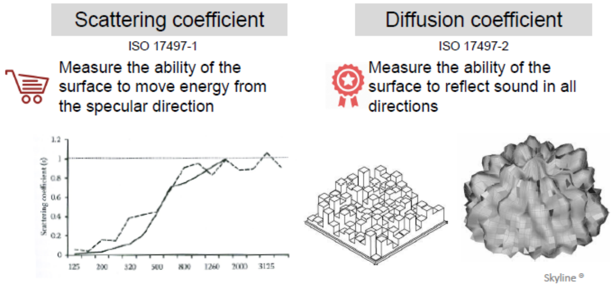

Fig.1. Random-incidence scattering and diffusion coefficients according to ISO 17497. A typical scattering coefficient curve and polar distribution for Skyline® diffuser [8].

f [Hz]	100	125	160	200	250	315	400	500	630	800	1000	1250	1600	2000	2500	3150	4000
a, h [m]	1.72	1.38	1.08	0.86	0.69	0.55	0.43	0.34	0.27	0.22	0.17	0.14	0.11	0.09	0.07	0.05	0.04

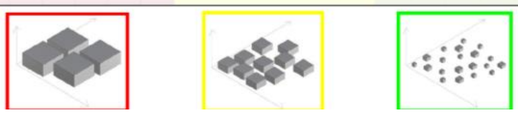

Fig.2. Effective frequency related to the dimensions of the elements as reported in the analytical model f=c/2a or f=c/2h [7].

2. DIFFUSERS OPTIMIZATION

The optimization of the diffusers performance concerns all the design aspects that can lead to both 1) a more uniform polar distribution of the scattered energy for any source angles, i.e. a diffusion coefficient values close to 1, and 2) a maximization of the scattered energy with respect to the specularly reflected energy, i.e. a random-incidence scattering coefficient close to 1. The geometrical aspects considered below refer in detail only to the second parameter. Moreover, it should be noted that besides the spatial dispersion, a good diffuser must also generate a distribution of the scattered reflection over time [8].

2.1 Diffusion coefficient optimization

As was shown in [13] a good diffuser has the ability to uniformly scatter in all directions, rather than just move energy away from the specular angles, i.e. dispersion *vs* redirection. To this aim, curved diffusive surfaces are the most common diffuser which can easily achieve higher uniformity of the polar distribution of the scattered energy. As it is shown in Cox and D'Antonio [8], geometrical elements organized in arrays and modulated, for example, as Schroeder diffusers are likely to generate a good spatial distribution. Therefore, an asymmetrical base shape as well as the reduction of periodicity are preferred.

2.2 Scattering coefficient optimization

2.2.1 Dimensions of the scattering elements

The dimensions of the scattering elements are the first design aspect that can be controlled. Based on the analytical model [7], that is f=c/2a or f=c/2h, there is a direct relation between the frequency and the dimensions (a=width or length, and h=height) of the scattering elements (Fig.2). This model gives an indication of the starting frequency from which the scattering becomes effective; below this frequency only the specular mode is reflected by the profile. However it should be kept in mind that in order to characterize the diffusers with a random-incidence scattering coefficient according to ISO 17497-1 [5], the height of the diffusive elements is restricted to a maximum of 1/16 of the diameter of the measurement rotating table(≈24cm).
Bradley et al. [17] verified that increasing the height of pyramids are achieved better scattering coefficients values. The test involved two types of pyramids (shallow and deep, that have an height that is three times that of the *shallow* pyramids) build in fiberboard and measured in a 1:4 scaled reverberation chamber. The height influences the scattering performance mainly in low and mid frequencies: scattering values are higher for increasing height.
The same results are confirmed by the work of Lin, Hong and Lee [18]. In this case the samples are built in wood and consist in a set of extruded profiles with different heights, where the variation is based on mathematical sequence as the Schroeder's diffusers. The surfaces are composed by the same profiles translated in *z* direction (the maximum height of 8 cm, 6 cm and 4 cm). Kim, Jang and Jeon [19] investigated the optimum height of 3D diffusers and found that a height of around 20cm (full scale) increases the scattering values at a frequency range 500-3150Hz.
Tsuchiya, Lee, and Sakuma [20] tested a variety of rib structures with a height of 1, 2.5 and 4.5 cm and width of 2.5 cm (scale 1:4). It was shown that the scattering values improve frequencies below 500Hz when higher elements are used. Furthermore, it was noticed that the use of elements with different heights (2.5 and 4.5 or 1, 2.5 and 4.5 cm) in the same panel improves the scattering values all over the frequency range of interest (125-4000Hz).This solution leads to more similar values

between adjacent frequencies, resulting in a smoother curve of the frequency dependent scattering.

The research of Choi [3] investigates periodic type diffusers based on rib structures in 1:5 scaled reverberation chamber. Three configuration are tested, ribs with a square cross section of 1cm, 2 cm, 4.4cm. The measured scattering coefficients increase in relation to the size of the ribs (width, length and height). Also in this case, the bigger elements led to higher scattering values at low and mid frequencies.

Lee, Tsuchiya, and Sakuma [21] showed that the combination of elements with different dimensions based on a fractal order leads to higher scattering values that covers the effective frequency ranges of the small and bigger elements. They also showed that the fractal typology has a higher uniformity in the polar distribution of the scattered energy. The Diffractal® is a similar example which imbeds high frequency diffusers within a low frequency diffuser to deal with periodicity and broader effective frequency range [8].

2.2.2 Configuration of the scattering elements

Different studies have investigated the effects of the periodic and aperiodic (randomized) configuration of the scattering elements of a diffusive surface. According to Jeon, Lee and Vorländer [22], the random array of cubes of 2cm (scale 1:10) produces a higher value of scattering coefficient for frequencies around 500-1000Hz and at high frequencies, starting from 3.15 kHz. The same result is found also in the research of Tsuchiya, Lee and Sakuma [20], for cubes of 5cm (scale 1:4) and cubes of 20cm (real scale) in Shtrepi at al. [23]. This is mainly evident at 500-1000Hz. Moreover, Lee et al. [21] obtained similar results based on the variations of a penrose configuration.

2.2.3 Coverage density of the scattering elements

Another geometric characteristic that should be considered is the coverage density of the scattering elements. According to the work of Tsuchiya, Lee and Sakuma [20], the scattering values are higher for a 50% density compared to a 25% or 75% coverage density of cubes of 5cm (20cm in real scale) distributed in a regular array. The improvement is noticed at medium and high frequencies.

This aspect has been investigated also in Jeon, Lee and Vorländer [22], through measurements with wooden hemispheres, radius 17.5 mm. The coverage densities of the hemispheres covering the base plate were 14, 28, 43, 57 and 71%. The most suitable coverage density was found to be around 57 - 58 % of the total surface. The improvement is noticed from averaging allover 1/3-octave band values. Kim, Jang and Jeon [19] studied coverage densities for 1D, 2D and 3D diffusers and reported that the optimal coverage density is around 38% , 46% and 57%, respectively.

2.2.4 Distance between the scattering elements

Tsuchiya, Lee and Sakuma [21]tested also the influence of the distance between the scattering elements. Structures of 2.5cm were put 10cm and 5cm (scale 1:4) apart from each other. It was shown that the scattering values improve at mid frequencies between 500-2000Hz when the more distant elements are considered.

However, the distance between the elements, reduces the coverage density, thus a compromise must be made between these two design aspects. Schmich-Yamane et al. [12] studied the scattering coefficients due to different configurations of periodic rectangular ribs of 4.7cm (real scale). They showed that increasing the distance between the periodic elements (e.g. series 4, 1000 and series 7, 1000000) leads to a decrease of the scattering values in the frequency range 500-3150Hz.

2.2.5 Shape profile of the scattering elements

The shape variation is also an important design variable. It was shown in section 2.1 that the shape influences the diffusion coefficient. Sakuma and Lee [24] investigated three types of samples with periodic surfaces, that is a rectangular, a triangular and a semi-circular profile. The shape affects the scattering performance at mid and high frequencies. High frequencies are improved by the triangular and semicircular shape, while the mid frequencies by the rectangular profile.

De Geetere and Vermeir [25] showed that a sine sweep profile improves the scattering at high frequencies compared to rectangular elements distributed as ribs and checkerboard.

The triangular profile has been shown to be a good diffuser only for specific generator angles. ($30° < \chi < 45°$); narrower or larger angles would lead to specular reflections or to absorption phenomenon, respectively [8].

It was shown that the alternation of concave and convex surfaces leads to higher scattering values [26]. These become higher when the convex surfaces are perpendicular to the concave ones.

Lee, Tsuchiya, and Sakuma [21] showed that prismatic elements lead to higher scattering values compared to pyramids or plates of the same dimensions.

3. EVALUATION OF THE DIFFUSIVE SURFACES

Different theoretical models have been used to analyse the sound waves reflected by a diffusive surface [10]. Most of these models are implemented based on FEM and BEM methods, which require advanced theoretical knowledge, very long calculation times and no immediate feedback is available. Therefore, these aspects leave apart designers from the acoustical investigation of the surfaces they design.

By the use of parametric modeling and computer programming techniques, acoustic performance can be integrated into architectural design workflows [27, 28]. Shtrepi et al. [28], showed an integrated evaluation method of the worth of diffusers (Fig.3). Both a 3D modeling software (Rhinoceros) and an acoustic ray tracing software (Pachyderm) have been used to optimize a complex diffusive surface, which has been designed based on the above mentioned criteria.
Moreover, the advancement of the production technologies has made possible the generation of very complex surfaces. Examples of the use of 3D printers, CNC milling machines, and industrial robots can be found in recent studies [27-30].

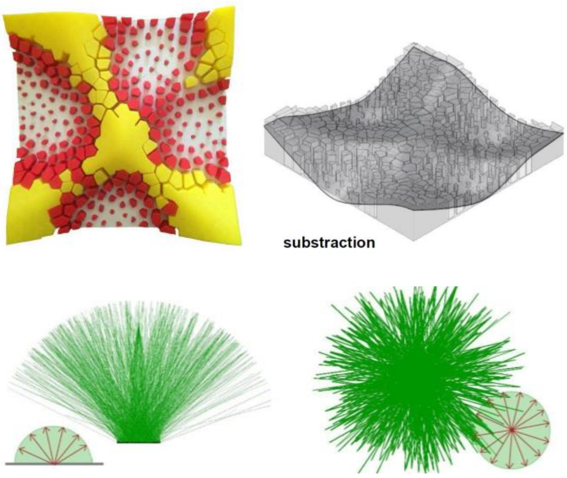

Fig.3. 3D print and spatial distribution of the scattered reflections of an optimized diffusive surface [28].

4. CONCLUSION

This paper has analyzed different studies, which have investigated the diffusive surface based on the ISO 17497-1 standard. The aim was to analyze the geometrical rules tested in each experiment in order to give useful and simple guidelines to designer for the optimization of the diffusers performance.
Finally, the geometrical rules could be summarized as follows:

- **Elements dimensions:** The geometrical dimensions of the elements are directly related to the effective frequency. In particular, the height of the scattering elements influences the scattering performance mainly at low and mid frequencies.
- **Elements configuration:** Mid frequencies seem to be the most affected by the randomization of the scattering elements.
- **Coverage density:** A coverage density of about 50-60% would improve the overall range of frequencies.
- **Distance between elements:** Distant elements improve scattering coefficients at mid frequencies between 500-2000Hz.
- **Shape profile:** Triangular and semicircular shape improve scattering coefficient at high frequencies, while a rectangular profile mainly affects mid frequencies.

Further aspects could be investigated through BEM simulations in a more systematic way in future work.

4. REFERENCES

[1.] C. Haan and F.R. Fricke: **An evaluation of the importance of surface diffusivity in concert halls**. Applied Acoustics 51(1), 1997, 53-69.

[2.] L. Beranek, ***Concert and opera halls: how they sound***. Acoustical Society of America, Woodbury, New York, 1996

[3.] Y.J. Choi: **Effects of periodic type diffusers on classroom acoustics**, Applied Acoustics, 74, 2013, 694-707

[4.] H. Onaga, J.H. Rindel, **Acoustic characteristics of urban streets in relation to scattering caused by building façades**, Applied Acoustics 68 (3), 2007, 310-325.

[5.] ISO 17497: Acoustics -- Sound-scattering properties of surfaces -- Part 1: Measurement of the random-incidence scattering coefficient in a reverberation room, 2004.

[6.] ISO 17497-2:2012: Acoustics -- Sound-scattering properties of surfaces -- Part 2: Measurement of the directional diffusion coefficient in a free field, 2012.

[7.] T. J. Cox1, B.-I. L. Dalenback, P. D'Antonio, J. J. Embrechts, J. Y. Jeon, E. Mommertz, M. Vorlander, **A Tutorial on Scattering and Diffusion Coefficients for Room Acoustic Surfaces**, Acta Acustica united with Acustica 92, 2006, 1-15

[8.] T. J. Cox and P. D'antonio Cox, ***Acoustic Absorbers and Diffusers: Theory, Design and Application***. Taylor and Francis, New York, USA, 2017.

[9.] M. Vorländer, **International Round Robin on room acoustical computer simulation**s. 15th International Congress on Acoustics Trondheim, Norway, 1995.

[10.] J.-J. Embrechts, L. De Geetere, G. Vermeir, M. Vorländer, and T. Sakuma: **Calculation of the Random-Incidence Scattering Coefficients of a Sine-Shaped Surface**. Acta Acustica united with Acustica 92(4), 2006, 593-603.

[11.] J.-J. Embrechts, and A. Billon: **Theoretical Determination of the Random- Incidence Scattering Coefficients of Infinite Rigid Surfaces with a Periodic Rectangular Roughness Profile**. Acta Acustica united with Acustica 97(4), 2011, 607-617.

[12.] I. Schmich-Yamane, M. Malgrange, and C. Rougier: **How absorptive can a diffuser be to accurately measure random incidence scattering coefficients?** Proceedings of Meetings on Acoustics, Montreal, 2013.

[13.] T. J. Hargreaves, T. J. Cox, Y. W. Lam, and P. D'Antonio: **Surface diffusion coefficients for room acoustics: Free-field measures.** The Journal of the Acoustical Society of America 108(4), 2000, 1710-1720.

[14.] T. J. Cox: **The optimization of profiled diffusers.** The Journal of the Acoustical Society of America 97(5), 1995, 2928-2936.

[15.] R. J. Orlowski: **Shape and diffusion in the design of music spaces**. 17th International Congress on Acoustics, Rome, Italy, 2001.

[16.] D. Takahashi: **Development of optimum acoustic diffusers**. Journal of the Acoustical Society of Japan (E) 16(2), 1995, 51-58.

[17.] D. T. Bradley, A. Sharma, and J. Adelgren: **Assessing the effectiveness of geometrically modified pyramidal diffusers: Scattering coefficient measurements**. 166th Meeting of the Acoustical Society of America, San Francisco, USA, 2013.

[18.] F.-M. Lin, P.-Y. Hong, and C.-Y. Lee: **An experimental investigation into the sound-scattering performance of wooden diffusers with different structures**. Applied Acoustics 71(1), 2010, 68-78.

[19.] Y. H. Kim, H. S. Jang, and J. Y. Jeon: **Characterizing diffusive surfaces using scattering and diffusion coefficients**. Applied Acoustics 72(11), 2011, 899-905.

[20.] Y. Tsuchiya, H. Lee, T. Sakuma: **Scale model measurements of the scattering coeffcients of rib/block structure walls**, AIJ J. Technol. Des. 19(41), 2013, 175-178.

[21.] H. Lee, Y. Tsuchiya, T. Sakuma: **Acoustic scattering characteristics of Penrose-tiling-type diffusers**, Applied Acoustics 130, 2018, 168–176.

[22.] J. Y. Jeon, S. C. Lee, and M. Vorländer: Development of scattering surfaces for concert halls. *Applied Acoustics* **65**(4), 2004, 341-355.

[23.] L. Shtrepi, A. Astolfi, G. D'Antonio, G. Vannelli, G. Barbato, S. Mauro, A. Prato**, Accuracy of the random-incidence scattering coefficient measurement**, Applied Acoustics 106, 2016, 23–35.

[24.] T. Sakuma and H. Lee, **Recent topics in acoustic scattering coefficient determination for wall surfaces.** International Symposium on Room Acoustics ISRA 2013, Toronto, Canada, 2013.

[25.] L. De Geetere, and G. Vermeir: **Investigations on real-scale experiments for the measurement of the ISO scattering coefficient in the reverberation room**. Forum Acusticum 2002: 3rd European Congress on Acustics, Sevilla, Spain, 2002.

[26.] C. Bibby, and M. Hodgson, **Characterization and improvement of absorption and scattering by profiled architectural surfaces without specialized test facilities**. Applied Acoustics 72(11), 2011, 889-898.

[27.] B. Peters, T. Olesen, **Integrating Sound Scattering Measurements in the Design of Complex Architectural Surfaces: Informing a parametric design strategy with acoustic measurements from rapid prototype scale models**, in Future cities: 28th eCAADe Conference Proceedings, 2010, 481 - 491,.

[28.] L. Shtrepi, J. Menichelli, A. Astolfi, T. Mendez, M. Masoero**. Improving scattering surface design with rapid feedback by integrating parametric models and acoustic simulation**, The Journal of the Acoustical Society of America 142, 2017, 2499.

[29.] Kohler, M Gramazio, and J Willmann. ***The robotic touch: How robots change architecture***, 2014.

[30.] D. Reinhardt, D. Cabrera, A. Jung, and R. Watt, **Robotic Fabrication in Architecture**, Art and Design, 2016.

8th Congress of the Alps Adria Acoustics Association
Zagreb, Croatia
20 – 21 September 2018

Hrvatsko akustičko društvo
HAD
Acoustical Society of Croatia

ACOUSTICS QUALITY OPTIMIZATION OF THE LISTENING ROOM

Vladimir Olujić, Siniša Fajt, Tin Obradović

University of Zagreb, Faculty of Electrical Engineering and Computing,
Unska 3, 10000 Zagreb, Croatia
vladimir.olujic@storm.hr

Abstract: *The paper analyzes the procedures for optimizing the acoustic quality of the listening room. Existing state of the objective acoustic parameters were modeled using application EASE (Enhanced Acoustic Simulator for Engineers) ver. 4.4. Measurements of the acoustic quality were carried out using the EASERA (Electronic and Acoustic System Evaluation and response Analysis) application conforming to the ISO3382 standard. These results are then compared to a computer simulated model. The following values of the objective parameters of the acoustic quality were measured: early decay time (EDT), the reverberation time (Tr), clarity (C) and definition (D). Subsequent optimization of the acoustics of space suggested solutions for its improvement, ie fine tuning.*

Key words: room acoustics, listening room, vibration system, reverberation time, acoustical measurements, acoustical parameters, coefficient of the absorption, computer simulation

1. Introduction

The sound process in the listening room can be modeled through the physical picture of the complex resonant system. The titration system, as in this case, the listening room or the combination of the resonant systems oscillates at the frequency emitted by the sound source. However, after the attenuation of the sound source in the room, it begins to stimulate the sound energy at the frequency of the nearest natural frequency of the room. As a result, we notice linear amplitude and phase distortion of the excitation signal at the reverberation of the sound pulse. Generally, a complex sound pulse will initiate more of them.

An additional problem arises when between each pair of parallel walls of the room, when acting the complex tone source signal, initiates and interferes with each other a series of standing waves.

This text describes the basic features of the acoustic space in the listening room based on a computer simulation of impulse response simulating reverberation time according to the frequency, the application of objective measurement methods for acoustic quality evaluation and the iterative procedure of alteration of the room wall material to improve acoustic quality.

2. Stages of the optimization process

As the processes of modeling, measuring, evaluating and optimizing the acoustics of the listening room are interrelated, it is instructive to state all the phases of the process, and then individually describe them:

1. Measurement of the size and physical form of the listening room with the measuring of the absorption surfaces dimensions,
2. Detection of features and coefficients of absorption of individual surfaces,
3. Input of measurement results into software application and drafting of the plan of the listening room,
4. The file entry of the floor plans, side views and absorption coefficients of the wall surfaces to the application support of the simulator,
5. Production of the physical model of the listening room,
6. Selection of objective parameters of room acoustical quality, measurement method, measuring equipment and test signals,
7. Arithmetic calculation of certain parameters of acoustic quality,
8. Computer simulation (modeling) of the listening room - impulse response and calculations with display of results,

9. Computer simulation by migrating test files and processing in specialized application support,
10. Evaluation of computer simulation results with regard to purpose of the listening room,
11. Measurement of objective acoustic parameters of the listening room (application support and peripheral measuring equipment),
12. Analysis of the obtained results and their comparison with the empirical curves of the reverberation and the estimate of the obtained results of objective parameters of acoustic quality of the listening room,
13. The testing of subjective parameters of acoustic quality,
14. Analysis of the quality of the subjective and objective parametars of the listening room
15. Corrective Process:
    a) correcting and redesigning of the wall surfaces
    b) implementation of wall coverings with corrected acoustic properties and return to phase 11.

2.1. Measurement of the size and physical form of the listening room with the measuring of the absorption surfaces dimensions

Measurement of dimensions and physical form of listening room is simple to be performed by laser device. It is important to keep in mind that each of the surfaces generally occupies specific features including the absorption coefficient.
Measured basic physical dimensions of the paralelepipedic listening room are: 6,223 [m] x 4,650 [m] x 3,02 [m]. The aforementioned physical dimensions are only a rougher representation of space dimensions. The more precise design was made by adding additional details and processed with the aid of adequate application support.

2.2. Detection of features and coefficients of absorption of individual surfaces

Detection of the features and absorption coefficients of individual surfaces is a more complex process. It is advisable to inspect the project documentation of the space, the bill of quantities, or the specification of the embedded materials and detect the type of installed lining, parquet, wooden planks, surfaces covered with plaster or concrete, as well as the surfaces of the doors and windows. For many of the built-in surfaces, it is possible to find the absorption characteristics and coefficients on the manufacturer's web site.

For the vast majority of standard wall surfaces, it is possible to find absorption coefficients in the simulation software database. For this purpose, the well-known application solution EASY (Enhanced Acoustic Simulator for Engineers) 4.4 was used, intended for acoustic space parameter estimations and sound system design.
For areas that cannot be properly detected it is recommended to perform a measurement.

2.3. Input of measurement results into software application and drafting of the plan of the listening room

Measured dimensions of the listening room are entered and plotted in Microsoft Visio software.

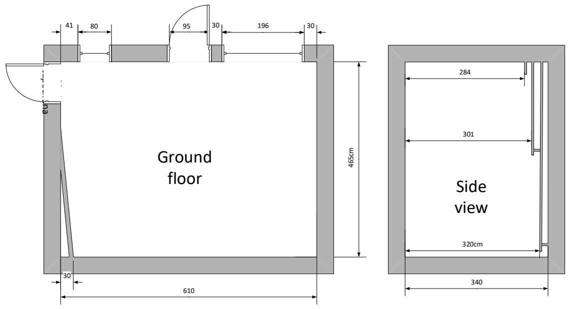

Fig. 1. The digitized drawing of the listening room

2.4. The file entry of the floor plans, side views and absorption coefficients of the wall surfaces to the application support of the simulator

The digitized drawing of the listening room is entered into the EASE application. This product incorporates all the surfaces and the relevant characteristics of the absorption materials of the listening room obtained from the lining manufacturer, as well as some of the simulator database.

2.5. Production of the physical model of the listening room

The EASE application can present 2D and 3D physical space display. Due to the 2D views in Visio's program support, the 3D model of the EASE software is shown here.

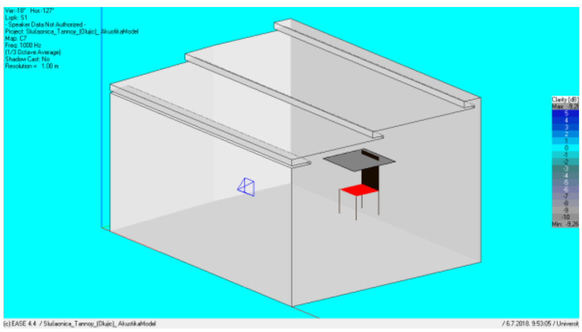

Fig. 2. 3D physical model of the listening room

2.6. Selection of objective parameters of room acoustical quality, measurement method, measuring equipment and test signals

Target acoustic quality parameters are determined by the ability to carry out objective measurement methods. They are also defined and recommended according to standard ISO 3382. The association of measured objective values with subjective parameters of acoustic quality correlates with the taste of the listener and his psychoacoustic experiences. The results of measurements and calculations of objective parameters must demonstrate a high degree of repeatability while simultaneously providing the same metering conditions. Below is coming up the more detailed description of the objective parameters of the acoustic quality assessment used in this paper.

2.6.1. Reverberation Time - Eyring

For low absorption values up to about 0.2, Sabine's formula is a special case of Eyring's expression.C. F. Eyring's formula is:

$$T_r(f) = 0{,}16\frac{V}{-S\cdot ln\,(1-\alpha(f))}\ [s] \tag{1}$$

2.6.2. Early Decay Time (EDT)

Early decline rates were suggested by Atal (1965) and Jordan (1975) as the sound energy deceleration time of 0 to -10 dB extrapolated to a 60 dB drop. The recommended measuring frequencies are: 125, 250, 500, 1000 and 2000 Hz.

2.6.3. Reverberation Time - *T_{20}* and *T_{30}*

For practically feasible measurements and inability to achieve the dynamic of the 60 dB real environment, the T20 and T30 were introduced, among other things, as sound-based reverberation estimates from -5 dB to -25 dB and from -5 dB to -35 dB, extrapolated to a level of 60 dB.

2.6.4. Clarity - *C_{50}* and *C_{80}*

Beranek and Schultz (1965), Reichardt (1975), Alim and Schmidt (1965) proposed Clarity as an objective parameter of the acoustic quality. The recommended measuring frequencies are: 125, 250, 500, 1000 and 2000 Hz. Generally it can be counted with different time parameter intervals.

$$C_{50} = \frac{E_{0-50ms}}{E_{50ms-\infty}} = \frac{\int_0^{50} p^2\,(t)dt}{\int_{50}^{\infty} p^2\,(t)dt} \tag{2}$$

$$C_{80} = \frac{E_{0-80ms}}{E_{80ms-\infty}} = \frac{\int_0^{80} p^2\,(t)dt}{\int_{80}^{\infty} p^2\,(t)dt} \tag{3}$$

$$C_{50} = 10\cdot\log\left(\frac{E_{0-50ms}}{E_{50ms-\infty}}\right) = 10\cdot log\left(\frac{\int_0^{50} p^2\,(t)dt}{\int_{50}^{\infty} p^2\,(t)dt}\right)[dB] \tag{4}$$

$$C_{80} = 10\cdot\log\left(\frac{E_{0-80ms}}{E_{80ms-\infty}}\right) = 10\cdot log\left(\frac{\int_0^{80} p^2\,(t)dt}{\int_{80}^{\infty} p^2\,(t)dt}\right)[dB] \tag{5}$$

2.6.5. Definition - *D_{50}*

The definition is the objective parameter of the acoustic quality proposed by Thiele (1953). The recommended measuring frequencies are: 125, 250, 500, 1000 and 2000 Hz.

$$D_{50} = \frac{E_{0-50ms}}{E_{0ms-\infty}} = \frac{\int_0^{50} p^2(t)dt}{\int_0^{\infty} p^2(t)dt} \tag{6}$$

$$D_{50} = 10\cdot log\left(\frac{E_{0-50ms}}{E_{0ms-\infty}}\right) = 10\cdot log\left(\frac{\int_0^{50} p^2(t)dt}{\int_0^{\infty} p^2(t)dt}\right)[dB] \tag{7}$$

2.7. Arithmetic calculation of certain parameters of acoustic quality

Using simple arithmetic terms, it is possible to calculate certain parameters of acoustic quality such as reverberation time, optimum reverberation time, and parameters such as the mean absorption coefficient, the mean free path length, and the associated number of reflections before the atenuation level to -60dB. The mean coefficient of absorption can be calculated according to the formula:

$$\alpha = \frac{a_1S_1 + a_2S_2 + a_3S_3 + \cdots + a_iS_i}{S} \tag{8}$$

What in the observed case results in α = 0,16. This simple arithmetic expression, of course, does not take into account the dependence of the reflection coefficient toward frequency.
The mean free path, under the condition of sufficient reflections, can be calculated from the formula: [1]

$$l = \frac{4V}{S}\ [m] \tag{9}$$

If we enter the values of the volume and the surface of the listening room we get a value for mean free path:
l = 2.57 m.

The following formula describes the relationship of the decrease in the intensity of sound due to N multiple reflections for 10^{-6} from the starting amount: [1]

$$(1-\alpha(f))^N = 10^{-6} \tag{10}$$

And with the previously calculated mean absorption coefficient, we get the average number of reflections before attenuation N = 79.
In Eyring's formula (1), the size, room surface, volume and the previously calculated mean absorption coefficient are known, from which it is possible to obtain the reverberation time $T_r(f)$ = 0.57 s.
According to the requirements of the Nordic Public Broadcasting Corporation, the optimum reverberation time for listening rooms can be determined according to the expression: [2]

$$T_{r\ opt} = T_0 \sqrt{\frac{S}{S_0}} \pm 0.05\ [s] \tag{11}$$

Where is:
S_0 = 60 m^2, T_0 = 0.35 s, S - floor surface of the room,
S = 6,223 x 4,650 = 28.94 m^2, which gives the result
$T_{r\ opt}$ = 0.24 ± 0.05 s.

The arithmetic calculation of the reverberation time, as has already been mentioned, does not show the frequency dependence and thus does not allow the selection of corrective absorbers for the purpose of interpolating the reverberation function in the spectral band required.
However, these terms provide the possibility of a rough estimate of the acoustic quality of the listening room, the calculation of the target value of the mean coefficient of absorption and the target value of the reverberation time.

Calculation shows that the reflection time of the tested listening room is 0.57 s, while its optimum time should be closer to 0.4 s. Some other authors for the listening rooms purpose further reduce reverberation time.

2.8. Computer simulation (modeling) of the listening room - impulse response and calculations with display of results

Computer simulation with EASE 4.4 may, inter alia, show a reverberation function toward frequency. Certain authors recommend achieving approximately uniform dependence of the reverberation time, which in this case is about 0.4 s.

However, it is shown that it is advisable to model the response time in accordance with empirically defined curves, where the purpose of the space and the type of musical expression define its shape.
The critical bandwidth of the frequency characteristic is between 500 Hz and 2 kHz, where small variations in reverberation time have a significant effect on acoustic quality. To achieve better music acoustics below this band, a small drop of the curve between 300-500 Hz and then its continued increase toward the lower boundary frequency is desirable.

Above the frequency of 3-4 kHz, in larger rooms there is a fall of the reverberation curve due to the absorption effect.

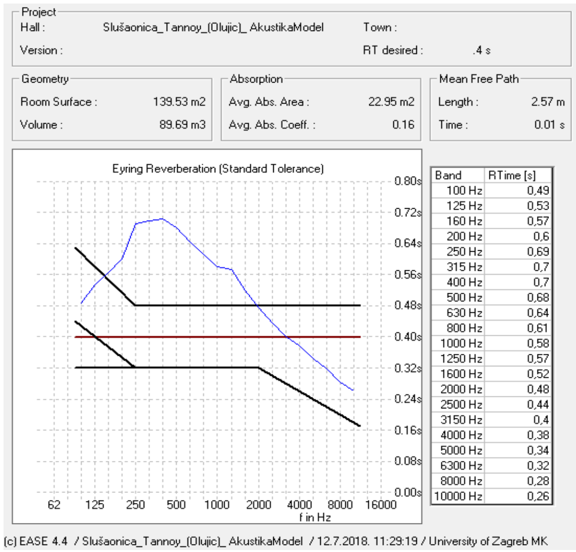

Fig. 3. Computer simulation of the reverberation curve and the recommended frequency band format before the surfaces correction

#	G	Item	Vis	Img	Face Material	Color	Surface [m2]	Shading	Locked	Sides
1		F1	Yes	Yes	ZLZ Mat - Gips ploca Knauf	15132390	8,47	Yes	No	12
2		F2	Yes	Yes	ZLZ Mat - Gips ploca Knauf	15132390	4,50	No	No	12
3		F3	Yes	Yes	ZLZ Mat - Gips ploca Knauf	15132390	16,96	No	No	4
4		F4	Yes	Yes	ZLZ Mat - Gips ploca Knauf	15132390	2,74	Yes	No	4
5		F5	Yes	Yes	ZLZ Mat - Gips ploca Knauf	15132390	0,30	Yes	No	4
6		F6	Yes	Yes	ZLZ Mat - Gips ploca Knauf	15132390	2,74	Yes	No	4
7		F7	Yes	Yes	ZLZ Mat - Gips ploca Knauf	15132390	0,77	No	No	4
8		F8	Yes	Yes	ZLZ Mat - Gips ploca Knauf	15132390	13,66	Yes	No	4
9		F9	Yes	Yes	ZLZ Mat - Gips ploca Knauf	15132390	0,31	Yes	No	4
10		F10	Yes	Yes	ZLZ Mat - Gips ploca Knauf	15132390	1,60	Yes	No	4
11		F11	Yes	Yes	ZLZ Mat - Gips ploca Knauf	15132390	0,80	Yes	No	4
12		F12	Yes	Yes	ZLZ Mat - Gips ploca Knauf	15132390	15,49	Yes	No	5
13		F13	Yes	Yes	ZLZ Mat - Gips ploca Knauf	15132390	0,31	Yes	No	4
14		F14	Yes	Yes	ZLZ Mat - Gips ploca Knauf	15132390	1,61	Yes	No	4
15		F15	Yes	Yes	ZLZ Mat - Gips ploca Knauf	15132390	0,81	Yes	No	4
16		F16	Yes	Yes	ZLZ Mat - Gips ploca Knauf	15132390	2,54	No	No	4
17		F17	Yes	Yes	ZLZ Mat - Gips ploca D127 12/25Q	65280	14,64	No	No	16
18		F18	Yes	Yes	CONCRETE S	12632256	2,06	No	No	4
19		F19	Yes	Yes	CONCRETE S	12632256	1,53	No	No	4
20		F20	Yes	Yes	CONCRETE S	12632256	12,03	No	No	16
21		F21	Yes	Yes	DRAPE THIN	65471	2,45	No	No	4
22		F22	Yes	Yes	DRAPE THIN	65471	0,96	No	No	4
23		F23	Yes	Yes	DRAPE MED	49151	2,06	No	No	4
24		F24	Yes	Yes	DRAPE MED	49151	1,71	No	No	4
25		F25	Yes	Yes	CARPT COMM	5000345	28,48	No	No	9
						Sum surface [m2]	139,53			

Table 1. Measured surfaces and types of the wall linings before the surfaces correction and computer simulation

2.9. Computer simulation by migrating test files and processing in specialized application support

The file obtained with EASE software is migrated to the EASERA application with a focus on measuring and calculating objective parameters of acoustic quality

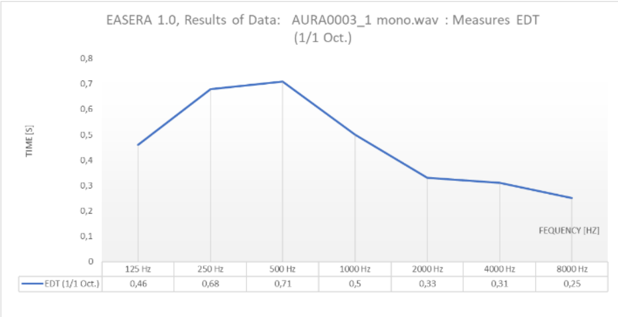

Fig. 4. EASERA simulation of the EDT curve

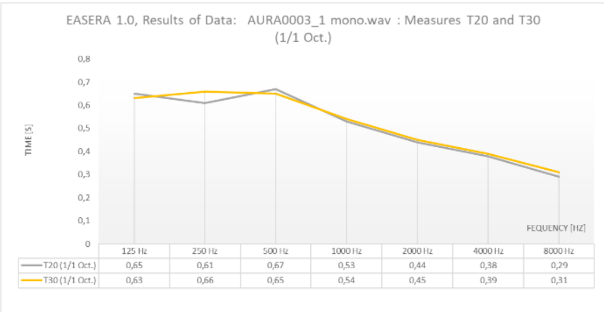

Fig. 5. EASERA simulation of the reverberation time curve -T_{20} and T_{30}

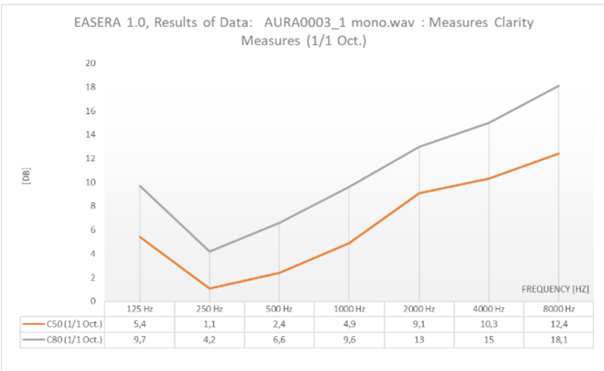

Fig. 6. EASERA simulation of the Clarity - C_{50} and C_{80}

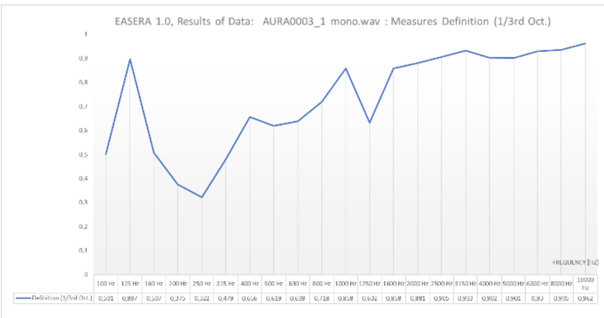

Fig. 7. EASERA simulation of the Definition - D_{50}

2.10. Evaluation of computer simulation results with regard to purpose of the listening room

The result of EASE software simulation of the computer acoustic quality of the room of the impulse response method in Figure 3 shows an average reverberation time of almost 0.6 s, while the spectrum curve in the band 150 Hz to 2 kHz does not match the expected limits of the reverberation time.
Computer simulation software EASERA shows the EDC - early decay time function in Figure 4, which coincides with the EASE simulator reverberation function.

The reverberation functions T20 and T30 on Figure 5 are of a similar shape with a somewhat more linear part in the band of 125-250 Hz. It is obvious that the energy signal drop trend slows down after about 15-25 ms.
In the band of 150-500 Hz where the amplitude of the reverberation function rises, there is a decrease of the objective parameters of the acoustic quality: Clarity C50 and C80 in Figure 6 and Definition D50 in Figure 7.

The reverberation functions, EDT, T20 and T30 in the upper part of the spectrum coincide for both simulations. The simulated reverberation curve is well interpolated in the empirically accepted reverberation boundaries in a band of 2 kHz to the upper boundary frequency.

2.11. Measurement of objective acoustic parameters of the listening room (application support and peripheral measuring equipment)

The scheme shows that the measurement was performed using an omnidirectional speaker as a source, output power amplifier, sliding tone as a test signal, omnidirectional microphone Behringer ECM 8000, Tascam US-144 sound card and processing with a portable computer with installed EASERA 1.0 support.

The measurement was performed by octave energy time curve (ETC) analysis.

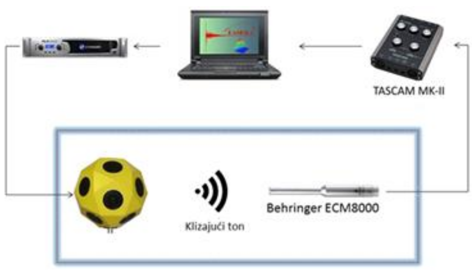

Fig. 8. Sheme of the metering[3]

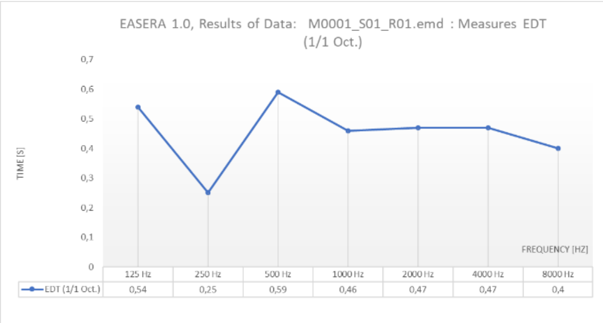

Fig. 9. EASERA measuring results of the EDT curve

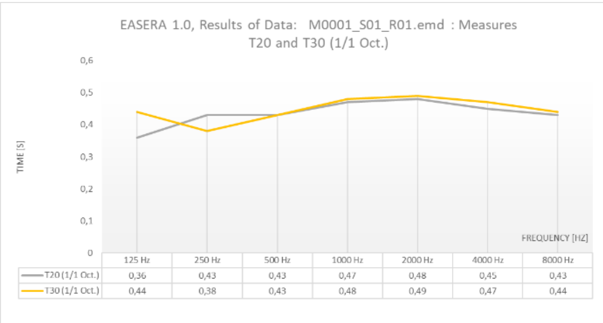

Fig. 10. EASERA measuring results of the reverberation time curve -T_{20} and T_{30}

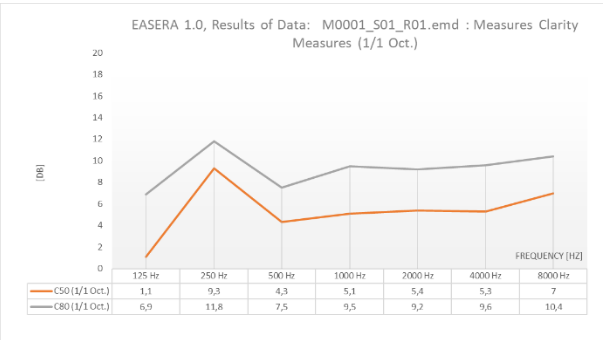

Fig. 11. EASERA measuring results of the Clarity - C_{50} and C_{80}

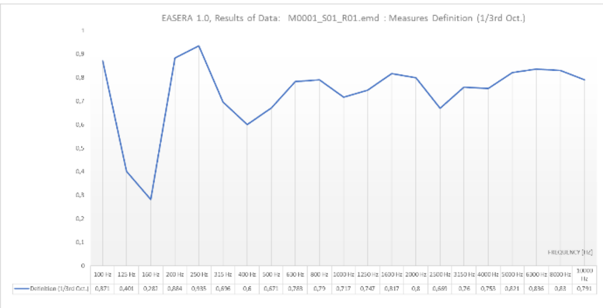

Fig. 12. EASERA measuring results of the Definition - D_{50}

2.12. Analysis of the obtained results and their comparison with the empirical curves of the reverberation and the estimate of the obtained results of objective parameters of acoustic quality of the listening room

Before the hearing room measurements were carried out, it was additionally entered an armchair, a massive carpet of 10 m^2, a pair of Tannoy Westminster Royal loudspeakers (volumes of 530 liters each), the other electroacoustic equipment and a dozen LP gramophone records.

We can expect that the changes in the materials and surfaces in the listening room will change some of the input parameters of the processing. To a certain extent, this will change the results of previously performed simulations. Looking at the EDT function obtained by measuring in Figure 9, we can notice a significant drop in the curve around the center frequency of 250 Hz and the associated band around +/- 100 Hz, according to the same but simulated function in Figure 4.

Measured T20 and T30 reverberation functions in Figure 10 are more linear in the upper frequency band and show a fall in reverberation time from an average of 0.6 ms during the simulation as shown in Figure 5, to an average level of a measured value of 0.4 ms toward the functions shown in Figure 10.

The described decline in the reverberation time measured around the frequency of 250 Hz result in the rise in the level of the objective parameters of the acoustic quality in the lower band, clarity C50 and C80 as shown in Figure 11 and Definition D50 at Figure 12.

It is obvious that the fall of the reverberation time level in certain circumstances implies an increase in the levels of said objective parameters of the acoustic quality.

2.13. The testing of subjective parameters of acoustic quality

In general, a whole set of subjective parameters that describe the acoustic quality of the listening room is known. Although not standardized, some of the common and most commonly mentioned subjective parameters are timbre, vividness, clarity, loudness, etc. In this case, statistical analysis of subjective parameter results was not performed. The overall quality of the acoustic space was good in the middle and upper spectrum of musical performance, demonstrating the quality timbre and definition.

In the lower spectrum, the sound showed significant nonlinearity of the amplitude at certain frequencies. The intensity of the sound was significantly unbalanced toward the middle and upper band of the frequency spectrum. The clarity of the musical performance was good enough, while the spatiality as a subjective parameter was below a minimum acceptable level. The overall rating of the subjective parameters of the acoustic quality of listening was for most listeners is estimated as insufficient.

2.14. Analysis of the the quality of the subjective and objective parametars of the listening room

In case of need of additional processing of the listening room, it is necessary to perform the correction phase. In the case of satisfying the expected acoustic quality, the optimization process can be concluded.

2.14. Corrective Process:

- **a) correcting and redesigning of the wall surfaces**
- **b) implementation of wall coverings with corrected acoustic properties and return to phase 11**

a) It is possible to perform correction of wall linings with the help of the arithmetic methods described in subheading 2.7 and computer simulations with impulse response in subheading 2.8.

Arithmetic methods can provide framework results for correcting the mean value of reverberation. For spectral correction of the reverberation curve, it is necessary to use a computer simulator database and manufacturer's database with corresponding function of the absorption coefficient toward frequency.

The simulator provides an easy calculation of the surface of a specific wall lining as appropriate corrective measures for interpolating the reverberation curve to the functional frame. The corrective process in this case was carried out by modeling the substitution of the material from Table 1, item 12, plaster wall covering of 15.49 m2, whose absorption function toward frequency is shown in Figure 14 for the same surface of D-127 type gypsum, whose absorption function is shown in Figure 15.

Table 2 shows the structure of surfaces after interpolating the replacement lining in item 12, and is the basis for performing corrective computer simulation. The process was carried out by the EASE simulation software, as in the first case. Figure 16 shows the result of the simulation, that is, the reverberation function after the imaginary replacement of the wall covering.

The corrected reverberation function is much better interpolated in the empirically acceptable boundaries of the function for the aforementioned purpose of the auditory room. This correction is just the first step in correcting the required acoustic quality.

Further steps can be made by replacing of suitable types of additional absorption surfaces and even more precise interpolation of simulated reverberation curves or other objective parameters of acoustic quality.

Then it is good to repeat the phase of the migration and simulation of the test file in the specialized EASERA application support like it is already described in subheading 2.9. and evaluation of computer simulation results described in subheading 2.10.

Like replacements of various wall coverings, corrective actions can be performed with the projecting and installation of different types of resonators. The best results can be achieved by combining both methods.

b) incorporation of wall linings with corrected materials of acoustic properties and return to phase of the optimization of the acoustic quality of the auditory room which is described in subheading 2.11.

#	G	Item	Vis	Img	Face Material	Color	Surface [m2]	Shading	Locked	Sides
1		F1	Yes	Yes	ZLZ Mat - Gips ploca Knauf	15132390	8,47	Yes	No	12
2		F2	Yes	Yes	ZLZ Mat - Gips ploca Knauf	15132390	4,50	No	No	12
3		F3	Yes	Yes	ZLZ Mat - Gips ploca Knauf	15132390	16,96	No	No	4
4		F4	Yes	Yes	ZLZ Mat - Gips ploca Knauf	15132390	2,74	Yes	No	4
5		F5	Yes	Yes	ZLZ Mat - Gips ploca Knauf	15132390	0,30	Yes	No	4
6		F6	Yes	Yes	ZLZ Mat - Gips ploca Knauf	15132390	2,74	Yes	No	4
7		F7	Yes	Yes	ZLZ Mat - Gips ploca Knauf	15132390	0,77	No	No	4
8		F8	Yes	Yes	ZLZ Mat - Gips ploca Knauf	15132390	13,66	Yes	No	4
9		F9	Yes	Yes	ZLZ Mat - Gips ploca Knauf	15132390	0,31	Yes	No	4
10		F10	Yes	Yes	ZLZ Mat - Gips ploca Knauf	15132390	1,60	Yes	No	4
11		F11	Yes	Yes	ZLZ Mat - Gips ploca Knauf	15132390	0,80	Yes	No	4
12		F12	Yes	Yes	ZLZ Mat - Gips ploca D127 12/25Q	15132390	15,49	Yes	No	5
13		F13	Yes	Yes	ZLZ Mat - Gips ploca Knauf	15132390	0,31	Yes	No	4
14		F14	Yes	Yes	ZLZ Mat - Gips ploca Knauf	15132390	1,61	Yes	No	4
15		F15	Yes	Yes	ZLZ Mat - Gips ploca Knauf	15132390	0,81	Yes	No	4
16		F16	Yes	Yes	ZLZ Mat - Gips ploca Knauf	15132390	2,54	No	No	4
17		F17	Yes	Yes	ZLZ Mat - Gips ploca D127 12/25Q	65280	14,64	No	No	16
18		F18	Yes	Yes	CONCRETE S	12632256	2,06	No	No	4
19		F19	Yes	Yes	CONCRETE S	12632256	1,53	No	No	4
20		F20	Yes	Yes	CONCRETE S	12632256	12,03	No	No	16
21		F21	Yes	Yes	DRAPE THIN	65471	2,45	No	No	4
22		F22	Yes	Yes	DRAPE THIN	65471	0,96	No	No	4
23		F23	Yes	Yes	DRAPE MED	49151	2,06	No	No	4
24		F24	Yes	Yes	DRAPE MED	49151	1,71	No	No	4
25		F25	Yes	Yes	CARPT COMM	5000345	28,48	No	No	9
						Sum surface [m2]	139,53			

Table 2. Measured surfaces and types of the wall linings after the surfaces correction and computer simulation

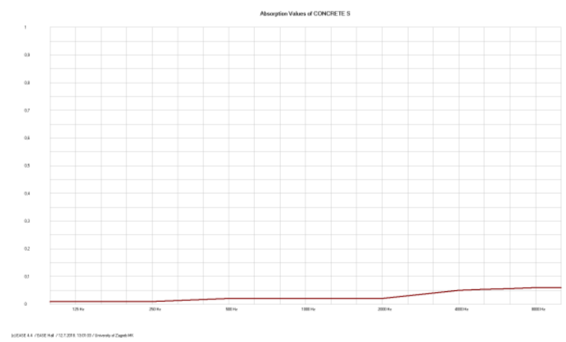

Fig. 13. The curve of the absorption toward frequency for classic concrete wall of the listening room

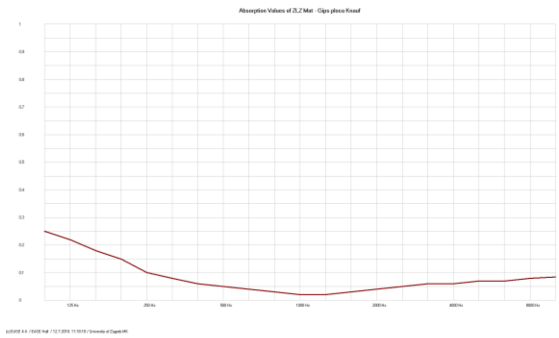

Fig. 14. The curve of the absorption toward frequency for wall lining made of gypsum

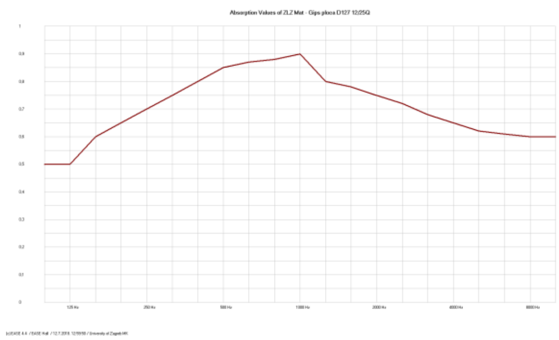

Fig. 15. The curve of the absorption for wall lining made of acoustic gypsum with high absorption value in the lower frequency band (20-400 Hz)

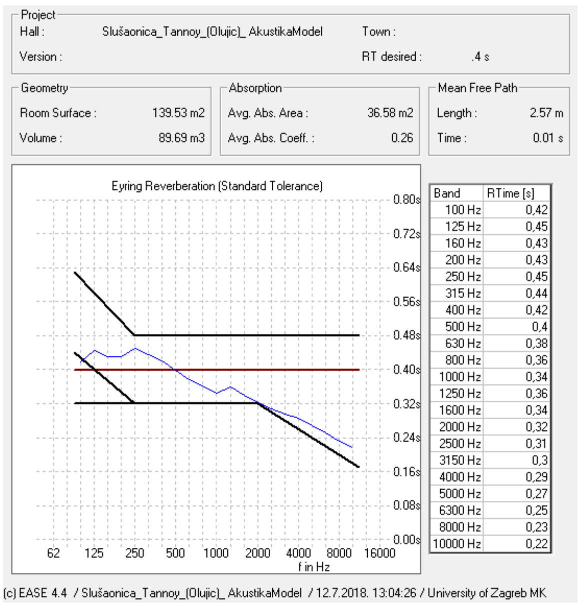

Fig. 16. Computer simulation of the reverberation curve and the recommended frequency band format after the surfaces correction

3. Conclusion

Acoustic quality is generally determined by the ratio of direct and reflected sound energy. By measuring early decay time (EDT) and reverberation time it is possible to evaluate the acoustic quality of the listening room.

This paper describes the optimization of the acoustic quality of listening rooms in realistic conditions of classical living space, ie smaller space areas and volumes. Such spaces are a common environment for day-to-day listening and therefore their optimization is a logical requirement for a more demand audience. Such hearing rooms inherently include some of the specific issues.

Since the number of resonant frequencies of a given spectral band depends on the volume of the auditory space and the square of the its frequency, low frequency sound will stimulate a smaller number of natural frequencies than the high frequency excitation sound.

The problem of the appearance of a small number of resonant frequencies in the lower band of the spectrum is particularly pronounced in small volume listening rooms, because their proportional volume is small, and thus the spacing is large. The increase in the amplitude of the signal at these frequencies has a detrimental impact on the low frequency spectrum of the playback and hence on the overall hearing experience.

The sound field in the lower area, in that case, cannot satisfy the assumption of diffusion or the nature of the sound dispersion.
After the reflection of the sound pulse the sound spectrum does not spread roughly evenly in all directions, so the intensity in the lower part of the spectrum is unevenly distributed in the space.

With conduction of the described phases of the optimization, it is possible to improve the acoustic quality of the hearing rooms.

Using the described simulation, metering methods and the potential application of multiple iterative corrective actions, it is possible that the music experience in its everyday environment will be brought up to significantly higher levels.

4. References

[1.] Tihomil Jelaković: ***Zvuk, sluh, arhitektonska akustika***, *Školska knjiga Zagreb*, 1978, 167-174

[2.] Nordic Public Broadcasting Corporation: ***N 12-A Sound Control Rooms and Listening Rooms***, *Second Edition*, 1992

[3.] Marin Milković, Miljenko Krhen, Siniša Fajt: ***Method of evaluating the quality of room acoustics based on energy relations of sound***, *Tehnički glasnik 8, 3(2014)*, 222-228

[4.] Siniša Fajt, Miljenko Krhen, Tončo Marušić: ***Correlation between objective and subjective acoustic quality parameters of professional sound control rooms***, *Technical Gazette 24, 2(2017), 543-550*

[5.] C. C. J.M. Hak, R.H.C.Wenmaekers, L.C.J.van Luxemburg: ***Measuring Room Impulse Responses: Impact of the Decay Rangeon Derived Room Acoustic Parameters***, Acta acustica united with acustica Vol. 98, 2012, 907–915

[6.] Miljenko Krhen, Siniša Fajt, Marin Milković: ***Principal component analysis in determining the best setup for acoustic measurements in sound control rooms,*** *Tehnički vjesnik 22, 2015, 1327-1335*

[7.] Siniša Fajt: ***Vrednovanje kvalitete akustički obrađenih prostora***, *Doktorska disertacija, Zagreb, 2000*

[8.] F. Alton Everest, Ken C. Pohlmann: ***Master Handbook of Acoustics***, Fifth Edition, The McGraw-Hill Companies, Inc., 2019

8th Congress of the Alps Adria Acoustics Association
Zagreb, Croatia
20 – 21 September 2018

Hrvatsko akustičko društvo
HAD
Acoustical Society of Croatia

THE CASE STUDY ON USER SATISFACTION IN RELATION TO COMFORT CONDITIONS IN MANİSA MOSQUES: ÇEŞNİGİR MOSQUE, İVAZ PAŞA MOSQUE, SULTAN MOSQUE AND HATUNİYE MOSQUE

Fatma Yelkenci Sert

Dokuz Eylül University, İzmir, Turkey, fatma.yelkenci@deu.edu.tr

Özgül Yılmaz Karaman

Dokuz Eylül University, İzmir, Turkey, ozgul.yilmaz@deu.edu.tr

Abstract

The historical mosques are important buildings for Islamic World because of not only representation of beliefs but also being cultural heritage for their community. The mosques have some acoustic problems with negative factors as speaker system, having large volume, incorrect repair solutions on historical ones, etc. These factors reduce the quality of auditory comfort conditions. Additionally, the background noise level must be between optimum values to ensure proper auditory comfort conditions. As results of these acoustic defects and unsuitable background noise level, worshipers can be affected negatively and the feeling of unity or integrity can be lost which are aimed to be created during the rituals.

This study, as a part of the studies that evaluating the acoustic comfort conditions of mosques built in different periods in Manisa, aimed to evaluate acoustic comfort conditions of historical mosques in Manisa through users' evaluations. As case studies, four historical mosques are selected because of having the same plan schema. The method of study consists of the measurement of noise level inside/ outside and the survey for prayers and imams/ muezzins. At the end of study, subjective evaluations about auditory comfort conditions are examined by comparing with the measured background noise levels.

Keywords: Mosque acoustics, architectural acoustics, survey, A-weighted sound levels.

1. INTRODUCTION

Mosque is an important building type for Muslims which is used for religious rituals such as prayer, Qur'an recitations, Khutba and sermon, etc. Historical mosques have an important position in the society having historical significances besides religious importance. The acoustical characteristics of mosques considered as cultural heritage are very important. There is a significant relationship between the cultural heritage building and its acoustics [1]. If some acoustic problems occur in the mosques such as high background noise level, long or short reverberation time, the quality of auditory comfort conditions will be affected badly. The results of acoustic defects prevent the feeling of unity or integrity aimed to be created during religious rituals.

In the literature, there are many studies about the acoustic properties of mosques. Oleg Grabar, one of the leading Islamic art historians, says that the self-representation of Islamic culture is based on hearing more than seeing [2]. In Ergin's study indicate that Ottoman architects sees the mosques as the original revelation is re-staged and they are musical instruments that provide the voices of the Qur'an [3]. Another study about mosques is CAHRISMA (Conservation of the Acoustical Heritage by Revival and Identification of Sinan's Mosques) which the acoustics of Sinan's Mosques and old Byzantine churches have been studied [4]. Gül, Çalışkan and Tavukçuoğlu aimed to investigate the effects of the architectural elements of the Süleymaniye Mosque, the materials used inside and repair solutions on the acoustics of the mosque [5]. Topaktaş studied the acoustic properties of the Süleymaniye, Rüstem Paşa, Mihrimah Sultan (Edirnekapı) and Cenabı Ahmet Paşa Mosques, designed by Mimar Sinan, using acoustic measurements and simulations [6]. In addition to these studies, there are some assessment studies about acoustic with single mosque, many mosques by comparisons each other and comparison studies of mosques to churches. Abdou searched 21 mosques in Saudi Arabia by measurements for evaluating room acoustic parameters [7]. Carvalho and Freitas investigate the acoustical characteristics of the Central Mosque of Lisbon by comparing results to other mosques and Catholic churches with similar volume [8]. 21 mosques in Saudi Arabia and 41 Roman Catholic churches in Portugal are assessed about their acoustical and architectural features in another study [9].

Manisa, in Turkey, has many cultural heritages, especially mosques, which are belongs to Ottoman Empire. The study has taken place four historical mosques as Çeşnigir Mosque, İvaz Paşa Mosque, Sultan Mosque and Hatuniye Mosque. The reasons of choosing these mosques as the case studies are that they were built in the same period and have the similar plan schema. As a subjective method, a survey study which is conducted with the mosque users (imams, muezzins and worshipers) and includes questions about evaluating auditory comfort conditions is presented. As an objective method, the background noise levels are measured in the main worship areas and outside of buildings determined as the study area. At the end of study, subjective evaluations about auditory comfort conditions are examined by comparing with the measured background noise levels.

2. THE EXAMINED MOSQUES

Manisa, whose history resides to the Palaeolithic period, is an important settlement named Magnesia and Sipylum in the antique period in Turkey. Manisa had an important position in the historical period because it was one of the cities to be sanjak in the Ottoman period where princes were educated and managed. Many important buildings were built in Manisa such as mosque, library, school, Turkish bath, commercial building, etc. Because the members of sultanate with princes and the people who are responsible for the princes' education dwelled in this city [10].

In the scope of study, four historical mosques are selected. All of them have the similar plan schema and built in the same historical period. The mosques examined in this study have a central position and circulated with some noise factors such as shops, pedestrian and vehicle circulation axes, houses. Therefore, it is aimed to investigate the effects of these factors on the acoustic conditions of mosques and the religious rituals.

2.1. Çeşnigir Mosque

The building, was built in 1474, has a rectangular plan and three sections [10]. The mosque has a floor area of 182.6 m². The mosque is covered with a large dome in the middle and 4 small dome in the side spaces. The main dome of mosque has a diameter of 9 m. The smaller domes have diameters of 3.30 m. The side spaces are covered by oval domes with pendentive transitional. At the north of main worship area, there is a four-parted narthex with pointed arches sitting on five circle columns (**Fig. 1**).

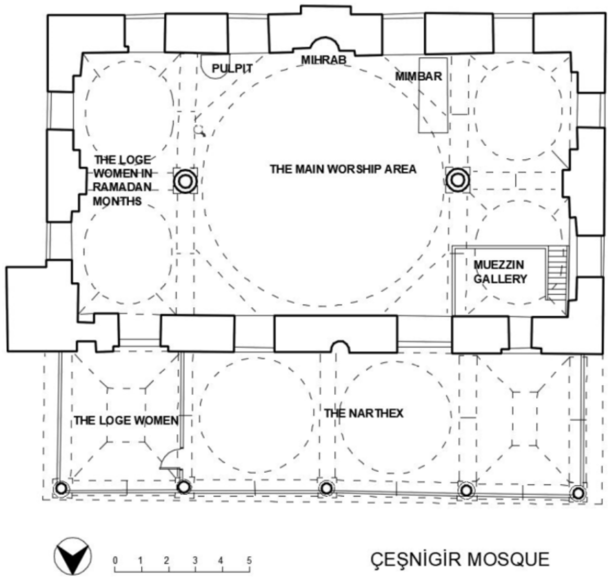

Fig. 1. The plan of Çeşnigir Mosque

Fig. 2. The North facade of Çeşnigir Mosque

The walls of mosque are made of rubble stone, the corners of walls and the narthex are made of cut stones, the arches and the domes are made of bricks (**Fig. 2**). The walls have approximately thickness of 1.10 m. The sermon chair is made of marble, mihrab is made of plaster and the mimbar is made of wood. The floor of mosque is covered with carpet. The narthex is closed by glass surfaces today. The maksoorahs which is elevated parallel to the side spaces was carried out. Instead of these maksoorahs, the east part of narthex is closed by panels for a loge woman. In the month of Ramadan, the east part of main worship area is closed with curtains for loge women. A public park, surrounded by lots of shops and coffee houses, is located at the north and east of mosque. There are dwellings in the south side, and car parking in the west side of the mosque. Because of the shops around the mosque, the community of the mosque is usually made up of shop staff and customers.

2.2. İvaz Paşa Mosque

The mosque was built in 1484, has a rectangular plan and three sections like Çeşnigir Mosque [10]. The mosque has a floor area of 130.5 m². However, they have some different architectural features as volume, transitions from wall to dome, narthex. Although the side spaces in Çeşnigir Mosque are symmetrical, the symmetry between the side spaces is destroyed by the entrance of the grave chamber into the building structure in İvaz Paşa Mosque (**Fig. 3**). Contrary to oval domes with pendentive transitionals in Çeşnigir Mosque, the domes on side spaces are round with triangular transitions. The mosque is covered by a main dome in front of mihrab and smaller domes at the side sections. The main dome of mosque has a diameter of 8.05 m. The smaller domes have diameters of 2.55 m and 3.30 m. The transition of the dome is provided by muqarnas. The maksoorah which is located parallel to the northern wall of the main building was carried out after restoration. A muezzin gallery is added to the northwest of mosque after restoration. The pulpit is made by marble. The mimbar is made by wood.

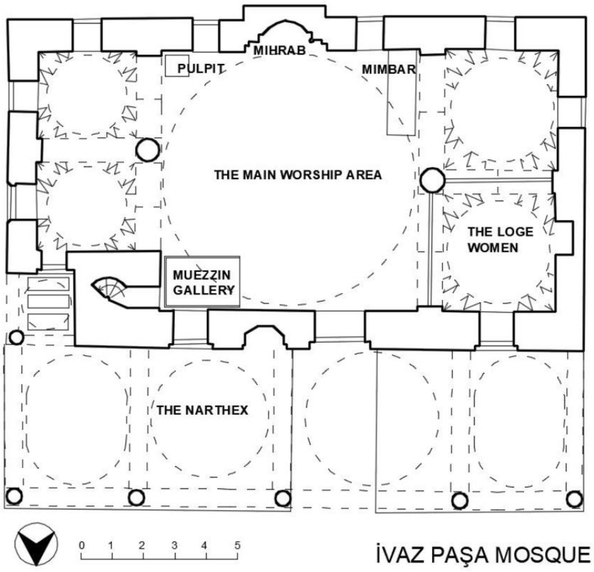

Fig. 3. The plan of İvaz Paşa Mosque

The floor of mosque is covered with carpet. The loge woman takes part at the northeast of mosque by leaving from main worship area with curtains. The muqarnas headed mihrab niche is located on the south wall and is covered by painted plaster. The narthex, which is bounded by five columns, is located 30 cm above the ground. The columns are connected with each other by pointed arches. The mosque is built on a masonry system by using brick and stone (**Fig. 4**). The walls have approximately thickness of 1.20 m.

Fig. 4. The North facade of İvaz Paşa Mosque

2.3. Hatuniye Mosque

The mosque was constructed in 1490, has the similar plan schema with Çeşnigir and İvaz Paşa Mosques [10] (**Fig.5**). The volume is bigger than the others. The structure has a main dome with diameter of 11 m and four smaller domes with diameter of 5 m at side spaces. The mosque has a floor area of 272 m². The mosque as a whole is built on a masonry system by using brick and stone like the other mosques (**Fig. 6**). The walls have approximately thickness of 1.20 m. The main dome is located on octagon hoop supported by walls and columns. The transition from the walls to octagon hoop is provided pendentives. Two columns in the main area have rectangular section and niches. The walls are covered by painted plaster and wooden panels. The pulpit and mimbar are made of wood. The floor is covered by carpets. The loge woman, elevated 30 cm from ground, takes part on the southeast of volume with curtains. The mihrab has a half cylindrical body with a muqarnas head. The five sectional narthex is on the north of mosque is elevated from the ground and covered by wood/ glass surfaces. Hatuniye Mosque is shown as an important structure in the course of the central plan with the effort of connecting the side spaces to the middle space due to 11 m diameter dome [10]. The difference of Hatuniye Mosque from the other mosques is that the central dome is carried by the south and north walls and the middle columns. In other mosques, the large dome is carried with the south and north walls and the hanger arches on the sides.

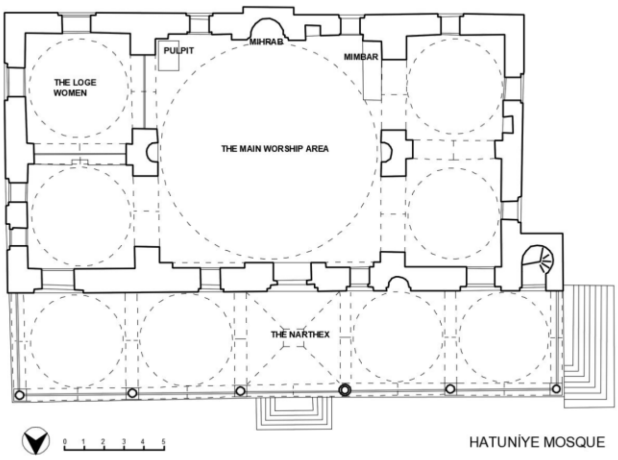

Fig. 5. The plan of Hatuniye Mosque

Fig. 6. The North facade of Hatuniye Mosque

2.4. Sultan Mosque

According to the inscription on the entrance gate, the Sultan Mosque was built by Ayşe Hafsa Sultan, the wife of Yavuz Sultan Selim, in 1522-1523. The architect of mosque is Acem Ali [10]. The Sultan Mosque is similar to the other mosques due to have a rectangular plan with three partitions (**Fig. 7**). The mosque has a volume of approximately 5000 m³ which is covered with a domed composition consisting of a main dome of about 22.5 m in height and two small domes in two sides. The main dome of mosque has a diameter of 11.5 m. The smaller domes have diameters of 5 m. The mosque has a floor area of 312.5 m². The main gate is in the center of five-sectional narthex and on the axis of the altar (**Fig. 8**). The main dome is carried with the south and north walls and the hanger arches on the sides like Çeşnigir and İvaz Paşa Mosques. The transition to the domes is provided by pendentives. Two niches, filled with cabinet elements today, are opened on the eastern and western walls. In the northwest of mosque, there is a maksoorah carried by five wooden masts with square cross-section. Under this place, there is another maksoorah located about 40 cm above the floor for muezzins. The southeastern part of mosque has been raised 50 cm from the ground. Nowadays, this part is divided from the main worship area by reflective panel elements which are later added to the structure and used for women's worship. There are 6 rows of muqarnas workmanship in the mihrab. Mimbar is made of white marble and is said to be preserved in its original state [10]. The entrance of the mimbar element is covered with a rug.

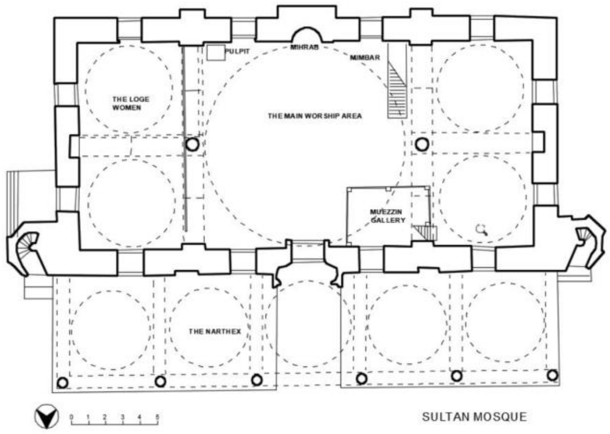

Fig. 7. The plan of Sultan Mosque

Fig. 8. The North facade of Sultan Mosque

The floor is covered by carpets. The interior surfaces of masonry stone walls are plastered and painted. The interior of the mosque has two windows on the east and west walls, and four window openings on the south and north walls. These windows are symmetrically located. The interior volume is naturally illuminated by these window openings. All windows and doors were made of wood. Window pedestals are covered with blue-white İznik tiles. There are stone, gypsum, wood, tile decorations throughout the building. Wood ornaments are in door and window wings. The gypsum ornament is used in the mihrabs.

3. EVALUATION OF MOSQUES

3.1. The measurements of A-weighted sound levels

A-weighted sound levels (LAeq) were measured for four mosques by using the Bruel &Kjaer sound level meter type 2250. The sound levels were measured inside and outside of mosques. The reason of performing inside and outside measurements is to understand the acoustical conditions around the mosques. In the measurements, the height of sound level meter is arranged as 1.5 m. The background noise levels were recorded over 10 minutes intervals. The mean LAeq values for inside and outside each mosque are listed. (**Table 1)**
It is expected that background noise should be between suggested interval limits for good speech intelligibility. The interval limits vary according to the function of building. In the literature, NC25-30 is the recommended noise interval for religious buildings [11]. Knudsen and Harris emphasized in their book that the religious buildings have the necessity for insulation from outside noise. They added the noise of inside doesn't exceed 30 db for religious buildings [12]. It is seen that the A-weighted sound levels of the examined mosques exceeded the recommended limits. The measurements were performed in summer months in which Quran courses are set up in all investigated Mosques in this study. During the measurements, the windows are opened and the courtyards of mosques are full of children playing games and their parents. The Sultan Mosque can be given as an example to understand the effect of varying environmental conditions on the background noise level. In another study, A-weighted sound level (LAeq) of Sultan Mosque is measured as 30 Dba which is in the suggested intervals [13]. The reason of appropriate value that, the air is not very hot, there is no Quran courses or children playing games and the building elements such as the doors and windows are in closed position during the measurement.

	Çeşnigir Mosque	İvaz Paşa Mosque	Hatuniye Mosque	Sultan Mosque
LAeq (inside)	42.3 dB	35.4 dB	50.5 dB	50.2 dB
LAeq (outside, in the courtyard)	52.8 dB	58.4 dB	57.6 dB	59.7 dB
LAeq (outside)	48.2 dB	63.6 dB	64.2 dB	60.0 dB

Table 1. The mean A-weighted sound level (LAeq) values for four mosques

For the Çeşnigir Mosque, resulting A-weighted sound levels (LAeq) is measured to be 42.3 db inside, 52.8 db in the courtyard and 48.2 db in the pathway beside south facade. The interior value is too much according to the recommended limits. There are green areas with seating units, coffee houses, shops in the north and east side, a parking area for cars in the west side and a pedestrian road in the south of mosque. The noise of traffic, the shops and workers can be partially prevented to reach the mosque by using the green areas as a sound bar. In summer months, the children who are playing games in the courtyard are a major noise factor in this mosque. It can be said that the high noise level results are caused by the children.
In the İvaz Paşa Mosque, A-weighted sound levels (LAeq) is measured as 35.4 db inside, 58.4 db in the courtyard and 63.6 db in the traffic way beside east facade. Although the background noise level of inside is lower than other mosques, the value (35.4 db) is obtained above the recommended range. There is a green area to the north, west and south of the building, and a vehicle and a pedestrian path to the east side. The lower inside sound level of Çeşnigir and İvaz Paşa Mosques can be explained by the fact that they are located farther away from the city center than the others. However, the number of child users increases in summer, so it causes an increase in the sound level. The road to the east of the building can be seen as an important noise factor.
Hatuniye Mosque is located in the most intensively used area of the city. In the north of the structure, there is a large square opposite to government office used for sitting or a transition space in the lower ground. There are many coffee houses and shops in the west and heavy traffic flow is on the south and east side of mosque. For the Hatuniye Mosque, resulting A-weighted sound levels (LAeq) is measured to be 50.5 db inside, 57.6 db in the courtyard and 64.2 db in the pathway beside south facade. The 50.5 db for inside of mosque is too much according to the recommended values. This value was obtained when the windows were opened and the fans were running since the mosques were measured in summer months. The Sultan Mosque is located next to the heavy junction. There are green areas with sitting arrangements in the north and west of mosque. The south and east side are surrounded by vehicles and pedestrian paths. It is separated from the surrounding noise factors by the garden wall. A-weighted sound levels (LAeq) are measured as 50.2 db inside, 59.7 db in the courtyard and 60.0 db in the traffic way beside south-east facade. In the courtyard measurements of mosques, the highest was obtained in the Sultan Mosque because the number of playing children was considerably higher than other mosques. While the measurements, the windows and the fans are opened.

3.2. The Survey

To address whether there is any noise problem during the worship, a survey study was designed and implemented in this study. The survey study consists of two questionnaire format. The first one is for reply by imam / muezzin and the other is replied by users'. To understand the participants' thoughts about aural comfort conditions, they were asked to respond to the questions after a prayer/ sermon. The questionnaire consists of 5 sections as personal, visual perception, interest of mosque, acoustical defects and general evaluation. The questionnaires were mostly made with male users because the prayer rituals include the male population dominantly. The number of female participants is too few for two mosques. 85% of participants in Çeşnigir Mosque and 82% of participants in İvaz Paşa Mosque are men. To record of prayers' thoughts, the participants were chosen after Friday pray/sermon in the examined mosques. The users in the examined mosques state that the Imam uses the microphone while commanding during prayer or preaching on Fridays. All of the users say that they clearly understand the Imam's speech most of time during the rituals.

The results of survey study in Çeşnigir Mosque show that 76% of users are over 40 years old. Although 31% preferred the front of the mihrab, 38% preferred the narthex on the day of the questionnaire, the 62% of users want to be front of the mihrab during the rituals. Moreover, some participants point out that the position in the mosque can vary according to the type of rituals. 54% of interviewed people say that they come too often and 31% of them used seldom. Therefore, the community of mosque consists of same users as imam says. The users stated that they came to mosque frequently five time salath and Friday prayer, then bairam prayer and mevlut. The most of people prefer this mosque due to close to their home and works. A small percentage of users prefer this mosque due to its architectural (6%) and historical features (13%) (**Fig. 9**).

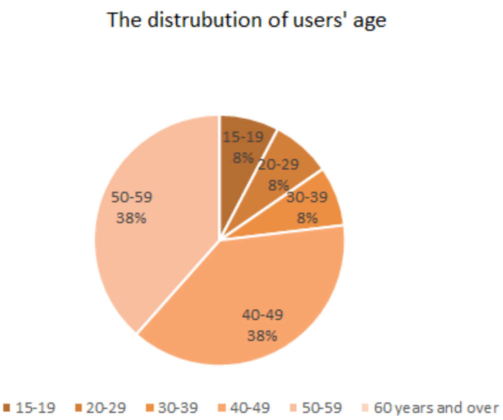

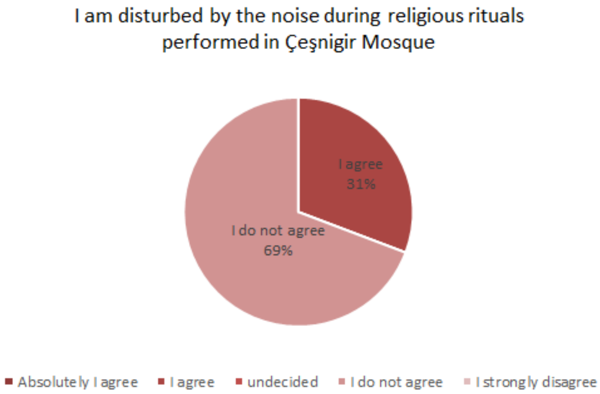

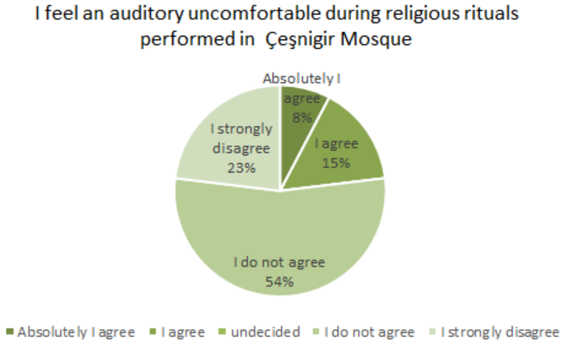

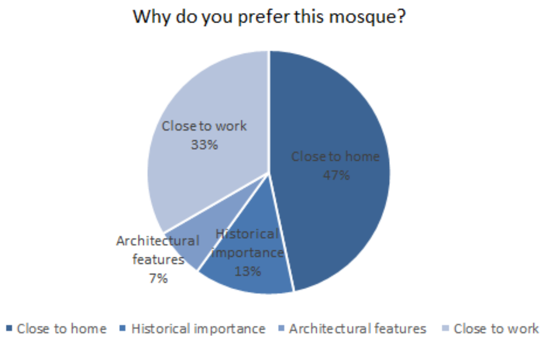

Fig. 9. The results of the surveys for Çeşnigir Mosque

54% of users don't agree and 23% strongly disagree to feel an auditory uncomfortable during religious rituals while 15% of them agree and 8% absolutely agree. 69% of people aren't disturbed by the noise during pray. The 31% of users with noise complaints state that they mostly complain about traffic and animal sounds. 77.5 of users evaluate the acoustic of mosque as good. The most of people say they are satisfied with the worship performed in the Çeşnigir Mosque.

The range of users' age in İvaz Paşa Mosque is more varied than Çeşnigir Mosque (**Fig. 10**). Although none of them are close to mihrab on the day of the questionnaire, the 73% of participants usually want to be front of the mihrab particularly during the prayer. While 45% of interviewed people say that they come seldom, 36% of them used often. Participants prefer this mosque for Friday prayers, individual worship and five time salath. The reason of 55% of participants for come to the İvaz Paşa Mosque is close to home.

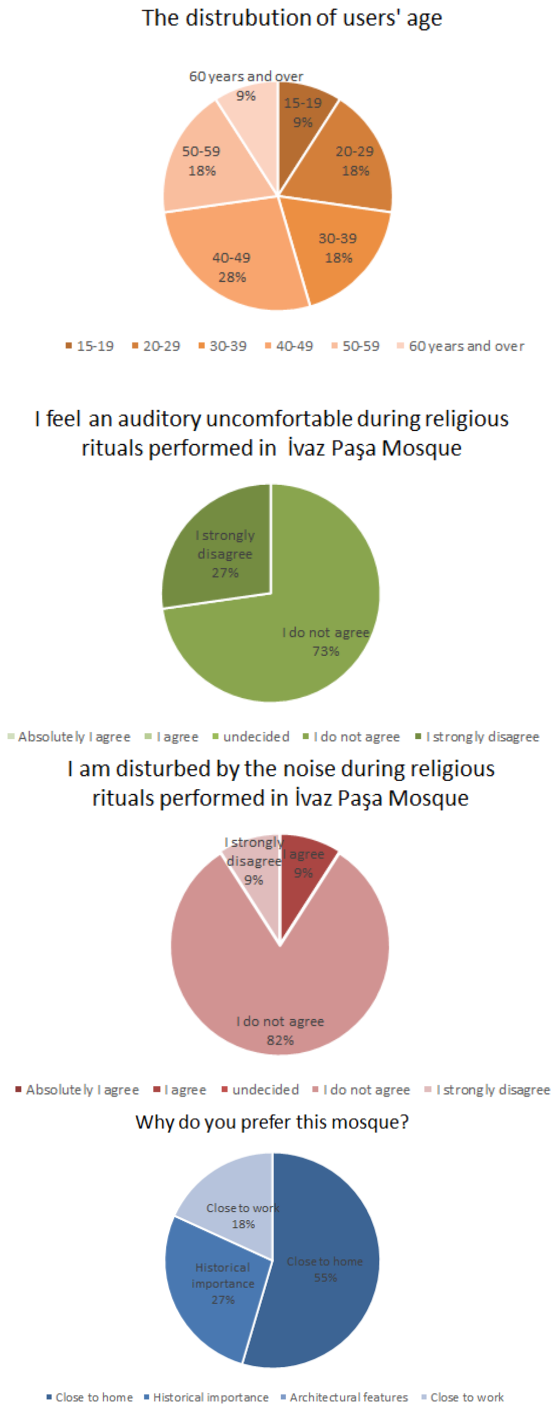

Fig. 10. The results of the surveys for İvaz Paşa Mosque

73% of users don't agree and 27% strongly disagree to feel an auditory uncomfortable during religious rituals. 91% of people don't disturb by the noise during pray. The 9% of users with noise complaints state that they mostly complain about traffic. Most of participants evaluate the acoustic of İvaz Paşa Mosque as good. The most of people say they are satisfied with the worship performed in the mosque.

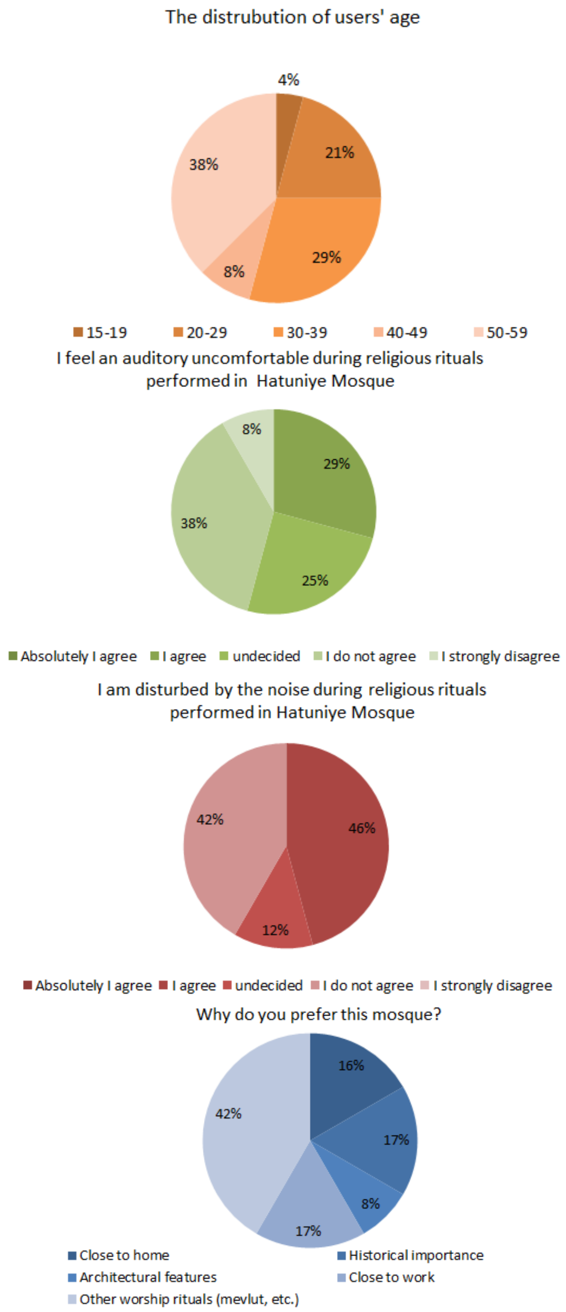

Fig.11. The results of the surveys for Hatuniye Mosque

The results of survey study in Hatuniye Mosque show that 75% of users are over 40 years old. 42% of participants are female. The most of users choose to be close to the mihrab axis due to religious causes. 42% of people state that they use this mosque seldom. The community consists of tourists, tradesmen and people who come to wedding hall so closed to Mosque. Therefore, the community of mosque consists of different users as imam says. The number of people using the mosque for the first time has a big percentage because the location of mosque is in the city center. The users stated that they came to mosque frequently five-time salath, personal prayer, Friday prayer, funeral

prayer, bairam prayer and mevlut. Most people prefer this mosque due to close to their works. A small percentage of users prefer this mosque due to its architectural features (8%).
According to the survey results, 38% of users don't agree and 8% strongly disagree to feel an auditory uncomfortable during religious rituals while 29% of them agree and 25% of users are undecided in Hatuniye Mosque. 42% of people aren't disturbed by the noise during pray. The 46% of users with noise complaints state that they mostly complain about traffic, people in the cafe houses, music and mechanical sounds. 77.5% of users evaluate the acoustic of mosque as good. The 79% of participants are satisfied with the worship performed in the Hatuniye Mosque (**Fig. 11**).
Survey study in the Sultan Mosque, where 43 percent of the participants were women, 24% is in the 20-29, 24% is in the 30-39, 9% is in 40-43, 19% is in 50-59 age range and 24% is 60 years and over. 19% of users preferred the front of the mihrab on the day of the questionnaire. Most of participants state that they want to be close to the mihrab axis during performing salath.

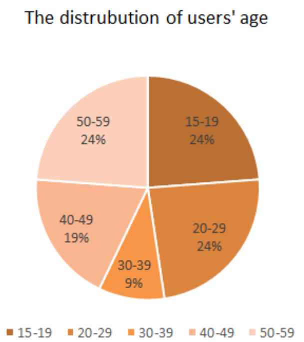

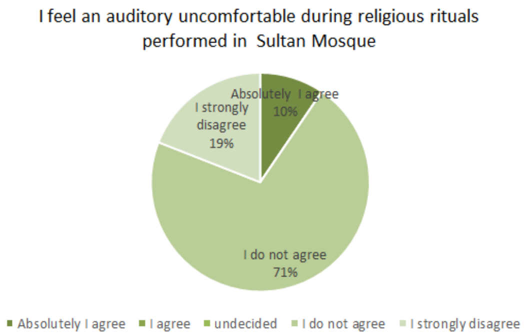

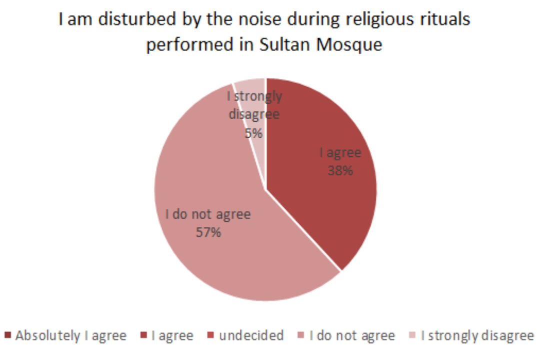

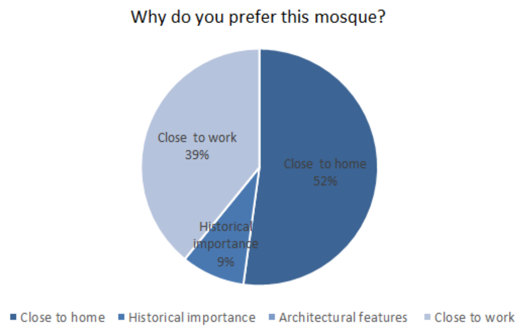

Fig. 12. The results of the surveys for Sultan Mosque

They choose whichever wall sides while the sermon or mevlut rituals. 43% of the participants are female, so they choose the women loge located east side to pray. The number of people with a big percentage used this mosque at the first time as a tourist. The Sultan (Mesir) Mosque has a privileged position due to reflect the Ottoman Classical Period architecture features. The mosque is used for worship and seen as a focus of interest because of hosting Mesir Festival which Mesir paste is scattered through the people on the mosque. For this reason, many tourists come to see the Sultan Mosque during the year. 57% of participants said that it is a historical importance as the reason for choosing this mosque.
While 71% of users don't agree and 19% strongly disagree to feel an auditory uncomfortable during religious rituals, 10% of people absolutely agree. 62% of people aren't disturbed by the noise during pray. The 38% of users with noise complaints state that they mostly complain about traffic, people, music and mechanical system. Although most of participants evaluate the acoustic of Sultan Mosque as good, 19% of participants comment as fair. Most people say they are satisfied with the worship performed in the mosque (**Fig. 12**).

4. THE EVALUATION OF OBJECTIVE AND SUBJECTIVE DATAS

When we look at the results of survey and measurements, participants' noise complaints seem to be related to the increase of sound levels measured in the mosques. For instance, the highest sound level was measured in the Hatuniye mosque and the highest percentages of the noise complaints were also obtained from this mosque. The İvaz Paşa Mosque, measured the lowest sound level inside, has the lowest percentages of the noise complaints (**Table 2**). The causes of noise generally consist of traffic, people, music, animal, mechanical system.
The courtyards of mosques, except for the Çeşnigir Mosque, are protected from the environmental noises by some factors like the garden walls and located at

different heights. Therefore, the sound level measured in the courtyard is the highest level. In other mosques, the sound levels in the courtyards are obtained at a lower level than the other points.

	LAeq (inside)	LAeq (courtyard)	LAeq (outside)	Feel an auditory uncomfortable (agreement)	Disturbed by the noise (agreement)
ÇEŞNIGIR M.	42.3 db	52.8 db	48.2 db	8% Absolutely I agree 15% I agree	31% I agree
İVAZ PAŞA M.	35.4 db	58.4 db	63.6 db	-	9% I agree
HATUNIYE M.	50.5 db	57.6 db	64.2 db	29% I agree	46% I agree
SULTAN M.	50.2 db	59.7 db	60.0 db	10% Absolutely I agree	38% I agree

Table 2. The results of measurement and survey studies

Background noise is a major contributor to improve the speech intelligibility in buildings [14]. According to the results, the indoor background noise level of 30 dB suggested for religious buildings seems to be exceeded in all the examined mosques. It can be shown that the measurements were made in the summer period as the reason for the high sound level values. Quran courses, children playing, opened windows and doors, ventilators and the location of mosques effect the sound level inside and outside. According to American National Standards, the average sound levels of land use of buildings are mentioned in terms of land use. This guideline states that land use for religious buildings can be accepted as 60 dB or less, 60-65 dB as normal, 65 - 75 dB not acceptable as normal, 75 dB and above as unacceptable [15]. The measured outside noise levels for the mosques are in the acceptable values according to this guideline. It can be said that the outdoor sound levels of four mosques are obtained at appropriate values although the traffic, pedestrian axis, shops, cafe houses near to the location of mosques. The environmental regulations and locations of historical mosques are important issues for being a guide to the next mosques projects.

5. CONCLUSION

This study intended to focus on the user satisfaction in relation to aural comfort conditions in Manisa Mosques with objective and subjective evaluations. Selected mosques are good examples to understand the differences in comfort conditions or noise levels. Because, the mosques have the similar plan schema in different locations of the city.

According to the results of the survey, no significant negativity was found about the aural comfort conditions of examined mosques. It can be explained by the design solutions and building materials used in the Ottoman Mosques. Negative effects that may arise from walls parallel to each other minimized by the elements such as niches, columns, maksoorah, mimbar opened on the wall surfaces. In addition, the pendentives used in transition to dome, the arches used in the side sections and columns contribute to distribution of sound energy properly in the volume. The dome, which is an important element of the main worship place, tends to gather the voices from the surfaces to one spot due to its concave form [16]. This can lead to sound bursts or dry / dead spots at some points in the volume, thus the homogeneous distribution of sound energy is damaged. The focal points of studied mosques are gathered out of the audience area. This is an acoustically desirable feature to prevent unwanted sound bursts, dry and dead space formation within the volume. In the survey study, the echo problem has not been addressed for mosques by the participants. The reason is that usage of carpets on the floor in mosques is an important material preventing the long reverberation time even when the volume is empty.

This study is done to support the documentation of the acoustic conditions of historical religious structures as intangible cultural heritage. The results of study show that subjective findings are connected with objective ones. These findings support the idea that the locations, the wall thickness of historical mosques, the user profile, the use of summer and winter affect the noise levels. Just having similar plan doesn't cause a resemblance to the interior background noise level. But the sound levels of mosques close to each other with the similar volume. There is a serious difference in noise levels both inside and outside despite the fact that the mosques are summer use. Design criterias such as wall thicknesses of mosques, garden walls, used building materials help to have suitable acoustic conditions inside. Therefore, it is possible to guide the future projects by taking the historical mosques as examples to provide noise control between inside and outside volume.

6. REFERENCES

[1.] L. Elicio, F. Martellotta: **Acoustics As A Cultural Heritage: The Case Of Orthodox Churches And Of The "Russian Church" İn Bari**, *Journal of Cultural Heritage*, 16 (6), 2015, 912-917.

[2.] O. Grabar: **"Symbols and Signs in Islamic Architecture", Architecture and Community: Building in the Islamic World Today**, ed. Renata Holod, Millerton, New York, 1983.

[3.] N. Ergin: **The Soundscape of Sixteenth-Century Istanbul Mosques: Architecture and Qur'an Recital**, *Journal of the Society of Architectural Historians* 67/2, 2008, 204-221.

[4.] Z. Karabiber: **A New Approachto An Ancient Subject: CAHRISMA Project,** *In Proceeding of the 7th International Congress on Sound and Vibration*, 2000, 1661-1668.

[5.] Z. Gül, M. Çalışkan, A. Tavukçuoğlu: **Geçmişten Günümüze Süleymaniye Camii Akustiği**, *Megaron*, 9(3), 2014, 201-216.

[6.] L. Topaktaş: **Acoustical Properties Of Classical Otoman Mosques Simulation And Measurements,** *PHD Thesis,* Middle East Technical University, Ankara, 2003.

[7.] A. Abdou: **Measurement of Acoustical Characteristics of Mosques in Saudi Arabia,** *The Journal of the Acoustical Society of America,* 113 (3), 2003, 1505-1517.

[8.] P.O. Carvalho, C.T. Freitas: **Acoustical Characterization of the Central Mosque of Lisbon,** Forum Acusticum, Aalborg, Denmark, 2011.

[9.] A.P.O. Carvalho, C.G. Monterio: **Comparison of the Acoustics of Mosques and Catholic Churches,** *The Sixteenth International Congress on Sound and Vibration*, Krakow, 5-9 July 2009.

[10.] H. Acun: **Manisa'da Türk Devri Yapıları,** Türk Tarih Kurumu Yayınları, Ankara, 1999.

[11.] L.L. Beranek: **Balanced noise criterion (NCB) curves**, *The Journal of the Acoustical Society of America,* 86 (2), 1989, 650-664.

[12.] V.O. Knudsen, C.M. Harris: **Acoustical Designing in Architecture**, John Wiley & Sons, America, New York, 1967.

[13.] F. Yelkenci Sert, H. İ. Alpaslan, Ö. Yılmaz Karaman: **Manisa Sultan (Mesir) Camisi'nin Akustik Özelliklerinin Değerlendirilmesi**, *Journal of Art History*, XXVI, October 2017, 243-259.

[14.] M. Mehta, J. Johnson, J. Rocafort: **Architectural acoustics principles and design,** New Jersey: Prentice-Hall, Inc., 1999.

[15.] S. Y. Demirkale: **Çevre ve Yapı Akustiği,** Birsen Yayınevi, İstanbul.

[16.] W. A. Orfali: **Sound parameters in mosques,** Proceedings of Meetings on Acoustics, Acoustical Society of America, 2007.

8th Congress of the Alps Adria Acoustics Association
Zagreb, Croatia
20 – 21 September 2018

Hrvatsko akustičko društvo
HAD
Acoustical Society of Croatia

COUPLING OF SOUND SPACES BY THE SURFACE IMPEDANCE APPROACH

Goran Pavić[1], Liangfen Du[2]

[1]Vibration-Acoustics Lab, National Institute of Applied Science, Lyon, France (goran.pavic@insa-lyon.fr),
[2]Department of Building, National University of Singapore, Singapore (dul060759@gmail.com)

Abstract: *The surface impedance approach is used to model acoustical properties of multi-connected sound spaces. This approach is particularly advantageous where a mathematical model of each individual space is available. Alternatively the properties of some or all of the spaces can be carried out by measurement while the coupling between them is obtained by subsequent computation.*
Two dissimilar surface impedance techniques are outlined: the patch technique and the surface harmonics technique. The advantages and disadvantages of the two techniques are discussed. Modelling examples of multi-connected rooms are shown which demonstrate the potential of the approach.

Key words: Acoustical impedance, sound transmission, acoustical coupling, room acoustics.

1. INTRODUCTION

Modelling of sound field in a closed space is an essential subject in various engineering applications, such as building, machinery and structural design. The simplest way to describe sound in a cavity is to attribute to it a single value of sound level. This can be done by means of statistical approximations, e.g. by Sabine-Franklin-Jaeger theory [1]. In such a case the value of sound pressure is obtained by averaging across the space and frequency. A simple formula provides the expected reverberation time T_{60} as a function of cavity volume V, surface S and mean absorption coefficient α, $T_{60} = 0.16V/S\alpha$. An alternative way of estimating the reverberation time is by Norris-Eyring approach which provides an expression equivalent to Sabine formula by replacing α with $\ln(\alpha\text{-}1)$. Once the reverberation time is known the average pressure level in a cavity can be then estimated from the frequency-averaged sound power level emitted in the cavity.
The statistical approach works well if the sound field is diffuse enough. The latter condition applies to spaces of large volume and low absorption which yield the sound field diffuse providing the frequency is high enough. The validity of this condition can be checked via the so called Schröder frequency, [2], which separates the low and high frequency regions by a transition zone.
In cases where more detailed modelling is required the statistical approach should be replaced by a numerical field discretization technique, such as FEM or BEM, or alternatively by some ray-tracing approach. In such a case the limitation to diffuse sound field is removed. In spite of advantages of numerical techniques regarding the cavity shape, some key acoustical problems remain delicate, e.g. sound modelling in open cavities. As a rule the acoustical coupling of connected spaces is a subject of growing importance in view of numerous applications which concern both the modelling and measurements.
In this paper an engineering approach based on surface coupling between acoustic spaces will be investigated. The approach focuses on the modelling of acoustical cavities composed of several sub-cavities of simple shape. For the sake of simplicity the coupled cavities of paralelepipedic shape will be considered as these can be modelled by analytical means. This restriction however does not limit the applicability of the approach to cavities other than paralelepipedic ones.

2. THE COUPLING PROCEDURE

Suppose that means are available for either computation or measurement of sound fields in several acoustical spaces taken separately. The question arises: how will the sound field be modified in these spaces are coupled to each other.
Statistical laws of room acoustics yield a simple answer to this question: the assembled space will be considered as a single space such that the basic space characteristics i.e. the volumes, surfaces, absorption areas etc, add up algebraically. If several sound sources run simultaneously the algebraic summation of their sound powers applies too providing the sources are uncorrelated.
This picure changes radically if the sound fields are not diffuse, as will be the case in low-frequency small-volume conditions. Another approach will then be needed.

Inn the present paper an approach will be outlined where the coupling between different acoustical spaces is done in a fairly detailed and rigorous manner. The medium is assumed to be linear and motionless. The analysis will be done in frequency domain. This allows the use of complex amplitudes and the suppression of time-dependent terms. The acoustical quantities will be indicated by lowercase symbols for instantaneous values and by uppercase symbols for complex amplitudes. Vectors and matrices will be denoted by bold characters.

2.1. The coupling continuity conditions: 1D case

The principles of acoustical coupling can be illustrated with no loss of generality using two spaces coupled via a single surface. To start with, suppose that in both spaces only plane waves exist, normal to the interface surface which itself is plane, Fig. 1. Two specific field variables will be used relative to each of the spaces:

- *Blocked sound pressure* at the interface; this is the sound pressure across the interface, created by the sound source(s) internal to the space, when the interface is made motionless (rigid).
- *Surface acoustical impedance* at the interface; the ratio of sound pressure at the interface and the normal particle velocity applied to it with the internal sources switched off.

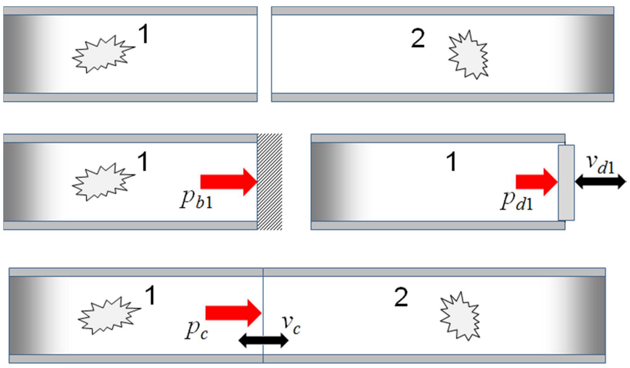

Fig.1. Coupling of two simple acoustical spaces. Top: decoupled spaces; middle: blocked pressure (left) and impedance (right); bottom: coupled spaces.

The interface impedance of the space 1 is: $Z_1 = P_{d1}/V_{d1}$ where V_{d1} is the amplitude of interface driving velocity while P_{d1} is the resulting interface sound pressure with the source 1 turned off. Analogous definition applies to the impedance of the space 2. The superposition applies owing to linearity; the pressure and velocity continuity at the interface yields a simple expression for the coupled velocity amplitude at the interface:

$$V_c = \frac{P_{b1} - P_{b2}}{Z_1 + Z_2} \tag{1}$$

Once the interface coupling velocity has been found, each of the two spaces can be considered independent; the resultant sound field will be then a superposition of two fields: one created by the operating source with the interface blocked, the other created by the motion of the interface with velocity v_c, the source turned off.

It can be seen that the impedances of the two spaces add to each other while the respective blocked pressures are subtracted from each other. If the blocked pressures in the two spaces were identical, the coupling would have produced no effect to the sound fields.

2.2. Computation of coupling in a general case

The preceding simple example just outlines the coupling principle. In a general case of two coupled spaces both the sound pressure and the particle velocity are unevenly distributed across the interface. The question is how to define the surface impedance in such conditions.

Two techniques will be described which can handle the spatially varying acoustical quantities in a purposeful way enabling the definition of surface impedance.

One of the techniques is the patch impedance, as used in [3]. The concept of dividing a surface into patches and of assigning to each patch a single value of sound pressure and particle velocity originates from [4]. This technique represents an approximation of continuous functions of space by discrete values. It is clear that by reducing the wavelength the required patch size should reduce too in order to make the interface sound field be represented with a sufficient accuracy.

The other technique uses continuous surface functions to express the sound pressure and particle velocity. Each of these two quantities is approximated by a finite number of some elementary continuous functions. Each of these functions is completely defined by one discrete value: its magnitude. The principle of the method was described in [5] where the objective was the characterization of an arbitrary sound source using a particular interface: a sphere. Application of the same principle to rectangular interface surfaces, considered to be more useful in practice, was done in [6-7].

Using either of the two representations of the surface impedance, the patch one and the continuous one, the pressure and the velocity across the interface surface become fully defined by a N-size vectors the elements of which are the patch-averaged amplitudes or the surface function magnitudes depending on the technique used. Consequently the surface impedances become $N\times N$-size matrices. The m-n^{th} element of an impedance matrix thus is the ratio between the m^{th} component of pressure vector and the n^{th} component of driving velocity vector. Eq. (1) stays valid once converted to a matrix form:

$$\mathbf{V}_c = (\mathbf{Z}_1 + \mathbf{Z}_2)^{-1}(\mathbf{P}_{b1} - \mathbf{P}_{b2}) \tag{2}$$

3. DEMONSTRATION

A simple example will be considered first with the aim of demonstrating the validity of the coupling approach. The entire acoustical space, a paralelepipedic room, will be divided into two unequal sections, Fig. 2, each of which will be modelled independently. Once the four quantities appearing in Eq. (2) are found, the coupled particle velocity at the interface of the two sections will be computed and the sound pressure in the two coupled sections will be worked out. The results will be compared to the values of sound pressure obtained by considering the entire space as a single room.
The use of paralelepipedic shapes of all the concerned spaces enabled analytical modelling of all the quantities involved.

3.1 The acoustical spaces

In the example shown the interface surface parallel to y-z plane was placed at 39% from the origin in x-direction of the room length. Seven monopole sources were placed in the room, and five response points were defined, both at positions selected at random. The interface divided the room in such a way that three sources and two response points were located in the first section (section 1), while the remaining four sources and two reponse points were in the section 2. The analysis was done in the frequency range 20-500 Hz with 1 Hz step. The complex amplitudes of volume velocities of all the sources were also selected by random number generator; the same amplitudes were used for the entire frequency range.

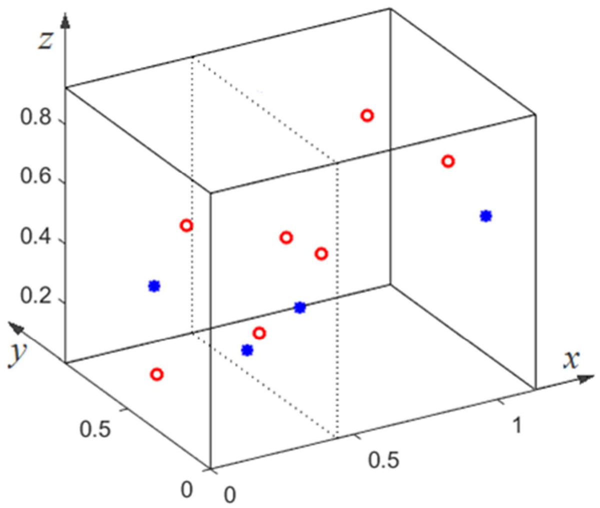

Fig.2. Model of acoustical space. Circles: source positions; dots: response positions.

3.2. The cavity response

The cavity pressure response to monopole excitation can be represented in terms of eigenfunctions Φ, [1]:

$$P(\mathbf{r}) = Q(\mathbf{r}_e)\sum_n \Phi_n(\mathbf{r},\mathbf{r}_e,\omega), \quad n = 1,2... \tag{3}$$

Here P - response pressure amplitude, Q – excitation volume velocity amplitude, r - response point, r_e - excitation point, ω - radian frequency. The functions Φ are given by the mode expansion rule:

$$\Phi_n(\mathbf{r},\mathbf{r}_e,\omega) = \mathrm{j}\frac{\omega\rho_0 c^2}{V}\frac{\varphi_n(\mathbf{r})\varphi_n(\mathbf{r}_e)}{\omega_n^2 - \omega^2 + 2\mathrm{j}\varepsilon\omega} \tag{4}$$

where ρ_0 – mean mass density of fluid, c – sound speed, V - volume, ε - damping coefficient and j – imaginary unit. The spatial functions φ_n and the values ω_n are the natural modes and natural frequency of the given space respectively.
The particle velocity vector $\mathbf{v}$ can be obtained from the 2nd Newton's law applied to an elementary fluid volume:

$$\frac{\partial \mathbf{v}}{\partial t} = -\frac{1}{\rho_0}\nabla p \tag{5}$$

The natural modes and frequencies of a paralelepipedic space of hard walls, the size of which is $a\times b\times h$, read, [1]:

$$\omega_n = \frac{\pi}{c}\sqrt{\left(\frac{m_x}{a}\right)^2 + \left(\frac{m_y}{b}\right)^2 + \left(\frac{m_z}{h}\right)^2} \tag{6}$$

$$\varphi_n = \zeta\cos(\frac{m_x\pi x}{a})\cos(\frac{m_y\pi y}{b})\cos(\frac{m_z\pi z}{h})$$

$$\zeta = \sqrt{2^s}, \quad s = \mathrm{sgn}(m_x) + \mathrm{sgn}(m_y) + \mathrm{sgn}(m_z)$$

$$m_x(n),\, m_y(n),\, m_z(n) = 0, 1, 2...$$

The modal summation (3) should theoretically extend to infinity but in practice the truncation is applied to terms having the natural frequencies well above the excitation frequency. This condition sets an upper limit to the natural frequency $\omega_n = \omega_{max}$. The three integers m are chosen in such a way that all the combinations of these integers giving $\omega_n \le \omega_{max}$ get covered.
Eqs. (3-5) provide the basis by means of which can be carried out all the computations needed to obtain the response of the main cavity as well as the impedances and blocked pressures of its parts, as required by Eq. (2). The elements of such computations will be skipped here for the sake of brevity; the details can be found in refs [3] and [6-7].

3.3. Coupling by patches

The interface surface of 0.877m×0.923m size was divided into 9×10 patches. This division was chosen to make the patch length fit roughly the 1/7 the shortest wavelength of 68.6 cm. The 90×1 vectors of blocked pressure, P_{b1} and P_{b2}, and the 90×90 impedance matrices Z_1 and Z_2 of the two sections were computed per each frequency point. The averaging across the patches was carried out by analytical integration as previously shown in [3]. The resulting patch-averaged surface velocities were thus obtained from Eq. (2).

Fig. 3 shows the sound pressure levels at two points in the room obtained by direct computation, considered as a reference, and then by the coupling procedure. The two plots refer to two different response points, one in the space in front of the coupling surface, the other in the space behind it. The peak values, occurring at natural frequencies, are indicated by dots for improved visibility.

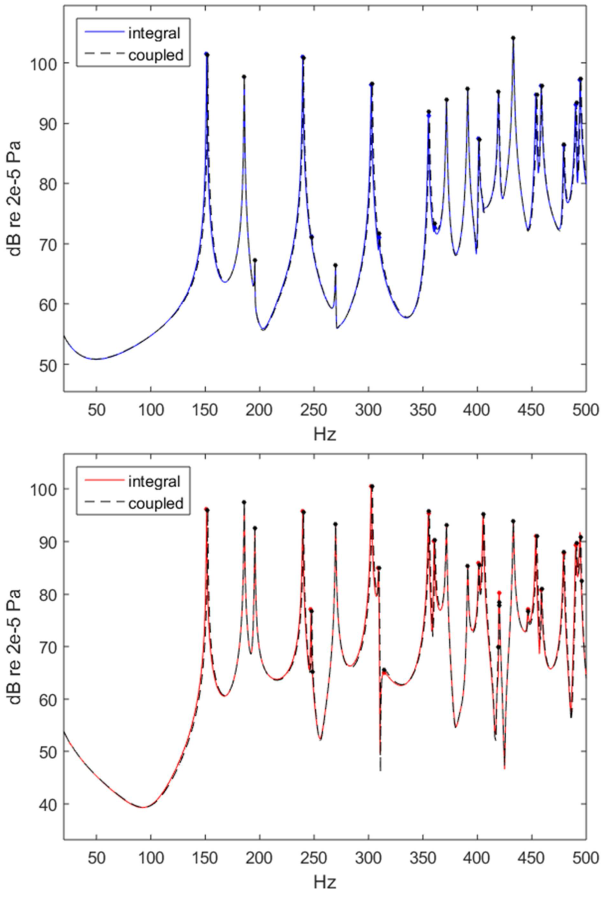

Fig. 3. Sound pressure level in the room. Top: point in space 1; bottom: point in space 2.

One can see that the results obtained by coupling match very well the reference ones throughout the frequency region concerned. The results obtained at other points show the same degree of matching. Shown for the sake of brevity are only the absolute values of sound pressure; the phase matching was found to be very good too.

There exists however a particular type of mismatch not easily discernible due to high modal density: the slight frequency shift between the peaks. The shift can be seen on Fig. 4 where the close-up was made of pressure levels within a narrow frequency band around the 4th natural frequency of 239.7 Hz. The shifts are not large, less than 1 Hz, and may be disregarded in most of practical cases, especially where band averaging is involved. The shifts result from the discretization of velocity and pressure patterns. This is equivalent to coupling the two spaces by weightless finite pistons which produces change in the original boundary conditions between these spaces.

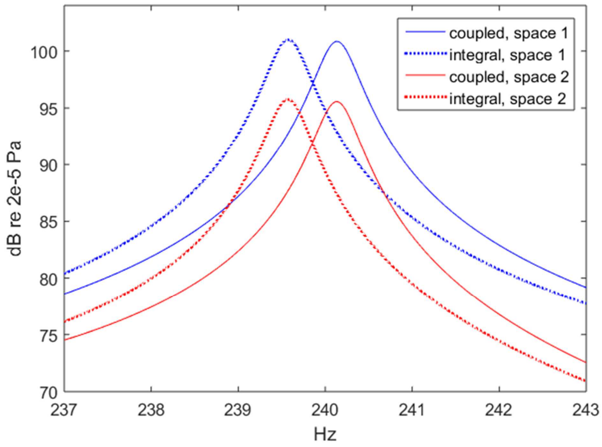

Fig. 4. Close up at the frequency shift effect.

It thus follows that the coupling of acoustical spaces by the discrete patch technique can produce good results but the frequency shift is inherent to this technique.

3.4 Coupling by surface functions

As the interface surface is in the present case a rectangle, the obvious way to represent the acoustical field across it is to use double trigonometric functions. In such a case the complex amplitudes of either the sound pressure p or the particle velocity v can be represented as:

$$P(y,z) = \sum_i \Gamma_i \phi_i, \quad V(y,z) = \sum_i \Xi_i \phi_i \tag{7}$$

The functions ϕ are the Laplacian eigenfunctions of a rectangular surface. These functions will be named here the "surface harmonics":

$$\phi_i(y,z) = q_y\left(\frac{m(i)\pi y}{b}\right) q_z\left(\frac{n(i)\pi z}{h}\right), \tag{8}$$
$$m \in \{m_1, \cdots M\}, \quad n \in \{n_1, \cdots N\}$$

The functions q are sine and cosine, corresponding to Dirichlet and Neumann boundary conditions. In a general case all of 4 combinations, i.e. cos-cos, cos-sin, sin-cos and sin-sin appear in the sum of Eq. (7).

Wile theoretically an infinite sum over i would be needed to exactly reproduce the field, for practical purposes a truncation will be made to M and N limiting values of the integers m and n as shown in Eq. (8). Since sine indices start from 1 and cosine indices from 0 the sum of Eq. (7) will have $H = (2M+1)(2N+1)$ harmonics.

In what follows the final results of computation will be shown; more details about the harmonics approach can be found in [6-7]. In the computation M=7 and N=8 top orders were used, resulting thus in 255 harmonics.

Fig. 5, top shows the sound pressure levels in all 4 points of the cavity obtained by computing the integral field. The continuous representation of sound field across the interface surface does not create frequency shift as does the discrete one. The matching of these results with the results obtained by the coupling techniqe is so close that the difference between the two becomes indiscernible on the same plot. Instead the level difference is shown on the bottom plot.

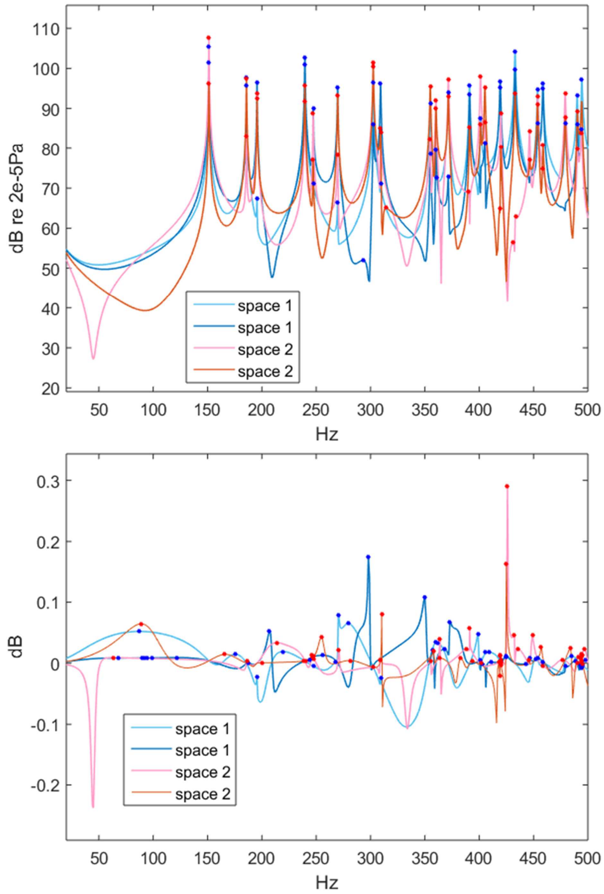

Fig. 5. Top: pressure spectra at 4 response points; bottom: level difference between results obtained by coupling technique and reference results; 255 harmonics.

It can be seen that the typical values of mismatch are of the order of 0.5 dB or lower. Even the extreme mismatch values are well under 1 dB. Equally good matching is obtained for the phase of sound pressure. The method of surface harmonics is thus seen to work extremely well.

Fig. 6 shows the level mismatch in the case where only 49 harmonics were used, $M = N = 3$. As expected, the matching is less good in comparison with the previous case, but it stays still remarkable.

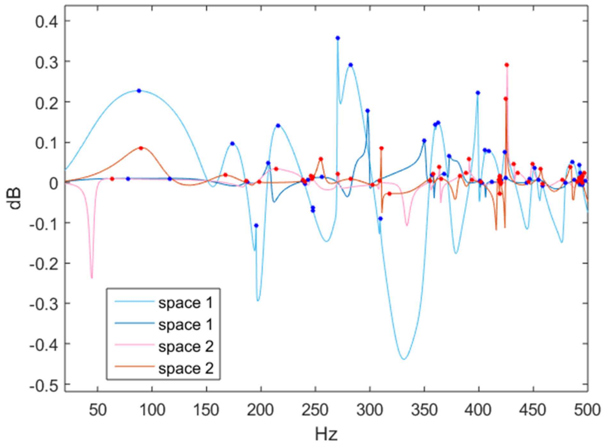

Fig. 6. Top: pressure spectra at 4 response points; bottom: level difference between results obtained by coupling technique and reference results; 255 harmonics.

4. CASE STUDY: CONNECTED ROOMS

Three rooms of 60m^3 total volume are shown on Fig. 7. A monopole source of uniform spectral density is placed in Room 1 at a position offset from the center. The sound pressure is computed in Rooms 2 and 3 across two surfaces indicated by dotted lines. The two 2m×1m doors act as interface surfaces between the rooms. Like in §3 the computation is done twice, once by modelling the entire acoustical space and subsequently by modelling each room separately and then by applying the interface coupling conditions. The method of surface harmonics is used to enable the inter-room coupling.

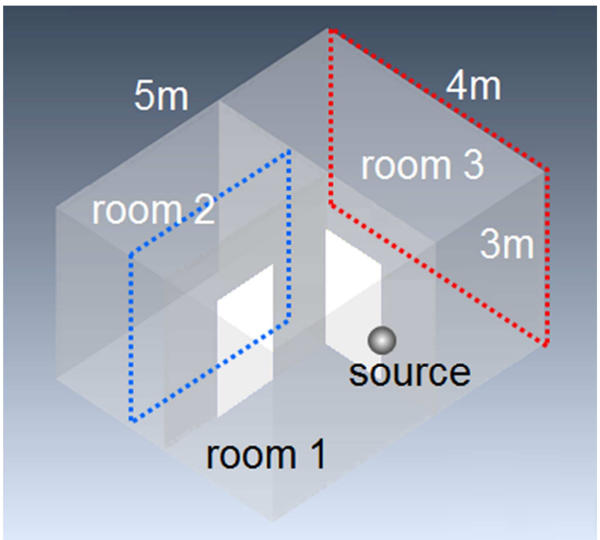

Fig. 7. Multi-connected acoustical space.

As the validation of the results obtained by coupling could not be done in this case by analytical computation, the entire modelling was done by Actran software. Two different sets of harmonics per coupling surface were applied: H = 15 (M = 2, N = 1) and H = 45 (M = 4, N = 2). The first of these two cases, H = 15, was used to test the relevance of the method in quite extreme conditions of spatial resolution.
Fig. 8 compares the results obtained by surface coupling with the reference ones obtained by direct computation of the entire space. In view of much higher modal density than in the demonstration case the pressure level is now shown in 1/3 octave bands. The matching with the reference values is quite good; as expected the accuracy of results drops with the number of harmonics.

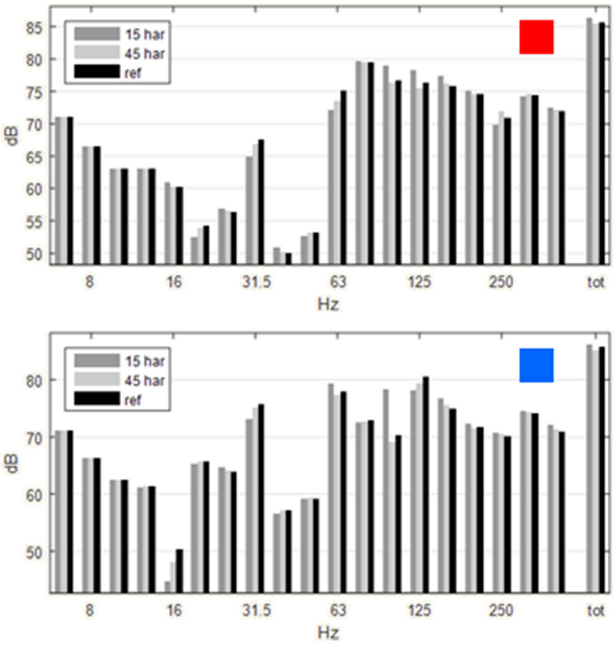

Fig. 8. The space-averaged sound pressure level in 1/3 octave bands. Top: Room 3; bottom: Room 2.

Table 1 lists the global RMS values in mPa of the sound pressure across the response surface of the Room 3 at three characteristic frequencies: resonance at 194 Hz, anti-resonance at 230 Hz and an intermediary frequence of 344 Hz. One can notice that the accuracy reduces with frequency increasing, as expected.

	194 Hz	230 Hz	344 Hz
15 har.	66.0	35.7	47.5
45 har.	65.5	34.8	41.0
reference	65.6	34.7	39.2

Table 1. Global RMS values of sound pressure in mPa

Fig. 9 shows the instantaneous sound pressure maps across the same surface at the three frequencies. Zero is in white while red and blue denote positive and negative sound pressure values. The scaling is adapted to each frequency but it stays the same for the three results (15 harmonics, 45 harmonics and reference). These results clearly indicate that the results are coherent not only in global values but in details too.

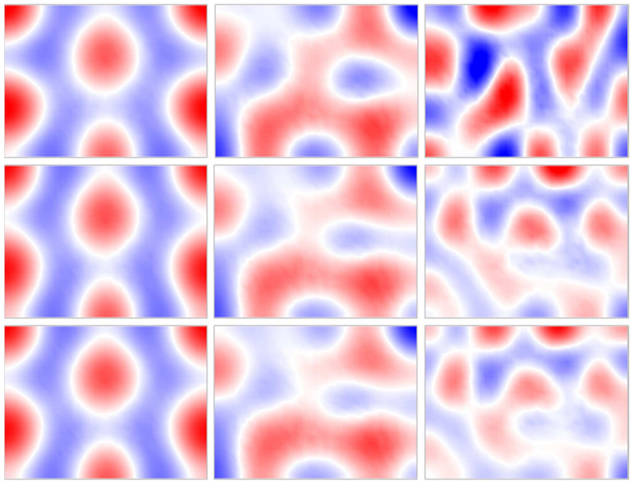

Fig. 9. Instantaneous sound pressure across the response surface in Room 3. Left: resonance, 194 Hz; centre: anti-resonance, 230 Hz; right: intermediary, 344 Hz. Top: 15 harmonics; middle: 45 harmonics; bottom: reference.

5. CONCLUSIONS

Using a simple demonstrator example followed by a case study it is shown how can acoustical spaces be connected by computation. A particular way of coupling the spaces consists of computing the impedance and the blocked sound pressure across the interface surface of each individual space. Out of these quantities the coupled particle velocity can be worked out across each interface. This velocity is then applied as the external excitation of each space taken on its own and the sound pressure gets thus accessible throughout the entire system.
Two coupling techniques are applied, the patch and the surface harmonic technique. While both are shown to produce acceptable results, the patch technique creates a small frequency shift at resonant frequencies. The surface harmonic technique thus seems to provide a powerful coupling tool in the prediction of sound levels of connected acoustical spaces.

6. REFERENCES

[1] A.D. Pierce: **Acoustics: an Introduction to its Physical Principles and Applications**, McGraw-Hill, New York, 1981.
[2] M.R. Schroeder, K.H. Kuttruff: **On Frequency Response Curves in Rooms. Comparison of Experimental, Theoretical, and Monte Carlo Results for the Average Frequency Spacing between**

Maxima, Journal of the Acoust. Soc. of America 34 (1), 1962, 76–80.

[3] G. Pavić, **Air-borne sound source characterization by patch impedance coupling approach**, Journal of Sound and Vib. 329, 2010, 4907-4921.

[4] M. Ouisse, L. Maxit, C. Cacciolati, J.-L. Guyader: **Patch Transfer Functions as a Tool to Couple Linear Acoustic Problems**, Journal of Vib. and Acoust. 127 (5), 2005, 458-466. 13.

[5] Yu.I. Bobrovnitskii, G. Pavić: **Modelling and Characterization of Airborne Noise Sources**, Journal of Sound and Vib., 261 (3) , 2003, 527-555.

[6] G. Pavić. **Air-borne sound characterisation by plane surface harmonics**. Proc. Internoise 2012, New York, August 19-22, 2012, 1493-1500.

[7] L. Du: **Characterisation of Air-borne Sound Sources using Surface Coupling Techniques**, PhD Thesis, Univ. of Lyon, 2016.

8th Congress of the Alps Adria Acoustics Association
Zagreb, Croatia
20 – 21 September 2018

NARROW BAND REVERBERATION TIME

Luka Čurović, Jure Murovec, Tadej Novaković and Jurij Prezelj

University of Ljubljana, Faculty of Mechanical Engineering, Aškerčeva 6, 1000 Ljubljana, Slovenia: luka.curovic@fs.uni-lj.si

Abstract: *A signal processing algorithm for reverberation time determination in narrow band spectral resolution is proposed based on short Fourier transform on overlapping blocks of the signal. The choice of the calculation parameters is based on study of their influence on the value of reverberation time. Narrow band reverberation time is evaluated against the conventional broadband analysis for both impulse response and interrupted noise methods. The algorithm can improve the results of the classical methods in the low frequency range in non-diffuse sound felds. The proposed algorithm can be applied in standard measuring equipment. No additional measurements have to be performed.*

Key words: reverberation time, narrow band

1. INTRODUCTION

The reverberation time (RT) [1] has numerous applications in acoustics. Due to the increasing presence of low frequency sound sources conventional room acoustic measurements should be performed in the extended frequency range below 100 Hz. Several authors have investigated and analysed the results of the RT measurement protocols [2, 3, 4, 5]. All authors concluded that the dispersion of RT measurementss is large, especially in the low frequency region below 250 Hz. Hopkins et al. [5] proposed that the measurements should be performed in the 63 Hz octave band, while others [6, 7] have investigated the use of impulsive sound sources to increase signal to noise ratio in the lowest frequency bands. The latest articles introduce the concept of modal RT [8]. The proposed procedure requires additional measurements as frequency response of the room has to be measured beforehand. Economou et al. [9] and Schultz [10] point out that the RT is not a continuous parameter and cannot be adequately presented in 1/1 or 1/3 octave spectrum. To improve the accuracy of the measurements one must be able to analyze the room response in high time and frequency resolution. None of the studies so far analyzed the measurements of RT in narrow band frequency resolution.

While high temporal resolution can be achieved with the increase of the sampling frequency, high frequency resolution is achieved with long sampling time. The inverse relationship between time and frequency resolution can be optimized with the use of overlapping time windows and short time Fourier transform. For this purpose, a signal processing algorithm, based on short Fourier transform and overlapping time windows was developed.

Section 2 presents the theoretical background of the RT measurements. A new algorithm based on digital signal processing is considered in section 3. In section 4, the experimental procedure and the results are presented. The analysis is presented in chapter 5.

2. THEORETICAL BACKGROUND

2.1. The decay of sound

The decay of sound can be studied in two ways [11]. At low frequencies the wave equation should be solved and acoustics should be studied in terms of modes and modal frequencies. At mid and high frequencies statistical models are used and the sound field is considered to be diffuse. The limiting frequency between the two regions is known as the Schroeder frequency. The modal approach assumes that each mode maintains its shape during the decay process. The sound energy in each mode decreases exponentially [11]. All modes are important. Axial (1D) modes die out at slightly slower rate than tangential (2D) and oblique (3D) modes. As a result of the different decay rates logarithmic decay functions recorded in rectangular rooms tend to be curved at low frequencies when the decay is studied in $1/n$ octave bands. In case of stationary diffuse sound fields (e.g. above Schroeder frequency) the decay is described by the Sabine's equation, oblique (3D) modes dominate, and the logarithmic decay curves tend to be linear.

2.2. Reverberation time measurements

Evaluation of RT is divided into two phases. In the first phase operator has to set up the measuring equipment including sound source and the receiving microphone by following a certain procedure (e.g. ISO 3382 [1]). In the second phase the recorded signal is further processed and RT is calculated. The signal processing is dependent on whether interrupted noise method (IN) or integrated impulse response (IIR) method was used. The partial or filtered signals are smoothed by the use of averaging, Hilbert transform and Schroeder integration and the decay curves (sound pressure level (L) vs. time) are obtained. If the curves are non-linear this may indicate a mixture of modes with different RTs and thus the result may be unreliable [1]. Correlation coeffcient of the regression model (r) can be used to evaluate the degree of non-linearity.

2.3. Short Fourier transform in the reverberation time measurements

The main use of the Fourier transform is to estimate the frequency power spectrum. The estimation is dependent on sampling frequency, signal length, use of windowing functions, averaging, octave smoothing etc. By consecutively applying the Fourier transform and appropriate windows on overlapping blocks of signal one can study time frequency characteristics of signal. Time frequency analysis can be implemented as the cumulative spectral decay (CSD) or as the short-time Fourier (SFT) transform. SFT is a function of frequency and time.

$$STF\big(x(t)\big) = X(t,\omega) = \int_{-\infty}^{\infty} x(t')w(t'-t)e^{-i\omega t}\,\mathrm{d}t' \tag{1}$$

where $w(t)$ is the window function (e.g. Hanning window), $X(t,\omega)$ is the Fourier Transform of $(t')w(t'-t)$. The result of SFT on overlapping block of samples is a matrix which records spectrum for each point in time and frequency. SFT is often used to detect occurrences of modes and resonances as well as recognition of peak energy patterns. The frequency resolution (Δf) of SFT is dependant on the size of the FFT block ($NWIN$) and the sampling frequency (f_S) as $\Delta f = f_S/NWIN$. One wants to choose large FFT block in order to get high frequency resolution. Large FFT block step size can not detect short transient events. One way to solve this is to use short step in time or large overlap.

3. METHOD

The RT is traditionally analyzed in $1/n$ octave bands. An algorithm written in python programming language was developed as a system for narrow band analysis of RT is currently not available.

3.1. The algorithm

In the first step SFT Eq. (1) is applied to the signal to calculate the frequency time matrix by using the following parameters: the sampling frequency (f_S), the size the FFT block ($NWIN$), the window function (e.g. boxcar) and the overlap (which determines the time step). The result of the SFT is a power spectrum density vs. time matrix. In the next step the energy level vs. time curves are averaged using the integration time constant (τ). If IIR method is used, backward integration [12] is performed as well. The steady state sound pressure level (L_0) and the background sound pressure level (L_b) are calculated. The part of the curve where sound pressure levels (L) are in the $L_0 - L_\mathrm{init}\,dB > L > L_\mathrm{b} + L_\mathrm{end}$ range, are used to calculate the RTs. The correlation coeffcient (r) associated with the fitted line is calculated, and only curves with r values higher than 0.99 are accepted. The calculation workflow for both IIR and IN methods is presented in Figure 1.

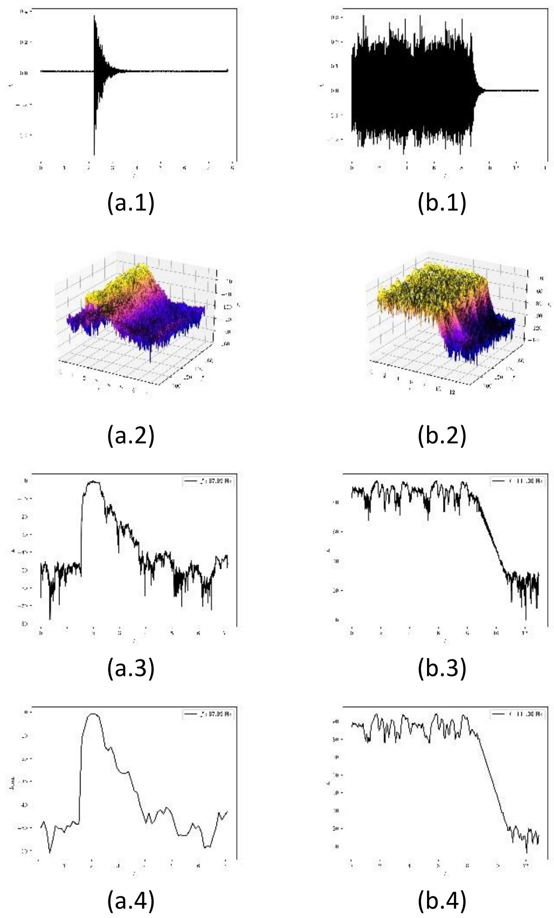

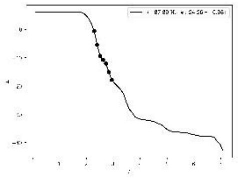

(a.5)

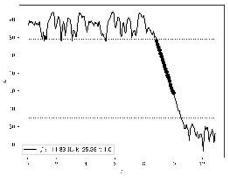

(b.5)

Fig.1. The figures show how decay curve is obtained using the narrow band method for the impulse response (a) and interrupted noise signals (b).

3.2. Choice of calculation parameters

The influence of the algorithm parameters on the calculation of RT was studied. One interrupted noise signal and one impulse response were recorded and analyzed. Both interrupted noise and impulse response algorithms were studied with 5 FFT block lengths ($NWIN$) between 4096 and 131072 samples. The effect of FFT block length on the resulting decay curves is shown in Figure 2. If long FFT block is used, the transient signal is not accurately followed. As shown on Figure 2 long FFT window distorts the original impulse and introduces lag (slow decay in the first part of the decay curve). This is not the case with the interrupted noise method. Due to high frequency noise one should also choose the length of the FFT window based on the frequency of interest. Low frequencies should be analyzed with longer FFT windows while high frequencies can be analyzed with shorter windows.

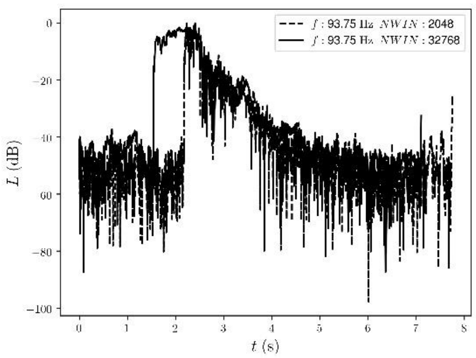

(a)

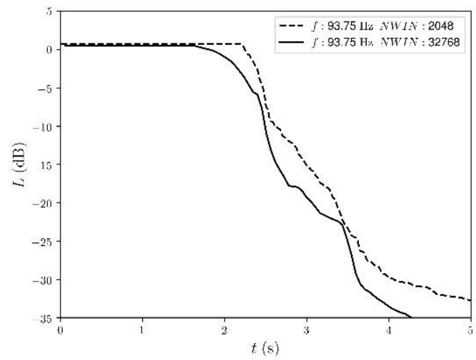

(b)

Fig.2. When long FFT block size is used, the impulse response signal is not accurately followed (a). The decay curve (b) is decaying slowly in the first part.

The influence of overlap on decay curves of the impulse signal was analyzed with the following parameters: $NWIN$ = 32768, τ = 0.1 s, L_{init} = 7 dB, L_{end} = 5 dB, while the value of overlap changed from 92% to 99.5%. The interrupted noise signal was analyzed with the following parameters: $NWIN$ = 65536, τ = 0.1 s, L_{init} = 5 dB, L_{end} = 5 dB. The influence of the overlap on the shape of the decay curves for both methods was not significant.

The choice of a part of a decay curve to be used for the evaluation of RT is especially important when impulse response is analyzed. The start of the curve is marked by the $L_0 - L_{\text{init}}$ level. In case of IIR method, higher r values are achieved when L_{init} is less than standard value of 5 dB, due to the lag in the signal. With the IN method the standard value of 5 dB can be used.

RMS averaging is used to smooth the decay curve and to remove high frequency noise. The appropriate integration constant τ has to be chosen. If the value of τ is too high the decaying process will not be accurately followed. If the value of τ is too small the averaging does not have the desired effect and high frequency noise is not removed. In our experiments the value τ = 0.1 s was chosen for the both methods.

4. EXPERIMENT AND RESULTS

Two measurements were performed to evaluate the performance of high resolution RT algorithm and to compare the results with the methods described in ISO 3382 [1].

4.1. Impulse response method

In the first experiment 10 impulse responses, downloaded from the isophonics [13] repository, were analyzed. The collection of room impulse responses was measured in a classroom at the Mile End campus of Queen Mary, University 130 of London in 2008. The measurements were created using the sine sweep technique with a Genelec 8250A loudspeaker and, an omnidirectional microphone DPA 4006. The RTs according to ISO 3382 [1] in 1/1 octave frequency bands were determined. The RTs were also calculated in the narrow band frequency resolution. The value of $NWIN$ = 32768 was used for frequencies below 177 Hz. The value of $NWIN$= 8192 was used for frequencies in the 177 Hz to 707 Hz range. The value of $NWIN$ = 2048 was used for frequencies higher than 707 Hz. Boxcar window, 99% overlap, L_{init} = 7 dB and integration time constant τ = 0.1 s were used for the whole frequency range. The results of calculation are shown in Figure 3 (left) and Table 1.

4.2. Interrupted noise method

The second experiment was conducted in a small test room at our faculty where interrupted noise method was applied. There were no additional objects inside the room except the measuring equipment. The walls and the ceiling of the room are made of plaster boards and the floor is made of concrete. The volume of the room is approximately 6.4 m^3. The measurements were performed with a omnidirectional loudspeaker (self made), a half inch microphone (Behringer ECM8000), an external soundcard (M-audio), an amplifier (M-audio) and a personal computer (HP, ProBook 440 G4). Pink noise was used as an excitation signal. 96 kHz sampling frequency and a 16 bit resolution was chosen. The sound source was placed 10 cm from the bottom corner of the room. 5 microphone positions were chosen and 10 interrupted noise signals were recorded at each position. The pink noise length was 15 s. Each recording was analyzed and standard 1/1 octave band and narrow band RT were determined. The value of $NWIN$ = 65536 was used for frequencies from 0 Hz to 175 Hz. The value of $NWIN$ = 8192 Hz was used for the 175 Hz to 500 Hz frequency range and the value of $NWIN$ = 2048 was used for frequencies above 500 Hz. Boxcar window, 99% overlap, L_{init} = 5 dB and τ = 0.1 s were used for the whole frequency range. The results of calculation are shown in Figure 3 (right) and Table 1.

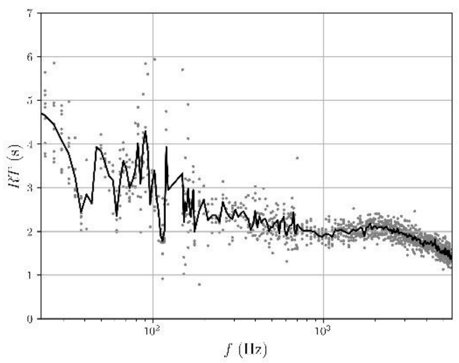

(a)

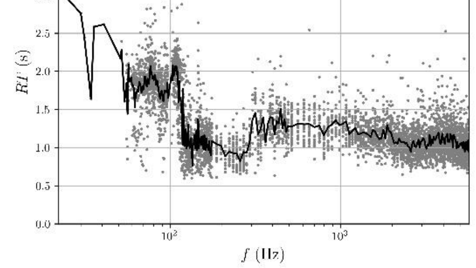

(b)

Fig.3. Narrow band RT for the IIR (a) and IN (b) procedures. The dots present individual measurments, the black line is average value for each frequency band.

In order to compare the new method with the conventional broadband analysis, octave band RT was determined as arithmetic average of narrow band RTs within the analyzed 1/1 octave band. Type A statistical error was determined as standard deviation of RTs. T_{20} was used for comparison. The results are summarized in Table 1.

$T_{20}\pm$ standard deviation (s)	*IIR*		*IN*	
1/1 OCTAVE BAND	ISO 3382	Narrow band	ISO 3382	Narrow band
31.5	$\mathbf{1.97 \pm 0.34}$	$\mathbf{3.73 \pm 0.34}$	$\mathbf{0.76 \pm 0.84}$	$\mathbf{2.52 \pm 0.44}$
63	3.29 ± 0.41	3.35 ± 0.33	2.00 ± 0.82	1.85 ± 0.29
125	$\mathbf{1.54 \pm 1.57}$	$\mathbf{3.17 \pm 0.74}$	1.42 ± 0.52	1.44 ± 0.49
250	2.04 ± 0.13	2.41 ± 0.38	0.99 ± 0.12	1.05 ± 0.26
500	2.04 ± 0.08	2.15 ± 0.34	1.28 ± 0.07	1.32 ± 0.22
1000	1.86 ± 0.03	1.97 ± 0.16	1.21 ± 0.04	1.24 ± 0.20
2000	1.99 ± 0.04	2.05 ± 0.15	1.10 ± 0.03	1.10 ± 0.19
4000	1.72 ± 0.03	1.7 ± 0.21	1.03 ± 0.03	1.08 ± 0.20

Table 1. Reverberation time and its standard deviation in octave bands for each experiment. Comparison between standard [1] and narrow band methods (note the differencies between the two methods below 125 Hz).

5. CONCLUSION

The uncertainty of low frequency RT measurements is still inadequate even with the use of the latest equipment. The RT in the low frequency region should be treated as discrete parameter. In this paper the analysis of the reverberation time in high frequency resolution was introduced. The influence of input parameters on the shape of the decay curve and calculation of RT is studied for both IIR and IN methods. Results of sensitivity analysis show important effect of the input parameters on linearity of the decay curve. Careful selection of these parameters is needed for both impulse response (IIR) and interrupted noise (IN) methods. The choice of time window length is dependent on the desired frequency resolution and the sampling frequency. In both presented experiments a frequency resolution of Δf = 1.46 Hz was selected as optimal. Time windows should be overlapped by as much as 99% and integration time constant (τ) should be in the 50 ms to 200 ms range. If the impulse response (IIR)method is used the calculation should start t levels which are more than 5 dB below the steady state part of the curve due to lag which is introduced when high frequency resolution is desired. The narrow band reverberation time algorithm is less sensitive to the selection of input parameters for the interrupted noise (IN) method which is thus preferred method. Narrow band reverberation time was compared with the conventional broadband analysis. At higher frequencies both methods give similar results and octave band reverberation time is equal to average of narrow band reverberation times within the octave band. In the low frequency region resonant frequencies determine the decay of sound and statistical averaging as adopted by conventional method gives results that are inadequate. Narrow band reverberation time gives results that are more reliable as only discrete frequencies are considered. Such procedure is also quite common in room acoustics.

6. REFERENCES

[1.] ISO 3382: ***Acoustics - measurement of room acoustic parameters - Part 2:reverberation time in ordinary rooms***, Standard, International Organiza tion for Standardization, Geneva, CH (2008)

[2.] C. Scrosati, F. Scamoni, G. Zambon: ***Uncertainty of facade sound insulation ain buildings by a round robin test***, Applied Acoustics 96 (2015) 27-38.

[3.] D. Masović, M. Oguc, **Analysis of reverberation time field measurement results in building acoustics**, Telfor Journal 5 (2) (2013) 145-150.

[4.] A. Lundeby, T. E. Vigran, H. Bietz, M. Vorlander, **Uncertainties of measurements in room acoustics**, Acta Acustica united with Acustica 81 (4) (1995) 344-355.

[5.] C. Hopkins, P. Turner, **Field measurement of airborne sound insulation between rooms with non-diffuse sound fields at low frequencies**, Applied Acoustics 66 (12) (2005) 1339-1382.

[6.] [6] F. Dezelak, L. Curovic, M. Cudina, **Determination of the sound energy level of a gunshot and its applications in room acoustics**, Applied Acoustics 105 (2016) 99-109.

[7.] M. R. Lamothe, J. Bradley, **Acoustical characteristics of guns as impulse sources**, Canadian Acoustics 13 (2) (1985) 16-24.

[8.] A. Prato, F. Casassa, A. Schiavi, **Reverberation time measurements in nondiffuse acoustic field by the modal reverberation time**, Applied Acoustics (2016) 160-169.

[9.] P. Economou, C. Economou, P. Charalampous, **Beyond sabine: Investigating the acoustical phenomenon of reverberation using room modal decay**, in: 24th international congress on sound and vibration, Vol. 1, International Institute of Acoustics and Vibration, 2017.

[10.] T. J. Schultz, **Problems in the measurement of reverberation time**, Journal of the Audio Engineering Society 11 (4) (1963) 307-317.

[11.] F. Jacobsen, P. M. Juhl, **Fundamentals of general linear acoustics**, John Wiley & Sons, 2013.

[12.] M. R. Schroeder, **New method of measuring reverberation time**, J. Acoust. Soc. Am. 37 (1965) 409.

[13.] R. Stewart and M. Sandler, **Database of omnidirectional and b-format impulse responses**, in Proc. of IEEE Int. Conf. on Acoustics, Speech, and Signal Processing (2010).

SINGLE DEGREE OF FREEDOM SYSTEMS WITH BOUC HYSTERESIS AND FILTERED WHITE NOISE

Holger Waubke

Austrian Academy of Sciences, holger.waubke@oeaw.ac.at

Abstract: *Using the Gaussian Closure Technique a system with a single degree of freedom will be presented, which is excited with filtered white noise. The system has a hysteretic behaviour described by Bouc. The filtered white noise is generated by an ordinary differential equation of the second order. The equations of a non-linear oscillator are added to the state vector. The result is a single sided coupled system with two degrees of freedom. Additionally, the amplitude of the white noise process can be smoothly modulated. In addition, viscose damping and restoring forces can be set to zero and an asymmetry applying a constant load can be added to the system. The results are compared with the Monte-Carlo method and the stability of the new method is investigated.*

Key words: Gaussian Closure, Bouc Model

8th Congress of the Alps Adria Acoustics Association
Zagreb, Croatia
20 – 21 September 2018

Hrvatsko akustičko društvo
HAD
Acoustical Society of Croatia

MUSIC DYNAMIC RANGE OF FM RADIO STATIONS IN ZAGREB

Ivan Djurek, Elena Maganić, Mia Suhanek

University of Zagreb, Faculty of EE and Computing, Unska 3, Zagreb, Croatia
ivan.djurek@fer.hr

Abstract: *Dynamic range of music nowadays is very limited. Additional dynamic processing in radio station signal chain could further limit this dynamic range, which could significantly reduce the reproduction quality. Therefore, signals of seven FM radio stations in Zagreb were analyzed in terms of dynamic range. It was found that the used dynamic range was reduced compared to the selected original songs. It was discovered that all included radio stations maintain constant smaller dynamic range and loudness, which change depending on music genre. Reasons for smaller dynamic range were analyzed and discussed and thus, appropriate dynamic range was proposed.*

Key words: dynamic range, FM radio, music

1. INTRODUCTION

Dynamic range gives music its liveliness, mood and character, and therefore is important for listening quality. In recent decades there is a trend in music to increase its loudness at the expense of its dynamic range. Some studies [1] showed that listeners prefer louder music, and in general say that louder music is better. The music producers and radio stations' owners, forced by commercial reasons, focuse on audio signal's loudness. In other words, the general opinion is that everything should be loud, since listeners prefer loud.

Taking into account nowadays modern world and our listening habits, this could be justified. Today, music is mainly listened in noisy environments, like trains, trams and cars. In order to be isolated from the outside world, people in public places usually wear earphones or earbuds. Furthermore, in cars, there is a problem of engine and wind noise. Those are environments, which do not allow listening with higher dynamic range.

This constant persuit for louder signals, resultet in so called "loudness war". Loudness war is a term which describes constant increase in loudness, and reduction of dynamics. Results of this "war" are evident in audio signal's shape. Figure 1 shows a signal of a song before and after it was processed in a radio station's equipment. It is clearly shown how extreme dynamic changes can be. Dynamic range of the song which in original format is around 30 dB, after broadcasted in a radio station, has a dynamic range less than 10 dB. In a last few years, audio engineers and music lovers started to question where and when this war will end. Do listeners can perceive difference between original and hyper-compressed material.

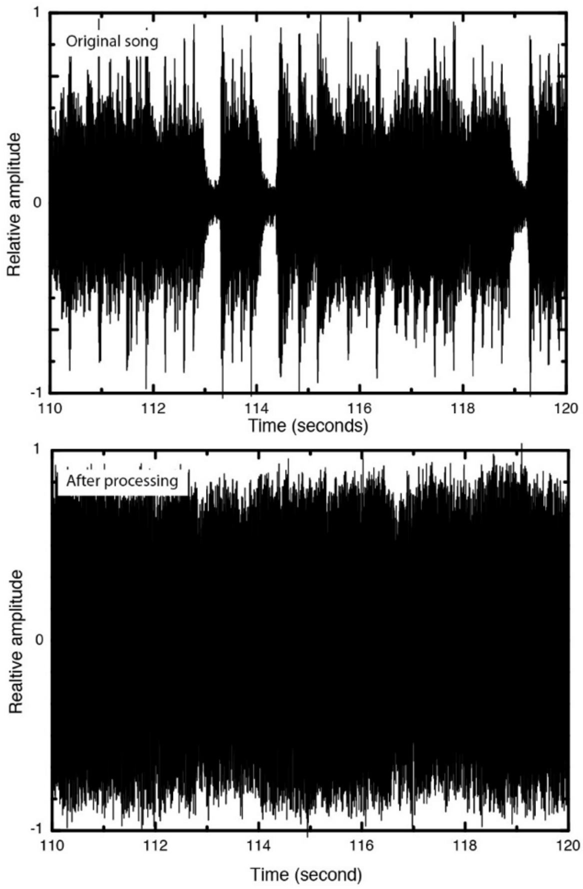

Fig 1. Comparisons of an audio signal before and after processing on a radio station.

One subjective listening test with original and hyper-compressed material showed that listeners preference depends on several factors, like music genre, age group, amount of exposure to different genres [2]. Taking loudness as the only factor for quality is oversimplification of the listeners' preferences. Some studies tried to address the assumption that hyper-compressed music is an advantage when environmental noise acts as a masking agent [3]. This studies showed that this not the case, and that hyper-compression will not make listeners to select louder music as a better choice in noisy environments. Finally, subjective tests with compressed music in several stages showed that the crest factor has a big influence on loudness and quality perception, however, this is largely influenced by genre [4,5,6].

This competition in loudness in radio broadcasting exists for at least 30 years. In the beginning, in order to get louder, radio stations used simple clipping. This method now has transferred in the music industry. Taking into account audio processing path in modern radio station, this tendency to increase music loudness does not well coexist with severely compressed audio signal [7].

In this paper, we analyzed the dynamics of seven FM radio stations in Zagreb, Croatia, in order to get information how big these changes can be. Today's modern music, especially pop music, is produced to be loud. Additional loudness increase, and dynamic range reduction could significantly reduce its quality. A legitimate question arises, whether loudness increase in radio stations is actually necessary.

2. THE ANALYSIS

In order to get a better overview of the FM radio stations' signal dynamics, we selected seven radio stations in Zagreb, Croatia. They differ in music program, predominant music genres and amount of spoken program. For recording of radio stations' signal we used a Sony FM tuner, whose output was connected to a sound card connected to a PC. For each radio station, we recorded about 90 minutes of the stereo signal. The audio signals included mainly music signals, and on the other hand spoken program. We selected two national and five commercial radio stations.

First, we analyzed the dynamics and ITU-R BS.1770-2 loudness value [8] of the whole audio signals, which included music and speech. In 2011, ITU has defined the recommendation ITU-R BS.1770-2, which proposes algorithms for measurement of audio programme loudness and true-peak level. The goal was to define a single level measuring algorithm which will be used by all video and audio broadcasting stations in order to ensure equal sound level across various digital platforms, especially when listeners change stations and during commercial brakes.

Second, we focused on three songs, selected from each station's audio signal. We wanted to find out how much music signal in each radio station is changed, before it is aired. As afore mentioned, before it is aired, an audio signal in a FM radio station goes through several phases, of which, dynamic processing and levelling are the most important. Selected songs represent the main genre of each radio station, from folk music to rock music. When each song was selected, we downloaded the original signal from the Internet and compared it to the aired song. This enabled us to better understand how songs, i.e. audio signal on radio stations is changed in terms of dynamics. Before the analysis, the recorded and downloaded songs were peak normalized.

We analyzed several signal's parameters, all connected with signal amplitude. For the analysis we used algorithms created in the Matlab. We focused on the parameters connected with the dynamics. Those were the peak amplitude, RMS amplitude, dynamic range used and ITU-R BS.1770-2 loudness value. Value "dynamic range used" represents average dynamic range between peak value and average RMS value not including too quiet parts, such as pauses etc. Those are just average numbers which show average values. Average values are suitable for a fast comparison, but do not give an overall picture of signal's dynamics.

In order to get a better understating how dynamics of a signal in FM radio stations is changed, we also calculated the probability density functions (PDFs) of each song signal's amplitude. The PDF shows a graphic representation how signal's amplitude is changed. From these diagrams, it is immediately clear if the signal has large or small dynamics.

3. RESULTS AND DISCUSSION

Results of the analysis are shown in the following tables and figures.

Table 1 shows dynamics and loudness of the complete audio signal of all analyzed seven radio stations.

Table 1. Calculated dynamics and loudness for the complete signal of all FM radio stations.

Station	1	2	3	4	5	6	7
Peak Amplitude (dB)	0,00	-0,03	-0,01	-0,04	0,00	-0,33	0,00
Average RMS Amplitude (dB)	-11,69	-12,42	-12,70	-12,60	-13,14	-14,99	-14,37
Dynamic Range Used (dB)	24,50	33,05	18,60	18,45	29,95	41,45	28,60
ITU-R BS.1770-2 Loudness (LUFS)	-7,95	-9,14	-9,22	-9,44	-9,08	-10,63	-10,91

As can be seen from Table 1, used dynamic range vary largely among these stations. This could be attributed to different program types of these stations, but also to different settings of radio broadcasting equipment. ITU-R loudness is similar to all stations and ranges between -8

and -11 LUFS. Commercial radio stations tend to be louder with smaller dynamics.
Tables 2 to 8 show calculated dynamics values for three songs for each of seven radio stations.

Table 2. Calculated values for signal of FM radio station 1. (commercial)

	Song 1		Song 2		Song 3	
	Internet	Radio	Internet	Radio	Internet	Radio
Peak Amplitude (dB)	-0,05	0,00	-0,53	-0,39	-0,31	-0,34
Total RMS Amplitude (dB)	-15,12	-10,67	-16,18	-9,88	-11,79	-10,79
Dynamic Range Used (dB)	45,25	34,80	**58,35**	**6,75**	22,65	20,75
ITU-R BS.1770-2 Loudness (LUFS)	-12,46	-7,97	-12,91	-6,88	-9,86	-7,53

Table 3. Calculated values for signal of FM radio station 2. (national)

	Song 1		Song 2		Song 3	
	Internet	Radio	Internet	Radio	Internet	Radio
Peak Amplitude (dB)	-0,55	-0,03	-0,14	-0,01	-0,28	-0,05
Total RMS Amplitude (dB)	-17,23	-10,77	-11,68	-10,08	-14,44	-9,90
Dynamic Range Used (dB)	20,85	12,05	15,05	9,80	39,60	30,65
ITU-R BS.1770-2 Loudness (LUFS)	-15,13	-8,80	-9,10	-7,72	-12,04	-7,71

Table 4. Calculated values for signal of FM radio station 3. (commercial)

	Song 1		Song 2		Song 3	
	Internet	Radio	Internet	Radio	Internet	Radio
Peak Amplitude (dB)	-0,24	-0,24	-0,01	-0,54	-0,30	0,00
Total RMS Amplitude (dB)	-17,72	-12,76	-14,56	-13,20	-12,63	-11,06
Dynamic Range Used (dB)	38,25	35,90	25,00	18,00	18,15	11,65
ITU-R BS.1770-2 Loudness (LUFS)	-13,63	-9,39	-13,22	-9,48	-9,43	-7,93

Table 5. Calculated values for signal of FM radio station 4. (commercial)

	Song 1		Song 2		Song 3	
	Internet	Radio	Internet	Radio	Internet	Radio
Peak Amplitude (dB)	-0,14	-0,04	0,00	0,00	0,00	-0,09
Total RMS Amplitude (dB)	-13,94	-11,43	-12,47	-11,18	-14,95	-11,81
Dynamic Range Used (dB)	**23,65**	**11,85**	22,70	10,30	**23,05**	**9,85**
ITU-R BS.1770-2 Loudness (LUFS)	-11,61	-8,30	-9,93	-8,38	-12,48	-8,72

Table 6. Calculated values for signal of FM radio station 5. (commercial)

	Song 1		Song 2		Song 3	
	Internet	Radio	Internet	Radio	Internet	Radio
Peak Amplitude (dB)	-0,05	0,00	-0,04	-0,69	-0,12	-0,16
Total RMS Amplitude (dB)	-14,91	-10,23	-14,84	-11,25	-11,22	-11,15
Dynamic Range Used (dB)	9,75	4,50	**73,25**	**11,25**	20,40	13,00
ITU-R BS.1770-2 Loudness (LUFS)	-11,70	-7,35	-10,91	-8,02	-8,75	-8,45

Table 7. Calculated values for signal of FM radio station 6. (national)

	Song 1		Song 2		Song 3	
	Internet	Radio	Internet	Radio	Internet	Radio
Peak Amplitude (dB)	-0,17	-0,75	-0,01	-0,19	-1,42	-0,24
Total RMS Amplitude (dB)	-15,17	-12,17	-16,55	-12,53	-20,16	-12,62
Dynamic Range Used (dB)	17,10	9,70	24,20	17,40	21,95	14,25
ITU-R BS.1770-2 Loudness (LUFS)	-12,90	-9,86	-13,83	-10,07	-17,37	-9,90

Table 8. Calculated values for signal of FM radio station 7. (commercial)

	Song 1		Song 2		Song 3	
	Internet	**Radio**	**Internet**	**Radio**	**Internet**	**Radio**
Peak Amplitude (dB)	0,00	-0,02	-0,04	-0,05	0,00	0,00
Total RMS Amplitude (dB)	-12,12	-10,09	-13,72	-8,69	-19,19	-11,63
Dynamic Range Used (dB)	10,70	8,85	**16,05**	**6,85**	38,55	34,15
ITU-R BS.1770-2 Loudness (LUFS)	-8,32	-7,37	-11,60	-6,59	-16,18	-9,05

The first thing that can be concluded from the presented tables is that all analyzed radio stations maintain uniform loudness for analyzed songs. As can be seen, average ITU-R loudness is around -8 LUFS. This ensures that all radio program is equally loud, regardless of the change in the program and music genre. However, when aired over the radio, songs are louder, in average for 5 dB. In this case, radio stations achieved their goal to be as loud as possible. On the other hand, there are large differences in dynamic range used, which influences listening quality. In order to maintain the same high value of loudness, radio stations' equipment is set up for amplification of quiet parts. In extreme cases, difference in dynamics of the original and aired song is 50 dB, like in case of the song 2 for radio station 1.

Much more information about signal's dynamics can be seen from PDFs. Figure 2 shows PDFs for selected song 1 of each analyzed radio station. Figures show left and right channels. They also show that each radio station tends to hold the audio signal in a narrow dynamic range of 5 to 10 dB. There are no quiet passages, and therefore dynamic range of the signal is degraded. Naturally, there are differences in amplitude distribution between different music genres, however in general, dynamic range is much narrower.

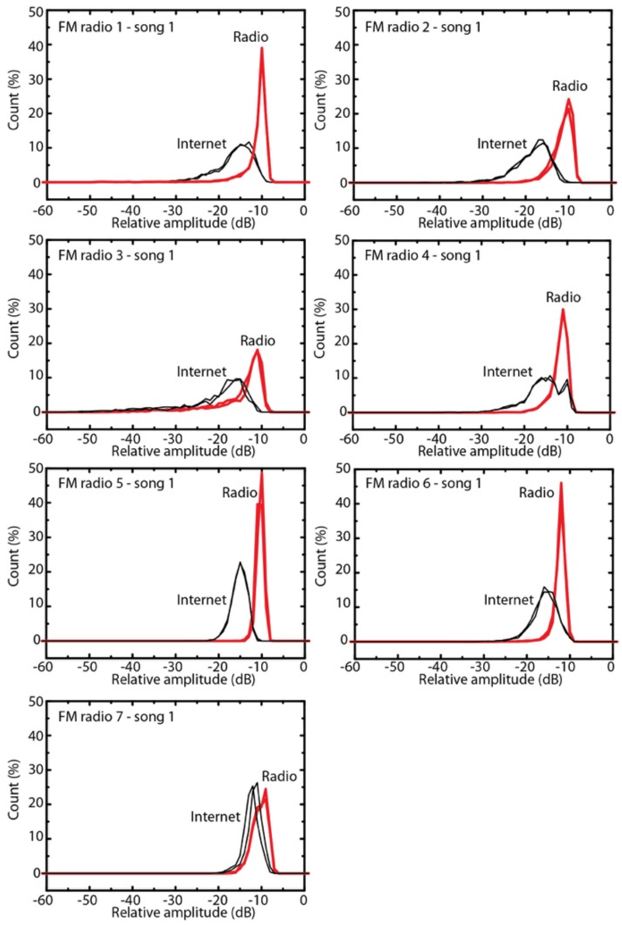

Fig. 2. PDFs of selected song 1 for each analyzed radio station (black line: downloaded original song, red line: recorded song from a radio station)

4. CONCLUSION

Audio signal of seven FM radio stations in Zagreb was analyzed. We analyzed dynamics of the audio signals by calculating the difference between the peak and average signal level. In order to make a comparison of the dynamics before the songs were emitted on the FM radio stations, we selected three characteristic songs from each radio stations' audio signals. Comparison showed that all analyzed radio stations use heavy compression with narrow dynamic range. In some cases, difference in dynamics, before and after processing audio signals in radio stations was greater than 50 dB.

Radio stations tend to have louder signal in order to be noticed when user dials radio stations on a tuner. This results in heavily compressed audio signal with very low dynamics. In some cases, heavy compression results with a degraded signal. Listening tests showed that listeners' preferences can be very different, and not only based on loudness.

Already heavily compressed music, when reproduced on radio stations is even more degraded. In some cases, distortions could be easily heard. In order to use the high

dynamic range of modern equipment, there should exist a compromise between music producers and radio station owners regarding dynamic range and signal quality.
Listening experience depends on many factors, and radio stations should not only focus on loudness. There are several other factors that should be considered. For example, the listeners should be asked how they choose their favorite radio stations. Future work will focus on these and other similar factors of listeners' preferences.

5. REFERENCES

[1.] E. Vickers: **The Loudness war: background, speculation and recommendations**, *Proceedings of 129th AES Convention, Convention paper 8175, 129th AES Convention*, 4-7 November, 2010, San Francisco, USA

[2.] R. W. Taylor, W. L. Martens: **Hyper-compression in music production: listener preferences on dynamic range reduction**, *Proceedings of 136th AES Convention, Convention paper 9022*, 26-29 April, 2014, Berlin, Germany

[3.] R. W. Taylor, L. Miranda: **Hyper-compression, Environmental Noise and Preferences for the Ear Bud Listening Experience**, *Proceedings of 141st AES Convention, Convention paper 9657*, 29.9-2.10., 2016, Los Angeles, USA

[4.] M. Wendl, H. Lee: **The Effect of Dynamic Range Compression on Loudness and Quality Perception in Relation to Crest Factor**, *Proceedings of 136th AES Convention, Convention paper 9021*, 26-29 April, 2014, Berlin, Germany

[5.] N. B.H. Croghan, K. H. Arehart: **Quality and loudness judgments for music subjected to compression limiting**, *The Journal of the Acoustical Society of America* **132**, 1177 (2012); doi: 10.1121/1.4730881

[6.] M. Ronan, N. Ward, R. Sazdov: **Identifying and validating program material: a hyper-compression perspective**, *Proceedings od 139th AES Convention, Convention paper 9383*, 29.10-1.11., 2015, New York, USA

[7.] R. Orban, F. Foti: **What happens to my Recording when it's played on the radio?**, *Proceedings of 111th AES Convention, Convention paper 5469*, 111th AES Convention, 21-24 September, 2001, New York, USA

[8.] **R 128: Loudness normalization and permitted maximum level of audio signals**, EBU Recommendation, Geneva, June 2014

8th Congress of the Alps Adria Acoustics Association
Zagreb, Croatia
20 – 21 September 2018

Hrvatsko akustičko društvo
HAD
Acoustical Society of Croatia

BLIND ESTIMATION OF REVERBERATION TIME – IT IS HOW YOU SAY IT THAT MATTERS

Andrea Andrijašević

Faculty of Engineering, University of Rijeka, Vukovarska 58, 51 000 Rijeka, Croatia
(andrea.andrijasevic@riteh.hr)

Abstract: *In this study, a set of recordings of phonetically balanced sentences uttered by speakers of both sex in six speaking styles was artificially reverberated. The ground truth values of reverberation time for the utilized measured room impulse responses were calculated in conformance with the ISO-3382 standard. Following that, blind estimation of reverberation time on those reverberant recordings was performed using three state-of-the-art algorithms. For all three algorithms assessed, statistical tests confirmed the hypothesis that speaking style influences the blind estimation process. It was also observed that the largest differences in the values of obtained estimates are present for the recordings that most strongly differ in loudness (soft versus loud), i.e. in the subglottal pressure, that the speaker utilized.*

Key words: reverberation time, estimation, speech, Kruskal-Wallis

1. INTRODUCTION

A number of algorithms for reverberation time (T_{60}) estimation from the received speech signal have been developed over the past two decades. These algorithms differ considerably in their complexity; from the algorithms that are based solely on a stochastic time-domain model of room impulse responses [1-6], to the ones for which there exists an intermediate feature whose value is estimated and from which a reverberation time estimate is obtained [7, 8], and finally to the machine learning approaches utilizing classifiers [9, 10].

In 2016, the results of a preliminary study done by Andrijašević and Domitrović [11] showed that, in addition to background noise [12], speaker's speaking style also influences the value of a time-domain algorithm's output [3]. Therefore, the main objective of this study is to assess whether the sensitivity of an algorithm's output to speaking style is inherent only to that one algorithm, or is generally present, i.e. regardless of the algorithm and of the domain in which it operates.

The remainder of the paper is structured as follows: in Section 2, the speech recordings, room impulse responses (RIRs) and algorithms for blind T_{60} estimation are introduced. Results of statistical analyses are presented and discussed in Section 3, while in Section 4, the conclusions are drawn.

2. METHODOLOGY

2.1. Algorithms for blind T_{60} estimation

In the ACE Challenge [12], the most recent comparative study of blind reverberation time algorithms' performance, the influence of the noise term on estimation quality was assessed. Based on the Challenge results, three of the best performing algorithms were selected and utilized in this study.

The first algorithm, which operates in the mel-STFT domain, was developed by Eaton et al. [7]. Matlab implementation of the algorithm provided on-line by its authors [13] was utilized. The values of the parameters were set as follows: frame length - 16 ms, overlap - 25 %, and the number of mel-frequency bands - 31. Since in this study no noise was added to the reverberant signal, in order to make the algorithm's results comparable to the ones of the remaining two algorithms that do not adapt to the changes in the SNR, the algorithm was adjusted so that it gives an estimate of T_{60} as if the estimated SNR was highest possible.

The second algorithm, developed by Prego et al. [8], also operates in the STFT domain. An implementation of the algorithm, in the form of Matlab code, was provided by its authors. For this algorithm, the values of the parameters were not changed from the original values, and were as follows: frame length - 50 ms, overlap - 25 %, and the number of frequency bins - 1025.

The last algorithm, which operates in the time-domain, was developed by Löllmann et al. [3]. A Matlab implementation of the algorithm was created by following the steps presented in Ref. 3. The values of the parameters were set as follows: frame length - 2 s, where each frame is partitioned into 30 subframes of equal length, and frame shift - 20 ms.

2.2. Room impulse responses and speech recordings

Acoustic impulse responses were taken from the Aachen Impulse Response database v1.4 [14]. Six of the room impulse responses were measured in the room designated as 'booth', six were from the room named 'office' and ten RIRs were from the room named 'meeting'. For each RIR, the associated ground truth value of reverberation time was obtained in fullband, from its energy decay curve, in the [-5 -25] dB interval, in accordance with the ISO-3382 standard [15].

The recordings of 50 phonetically balanced sentences in French language, uttered in six different speaking styles (fast, slow, loud, soft, questioning and normal) by nine speakers of both sex were taken from the OLdenburg LOgatome (OLLO) corpus ver. 2.0 [16]. The corpus IDs for the speakers are as follows: women - 41, 45, 47 and 49, and men – 42, 43, 44, 46 and 48.

For each speaker and speaking style combination, the 50 recordings were concatenated, convolved with a RIR, and used as the input for the algorithms from which the blind estimates of T_{60} were acquired. Finally, the errors were calculated as the difference between the estimated and ground truth value of reverberation time.

3. RESULTS

Since the Jarque-Berra normality test indicated that the data is not normally distributed for some of the groups, 3-way ANOVA statistical tests could not be performed. Instead, Kruskal-Wallis one-parameter tests were carried out, with data grouped based on one of the following factors: speaker, speaking style and true value of reverberation time.

3.1. Speaker

Table 1 shows the results for the Kruskal-Wallis tests when the grouping was based on the speaker. For all three algorithms, speaker is a statistically significant factor influencing the value of the T_{60} estimate. Its influence is strongest for the second algorithm, which can be confirmed in the Fig. 1. Also visible is that the distributions exhibit very similar trends across the speakers for the two time-frequency operating algorithms.

Algorithm	SS, %	χ2	p > χ2
Eaton	15.25	181.03	<0.001
Prego	28.99	344.11	<0.001
Löllmann	3.31	39.25	<0.001

Table 1. Kruskal-Wallis. Groups based on speakers. Sum of squares (SS) is expressed as the percentage of its total value.

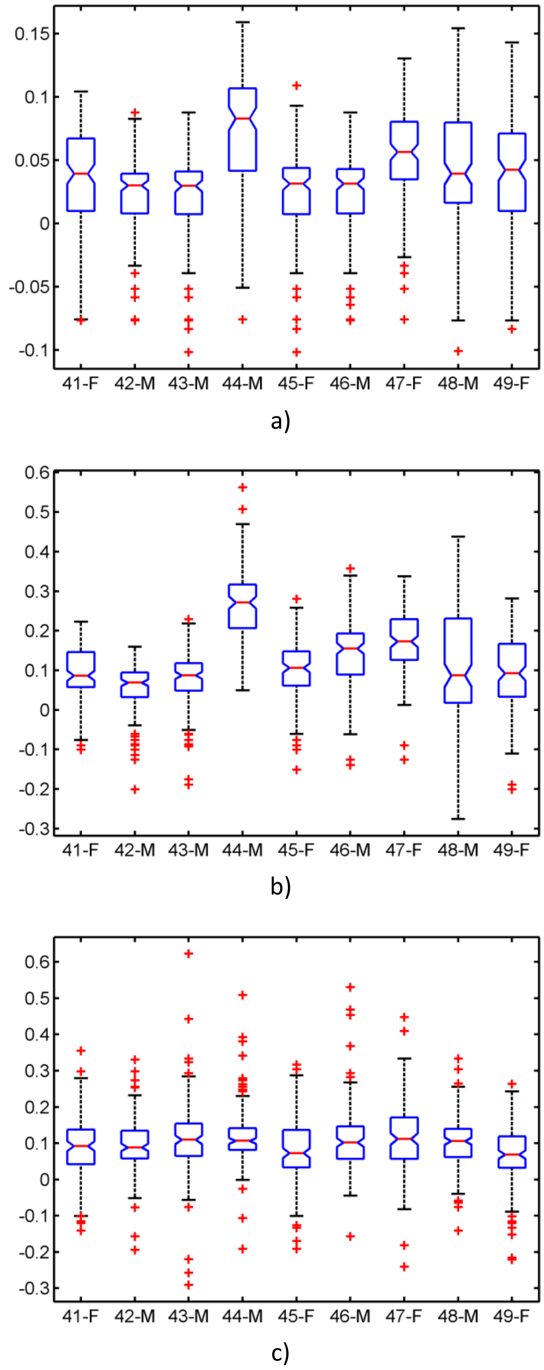

Fig. 1. Kruskal-Wallis boxplots of data. Groups based on speakers: a) Eaton, b) Prego, c) Löllmann.

3.2. Speaking style

In Table 2, the results of statistical tests for the data grouped by speaking style are summarised while Fig. 2 shows the accompanying boxplots. Again, the algorithm most sensitive to the grouping factor is Prego's. Moreover, the changes of the distributions across speaking styles are again very well aligned for the two time-frequency operating algorithms, with loud and soft speaking styles showing the largest difference of their medians among the six groups. For Löllmann's algorithm, the distributions for the soft and loud style also show different median values, but for this algorithm, the distribution for the soft style is also very similar to the distribution for the slow group.

Algorithm	SS, %	χ2	p > χ2
Eaton	9.94	118.02	<0.001
Prego	40.54	481.22	<0.001
Löllmann	7.63	90.6	<0.001

Table 2. Kruskal-Wallis. Groups based on speaking style. Sum of squares (SS) is expressed as the percentage of its total value.

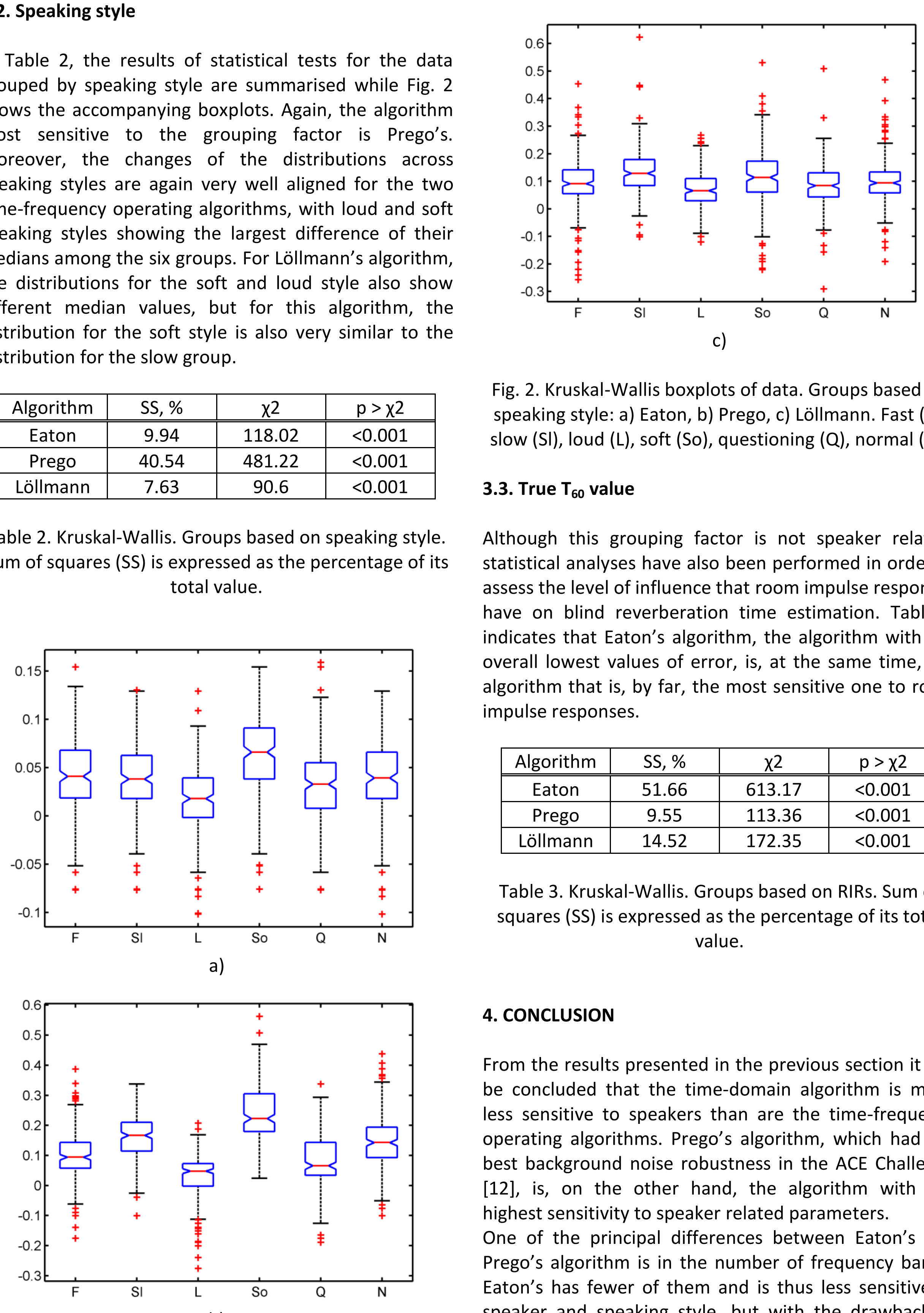

Fig. 2. Kruskal-Wallis boxplots of data. Groups based on speaking style: a) Eaton, b) Prego, c) Löllmann. Fast (F), slow (Sl), loud (L), soft (So), questioning (Q), normal (N).

3.3. True T_{60} value

Although this grouping factor is not speaker related, statistical analyses have also been performed in order to assess the level of influence that room impulse responses have on blind reverberation time estimation. Table 3 indicates that Eaton's algorithm, the algorithm with the overall lowest values of error, is, at the same time, the algorithm that is, by far, the most sensitive one to room impulse responses.

Algorithm	SS, %	χ2	p > χ2
Eaton	51.66	613.17	<0.001
Prego	9.55	113.36	<0.001
Löllmann	14.52	172.35	<0.001

Table 3. Kruskal-Wallis. Groups based on RIRs. Sum of squares (SS) is expressed as the percentage of its total value.

4. CONCLUSION

From the results presented in the previous section it can be concluded that the time-domain algorithm is much less sensitive to speakers than are the time-frequency operating algorithms. Prego's algorithm, which had the best background noise robustness in the ACE Challenge [12], is, on the other hand, the algorithm with the highest sensitivity to speaker related parameters.
One of the principal differences between Eaton's and Prego's algorithm is in the number of frequency bands; Eaton's has fewer of them and is thus less sensitive to speaker and speaking style, but with the drawback of higher sensitivity to RIRs. Since, in general, Eaton's algorithm produces the lowest values of errors, it can be concluded that the speech versus RIR sensitivity trade-off

encoded in the number of frequency bands produces better overall results than for Prego's algorithm.
Lastly, for Löllmann's algorithm, it should be noticed that a very large share of SS could not be explained when speaker, speaking style and RIRs were considered as grouping factors; since in Ref. 11 it was shown that the algorithm's output is sensitive to speaking style but also to the phonemes present in words, it might be the latter factor that could possibly explain the remainder of SS.

5. REFERENCES

[1] R. Ratnam, D. L. Jones, B. C. Wheeler, W. D. O'Brien, C. R. Lansing, A. S. Feng: **Blind estimation of reverberation time**, *J. Acoust. Soc. of Am*., 114(5), 2003, 2877–2892
[2] R. Ratnam, D. L. Jones, W. D. O'Brien: **Fast algorithms for blind estimation of reverberation time**, *IEEE Signal Process. Letters*, 11(6), 2004, 537–540
[3] H. W. Löllmann, E. Yilmaz, M. Jeub, P. Vary: **An improved algorithm for blind reverberation time estimation**, *Proceedings of the International Workshop on Acoustic Echo and Noise Control (IWAENC)*, Tel Aviv, Israel, 2010, 1-4
[4] H. W. Löllmann, A. Brendel, P. Vary, W. Kellermann: **Single channel maximum-likelihood T60 estimation exploiting subband information**, *Proc. ACE Challenge Workshop (a satellite of IEEE WASPAA)*, New Paltz, NY, USA, 2015, 1-5
[5] P. Kendrick, T. J. Cox, F. Li, Y. Zhang, J. Chambers: **Monaural room acoustic parameters from music and speech**, *J. Acoust. Soc. Am.,* 124, 2008, 278-287
[6] A. Keshavarz, S. Mosayyebpuor, M. Biguesh, T. A. Gulliver, M. Esmaeili: **Speech-model based accurate blind reverberation time estimation using an LPC filter**, *IEEE/ACM Trans. Audio, Speech, Language Process*., 20(6), 2012, 1884-1893
[7] J. Eaton, N. D. Gaubitch, P. A. Naylor: **Noise-robust reverberation time estimation using spectral decay distributions with reduced computational cost**, *Proc. IEEE International Conference on Acoustics, Speech and Signal Processing (ICASSP)*, Vancouver, Canada, 2013, 161-165
[8] T. M. Prego, A. A. Lima, S. L. Netto: **A blind algorithm for reverberation-time estimation using subband decomposition of speech signals**, *J. Acoust. Soc. of Am.*, 131, 2012, 2811–2816
[9] T. H. Falk, W. Y. Chan: **Temporal dynamics for blind measurement of room acoustical parameters**, *IEEE Trans. Instrum. Meas.,* 59(4), 2010, 978-989
[10] F. Xiong, S. Goetze, B. T. Meyer: **Blind estimation of reverberation time based on spectro-temporal modulation filtering**, *Proceedings of the International Conference on Acoustics, Speech and Signal Processing (ICASSP)*, Vancouver, Canada, 2013, 443-447
[11] A. Andrijašević, H. Domitrović: **Effects of word phonetic contents and speaking style on blind estimation of reverberation time**, *Proc. of Alps Adria Acoustics Association Congress on Sound and Vibration*, Ljubljana, Slovenia, 2016, 201-208
[12] J. Eaton, N. D. Gaubitch, A. H. Moore, P. A. Naylor: **Estimation of room acoustic parameters: The ACE Challenge**, *IEEE/ACM Trans. Audio, Speech, and Language Process.*, 24(10), 2016, 1681-1693
[13] Available online: http://www.commsp.ee.ic.ac.uk/~sap/projects/blindestimation-of-acoustic-parameters-from-speech/blind-t60-estimator/. Last viewed on: 16th May 2018
[14] M. Jeub, M. Schäfer, P. Vary: **A binaural room impulse response database for the evaluation of dereverberation algorithms**, *Proceedings of the International Conference on Digital Signal Processing*, Santorini, Greece, 2009, 1-4.
[15] Acoustics - Measurement of the reverberation time of rooms with reference to other acoustical parameters, Intl. Org. for Standardization (ISO) Recommendation ISO-3382, 2008.
[16] B. T. Meyer, T. Jürgens, T. Wesker, T. Brand, B. Kollmeier: **Human phoneme recognition depending on speech-intrinsic variability**, *J. Acoust. Soc. of Am*., 128(5), 2010, 3126–3141

SPEECH INTELLIGIBILITY IMPROVEMENT FOR HEARING IMPAIRED WITH HEARING INSTRUMENTS AND FM SYSTEMS

Davor Šušković, Siniša Fajt, Domagoj Matić

davor.suskovic@microton.hr, sinisa.fajt@fer.hr, domagoj.matic@fer.hr

Abstract: *Speech, as an electrical signal, presents its most complicated form. Phonemes cover wide frequency range. Most types of hearing losses are characterized with higher level of hearing loss toward the higher frequencies. As a result, high frequency piece of a phonem becomes inaudible, and hearing impaired persons have a feeling that they can hear but can not understand the speech. The primary goal of the hearing instruments is to give better speech intelligibility. Modern digital hearing instruments use many algorithms to improve speech intelligibility in a head to head communication, even in the most challenging hearing situations with the surrounding noise. However, if the speech is coming from bigger distance, it is necessary to improve the hearing solution with the FM technology. FM systems brings a major benefit in speech inteligibility in difficult hearing situations and are recommended for hearing impaired children during their education.*

Key words: speech intelligibility, formants, hearing instruments, noise reduction, FM systems

1. SPEECH INTELLIGIBILITY WITH HEARING IMPAIRED

Speech signal is very complex, considering its formation, processing and propagation. Observed as an electric signal, it represents its most complex type. The signal is non-stationary, it is variable in frequency and intensity and predominantly transient nature with the sudden emergence and disappearance of certain speech phenomena. Signals use amplitude and frequency modulation [10].

By observing the speech signal spectrum, we notice places of greater energy. Such total or local maxima are called formants. The frequency of the base tone is most often indicated with F0. In phonetics, it is a very important element of the description because its changes on the perceptual plan represent changes in pitch (intonational change). The symbols F1, F2, F3, etc. are accepted for formants and their frequencies. The F0 symbol refers only to the first harmonic and its frequency, which is the frequency of opening and closing the vocal. The first 2 formants (F1 and F2) are important in the determination of speech patterns, ie the recognition or understanding of speech [1]. In Figure 1. you can clearly see the position of the formant in the voice signal.

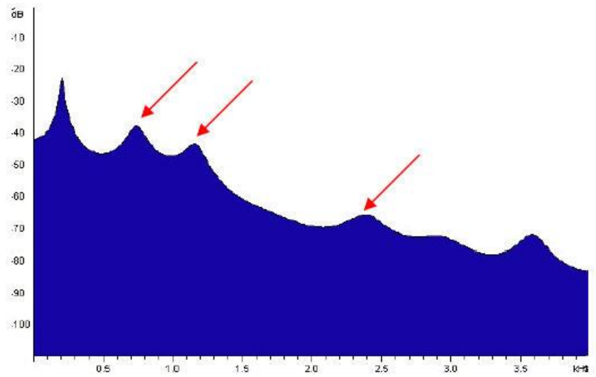

Fig.1. Position of the formants

Hearing loss is a multifaceted loss of listening ability 5. Sensorineural hearing loss results in several consequences:

1.1. Reduced hearing ability

People with hearing loss are unable to hear some sounds. People with the severe hearing loss (hearing loss over 60 dB [9]) can't hear speech, unless it is a loud one or the speaker is standing really close. The problem of understanding speech is the result of the lack of hearing of a part of the phoneme. Hearing loss characterized by a decrease in hearing from lower to higher frequencies (from 500 Hz to 4 KHz), occurring in more than 90% of hearing impaired adults and 75% of children[14], prevents the hearing of higher formants, which leads to a reduction of speech intelligibility. In Figure 2. and in Table 1. the similarity of the first formant of the phonemes „o“ and „e“ is seen, which can cause uncertainty in understanding if the second formant is inaudible.

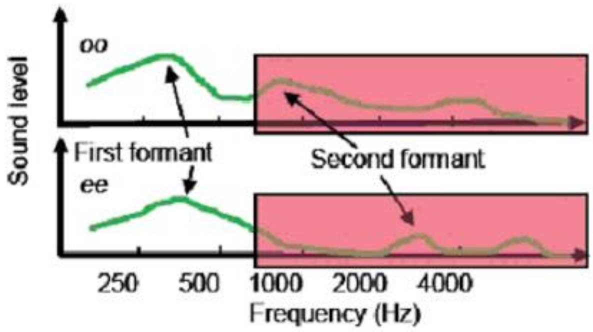

Fig.2. Position of F1 and F2 at „o“ and „e“

phoneme	e	o
F1	471	482
F2	1848	850
F3	2456	2472

Table 1. Position of formants (Hz)

As low-frequency parts of the speech signal cause volume, hearing impaired people often do not perceive the lack of audibility and we can hear the phrase "I hear, but I do not understand".

1.2. Reduced Dynamic Range

Sensorineural hearing loss raises the hearing threshold, but the UCL (uncomfortable level) is slightly changing, especially in mild and moderate hearing losses. This results in a reduced dynamic range compared to normal hearing people (Figure 3.).

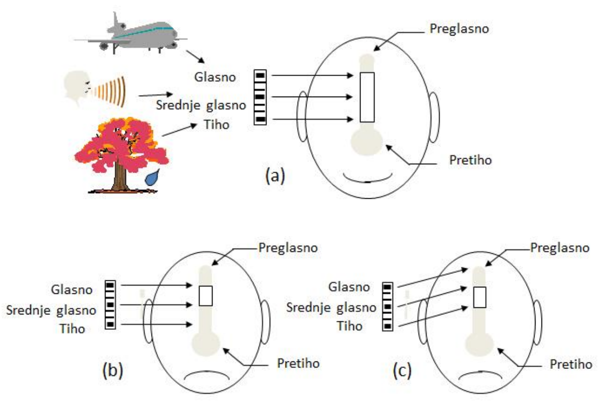

Fig.3. Reduced dynamic range with hearing impaired

1.3. Reduced frequency resolution

If the surrounding noise contains frequencies close to those of the speech signal, the normal hearing ear can send separate brain signals. Based on the information it receives, hearing and visual (reading from the lips) and with the knowledge of the direction of the sound, the brain can partially neglect part of the signal that contains noise and focus on listening to speech.
The frequency resolution potencial is reduced for persons with sensorineural hearing loss. The frequency allocation can be reduced even if there is no surrounding noise. Relatively intense low frequency sounds can mask silent high frequencies (second and third formants). This phenomenon is called upward spread of masking [4].

1.4. Reduced resolution due to masking

Loud sounds can mask silent sounds that come just before or after them. This phenomenon is more frequent in people with hearing loss and directly affects speech intelligibility [8,16].
Many everyday situations include noise that dynamically varies with its intensity. Normal hearing people have the ability to listen during quiet moments and based on acquired parts to form complete information. Hearing impaired people partially lose this ability, especially if they are older [6].
Any of the mentioned consequences of the sensorineural hearing loss can cause a lower understanding in a given situation, comparing it with a normal hearing person. Generally, a hearing impaired person needs a higher signal-to-noise ratio (SNR) than a normal hearing person if he or she wants to achieve the same result of speech intelligibility.

2. HEARING AIDS

The purpose of hearing aids is primarily to enable hearing impaired people to hear and understand speech. Although a normal hearing person is able to listen to sound frequencies up to about 20 kHz, hearing aids, due to their technical limitations, set the upper limit of their operation between 6 kHz and 9 kHz depending on their performance and sound transmission (classic earmould or RIC hearing aids).
In today's digital world of hearing aids, the simplest ones, with its features and capabilities, are suitable for hearing situations without background noise and for the participation in face-to-face communication. Technologically more complex hearing aids allow for easier communication in more demanding hearing situations with the presence of background noise. For longer distance communication an extension of the audio system is required.
Hearing aids are intended to make use of the remaining hearing area with sounds being amplified a certain value

so that they can be heard in a pleasant and understandable way. The required amplification at certain frequencies, depending on the hearing loss, is determined by fitting formulas. Today the most popular are NAL-NL2 and DSL v5. DSL (Desired Sensation Level) has a prime goal to normalize the volume across the entire frequency range, enabling maximum hearing of all sounds, which is why DSL is the recommended fitting formula for children. NAL-NL2 (National Acoustic Laboratories - nonlinear) is doing the normalization in the medium frequency range for the purpose of highlighting the spoken area and increasing the understanding of speech, especially in situations with the present noise [11].

As the hearing range of hearing impaired people is significantly reduced in relation to normal hearing people, hearing aids use compression when amplifying the sounds of different volume. With compression, it is possible to apply greater amplification for quiet sounds so that they become audible, then less amplification for medium loud sounds and the least amplification (or limitation) of loud sounds so that they do not cross the UCL (Figure 4.).

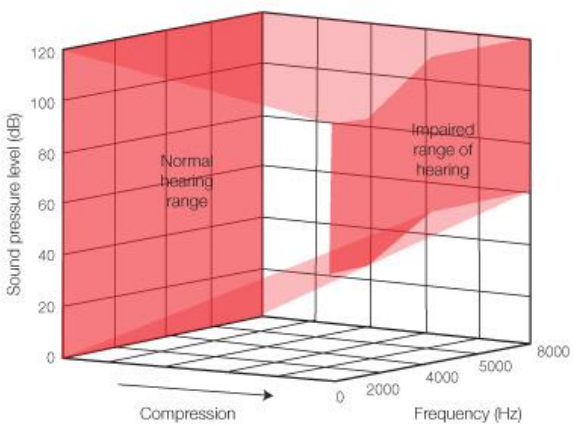

Fig.4. Hearing aids compression

In the listening situation with the present noise, the best results of improving speech intelligibility are achieved by the use of directional microphones. The benefit of using the directional microphones depends on the degree of direction, reverberation, distance from speaker and noise level. During the face-to-face conversation, the gain (increase in SNR) from the use of the directional microphones is 3-5 dB, and if the noise source is behind the hearing aid users, the improvement of the SNR can reach 10 dB[3].

Using the noise reduction or elimination algorithms for improving speech intelligibility with hearing aids, not taking into account the benefit of directional microphones, is a major problem that has still not been solved yet, and which was predicted by Harry Levitt in 1997 [12]:

Our understanding of this problem is so limited that we have not only been unsuccessful in finding a solution, but we do not even know whether it is possible to improve the intelligibility of speech in noise by any significant amount.

Noise reduction algorithms analyze narrow bandwidth, and if they recognize the existence of noise they reduce the prescribed amplification. By increasing the number of frequency bands in the digital signal analysis and increasing the number of channels of the hearing aids, these algorithms can work very precisely and only affect the frequency band in which the noise is present. However, the decrease of amplification within a given frequency band will reduce not only the noise level, but also the level of the speech signal present in that frequency band. Because of that, the SNR in that band will remain the same, and thus the overall SNR. Equally, no improvement in speech intelligibility will be achieved. Subjective benefit is gained in users of hearing aids, which is reflected in increasing the feeling of pleasant listening and reducing the listening efforts [2].

Most hearing impaired people have greater hearing loss at higher frequencies than the lower ones. Due to the reduced hearing range at higher frequencies, the difficulty of discerning the phonemes and the technical limits of hearing aids (limited amplification at higher frequencies) special hearing aid algorithms are required that will allow the hearing of high-frequency sounds, especially the occlusive „p“, „t“ and „k“ and the frightening „s“. „š“, „f“, „h“, „z“ i „ž“. There are various frequency lowering techniques that lower the high frequency sounds to the lower frequency range, depending on the hearing aid manufacturer. Generally, such algorithms result in improved understanding of speech, but also in the development of speech with the prelingually hearing impaired children [7].

3. FM SYSTEMS

If you want to improve the speech intelligibility in the listening situations where the speaker is at a greater distance from the hearing aids user or is not facing him, it is necessary to extend the hearing aids system. The solution that achieves excellent results, even in situations with higher levels of background noise, is the use of the FM system (Figure 5.).

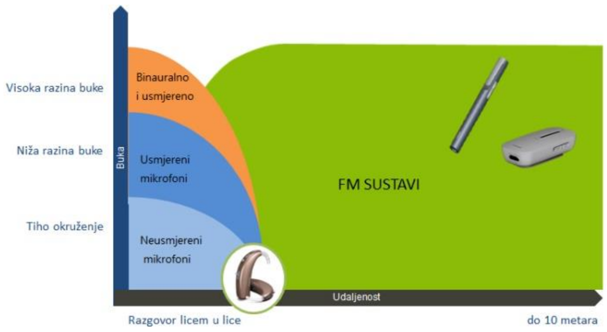

Fig.5. Usage of the FM systems and hearing aids depending on noise level and distance from the speaker

The FM system uses frequency modulation for signal transmission. The advantages of the frequency modulation of the signal are the high interference resistance for transmission, both amplitude and frequency disturbances. For the transmission performance the nonlinear amplifiers are sufficient, and they have a much greater efficiency than the linear.
The modern FM system uses the ISM (Industrial, Scientific, Medical) frequency band at 2.4 GHz frequency. Theoretically, it is possible to use an unlimited number of devices within an FM system, which makes the system suitable for use during the education for students using hearing aids and an FM system.
The FM system consists of an FM signal transmitter and an FM signal receiver. The FM transmitter has a microphone and it transmits the frequency modulated sound (speech) to the FM receiver. The FM Receiver signal then transmits it to the hearing aid. There is no need for line of sight between the transmitter and the receiver and the signal can be transmitted to the distance of up to 30 meters. The time required for modulation, demodulation and signal transmission is less than 10 ms and does not affect the sound quality. The frequency range of the signal transmission is from 200 Hz to 7300 Hz (for comparison, the upper limit frequency of the bluetooth is 4000 Hz and the delay in transmission is about 50 ms).
Improving speech intelligibility with FM systems in situations with present noise can be really substantial. The transmitter microphone has an expected 20 dB SNR gain in relation to the hearing aid microphone, solely due to it's position close to the speaker. Figure 6. shows the difference in the speech reception threshold (SRT): without the use of hearing aids, with hearing aids without directional microphones, with directional microphones, with an FM receiver on one hearing aid and with FM receivers on both hearing aids [13].

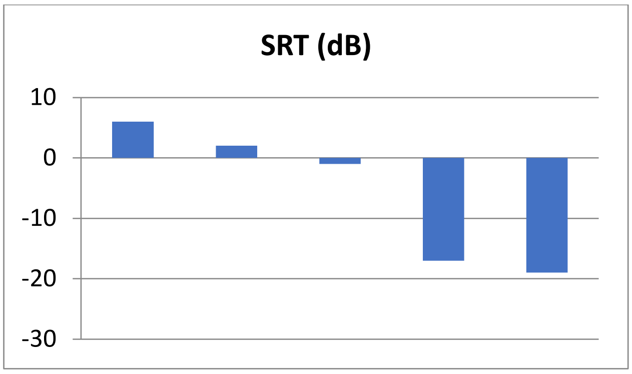

Fig.6. SRT with and without FM system

In the presence of a background noise of 68 to 73 dB it is possible to improve the speech intelligibility of about 50% compared to the standard FM systems and 80% compared to the non-use of the FM system [15].
FM systems are irreplaceable in assisting the hearing impaired children during schooling. The FM system's flexibility makes it possible to maintain a constant SNR regardless of the noise level created by other students or environments. FM systems can be used in adults as well, and they complement the hearing system of the hearing aids, in situations of higher levels of surrounding noise and when listening to a distant speaker. Most digital hearing aids support the use of FM systems. The connection between the FM receiver and the hearing aid can be direct (built-in receiver in the hearing aid) or via the T-coil.
In Croatia, The Ordinance on orthopedic and other aids (NN 7/12) with the List of Aids (NN 106/16) provides children upon completion of the 7th year of age and during the regular education, the right to use one FM transmitter and one FM transmitter with a 5 year term.

4. REFERENCES

[1.] Bakran J., **Zvučna slika hrvatskoga govora**, Zagreb: Ibis grafika., 1996.
[2.] Bentler R.A. et al: **Digital Noise Reduction: outcomes from laboratory and field studies**, Int J Audiol, 47(8):447-460, 2008.
[3.] Compton-Conley at al: **Performance of directional microphones for hearing aids, real world versus simulation**, J Am Acad Audiol, 15(6):440-455, 2004.
[4.] Danaher ES, Pickett JM.: **Some masking effects produced by low-frequency vowel formants in persons with sensorineural loss**, J Speech Hear Res, 18:79-89, 1975.
[5.] Dillon H.: **Hearing Aids**, 2nd ed, Boomerang Press, Sydney, 2012.
[6.] Festen J., Plomp R.: **Effects of fluctuating noise and interfering speech on the speech-reception threshold for impaired and normal hearing**, J Acoust Soc Amer, 88(4):1725-36, 1990.

[7.] Glista D. et al: **Evaluation of nonlinear frequency compression: Clinical outcomes**. International Journal of Audiology, 48, 632-644, 2009.

[8.] Glasberg BR, Moore BCJ.: **Psychoacoustic abilities of subjects with unilateral and bilateral cochlear hearing impairments and their relationship to the ability to understand speech**, Scand Audiol Suppl, 32:1-25, 1989.

[9.] Gortan D.: **Audiologija**, Spiridion Brusina, Zagreb, 1995.

[10.] Ivančević B., **Elektroakustika**, elektroničko izdanje 3.2, Sveučilište u Zagrebu, 2007.

[11.] Kulak et al.: **The effect of fitting formulas in programmable hearing aids on speech discrimination in noise**, National Center for Biotechnology Information, 17(5):278-82, 2007.

[12.] Levitt H.: **Digital hearing aids: past, present and future, Practical hearing aid selection and fitting**, Tobin H (ed) xi-xxiii, Dept of Veterans Affairs, Washington DC, 1997.

[13.] Lewis M.S. et al: **Speech perception in noise: directional microphones versus frequency modulation (FM) systems**, J Am Acad Audiol, 15(6):426-439, 2004.

[14.] Macrae JH, Dillon H.: **Gain, frequency response and maximum output requirements for hearing aids**, J Reahab Res Dev, 33(4):363-376, 1996.

[15.] Thibodeau L.: **Benefits of adaptive FM systems on speech recognition in noise for listeners who use hearing aids**, Am J Audiol,19(1):36-45, 2010.

[16.] Zwicker E., Schorn K.: **Temporal resolution in hard-of-hearing patients, Audiology**, 21:474-494, 1982.

SUBJECTIVE AND OBJECTIVE NOISE ANALYSIS OF NEW CENTRIFUGAL IMPELLER DESIGN

Tadej Novaković*, Jure Murovec*, Luka Čurović*, Jurij Prezelj*

*University of Ljubljana, Faculty of Mechanical Engineering, Aškerčeva 6, 1000 Ljubljana, Slovenia
e-mail: tadej.novakovic@fs.uni-lj.si

Abstract: *Household vacuum cleaners are one of the dominant noise sources among household. Over the years, there were numerous efforts to reduce the centrifugal impeller noise. Years of optimization have led to a stage, where further noise reduction is not financially feasible. However, the subjective response to noise is not influenced only by its sound levels. We can also influence the sound quality of the machine. We proposed a new impeller design featuring triangular shaped flow channels. Psychoacoustic metrics loudness, roughness, tonality and fluctuating strength were used for evaluating the new designs. A psychoacoustic annoyance model was used to evaluate the impeller designs. It was shown the triangular flow channel with logarithmic blade curvature was the best design opposed to the classical rectangular flow channel impeller. Listening tests were performed with two groups of people to further validate the new design. Each subject listened to the sound recordings of the tested suction units and rated the sounds using semantic differentials. The results of the subjective tests were compared to the calculated metrics. It was found the objective and subjective results were in good correlation thus proving the usefulness of the calculated psychoacoustics metrics for suction unit noise evaluation and validating the new centrifugal impeller design.*

Key words: noise psychoacoustics impeller suction unit

1. **INTRODUCTION**

The noise generated by vacuum cleaners is the most recognizable noise source among all household appliances. The dominant noise source in the suction unit is the centrifugal impeller. The suction unit generates noise due to its vibrating surfaces and due to pressure pulsations in the airflow. In the case of small fans and blowers such as suction units used in vacuum cleaners the aerodynamically induced noise is typically dominant [1, 2]. Aerodynamically generated noise is both tonal and broadband in nature. Discrete or narrowband noise is associated with rotational and blade passing frequencies with their respective higher harmonics. Turbulent noise is characterized by a broadband frequency spectrum [3]. Tonal noise is usually dominant and the most annoying feature of the overall noise. Reduction of tonal noise was one of the most important topics for many researchers. Several solutions have been proposed by various authors to reduce the tonal component of noise, among them irregular blade spacing, acoustically optimized fan casing, use of resonators, etc. [4, 5]. Some alternative approaches of centrifugal fan noise control have also been proposed, among them active noise control [6, 7, 8], implementation of open cell metal foam [9, 10] and a psychoacoustic approach to fan design [11, 12, 13].

Researchers reached a point where considerable reduction of the noise levels is hard to achieve or financially not feasible. However, even if the noise levels are unchanged, we can alter the subjective perception of sounds. For this reason we adopted a psychoacoustic approach at the design stage of the centrifugal impeller, [13]. The emitted noise and sound quality widely depend on the suction unit operating point which depends on the resistance of the flow passages in the assembly, such as the piping, inlet nozzle, vacuum cleaner housing and most importantly the dust collection bag. The sound quality of products is increasingly gaining in importance. One of the earliest research was done by Zwicker [14] and Fastl [15]. Since that time, psychoacoustic evaluation of products has found its way into numerous applications and industries [11, 17-19]. Sound quality estimation was traditionally based on the subjective perception of sound. However, the human response to noise tends to be highly unreliable due to the listener's affective reactions, [20]. Consequently, the best option is to perform validation measures for the calculated psychoacoustic metrics, usually by performing listening tests. Listening tests are usually performed using semantic differentials [21, 22]

There are several standardized metrics for evaluating the subjective response to noise such as Loudness *N* (DIN 45631/A1), tonality *T* (DIN 45681) and sharpness *S* (DIN 45692). In our research we also used fluctuating strength *F*, roughness *R* [23] and a joint parameter of psychoacoustic annoyance *PA* by Guoqing [24].

In this paper, we presented the psychoacoustic analysis of a newly proposed design for centrifugal fan impeller with triangular flow channel geometry with logarithmic blade curvature. Standardized psychoacoustic metrics in combination with jury based listening tests were adopted alongside with flow characteristic measurements in order to further validate the novel design.

2. EXPERIMENTAL METHODOLOGY

A set of experiments was carried out to validate the design of the new impellers (Fig.1). The impellers were 3D printed using a composite material called alumide. Three different impellers were examined; a classical geometry, an impeller with triangular flow passages and logarithmic blade curvature and an impeller with triangular flow passages and simple arc blade curvature. Flow characteristics were measured according to IEC-60312:2007 and DIN-44956(2):1981.

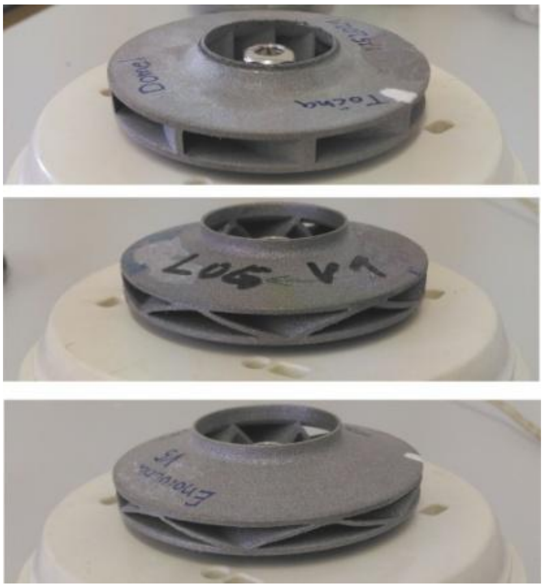

Fig. 1. Tested impellers; original A1 (top) triangular with logarithmic blade curvature F1 (center) and triangular with arc blade curvature F4 (bottom)

All three impellers were mounted on the same type of electric motor and were dynamically balanced as an assembly. The rotational speed was 32000 RPM during the whole test procedure. Every suction unit was switched on for 10 minutes prior to the measurement procedure to ensure stable operating conditions. Operational point of the suction units was varied using seven throttling orifices with opening diameters from 13 mm to 50 mm.

Sound signals were recorded with an M-AUDIO 2626 sound card, using an artificial head for binaural recordings (Fig.2). Back-electret microphone cartridges were used on the outside surface of the ear and inside the ear canal. The ear canal was represented by a rubber tube, adjusted according to the frequency response of a human ear.

We used a B&K s2032 sound signal analyzer in parallel to the binaural recordings which provided a reference value for the sound pressure level. All measurements were performed inside an anechoic chamber (Fig.3).

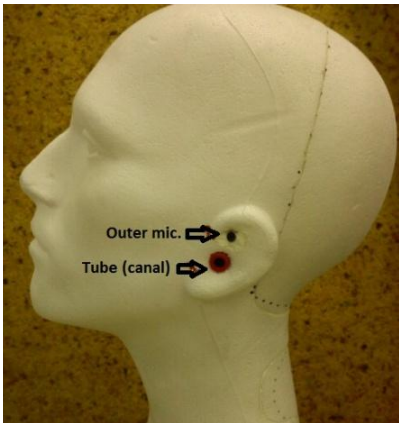

Fig. 2. Artificial head for binaural recordings

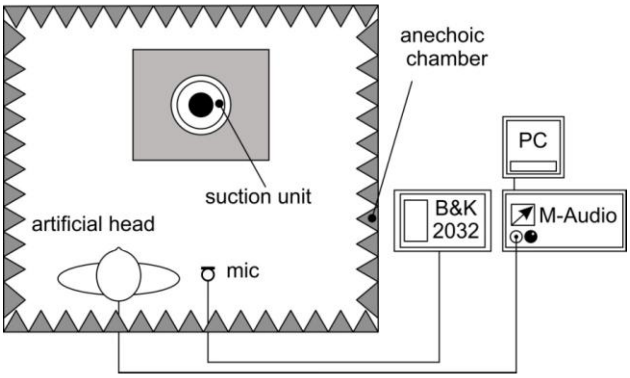

Fig. 3. Measurement setup

After the sound recording, we performed jury-based listening tests on a group of 40 students. The subjects were between 20 and 25 years old, both male and female. Each subject was given the same headset with calibrated levels and listened to the recordings. While listening, the individuals rated the sounds with a given set of semantic differentials, using a score system ranging from -3 to 3, 3 being the least annoying.

The semantic differentials used in the study are presented in Table 1 in English and Slovenian language as the tests were performed in Slovenian.

English	Slovenian
-3 – 0 – 3	-3 – 0 – 3
Weak - Powerful	Šibak - Močan
Inefficient - Efficient	Učinkovit - Neučinkovit
Broken - Functioning	Pokvarjen - Delujoč
Cheap - Prestige	Cenen - Prestižen
Disturbing - Pleasant	Moteč - Prijeten
Loud – Quiet	Glasen – Tih
Rough – Soft	Hrapav - Mehak
Sharp – Muffled	Oster - Zadušen
Fluctuating – Stable	Nihajoč - Stabilen
Tonal – Humming	Tonalni - Šumeč

Table 1. Semantic differentials used in the study

3. RESULTS AND DISCUSSION

The results are divided into two sections. At first, we discussed the psychoacoustic metrics calculated from sound signals for suction units operating at seven different flow rates. Secondly, we discussed the correlation between the calculated metrics to the subjective listening tests results.

Only if psychoacoustic metrics are calculated over a wide operating points, they reveal the true impact on the user's subjective perception of noise. The results from the calculation of psychoacoustic metrics are depicted in Fig. 4. The results for tonality showed the original impeller's optimal operating point (orifice diameter 19 mm), which is in agreement with turbo machinery noise theory. The triangular flow channel impellers show more stable psychoacoustic noise properties over the operating range. The triangular impeller with logarithmic blade curvature was the best design as seen from psychoacoustic annoyance results. The novel geometry of the flow channel cross-section also exhibited a more stable operation in the low flow rate area, which is also seen from the results for fluctuation strength.

The subjective test results are displayed in Table 2. We calculated the mean score values for each semantic differential using the scores from all 40 listeners. The sum of the scores was used to evaluate the impeller designs. The results show that the triangular impeller with logarithmic blade curvature is scored as the least annoying which is in good agreement with the calculated metrics. Additionally, the subjective tests confirmed the annoyance of noise being more stable with the change of flow rate. The stability of annoyance is of prime importance for vacuum cleaner use as the operating point changes greatly with time. The operating point is dependent on the piping, inlet nozzles, vacuum cleaner case and changes with the quantity of dust particles in the dust bag.

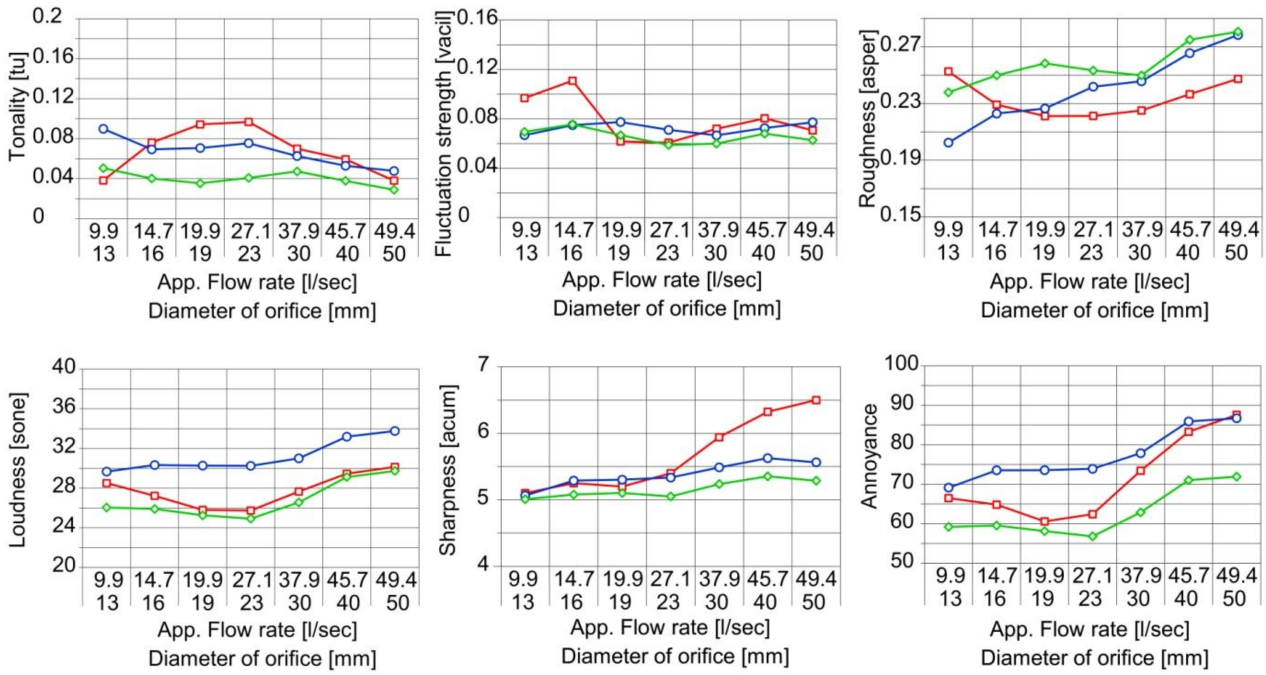

Fig. 4. Psychoacoustic metrics of impellers as a function of flow rate;

Original “A1”, Triangular ARC “F4” and Triangular LOG “F1”

Semantic		Impeller *Operating point	Original "A1" L	Original "A1" Opt	Original "A1" H	Triangular LOG "F1" L	Triangular LOG "F1" Opt	Triangular LOG "F1" H	Triangular ARC "F4" L	Triangular ARC "F4" Opt	Triangular ARC "F4" H
Weak	- 0 -	Powerful	1.0	0.0	0.6	0.7	0.1	0.5	2.3	1.3	0.8
Inefficient	- 0 -	Efficient	0.7	1.4	0.4	1.3	1.2	1.0	1.1	1.0	0.9
Broken	- 0 -	Functioning	1.4	2.2	1.1	2.1	2.1	2.1	1.2	1.0	1.6
Cheap	- 0 -	Prestige	-0.7	0.4	-0.6	0.2	0.5	0.0	-0.8	-1.4	-0.3
Disturbing	- 0 -	Pleasant	-1.2	0.8	-0.3	-0.1	0.5	0.4	-1.6	-0.8	-0.4
Loud	- 0 -	Quiet	-1.5	0.6	0.4	0.6	1.3	0.4	-2.1	-1.0	-0.4
Rough	- 0 -	Soft	-0.9	1.0	0.6	0.8	1.3	0.8	-1.3	-0.2	0.5
Sharp	- 0 -	Muffled	-1.0	1.2	0.5	0.7	0.7	1.2	-1.2	-0.5	0.1
Fluctuating	- 0 -	Stable	2.4	2.9	1.9	2.9	2.9	2.5	2.0	1.6	2.8
Whistling	- 0 -	Humming	0.5	1.0	1.0	1.9	1.3	1.4	0.6	0.3	-0.4
SUM			0.6	11.6	5.6	11.0	12.0	10.4	0.3	1.3	5.2

**L is the low flow rate condition, Opt the optimal operating point and H the free delivery point*

Table 2. Subjective test scores

A comparison of the sum of semantic differential scores to the calculated psychoacoustic annoyance is depicted in Fig. 5.

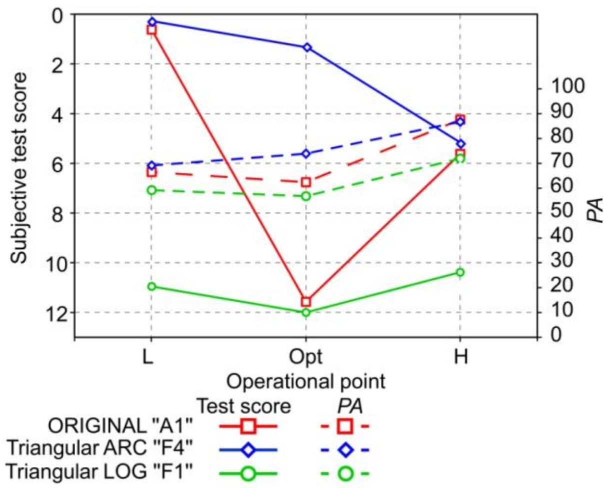

Fig. 4. Comparison of subjective test results to the calculated psychoacoustic annoyance

The subjective results are generally consistent with the calculated metrics. The psychoacoustic annoyance *PA* somewhat underestimates the annoyance of the impellers operating at low flow rates. The difference between the annoyance of A1 and F1 impellers is small at optimal operating conditions. However, when the suction units operate outside the optimal operating zone, the annoyance of the original impeller rises much higher than that of the triangular flow channel with logarithmic blade curvature impeller. At low flow rates the difference most probably arises from the unstable operation of the original impeller. The F4 impeller was the most annoying impeller in the study. The reason lies in a different blade geometry, inlet and outlet angles. Its optimal operating point was well above the other two impellers, thus making it unsuitable for the application.

4. CONCLUSIONS

The study demonstrates the impellers should be analyzed over the wide operating range as the results vary greatly with flow rate. The centrifugal fan can be designed to be less annoying to the user while its efficiency is left unchanged. Triangular shaped flow channels are proven to significantly alter the sound quality of the impeller. The results suggest the psychoacoustic metrics and the psychoacoustic annoyance model are in good correlation with the listening tests. The triangular flow channel impeller with logarithmic blade curvature has shown surpassing sound quality in a wide operating region which is of great importance for the application in vacuum cleaner suction units.

4. REFERENCES

[1] W. H. Jeon Overview of numerical analysis of fan noise, Fan noise 2003, International Symposium Senlis, 23–25 September (2003), pp. 1–8.

[2] J. Prezelj, M. Čudina Quantification of aerodynamically induced noise and vibration-induced noise in a suction unit, Proceedings of the Institution of Mechanical

Engineers – Part C, Journal of Mechanical Engineering Science, Mar. (2011), 225 (3), pp. 617–624.

[3] S. Velarde-Suárez, R. Ballesteros-Tajadura, J. P. Hurtado-Cruz , C. Santolaria-Morros Experimental Determination of the Tonal Noise Sources in a Centrifugal Fan, J Sound Vib, (2006), 295, 781–796.

[4] W. Neise Noise reduction in centrifugal fans: A literature survey, J Sound Vib (1976) 45(3), 375–403.

[5] W. Neise Review of noise reduction methods for centrifugal fans, Journal of Engineering for Industry, (1982), 104/151, pp. 151–161.

[6] J. Prezelj, M. Čudina A Secondary Source Configuration for Control of a Ventilation Fan Noise in Ducts, Strojniški vestnik – Journal of Mechanical Engineering, 57 (6), (2011), pp. 468–476.

[7] T. B. Patil, K. R. Borolek, S. B. Sanap Noise reduction of centrifugal fan by use of resonator and active noise control technique, IJME, 2 (4) (2003), pp. 9–20.

[8] J. Prezelj, M. Čudina Dipole in orthogonal direction as a secondary source for active noise control in ducts, Acta Acustica united with Acustica, 93(1) (2007), pp. 63–73.

[9] C. Xu, Y. Mao. Passive control of centrifugal fan noise by employing open-cell metal foam, Applied Acoustics, 103 (2016), pp. 10–19.

[10] G. Benedik, et.al. Flow Characteristics of Bladeless Impeller Made of Open Cell Porous Material, Strojniški vestnik – Journal of Mechanical Engineering, 56 (2010), pp. 464–476.

[11] G. Minorakava, T. Yamaguchi Study on evaluation method of tonal noise for small fan, ICSV22, Florence, Italy, 12 – 16 July, (2015), pp. 1–8.

[12] M. Schneider, C. Feldmann Psychoacoustic evaluation of fan noise, Fan 2015, Lyon, France, 15–17 April (2015), pp. 1–12.

[13] J. Prezelj and T. Novaković, 2018, Centrifugal fan with inclined blades for vacuum cleaner motor. Applied Acoustics. 2018. Vol. 140, p. 13-23. DOI 10.1016/j.apacoust.2018.05.010. Elsevier BV

[14] E. Zwicker: Procedure for calculating loudness of temporally variable sounds. Journal of the acoustical society of America 62, 675-682 (1978).

[15] H. Fastl Hearing sensations and noise quality evaluation. Journal of the acoustical society of America 87(S1), S134-S134 (1990).

[16] M. Schneider, C. Feldmann Psychoacoustic evaluation of fan noise. Fan 2015. Lyon. France. 15–17 April (2015). pp. 1–12.

[17] R. Jurc, O. Jiricek Sound quality evaluation of fan computer. Fan Noise 2003. International Symposium Senlis. 23–25 September (2003).

[18] P. Lipar, et. al. Psychoacoustic approach used for developing the model of sound pleasantness of vacuum cleaners and suction units. based on objective and subjective analysis. 5th Congress of Alps-Adria Acoustics Association. 12–14 September (2012). Petrčane. Croatia. pp. psy02/1–psy02/8.

[19] V. Hodor, et.al. CFD predictions with LES for psycho acoustic relevance in ventilation. Energy Procedia. 85 (2016). pp. 252–259.

[20] H. Fastl The psychoacoustics of sound-quality evaluation. Acustica-Acta acustica, Vol. 83 1997.

[21] D. Dal Palù, et.al. The use of semantic differential scales in listening tests: A comparison between context and laboratory test conditions for the rolling sounds of office chairs. Applied Acoustics. 2017. Vol. 127, p. 270-283. DOI 10.1016/j.apacoust.2017.06.016. Elsevier BV

[22] P. Susini, et. al. Instruction’s effect on semantic scale ratings of interior car sounds. Applied Acoustics. 2009. Vol. 70, no. 3, p. 389-403. DOI 10.1016/j.apacoust.2008.06.008. Elsevier BV

[23] Fastl, Zwicker E. Psychoacoustics – Facts and Models, page (325), third edition, Springer-Verlag Berlin, Heidelberg (2007).

[24] Guoqing D. An improved psychoacoustic annoyance model based on tonal noises, Internoise (2016), 21–24 August, Hamburg, Germany.

NVH SIGNAL ANALYSIS VIA PATTERN RECOGNITION ANNs: AUTOMOTIVE BRAKE CREEP GROAN AS CASE STUDY

Manuel Pürscher, Stefan Schöpf, Peter Fischer

Institute of Automotive Engineering (office.ftg@tugraz.at), Graz University of Technology, Austria

Abstract: *Automotive Noise, Vibration and Harshness (NVH) issues often cause costly customer complaints. In particular, NVH of the brake system is critical for subjective ratings of vehicle safety and passenger comfort. Recently, especially a stick-slip induced low-frequency phenomenon, the so-called brake creep groan, has become increasingly relevant. In order to avoid this brake NVH problem within upcoming automobile fleets, simulative and/or experimental parameter studies throughout all industrial brake development stages are indispensable. To this end, reasonable and efficient data analysis methods are necessary too. This kind of signal assessment challenge is addressed here by means of a method which applies techniques of Artificial Intelligence (AI) or Artificial Neural Networks (ANNs) respectively. The basis for this is a large number of generically synthesised brake component acceleration spectra which represents data in the frequency domain with and without creep groan. This generic data is used to create specifically elaborated pattern recognition ANNs. Eventually, the proposed approach provides an integrated framework of conditioned ANNs which is supposed to detect and separate non-linear signatures of different brake creep groan vibrations. In order to examine the method's practical limitations, additional data sets of synthetic accelerations including generic noise have been considered, and moreover, gauged accelerations concerning two test rig setups have been taken into account. Although the devised creep groan analysis approach is designated for automotive brake development workflows, its principle could be appropriate for similar NVH problems or signal analysis tasks in other engineering fields alike.*

Key words: artificial neural networks, brake vibrations, creep groan, pattern recognition, signal analysis, stick-slip

1. INTRODUCTION

1.1. Automotive Brake NVH

For some years now, the automotive industry has been facing immensely increasing requirements for technical, economical, environmental and people-oriented aspects for a manifold range of ever faster developed vehicle types. This also counts for automotive Noise, Vibration and Harshness (NVH) issues which are potentially misconstrued by drivers and passengers as serious quality deficits, or even as system malfunctions. Hence, automotive NVH requirements involve inherently safety-critical friction brake systems in particular.

Beyond aspects related to car occupants exclusively, offer sound-emitting brakes annoyance potential for external individuals too. Akay [1] mentioned a survey from the 1930s which stated brake noise as a top-ten urban noise pollution problem of New York City. Nowadays, in case of up-to-date (semi-) automated vehicle driving modes such as *Parking-Pilot* or *Garage-Pilot*, an externally affected person could even be the actual "driver", see Fig. 1 and [2] respectively.

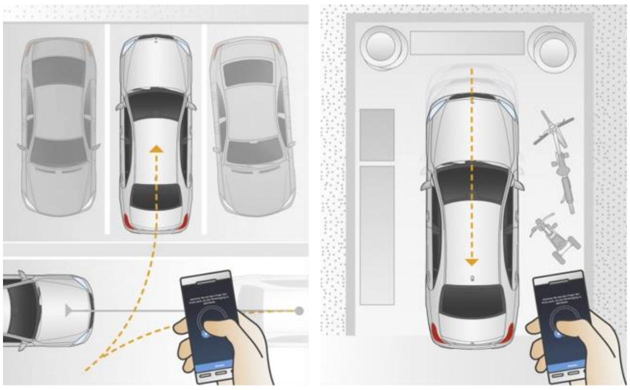

Fig. 1. *Parking-Pilot* / *Garage-Pilot* enable remote operability by external "driver", adapted from [2].

However, brake NVH affected the subjective perception of a car's and/or brand's comfort and reliability long before advanced technologies such as those just referenced entered the market. In 1991, Crolla and Lang [3] presented research data concerning reported brake faults after the market launch of five different European passenger car series. For each up to 1-year-old type, brake noise was indicated with a dominant quantity. In the early 2000s, Akay [1] referenced to industry studies which assessed annual costs of brake NVH warranty claims on the North American market around one billion dollar. According to a paper of Abendroth and Wernitz [4] from the same period, leading automotive friction material companies spend almost 50 % of their engineering budgets directly or indirectly on measures against brake NVH problems. A few years later, Bittner [5] mentioned a comparable cost component for the automotive brake system supplier as a whole. A *J.D. Power Studies* North American market survey from 2014 [6], which rested upon more than 40.000 responses by original owners of up to 3-year-old automobiles, yielded two different brake NVH problems within the top-five complaints. A Japanese market study from 2017 [7] reported NVH of friction brakes as a major inconvenience for around 2 % of roughly 19.000 involved purchasers.

Thus, vibro-acoustic friction brake emissions entail an undesirable circumstance of high priority. One of these, the so-called brake creep groan phenomenon, is in focus within this article. In the typical automotive (disk) brake NVH classification chart in Fig. 2, which is based on an adapted literature condensation including [5] by Huemer-Kals [8], one can imagine via the sensibility examples in [9] that self-excited creep groan is situated in the tactile/audible frequency range of human perception.

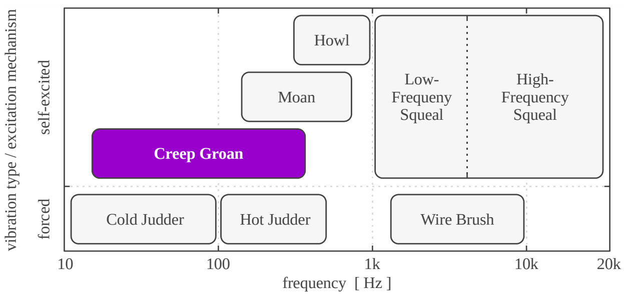

Fig. 2. Typical classification of common (disk) brake NVH phenomena, adapted from [8].

A comparable verbalised classification can be found in [10]. Although further fragmentation in terms of brake NVH is possible, e.g. 10 spectral and/or phenomenological subdivisions in [9], or even 15 terminologies in [1], the creep groan issue remains one of the most salient ones.

According to the typical distribution of warranty claims, which has been outlined graphically by Barton and Fieldhouse [10] based on the report of a high performance vehicle manufacturer, it owns the third largest share. Independent of that exemplary claim distribution, creep groan has a steadily increasing relevance for all commonly installed brake types and chassis designs within all vehicle segments due to several reasons such as described hereafter.

1.2. Topicality and Phenomenology of Creep Groan

The main reasons for a growing attention towards the creep groan issue are an increased customer expectation in conjunction with a reduced vibro-acoustic background sound level of advanced engines and powertrains. Therefore, creep groan is problematic for high-priced and/or electrified passenger cars with disk brake systems in particular. Nevertheless, it is also present for drum brakes and/or commercial vehicles which is pointed out in a publication by Karabay et al. [11]. Their work includes market surveys, value and failure analyses as well as troubleshooting measures concerning a specific light truck.

Various creep groan phenomena of all systems have comparable origination situations with associated characteristic spans of certain operational parameters in common. Accordingly, the brake pressure is moderate and a very slow vehicle velocity near standstill is present, whereby the occurrence of creep groan is favoured from cold and/or wet environments in particular. Since the mentioned simultaneity of both operational parameters is in some (semi-) automated driving modes a potentially mandatory situation for safety reasons, e.g. for remote controlled parking or during activated stop-and-go driver assistance features, creep groan tends to become progressively more relevant within automobile fleets of the next decade. However, concerning previous vehicles with standard automatic gearboxes it has been a known, but often secondarily treated brake NVH problem.

Oscillation characteristics of creep groan phenomena with mechanical and tribological component influences have not only been outlined in former works of the authors, e.g. [12, 13, 14], but also in specific book chapters and in studies of other research groups, e.g. [9, 10, 11]. Accordingly, creep groan is related to a physically unstable triggering mechanism which is in tribology fields described as stick-slip effect. This self-excited process at the main friction interfaces leads to periodic non-linear low-frequency brake and chassis vibrations with large component deflections. Accompanying short-term structure-borne noise disturbances appear inside and outside the car with relevant contents up to 500 Hz.

1.3. AI and ANNs for Pattern Recognition

More and more companies have started to see real-life benefits of Artificial Intelligence (AI) implementations. Early adopters of AI are mainly from sectors with a data-driven background such as the financial service industry or the automotive area, e.g. concerning stock trading or in terms of low-frequency interior noise evaluation [15]. Beyond such initial adopters, is nowadays a wide range of strongly digitalised business sectors just like complex technology fields supported by assorted varieties of AI, as outlined by Bughin et al. [16].

A typical application of AI is machine learning with pattern recognition as one of its major branches. Rosenfeld and Wechsler [17] summarised historical perspectives and expected future directions of pattern recognition within their article almost 20 years ago. They described pattern recognition as one of the most important functionalities for intelligent behaviour which is displayed in biological and artificial systems alike. A prominent biological example is the detection of foreign intruders in an organic body by specific cellular antibodies in order to ensure the host's survival. For man-made tasks, a prepared AI seeks to apply approximating functions with the lowest possible probabilities of misallocations for the evaluated data set. Thus, the pattern recognition problem is akin to the more general issue of statistical regression. Typical artificial use cases are optical character readers to comprehend and separate written letters or text modules, biometrical algorithms to identify persons by means of fingerprints, iris, face or speech, and furthermore, medical analysers to find anomalies in heart electrocardiograms. Liu et al. [18] have listed further application fields such as linguistics, meteorology like exemplarily shown in [19], philosophy, psychology, robotics, or even very specialised areas, e.g. ethology. They traced the latest progresses especially to recent technology trends such as social computing.

However, modern mathematical/empirical functions for pattern recognition rest upon Artificial Neural Networks (ANNs). According to [15, 17, 19, 20], two coherent data sets are necessary in order to obtain the requested functionalities. For so-called supervised learning, these are input signals (variables) which are available in the functions' development procedure as well as in the later application, and furthermore, output targets (variables) which are usually known in the set-up process exclusively.

1.4. Problem Definition / Aim of Study

Creep groan phenomena are challenging for automotive NVH engineers. In view of this circumstance, innovative investigation methods and industrially implementable routines are necessary. These should help to devise and optimise efficient remedial technical measures in upcoming vehicle development projects. For this purpose, the authors have already published concepts of new experimental and/or simulative methods, e.g. [12, 13, 14].

It is only natural that comprehensive creep groan investigations, which lead to a vast amount of data, require reasonable and efficient data assessment tools. This kind of signal analysis task is addressed here via an innovative creep groan classification method based on pattern recognition ANNs.

1.5. Article Structure

Representative brake component acceleration signals of creep groan appearances, which were recorded with two different setups in similar operational parameter studies at corner test rig level, are discussed in section 2. The idea behind the simplification of characteristic creep groan signatures in order to synthesise a high amount of more or less realistic acceleration frequency spectra generically is presented in chapter 3. These specifically synthesised data sets are used to develop differently elaborated pattern recognition ANNs which are content of section 4. Then, a data set of synthetic spectra including noise is processed to check the well-considered framework of conditioned ANNs. In addition, sets based on measured acceleration data get involved to assess the framework's capabilities in a more realistic way. Both verification strategies with previously unseen spectra are discussed in section 5. Summary and conclusion of the new application method are drawn in chapter 6. Eventually, prospects on feasible refinements and further research steps are content of section 7.

2. REPRESENTATIVE CREEP GROAN SIGNATURES

2.1. Corner Test Rig Experiments with Two Setups

Typical signatures of creep groan vibrations are discussed here via brake component acceleration signals. The accelerations were gauged at the disk brake callipers of two dissimilar automobile front corner setups. Design models of these excluding the wheels are shown true to scale together in Fig. 3 and [14] respectively.

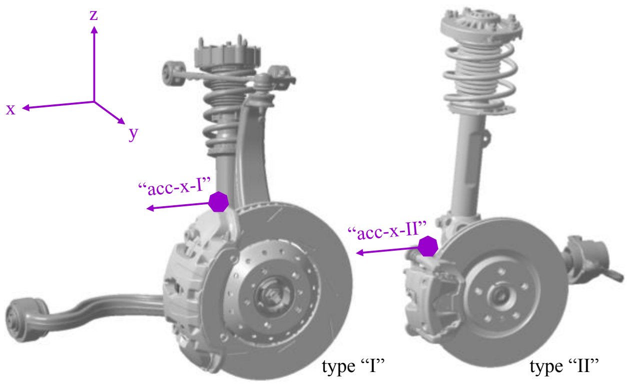

Fig. 3. Calliper accelerometer positions "acc-x-I" and "acc-x-II" on front corner systems type "I" and type "II", adapted from [14].

The design on the left, named type "I", belongs to a sporty grand tourer, whereas type "II" on the right illustration is implemented in a compact van. As one can see, type "I" follows the double wishbone suspension principle with fixed calliper brake module. Type "II" on the right is built with a MacPherson suspension assembly including floating calliper brake construction. Both setups had, among other sensors, a miniature triaxial accelerometer glued to the upper surface of the calliper. Nevertheless, only the signals according to vehicle x-direction, named "acc-x-I" and "acc-x-II", are actually of relevance.

Creep groan of both setups was investigated at a drum driven suspension and brake test rig. It is pictured with an exemplary front corner setup of the left vehicle side in Fig. 4 and [14] respectively.

Fig. 4. Drum driven suspension and brake test rig for creep groan parameter matrix experiments, adapted from [14].

Information about the test rig's sophisticated structure with adaptable functionalities as well as its interface constructions for the mounting of automobile corners, and furthermore, the test rig's capabilities regarding main operational parameters and basic environmental conditions under control can be found in [12]. The previous work also describes an innovative systematic creep groan investigation approach with its well-defined sensitivity experiments in detail. This test matrix procedure leads to rather extensive acceleration data sets. Basically, these data sets allow comparisons of defined combinations of brake pressure and drum (vehicle) velocity for different mechanical and/or tribological component variants.

The two mentioned operational parameters were gauged and adjusted via the test rig's control management with a given rate of 100 Hz, whereas "acc-x-I" and "acc-x-II" have been recorded separately with 10 kHz.

2.2. Calliper Acceleration Signal Patterns

In the following, a diagram with an acceleration recording including its computed Fast-Fourier-Transform (FFT) is presented for each of three distinctive brake creep groan vibrations of type "I" and type "II" respectively. The FFT with an upper calculation limit adjusted to 2 kHz applies a *Hanning* window of 50 % overlap to an 1 s time segment which contains the depicted short segment of 0.18 s in each case. This results in an appropriate frequency resolution of exactly 1 Hz up to the practically chosen boundary of 1 kHz.

Detailed explanations of creep groan phenomena with extensive interpretations of similar self-measured calliper accelerations have already been documented in [12, 13, 14]. Apart from that, Akay [1] showed and explained comparable time plots and frequency spectra related to other friction-induced vibration mechanisms.

The two diagrams without creep groan show comparable acceleration patterns, see Fig. 5 and Fig. 6. It makes no difference that dissimilar setups were tested regarding opposed oriented drum rotations with velocities unequal by the factor 4. Thus, both comparable time signals contain low fluctuations which are just related to small corner setup oscillations as well as subordinate test rig vibrations and/or unproblematic measurement noise. A FFT leads to spectra with flat broadband bumps and relatively low and narrow decibel (dB) peaks.

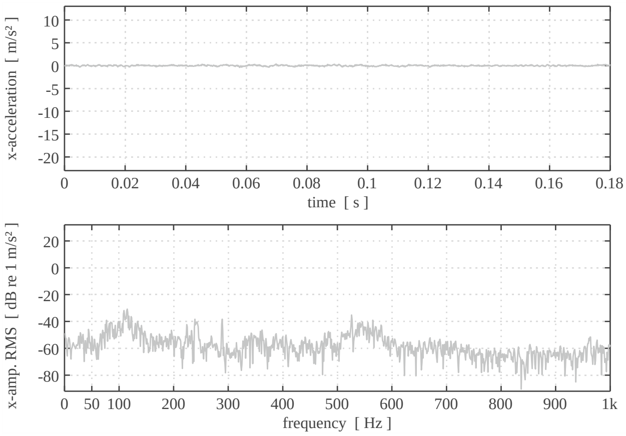

Fig. 5. Acceleration "acc-x-I" without creep groan, 4 bar / 0.04 km/h.

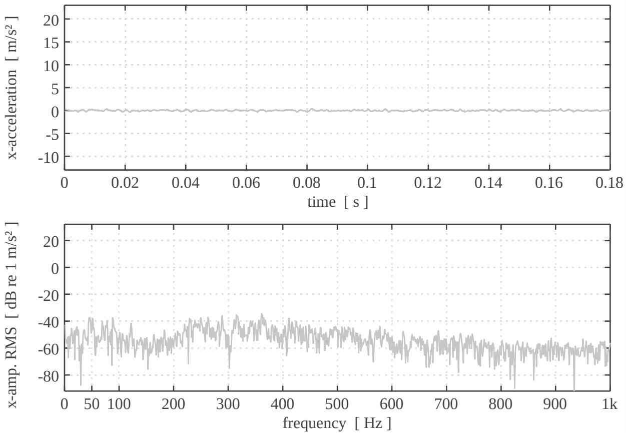

Fig. 6. Acceleration "acc-x-II" without creep groan, 4 bar / -0.16 km/h.

The two typical examples of creep groan within the deeper frequency area, depicted in Fig. 7 and Fig. 8, reveal strong accelerations with more or less pronounced non-linear characteristics.

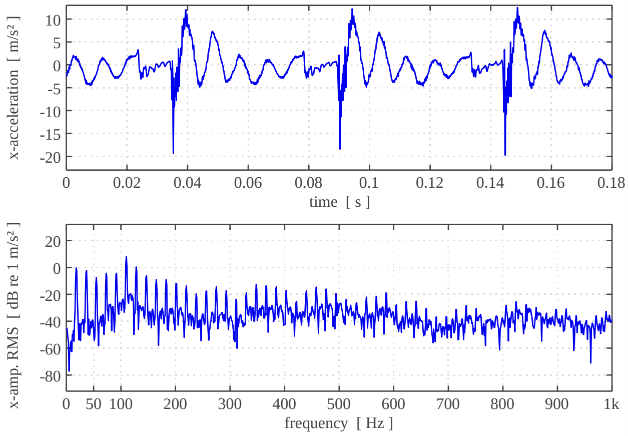

Fig. 7. Acceleration "acc-x-I" with 18 Hz creep groan, 10 bar / 0.16 km/h.

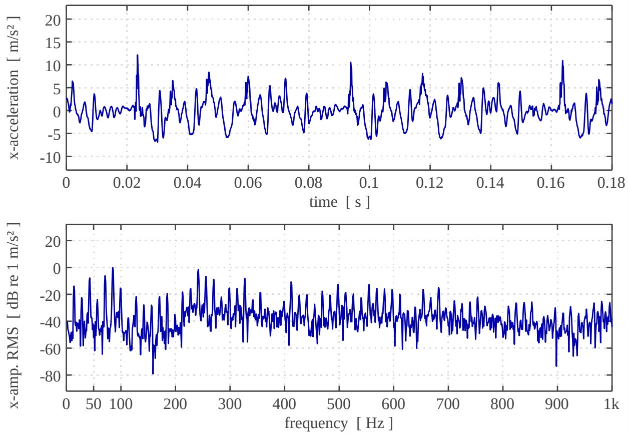

Fig. 8. Acceleration "acc-x-II" with 14 Hz creep groan, 10 bar / -0.04 km/h.

Moreover, the two calliper x-accelerations concerning creep groan vibrations within the upper frequency area, shown in Fig. 9 and Fig. 10, also represent distinctive non-linear signatures.

All four acceleration time data plots have a relatively steep and rather high amplitude (amp.) peak which is followed by some less intense fluctuations or damped natural oscillations respectively. This striking signal pattern repeats accurately with a specific interval according to the dominant stick-slip transition. The tribological switch-over appears in the shown instances with 18 Hz, 14 Hz, 107 Hz and 86 Hz respectively. If applying a FFT on such kind of periodic non-linear signal, prominent Root Mean Square (RMS) dB peaks of usually different heights will result at multiple intervals of the basic frequency. This can be seen in the spectra of all four creep groan phenomena. Therefore, the characteristic spectral behaviour is found to be an appropriate criterion within the introduced AI approach. Accordingly, the observable regular patterns of the spectra are of relevance.

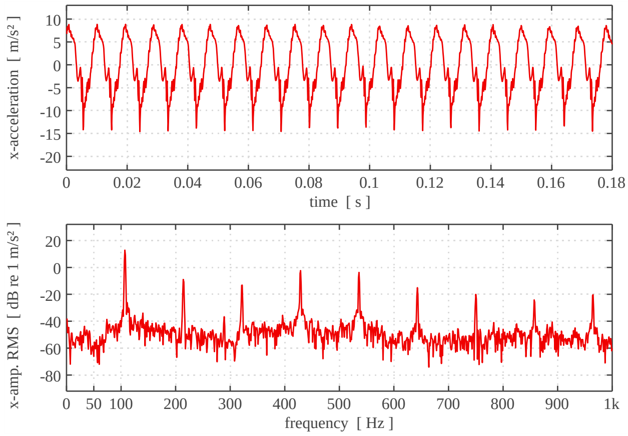

Fig. 9. Acceleration "acc-x-I" with 107 Hz creep groan, 7 bar / 0.08 km/h.

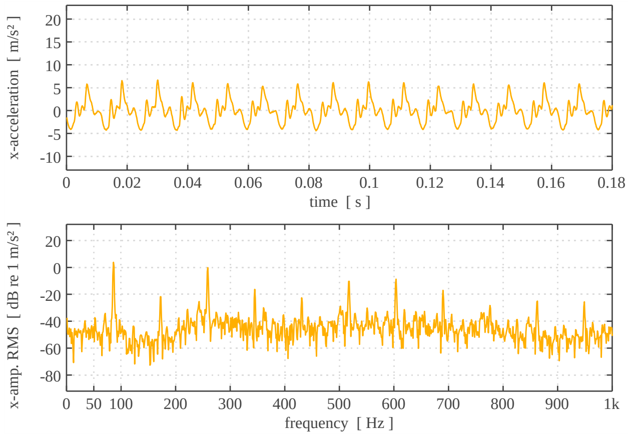

Fig. 10. Acceleration "acc-x-II" with 86 Hz creep groan, 7 bar / -0.08 km/h.

All shown instances of "acc-x-I" and "acc-x-II" refer to differently combined operational parameters which were representatively chosen out of the existing test matrices. Further comparable experimental and/or simulative creep groan signatures regarding both setups can be found in [12, 13, 14]. The related master thesis by Huemer-Kals [8] contains additional experimental examples.

2.3. Operational Parameter Sensitivity Studies

Although friction at micro- and macroscopic scale with respect to vibro-acoustic effects has been intensively studied by many authors, e.g. reviewed in [1], there are open questions on specific friction-induced mechanisms in various engineering fields. To a certain extent, this applies to the non-linear behaviour of creep groan vibrations. However, the systematic investigation approach published in [12] enables already a better detection of other non-linear influences apart from the evident tribological interface, e.g. those of axle elastomer bushings. Therefore, changing subsystem oscillations with specific component participations are also identifiable.

The non-linear influences due to operational parameter variations can be recognised in the form of zonally switching basic creep groan frequencies in the so-called Creep Groan Map (CGM). It was introduced in [12] with 190 operational parameter combinations of brake pressure and drum velocity. An adapted CGM with merely 49 test matrix entries and reduced complementary information is illustrated in Fig. 11 for type "I" and in Fig. 12 for type "II" respectively.

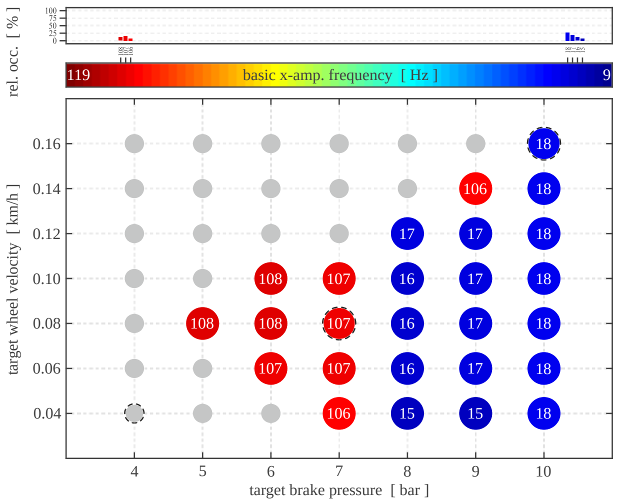

Fig. 11. CGM of type "I" with 49 test matrix entries of brake pressure / forward drum velocity.

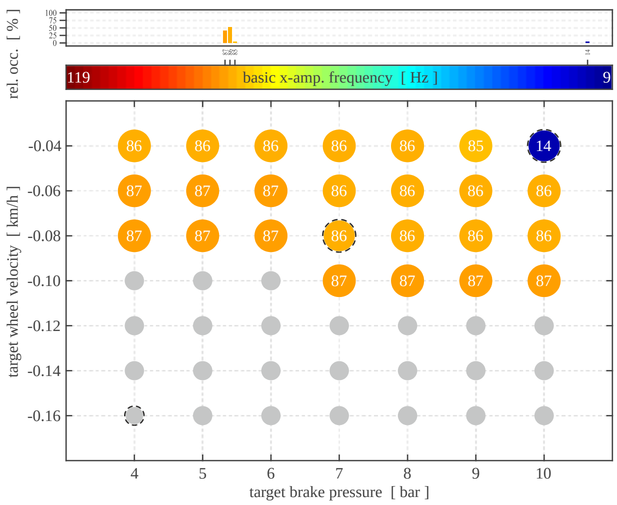

Fig. 12. CGM of type "II" with 49 test matrix entries of brake pressure / reverse drum velocity.

Both evaluations are based on comparable operational parameter spans with identical brake pressures regarding opposed drum rotations. As one can see, each chart reveals two different frequency areas for the basic stick-slip interval which is indicated via a certain colour and the corresponding numeric frequency value. Moreover, a relative occurrence (rel. occ.) of each enabled basic frequency is reported. Since comparable frequency areas have evinced for all automobile front corner setups tested so far, the adjusted frequency window between 9 Hz and 119 Hz results just from the authors' experience. A presence of two prominent stick-slip frequency areas in each CGM becomes especially clear, if brake pressures higher than 10 bar are considered, compare to [12, 13]. Nevertheless, the shown test matrices contain all relevant subsystem interactions which are potentially activated during creep groan appearances. Note that the previously discussed x-acceleration examples are bordered with dotted circles.

In order to derive a CGM, the evaluation algorithm presented in [12] is applied. It rests upon spectral analyses with well-considered adaptable queries. Thereby, the method is fairly well able to distinguish x-accelerations with creep groan vibrations from those without. As depicted before, the deterministic algorithm is also intended to categorise the basic frequency of creep groan. Because only if it is determined, the brake NVH issue is treatable holistically. Of course, also super-harmonic spectral contents of the friction-induced excitation are examinable via the algorithm. In prospective development steps, source-drain properties towards a passenger's perception, according to a vibro-acoustic chain of effects such as pictured by Marschner et al. [9], might be calculated and improved. Independent of that vision, an evaluation of the exact frequency contents supports the interpretation of design benchmarks and/or material studies and gives feedback on potentially switching subsystem interactions from the upper to the deeper frequency area or vice versa.

Nevertheless, reliability and accuracy of the currently applied deterministic evaluation method suffer, if fuzzy acceleration time signals such as depicted in Fig. 8 appear, or even if the adaptable queries are improperly chosen. The proposed AI approach aims to deliver step-by-step advancements in order to overcome these present deficiencies. Whether and how this is realisable is under investigation within this study.

3. GENERIC SYNTHESIS OF ACCELERATION DATA SETS

3.1. Functionality Set-Up: Input Signals / Output Targets

Besides the capabilities of the *Pattern Recognition app* within the *ANN Toolbox* provided by *MATLAB R2016a*, the presented approach's principle rests upon comprehensive data sets of different acceleration frequency spectra in particular. These are relevant to generate an integrated framework of 112 autarchic ANNs (see also chapter 4.2.) in total.

Since not enough measurements regarding possible creep groan manifestations (between 9 Hz and 119 Hz) were available in order to do so, an acceleration generation formalism has been designed. It evolved from subjective inspections of hundreds of frequency spectra with and without creep groan vibrations. Additionally, it has similarities to the evaluation algorithm proposed in [12]. As hinted, the generic formalism enables a reproducible creation of extensive data sets of synthetic x-accelerations or input spectra respectively. To this end, typical creep groan signatures are simplified via 10 adjustable spectral attributes which are visualised in Fig. 13.

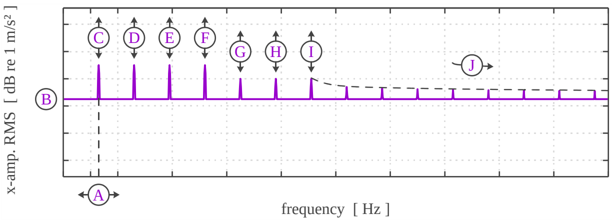

Fig. 13. Attributes of the generic spectra.

By means of these well-considered attributes, 112 separate data sets of input signals have been processed. Of course, related output targets were defined alike. It should be noted that the basic concept in terms of synthesised data sets for the elaboration of pattern recognition ANNs has already been followed in the broad area of automotive NVH, e.g. by Lee and Chae [15].

The so-called “primary-ANN” (see also chapter 4.4.) deals with the basic frequency categorisation. It refers to a reproducible data set of 242.757 input spectra. The 111 so-called “secondary-ANNs” (see also chapter 4.5.), which are meant for creep groan judgement, are based on 82.944 reproducible input spectra per relevant basic creep groan frequency. All synthetic x-acceleration signals have a frequency resolution of 1 Hz up to the useful boundary of 1 kHz. The demanded acceleration amplitude peaks are achieved via addition of super-harmonic in-phase sine oscillations below a given limit of 1 kHz. To this end, a time domain resolution of 10 kHz is provided and the basic frequency of the fundamental sine wave is varied stepwise from 9 Hz to 119 Hz. The superimposition is followed by a FFT similar as described in the previous chapter. Thus, all equally spaced peaks are realistically supported from adjacent frequencies. An adaptable bandwidth of white noise as well as an amplitude attenuation, which diminishes super-harmonic orders above an initial attenuation frequency equal to the seventh acceleration amplitude peak with 1 dB/octave, are both implemented in the frequency domain.

The values for each of the 10 spectral attributes used to compile the 242.757 unique input spectra for the only “primary-ANN” can be extracted out of Table 1. Note that eight of these attributes are actually varied.

		attributes									
	index	A	B	C	D	E	F	G	H	I	J
	variable [unit]	basic frequency [Hz]	white noise [→]	x-amp. RMS [dB re 1 m/s²]							x-amp. RMS attenuation [dB/octave]
values	minimum	9	-35 (no)	-30	-30	-30	-30	-30	-30	-30	-1
values	increment	1	–	20	20	20	20	10	10	10	–
values	maximum	119	–	10	10	10	10	-10	-10	-10	–
		input spectra (1 Hz ... 1 kHz)									
options [#]	per attribute	111	1	3	3	3	3	3	3	3	1
options [#]	cumulative - all	111	111	333	999	2.997	8.991	26.973	80.919	242.757	242.757
options [#]	… - frequency	1	1	3	9	27	81	243	729	2.187	2.187

Table 1. Attributes of 242.757 generic input spectra to obtain one “primary-ANN” for basic frequency categorisation.

As one can read on the right side of the lowest table row, 2.187 spectrum options per creep groan frequency are available. This quantity is broken down in the listed combinatorial calculation. In the following, four examples illustrate the considered amplitude range limits. Fig. 14 shows the two borderline cases of all 9 Hz input spectra and Fig. 15 those of 119 Hz respectively. Even though both instances at the lower range would not be rated as creep groan vibrations in the end, it has no relevance for the determination of a basic frequency which is the exclusive task of the “primary-ANN”.

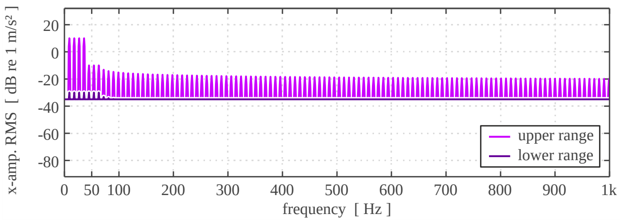

Fig. 14. Amplitude range limits of 2.187 generic input spectra to describe 9 Hz basic frequency.

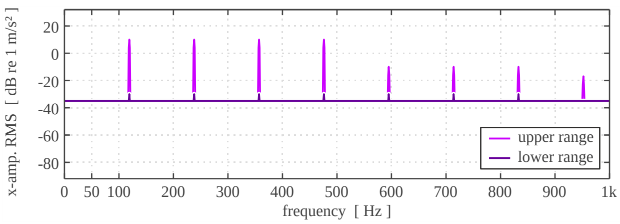

Fig. 15. Amplitude range limits of 2.187 generic input spectra to describe 119 Hz basic frequency.

The values for each of the 10 attributes used to compile the 9.206.784 singularly combined input spectra for the 111 alternative “secondary-ANNs” can be seen in Table 2.

Once again, merely eight of these spectral attributes are actually varied.

		attributes									
	index	A	B	C	D	E	F	G	H	I	J
	variable [unit]	basic frequency [Hz]	white noise [→]	x-amp. RMS [dB re 1 m/s²]							x-amp. RMS attenuation [dB/octave]
values	minimum	9	-35 (no)	-26	-26	-26	-26	-27	-27	-27	-1
	increment	1	–	–	–	–	–	–	–	–	–
	level I	–	–	-21	-21	-21	-21	-22	-22	-22	–
	level II	–	–	-19	-19	-19	-19	-18	-18	-18	–
	level III	–	–	-14	-14	-14	-14	–	–	–	–
	level IV	–	–	-4	-4	-4	-4	–	–	–	–
	maximum	119	–	6	6	6	6	-13	-13	-13	–
		input spectra (1 Hz ... 1 kHz)									
options [#]	per attribute	111	1	6	6	6	6	4	4	4	1
	cumulative - all	111	111	666	3.996	23.976	143.856	575.424	2.301.696	9.206.784	9.206.784
	… - frequency	1	1	6	36	216	1.296	5.184	20.736	82.944	82.944

Table 2. Attributes of 9.206.784 generic input spectra to obtain 111 autarchic "secondary-ANNs" for creep groan judgement.

The attribute values are different compared to those of Table 1. On one hand, tighter range limits for the x-acceleration amplitude peaks are taken into account here in order to create more realistic input spectra. On the other hand, the relevant attribute values have smaller increments in unequal intervals which results from an intended relation to the original evaluation algorithm introduced in [12]. However, this input signal mixture is supposed to provide "secondary-ANNs" which are able to recognise the requested regularities of creep groan vibrations within typical acceleration spectra.

Basically, at least one consistent output target formulation is necessary if an ANN for pattern recognition is elaborated. In case of the "primary-ANN", each equivalent output target contains the prescribed information about the associated spectrum's embedded basic frequency. This is realised via an 111 times 242.757 data matrix containing zeroes or ones, whereby a correct column entry is indicated by means of the value one. By contrast, the 111 output target data matrices used to define the "secondary-ANNs" have the sizes 2 times 82.944 respectively. The unique value one in a first column entry implies absence of creep groan for the related input spectrum. The single value one in the second column entry indicates contrary terms. Eventually, creep groan is prescribed in each of the 111 equivalent set-up data clusters for approximately 55 % of the input signals which is not a mandatory share.

3.2. Functionality Check: Unseen Noisy Verification Signals

In order to examine operability and capability of the designed framework with 112 self-sufficient ANNs at a later stage, also a generic verification data set is designed. Its mixture made of 909.312 unique input signals is gathered in Table 3.

		attributes									
	index	A	B	C	D	E	F	G	H	I	J
	variable [unit]	basic frequency [Hz]	white noise [→]	x-amp. RMS [dB re 1 m/s²]							x-amp. RMS attenuation [dB/octave]
values	minimum	9	-35 (no)	-25	-25	-25	-25	-25	-25	-25	-1
	increment	1	low medium high	10	10	10	10	10	10	10	–
	maximum	119		5	5	5	5	-15	-15	-15	–
		evaluation spectra (1 Hz ... 1 kHz)									
options [#]	per attribute	111	4	4	4	4	4	2	2	2	1
	cumulative - all	111	444	1.776	7.104	28.416	113.664	227.328	454.656	909.312	909.312
	… - frequency	1	4	16	64	256	1.024	2.048	4.096	8.192	8.192

Table 3. Attributes of 909.312 generic verification spectra including different white noise bandwidths to check framework of 112 ANNs.

The chosen attribute values are meant to be different compared to those of Table 1 and Table 2. Even though this applies neither to the described basic frequencies of the first column nor to the considered amplitude attenuation of the last column, there are still previously unseen verification spectra provided for the purpose of AI examination. This is even more true in view of three optional bandwidths of white noise superimposed to each of the 227.328 unique synthetic spectra, see Fig. 16.

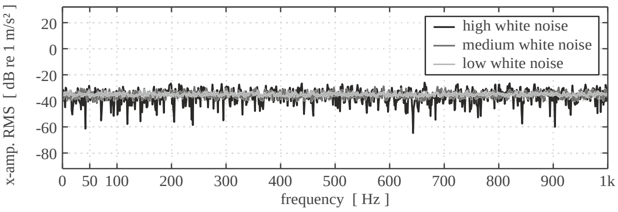

Fig. 16. Optional white noise variants superimposed to 227.328 generic verification spectra.

Each reproducible white noise spectrum is adjusted up to a limit of 1 kHz in order to reach a summarised overall RMS of 25 dB re 1 m/s² respectively. This also counts for the initial option without noise at all. Independent of that, the procedure to obtain the output targets concerning the more or less noisy verification signals is the same as discussed in the prior section. Note that output target values related to Table 3 are only necessary to examine the predictions of the proposed AI approach.

4. ELABORATION OF PATTERN RECOGNITION ANNs

4.1. Basic Model and Practical Implementation

As explained in the fundamental book of Hertz et al. [20], the basic scheme of a multilayer feed-forward pattern recognition ANN commonly contains a passive input layer which is followed by a number of active hidden layers and a mostly active output layer in the end, see model in Fig. 17 and literature sources [15, 19, 20].

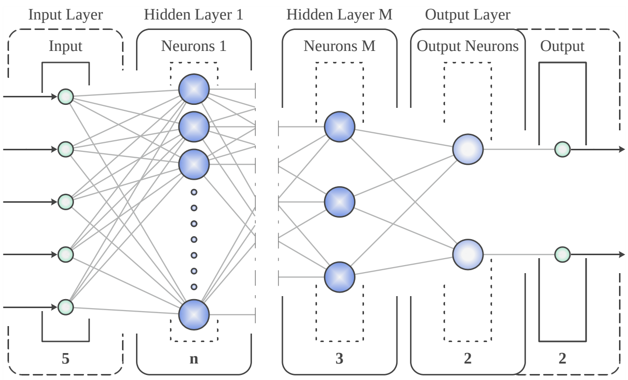

Fig. 17. Exemplary multilayer feed-forward ANN model, adapted from [15, 19, 20].

In simple terms, the number of hidden layers determines whether the ANN adapts the philosophy of either shallow or deep learning, whereby this distinction is not strictly defined. Each of these hidden layers accommodates a manually predefined amount of the substantial neurons, see neuron model explanations in [15, 20]. Accordingly, the neurons of the first hidden layer receive a stimulating signal via the input variables, manipulate the obtained values pursuant to specific inherent functions and then forward differently weighted values to the neurons of the next hidden layer or to those of the output layer respectively. If this output layer is active, the values get altered once more. The obtained result is a list of confidence values for each prescribed output variable.

It should be noted that the external connectors at input layer and output layer are often equivalently named input neurons and output neurons or just simply input and output, and furthermore, neurons are sometimes designated as nodes just like layers as units. A couple of these specialised terms are used within the referenced works [15, 17, 19, 20].

During an ANN's creation procedure, each active neuron's specific function is continuously adapted in order to minimise misallocations. For the topical implementation, this prefabricated process refers to supervised learning which means that output targets with preferable solutions are available for a comparison to predictions of the ANN. Of course, this pertains to the available algorithm for training/validation/testing in particular.

ANNs implemented within this work have been created by means of several modified scripts derived from the *Pattern Recognition app* within *MATLAB R2016a*.

Due to high data volumes provided for the creation process, out-of-memory issues appeared for the authors' premature plan to combine all set-up data clusters simultaneously in order to build one comprehensive ANN with abilities in basic frequency categorisation as well as creep groan judgement. However, this data volume problem of *MATLAB R2016a*, which was running here on *Windows 10 Pro 64 Bit* either at a *dual core i7* or at a *quad core i7* including 8 GB RAM respectively, has already been resolved by the software's developers via the so-called tall arrays. These allow the additional use of out-of-memory data, see description in [21] concerning more recent software releases. Nevertheless, the faced data volume restrictions made a workaround necessary.

4.2. Integrated Framework of 112 ANNs

The workaround is based on the separation of basic frequency categorisation and creep groan judgement. Therefore, an integrated framework including one "primary-ANN" and 111 autarchic "secondary-ANNs" has evolved. Due to this strategy, the memory requirements for training/validation/testing were strongly reduced. Certainly, the overall data volume was approximately the same, or even larger. However, the framework's task distribution and information flow can be seen Fig. 18.

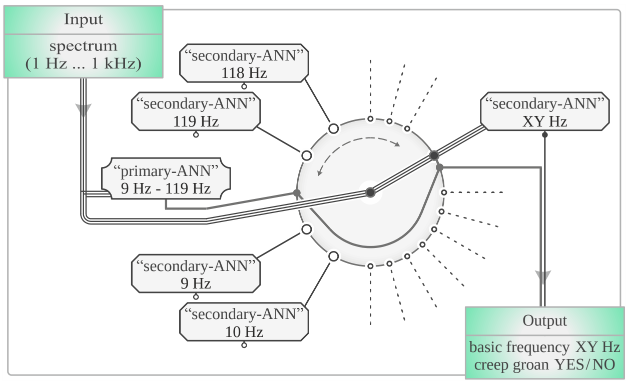

Fig. 18. Task distribution and information flow within framework of 112 self-sufficient ANNs.

Accordingly, the framework input reads a spectrum. It has a more or less embedded basic frequency which should be detected via the "primary-ANN" based on the highest of 111 probabilities. After this initial categorisation is done, the developed script routine forwards the spectrum to the "secondary-ANNs", whereby only the previously determined one is executed. It computes a probability approximation for both only possible states which means presence of creep groan or no occurrence. After all, the framework output includes the most likely stick-slip frequency of the imported spectrum and its related state concerning creep groan.

4.3. Split of Set-Up Data for Training/Validation/Testing

The "primary-ANN" is based on an 1.000 times 242.757 input signal data matrix and an 111 times 242.757 output target data matrix, whereas the other 111 autarchic "secondary-ANNs" rest upon 1.000 times 82.944 input signal data matrices and 2 times 82.944 output target data matrices. All 112 separate set-up data clusters were separately processed one after the other within the functionality generation phase.

Therefore, a well-considered split of each data matrix affiliation according to training/validation/testing was necessary. Eventually, a training data package is used to adapt an ANN in order to let it comply with as many known output targets as possible with respect to given input signals. A validation data package is mainly applied in terms of generalisation of an ANN. It is necessary to systematically decide whether and/or when to stop training. This leads to a ranking of the varied designs. Moreover, testing is important to independently quantify the effectiveness of an ANN's concluded design on previously unseen set-up data packages. Thus, it becomes feasible to avoid unfavourable data memorisation effects.

In order to ensure a comparability of different versions and parameter settings, the initial set-up data split is done here via a predetermined index and not randomly.

4.4. "Primary-ANN" for Basic Frequency Categorisation

The "primary-ANN" is modelled with one hidden layer including 80 neurons of function type *tan-sigmoid* which is described in [15]. The data matrices of the already mentioned input signals and output targets determine the amount of 1.000 passive input neurons and 111 *softmax* function output neurons. This structure is shown in Fig. 19 based on the standardised ANN visualisation provided by the *Pattern Recognition app*.

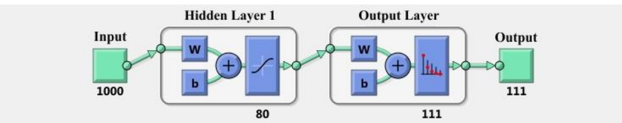

Fig. 19. Refined *MATLAB* representation for "1000-80-111" structure of the "primary-ANN".

A percentual set-up data division of 80/10/10 for training/validation/testing and a regression value of 0.1 within the well-considered Scaled Conjugate Gradient (SCG) backpropagation training method, which is treated in [19], have been applied.

Compared to other options, the applied data split in combination with the mentioned regression value seem to deliver the best results while avoiding over-fitting on the given set-up data clusters. The main reason to choose SCG over other equally well performing training techniques is its memory efficiency. This correlates with the findings of Azhar Omar et al. [19] concerning an ANN for meteorological issues.

The built-in stop criteria for training of the "primary-ANN" were set to 2.500 epochs, which is the maximum number of design iterations allowed for the entire layer composition, and moreover, to a limit of 500 consecutive validation checks which do not show improvements compared to the previously best. Only these two criteria are activated here in order to end the training iterations of the "primary-ANN".

The final training cycle of the "primary-ANN" results in less than 1 % misclassifications, if considering the testing data package not used for training or validation. Basically, all attempted layer compositions and optional parameter settings were varied largely automated until no further significant improvements regarding the minimisation of misclassifications occurred.

4.5. "Secondary-ANNs" for Creep Groan Judgement

Each of the 111 self-sufficient "secondary-ANNs" contains two hidden layers including 120 *tan-sigmoid* neurons respectively. The sizes of the data matrices according to Table 2 lead to the amount of 1.000 passive input neurons and two *softmax* output neurons. The consistent structure of each "secondary-ANN" is shown abstractly in Fig. 20.

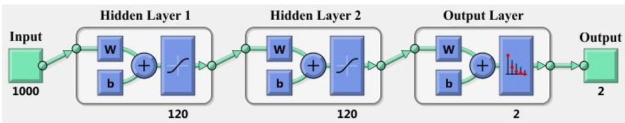

Fig. 20. Refined *MATLAB* representation for "1000-120-120-2" structure of each "secondary-ANN".

In light of positive experiences, the percentual set-up data split for training/validation/testing was adjusted to 80/10/10 alike, and moreover, the SCG backpropagation training method and a regression value of 0.1 were chosen again.

An extension from one towards two hidden layers, which can be interpreted as adaption from a shallow to a deep learning philosophy, was necessary due to a former share of around 20 % misjudgements on average, if considering the testing data package not used for training or validation. Based on trial and error, two times 120 neurons achieved good results for this problem, whereby computational times were reasonable compared to ANN compositions with more extensive hidden layer numbers and/or neurons. Thus, the mentioned errors regarding both only possible states, which means presence of creep groan or no occurrence, were reduced within all 111 “secondary-ANNs” to less than 2 % on average.

In order to achieve this optimisation while keeping the computational effort reasonable, the built-in stop criteria for training of each autarchic ANN concerning creep groan judgement were set to the upper limit of 10.000 epochs or training cycles respectively, to the maximum threshold of 500 consecutive validation checks without refinements compared to the previously best, to a demanded performance value lower than 0.00015 in terms of a cross-entropy calculation with a regularisation value of 0.05, and furthermore, to the upper time limit of 2 hrs. An optional gradient criterion related to the performance value curve is not used in order to avoid premature stops at local minima.

The additional stop criteria compared to those of the ANN for basic frequency categorisation were considered to ensure a predictable and manageable creation time across all 111 implementations. Accordingly, the cumulative time for training/validation/testing of the finally chosen layer compositions and parameter settings was approximately 130 hrs. However, specific “secondary-ANNs” have been retrained due to significantly worse reliabilities than the majority of the others. This would make clear that the realised branched ANN approach allows a simple comparison of identically created ANNs with a quick retraining possibility, whereas this is more problematic in a single ANN architecture.

5. VERIFICATION OF NEW CREEP GROAN PATTERN RECOGNITION METHOD

5.1. Check via Noisy Synthetic Input Signals

In the first part of the verification, the four variants with 227.328 unique synthetic spectra in each case are of relevance, see Table 3. Certainly, all prescribed output targets per variant are considered alike. Hence, each singular spectrum has a proper basic frequency as well as a preferable state whether creep groan should be allocated or not. Eventually, the elaborated framework’s reliability is quantified here in terms of pro-rata misevaluations per basic stick-slip frequency between 9 Hz and 119 Hz.

On one hand, “creep groan - underrated” means that the negatively signed percentual share, which is always normalised to roughly 65 % of all 2.048 spectra at a certain stick-slip frequency, is not judged by the “secondary-ANN” as creep groan, although it should be.

On the other hand, the positive percentual value regarding “no creep groan - overrated” means that this share, which pertains to the other approximately 35 % of all 2.048 spectra at a certain basic frequency, is evaluated by the AI as creep groan, although the prescribed output targets of the related unseen verification spectra suggest contrary terms.

Of course, this interpretation implies that the upstream “primary-ANN” performs very well. Indeed, concerning all four variants this counts for at least 99.70 % of the generic verification spectra, whereby the highest success rate is reached without white noise and the worst one with high white noise. Independent of that, the very small shares of incorrect basic frequency categorisations are primarily a result of misclassifications towards whole-numbered multiples or dividers, e.g. 9 Hz categorised as 18 Hz or vice versa. It should be noted that the ensuing judgement of a wrongly assigned “secondary-ANN” is possibly still correct in case of absent creep groan vibrations. However, the aftereffects based on errors of the “primary-ANN” are included in the four bar graphs hereafter.

The AI misevaluations regarding the generic data set without white noise are shown in Fig. 21. As it can be seen via the left-most cumulative bars which are differently scaled by the factor 7, there is around -0.22 % underrating and 4.97 % overrating for the entire verification data set. However, the reliabilities of the 111 “secondary-ANNs”, which affect both cumulative percentual values much more than the “primary-ANN”, are very specific. An almost negligible underrating does not appear above 35 Hz at all, whereas a widely more significant overrating tends to occur there instead in particular. By contrast, the tendency towards misevaluations of the subjacent frequencies is rather opposed, but with less intensity. Obviously, the basic frequencies with 10 Hz, 12 Hz, 20 Hz, 114 Hz, 118 Hz and 119 Hz are a few exceptions of that rough rule of thumb. Hence, these “secondary-ANNs” have potentially stronger biases than the majority of the others.

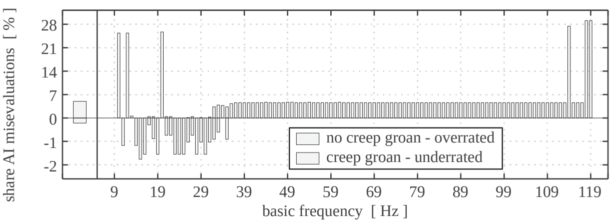

Fig. 21. AI misevaluations concerning 227.328 synthetic spectra without white noise.

The AI misevaluations regarding the generic data set with low white noise are broken down in Fig. 22. In general, there is a very similar distribution across the entire frequency window between 9 Hz and 119 Hz as discussed before via Fig. 21. Thus, low white noise is not an additional challenge for the framework of conditioned ANNs.

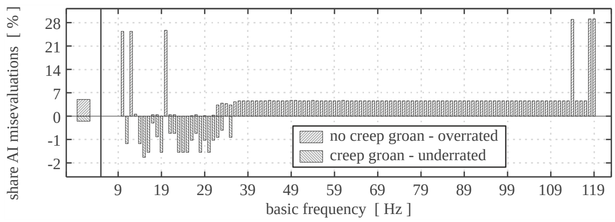

Fig. 22. AI misevaluations concerning 227.328 synthetic spectra including low white noise.

In comparison to both previous data sets, superimposed medium white noise leads already to slightly different verification results, see Fig. 23, whereby it is unfeasible to comprehend why just some basic frequencies are noteworthy affected. However, the main difference lies in an inferior success rate of the "secondary-ANNs" at 10 Hz, 22 Hz, 26 Hz, 45 Hz, 61 Hz, 70 Hz and 102 Hz. This leads to an average underrating of approximately -0.26 %. The opposite situation concerns around 5.17 %.

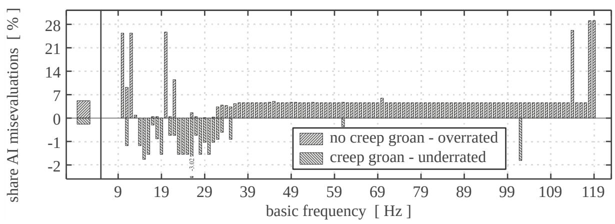

Fig. 23. AI misevaluations concerning 227.328 synthetic spectra including medium white noise.

Lastly, as indicated in Fig. 24, the synthesised data including high white noise leads to the largest percentual shares of misevaluations with rounded overall values of -0.56 % and 8.30 %. Once again, certain "secondary-ANNs" are more sensitive on noisy signal components than the majority of the others.

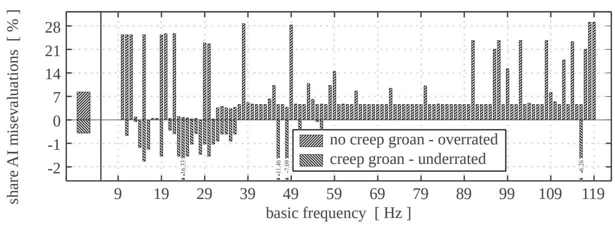

Fig. 24. AI misevaluations concerning 227.328 synthetic spectra including high white noise.

In summary, a clear bias towards overrating can be noticed within these four verifications. An interesting aspect is that "secondary-ANNs" with initially worst overrating, e.g. those of 10 Hz or 118 Hz, undergo no additional deterioration throughout all considered bandwidths of white noise.

5.2. Check via Measured Creep Groan Accelerations

In the second part of the verification, the integrated framework of conditioned ANNs is checked by means of measured calliper x-accelerations available from both automobile front corner test setups. Thus, the data sets applied for this are identical as discussed in section 2, and moreover, comparable visualisations as depicted in Fig. 11 and Fig. 12 can be generated. Hence, an AI-based CGM with 49 test matrix items is illustrated in Fig. 25 for type "I" and in Fig. 26 for type "II" respectively.

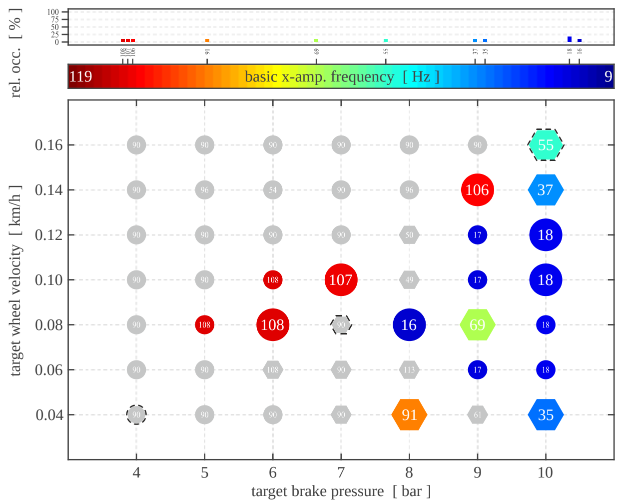

Fig. 25. AI-based CGM for test matrix of front corner system type "I".

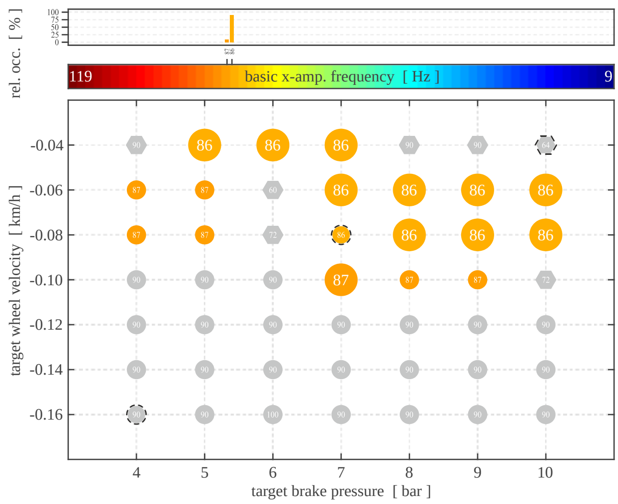

Fig. 26. AI-based CGM for test matrix of front corner system type "II".

A numeric value at each test matrix item clarifies the decision of the "primary-ANN". It corresponds to the calculated option of highest probability. For this purpose, frequency values from 9 Hz to 119 Hz are enabled exclusively.

Colour-filled circles refer to appropriately assigned "secondary-ANNs" in case of actually present creep groan, whereby the large ones indicate its proper approval and the small ones its incorrect denial. Uniformly grey-shaded small circular areas represent the adequate rejection of creep groan in case of its actual absence which makes the included numeric values somehow dispensable. However, it is interesting that 90 Hz is assigned for most of these instances without creep groan vibrations.

Hexagons are used to illustrate faulty declared outputs of the "primary-ANN". The larger ones in colour indicate a proper approval of creep groan. Unfortunately, always at inherently false basic frequencies. The smaller hexagons in grey show a false denial of creep groan. Even though it could be correct for wrongly assigned "secondary-ANNs", these evaluation results are still errors in a holistic view.

Consequently, large coloured circles just like small grey ones are the only items that show the requested verification results in a similar manner as in the initial evaluations, compare to Fig. 11 and Fig. 12.

As one can see in Fig. 25 and Fig. 26, hypothetically correct test matrix entries are distributed rather patchy. Overall, around 59 % and roughly 71 % matches are reached. A further breakdown reveals that the "primary-ANN" performs appropriately for approximately 73 % of the considered test matrix x-accelerations of type "I". For type "II", this applies to about 86 % of the 49 items. Furthermore, the charts show that there is a conspicuous bias towards underrating of creep groan vibrations in case of correctly assigned "secondary-ANNs", whereas overrating never occurred. Hence, all percentual values described most recently depend on the incidence of creep groan within the test matrix entries. Of course, this means that reliability and accuracy of the new evaluation approach are not objectively quantifiable based on measured creep groan accelerations.

6. SUMMARY AND CONCLUSION

This work's main objective relates to the development of an integrated framework of pattern recognition ANNs in order to detect and separate potentially existing non-linear low-frequency brake creep groan vibrations within comprehensive measurements and/or simulations.

On one hand, the method rests upon several millions of generically synthesised acceleration spectra which feign data with and without creep groan more or less realistic.

The data sets have been synthesised in a well-considered manner after subjective analyses on thousands of available calliper acceleration spectra, see also examples in [12, 13, 14]. The frequency window for recognisable basic stick-slip intervals of creep groan vibrations was adjusted from 9 Hz to 119 Hz. However, these are not mandatory values

On the other hand, the presented AI application method deploys the capabilities of the *Pattern Recognition app* within *MATLAB R2016a* in order to process the generic data in view of 112 self-sufficient ANNs in total.

However, only the faced data volume restrictions within this available software version led to the need for a workaround by means of these 112 autarchic ANNs in a branched architecture. In a positive sense, the distribution allows a simple comparison of identically created ANNs with a quick retraining possibility, whereas this would not be possible in a single ANN approach.

The so-called "primary-ANN", which is used for basic frequency categorisation, has a form "1000-80-111". By contrast, the other 111 so-called "secondary-ANNs", which are used for creep groan judgement, are designed with more *tan-sigmoid* neurons and an additional hidden layer according to a form "1000-120-120-2" respectively.

Both multilayer feed-forward ANN types rest upon supervised learning, a reproducible index-based 80/10/10 percentual data division for training/validation/testing and a regression value of 0.1 in combination with the SCG backpropagation training function. Iteration stop criteria were adjusted within an automated training procedure in order to ensure reasonable computational times while avoiding premature stops.

As a whole, the computational times in terms of the finally chosen layer compositions and parameter settings including retraining of specific "secondary-ANNs" took nearly 200 hrs. Eventually, the final training cycles revealed for all 112 ANNs less than 2 % errors on average, if considering each testing data package not used for training or validation.

The framework's practical limitations are determined by means of four additional synthetic acceleration spectrum compilations including different reproducible white noise bandwidths, and moreover, via two independent data sets of accelerations gauged for two typical passenger car front corner setups at a drum driven suspension and brake test rig. Thus, 909.312 generic verification spectra just like 98 measured ones have been considered in particular.

Each unique verification spectrum has a proper basic frequency and a preferable state whether creep groan should be allocated or not. Since these prescribed output targets are based on the deterministic creep groan evaluation algorithm presented in [12], which can be questioned critically on its own, there are uncertainties involved in case of fuzzy acceleration spectra in particular.

Nevertheless, it is assumed here that Fig. 11 and Fig. 12 reflect correct results.

In terms of all 909.312 generic verification spectra with a prescribed proportion of roughly 35 % absent creep groan, a tendency towards “no creep groan - overrated” can be noticed.

This overrating appears for 4.97 % to 8.30 % on average, whereas “creep groan - underrated” with respect to the other roughly 65 % counts for -0.22 % to -0.56 % on average. Both smaller values correspond to the data compilation without white noise and the larger values refer to high white noise respectively. The rounded overall success rates for these examples reach 98.12 % and 96.73 % respectively. Since the “primary-ANN” classifies at least 99.70 % of the spectra within each data set of the four synthetic verification variants very well, the major share of the emerged AI misevaluations can be traced to misjudgements of the “secondary-ANNs”.

A not fully understood aspect is that certain of these ANNs significantly change the reliability with increasing white noise bandwidths, whereas others do not show this behaviour, compare Fig. 21 with Fig. 24. Furthermore, it is interesting that underrating is rather omitted above 35 Hz.

In terms of the 98 examples of measured calliper x-accelerations with a known proportion of around 47 % absent creep groan vibrations, a clear bias towards underrating can be noticed via Fig. 25 and Fig. 26.

By contrast, overrating never occurred. The investigation shows that the “primary-ANN” performs adequately for approximately 80 % of the 98 considered test matrix items. Subsequently, the elaborated framework of conditioned ANNs reaches an overall hit rate of around 65 %.

However, a major concern in this verification part is the fact that these percentual values described most recently depend on the incidence of creep groan within the test matrix entries. Hence, a slightly higher overall hit rate of approximately 70 % is reached in case of considering both creep groan parameter matrices of [12] with 190 items respectively. On the downside, matches for the 190 test matrix items of [13] emerge only for roughly 37 %.

Based on verifications with these 570 additional items should be noted that potential for improvements seems to lie within a sophisticated treatment of typical misclassifications of the “primary-ANN”. These are often related to a detection of whole-numbered basic frequency multiples or dividers, and furthermore, to rounded basic frequency decimals which were not yet taken into account.

7. OUTLOOK

The developed approach’s principle rests upon not yet fully exploited capabilities of a specific software. Moreover, ANN models for pattern recognition can be adapted in many ways. Hence, more experienced software users and/or AI specialists probably detect potential for improvements. However, the fundamental set-up data clusters are always essential.

Millions of generically synthesised acceleration spectra have been considered. Nevertheless, there could be a lack of information in the attempt to imitate the evaluation algorithm introduced in [12]. Further attribute values might be tested or realistic spectral noise could be added, whereby a higher amount of generic input spectra for more training/validation/testing options should not be a main aim. Of course, the dimensions of the input signal data matrices might be reduced in order to decrease the computational effort, e.g. to 500 Hz.

Alternatively, measured creep groan accelerations could be considered during the set-up phase. Preliminary studies have shown a large potential with good matching rates around 90 % concerning this adapted single ANN strategy. Nevertheless, the available data pool from test rig measurements regarding different creep groan manifestations within the relevant frequency window is not yet enough. In view of upcoming creep groan experiments, or even with prospective transient simulations such as demonstrated in [13], this alternative approach with only one ANN is practicable at the soonest in a few years.

Lastly, it should be noted that the principle of the devised AI application method could be suitable for similar NVH problems or signal analysis tasks in other engineering fields alike. However, refinements have to be made in order to enable an implementation.

8. REFERENCES

[1] A. Akay: **Acoustics of friction**, *The Journal of the Acoustical Society of America*, 111(4), 2002, 1525-1548, doi:10.1121/1.1456514

[2] A.L. Dorofte: **The new Mercedes-Benz S-Class: The automotive benchmark in efficiency and comfort**, MERCEDES-BENZ / AUTOMOBILES / LIMOUSINE / *S-CLASS*, Mercedes-Benz-Blog, Bucharest, 2017, https://mercedes-benz-blog.blogspot.com/2017/04/the-new-mercedes-benz-s-class_19.html, accessed July 2018

[3] D.A. Crolla and A.M. Lang: **Brake Noise and Vibration - The State of the Art**, *Tribology Series*, 18, 1991, Paper VII (i), 165-174, doi:10.1016/S0167-8922(08)70132-9

[4] H. Abendroth and B. Wernitz: **The Integrated Test Concept: Dyno - Vehicle, Performance - Noise**, SAE Technical Paper 2000-01-2774, 2000, doi:10.4271/2000-01-2774

[5] C. Bittner: **Reduzierung des Bremsenrubbelns bei Kraftfahrzeugen durch Optimierung der Fahrwerkslager**, Doctoral thesis, Technical University of Munich, Institute of Automotive Technology, Munich, 2006

[6] J. Youngs: **Vehicle Dependability Study: Top 10 Problems in 3-Year-Old Vehicles**, *J.D. Power Studies*, J.D. Power, Westlake Village, 2014, http://www.jdpower.com/cars/articles/jd-power-studies/vehicle-dependability-study-top-10-problems-3-year-old-vehicles, accessed July 2018

[7] G.O. Davies: **Vehicle dependability in Japan declines, J.D. Power finds**, *Automotive World*, Automotive World Ltd, Penarth, 2017, https://www.automotiveworld.com/news-releases/vehicle-dependability-japan-declines-j-d-power-finds/, accessed July 2018

[8] S. Huemer-Kals: **Complex Eigenvalue Analysis of Friction Induced Low-Frequency Vibrations in Vehicle Disc Brake Systems**, Master thesis, Graz University of Technology, Institute of Automotive Engineering, Graz, 2018

[9] H. Marschner, A. Pfaff, P. Leibolt and G. Maggi-Trovatoto: **Schwingungen und Geräusche**, 627-648, In: *Bremsenhandbuch*, B. Breuer and K. Bill (eds), 2017, Springer, doi:10.1007/978-3-658-489-9_28

[10] D.C. Barton and J.D. Fieldhouse: **Noise, Vibration and Harshness (NVH)**, 255-317, In: *Automotive Chassis Engineering*, D.C. Barton and J.D. Fieldhouse (eds), 2018, Springer, doi:10.1007/978-3-319-72437-9

[11] S. Karabay, K. Baynal and C. İğdeli: **Detecting Groan Sources in Drum Brakes of Commercial Vehicles by TVA-FMEA: A Case Study**, *Strojniški vestnik - Journal of Mechanical Engineering*, 59(6), 2013, 375-386, doi:10.5545/sv-jme.2012.809

[12] M. Pürscher and P. Fischer: **Systematic Experimental Creep Groan Characterization Using a Suspension and Brake Test Rig**, SAE Technical Paper 2017-01-2488, 2017, doi:10.4271/2017-01-2488

[13] M. Pürscher, S. Huemer-Kals and P. Fischer: **Experimental and Simulative Study of Creep Groan in Terms of MacPherson Axle Bushing Elasticities**, *Proceedings of EuroBrake 2018*, EB2018-SVM-011, May 22-24, The Hague, 2018

[14] M. Pürscher, S. Huemer-Kals and P. Fischer: **Experimental Investigation of Low-Frequency Vibration Patterns in Automotive Disk Brake Systems: Utilization Study for Modal Simulation Methods**, SAE Technical Paper 2018-01-1513, 2018, doi:10.4271/2018-01-1513

[15] S.K. Lee and H.C. Chae: **The application of artificial neural networks to the characterization of interior noise booming in passenger cars,** *Proceedings of the Institution of Mechanical Engineers, Part D: Journal of Automobile Engineering*, 218(1), 2004, 33-42, doi:10.1243/095440704322829146

[16] J. Bughin et al.: **Artificial Intelligence: The Next Digital Frontier?**, *McKinsey Global Institute Discussion Paper*, McKinsey & Company, 2017

[17] A. Rosenfeld and H. Wechsler: **Pattern Recognition: Historical Perspective and Future Directions,** *International Journal of Imaging Systems and Technology*, 11(2), 2000, 101-116, doi:10.1002/1098-1098(2000)11:2<101::AID-IMA1>3.0.CO;2-J

[18] H. Liu, J. Yin, X. Luo and S. Zhang: **Foreword to the special issue on recent advances on pattern recognition and artificial intelligence,** *Neural Computing & Applications*, 29(1), 2018, 1-2, doi:10.1007/s00521-017-3243-x

[19] M. Azhar Omar, M. Khair Hassan, A. Che Soh and M.Z.A. Ab Kadir: **Lightning severity classification utilizing the meteorological parameters: A neural network approach,** *Proceedings of 2013 IEEE International Conference on Control Systems, Computing and Engineering,* 111-116, Nov. 29 - Dec. 1, Minden, 2013, doi: 10.1109/ICCSCE.2013.6719942

[20] J. Hertz, A. Krogh and R.G. Palmer (eds): **Introduction to the Theory of Neural Computation**, 1991, Addison-Wesley, ISBN 0-201-50395-6

[21] J. Little and C. Moler: **Matlab Release Notes**, *MATLAB Documentation*, The MathWorks, Inc., Natick, 2018, https://de.mathworks.com/help/matlab/release-notes.html?rntext=&startrelease=R2017a&endrelease=R2018a&category=data-analysis&groupby=release&sortby=descending&searchHighlight=, accessed August 2018

8th Congress of the Alps Adria Acoustics Association
Zagreb, Croatia
20 – 21 September 2018

Hrvatsko akustičko društvo
HAD
Acoustical Society of Croatia

LINEARIZED SIMULATIVE APPROACH FOR THE INVESTIGATION OF A FRICTION-INDUCED LOW-FREQUENCY BRAKE MOAN OSCILLATION PHENOMENON WITHIN PASSENGER VEHICLE FRONT AXLES

Severin Huemer-Kals, Manuel Pürscher, Peter Fischer

Graz University of Technology, Institute of Automotive Engineering (FTG)
Inffeldgasse 11/II, 8010 Graz, Austria
Contact: severin.huemer-kals@tugraz.at

Abstract: *Noise, Vibration and Harshness phenomena regarding a passenger vehicle's brake and suspension system can imply a reduced sense of quality as well as significant warranty costs. In contrast to well-researched mid- to high-frequency brake squeal, low-frequency vibrations have gained popularity only most recently. Brake moan is one of these effects, featuring frequencies from 350-600 Hz. Among others, independent wheel suspension systems at the front axle can exhibit moan-related oscillations. Here, evaluations imply high familiarity to disk brake squeal, which can be explained by a coupling of different eigenmodes of suspension and brake system, induced by the frictional contact between disk and pads. Consequently, simulation techniques used for squeal evaluation should be applicable for moan phenomena too. Hence, the linearized approach of the Complex Eigenvalue Analysis was investigated for a Finite Element model of a vehicle's front corner. Parameter variations within a relevant operating range were performed for two different rim designs. A validation based on experimental tests reveals the simulative method's ability to predict the eigenfrequency of characteristic torsional rim oscillations. However, stability was computed divergent to the systems' real-life behaviors: Further examination and correct implementation of sensitive parameters seem necessary for a predictive application of this linearized, simulative approach.*

Key words: brake vibrations, complex eigenvalue analysis, friction-induced vibrations, moan, stability analysis

1. INTRODUCTION

Within a conventional vehicle, the internal combustion engine ensures a certain amount of background noise during driving. For the increasing numbers of Battery Electric (BEV) and Plug-in Hybrid Vehicles (PHEV), this sound source drops out and increases the influence of low-frequency (<1000 Hz) suspension and brake Noise, Vibration and Harshness (NVH) issues. What is more, new driving modes such as automated parking utilize the brakes while a certain drive torque is present at the same time. Because friction-induced low-frequency vibrations essentially occur for the combination of low speed and low brake pressure, as explained in [1, p. 630], their impact on quality and warranty costs is rising.

Brake moan is one of the relevant phenomena, see fig. 1 for an overview. Based on the authors' experience, its main frequency can be found between approx. 350-600 Hz. However, [2] concatenates results from several studies to an even wider range of 200-1000 Hz.

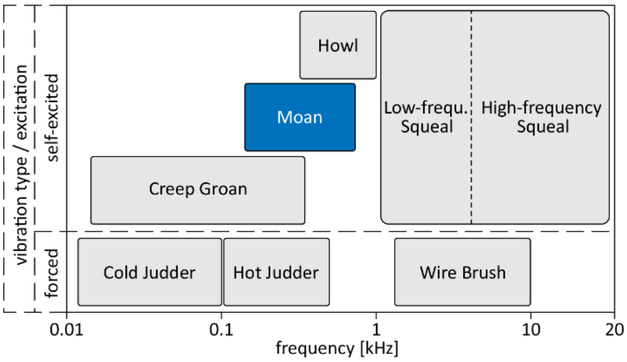

Fig. 1. Brake NVH phenomena classified by vibration type and first dominant frequency, adapted from [3–8]

The exact excitation mechanism of this NVH effect, induced by the frictional contact between the rotating brake disk and the brake pads, is still not perfectly clear. Whereas some researchers refer to the stick-slip effect, e.g. [9, p. 1392, 10, p. 1, 11], others claim modal coupling similar to brake squeal to be responsible, see e.g. [2, 12]. Supporting the authors' opinion given in [13], the research group of [2] states that this discrepancy could probably relate to the distinction by frequency: Depending on each individual axle's stiffness and mass parameters, either "global" stick-slip transitions – i.e. breakaway throughout the whole pad/disk contact – or modal coupling can lead to NVH issues in a similar frequency range.

Brake moan is mostly known to occur at a car's rear axle: E.g., [2] explains a moan phenomenon at a twist-beam suspension setup. Operational deflections were dominated by rotations of the caliper about its vertical axis, the vehicle roll axis and the wheel axis. Furthermore, a coupling between left and right brake system was discovered. For front axle systems with double wishbone suspension, [14] describes a torsional rim mode in combination with control arm bending oscillations.

Similar to the well-researched, higher-frequency brake squeal, frequency analyses typically show a distinct first peak accompanied by several superharmonic contents of lower energy, see e.g. [15, p. 5]. An example is given by the frequency plot of measured brake pad accelerations in fig. 2.

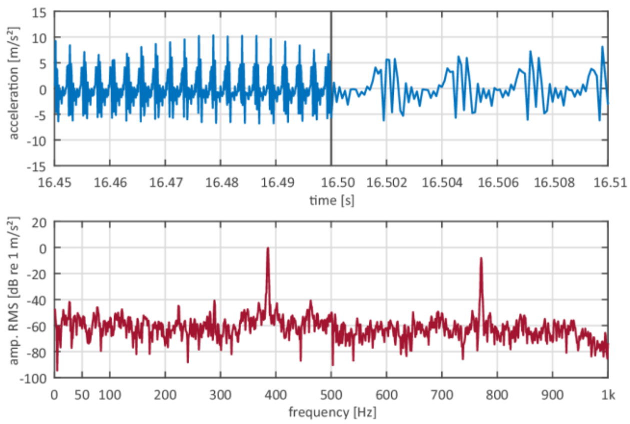

Fig. 2. Longitudinal pad acceleration during 386 Hz moan, adapted from [13, 16]

Similar to other applications within the automotive industry, early simulative prediction is desired for a short and cost-effective vehicle development. In terms of brake NVH, two basic computational methods can be distinguished, [17, p. 1206]:

- Time domain approaches
- (Linearized) stability analyses

Even if they feature promising capability for low-frequency brake phenomena such as creep groan, see e.g. [18], time domain approaches are typically limited to the application on strongly reduced systems for research due to the high computational effort. By contrast, linearized stability analyses in the form of the Complex Eigenvalue Analysis (CEA) are widely used for the prediction of higher-frequency squeal. Within this work, its ability to predict moan-related phenomena shall be investigated.

2. COMPLEX EIGENVALUE ANALYSIS

In this chapter, mathematical and theoretical essentials regarding the CEA in terms of its usage for brake NVH evaluation are explained, based on the more detailed contents of [19] and the authors' related publication, [13]. As large-scale simulations were carried out with the Finite Element solver PERMAS, some formulations relate to this software package, [20].

2.1. Theorem of Hartman and Grobman

Based on the theorem of Hartman and Grobman, the stability of a non-linear system near a fixed point can be determined by an evaluation of the linearized system: If the related eigenvalue has a non-zero real part, i.e. a so-called hyperbolic fixed point is existent, the stability behavior of linear and non-linear system are identical. This principle provides the theoretical basis for stability studies by CEA. [21]

2.2. Basic Equation and Procedure

Eventually, the dynamic system equation – typically given in modal coordinates – needs to be solved, see eq. 1.

$$\begin{aligned}\vec{0} = {} & \widetilde{\boldsymbol{M}} \cdot \ddot{\vec{q}} + \\ & \left[\widetilde{\boldsymbol{D}}_{\mathrm{V}} + \widetilde{\boldsymbol{D}}_{\mathrm{Ct}}(\Omega) + \widetilde{\boldsymbol{D}}_{\mathrm{G}}(\Omega)\right] \cdot \dot{\vec{q}} + \\ & \left[\widetilde{\boldsymbol{K}}_{\mathrm{el}} + \widetilde{\boldsymbol{K}}_{\mathrm{Ct}} + \widetilde{\boldsymbol{K}}_{\mathrm{G}}(\Omega) + \widetilde{\boldsymbol{K}}_{\mathrm{C}}(\Omega) + \mathrm{i}\widetilde{\boldsymbol{H}}\right] \cdot \vec{q}\end{aligned} \quad (1)$$

In order to form this equation, an extensive model build-up consisting of several steps is necessary. This four-step process including its crucial simplifications is shown in fig. 3.

After finding the fixed point by application of a static, non-linear contact simulation in step 1, a (critical) linearization is performed. Here, the Coulomb sliding friction force within the disk/pad contact, relating to normal contact force, coefficient of friction and direction of the relative velocity according to eq. 2, is linearized by means of a Taylor series approximation.

$$\vec{f}_{\mathrm{R}} = -\mu \left\|\vec{f}_{\mathrm{N}}\right\| \frac{\vec{v}_{\mathrm{rel}}}{\left\|\vec{v}_{\mathrm{rel}}\right\|} \quad (2)$$

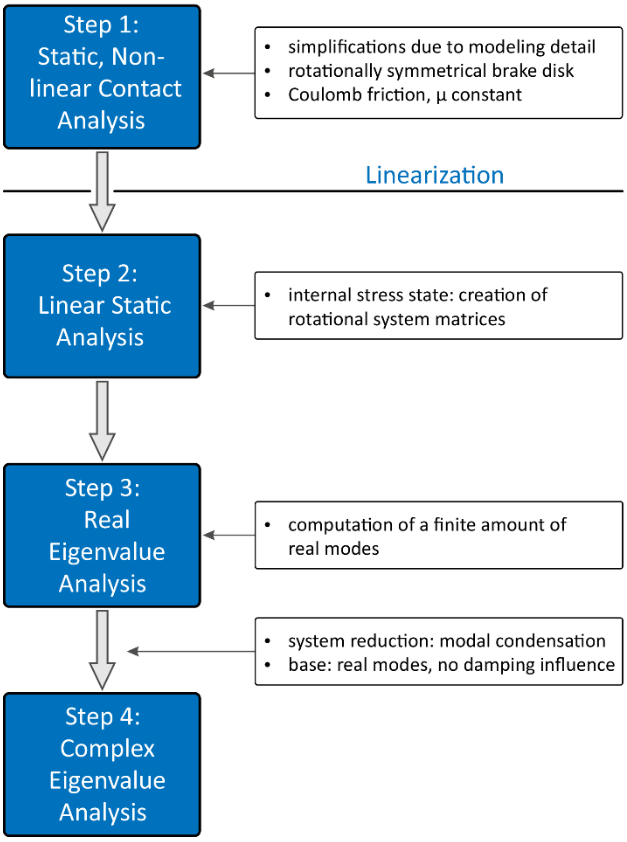

Fig. 3. Procedure for disk brake NVH Complex Eigenvalue Analysis, adapted from [13]

As presented within the related publication [13], the application of CEA is only meaningful for clearly non-zero relative speeds. Because of highly non-linear behavior near the state of sticking, predicted stability behaviors would be valid for exceptionally small intervals about the fixed point only. See fig. 4 for additional clarification.

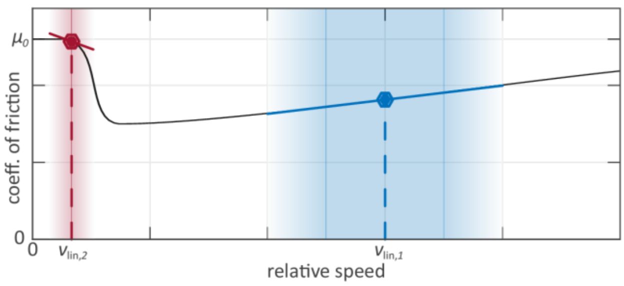

Fig. 4. Friction linearization at different fixed points, adapted from [13]

Especially for stick-slip-related creep groan phenomena, additional non-linearities such as e.g. elastomer bushing stiffnesses can be of influence, see [18]. Certainly, these effects are part of the linearization too.

Subsequently, supplemental rotational terms are created in a linear static analysis. On the one hand, geometric and convective stiffness contents relate to the square of the rotational speed. Especially for very low velocities, which are characteristic for creep groan and moan occurrence, these terms were found negligible according to [13]. On the other hand, linearly speed-dependent gyroscopic terms are known to alter the stability behavior even if the actual magnitude order is small, see e.g. [22, p. 143].

Due to a desired reduction of computational effort, the investigated vehicle corner Finite Element models are typically reduced based on a modal condensation. Therefore, real modes – without the influence of damping – are computed to assemble a new, smaller set of basis (eigen)vectors $\boldsymbol{\Phi}$. See eq. 3 and eq. 4.

$$[\boldsymbol{K}_{\mathrm{el}} - \omega^2 \boldsymbol{M}] \cdot \vec{\phi} = \vec{0} \tag{3}$$

$$\boldsymbol{\Phi} = [\vec{\phi}_1, \vec{\phi}_2, \dots, \vec{\phi}_{\mathrm{n}}] \tag{4}$$

Eventually, the coordinate transformation and a left multiplication by the transposed modal matrix $\boldsymbol{\Phi}^{\mathrm{T}}$ according to eq. 5 leads to the equation to solve, eq. 1.

$$\underbrace{[\boldsymbol{\Phi}^{\mathrm{T}} \boldsymbol{M}\, \boldsymbol{\Phi}]}_{\widetilde{\boldsymbol{M}}} \cdot \ddot{\vec{q}} + \underbrace{[\boldsymbol{\Phi}^{\mathrm{T}} \Sigma \boldsymbol{D}_i\, \boldsymbol{\Phi}]}_{\widetilde{\boldsymbol{D}}} \cdot \dot{\vec{q}} + \underbrace{[\boldsymbol{\Phi}^{\mathrm{T}} \Sigma \boldsymbol{K}_i\, \boldsymbol{\Phi}]}_{\widetilde{\boldsymbol{K}}} \cdot \vec{q} = \vec{0} \tag{5}$$

By usage of a complex approach consisting of complex eigenvector and complex eigenvalue as in eq. (6), the equation then is solved.

$$\vec{q} = \vec{\phi}_{\mathrm{c}} \cdot \mathrm{e}^{(\delta + \mathrm{i}\omega_{\mathrm{c}})t} \tag{6}$$

In terms of stability, the equivalent viscous damping ratio is typically evaluated. This characteristic number, given in eq. (7), indicates unfavorable, unstable behavior by a negative sign related to the eigenvalue's real part.

$$\xi_i = \frac{-\delta_i}{\delta_i^2 + \omega_{\mathrm{c},i}^2} \tag{7}$$

It has to be noted that this value only relates to the stability about the fixed point computed in step 1, no conclusion about resulting oscillation amplitudes can be drawn by the CEA. One big drawback of this method is the fact that stability is regularly over- or underestimated in industrial applications. Nevertheless, CEA is capable to efficiently handle large parameter variations, which is an important reason for its wide usage.

2.3. Application for Brake Moan

As stated above, the application of CEA for predictive brake NVH evaluation is only meaningful for clearly non-zero relative speeds. In terms of brake moan, this corresponds to phenomena which occur in the relevant frequency range and are rather excited by modal coupling than by global stick-slip transitions in the disk/pads contact zones. If this is the case, moan can be assumed as a dynamic instability or a kind of "low-frequency brake squeal": Based on [2] and the related work [13], CEA stability analysis should be applicable.

3. SIMULATIVE INVESTIGATIONS

3.1. Model Description

Starting from a Finite Element model provided by an industrial project partner, a full corner model appropriate for moan evaluation was built up. In this case, two different rim designs were compared. Within [13], this model's predecessor is explained.

As one can see in fig. 5 and fig. 6, the corner model features all main components between wheel contact point and chassis of the car. This includes the fixed caliper brake system with brake disk, caliper and pads as well as the double wishbone suspension with wheel carrier and steering link. Anti-roll bar and drive shaft were removed due to the corresponding experimental setup.

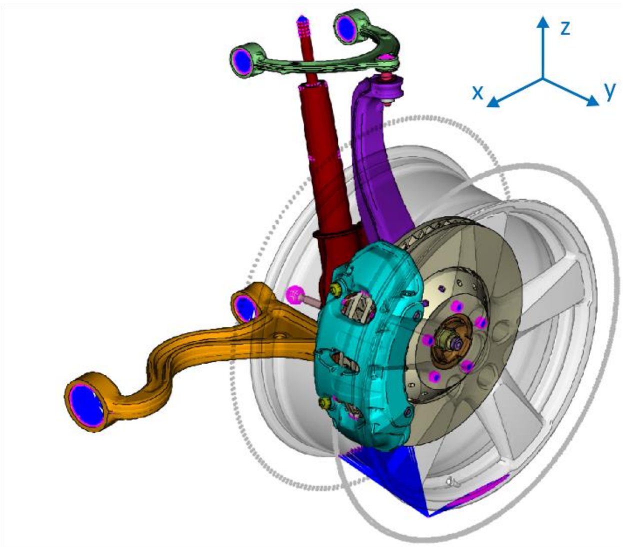

Fig. 5. Investigated Finite Element model with rim A, [16]

Furthermore, a rim model consisting of 2nd order tetrahedron elements in combination with mass points representing the tire inertia and a three-dimensional stiffness/damping element in the wheel contact point introduce wheel influences. Two different rim designs were compared: Rim A with 5 separate, broader spokes and rim B with 20 slim spokes – see fig. 5 and fig. 6 for a depiction. Regarding the mass moment of inertia about the wheel axis, a swing experiment delivered rather accurate values of rim A. For rim B, identical rotational inertia was assumed and introduced by arranging the tire mass points' radial center distance accordingly.

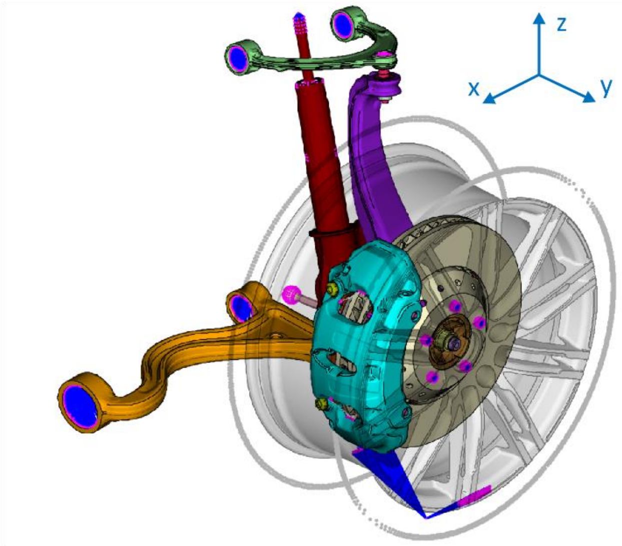

Fig. 6. Investigated Finite Element model with rim B, [16]

Depending on rim design, the overall number of nodes was 690 000 (rim A) and 1 000 000 (rim B) respectively. Boundary conditions were applied at the interfaces to the chassis in Degrees of Freedom (DOFs) 123456 and at the wheel contact point with the road surface (DOFs 123). Moreover, the steering link was supported translational and in one torsional rotation direction (local DOFs 1235).

Compared to the model presented in [13], measures were taken to improve its ability for predicting moan phenomena: Firstly, less damping was introduced at the wheel contact point. Secondly, rim nodes of the Multi-Point Constraint connecting the rim to the ground were reduced. Thirdly, real modes were computed up to a higher frequency of 2.5 kHz.

Operational parameters can be found in table 1. Even though moan can occur also at slightly higher speeds and even lower brake pressures, it basically emerges in operating ranges similar to creep groan, [1, p. 630, 23]. Hence, parameters were chosen in the low brake pressure / low vehicle speed range identical to [13], which also corresponds to experimental test results.

Brake pressure p_B	4 - 16 bar	Δ 2 bar
Vehicle speed v_{veh}	0.04 - 0.4 km/h	Δ 0.004 km/h
Coeff. of friction μ	0.25 - 0.55	Δ 0.05

Table 1. Simulative parameter variation ranges

Within [13] and [18], influences of non-linear elastomer bushing stiffness and damping behavior were proven to be highly relevant for low-frequency creep groan. As the study presented here builds up on a corresponding model, these parameters were modeled with special care: E.g., bushing stiffnesses were implemented in a non-linear parameter-dependent manner. However, the results reveal less relevance for moan, hence, a detailed explanation regarding these aspects is not featured here.

3.2. Simulative Results

In the following, CEA was performed for both rim designs using a vehicle reference speed of 0.2 km/h – rotational terms vary for deviations. Modal displacements as well as eigenfrequency and stability behavior were evaluated. Therefore, depictions of modal displacements and multi-dimensional stability diagrams are shown.

For rim A, only one moan-relevant mode was found unstable. Within fig. 7, its displacements are shown: Torsion between wheel hub and the rim's outer part dominates the oscillation. Furthermore, higher order bending modes of the control arms and the spring with damper assembly can be detected.

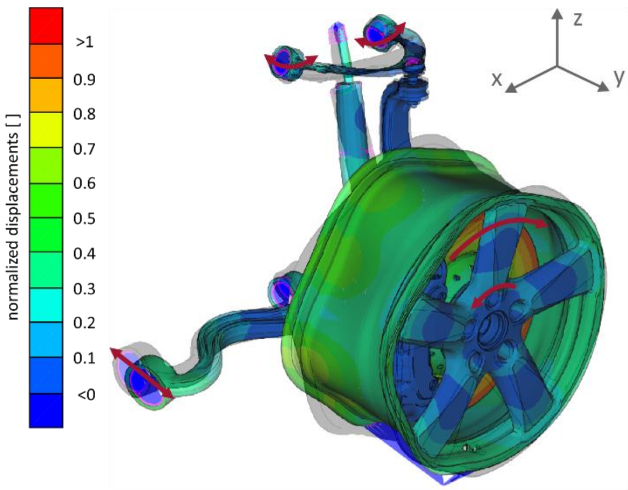

Fig. 7. Normalized displacements of the (partly unstable) moan-relevant mode with rim A for μ=0.55 and p_B=10 bar, adapted from [16]

Fig. 8 shows the corresponding eigenfrequency and stability behavior. This diagram contains 7 surfaces, drawn over the whole parameter range of brake pressures and vehicle speeds as x- and y-axis. Each of these surfaces is related to a coefficient of friction. Moreover, the vertical coordinate of each surface point corresponds to the resulting eigenfrequency. In addition, another dimension is introduced by color: unstable parameter combinations are marked blue, depending on the equivalent viscous damping ratio. Stable zones remain white.

In fig. 8, only one parameter combination was computed unstable, recognizable by the slightly blue color zone at the operating point μ=0.55, p_B=10 bar and v_{veh}=0.04 km/h. Generally, eigenfrequency was in the range of 562.5 – 563.4 Hz, changing only little for different parameters. Nonetheless, two combinations of brake pressure and coefficient of friction, including the unstable spot, feature slightly lower frequencies.

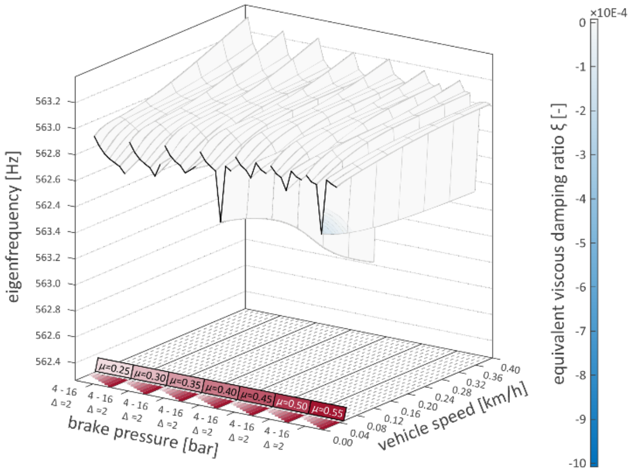

Fig. 8. Multi-dimensional stability diagram for the torsional rim mode with rim A, adapted from [16]

For rim B, no unstable mode was found within the moan-relevant frequency range at all. However, due to the resulting mode with rim A and experimental/literature results according to chapter 4, a torsional rim mode was evaluated. Fig. 9 shows the mode's displacements: By contrast to the mode with rim A, bending of suspension components such as control arms or spring with damper assembly cannot be found here.

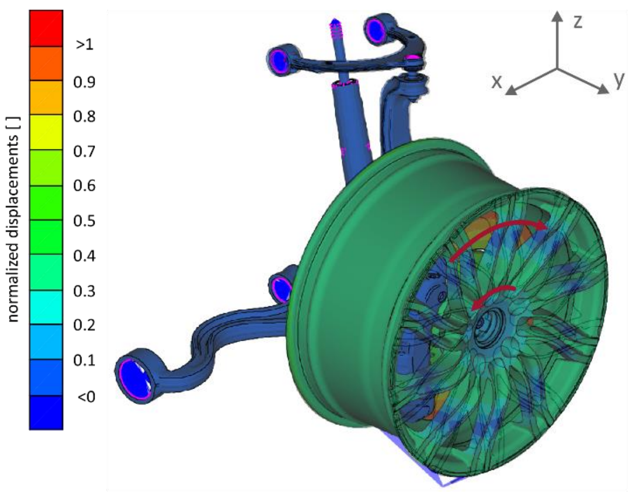

Fig. 9. Normalized displacements of the (stable) moan-relevant mode with rim B for μ=0.4 and p_B=16 bar, adapted from [16]

Fig. 10 shows no unstable parameter points for rim B. Furthermore, frequency changed only in its third decimal place in the whole parameter range at approx. 358.7 Hz.

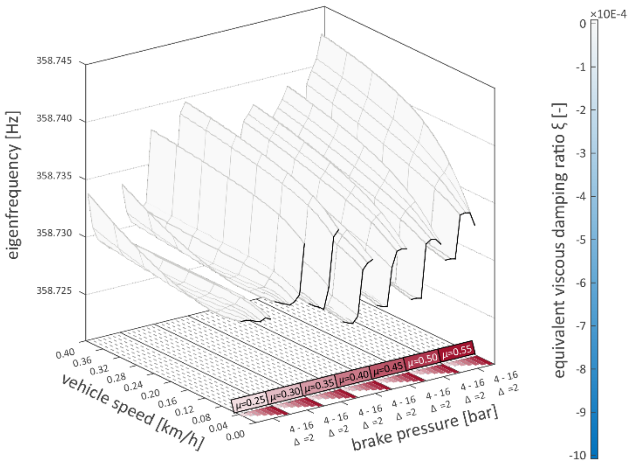

Fig. 10. Multi-dimensional stability diagram for the torsional rim mode with rim B, adapted from [16]

4. EXPERIMENTAL VALIDATION

For validation, experimental tests were performed on a drum-driven suspension and brake test rig. An example setup can be seen in fig. 11. By use of special adapters, the components of the vehicle's front left corner were mounted to the test bench plate according to the real vehicle. Analogously to the simulative investigations, anti-roll bar and drive shaft were omitted.

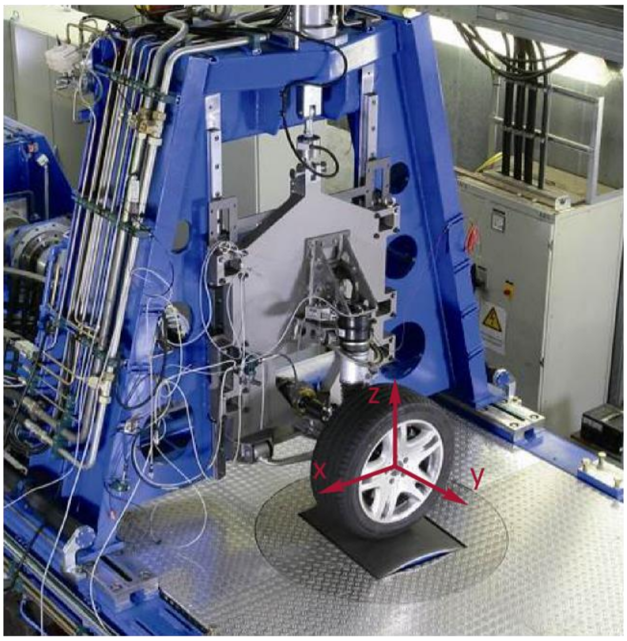

Fig. 11. Exemplary setup on the combined suspension and brake test rig at FTG / Graz University of Technology, adapted from [13]

During the tests, certain brake pressure and speed profiles according to [24] were retraced by the hydraulic unit and the speed-controlled drum. The coefficient of friction between disk and pads was estimated at approx. 0.35 by a method described within [25]. Furthermore, effects resulting from the vehicle's unladen weight were considered via a vertical pre-tension by a hydraulic cylinder.

In the following, data from several pad acceleration sensors and an incremental rotary encoder sampled with 10 kHz was used for the evaluation of dominant frequencies as well as relative speeds at the theoretic friction radius. The sensor positions can be found in fig. 12, details about measurement and procedure are given within [26].

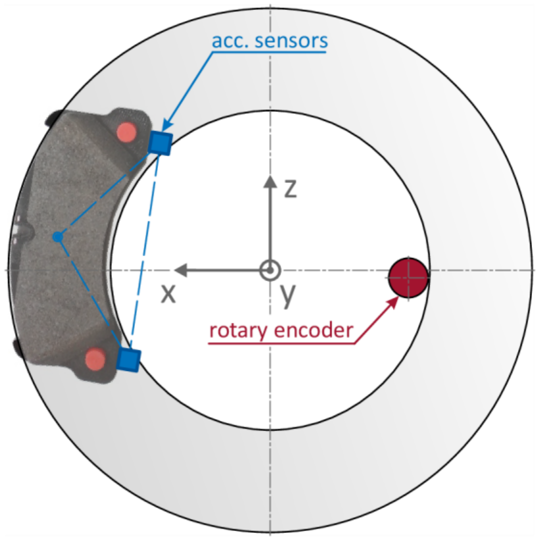

Fig. 12. Approximated sensor positions for acceleration measurement and evaluation of relative speed, adapted from [16]

In addition to the in-house experiments, literature results of similar or even nearly identical setups were consulted for validation purposes. Within [14], a project partner's work on an almost identical system is described.

4.1. Moan-Relevant Mode for Rim A

According to the simulative investigations, unstable behavior could probably occur in case of high coefficients of friction, moderate brake pressures and very slow speeds. However, as already mentioned in [13], moan was not found on the test bench for this rim.

What is more, personal correspondence with the main author of [14] further emphasized this setup's moan stability. Nonetheless, a noise phenomenon of almost identical frequency was said to be 'enforced' on test bench by this project partner. In addition, the torsional rim mode was verbally confirmed.

Interestingly, simulations have predicted a strongly parameter-dependent moan occurrence. However, this contradicts the theory of a dynamic instability, see [2].

4.2. Moan-Relevant Mode for Rim B

The torsional rim mode at approx. 358.7 Hz was computed stable for all parameter combinations. Even in an increased parameter range with coefficients of friction from 0.25 – 0.8, no unstable operating points were found. By contrast, experiments with this setup revealed moan oscillations at an approximately similar frequency of 386 Hz, see already published results within [13] and [26].

Meaningful averaging, filtering and integration of the signals from rotary encoder and acceleration sensors led to an evaluation of tangential velocities at the theoretic friction radius, [13]. The lower subfigure in fig. 13 displays constantly positive relative speed between brake disk and pads during moan operation. This relates to a dynamic instability and points out the principal capability of CEA prediction for this moan phenomenon.

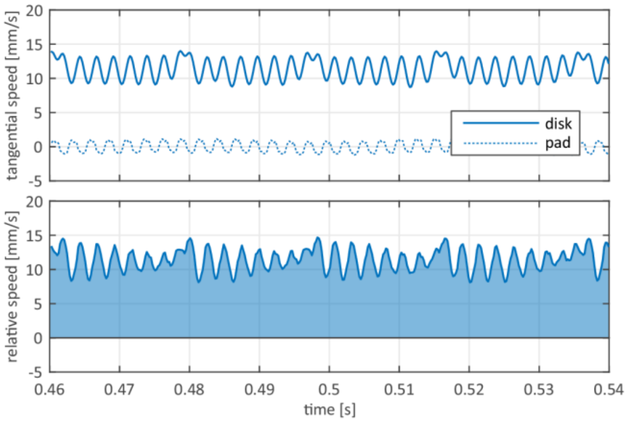

Fig. 13. Tangential disk/pad speeds and resulting relative speed during 386 Hz moan action, adapted from [13]

Furthermore, fig. 2 displays a time and a frequency plot of the longitudinal pad acceleration for this moan effect.

Within [14], a moan mode consisting mainly of torsional rim displacement was measured via laser vibrometry for an almost identical system. Here, the frequency found at 512 Hz was essentially higher, probably due to a different slim-spoke rim design.

5. CONCLUSION

Test bench experiments have shown, that brake NVH phenomena within a frequency range related to the so-called moan can (in the present case) be described by a dynamic instability. Hence, the linearizing CEA should be able to predict possibly critical eigenmodes.

However, simulative investigations of two different rim designs within a chosen parameter range of low brake pressures and vehicle speeds have delivered a stability behavior exactly opposite to the real-world behavior: Whereas rim A was computed unstable at least for one parameter set, rim B was predicted stable.

Most probably, this discrepancy results from an insufficient Finite Element model: Due to modal deflections, it can be assumed that a more sophisticated tire model paired with the implementation of more accurate parameters is necessary. Because of their high influence on stability behavior, damping influences resulting from elastomer bushings could also be a starting point, see [27, pp. 524-525]. In addition, more detailed treatment of the tribological contact, e.g. by augmented state vectors as explained in [17] or an improved condensation method according to [28], could alter the simulative output in a positive manner.

Nonetheless, the computed torsional rim modes and their influence on the dominant moan frequency were in good correspondence with tests performed on similar or even almost identical systems.

6. REFERENCES

[1] B. Breuer and K. H. Bill, Eds.: ***Bremsenhandbuch: Grundlagen, Komponenten, Systeme, Fahrdynamik,*** 5th ed., Wiesbaden, Springer Fachmedien, 2017.

[2] J. Bauer, M. Körner, and A. Pfaff: **Moan Noise - The Phenomenon and Solution Approaches,** *EuroBrake 2017: Conference Proceedings*, Dresden, 2017.

[3] Y. Dai, T. C. Lim: **Suppression of brake squeal noise applying finite element brake and pad model enhanced by spectral-based assurance criteria,** *Applied Acoustics*, vol. 69, no. 3, pp. 196–214, 2008, DOI: 10.1016/j.apacoust.2006.09.010.

[4] D. Wallner: ***Experimental and numerical investigations on brake squeal: Development of a smart friction force measuring sensor,*** Dissertation, Graz, Verl. der Techn. Univ. Graz, 2013.

[5] R. Allgaier: ***Experimentelle und numerische Untersuchungen zum Bremsenquietschen,*** Dissertation, Düsseldorf, VDI-Verlag, 2002.

[6] R. Nunes, A. Shivaswamy, and M. Könning: **A Time Domain Approach Towards Analysing Creep Groan Noise in Automobile Brakes,** *EuroBrake 2016: Conference Proceedings*, Milan, Italy, 2016.

[7] C. Bittner: ***Reduzierung des Bremsrubbelns bei Kraftfahrzeugen durch Optimierung der Fahrwerkslagerung,*** Dissertation, Technical University of Munich, Munich, Germany, 2006.

[8] J. Wallaschek, K.-H. Hach, U. Stolz, and P. Mody: **A Survey of the Present State of Friction Modelling in the Analytical and Numerical Investigation of Brake Noise Generation,** *Proceedings of the ASME Design Engineering Technical Conferences:* Las Vegas, NV, USA, 1999, pp. 2299–2310.

[9] Y. D. Kim et al.: **Identification of moan-noise generation mechanisms by an experimental method and verification of the mechanism by finite element analysis,** *Proceedings of the Institution of Mechanical Engineers, Part D: Journal of Automobile Engineering*, vol. 229, no. 10, pp. 1392–1405, 2015, DOI: 10.1177/0954407014562618.

[10] A. Wang, L. Zhang, N. Jaber, and J. Rieker: **On Brake Moan Mechanism from the Modeling Perspective,** *SAE Technical Papers*, 2003, DOI: 10.4271/2003-01-0681.

[11] M. Donley, D. Riesland: **Brake groan simulation for a McPherson strut type suspension,** *SAE Technical Papers*, 2003, DOI: 10.4271/2003-01-1627.

[12] H. Marschner, P. Leibolt, A. Pfaff, and C. Morschel: **Untersuchung der Wirkmechanismen reiberregter Haft-Gleit-Schwingungen am Beispiel des Bremsenknarzens und analoger Schwingungsphänomene,** *XXXV. Internationales µ-Symposium - Bremsen-Fachtagung:* Bad Neuenahr, pp. 84–104, 2016.

[13] S. Huemer-Kals, M. Pürscher, and P. Fischer: **Application Limits of the Complex Eigenvalue Analysis for Low-Frequency Vibrations of Disk Brake Systems,** *SAE Technical Papers*, 2017, DOI: 10.4271/2017-01-2494.

[14] D. Müller, D. Wallner, S. Carvajal, and F. Gauterin: **Simulation der Frequenzantwort des Rad-Bremse Verbundes auf gemessene Anregungssignale,** *18. Kongress SIMVEC - Simulation und Erprobung in der Fahrzeugentwicklung: Berechnung, Prüfstands- und Straßenversuch*, Baden-Baden, pp. 491–508, 2016.

[15] A. K. Kléperon, R. D. Abreu, R. M. Bitencourt, and F. J. Almeida: **Brake Moan Noise Study through Experimental and Operational Modal Analysis Techniques in a Passenger Car,** *SAE Technical Papers*, 2014, DOI: 10.4271/2014-36-0768.

[16] S. Huemer-Kals: ***Complex Eigenvalue Analysis of Friction Induced Low-Frequency Vibrations in Vehicle Disc Brake Systems,*** Master Thesis, Institute of Automotive Engineering, Graz University of Technology, 2018.

[17] A. Völpel, G. P. Ostermeyer: **Investigation of the Influence of ODE Based Friction Models on Complex FEM Brake Models in the Frequency Domain,** *SAE International Journal of Passenger Cars - Mechanical Systems*, vol. 9, no. 3, pp. 1206–1213, 2016, DOI: 10.4271/2016-01-1931.

[18] M. Pürscher, S. Huemer-Kals, and P. Fischer: **Experimental and Simulative Study of Creep Groan in Terms of MacPherson Axle Bushing Elasticities,** *EuroBrake 2018: Conference Proceedings*, The Hague, 2018.

[19] N. Gräbner: ***Analyse und Verbesserung der Simulationsmethode des Bremsenquietschens,*** Dissertation, Technische Universität Berlin, Berlin, 2016.

[20] INTES GmbH: ***PERMAS-Workshop - Dynamik II: Erweiterungen und spezielle Anwendungen,*** Stuttgart, Germany, Oct. 2015.

[21] J. Guckenheimer, P. Holmes: ***Nonlinear oscillations, dynamical systems, and bifurcations of vector fields,*** 7th ed., New York, NY, USA, Springer, 2002.

[22] Hartmut Hetzler: ***Zur Stabilität von Systemen bewegter Kontinua mit Reibkontakten am Beispiel des Bremsenquietschens,*** Dissertation, Karlsruhe, Universitätsverlag Karlsruhe, 2008.

[23] B. Siegl: **Output-only Modal Analysis for System Identification Before Brake Squeal,** *presented at ISNVH 2018*, Graz, Austria, Jun. 22, 2018.

[24] M. Pürscher, P. Fischer: **Systematic Experimental Creep Groan Characterization Using a Suspension and Brake Test Rig,** *SAE Technical Papers*, 2017, DOI: 10.4271/2017-01-2488.

[25] M. Pürscher, P. Fischer: **Strain Gauge Application at Pad Backing Plates to Investigate Friction Force and NVH Issues,** *EuroBrake 2017: Conference Proceedings*, Dresden, 2017.

[26] M. Pürscher, S. Huemer-Kals, and P. Fischer: **Experimental Investigation of Low-Frequency Vibration Patterns in Automotive Disk Brake Systems: Utilization Study for Modal Simulation Methods,** *SAE Technical Papers*, 2018, DOI: 10.4271/2018-01-1513.

[27] N. Hoffmann, L. Gaul: **Effects of damping on mode-coupling instability in friction induced oscillations,** *ZAMM - Zeitschrift für Angewandte Mathematik und Mechanik*, vol. 83, no. 8, pp. 524–534, 2003, DOI: 10.1002/zamm.200310022.

[28] N. Gräbner, S. M. Quraishi, C. Schröder, V. Mehrmann, and U. von Wagner: **New numerical methods for the complex eigenvalue analysis of disk brake squeal,** *EuroBrake 2014: Conference Proceedings*, Lille, France, 2014.

8th Congress of the Alps Adria Acoustics Association
Zagreb, Croatia
20 – 21 September 2018

ELECTROMECHANICAL AND ACOUSTICAL CHARACTERIZATION OF PIEZOCERAMIC ELEMENTS AND ULTRASOUND TRANSDUCERS

Petar Franček[1], Antonio Petošić[1], Marko Budimir[2], Iva Brkić[1]

[1]University of Zagreb, Faculty of Electrical Engineering and Computing, Unska 3, 10 000 Zagreb, Croatia
(petar.francek@fer.hr)
[2]INETEC d.o.o., Dolenica 23, Lučko, 10 250 Zagreb, Croatia

Abstract: *Usage of a piezoceramic actuators and ultrasound transducers in modern applications requires very high efficiency and stability in real operating conditions. Whether if it's used in medicine as a diagnostic, therapeutic or invasive device, in industry for non-destructive testing, for cleaning overall or for other purposes, usage of an ultrasound element should be optimized to obtain as higher radiation power as possible or better resolution by optimizing the pulse shape and its duration. To enhance and optimize utilization of an ultrasound transreceiver a proper characterization is needed. Mostly used methods for characterization (frequency sweeping, amplitude sweeping) are described in EN standards (50324) [1]. In this paper an overview of mostly used and some recently published methods is given. Algorithms for laboratory equipment are implemented and setups are adjusted for each considered method. Laboratory measurements are created, and results are presented. Results of electromechanical characterization for different types of bulk piezoceramic materials and transducers are analyzed and discussed. An introduction to novel automated method for determining properties of a piezoceramic elements and ultrasound transducers driven by continuous signal at resonant frequency which depends on the excitation level is also shown and discussed.*

Key words: electromechanical and acoustical characterization, standardized methods, optimization of impedance matching, impulse excitation, characterization at resonant frequency

1. INTRODUCTION

Nowadays, accessibility and usability of a devices with high computational power, small overall dimensions and low power consumption has become ordinary. Decreasing manufacturing costs, devices with various sensors, setups and with the ability to compute gathered information can be found in every household [2]. This increase can be noted also in use of ultrasound devices, whether the usage is in medicine, research, industry, or some other branch. Ability to minimize power consumption and to optimize speed and size drastically increase the utilization of such devices [3]. Best increase and an overall optimization are obtained by driving the device at series resonance frequency where the impedance magnitude has minimum and current, displacement and pressure have maximum values. For that reason, an additional research must be performed in the area near the serial and parallel resonant frequencies of piezoceramic elements and overall ultrasound transducers.

Characterization of a piezoceramic elements is performed to determine their properties (mechanical quality factor, electromechanical coupling coefficient, dielectric, piezoelectric and elastic properties). Those parameters are the result of standardized methods for electromechanical characterization [1]. They can be used as input parameters for modelling of overall transducer behavior before assembling the transducer.

Most common methods for full electromechanical characterization of device under tests (DUTs) are with low excitation voltage and current magnitude by using frequency sweeping signals at the room temperature. In real operating conditions that excitation parameters can be changed when compared to measurements in laboratory conditions, the temperature and for example voltage or current excitation level are much higher from the used ones during laboratory characterization and those parameters can be significantly different during usage of piezoceramic elements in ultrasound transducers.

As the result, it is possible to drive an ultrasound transducer that is not well fitted for a designed excitation in real operating conditions.

This paper will compare results from methods for piezoceramic elements and overall ultrasound transducers characterization in usually used conditions for characterization (room temperature, low excitation, …) with the results measured in the conditions close to the real operating conditions (DUT driven at some high excitation level (up to 100 W) and increasing the working temperature because of driving the device at series resonance frequency)

2. THEORETICAL BACKGROUND

To enhance and optimize utilization of an ultrasound transreceiver a proper characterization in real operating conditions is needed. Measurements by using different excitation levels (expressed in voltage, current or applied electrical power) or exciting DUTs on elevated temperature, results with series resonant frequency shifting and increase of the impedance magnitude at resonance frequencies. Difference can be in excitation voltage, current, applied electrical power and in response mechanical and acoustical signals and obtained mechanical and radiated acoustic power in different types of ultrasound transducers for medical (surgery, therapy) and industrial application (NDT). Also, the electrical excitation can be formed from various shapes, intervals, repetitions or it can be the sum of other more complex waveform shapes (for example in NDT applications). All mentioned above, can be found in real operating conditions in ultrasound transducers, what can mislead expected behavior if input parameters are determined at linear driving conditions and at room temperature.

1.1. Impedance spectroscopy

Electrical impedance spectroscopy (by using frequency sweeping signal) method is mostly used as characterization method. It can be used in combination with impedance bridge and keeping constant voltage, current and/or displacement magnitudes at each frequency considered around the mode of interest (radial, thickness extensional). For full and optimal characterization of piezoceramic elements and ultrasound transducers these methods do not consider all parameters that have influence on their behavior (dynamical change of excitation level in medical applications of horn ultrasound transducers, sonotrode types of transducers in food processing).

1.2. Pulse-echo method

Impulse excitation is often used in real operating conditions in NDT usage so characterization with this type of excitation assures conditions similar to in-situ situations. While Impedance spectroscopy uses continuous sine signal with targeted frequency, in this method impulse signal has power in small portion of a period of a whole signal, so this type of method takes the measurements avoiding overheating which can cause the changes in piezoceramic sample properties. The method enables determination of material parameters only at one frequency of interest (near resonance frequency) so the measurement should be repeated at some other frequencies near resonance to validate the data in the frequency range of interest [4].

1.3. Novel methods

Proposed novel method uses signal with continuous sine voltage as excitation. Method tracks series resonance behavior by changing excitation magnitude and monitoring different DUT parameters (electrical, mechanical and acoustical) when excitation level is changed, and new series resonance frequency is found. In electrical domain, voltage and current have been monitored with a corresponding phase shift. In acoustical/mechanical domain a sound pressure, displacement and temperature have been monitored and stored for analysis with available theoretical models which can describe the change of resonant frequency due to nonlinear effects or elevated temperature. Goal of using novel methods to characterize piezoceramic elements or ultrasound transducers is to find changed resonant frequency due to nonlinear effects and elevated temperature.

3. EXPERIMANTAL SETUP

All the measurements have been performed in controlled and monitored laboratory setup. All the equipment is used according to its manuals and guides, following advices and tips. Current sensor has been adequately calibrated on every turning on and displacement sensor has been well positioned for proper measurement results. Temperature sensor is developed especially for these measurements. As a result of self-heating during measurements at higher excitation levels surface temperature of the DUT is monitored. To get optimal heat spectrum from the DUT and appropriate temperature results positioning of contactless sensor is extremely important. Sensor has to be close to DUT, facing area with high temperature dissipation, which is a challenge to realize for some tested elements regarding its size and shape.

Equipment used for Impedance spectroscopy measurements is shown in **Fig. 3.1.** The BODE impedance analyzer is used for measuring the input electrical impedance by using low voltage magnitude (1 V_{RMS}) frequency sweeping signal around series resonance frequency. To ensure better measurement results an impedance adapter is used in a combination with network analyzer. Setup with impedance adapter has to be calibrated for each measurements.

The scheme of an experimental setup used for characterization with pulse-echo method and with novel methods can be seen in **Fig 3.2**.

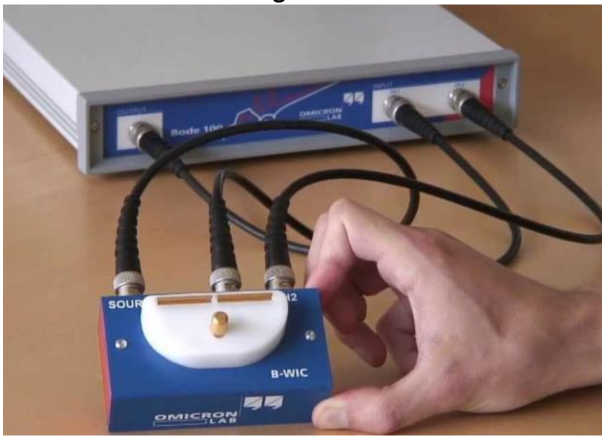

Fig.3.1. BODE100 network analyser with impedance adapter used for Impedance spectroscopy

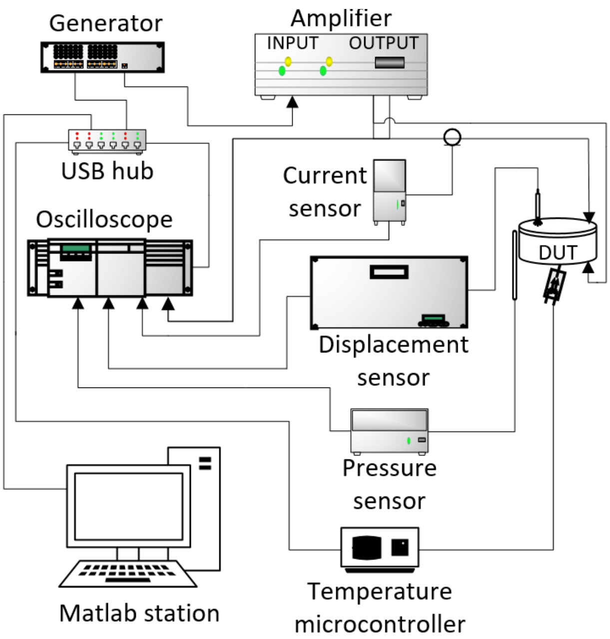

Fig.3.2. Laboratory measurement setup used for pulse-echo and novel methods

As a central processing, storing, managing and supervising unit a PC with preinstalled Matlab is used. PC is connected to peripheral laboratory equipment via USB interface. Keysight 33512b arbitrary waveform generator with resolution of 100µV and 0.1Hz [5] is used as a generator for the sine signals of different excitation levels and frequencies. Signal is amplified by the TOA 300M [6] power amplifier and amplified signal is connected to a DUT. A series of sensors used to control and gather a DUT parameters are connected to the following inputs of the MSO-3024A oscilloscope [7]:

- CH1: Voltage probe Testec TT-SI 9001 with frequency range up to 25MHz and levels up to 700Vpp [8] is directly connected to ceramic electrode (DUT)
- CH2: Current probe Tektronix TCP312 [9] with frequency range up to 100 MHz and levels from mA up to 30 A, whose signal is processed through its own amplifier TCPA300 [10], spans one wire of a DUT
- CH3: The signal of Acoustic Pressure Sensor Bruel&Kjaer 8103 [11], positioned exactly at DUT, is amplified with the associated Bruel&Kjaer Nexus Amplifier [12] making the measurements more accurate
- CH4: Displacement signal obtained from an amplifier MTI 2100 [13] whose photonic sensor is positioned exactly along the DUT surface

Next to the aforementioned sensors, there is a temperature contactless sensor with accuracy of 0.5 °C in range -40 °C to 125 °C and resolution of 0.02 °C [14]. It is controlled by a NodeMCU microcontroller connected to the computer via a LAN connection.

4. MEASUREMNT RESULTS

During measurements ambient temperature was in range 26°C – 28°C. As a commercial NDT transducer, a Krautkrämer transducer with declared 2.25 MHz series resonance frequency is used and as a bulk piezoceramic three (2 hard and 1 soft) bulk ceramic samples were used:

1. APC50 – APC 851 hard sample from American Piezo, APC International, Ltd
2. PiHard – PIC 181 hard sample from PI Ceramic GmbH
3. PiSoft – PIC 151 soft sample from PI Ceramic GmbH

For the bulk samples the resonance frequency of radial mode of working has been chosen and for commercial transducer a thickness mode of working has been chosen. Bulk testing samples dimensions are shown in the **Table 1.**

DUT	Diameter [mm]	Thickness [mm]	Mass [grams]
APC50	48.98	9.94	150
PiHard	49.76	4.92	78
PiSoft	49.74	4.84	76

Table 1. Sample physical parameters [15][16]

It is obvious that bulk samples dimensions important for radial mode of working (diameter) are almost the same (cca. 5cm).

Measurement results have been divided following characterisation methods described in 2nd chapter respectively.

Commercial Krautkrämer NDT transducer is characterized using Impedance spectroscopy method and two different impulse excitation signals (unipolar and bipolar) with pulse width 217.5 ns. First figure (**Fig. 4.1.a)**) shows characterisation results (transducer impedance) without sonogel applied to transducer surface standing clear in the air and second figure (**Fig. 4.1.b)**) represents measurements with applied sonogel on the steel block (measurement with conditions closer to the real operating conditions).

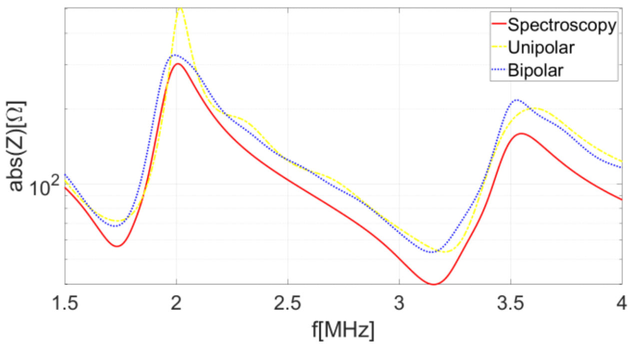

Fig.4.1.a) Measured transducer impedance without sonogel applied to transducer surface

There are visible two resonance peaks in **Fig 4.1.a)**. (1.7-2.1 MHz and 3.2-3.6 MHz) and second resonance is supressed while performing same characterisation with applied sonogel (**Fig. 4.1.b)**). Impedance magnitude is higher by using impulse excitation signals (bipolar and unipolar).

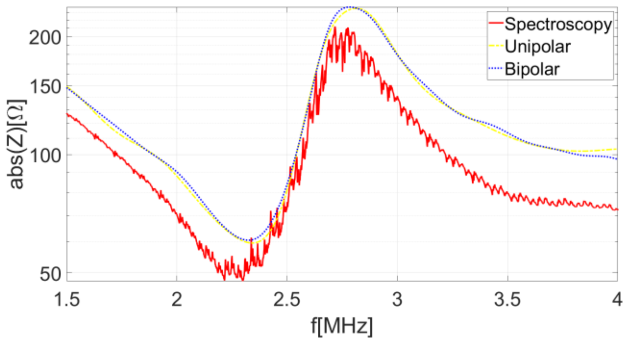

Fig.4.1.b) Measured transducer impedance with sonogel

There is no significant difference for the impedance magnitude determined using bipolar and unipolar pulse as shown in **Fig. 4.1.b)**. Also, in this figure there are visible multiple ripples on Impedance spectroscopy curve. Ripples can be explained with multiple reflections from sonogel and block.

The same transducer is used to compare various types and widths in impulse excitation characterization method. Comparison of two commonly used types (bipolar and unipolar) with 2 different pulse widths (217.5 ns and 263.2 ns) is shown in **Fig. 4.2.**

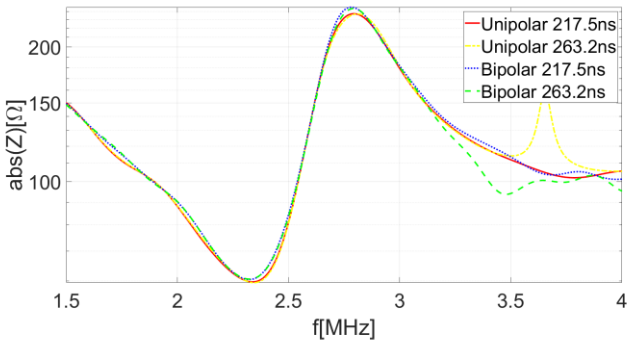

Fig.4.2. Comparison of impulse excitation with two different pulse types and widths

It is visible in **Fig. 4.2.** that bipolar impulse excitation has slightly higher impedance magnitude compared to the unipolar impulse excitation.

In process of designing and developing novel characterization methods preliminary measurements are created on bulk piezoceramic samples. Results are shown in **Fig. 4.3.a)** and **Fig. 4.3.b)**.

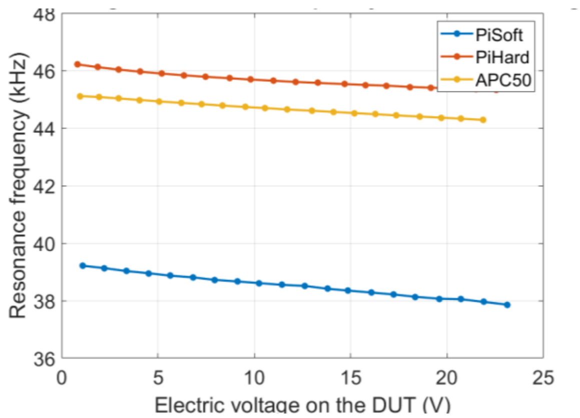

Fig.4.3.a). The change of serial resonant frequency with electric voltage

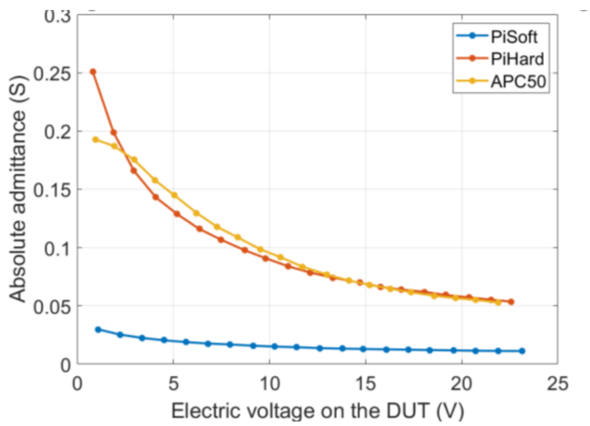

Fig.4.3.b). The change of admittance in resonance with electric voltage

Characterization results are showing that determined parameters are not constant but have some regularities. With raising excitation magnitude resonant frequency is becoming lower and absolute admittance is becoming lower. The trend of change depends on the piezoceramic sample material and shape.

5. CONCLUSION

Presented measurement results created with characterization methods described in this paper are showing that characterisation results strongly depends on a various conditions while performing characterisation. As shown in aforementioned results, piezoceramic or ultrasound transducer resonant parameters are tightly connected with excitation type (continuous, pulse, burst,…), shape (sine, square, bipolar/unipolar pulse,…), frequency (and pulse duration) and magnitude. Also, those parameters are tightly connected to a piezoceramic or ultrasound transducer material content, working temperature, mass and applied pressure.

For characterisation with high continuous excitation piezoceramic characteristic of a self-heating is very expressed. Proposed novel method is trying to minimize influence of a piezoceramic self-heating by measuring ceramic sample temperature in every step of the characterisation. With monitoring and gathering voltage, current, displacement, sound pressure, phase shift of mentioned signals and time data for each characterisation step this method is designed to characterize piezoceramic or ultrasound transducer taking into account electrical, mechanical and acoustical parameters overall.

6. ACKNOWLEDGEMENT

Part of this research is funded by project “An ultrasonic non-destructive testing system for detection and quantification of early stage subsurface creep damage in the thermal power generation industry (CreepUT)” (Project ID: 760232) funded by European Union from the programme “H2020-EU.2. - PRIORITY 'Industrial leadership'” and programme “H2020-EU.3. - PRIORITY 'Societal challenges'“..

7. REFERENCES

[1.] „**IEEE Standard on Piezoelectricity , ANSI/IEEE 176-1987**“, IEEE, New York, 1987. [Online] (http://ieeexplore.ieee.org/stamp/stamp.jsp?arnumber=26560).

[2.] A. González, Á. García, C. Benavente-Peces, L. Pardo, “**Revisiting the Characterization of the Losses in Piezoelectric Materials from Impedance Spectroscopy at Resonance**”, Materials (Basel). 2016 Feb; 9(2): 72.

[3.] Liao X, et al., “**Functional Piezocrystal Characterisation under Varying Conditions**”, Materials 2015; 8(12):5456.

[4.] H. Shekhani: “**Characterization of the high power properties of piezoelectric ceramics using the burst method: methodology, analysis and experimental approach**”, A Dissertation in Electrical Engineering, The Pennsylvania State University The Graduate School College of Engineering.

[5.] **Keysight 33512b datasheet** [Online] (URL: https://literature.cdn.keysight.com/litweb/pdf/5992-2572EN.pdf?id=2937598).

[6.] **TOA 300M datasheet** [Online] (URL: http://www.gbaudio.co.uk/data/p300.htm).

[7.] **MSO-3024A datasheet** [Online] (URL: http://www.testequipmenthq.com/datasheets/Agilent-MSOX3024A-Datasheet.pdf).

[8.] **Testec TT-SI 9001 datasheet** [Online] (URL: www.testec.de/en/assets/pdf/TT-SI/TT-SI-9001-9002_EN.pdf).

[9.] **Tektronix TCP312 datasheet** [Online] (URL: https://www.tek.com/sites/default/files/media/media/resources/TCPA-Amplifiers-and-TCP300-400-Probes-Datasheet-60W1645811.pdf).

[10.] **TCPA300 datasheet** [Online] (URL: https://www.tek.com/datasheet/ac-dc-current-measurement-systems).

[11.] **Acoustic Pressure Sensor Bruel&Kjaer 8103 datasheet** [Online] (URL: https://www.bksv.com/doc/bp0317.pdf).

[12.] **Bruel&Kjaer Nexus Amplifier datasheet** [Online] (URL: https://www.bksv.com/doc/bp1702.pdf).

[13.] **MTI 2100 datasheet** [Online] (URL: https://www.mtiinstruments.com/wp-content/uploads/2017/08/Fotonic.pdf).

[14.] **MLX90614 datasheet** [Online] (URL: https://www.sparkfun.com/datasheets/Sensors/Temperature/MLX90614_rev001.pdf).

[15.] **American Piezo datasheet** [Online] (URL: https://www.americanpiezo.com/apc-materials/piezoelectric-properties.html).

[16.] **PiCeramic datasheet** [Online] (URL: https://www.piceramic.de/fileadmin/user_upload/physik_instrumente/files/datasheets/disc-Datasheet.pdf).

Index of authors